Isotope geochemistry of black shales and Recent marine sediments

A THESIS

Submitted for the Award of Ph. D degree of

MOHANLAL SUKHADIA UNIVERSITY
In the
Faculty of Science

by

Gyana Ranjan Tripathy

Under the Supervision of

Dr. Sunil Kumar Singh
ASSOCIATE PROFESSOR

Physical Research Laboratory,
Ahmedabad-380009, India.

DEPARTMENT OF GEOLOGY

MOHANLAL SUKHADIA UNIVERSITY

UDAIPUR

2011

DECLARATION

I, **Mr. Gyana Ranjan Tripathy**, S/o Mr. Uma Charan Tripathy, resident of A-4, PRL residences, Navrangpura, Ahmedabad – 380009, hereby declare that the research work incorporated in the present thesis entitled ***"Isotope geochemistry of black shales and Recent marine sediments"*** is my own work and is original. This work (in part or in full) has not been submitted to any University for the award of a Degree or a Diploma. I have properly acknowledged the material collected from secondary sources wherever required. I solely own the responsibility for the originality of the entire content.

Date: (Gyana Ranjan Tripathy)

CERTIFICATE

I feel great pleasure in certifying that the thesis entitled "**Isotope geochemistry of black shales and Recent Marine sediments**" by **Gyana Ranjan Tripathy** under my guidance. He has completed the following requirements as per Ph.D. regulations of the University

(a) Course work as per the university rules
(b) Residential requirements of the university
(c) Presented his work in the departmental committee
(d) Published/accepted minimum of two research paper in a referred research journal.

I am satisfied with the analysis of data, interpretation of results and conclusions drawn.

I recommend the submission of thesis.

Date: *Name and designation of supervisor*

Sunil Kumar Singh,
Associate Professor

Countersigned by
Head of the Department

Dedicated

To

My Parents,

Sri Uma Charan Tripathy & Smt. Monorama Tripathy

Acknowledgement

This thesis work would not have been possible without the help and support of many people. I sincerely thank all of them for their selfless cooperation.

Since my first day at PRL, Dr. Sunil Kumar Singh, my thesis supervisor, was always there to share his knowledge and expertise in geochemistry and instrumentation. He introduced me to the field of isotope geochemistry and mass spectrometry. Without him, my transition from physics to geochemistry would have been unexciting. He was very instrumental in educating me with every minute detail of isotope geochemistry, chemical processing of samples, working with TIMS, data analysis and interpretation. His friendly and informal nature helped me to boldly present my views during scientific discussions. I acknowledge him for providing me ample freedom to work and for his support and guidance.

I express my gratitude to Swami (Prof. S Krishnaswami) for his valuable comments and suggestions during this work. Discussions with him were always beneficial in my growth as a researcher. Scientific integrity, in-depth knowledge in geochemistry and his meticulous approach towards research makes him very special; it was truly an honor to be associated with such a great geochemist. His requirement for perfection in every aspect of science, although makes it tough to work with him, but has been very educative. I am immensely thankful to Prof. Swami for his valuable time and constructive views. I thank Prof. M M Sarin for his support and suggestion during my thesis work. His systematic approach towards scientific problems has been very encouraging and discussions with him, particularly on U-Th isotopic systematics, river water chemistry and instrumentation were very beneficial. I owe my sincere thanks to Prof. SVS Murthy for his guidance during my course work project.

I am extremely thankful to Prof. J. N. Goswami, the Director, Prof. Utpal Sarkar, Dean and Prof. S K Bhattacharya and A.K. Singhvi, former Dean, Physical Research Laboratory, for providing me support and facilities for my thesis work. I thank academic committee members for timely review of my work. Special thanks to Profs. R Ramesh, S K Gupta, Dr. D Banerjee for their informative lectures during course work.

I am thankful to all members of the Chemistry Lab for their help and support during my thesis work. I thank Dr. Santosh K Rai for his guidance during chemical processing of samples and TIMS operation. I thank Dr. Ravi Bhushan for encouragement and support during my thesis. Working with him has always been a pleasure, whether on a cruise or during scientific discussions. I acknowledge the help of Dr. R Rengarajan for his co-operation and suggestions during my thesis work. Thanks to Sudheer for his help during geochemical analyses of river water samples. It's my pleasure to thank J P Bhavsar for his help and for providing a homely environment in the lab. I thank Rahaman, Kirpa, Ashwini, Timmy, Vineet, Satinder, Jayati, Srinivas and Prashant for their help and support. Discussion and support of my seniors, Tarun, Anirban and Neeraj was always helpful in my work. I duly acknowledge the help of Vishwanathan, Sneha, Komal and Shantaben.

I am thankful to Drs. J.S Ray, Navin Juyal, M.G. Yadava, Vinai K. Rai and Mr. A D Shukla for their reassurance towards my work. Thanks are also due to Drs. P. Sharma, R.D. Deshpande, Kuljeet Kaur, D. K. Rao, R.A Jani, D. Panda, Dibyendu Chakravarty, Som K. Sharma and Bhushit Vaishnav for their kind support. I am grateful for the instrumentation facility in Planex and to Durgaprasad, Jayesh and Narendra for his help during measurements. I thank Drs. Rajesh Agnihotri and Koushik Dutta for their help and support. I thank Dr. V Ramaswamy, Prof. H. Bhu and Prof. G J Chakrapani for their suggestions in our collaboration work. Discussions with Profs. A. Tarantola and P Gupta were very helpful during inverse modeling course at C-MMACS, Banglore. My sincere thanks to Drs. Subimal Deb, Sanat Kumar Das and Uma Das for their help in computer programming.

I am grateful to all the staff-members of Library, Computer Centre, Workshop, Administration, Dispensary, Maintenance section of PRL for their assistance and cooperation. Thanks to Bankim for fabricating Carius tube required for osmium chemistry.

The memorable moments of PRL tea-time, TV room, Volleyball and TT matches are pleasant and unforgettable. Thanks to my first friend at PRL, Lokesh for his care and support. I thank Naveen, Arvind, Bhavik, Sanjeev, Vishal, Anil, Kallol, *Pathak, Bindu and Charu for making my initial days of PRL joyful. I spent pleasant moments at PRL hostel with my close friends. Company of my batch-mates (Alok, Sumanto, Brajesh, Sumita, Bhatt, Tyagi, Shuchita, Harinder, Manan, Ram, Chandra Mohan (CM), Ayan, and Rohan), my seniors (Rajesh, Shreyas, Morthekai, Salman, Zeen, Mourya, Sunil, Amitavab, Sharma, Rohit, Ritesh, Satya, Antra, Vandana, Jayesh and Sasadhar) and my juniors (Arvind Saxena, Suratna, Rohit, Amjad, Chauhan, Rabiul, Neeraj, Ashish, Tapas, Sunil, Arun, Suruchi, Moumita, Chinmay, Iman, Patra, Suman, Ashok, Praveen, Bhaswar, Anand, Sandeep, Srikant, Soumya, Subrata, Vimal, Yogita, Prayakta, Pankaj, Zulfikar and Rajpurohit) made my stay pleasant and enjoyable at PRL.*

I thank Mrs. Renu Singh for making me feel like part of her family. Thanks to Mrs. Krishnaswami, Mrs. Sarin, Mrs. Bhushan, Mrs. Rengarajan and Mrs. Sudheer for their care and nice get-togethers. My sincere thanks to Mrs. Pauline Josheph for her help, support and affection. Presence of Markandeya, Monu, Golu and Mahin always made me joyous. I thank Preeti and Reshma for their care, and of course for the delicious food.

I owe my sincere thanks to my brothers (Sarada Prasad, Simanchal, Biswa and Rashmi Ranjan) for extending every possible comfort and support to me during this work. I am deeply grateful to Satya and Sujata for their affection, encouragement, care and support. Thanks are due to Minati, Vijaya, Jyotchna for their faith and confidence on me. Love and affection to Sipra, Sambit, Smruti, Sriya, Srija, Bhabhani (Suraj) and Snigdha for making my life cheerful. Its my pleasure to thank Bini, Sudhansu, Sasank, Pinku and Raju; I really enjoyed every moment that I shared with them. I thank Swapn for his rational and mature suggestions. I would cherish his friendship forever.

Lastly, but most importantly, pranam to my parents (Sri Uma Charan Tripathy and Smt. Monorama Tripathy) for their love, care, affection and support during this work. It was their confidence that inspired me the most to complete this work, and hence, I take this opportunity to dedicate this thesis to them.

ABSTRACT

The focus of this thesis is on the applications of radiogenic isotopes of Os, Sr and Nd to determine chronologies of key sedimentary deposits in India and temporal variations in provenances of sediments from the Bay of Bengal (BoB). Black shales from the Vindhyan, Lesser Himalaya (LH) and Aravalli were analyzed for ^{187}Re-^{187}Os systematics to constrain their depositional ages and to assess their potential to track atmospheric oxygen evolution during the Proterozoic to Early Cambrian. These studies have provided precise depositional ages for the Vindhyan (Kaimur) and outer belt of LH, in contrast samples from the Aravalli and inner belt of LH show "open system" behavior of Re-Os due to the post-depositional alterations. The ^{187}Re-^{187}Os isochron of black shales from the Upper Vindhyan yield an age of 1196±41 Ma with an initial ^{187}Os/^{188}Os of 0.74±0.27. The shales lying just above the Pc-C boundary of the outer LH provided a Re-Os age of 541±4 Ma, in excellent agreement with U-Pb ages for the Pc-C boundary reported from other locations. Results suggest more intense reducing condition during their deposition with higher supply of mantle like Os. The initial ^{187}Os/^{188}Os obtained in this study along with those available in literature on the Proterozoic ocean show consistent trend of atmospheric oxygen, attesting to the potential of ^{187}Os/^{188}Os as a suitable proxy for paleo-oxygen record.

The Sr-Nd isotopes of sediments from a piston core from the western BoB indicate that their dominant supply from the Himalaya and Peninsular India. Temporal variations in the Sr-Nd isotopes suggest source variability in the past with relatively reduced contribution from the Himalaya during LGM indicating a strong erosion-climate link. Lower erosion over the Himalaya is due to lower southwest monsoon intensity and higher snow cover over the Higher Himalaya during LGM.

Efforts to characterize the chemical erosion pattern of the Ganga basin and to apportion the sources of solutes, inverse modeling of available literature data on elemental and Sr isotopic composition of the Ganga headwaters was carried out. These results show that on average ~25% of major cations are from silicates and balance from carbonates. The chemical erosion rates of the basin bring out the importance of lithology in controlling the erosion pattern.

Table of Contents

LISTS OF TABLES

LISTS OF FIGURES

CHAPTER 1

Introduction

1.1. INTRODUCTION

Oxygenation of atmosphere, growth and erosion of continental crust and diversification of biosphere are the vital processes in making our planet habitable. These processes are inter-linked and are responsible to provide key macro- and micro-nutrients to the hydrosphere, which in turn shaped the modern biogeochemical cycle of the Earth [*Frimmel*, 2005]. Significant changes in these reservoirs occurred during the Precambrian period and information on their evolution history are contained in various sedimentary sequences deposited during that time and present on the Earth today. Sedimentary successions of various ages from the Paleoproterozoic to Recent are present in India that includes the Aravalli, Vindhyan, and the Himalaya. These formations preserve the records of history of Earth, atmospheric and biological evolutions in them and can be used to extract these paleo-informations. However, application of these deposits to infer early evolution of Earth has been largely hampered by their limited reliable age information. Attempts are made in this thesis to use Re-Os chronometer to date black shales from the Aravalli, Vindhyan and the Lesser Himalaya. The basic idea behind studying shales from these three geological successions is to reconstruct the geochronological framework for a time period spanning from the Proterozoic to Early Cambrian, an important time slice of the Earth history witnessing the evolution of atmosphere from an anoxic to oxic world, biological diversification *etc*.

The chemical and isotopic signals of sedimentary rocks though has a potential to provide useful information about past marine oxic-anoxic conditions, paleooceanography, paleoprovenance *etc*.; their use, however, is largely hampered due to difficulty in constraining their depositional ages. Among the various available dating schemes, the U-Pb dating of magmatic zircon interbedded with sedimentary sequences are found to provide reliable depositional ages. However, they are often too small in size (<10 μm) for their separation from other minerals and the limited availability of interbedded volcanic sequences in sedimentary basins often restrict their application [*Rasmussen*, 2005]. U-Pb dating of detrital zircon has also been used to constrain ages for Precambrian sedimentary deposits. The merit of using zircon lies in its potential to retain age information despite post-depositional thermal events [*Rasmussen*, 2005], however, application of this geochronometer is limited as it provides provenance age of the grains, which may be significantly higher compared to the sedimentary depositional age. The radiometric dating (Ar-Ar, K-Ar, Rb-Sr and Sm-Nd) of detrital minerals (*e.g*. gluconite, illite, K-feldspar, apatite, monazite, fine fractions of mud-rocks *etc*.) are also being used to constrain depositional ages of sedimentary deposits, however these techniques suffer from post-depositional alterations and provide the age information of the sources of the sedimentary succession not their depositional time. The Rb-Sr and Ar-Ar dating of lava flow and tuffs present in sedimentary successions are used to date them. Though these methods have the potential to find precise age of sedimentary rocks, thermal resetting of these igneous objects in post-depositional processes hinder their extensive application. The U-Pb and Pb-Pb systematics of carbonates have shown potential to constrain the depositional ages of sedimentary deposits, however presence of “older” detrital carbonates and post-depositional alterations also challenged this approach [*Rasmussen*, 2005]. During last few decades, Re-Os isotopic systematics has been found successful in better constraining the depositional ages of sedimentary deposits, especially those of organic-rich shales [*Ravizza and Turekian*, 1989; *Cohen et al.*, 1999; *Singh et al*., 1999; *Selby and Creaser*, 2003; *Kendall et al.*, 2004; *Yang et al.*, 2009]. Organic matter rich shales are available in most of the sedimentary deposits making this systematic suitable for dating them.

The ^{187}Re-^{187}Os isotopic systematics proved to be a useful geochronometer to obtain the depositional ages of organic-rich shales [*Ravizza and Turekian*, 1989; *Kendall et al.*, 2009a]. The Re-Os chronometer, like any other radiometric dating method, for sedimentary rock is based on the assumptions that (i) both Re and Os remain closed subsequent to their deposition (ii) initial ^{187}Os/^{188}Os are homogeneous and *i.e*., Re and Os present in the sedimentary deposits are predominantly authigenic, *i.e.* contribution from detrital and cosmic dust is insignificant [*Kendall et al.*, 2009a].

These assumptions seem to be valid for the Re-Os systematics in black shales. During the deposition of these organic-matter rich sediments in reducing condition, organophillic and redox-sensitive elements, Re and Os from seawater gets scavenged in these sediments. Hence, in general the Re and Os contained in black shales are mostly authigenic in nature as their abundances in upper continental crust are very small and hence, the Re-Os systematics of these shales preserve the age information of their deposition. Subsequent to the study of *Ravizza and Turekian* [1989], large number of studies has been carried for last two decades to constrain the depositional ages of black shales from various geological formations using Re-Os chronometer [*Cohen et al.*, 1999; *Singh et al.*, 1999; *Creaser et al.*, 2002; *Selby and Creaser*, 2003; *Schaefer and Burgess*, 2003; *Hannah et al.*, 2004, 2008; *Kendall et al.*, 2004, 2006, 2009b; *Anbar et al.*, 2007; *Jiang et al.*, 2007; *Turgeon et al.*, 2007; *Kato et al.*, 2009; *Yang et al.*, 2009; *Rooney et al.*, 2010]. Along with the depositional ages, these studies on Re-Os systematics of black shales also have provided the ^{187}Os/^{188}Os ratio of seawater prevailing at the time of their deposition. The Re-Os chronometer can yield accurate and precise age of black shales (~±1% uncertainity). For example, the Re-Os age of black shales [361.3±2.4 Ma; *Selby and Creaser*, 2005] from the Devonian-Mississippian boundary of the Exshaw formation is found to be in excellent agreement with the U-Pb age of zircons [360.7±0.7 Ma; *Trapp et al*., 2004] extracted from metabentonites. This thesis is aimed to constrain depositional ages of black shales from different sedimentary sequences of India (*e.g.* the Aravalli, Vindhyan and the Lesser Himalaya) using Re-Os chronometer.

The Re-Os isotopic systematics does not seem to undergo alteration during thermal events [*Creaser et al.*, 2002; *Jaffe et al*., 2002], however post-depositional alteration and weathering of organic-rich shales can mobilize Re and Os from the system, which can alter their ages. Studies on soil profiles showed that ~70% of organic carbon gets lost during weathering of black shales [*Jaffe et al*., 2002], which in turn can result in loss of organophillic elements, such as Re and Os. Among these two elements, Re is found to be more mobile compared to Os. The weathering of black shales, despite being a minor lithology in river drainages seem to contribute significantly to osmium budget of seawater [*Ravizza and Esser*, 1993; *Singh et al.*, 1999]. Similar to osmium, the important role of black shale weathering in supplying rhenium was borne out from the research of *Dalai et al.* [2002], which showed a strong correlation between the dissolved Re and SO_4 (an index of pyrite weathering) in the Yamuna river basin. It would be necessary to asses the impact of mobilization of Re and Os during weathering on the Re-Os isochron and ages of the black shales. In this thesis, attempts were also made to understand the mobility of Re and Os during weathering and its impact on Re-Os ages.

In the Indian sub-continent, pioneering study on Re-Os chronometry was done by *Singh et al.* [1999] to date black shales from the inner and outer belts of the Lesser Himalaya. These authors also made preliminary attempts to obtain chronology of black shales from the Kaimur group, Vindhyan Supergroup [*Singh et al.*, 2002]. Available techniques during those days, precluded them to analyze Re and Os concentrations and Os isotope composition of the black shales in the same aliquot of the black shale sample and hence the preliminary age provided by *Singh et al.* [2002] is less reliable owing to the large heterogeneity present in these black shales and necessitates their measurement in the same aliquot. This makes the resolution of the long-standing controversial issue of the age of the Vindhyan Supergroup an important application of Re-Os chronometer [*Ray*, 2006; *Azmi et al.*, 2008]. The Vindhyan Supergroup is a well preserved sedimentary sequence exposed in the Central India. The radiometric ages for the Supergroup indicates that it preserves the geological record from late Paleoproterozoic to late Neoproterozoic (1600-600 Ma) age [*Ray*, 2006]. In contrast, the biochronlogical ages claims the Supergroup to be much younger and is a record of short duration of Vendian to early Cambrian [~650-520 Ma; *Azmi et al.*, 2008]. The discovery of small shelly fossils [*Azmi*, 1998] in the Rohtas sub-group of the Lower Vindhyan, which are generally found in early Cambrian ages, is the basis of the biochronologists for constraining the chronology of the Vindhyan. Recently, *Bengston et al.* [2009] confirmed the presence a Paleoproterozoic age (1650 Ma) of multi-cellular fossils in Lower Vindhyan group following an integrated palentological-geochronological study. This reported age for Lower Vindhyan group is consistent with the earlier radiometric ages reported by various workers [*Rasmussen et al.*, 2002; *Ray et al.*, 2002, 2003; *Sarangi et al.*, 2004]. Therefore, the existing radiometric ages for the Lower Vindhyan which cluster around ~1600 Ma constrain their depositional ages with reasonable confidence. On the contrary to the Lower Vindhyan, there have been limited efforts to obtain depositional ages for the Upper Vindhyan, data that is required to constrain the time duration for the deposition of the Supergroup. Further, this information can be helpful in evaluating and quantifying the inference of presence of sedimentary hiatus between the deposition of the Lower and Upper Vindhyan sedimentary deposits based on their sedimentological evidences. The Pb-Pb age along with $^{87}Sr/^{86}Sr$ stratigraphy of the Bhander Limestone [*Ray et al.*, 2003], an age range of 750-650 Ma was assigned for the top-most succession of the Upper Vindhyan. In addition, there have been a few attempts to date the Majhgawan kimberlite pipe that intrudes the Kaimur sandstones of the Upper Vindhyan by radiometric techniques (Ar-Ar, K-Ar and Rb-Sr ages). These ages have a large range [~1630-950 Ma; *Gregory et al.*, 2006]. To better constrain the age of the Upper Vindhyan and hence, to infer about the time duration of the gap in sedimentation between the Upper and Lower Vindhyan, Re-Os dating of Bijaigarh shales from Kaimur group is attempted in this thesis work.

Another interesting issue is to provide reliable radiometric chronology of the biochronology-based Pc-C boundary in India, *i.e.* the Krol-Tal boundary of the outer Lesser Himalaya and also to the sediments deposited in the inner Lesser Himalaya to provide stratigraphic correlation between them. Further, study of Re-Os systematics in the Lesser Himalayan black shales help resolving the controversy pertaining to the state of anoxia prevailing during Pc-C transition and immediately after it. The remarkable change in the biosphere of the planet Earth at around Pc-C boundary is well documented through world-wide deposits of sedimentary rocks. However, the actual cause resulting into this transition from single cellular to multi-cellular dominating biosphere still remains unclear. Recent study [*Wille et al.*, 2008] based on records of Mo isotopic variations of seawater, decoded from black shales, concluded that during the Pc-C transition the surface seawater was euxinic resulting from upwelling of H_2S-rich bottom water. This “sulphide poisoining” caused a mass extinction which subsequently led to biological diversification. In contrast, *Jiang et al.* [2009] highlighted the importance of hydrothermal vents in causing reducing seawater and with a more precise U-Pb zircon age challenged the view of “sulphide poisoing” as the prime cause for Cambrian explosion. The importance of hydrothermal vents in contributing to the Pc-C seawater chemistry was also inferred from the enrichment of redox-sensitive elements in the sedimentary successions of south China [*Jiang et al.*, 2007]. These diverging views on the cause for Pc-C seawater chemistry demand more studies to understand causes for the Cambrian Explosion of life. In light of this, it would be useful to investigate the Re-Os isotopic systematics in the sedimentary deposits before, during and after the Pc-C boundary. The merit of using redox-sensitive Re-Os isotopic systematics to understand the Pc-C seawater chemistry lies in the fact that the isotopic composition of osmium supplied by hydrothermal vents (~0.12) is less radiogenic by an order of magnitude compared to riverine supply (~1.4). Hence, the proposition of enhanced hydrothermal supply during the Pc-C transition to the seawater can be best evaluated by inspecting the marine $^{187}Os/^{188}Os$ ratio at the Pc-C. In this study, Re-Os isotopic systematic of black shales deposited around the Pc-C boundary was investigated to understand the Pc-C seawater chemistry and its causative factors. Further an attempt was made to date black shales from the inner belt of the Lesser Himalaya to provide a reliable comparison between the sedimentary deposits of the inner and outer belts of the Lesser Himalaya.

Reconstructing and understanding the evolution of atmospheric oxygen through geological time scale is of great interest as it is closely related to evolution of the life on the earth. However, tracking the atmospheric oxygen level over geological time period is not straightforward and requires suitable proxies. Earlier researches, based on sulphur and iron isotopic fractionations, on reconstructing the evolution of atmospheric oxygen through geological timescale concluded that the oxygen content of the atmosphere started growing only after ~2.45 Ga [*Canfield et al.*, 2000; *Kasting*, 2001; *Farquhar and Wing,* 2003; *Kah et al.,* 2004; *Canfield,* 2005; *Rouxel et al.,* 2005], precisely after 2.32 Ga [*Bekker et al.,* 2004]. However, recent studies on this aspect based on S/C, Fe/Ti elemental ratios and S, Mo and Cr isotopes indicated presence of appreciable amount of oxygen before 2.45 Ga [*Ohmoto,* 1996; *Ohmoto et al.,* 2006; *Anbar et al.,* 2007*; Wille et al.,* 2007; *Frei et al.,* 2009]. Conflicting propositions pertaining to the rise of atmospheric oxygen pattern require suitable proxy having potential to track the oxygen evolution trend to settle this issue. In this work, the feasibility of temporal variation of seawater ^{187}Os/^{188}Os as a proxy to track the atmospheric oxygen evolution trend has been evaluated.

The present-day seawater osmium isotopic composition is regulated by its relative supply of radiogenic Os (^{187}Os/^{188}Os ~1.4) from continental weathering and unradiogenic Os (^{187}Os/^{188}Os ~0.12) from hydrothermal vent and cosmic dusts inputs. The contemporary global seawater ^{187}Os/^{188}Os is homogenous (1.06), as expected from its higher residence time [~10-40 ka; *Oxburgh,* 2001] compared to mixing time (~1 ka) of ocean. Osmium is a redox sensitive element and its dominant source to seawater is continental weathering through riverine input and its flux at any given time depends on its oxidative weathering from continents. In oxic condition, Os is highly mobile [*Hannah et al.*, 2004], indicating the significant impact of atmospheric oxygen level in controlling its continental supply. This coupling between Os supply *via* rivers and atmospheric oxygen level would control the supply of radiogenic Os to the ocean which in turn control the marine ^{187}Os/^{188}Os evolution. Therefore Os isotope evolution of seawater seems to have potential to track the atmospheric oxygen evolution trend. This proposition can be investigated through the Re-Os isotopic signals preserved in the sedimentary rocks, particularly that of reducing marine sediments (black shales). In this thesis, an effort has been made to reconstruct the global marine ^{187}Os/^{188}Os during the Precambrian using Re-Os systematics of black shales of various ages from the Aravalli, the Vindhyan and the Himalaya.

Along with depositional ages and paleo-seawater conditions, radiogenic isotopic signals preserved in marine sedimentary deposits, particularly Sr and Nd isotopes can be useful in inferring the sources of the detrital material of the sediments and erosion pattern of drainage basins in the past. Information on past continental erosion and their controlling factors would be useful in understanding the marine biogeochemical cycle as it plays a key role in driving the oxic-anoxic state of the seawater by controlling the supply of nutrients. The major driving factors for these erosion processes, both physical and chemical erosion, have been suggested to be different for different basins. The intensity of physical erosion pattern in river basins is often suggested to be controlled by the climatic and tectonic parameters, however their individual role in regulating the denudation process in a basin have remained a matter of debate. Similar to physical erosion, the chemical erosion also has been suggested to be governed by different parameters; of them, rainfall, elevation, lithology, temperature are a few suggested controlling factors. In order to understand the marine geochemical cycles in the past, it would be required to gain better information on the controlling factors of erosion process over continents. In this thesis, efforts are made to infer about the controlling factors of physical and chemical erosion of river basins over kilo year timescale, with a special emphasis to the Himalayan basin.

Chemical and physical erosion of the Himalaya, a young orogenic belt is an important regulator of the marine geochemical cycles and global atmospheric budget of various elements. Studies from PRL group over the years have addressed in detail the issue of the contemporary physical erosion pattern of the Himalayan river basins, for example, the Ganga [*Singh et al.*, 2008] and the Brahamaputra [*Singh and France-Lanord*, 2002] and their controlling factors. In addition, there have also been a few attempts to understand past erosion pattern over the Himalaya [*France-Lanord et al.*, 1993; *Colin et al.*, 1999; *Clift et al.*, 2008; *Rahaman et al.*, 2009; *Galy et al.*, 2010] based on chemical and isotopic signals preserved in sediments from the Ganga plain and the Bay of Bengal (BoB). These sediments archive the erosional history of the Himalaya and nearby landmass influenced by varying climate over thousands of years time scale and study of these sediments, therefore, could provide important information regarding the relation between climate and erosion. Earlier studies have observed that the erosion pattern of the Himalaya remained fairly stable over million year time scales [*France-Lanord et al.*, 1993; *Galy et al.*, 2010]. On a millennial timescale, there have been limited studies on the Himalayan erosion pattern, where climate have been proposed to play a significant role in controlling the continental erosion [*Ahmad et al.*, 2005; *Clift et al.*, 2008; *Rahaman et al.*, 2009]. Contradictory to this proposition, there have been also suggestions of constancy of Sr-Nd isotopes of the BoB sediments [*Galy et al.*, 2008a] since Last Glacial Maximum (LGM), indicating insignificant change in the sedimentary sources to the Himalaya over shorter timescales. These diverging views on the Himalayan physical erosion pattern over millennial timescale warrants more studies in this regard. Sr and Nd isotopes of sediments have been used successful to track the sediment provenances and their relative contributions [*Goldstein and O'Nions*, 1981; *France-Lanord et al.*, 1993; *Singh and France-Lanord*, 2002; *Singh et al.*, 2008]. The source signature of Nd isotopes is well preserved during weathering and transport. The Sr isotopes signatures, however, are prone to fractionation due to size sorting and preferential weathering of minerals [*Tutken et al.*, 2002; *Colin et al.*, 2006]. A combined study of Sr-Nd isotopes have been carried out in this study of BoB sediments to understand the continental erosion pattern (provenances changes) of the Himalaya and Peninsular India and their controlling factors over a ka time scale.

Chemical weathering in river basins is an important component of marine biogeochemical cycles of elements as it supplies nutrients and dissolved elements to the ocean. Again, the global importance of chemical (silicate) weathering lies in the fact that it acts as a major sink for atmospheric CO_2 over a geological timescale [*Walker et al.*, 1981; *Berner et al.*, 1983]. Among the various river basins, the chemical weathering of the Himalayan Rivers, particularly that of the Ganga has been studied extensively as these rivers have been suggested to have an important role in controlling global atmospheric CO_2 since the Cenozoic [*Raymo et al.*, 1988; *Raymo and Ruddiman*, 1992; *Richter et al.*, 1992; *Tripathy et al.*, 2010a]. This hypothesis have been invoked based on the steady increase of marine $^{87}Sr/^{86}Sr$ for the last 40 Ma which has been attributed to enhanced silicate weathering over the Himalaya river basins, which are highly radiogenic in Sr [*Krishnaswami et al.*, 1999]. In order to understand the chemical weathering pattern of the Ganga river basin and its impact on global atmospheric CO_2, large number of geochemical and Sr isotopic studies of the Ganga headwaters have been carried out during the last two decades [*Sarin and Krishnaswami*, 1984; *Sarin et al.*, 1989, 1992; *Krishnaswami et al.*, 1992, 1999; *Harris et al.*, 1998; *Galy and France-Lanord*, 1999; *Galy et al.*, 1999; *English et al.*, 2000; *Bickle et al.*, 2001, 2003, 2005; *Dalai et al.*, 2002, 2003; *Evans et al.*, 2001; *West et al.*, 2002; *Oliver et al.*, 2003; *Quade et al.*, 2003; *Tipper et al.*, 2006; *Tripathy et al.*, 2010b]. These studies were carried out either on individual minor river basins or on relatively large river systems of the Ganga tributaries or sub-tributaries to understand the processes regulating the chemical erosion of the basin, specifically to quantify the contribution from different lithological units to the stream chemistry. A detailed and coordinated study encompassing the major sub-basins of the Ganga headwaters would provide a better understanding of the contemporary weathering processes and the factors influencing them over the entire Himalaya. In the present study, the existing geochemical and isotopic information on the various sub-basins of the Ganga headwaters are reanalyzed. This has been done by both the forward and inverse models for source apportionment of the dissolved solutes and to derive silicate (SER) and carbonate (CER) erosion rates. An inverse model has been suitably developed [*Tarantola*, 2005] as a part of the thesis work to apportion the sources of dissolved material to the rivers and to estimate the chemical erosion rates and CO_2 consumption rates due to silicate weathering in their respective basins. The inverse model also provided a unique approach to estimate the loss of Ca from these headwaters due to calcite supersaturation during lean flow seasons.

1.2. OBJECTIVES OF THE THESIS

1. To determine the depositional ages of black shales from the Vindhyan and the Himalaya using Re-Os chronometer and to infer about their depositional environment.
2. To evaluate the potential of $^{187}Os/^{188}Os$ evolution of seawater as a proxy to track the atmospheric oxygen evolution trend.

3. To investigate the climate-erosion link based on Sr-Nd isotopic compositions of sediments from a core raised from the Bay of Bengal.
4. To study the chemical erosion pattern of the Himalaya (the Ganga headwaters) basin and their controlling factors through inverse and forward models.

1.3. STRUCTURE OF THE THESIS

Chapter 1 introduces the topics addressed in this thesis. It highlights the present state of understanding in these topics and existing research gaps. The objectives of the thesis are also presented in this chapter.

Chapter 2 provides the details of the materials and analytical methodologies used in this thesis work. The first section of the chapter contains the geological description of the sampling locations and sampling procedures followed, whereas the second section discusses the analytical techniques adopted for the geochemical and isotopic analysis of black shales and marine sediments.

Chapter 3 presents the results and discussions pertaining to the Re-Os isotopic compositions of black shales from the Lower Aravalli, Upper Vindhyan and the Lesser Himalaya analyzed during this thesis. These data sets are discussed in light of their depositional ages and impact of weathering of black shales on their Re-Os systematic. This chapter also evaluates the feasibility of tracking atmospheric oxygen evolution trend through past seawater ^{187}Os/^{188}Os.

Chapter 4 deals with the Sr-Nd isotope composition of sediments of a core from the western Bay of Bengal to asses the impact of climate on the past continental erosion pattern over the Himalaya and the Peninsular India.

Chapter 5 describes the application of an inverse model to apportion the sources of dissolved load of the Ganga headwaters and to derive their chemical erosion rates using the available data of major ions, Sr and $^{87}Sr/^{86}Sr$ from the literature.

Chapter 6 concludes the major findings of the thesis and also presents the future perspectives related to these studies.

CHAPTER 2

Materials and Methods

The major objectives of this thesis, as discussed earlier, are (i) to determine the depositional ages of sedimentary (*e.g.* black shale) sequences using Re-Os chronometry and (ii) to infer about changes in the marine oxic-anoxic conditions during specific periods in past using ^{187}Os/^{188}Os and geochemistry of Precambrian and Early Cambrian carbonaceous shales. This thesis also has carried out research to reconstruct erosion pattern of the Himalaya and the Peninsular India and their controlling factors over a millennial timescale based on the provenances of sediments from the Bay of Bengal and their variations in the past (ka time scale), which is traced using Sr-Nd isotopes as proxies. The achievement of these scientific goals requires proper sampling and isotopic and geochemical analyses of carbonaceous shales and marine sediments. This chapter provides detailed geological description of samples (black shales and marine sediments) and their sampling locations along with the methodology used for their isotopic and geochemical analyses. Quantitative information on the chemical erosion pattern of the Himalaya is also inferred in this study through an inverse model calculation of available data in the literature on the major ions, Sr and ^{87}Sr/^{86}Sr of the Ganga headwaters.

2.1. MATERIALS

2.1.1. Black Shales

For this thesis, black shales from various geological sequences from the Proterozoic and Early Cambrian are studied. These geological sequences, namely the Aravalli, Vindhyan and the Lesser Himalaya, exposed in India (Fig. 2.1) cover a wide age range of about 2200-540 Ma. Samples from the Lower Aravalli are collected during this thesis work, whereas black shales from the Vindhyan and the inner and outer belts of LH are from the sample archives of our group. The geological settings of these sequences and details of sampling locations are presented below.

(I) Aravalli Supergroup

(a) Geological Details:

The Aravalli Supergroup, exposed in the northwestern part of the Indian shield, covers an area of ~1,00,000 km^2. The Aravalli craton is broadly classified into three startigraphic sequences, *viz.* (i) Banded gneissic complex (BGC) basement (3500-2500 Ma), (ii) Aravalli Supergroup (2500-2000 Ma) and (iii) Delhi Supergroup rocks (2000-1700 Ma) [*Ahmad et al.*, 2008]. The major lithological units of the BGC are granitic gneisses, granitoids, amphibolites and metasediments, whereas the Delhi Supergroup contains Mesoproterozoic rocks of shallow marine depositional environment.

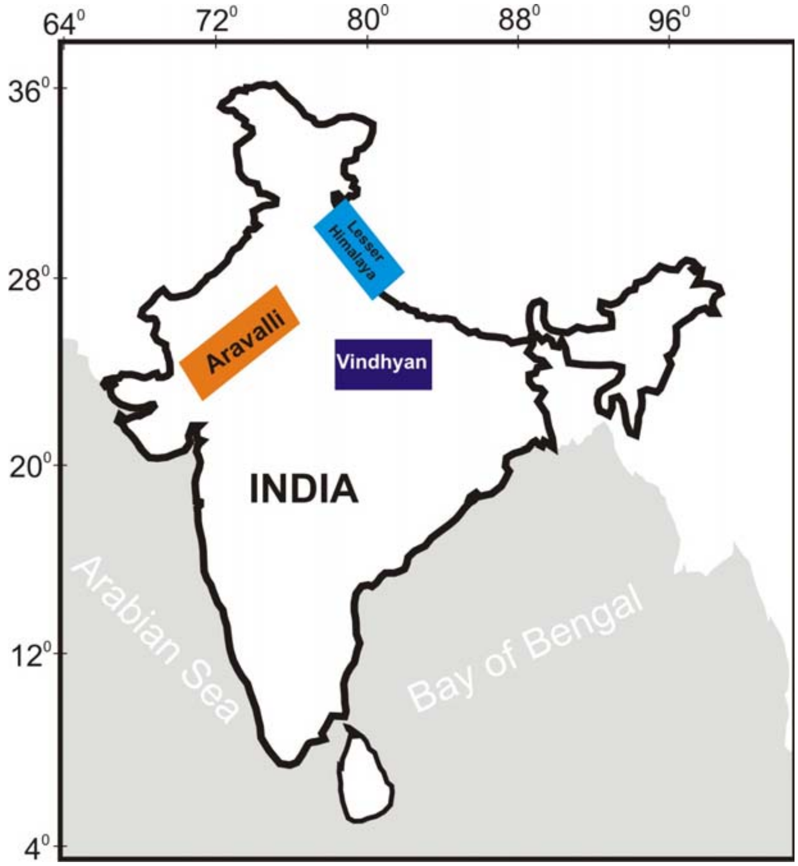

Figure 2.1: *Location of geological successions of India from where black shales for this study are analyzed.*

Frequent overlap of litho-units and repetition by isoclinal folding resulted from thrusting/shearing of rocks [*Ramakrishnan and Vaidyanadhan*, 2008] have complicated the geological mapping of the Aravalli Supergroup. Broadly, the Supergroup is composed of two contrasting lithofacies associations, (i) shale-sand-carbonate assemblage representing near-shore shelf deposition and (ii) carbonate-free shale facies, a deep-sea facies. The Supergroup consists of three unconformity-bounded stratigraphic successions, namely Lower, Middle and Upper Aravalli [Table 2-1; *Roy and Jakhar*, 2002].

Lower Aravalli: The Lower Aravalli overlies the BGC basement. The Delwara formation of the Lower Aravalli dominantly constitutes mafic and ultramafic volcanic rocks and intercalated quartzite sequences. The Jhamarkotra formation, superimposes the Delwara formation, contains shallow-marine dolomites and carbonaceous shales. The carbonate rocks are dolomitic in nature. The Jhamarkotra formation has been studied in some detail for its sedimentological, isotopic and geological information [*Sreenivas et al.*, 2001; *Roy and Jakhar*, 2002; *Papineau et al.*, 2009]. The depositional condition of phyllites present in this formation, based on V/Cr ratio, is suggested to be anoxic [*Roy and Jakhar*, 2002]. The depositional age for this formation was inferred from Pb-Pb ages of the carbonates [*Sarangi et al.*, 2006]. For this study, the carbonaceous black shales from this formation are strategically collected to infer about its depositional age and environment of Paleoproterozoic seawater.

Middle Aravalli: The Udaipur formation contains (meta-) greywacke and phyllites and it is separated from carbonate-rich Jhamarkotra formation by a prominent unconformity. These sediments are continent-derived [*Roy and Jakhar*, 2002]. The Mochia formation, lying above the Udaipur formation, is mainly composed of rocks with association of massive dolomite to phyllite and arkose. Above the carbonate horizon of the Mochia formation is the Bowa formation containing quartzite, quartzose phyllite along with conglomerate lenses. The Tidi formation consists of thinly bedded slate and phyllites with dolomitic and quartzite association.

Upper Aravalli: The Debari formation contains poorly sorted, polymictic conglomerate bed with quartzite and vein quartz pebbles, cobbles and boulders. The Debari formation is followed by Kabita dolomite sequence and the youngest formation of the group, Lakhawali phyllites and serpentinites. The triangular shaped Jharol formation of the Upper Aravalli is a deep-sea facies, composed mainly of argillaceous unit with thin beds of quartzite.

Table 2-1: Stratigraphic sequence of the Aravalli Supergroup along with their corresponding chronology [*Roy and Jakhar*, 2002; *Ahmad et al.*, 2008 *and references therein*].

	Group	**Shelf sequences**	**Deep-sea sequences**	**Chronology**
DELHI SUPERGROUP				2000-1700 Ma
ARAVALLI SUPERGROUP	**Upper Aravalli**	Serpentinites Lakhawali Phyllite Kabita Dolomite Debari Formation	Jharol Formation	
	Middle Aravalli	Tidi Formation Bowa Formation Mochia Formation Udaipur Formation		1700 Ma
	Lower Aravalli	Jhamarkotra Formation Delwara Formation		2200-2000 Ma
BANDED GNEISS COMPLEX, GRANTOIDS				3300-2500 Ma

(b) Chronological Perspective:

The geochronological evidences for the Aravalli Supergroup are scarce (Table 2-1). The radiometric ages of the BGC basement show a wide spread ranging from 3.3 to 2.5 Ga [*Gopalan et al.*, 1990; *Wiedenbeck and Goswami*, 1994; *Roy and Kroner*, 1996; *Wiedenbeck et al.*, 1996]. The model Pb isotopic age for galena from Delwara formation of the Aravalli was reported to be 2200-2000 Ma [*Deb and Thorpe*, 2004]. The reported ages for the Archean basement compared with the maximum age of Aravalli Supergroup hints towards ~ 300 Ma hiatus between the two geological sequences. Recently, *Sarangi et al.* [2006] obtained a Pb-Pb age of 1921±67 Ma for carbonates from Jhamarkotra formation, but suggested a 200-300 Ma further older depositional age for the formation compared to the Pb-Pb age for these carbonates based on the reported positive $\delta^{13}C$ anomalies of these rocks

[*Sreenivas et al.*, 2001]. Based on a Rb-Sr ages of synkinematic Darwal granite, *Choudhary et al.* [1984] indicated the minimum age of the Aravalli to be 1900±80 Ma. An active volcanism at ~2.3-1.8 Ga is inferred from the Sm-Nd isotopic systematics of komatites and tholeiites exposed in the Lower Aravalli [*Ahmad et al.*, 2008]. *Biju-Sekhar et al.* [2003] indicated that the Aravalli Supergroup was metamorphosed at lower to upper greenschist facies around 1.7-1.8 Ga.

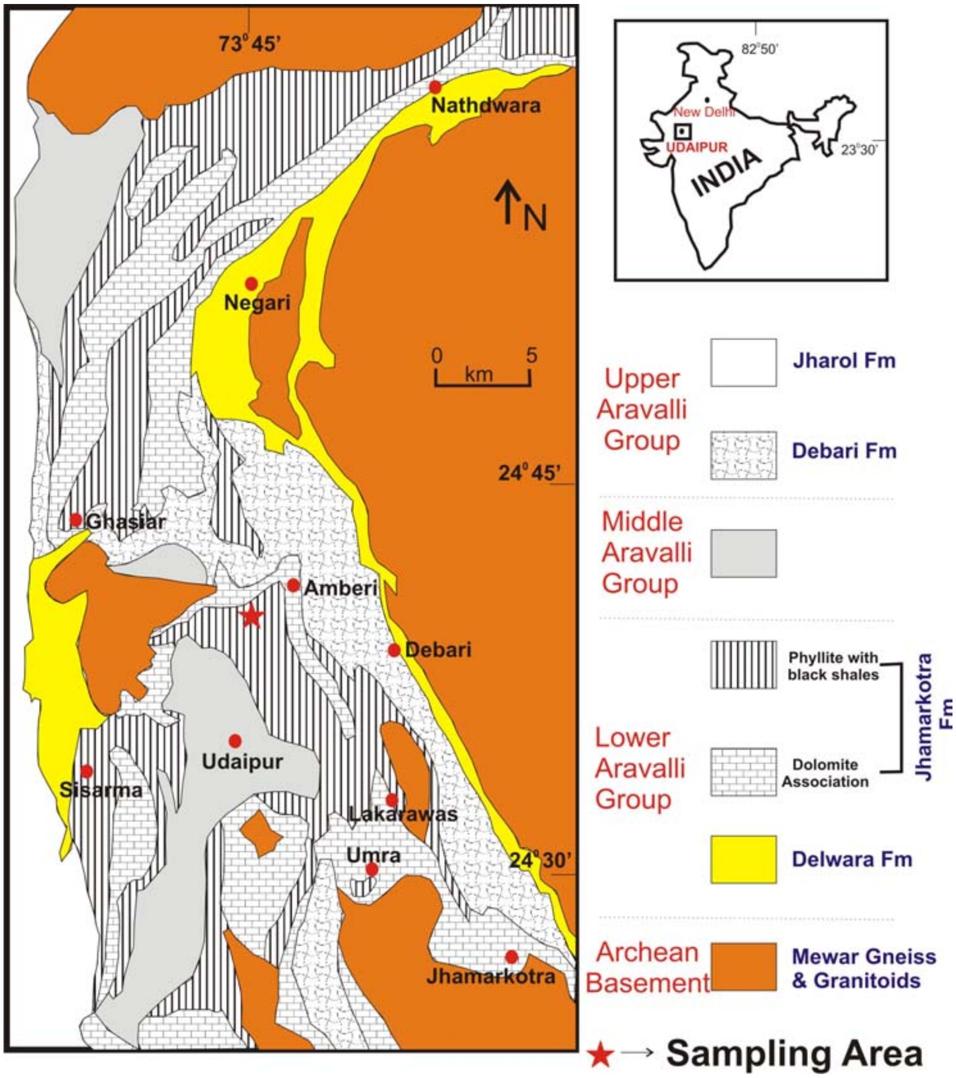

Figure 2.2: *Sampling location of black shales from the Aravalli Supergroup [modified after Papineau et al., 2009].*

(c) Sampling:

Suites of black shales from the Jhamarkotra formation of the Lower Aravalli group (Fig. 2.2) were collected in two field trips during 2006 and 2010. The black shales collected during 2006 trip are sampled near Meera Ka Goda (24°39.220'N; 73°44.099'E) and that collected during 2010 are from a fresh cut road-section near the Udaipur bypass road (Amberi, 24°39.236'N; 73°44.149'E). These two sampling locations are geographically close to each other. The collected shales are sampled after removing ~1 m of the exposed surfaces of black shales to minimize the effect of mobilization of Re and Os due to weathering. The samples during each filed trip were collected over a stretch of few meters of the same sequence of Jhamarkotra formation. In hand specimen, the collected samples were observed to be gone through less or minimal weathering.

(II) Vindhyan Supergroup

(a) Geological Details:

The Vindhyan Supergroup, a Proterozoic sedimentary sequence, is exposed over an area of ~1,04,000 km^2 in the Central India (Fig. 2.1) and large part of the Supergroup is concealed below the Deccan traps and the Ganga alluvium. The sedimentological occurance of the Vindhayn basin indicates its shallow [*Mitra*, 1996] to deep marine environments. Stratigraphically, the Supergroup, situated on the Bundelkhand granite massif (3.3-2.5 Ga), is sub-sectioned into the Lower (Semri) and Upper (Kaimur, Rewa, Bhander) Vindhyan (Table 2-2).

Lower Vindhyan: The dominant litho-units of the Lower (Semri group) Vindhyan (thickness ranging from 20-4345 m; Fig. 2.3) are mainly composed of sandstones, limestone, porcellanite and shales. This group rests on the Bundelkhand granites with prominent angular unconformity [*Ramakrishnan and Vaidyanadhan*, 2008]. Occurrence of lenses of chert and limestone with gluconitic sandstone in the Deoland sandstones suggest a transgressive marine environment [*Ramakrishnan and Vaidyanadhan*, 2008]. However, the presence of sulphur, pyrite in black shales and pyroclastic rocks in the upper part of the group indicates its volcanic and euxinic environment.

Table 2-2: Sedimenatry sequence of the Vindhyan Supergroup *[Ray, 2006; Azmi et al., 2008]*.

Geological stratigraphy				**Thickness**	**Lithology**	**Radiometric ages**
VINDHYAN SUPERGROUP	**UPPER VINDHYAN**	Bhander Group		1300-1500 m	Sandstone, shale, stromatolitic limestones	~600 Ma
		Rewa Group		100-300 m	Shales, sandstones, siltstones, barites	
		Kaimur Group		400 m	Sandstone, black shales, grit	~1150 Ma
	SEDIMENTARY HIATUS					
	LOWER VINDHYAN	Semri Group	Rohtas Subgroup	3000-4000m	Limestone, Black Shales, porcellanite	~1600 Ma
			Khenjua Subgroup			
			Mirzapur Subgroup			
BIJAWAR SUPERGROUP **BUNDELKHAND GRANITE-GNEISS COMPLEX**						~2500 Ma

Upper Vindhyan: The Upper Vindhyan is broadly sub-sectioned into three groups, *viz*. Kaimur, Rewa and Bhander group.

(i) **Kaimur Group:** The Kaimur group, the lower section of the Upper Vindhyan, is mainly a sandstone-shale association compared to shale-limestone association of the Semri group. The thickness of the Kaimur group is about 400 m. The Kaimur group mainly contains sandstone, black shales, grit and conglomerate. The sandstones exposed in this group are thick and cross bedded and ripple marked [*Roy and Jakhar*, 2002]. Occurrence of clasts of the Semri sequence in the basal conglomerate of the Kaimur indicates significant time gap between the two groups. The black shales for this study are collected from the Bijaigarh formation of the Kaimur Group. The sedimentary structure and lithology of the Bijaigarh shales of the Kaimur group suggests their lagoonal Precambrian deposits [*Singh*, 1980].

(ii) **Rewa Group:** This group lies in between the Kaimur and Bhander group of the Upper Vindhyan section (Table 2-2) with a thickness ~100-300 m. The basal succession of the group has no conglomerate, indicating continuous depositional record following that of the Kaimur group. The group mainly composed of shales and sandstones. Presence of red shale, limestone, barites and gluconite siltstone indicates lagoonal deposition of the sequence.

(iii) **Bhander Group:** The Bhander group is mainly a sandstone-shale-sandstone-stromatolitic limestone depositional sequence. The basal unit of the Bhander group, the youngest succession of the Vindhyan, is the Ganugarh shale. These shales associated with stromatolitic limestone, indicates its shoreline-lagoon-tidal flat complex. The Lakheri limestones are suggested to be from an evaporitic environment, whereas other exposures of limestones of the group are formed in tidal flat-lagoon environment. The sedimentary structures of sandstones indicate their tidal flat to near shore littoral environment. Presence of purple Sirbu shale with halite clasts indicates oxidizing to arid conditions.

(b) Chronological Perspective:

The depositional age of the Vindhyan sedimentary succession has remained unclear since the discovery of non-Ediacaran trace fossils and animal body fossils

[*Seilacher et al.*, 1998; *Azmi*, 1998] in the Lower Vindhyan. The controversy regarding the age of the Vindhyan exists due to disagreement between the radiometric ages and paleontological records [*Azmi et al*., 2008]. As one of the objectives of this study is to constrain the depositional age of the Kaimur group, the chronology aspect of the Vindhyan is highlighted here (Table 2-2) and detailed description will be presented in chapter 3.

The existing fossil records for the Vindhyan Supergroup infer contrasting depositional ages compared to radiometric dates. Paleobiological studies suggested an age range of ~900-1300 Ma for the Semri to the Kaimur Groups, which was in accordance with the inference of Lower Riphean (1200 Ma) age for the Semri series [*Venkatachala et al.*, 1996]. *Venkatachala et al.* [1996] also inferred a late Precambrian age (1045 Ma) for the Upper Vindhyan. Contrary to these ages, *Heron* [1953] suggested a Cambrian age for the Vindhyan "system". Based on the occurrence of non-Ediacaran trace fossils and animal body fossils [*Seilacher et al.*, 1998; *Azmi*, 1998] in the Lower Vindhyan, a Vendian to Early Cambrian age (~650-220 Ma) was proposed. Recent paleontological-radiometric integrated study by *Bengston et al.* [2009], however, confirmed the older ages of the Vindhyan and that these Cambrian-like small shelly fossils were present at 1650 Ma.

According to the radiometric ages, the Vindhyan Supergroup contains sedimentary records of age range ~1800-600 Ma [*Ray*, 2006]. The zircon Pb-Pb age of the Bundelkhand granitic basement rock of the Vindhyan is found to be 2492±19 Ma [*Mondal et al.*, 2002], consistent with previously reported Rb-Sr age of 2560 Ma [*Crawford and Compston*, 1970]. The ages reported for the rocks of the Semri group were observed to cluster around 1600 Ma [*Kumar et al.*, 2001; *Rasmussen et al.*, 2002; *Ray et al.*, 2002, 2003; *Sarangi et al.*, 2004; *Bengston et al.*, 2009]. Available ages of the Upper Vindhyan, however, are limited. Based on Rb-Sr age of Majhgawan lamproite intrusion, *Kumar et al.* [1993] suggested a depositional age of >1067 Ma for the Kaimur Group, consistent with few more radiometric ages reported for the kimberlite pipe that intrudes to the Kaimur sandstones [*Gregory et al.*, 2006 and *references therein*]. *Ray et al.* [2003] based on Pb-Pb ages for limestone and Sr isotopic stratigraphy indicated an age of ~700 Ma for the Bhander group. The lack of sufficient age information on the Upper Vindhyan demands more chronological studies to assign proper ages for these sedimentary deposits. Hence, efforts are made in this thesis to constrain the depositional ages of Kaimur group using Re-Os chronometer.

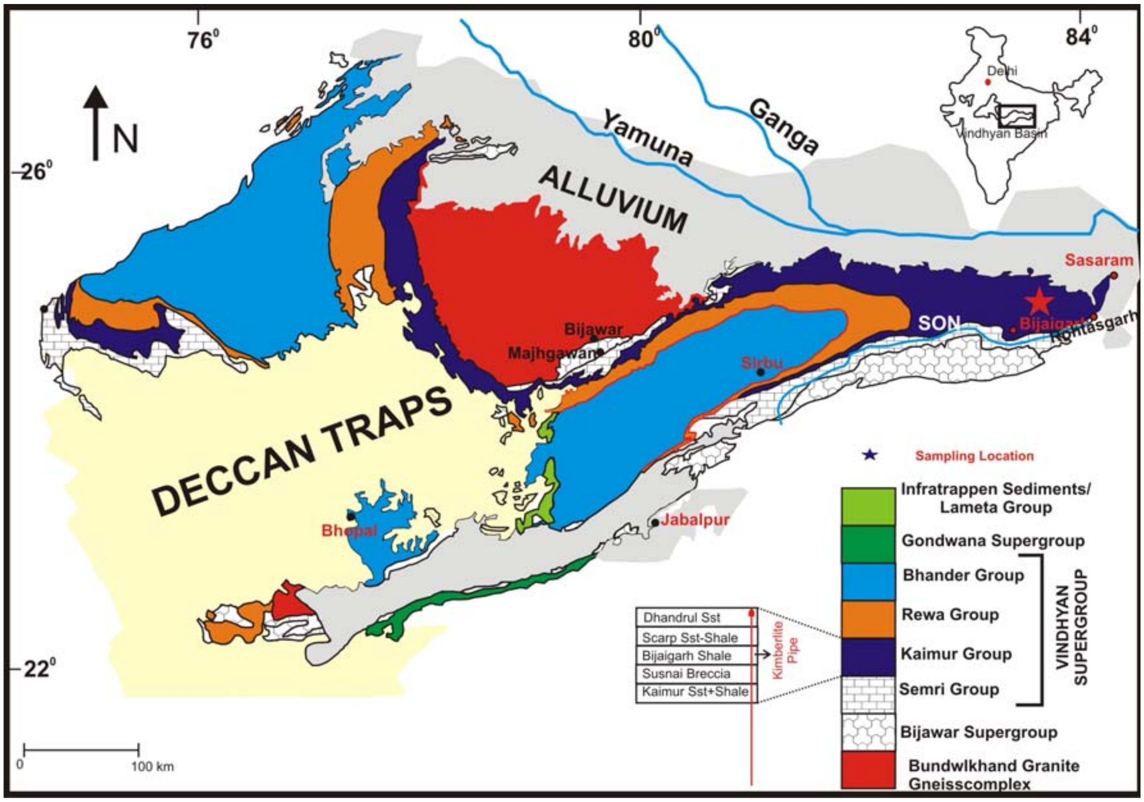

Figure 2.3: *Geological distribution of the Vindhyan Supergroup [modified after Azmi et al., 2008]. Sampling location of black shales is marked by star. The samples are from a pyrite underground mine.*

(c) Sampling:

Black shales from the Vindhyan Supergroup were collected by Dr. Sunil K Singh and colleagues during a field trip during 1999. Fig. 2.3 shows the sampling location along with the geological (spatial) distribution of the Vindhyan Supergroup. These shales are from an underground pyrite mine at Amjhore, Rohtas, Bihar (24°43.731’N;

83°59.488’E). In this mine, 1-2 m thick pyrite layer is sandwiched between two shale layers. These shales belong to the Bijaigarh formation, which forms the lower part of the Kaimur group (Fig. 2.3). Samples from the pyrite layer along with the top and bottom layers of black shales were collected over a stretch of few meters for Re-Os chronology. These shales, in hand specimen, are hard and black. Shining pyrite nodules of different sizes were present in them. The presence of shining pyrites and the fact that the samples are from underground mine are indication that these samples are unlikely to be subjected to chemical weathering. The main objective for sampling the lower Kaimur is to provide a well constrained depositional (Re-Os) age of this group which lies above the Rohtas subgroup where Cambrian-like fossils were discovered [*Azmi*, 1998].

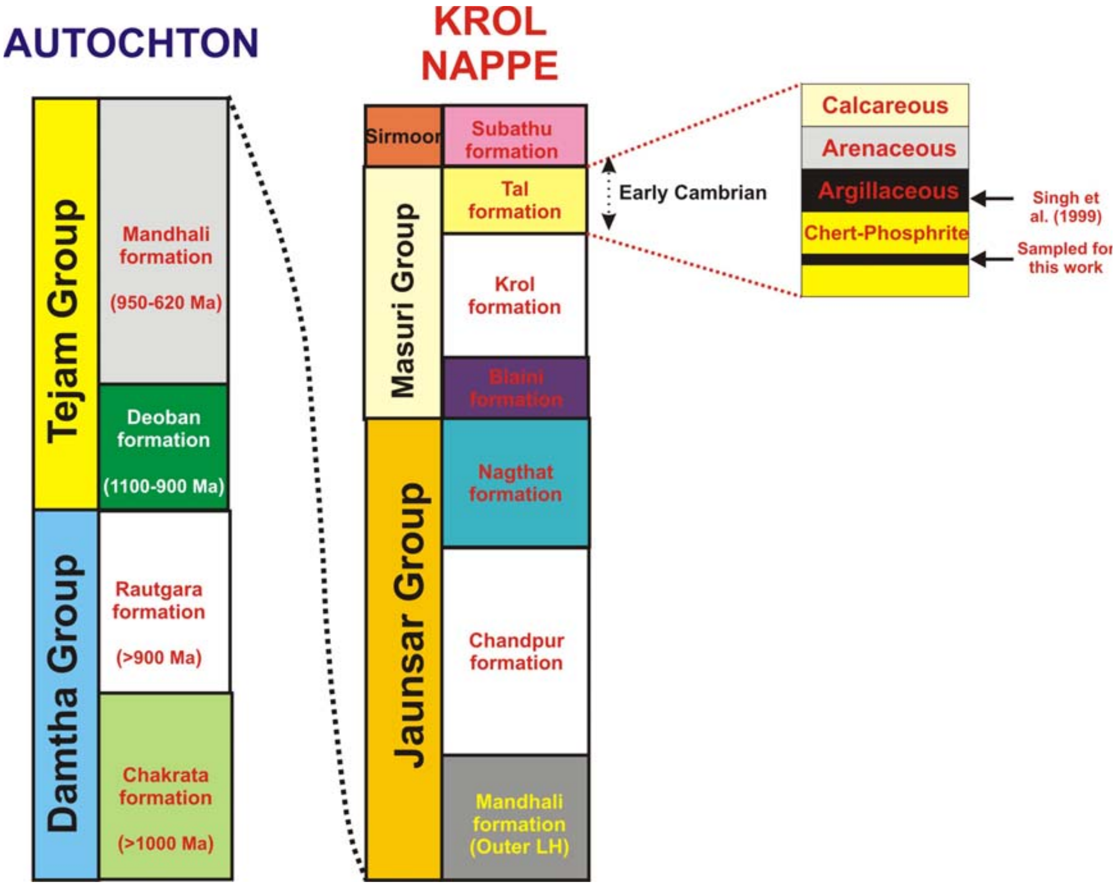

Figure 2.4: *Lithological startigraphy of the Lesser Himalaya [Valdiya, 1980; See text].*

(III) Lesser Himalaya

(a) Geological Details:

The Lesser Himalaya (LH) is a major part of the Himalayan chain extending from the Naga Parbat in the northwest to Namche-Barwa in the southeast and lies to the south of the Higher Himalaya (HH) and to the north of the Siwalik and is demarcated from these units by Main Central Thrust (MCT) in the north and Main Boundary Thrust (MBT) in the south respectively. The LH contains sediments, age ranging from ~1800 Ma to 500 Ma [*Ramakrishnan and Vaidyanadhan*, 2008]. The northern part of the sequence is known as inner belt and the southern part is the outer belt. The present study is carried out in samples from the Tal formation in the outer LH and the Mandhali formation exposed in the inner LH (Fig. 2.4). The geological description of these litho-tectonic units is detailed below.

Inner Belt of LH

1. *Deoban Formation*: The Deoban formation lies above the Rautgara formation (Fig. 2.4) and is a carbonate dominating formation, containing both dolomites (stromatolite-bearing) and calcites [*Valdiya*, 1980]. Based on sedimentary structure and associated stromatolites, a shallow, warm and agitating marine environment is suggested for the deposits of this formation.

2. *Mandhali Formation*: The Mandhali formation lies above the Deoban in the inner belt (Fig. 2.4). This formation is mainly composed of grayish to black carbonaceous shales interbedded with blue-banded limestones and paraconglomerates. The sedimentary structure of these rocks indicates their deposition in poorly ventilated euxinic marine environment [*Valdiya*, 1980].

Outer Belt of LH

Blaini Formation: The Blaini formation mainly contains conglomerates, siltstones, shales and dolomitic limestones. This formation has been suggested to be formed in glacio-marine environment [*Shanker et al.*, 1993]. The Infra-Krol formation lies above the Blaini formation and contains grayish black and bleached shale/slate interbedded with thin slit layers. The sedimentary structure of the sediments from Infra-Krol indicates their low energy tidal flat and lagoonal depositional environment.

Krol Formation**:** The Krol formation lies above the Blaini formation (Fig. 2.4). The lithology of Lower Krol overlaps with that of the Upper Blaini formation, which makes it difficult to properly demarcate the formations. Towards top of the formation, the phosphatic horizon of the Tal formation marks as a sequence of unconformity. The Krol formation is mainly composed of limestones, slates, siltstones and dolomites. *Awasthi* [1970] based on trace elements and insoluble residues inferred that the sedimentation in the Krol formation started in shallow coastal lagoons behind the barrier beach which changed with the passage of time into tidal-flat near mean sea level.

Tal Formation: The Tal formation overlies the Krol formation and is mainly composed of chert-phosphrite and calcerous rocks [Fig. 2.4; *Valdiya*, 1980]. The Lower Tal formation is composed of black chert interbedded with shale and rock phosphate, black shales, calcareouc siltstone and siliceous limestone. The Upper Tal exposes quartz arenite, shale, siltstone and limestone. Sedimentological evidences in Lower Tal succession are suggested to represent relatively deeper and sheltered depositional basin with restricted water circulation [*Valdiya*, 1980]. Based on sedimentary structures, *Banerjee and Narain* [1976] indicated that the depositional environment of Upper Tal was considerably shallowed and was converted into tidal flats and lagoons later. A suite of black shales for this study were collected from the Lower Tal formation from underground phosphorite mines at Maldeota.

(b) Chronological Perspective:

There have been considerable amount of efforts to study the fossil record of the outer and inner belts of the LH (Fig. 2.4). The occurrence of stromatolites, *e.g. Baicalica baicalia, Masloviella Columnaris* in the Deoban formation constrain its depositional age to Middle Riphean period. The testimony of the stromatolites from the Mandhali formation indicates its upper Riphean to Vendian age [*Valdiya*, 1980]. The major focus of the outer belt of the LH is the Blaini–Krol–Tal sequence as it contains the Neoproterozoic to Cambrian transition period. Until 1980s, the Tal formation was considered to span sedimentary deposits from Permian to Jurassic [*Auden*, 1933]. The discovery of small shelly fauna [*Azmi*, 1983] in the Tal formation indicated that this formation is deposited in the Early Cambrian. This age of the formation was supported by various subsequent studies based on paleontological records [*Shanker et al.*, 1993; *Hughes et al.*, 2005] and carbon, oxygen stratigraphy [*Banerjee et al.*, 1997, *Mazumdar et al.*, 1999; *Kaufman et al.*, 2006]. Based on the sedimentary sequences and their isotopic compositions, the Krol–Tal formation of the outer LH has been successfully correlated with other Pc-C boundaries exposed in south China, Russia and Sibearia [*Aharon et al.*, 1987; *Singh*, 1999; *McCall*, 2006, *Jiang et al.*, 2003].

There have been limited efforts to constrain the depositional ages of various sedimentary formations of the LH using radiometric dating methods compared to paleontological studies. *Sharma et al.* [1992] have obtained a Rb-Sr age of 626±13 Ma for the black shales belonging to the chert-phosphrite sequence from the Lower Tal. This age is found to be a few million years older compared to the ages reported for Pc-C boundary from other geological sections from China, Canada, South Australia [*Bowring et al.*, 1993; *Brasier et al.*, 1994]. *Singh et al.* [1999] found a Re-Os age of 535±11 Ma for black shales from the strata immediately above the chert-phosphrite sequence in the Tal formation. This age seem to be consistent with the carbon and oxygen stratigraphy [*Aharon et al.*, 1987; *Banerjee et al.*, 1997; *Kaufman et al.*, 2006] and the paleontological records [*Azmi*, 1983; *Hughes et al.*, 2005] of the Krol-Tal formation.

(c) Sampling:

Black shales for this study were collected from the Maldeota mine near Dehradun in 1999 (Fig. 2.5) are studied for their geochemical and isotopic compositions to understand the anoxic condition of the seawater near the Pc-C boundary. Earlier studies on Re-Os isotopic systematics of black shales from the Lower Tal have established their age 535±11 Ma [*Singh et al.*, 1999]. The stratigraphy of the sampling section shows that in addition to the layer of black shale analyzed by *Singh et al.* [1999], there is another layer of black shales below it. The samples studied in this thesis are stratigraphically below the phosphrite band exposed in the Lower Tal formation of the Mussoorie group of LH (Fig. 2.4). These samples are from the archives of Dr. Sunil Kumar Singh, collected from the Maldeota mine during a field campaign undertaken in 1999. Sampling of black shales from underground mine ensures their minimal weathering and mobilization of elements. The sampled mine at Maldeota is presently closed and inaccessible.

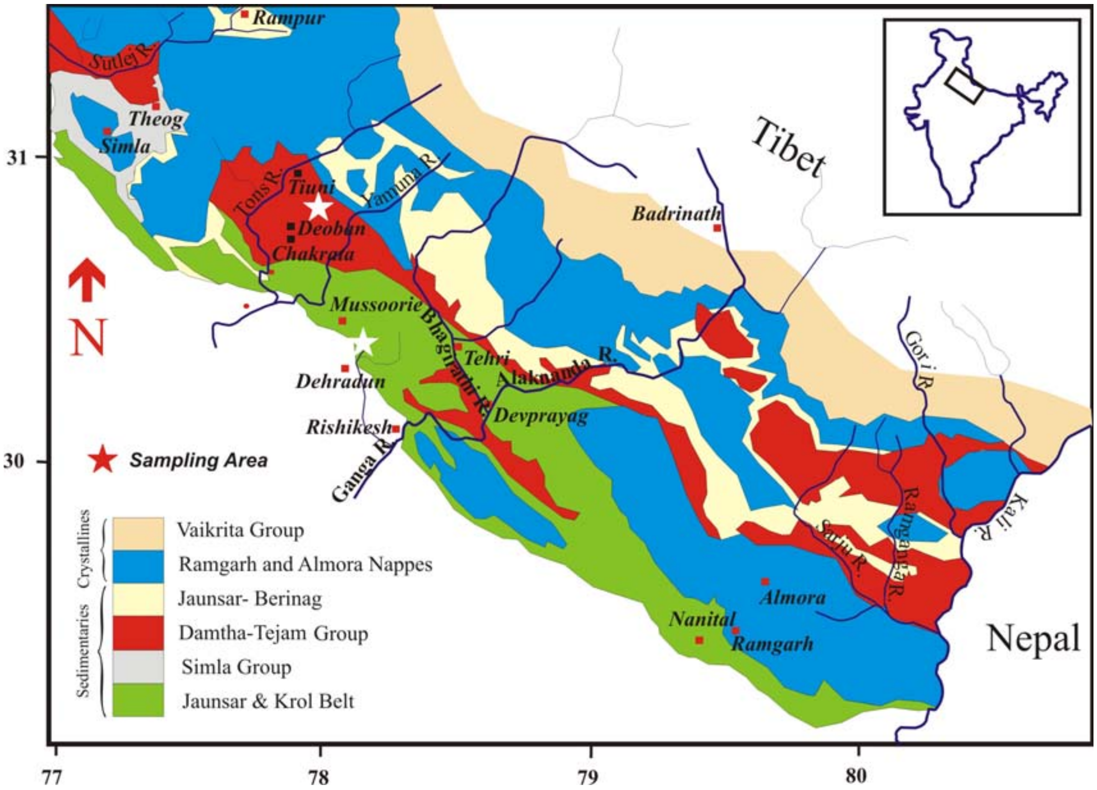

Figure 2.5: *Sampling locations of the black shales in the LH is shown here along with their geological details.*

A number of black shales were taken from a stretch of few meters from the same strata for Re-Os chronology. The collected samples, in hand specimen, were black, hard and have compact laminations. Fresh and shining pyrite nodules were present in these shales attesting their least alteration due to weathering. Based on available information on the oxygen isotope stratigraphy and biochronology, this sequence has been placed just above the Pc-C boundary [*Aharon et al*., 1987; *Brasier and Singh*, 1987; *Banerjee et al*., 1997]. An earlier attempt to provide radiometric age of this formation, using Rb-Sr on clay fraction of black shales from the Tal formation yielded an age of 626±13 Ma [*Sharma et al*., 1992], few million years older compared to other Pc-C sections of the world [*Bowring et al.*, 1993; *Brasier et al.*, 1994; *McCall*, 2006]. The geochemical and Re-Os isotopic systematics of these samples near to the Pc-C boundary together with that reported for black shales from an overlying sequence [*Singh et al.*, 1999] will be useful in gaining knowledge about the marine anoxicity around the Pc-C boundary.

A set of black shales was also collected during 1999 from the Mandhali Formation of the Tejam Group of the inner LH (Fig. 2.5) to understand the marine anoxic state during Neoproterozoic. These samples are from a road-cut on Tiuni-Chakrata road, near Lal Pol bridge located ~5 km from Lokhandi village towards Tiuni (Fig. 2.5). These samples were taken after removing ~1 m of the exposed surface of black shale from the road cut to get fresh samples. The shales were found to have black carbonaceous nodules and are found to be associated with sulphides. The collected samples, in hand specimen, are found to be hard and black. These samples are from the Mandhali group of the LH and paleontological evidences infer their upper Riphean to Vendian age [~950-620 Ma; *Valdiya*, 1980].

2.1. 2. RECENT MARINE SEDIMENTS

One of the objectives of this thesis, as discussed earlier, is to asses the impact of climate on continental erosion over millennial time scale. In light of this, marine sediments deposited in the Bay of Bengal can be useful to address this issue as it receives sediments from some of the major global rivers (*e.g.* Brahmaputra, Ganga, Irrawaddy, Salween, Godavari, Mahanadi, Krishna, *etc*.) and archived the erosional information of their source areas. The sedimentological and hydrogeological details of the BoB are provided below.

The Bengal Fan:

The sedimentary basin of the BoB extends over a length of ~3000 km, width of ~1000 km and maximum thickness of ~17 km [*Curray*, 1994; *Curray et al.*, 2003]. This largest sub-marine basin contains 12.5×10^6 km^3 of post India-Asia collision sediments together with 4.36×10^6 km^3 of pre-collision sediments [*Curray*, 1994]. Presently, the BoB receives large amount of sediments eroded by the rivers (Table 2-

3) and these sediments, mainly from the Ganga and Brahmaputra, get transported to the open ocean via an active submarine canyon, *Swatch of No Ground* [*La Fond*, 1957; *Kuehl et al.*, 1989]. The fan gradients of this canyon are significantly different, in the continental margin it is ~20-50 m/km whereas in upper, middle and lower BoB, it is 5.7 m/km, 1.7 m/km and 0.9 m/km respectively [*Curray et al.*, 2003].

Table 2-3: Hydrological and geological details of rivers supplying sediments to the BoB.

Basin	**River**	**Major Litho-units**	**Area** 10^6 km^2	**Runoff** mm/yr	**Water discharge** km^3/yr	**Sediment flux** 10^6 tons/yr
Himalaya	**Ganga**	HH, LH, Deccan	0.95	619	460	520
	Brahmaputra	HH, LH, Mishmi Hills, Indo-Burman Ranges	0.58	1087	630	540
Peninsular India	**Mahanadi**	Archean Crust	0.132	500	66	60
	Godavari	Archean Crust, Deccan	0.31	350	92	170
	Krishna	Archean Crust	0.252	266	67	16
Indo-Burman	**Irrawady**	Indo-Burmese Ranges, Arakan Mountains	0.414	1034	428	355
	Salwene	Mishmi Hills, Indo-Burmese Ranges	0.325	649	211	337

Hydrological parameters from http://www.gemswater.org/atlas-gwq/table3-e.html; Robinson et al., 2006

The Brahamaputra, Ganga, Irrawaddy, Salween, Godavari, Mahanadi, Krishna rivers are the major supplier of sediments to the Bay of Bengal . The annual sediment supply by these river systems are dominated during the southwest monsoon, however the sediment supply by the Irrawady, Salween, Krishna and the Godavari get influenced by the northeast monsoon too. Rainfall during the southwest monsoon (June-September) is the major source of water to the rivers draining into the BoB. The annual sediment supply and the major lithology of the drainage basin of these rivers are listed in Table 2-3. In terms of sediment supply to the ocean, the Ganga-Brahamputra (GB) river system ranks first among the global rivers [*Milliman and Meade*, 1983; *Milliman and Syvitski*, 1992]. The sediment deposition pattern of the BoB is largely governed by the GB river system with subordinate contribution from other river systems. This fact is well evident from the sediment trap studies [*Ramaswamy and Nair*, 1994], which finds that the average annual lithogenic particle flux to the BoB is highest in the northern part (21.2 gm m^{-2} yr^{-1}) compared to that in its central (15.7 gm m^{-2} yr^{-1}) and southern part (8.6 gm m^{-2} yr^{-1}), consistent with their proximity from the G-B river mouth.

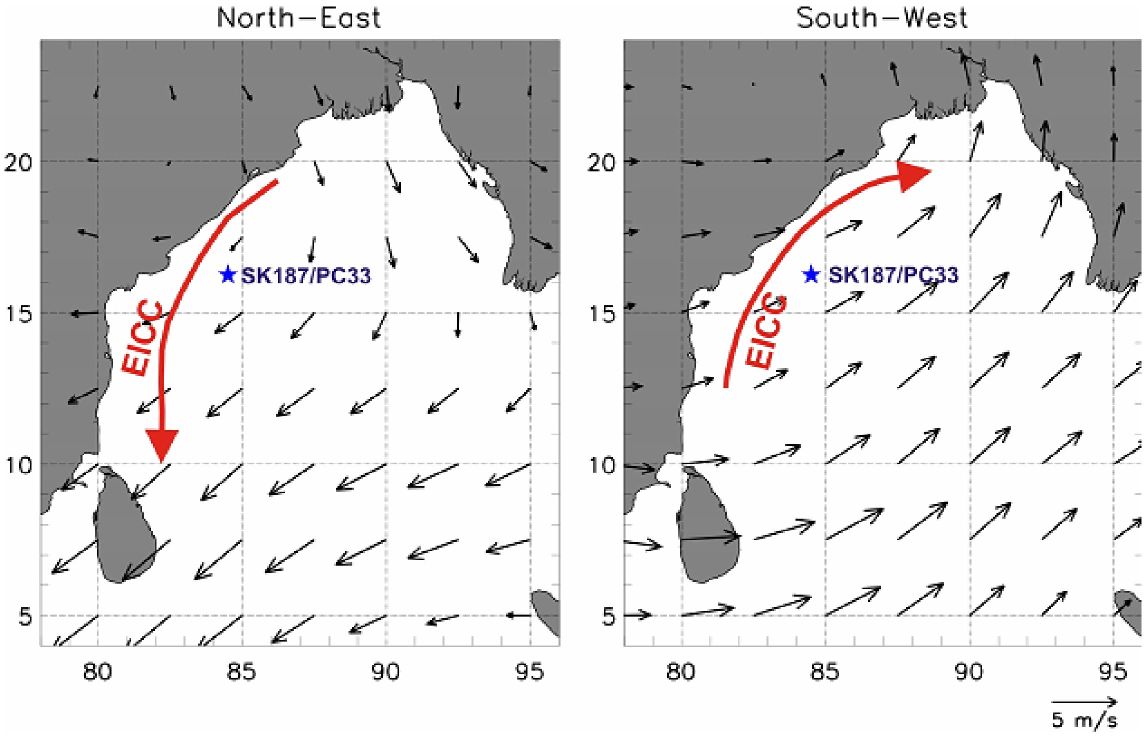

Figure 2.6: *Wind and water circulation pattern over the BoB during southwest and northeast monsoon period. Both the wind (black arrows) and East Indian coastal current (EICC; shown as red arrow) gets reversed during the two different monsoon seasons. The star mark in the figure represents the location of the core studied.*

The sediment dispersal pattern in the fan largely depends on the surface water circulation and hence on the annual wind pattern. The wind pattern over the BoB gets reversed twice a year (Fig. 2.6). The wind flow is towards south-west in summer (May-September), whereas relatively less stronger north-east wind blows in winter (November-February) [*Shankar et al.*, 2002]. The East Indian coastal current (EICC) in the BoB flows in northeast direction during the summer, whereas it is towards southwest during the winter [*Shetye et al.*, 1993].

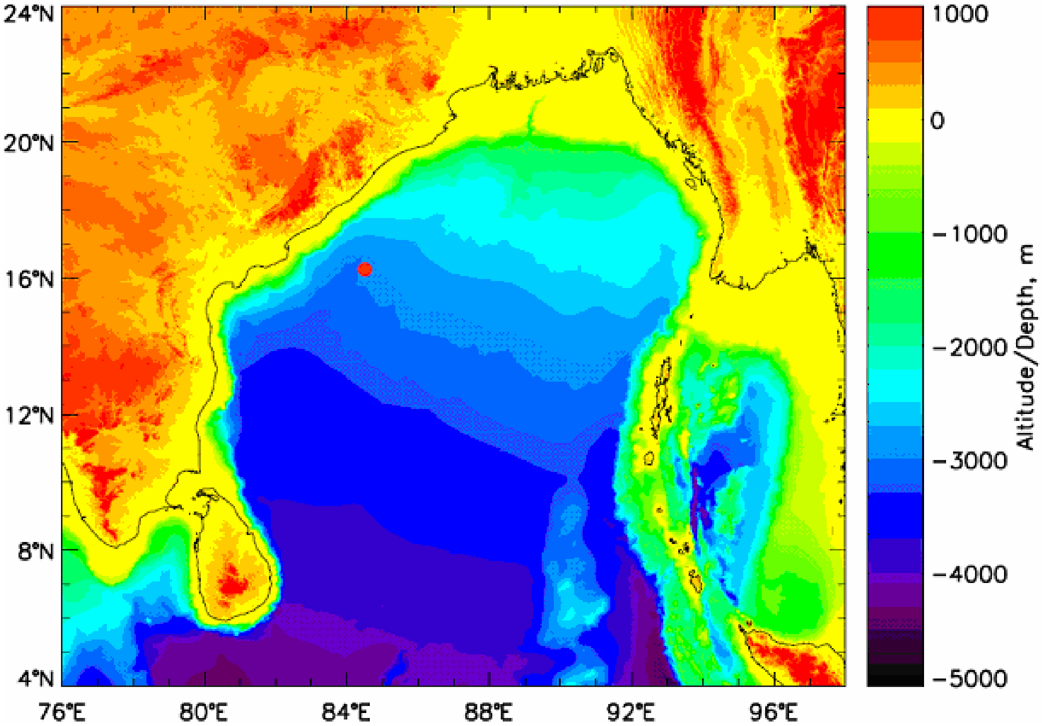

Figure 2.7: *Location of the studied core SK187/PC33 (marked as red circle) in the BoB.*

(a) Sampling:

The marine sediments studied in this study are from a 12.8-m-long piston core (SK187/PC33) raised from the western BoB (16° 16′ N, 84° 30′ E; Fig. 2.7; water depth: 3003 m) during the 187th expedition of the *ORV Sagar Kanya*. These sediment samples were provided by Dr. V. Ramaswamy from NIO, Goa. Utmost care was taken during coring to avoid slope deposits, slumping or turbidities (Fig. 2.7). The sediment core was divided into two halves; first part was archived and second part was sub-sampled at a resolution of 2 cm. The archive and the sub-samples were preserved at ~-5°C at NIO. From the sub-sampled core, few grams of sediments were brought to PRL and are used for their isotopic and geochemical studies in this work.

Compared to eastern and central BoB, the sediments from the western BoB have limited sources, viz. Himalayan and peninsular region. The present core location receives sediments predominantly from the Himalaya and the peninsular India and therefore is strategically situated to study the erosional process over these regions.

Table 2-4: Techniques followed in this study to analyze various elemental and isotopic compositions of black shales and the BoB sediments.

Parameters	**Technique**	**Instrument**
^{14}C	Liquid Benzene synthesis	Liquid scintillation counter
Os isotopes	Carius tube digestion, solvent extraction	N-TIMS
Sr, Nd isotopes	decarbonated samples, column chemistry	TIMS
Os, Sr, Nd	Isotope dilution method	TIMS
Re	Isotope dilution method	Q-ICP-MS
U, Mo	Standard calibration method	Q-ICP-MS
Na,K	Standard calibration method	Flame AAS
Ca, Mg, Al, Fe, Ti, V, Sr, Ba, Mn, Cr, Co, Cu, Zn, Ni	Standard calibration method	ICP-AES
Total carbon, nitrogen	Standard calibration method	CN analyzer
Inorganic carbon	Titration of CO_2	Coulometer
Magnetic Susceptibility	Using 0.47 kHz frequency	Susceptibility meter

2.2. ANALYTICAL METHODOLOGY

This section details the methodologies adopted for isotopic and geochemical analyses of black shales and marine sediments during this thesis work. In the course of this study, the chemical purification of osmium using Carius tube digestion and Br_2 solvent extraction procedure has been streamlined in our laboratory. These procedures are followed from *Shirey and Walker* [1995] and *Birck et al.* [1997], but differ from those used earlier in our laboratory by *Singh* [1999] using NiS fusion and large volume distillation [*Trivedi et al.*, 1999]. Therefore, the analytical methods used for osmium analysis of black shales have been presented in some detail in this chapter. The other methodologies (Table 2-4) are highlighted briefly, as these have been regularly used in our laboratory and their details are presented in various publications.

2.2.1. Osmium: Isotopes and Geochemistry

Osmium, a platinum group element (PGE) with seven naturally occurring isotopes [^{184}Os (0.023 %), ^{186}Os (1.600 %), ^{187}Os (1.510 %), ^{188}Os (13.286 %), ^{189}Os (16.251 %), ^{190}Os (26.369 %), ^{192}Os (40.957 %); *Faure*, 1986], among these, ^{186}Os and ^{187}Os are radiogenic. ^{190}Pt decays with a half life of 469 Ga to stable ^{186}Os by emitting an alpha particle, whereas ^{187}Re decays to ^{187}Os by emitting a beta particle with an energy of 2.5 keV. *Lindner et al.* [1989] measured the decay constant of ^{187}Re to be 1.64×10^{-11} yr^{-1} with a half life of 42.3±1.3 Ga by measuring the growth of ^{187}Os in 1 kg purified $HReO_4$ by spiking it with two Os tracers (^{190}Os and ^{192}Os). These values were later modified by *Smoliar et al.* [1996] to 1.666×10^{-11} yr^{-1} and 41.6±0.4 Ga from the Re-Os isochron of iron meteorites (Group-IIIA) of known age.

Table 2-5: Typical Re and Os elemental and isotopic composition in geological samples [*Esser and Turekian*, 1993; *Peucker-Ehrenbrink and Ravizza*, 2000; *Peucker-Ehrenbrink and Jahn*, 2001; *Rahaman and Singh*, 2010].

	Re	**Os**	**^{187}Re/^{188}Os**	**^{187}Os/^{188}Os**
	pg/kg			
Seawater	7450	10	4270	1.06
Upper Continental Crust	$2x10^{5}$	$3x10^{4}$	34.5	1.4
Rivers	428	9.1	227	1.4
Aeolian Dust	$3x10^{5}$	$3.1x10^{4}$	50	1.05
Cosmic dusts	$3.7x10^{7}$	$5x10^{8}$	0.4	0.127
Low Temperature Hydrothermal vents	-	98	-	0.11
High Temperature Hydrothermal vents	-	2.8-38	-	0.129-0.388

Os and Re both are siderophile and chalcophile in nature. They are often found to be enriched in the organic rich sediments due to their redox-sensitive nature. These elements found in trace amounts in most environmental samples (Table 2-5). The concentration of dissolved Re (8240 pg/kg) is higher compared to that of Os (10 pg/kg) in present-day seawater. The residence time of Re in seawater is estimated to be 0.75 Ma [*Colodner et al.*, 1993] whereas the residence time of Os is in the range of 10-40 ka [*Oxburgh*, 2001], much higher than mixing time of ocean (~1 ka). The osmium isotopic composition of contemporary seawater (1.06) is controlled by the mixing proportion of its various sources, *viz*. rivers (1.4), cosmic dust (0.12) and hydrothermal supply (0.12). Among these sources, both Re and Os in seawater are dominantly supplied by rivers. In oxic conditions, Re (ReO_4^-) and Os (probably as octavalent oxyanions, $HOsO_5^-$, $H_3OsO_6^-$) remains in dissolved form in seawater. However, in reduced conditions, Re reduces to +IV and Os first to +IV and then to +III and get removed from seawater to sediments. Re-Os isotopic systematics, owing to their geochemical behavior, has been used successfully to date various geological samples, particularly depositional ages of organic rich shales [*Ravizza and Turekian*, 1989, *Singh et al.*, 1999; *Selby and Creaser*, 2003; *Hannah et al.*, 2004; *Anbar et al.*, 2007; *Kendall et al.*, 2009a].

POWDERING:

For the geochemical and isotopic analyses, the Bay of Bengal sediments and hand specimens of black shales were powdered using Fritsch Planetary Mill PULVERISETTE in agate grinding bowl. While powdering the samples, care was taken to avoid any metal contamination. The BoB sediments were oven dried prior to powdering. The powdered samples, both the shales and sediments, were sieved using nylon mesh of 100 μm pore size and coarser fractions were repowdered, mixed and homogenized with <100 μM size sample.

Table 2-6: Calibration of Re-STD A using CRPG Spike (41.26 ng/g).

	Wt of Re STD-A (g)	Wt of Spike (41.26 ng/g), in g	[Re], ng/g
SPK-a	0.05248	0.50226	518
SPK-b	0.06301	0.50238	528
SPK-c	0.05227	0.24936	504
SPK-d	0.05278	0.25036	503
		MEAN	513
		STDEV (1σ)	12

2.2.2. Re AND Os SPIKES AND STANDARDS

Re and Os concentrations in black shales are measured using isotope dilution technique. Depending on the concentration in the samples, suitable amount of Re spike, enriched in ^{185}Re and Os spike, enriched in ^{190}Os are added to the samples to determine their concentration. To get the concentration of Re using isotope dilution method, three sets of spike solution (Re-Spk 1, Re-Spk 2, Re-Spk 3) with different strength have been used in this work. The strength of spike solutions were calibrated against two Re standard (Re-STD A, Re-STD B) prepared in our laboratory by dissolving pure Re metal in 2N HNO_3. The Re-STD B has been calibrated during a previous study from our group [*Rahaman and Singh,* 2010]. The Re STD-A standard was calibrated (Table 2-6) using a spike (with known concentration (41.26 ng/g) and isotope abundances (^{185}Re: 97.40 % and ^{187}Re: 2.60 %)) procured from CRPG, Nancy, France.

Table 2-7: Calibration of Re spikes using Re standards of known strength.

	Wt of Re STD-B (g)	Wt of Re Spike, in g	Re concentration of the spike, ng/g
Re-A1	1.08608	0.0565	54.0
Re-A2	0.92862	0.06129	53.4
Re-A3	0.90837	0.05642	53.5
		MEAN	53.6
		STDEV (1σ)	0.3

	Wt of Re STD-A (g)	Wt of Re Spike, in g	Re concentration of the spike, ng/g
Re-B1	0.10398	0.41499	293
Re-B2	0.1375	0.65299	293
Re-B3	0.11825	0.8106	290
		MEAN	292
		STDEV (1σ)	2

	Wt of Re STD-A (g)	Wt of Re Spike, in g	Re concentration of the spike, ng/g
Re-C1	0.31481	0.10524	4162
Re-C2	0.26575	0.06794	4110
Re-C3	0.34985	0.1002	4002
		MEAN	4091
		STDEV (1σ)	82

Calibration of Re-STD A:

Four aliquots of Re-STD A were equilibrated with the CRPG spike of concentration of 41.26 ng/g. The equilibrated standard-spike solutions were diluted to ~400 pg level and measured in Q-ICP MS for their Re isotopic compositions. Table 2-6 lists the results of the Re concentration of the Re-STD A.

Calibration of Re Spikes:

Three Re Spike solutions (Re-A, B, C) were calibrated using the Re STD-A (or B) of known strength (Table 2-7). For this, three set of aliquots for each spike solution were equilibrated with the Re STD. The standard-spike solution were diluted and measured in the Q-ICP-MS to obtain the Re strength of each of the spike solutions accurately (Table 2-7).

Calibration of Os Spikes:

The Os spike (Os-Spk 1) solution used for this work is calibrated using an Os standard, Os-STD B with concentration of 16.25 ng/g, provided by Dr. L. Resiberg, CRPG, Nancy. Five aliquots of the standard were equilibrated with Os-Spk 1 for 48 hrs. After equilibration, the Os isotopic composition for these standard-spike mixtures was measured using Thermal Ionization Mass Spectrometer in negative mode. The calibrated concentrations of these Os spikes are provided in Table 2-8.

Table 2-8: Calibration of osmium Spike using an Os standard of known strength.

	Wt of Os STD-B, g	Wt of Os Spike, in g	Os concentration of the spike, ng/g
Calib-1	0.10336	0.19155	6.73
Calib-2	0.10427	0.18522	6.65
Calib-3	0.10435	0.20866	6.21
Calib-4	0.10439	0.19947	6.43
Calib-5	0.10425	0.20425	6.37
		MEAN	6.48
		STDEV (1σ)	0.21

The calibrated concentrations of Re and Os spikes, given in Table 2-7 and 2-8 were used to measure Re and Os concentrations in black shales from the Aravalli, Vindhyan and the Himalaya.

2.2.3. OSMIUM PURIFICATION CHEMISTRY

The pure fraction of osmium from the black shales is extracted using Carius tube digestion [*Shirey and Walker*, 1995], solvent extraction and micro-distillation method [*Birck et al*., 1997]. This purification process for osmium (Fig. 2.8) enables to measure Os and Re from the same aliquot of the samples, which is essential to determine precise Re-Os age of the shales.

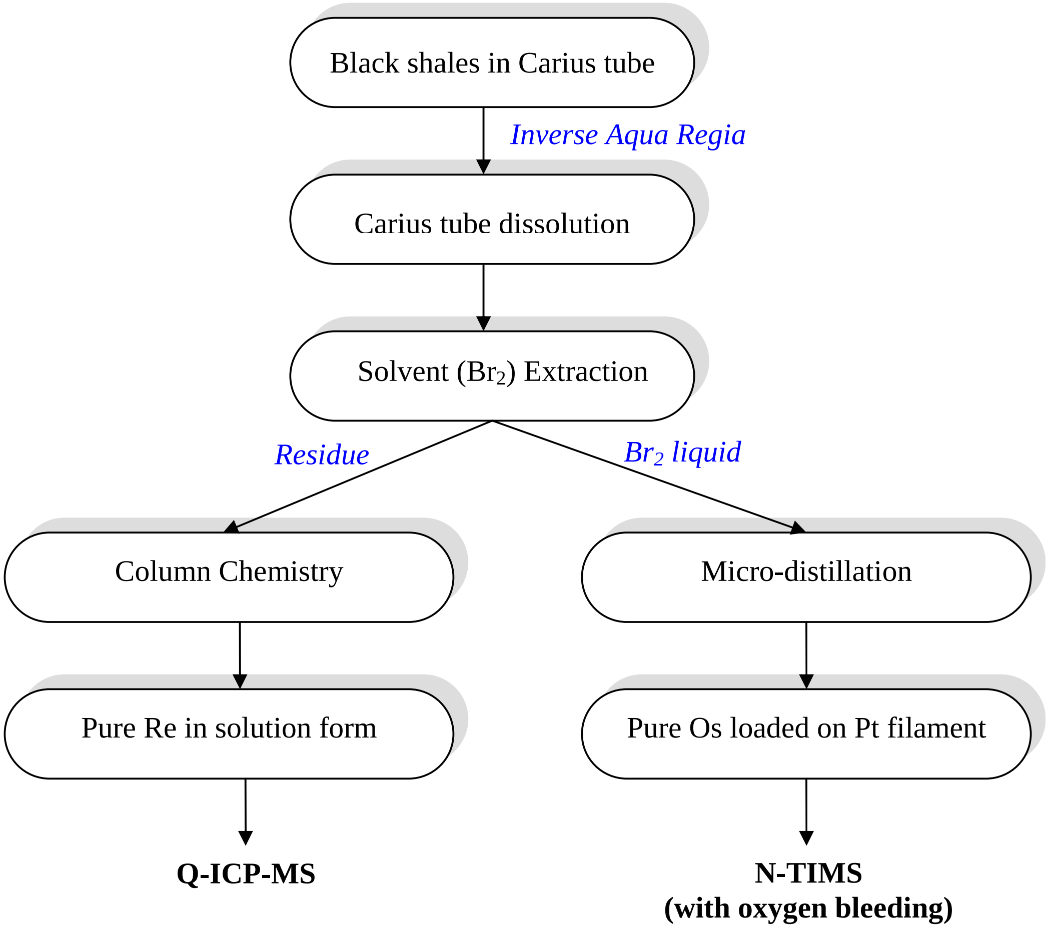

Figure 2.8: *Flow chart showing sample dissolution and Re-Os separation and purification.*

Sample Digestion:

In this thesis work, Carius tube digestion method [*Shirey and Walker*, 1995] is adopted for the digestion of shales with inverse aqua regia as the digestion medium. Carius tubes were made of borosilicate glass with a length of 340 mm and wall thickness of 3 mm [Fig. 2.9; *Pierson-Wickmann*, 2000]. Prior to its use for digestion, the Carius tube was boiled in an HNO_3 acid bath and cleaned properly with Milli-Q H_2O. The HCl and HNO_3 acid used for Re-Os purification were distilled twice using quartz distillation under sub-boiling conditions. The nitric acid, after quartz distillation, was further sub-boiled at ~80°C in a round bottom flask with its mouth open to oxidize osmium, if any, from it.

About 1 gm of sample (black shale) is taken in a pre-cleaned carius tube. To it, known amount of ^{190}Os spike is added. Before adding ^{185}Re spike, 2ml of HCl is added. Addition of HCl prior to ^{185}Re avoids any possibility of volatilization of Os from the samples due to oxic medium of Re spike solution. In addition, it also reacts with carbonate present, if any, in the sample and removes the CO_2 and reduces pressure inside the tube during dissolution of sample. After adding Re spike, the Carius tube is kept in a liquid nitrogen-alcohol/acetone slush with a temperature of ~-100°C. At this low temperature, 5ml of HNO_3 is added in the Carius tube and immediately, the Carius tube is evacuated by a hand vacuum pump and sealed using LPG-oxygen flame. The low temperature environment to add HNO_3 in the sample-spike mixture is required to avoid in any loss of osmium due to oxidation. After sealing the carius tube, the sealed portion of the tube is strengthened by annealing it for 4 hrs at 550°C. The sealed carius tube placed inside a metal jacket which is kept in an oven at 240°C for 24 hrs to digest the sample. This procedure for sample digestion ensures the sample-spike equilibration.

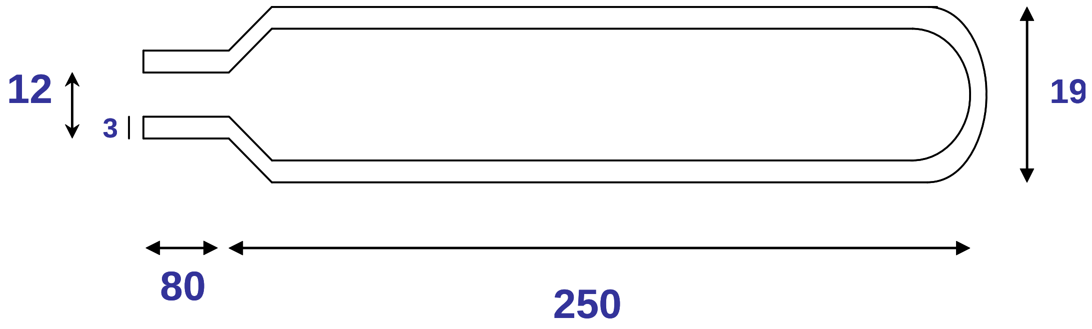

Figure 2.9: *Dimension (in mm) of carius tube used for the digestion of black shales for Re-Os chemical separation and purification.*

Solvent (Br_2) Extraction:

The Carius tube digestion method leaches osmium from the sample, brings to the solution and equilibrates the sample-spike Os. After the digestion, the Carius tube is kept in a container of liquid nitrogen and the tube was opened. The solution, which is in oxic medium, is transferred into a 60 ml Savillex Teflon bomb and 1 ml of double-distilled Br_2 liquid is immediately added to it. The bomb containing digestion solution and Br_2 liquid is properly tightened using a teflon wrench and kept over a hot plate ~65°C. The merit of using Br_2 liquid for the solvent extraction method [*Birck et al.*, 1997] to purify osmium is its affinity to form osmium bromate complexes in oxic conditions. Further, Br_2 liquid has a boiling point ~59°C and high density (~3 gm/ml). While refluxing the solutions at ~65°C in the bomb, the Br_2 liquid gets evaporated and condenses inside the lid. During the course of refluxing, Br_2 liquid within 3-4 hrs efficiently extracts the osmium present in the solution. After 3-4 hrs, the bomb is cooled in refrigerator to avoid volatilization of osmium. 1 ml of the Br_2 liquid containing the osmium is pipetted out and poured into a 7ml Teflon vial containing chilled H_2O to reduce evaporation. The Br_2 extraction method is repeated second time to extract the remaining Os. Now, the 7 ml Teflon vial containing 2 ml of Br_2 liquid contains the osmium, whereas the residue present in the bomb can be processed further to extract Re using chromatography.

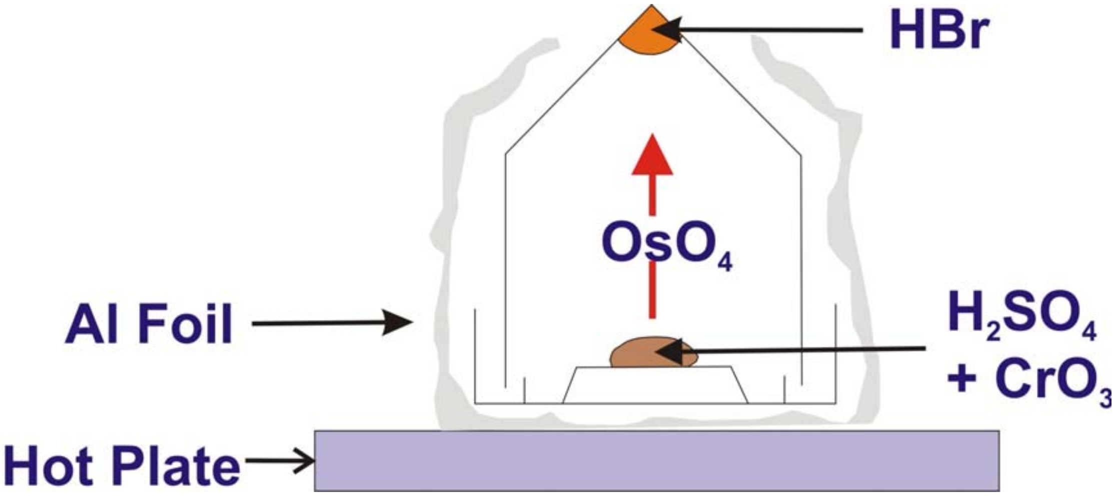

Figure 2.10: *Micro-distillation procedure used in this study to extract pure Os [Birck et al., 1997].*

Micro-distillation:

The chilled H_2O present along with 2 ml of Br_2 liquid is pipetted out and to the Br_2, 0.5 ml of Teflon-distilled HBr is immediately added to make the medium reducing, which is required to avoid volatilization of osmium from the solution. Br_2 is then evaporated from the vial at room temperature and the HBr solution containing Os was dried to a drop which was transferred to the lid of a 5 ml conical vial to dry it completely. In this condition, Os remains in $OsBr_6^{2-}$ form. The residue present in the lid further purified using micro-distillation following the method of *Birck et al.* [1997; Fig. 2.10]. After micro-distillation, the HBr containing the pure osmium is dried and used for isotopic and elemental analysis by negative thermal ionization mass spectrometer.

Extraction of Re

After the solvent extraction (Fig. 2.8), the residue in the Savillex bomb containing Re is dried and redissolved in 5 ml 0.8 N HNO_3. This solution was centrifuged and loaded on an anion exchange resin (AG1X8, 100-200 mesh), washed with 0.8N HNO_3 and the pure Re is collected by eluting the column with 8N HNO_3 [*Dalai*, 2001]. This extracted pure Re is dried and diluted properly in 2% HNO_3 medium for its measurement using Qudrapole Inductive Coupled Plasma Mass Spectrometer [*Rahaman and Singh*, 2010].

Mass Spectrometric analysis of osmium

High ionization potential of osmium along with its pico-to-nano gram level concentration in black shales, make its isotopic analysis challenging in positive mode of thermal ionization mass spectrometer. In this work, osmium isotopic analysis was carried out in the negative mode of Isoprobe-T Thermal Ionisation Mass Spectrometer with oxygen bleeding [*Creaser et al.*, 1991; *Volkening et al.*, 1991; *Walczyk et al.*, 1991].

Sample Loading: The extracted pure Os is loaded using HBr on a zone-refined Pt filament (99.999% purity, H. Cross Co.). Prior to loading, the Pt filament was annealed at 3 A for 30 mins to oxidize any osmium and rhenium present in the filaments and allowed it to cool for 24 hrs to avoid any spreading during loading. After loading the Os in the filament at ~0.6 A, $Ba(OH)_2$ in 0.1 N NaOH is loaded over it which acts as an ion enhancer [*Birck et al.*, 1997; *Chen et al.*, 2009]. This ion enhancer was prepared by refluxing a mixture of ~0.1 gm of NaOH, 0.7 gm of $Ba(OH)_2$ and ~30 ml H_2O in a vial for 3 hrs at 80°C. This supersaturated solution can be used effectively for more than 2 months with its minimal atmospheric exposure [*Luguet et al.*, 2008].

Table 2-9: Technical details of Isoprobe-T Negative-TIMS for Os analysis.

Accelerating Potential	6000 V	
Filament Current	~1.9 A	
Ion Counting:		
	Daly Discriminator (V)	0.3
	Photo multiplier (kV)	2.5
WARP Properties:		
	Retardation Lens	2.05
	Entrance Lens	350
	Exit Lens	735

Mass Spectrometric measurements**:** The pure Os metal loaded on the Pt filament is analyzed for their isotopic compositions using the Isoprobe-T Thermal Ionization Mass Spectrometer in negative mode (N-TIMS) with oxygen bleeding. The isotopic measurements for Os in OsO_3 form were carried out in a peak jumping mode using an electron multiplier detector. A small amount of pure oxygen is purged into the source of the mass spectrometer using a leak valve which drops down the vacuum of the source chamber to ~2×10^{-7} mbar. Osmium isotopic analysis was performed at this pressure level of the source chamber. Four isotopes of the Os ($^{187}OsO_3$, $^{188}OsO_3$, $^{190}OsO_3$ and $^{192}OsO_3$) were analyzed with an integration time of 10 sec. Each isotope was measured 100 times to get a precise isotopic composition and the average value of these 100 runs was reported in this work. A minimum of 1000 cps was accumulated under the $^{187}OsO_3$ peak during each run of the sample. Further, during analysis, mass 233 was monitored to look for any Re contamination ($^{185}ReO_3$);

generally the count rates in the mass, if any, was very low suggesting no potential interference of $^{187}ReO_3$ on mass $^{187}OsO_3$. A typical spectrum of OsO_3 isotopes is given in Fig. 2.11.

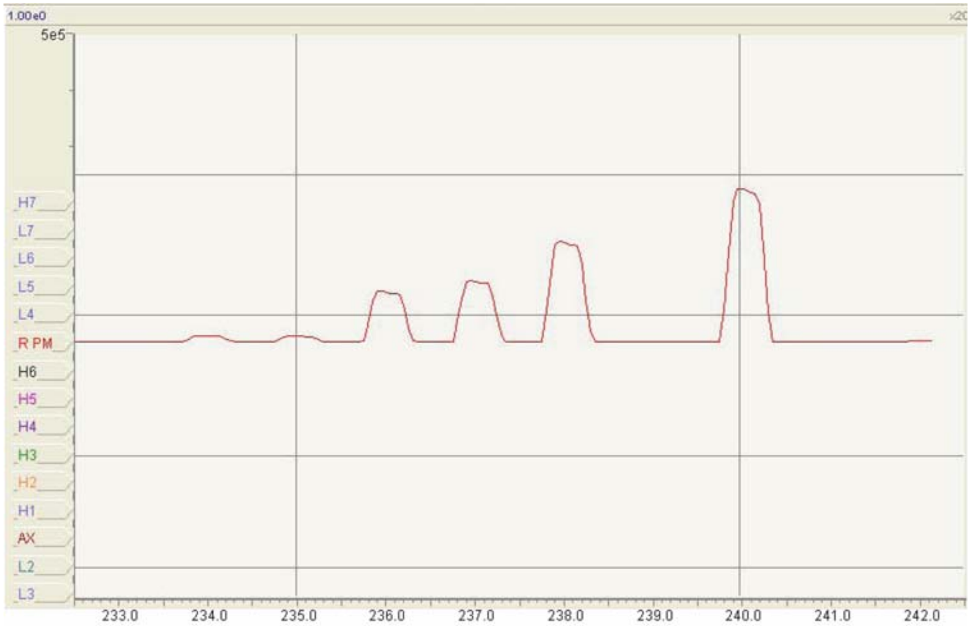

Figure 2.11: *A typical spectrum of isotopes of OsO_3 during their measurements in ISOPROBE-T N-TIMS.*

The negative ion beams of Os produced in the sources after passing through the magnetic field have to cross the Wide Apperture Retarding Potential (WARP) filter prior to reaching the electron multiplier detector. The WARP filter units were tuned properly (Table 2-9) to get a stable and flat-top peak of Os.

Data Reduction, Precision and Accuracy:

The Os isotope composition, as discussed earlier, was measured in its OsO_3 form in peak jumping mode. To get a precise Os isotopic ratio from the OsO_3 signals, these data have to be corrected for time correction, instrumental mass fractionation, isobaric interference due to various OsO_3 combinations and spike contribution. These were done following standard data reduction procedure followed in our laboratory [*Singh et al.*, 1999; *Trivedi et al.*, 1999]. The measured isotopic ratios were normalized with respect to $^{188}Os/^{192}Os$ of 0.32439 [*Nier*, 1937] to correct for the instrumental mass dependent isotope fractionation.

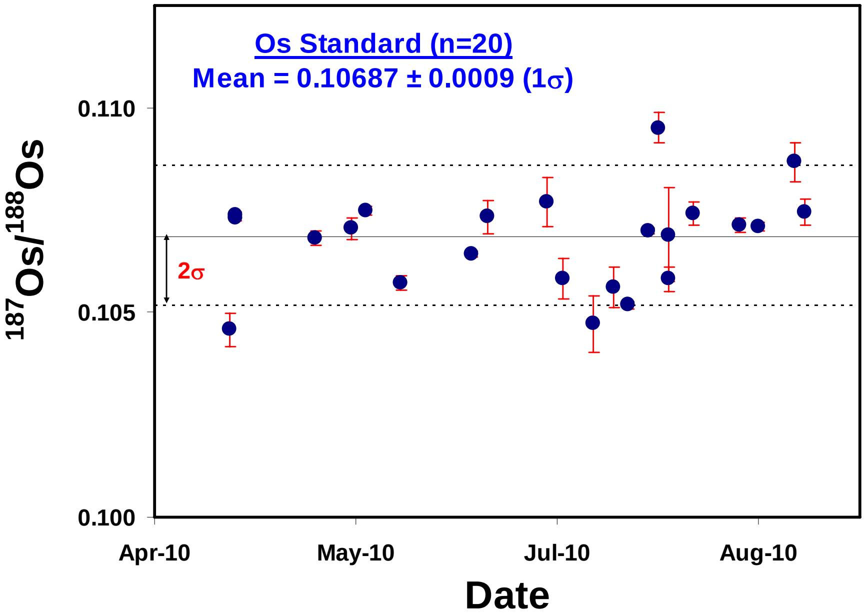

Figure 2.12: *Measurement of ^{187}Os/^{188}Os of standard versus time.*

An Os standard has been measured repeatedly for its isotopic composition over the period of this work (Fig. 2.12). The osmium standard used in this study was obtained from G. Ravizza and W. Pegram and is the same as used in the study of *Singh* [1999]. 50 to 2000 pg of Os standards were loaded on filaments to measure in N-TIMS, the average ^{187}Os/^{188}Os measured for the standard is found to be 0.10687±0.0009 (1σ, n=20), consistent with its reported value [0.1069±0.0024; *Singh*, 1999]. Along with the samples, few samples were also measured in duplicates to check the reproducibility of the measurements. The details of these repeat measurements are provided in Table 2-10. The CV for the repeat measurements for analyses of osmium concentration is found to be 3.8%.

The Re isotope measurements were carried out using Q-ICP-MS. The background signal for Re was monitored between analyses of the samples, which (~5 cps) is found to be negligible compared to count rates of few tens of thousand obtained for Re from shale samples. Measurement of every ~5 samples was bracketed by analyses of two Re standards and difference between ^{185}Re/^{187}Re of the standards is linearly interpolated to correct the measured isotopic data of samples for instrumental fractionation. The fractionation corrected Re data is used to determine the Re concentration of the samples using isotope dilution method. Few samples were measured in replicates and the repeat measurements for Re concentrations (Table 2-10) show reproducibility (CV) of 3.7%.

Table 2-10: Repeat measurements of Re, Os and ^{187}Os/^{188}Os in black shales.

Sample ID	Os, pg/g	^{187}Os/^{188}Os	Re, ng/g
UK99-1 (i)	8403	2.043	191
UK99-1 (ii)	8816	2.077	199
UK99-2 (i)	20160	1.892	382
UK99-2 (ii)	20499	1.931	371
UK99-3 (i)	9282	1.901	190
UK99-3 (ii)	9926	1.867	190
V99-1A (i)	397	6.705	14.4
V99-1A (ii)	440	6.649	14.5
V99-5A (i)	217	4.664	5.8
V99-5A (ii)	231	4.326	5.6
LA06-34 (i)	2602	9.480	0.5
LA06-34 (ii)	2635	9.701	-
LA10-9 (i)	4711	7.431	4.1
LA10-9 (ii)	4592	7.482	3.7

Re and Os Procedural blanks

During the course of measurements, complete procedural blanks for Re and Os were determined. Towards this, the complete chemical procedure was carried out without the sample, but with the same amount of reagents. Os and Re spikes were also added as was done for samples. The procedural blanks measured for Re and Os are found to be few orders lower (Table 2-11) compared to total Os and Re processed from the samples and hence, no blank corrections were made in this work.

Table 2-11: Procedural blank level for Re and Os measurements.

SampleID	[Os], pg/g	[Re], pg/g
BLK-A	0.29	32
BLK-B	0.42	26
BLK-C	0.31	45
BLK-D	0.11	39
Mean	0.28 ± 0.13	36 ± 8

In the initial period of streamlining the Re-Os measurements, the procedural blanks for osmium were higher (~30 pg). This higher blank was found to result from inadequate cleaning of the Teflon bombs. Diffusion of osmium bromate into the walls of the Teflon bombs during solvent (Br_2 liquid) extraction can be a potential source of blank contamination if not properly cleaned. This was a problem in the initial stage and the problem was identified and corrected after a few analyses by adopting a more rigorous cleaning procedure of all the Teflon and Savillex containers. The Teflon bombs, after boiling in a nitric acid bath, are filled with a washing solution (mixture of HF, HNO_3 and H_2O) and kept in an oven at 150°C. After a week, the washing solution was discarded and fresh solution was filled and the procedure repeated. After ensuring proper cleaning of the bomb, it is cleaned with Milli-Q H_2O and air dried prior to using for Re-Os analyses of samples. This cleaning procedure reduced the blank levels of osmium significantly from 30 pg to 0.3 pg. The results of samples analyzed for Re and Os during the initial phases of this study with high blank levels were discarded. The Re and Os data of black shales provided in this study are analyzed after ensuring low procedural blank levels (Table 2-11).

2.2.4. Sr-Nd CONCENTRATIONS AND ISOTOPE ANALYSIS

The Sr and Nd concentration and their isotope analyses are carried out in the decarbonated and organic matter free fractions of the black shales and the Bay of Bengal sediments to track their provenances following the procedure of *Singh et al.* [2008]. Briefly, sediment samples were decarbonated by treating them with 0.6 N HCl at ~70°C followed by washing with distilled water. Initially, there were concerns about the effectiveness of the procedure in completely decarbonating the marine sediments, particularly samples with high $CaCO_3$ (e.g. 221-223, 440-442, 899-901 cmbsf). Therefore, the high carbonate samples were reanalyzed after treating them one more time with 0.6 N HCl. The decarbonated and washed samples were ashed at 600ºC to combust the organic matter. The residue (silicate phase), spiked with ^{84}Sr and ^{150}Nd, was digested with HF, HCl and HNO_3. The samples were brought to complete solution and pure fractions of Sr and Nd were separated from the solution using conventional column chromatography [*Singh et al.*, 2008]. For the mass spectrometric analysis, pure Sr is loaded on a vacuum-baked Ta filament, whereas Nd is loaded on the outer side Ta filament of the triple filament assembly.

Table 2-12: Reproducibility of elemental and isotopic composition of Sr and Nd for the sediment samples.

Sample ID	**$^{87}Sr/^{86}Sr$**	**[Sr], μg/g**
V99-1 (i)	0.905947	38
V99-1 (ii)	0.906053	38
SK187-18-20 cm (i)	0.750514	87
SK187-18-20 cm (ii)	0.750698	97
SK187-300-302 cm (i)	0.735255	69
SK187-300-302 cm (ii)	0.734054	73
SK187-350-352 cm (i)	0.751504	82
SK187-350-352 cm (ii)	0.751241	74
SK18-_500-502 cm (i)	0.755147	71
SK187-500-502 cm (ii)	0.755939	79
SK187-650-652 cm (i)	0.725281	99
SK187-650-652 cm (ii)	0.726381	97

Sample ID	**$^{143}Nd/^{144}Nd$**	**ε_{Nd}**	**[Nd], μg/g**
V99-1 (i)	0.511627	-19.7	24.5
V99-1 (ii)	0.511624	-19.8	27.1
SK187-320-322 cm (i)	0.511865	-15.1	19.1
SK187-320-322 cm (ii)	0.511884	-14.7	19.7
SK187-400-402 cm (i)	0.511851	-15.3	18.5
SK187-400-402 cm (ii)	0.511811	-16.1	15.0

The isotopic ratios of Sr and Nd are measured using Isoprobe-T TIMS in static multi-collection mode. The measured $^{87}Sr/^{86}Sr$ and $^{143}Nd/^{144}Nd$ were corrected for instrumental mass fractionation by normalizing measured $^{86}Sr/^{88}Sr$ and $^{146}Nd/^{144}Nd$ with respect to their natural values, *viz*. 0.1196 and 0.7216 respectively. The Sr and Nd elemental composition for these samples were obtained through the isotope dilution method. Along with samples, Sr and Nd standards were measured repeatedly during the study period. The $^{87}Sr/^{86}Sr$ of the standard NBS 987 is found to be 0.710227±0.000014 (1σ, n=110) consistent with its reported value. The $^{143}Nd/^{144}Nd$ of JNdi standard is measured to be 0.512107±0.000008 (1σ, n=35), overlaps well with its reported values. To check the overall reproducibility of the Sr-Nd isotopic and elemental measurements, several samples were measured in duplicates, these results are presented in Table 2-12. The total procedural blanks of Sr (6, 4, 10 ng; mean: 6.7 ng) and Nd (1.6, 3.3 ng; mean: 2.5 ng) measured are order of magnitude lower than the total amount of Sr and Nd processed from the samples.

2.2.5. RADIOCARBON CHRONOLOGY OF SK187/PC33 CORE

The depth-age relation for the core SK187/PC33 has been constrained using ^{14}C ages of bulk inorganic carbonates. The low abundance of carbonates in the sediment samples required processing of ~100 grams of bulk samples for ^{14}C analysis [*Bhushan et al.*, 1994]; briefly, the dried sediments were treated with H_3PO_4 in vacuum to convert the carbonate to CO_2; from the CO_2, benzene was synthesized for ^{14}C measurements. ^{14}C activities were assayed using a low background liquid scintillation counter [*Bhushan et al.*, 1994]. The measured ^{14}C ages were calibrated using Calib 5.2 [*Stuiver and Reimer*, 1993] with a reservoir age correction of ΔR = -60±50 [*Dutta et al.*, 2001].

Inorganic and Organic Carbon

The powdered black shales and the BoB sediments were analyzed for their total carbon and nitrogen content using a CN analyzer (FISONS NA1500 CN elemental analyzer). In this regard, ~20 mg of dried sample is packed in an Al cup and is combusted in a closed chamber at ~1080°C. The CO_2 and N_2 gases produced during combustion were separated and purified through conventional chromatography and are quantified using standard calibration method to obtain the total carbon and nitrogen content in the samples [*Bhushan et al.*, 2001].

Table 2.13: Reproducibility of total and inorganic carbon and total nitrogen measurements.

Sample ID	**Nitrogen**	**Carbon**
	(wt %)	
2-4 cm (i)	0.07	1.12
2-4 cm (ii)	0.07	1.08
189-191 cm (i)	0.12	1.31
189-191 cm (ii)	0.12	1.25
360-362 cm (i)	0.07	1.89
360-362 cm (ii)	0.08	1.60
390-392 cm (i)	0.14	2.25
390-392 cm (ii)	0.13	2.23
440-442 cm (i)	0.04	7.93
440-442 cm (ii)	0.04	7.75
520-522 cm (i)	0.08	2.07
520-522 cm (ii)	0.08	2.09
590-592 cm (i)	0.03	3.40
590-592 cm (ii)	0.05	3.34
750-752 cm (i)	0.03	1.19
750-752 cm (ii)	0.03	1.26

Sample ID	**Nitrogen (wt %)**	**Carbon (wt %)**
WPA06-7 (i)	0.00	5.75
WPA06-7 (ii)	0.02	5.82
LA06-30 (i)	0.03	4.41
LA06-30 (ii)	0.00	4.58
LA06-31 (i)	0.02	2.73
LA06-31 (ii)	0.00	2.71

Sample ID	**Inorganic C (wt %)**
LA06-36 (i)	0.01
LA06-36 (ii)	0.01
UK99-4 (i)	0.77
UK99-4 (ii)	0.79
UK99-12 (i)	0.01
UK99-12 (ii)	0.01
420-422 cm (i)	0.71
420-422 cm (ii)	0.75
1159-1161 cm (i)	0.40
1159-1161 cm (ii)	0.42

Carbonate content in the samples were measured using UIC coulometer (Model 5012, UIC Inc., Illinois, USA). Toward this, ~100 mg of dried samples were treated with 40% H_3PO_4 at ~85°C and the liberated CO_2 gas is measured in the titration cell. The inorganic carbon content of the samples was calibrated with Na_2CO_3 solution of known strength, this standard was run repeatedly during analysis to check reproducibility of the measurements. The organic carbon content in the samples was estimated from the difference of total carbon and the inorganic carbon. Along with

Table 2-14: Repeat measurements of major and trace elements of the black shales and the BoB sediments.

Elements		**SK187 (320-322 cm)**		**SK187 (400-402 cm)**		***WPA06-2***		***WPA06-7***		**UK99-8**		**LA06-37**	
		(i)	***(ii)***	***(i)***	***(ii)***	***(i)***	***(ii)***	***(i)***	***(ii)***	***(i)***	***(ii)***	***(i)***	***(ii)***
Na	**(wt %)**	1.09	1.10	1.36	1.28	-	-	-	-	-	-	-	-
K		1.91	1.88	2.07	2.00	-	-	-	-	-	-	-	-
Ca		13.00	13.41	10.75	9.73	2.75	2.83	17.47	16.26	3.25	3.17	0.04	0.05
Mg		2.61	2.59	2.68	2.40	0.54	0.54	0.42	0.39	1.68	1.69	0.50	0.53
Al		6.61	6.28	6.41	6.42	4.53	4.55	4.22	3.88	4.01	4.07	3.67	3.95
Fe		4.06	3.97	3.87	3.95	1.75	1.82	1.07	0.98	1.70	1.72	0.78	0.81
Ti		0.34	0.36	0.36	0.38	0.22	0.28	0.18	0.14	0.30	0.28	0.21	0.22
Ba	**(µg/g)**	363	365	444	451	263	264	235	230	-	-	395	436
Cr		85	86	80	83	95	96	89	86	982	965	162	174
Mn		1685	1689	1356	1375	202	203	32	31	185	178	11	15
Sr		531	500	402	405	228	228	493	516	84	81	122	133
Co		23	25	24	26	25	28	23	20	32	30	22	21
Cu		36	36	40	39	148	144	223	211	186	173	107	120
Ni		68	68	79	86	48	52	59	60	231	234	66	68
Zn		397	430	461	396	91	95	43	40	295	274	66	62
V		77	80	78	82	174	174	241	239	3570	3606	1287	1368
U		-	-	-	-	-	-	-	-	19	19	14	15
Mo		-	-	-	-	-	-	-	-	37	32	35	38

the samples, a few samples were measured for inorganic carbon and total C and N, in duplicate to check the reproducibility of the measurements. The results of these repeat measurements are listed in Table 2-13. The analytical precision of the total and inorganic carbon measurements is better than 2% and 7% respectively, whereas for total nitrogen it is 3%.

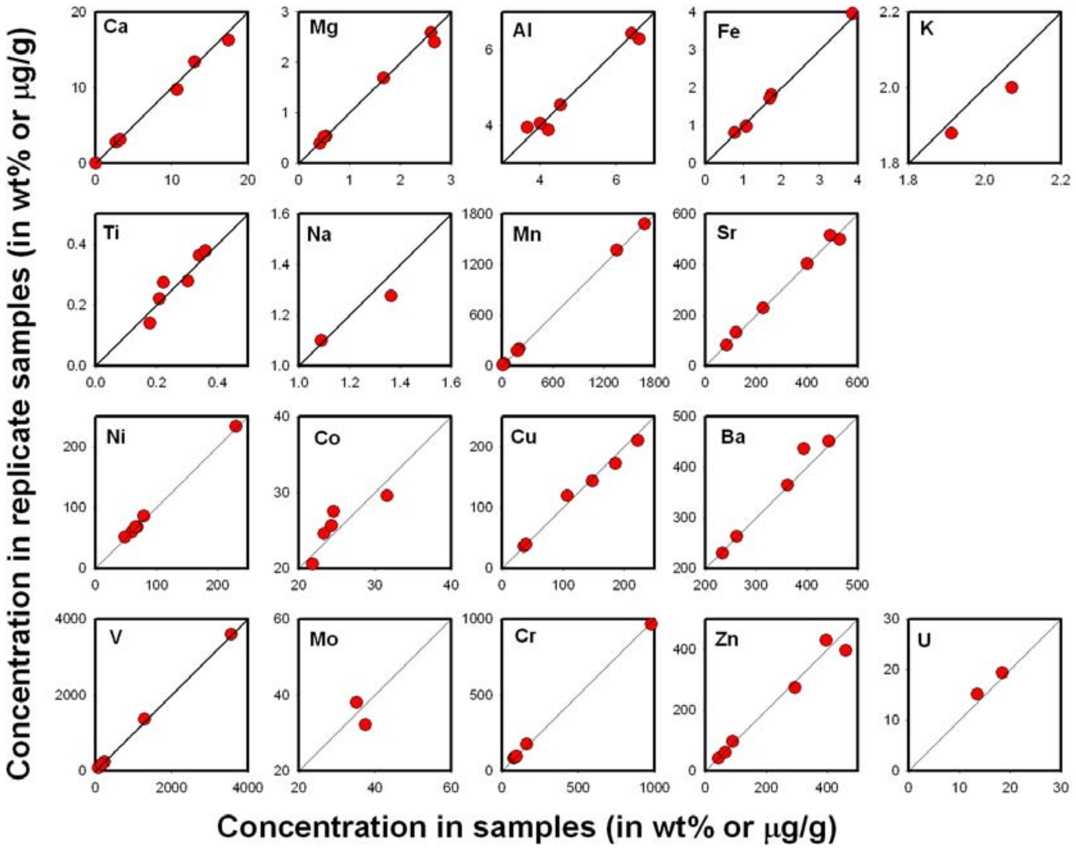

Figure 2.13: *Replicate analyses of geochemical composition of the black shales and the BoB sediments. The straight line in each sub-plot represents the 1:1 line*.

2.2.6. MAJOR AND TRACE ELEMENTS

Major, minor and trace elements were measured in sediments of the BoB and black shales. In the BoB sediments, prior to their complete dissolution, they were washed witth water to remove the sea salts present in them and dried at 80°C. These water-washed sediments were processed for their geochemical analysis. About 0.5 gm of shales and sediments were ashed at 600°C to oxidize the organic matters present in

Table 2-15: Coefficient of variance for different elements, calculated based on repeat measurements given in Table 2-13.

Element	CV (%)	Element	CV (%)
Na	3.4	**Ba**	3.3
K	2.0	**Cr**	2.6
Ca	5.6	**Mn**	9.8
Mg	4.1	**Sr**	3.5
Al	3.6	**Co**	6.8
Fe	3.2	**Cu**	4.2
Ti	9.8	**Ni**	3.4
		Zn	6.2
		V	2.5
		U	6.0
		Mo	8.5

them. The organic-matter free sediments were dissolved completely by treating with HF-HCl-HNO_3 repeatedly. The dissolved solutions of the sediments and shales were taken in 2% HNO_3 medium and were analyzed for geochemical composition using various techniques (Table 2-4). The approaches were all calibrated for relevant elements following standard procedure used in our laboratory [*Singh*, 1999; *Dalai et al.*, 2004; *Das and Krishnaswami*, 2007; *Rai*, 2008]. The measurements of Na and K were done using Flame AAS, whereas most of other elements (Ca, Mg, Al, Fe, Ti, V, Sr, Ba, Mn, Cr, Co, Cu, Zn, Ni) are measured using ICP-AES. Elemental compositions of Mo and U in the black shales were measured using Q-ICP-MS. The U and Mo concentrations were measured by calibrating ICP-MS using the standards with known strength [*Rahaman et al.*, 2010] and monitoring the signals of ^{238}U and ^{98}Mo isotopes.

To check the external precision of these measurements, few samples were dissolved in duplicates and measured (Table 2-14; Fig. 2.13). The reproducibility for different elements is found to be different and hence, the coefficient of variance (CV; Equation 2-1) for analysis of these elements were calculated based on the repeat measurements and are given in Table 2-15.

$$CV(\%) = 100 \times \sum_i \frac{1}{2n}\left(\frac{d_i}{x_i}\right)^2 \qquad \text{--------- (2-1)}$$

where, n is the number duplicates measured for the element and d_i is the difference of the duplicates of the i^{th} sample which has a mean value of x_i. Along with the samples, USGS sediment standard, G2 was also analyzed to check the accuracy of the measurements. The measured values of G2 during this study are listed and compared with reported values in Table 2-16. The measured values for G-2 are found to be in good agreement with their corresponding reported values (Fig. 2.14).

Magnetic Susceptibility:

The MS of the sediments are measured at ~10 cm interval using 0.47 kHz frequency in MS2 Bartington Magnetic susceptibility meter [*Kessarkar et al.*, 2005] at National Institute of Oceanography, Goa.

Table 2-16: Measured values of the USGS G2 standard compared to their corresponding reported values.

		Reported		**Measured**	
		Mean	Stdev	Mean	Stdev
Na	**(wt %)**	3.03	0.17	3.04	0.10
K		3.72	0.13	3.75	0.07
Ca		1.4	0.3	1.36	0.08
Mg		0.45	0.08	0.44	0.02
Al		8.15	0.03	8.18	0.29
Fe		2.07	0.13	1.85	0.06
Ti		0.29	0.02	0.31	0.03
Ba	**(µg/g)**	1880	23	1870	61
Cr		8.7	-	6.4	0.2
Mn		250	83	244	24
Sr		478	2	486	17
Co		4.6	0.7	8.0	0.5
Cu		11	-	8.6	0.4
Ni		5	-	b.d.	-
Zn		86	8	87	5
V		36	4	33	1

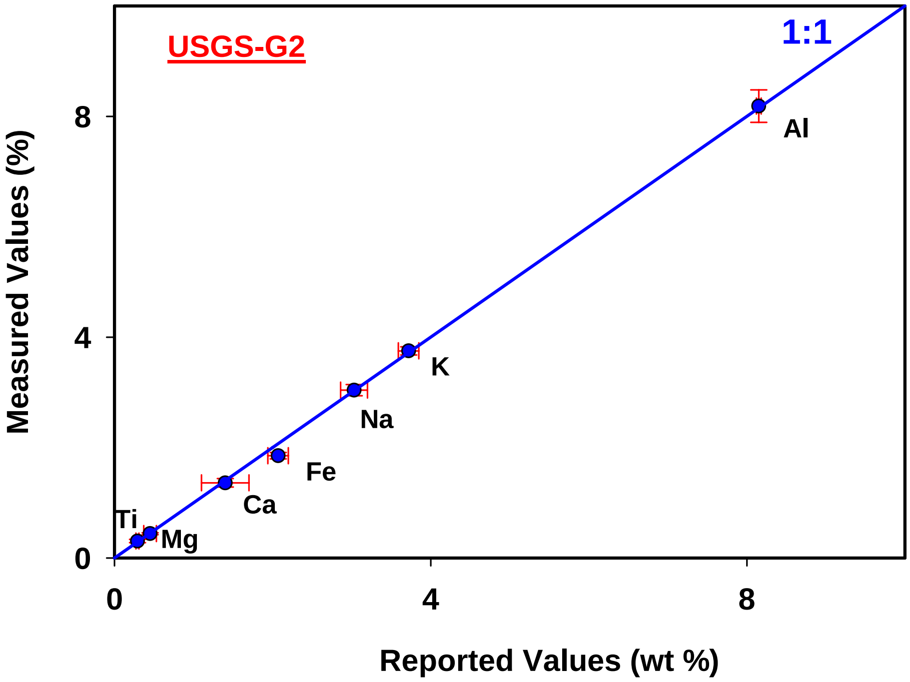

Figure 2.14: *The measured values for major elements of the USGS sediment standard G2 show good agreement with their corresponding reported values*.

CHAPTER 3

Re-Os isotopic systematics and Geochemistry of Black Shales from the Vindhyan, Himalaya and Aravalli: Implications to their ages, alteration and atmospheric oxygen evolution trend

3.1. INTRODUCTION

Marine black shales from various geological formations world-wide have been used to infer about the evolutionary history of the Earth. The chemical and isotopic signals preserved in these sedimentary rocks provide useful information on key geological processes, such as the evolution of atmosphere oxygen, diversification of life, past glacier epochs and their impacts and paleo-seawater conditions. In India, black shales are well preserved in various sedimentary formations in the Himalaya, Vindhyan, Aravalli, Cuddapah and the Dharwar [*Ramakrishnan and Vaidyanadhan*, 2008]. However, their potential to yield information on paleo-seawater conditions at the time of deposition has been limited owing to insufficient information on their depositional ages. In this thesis, efforts are made to date selected black shales from the Vindhyan, Himalaya and the Aravalli. The strategy behind studying samples from these three formations (Bijaigarh shales, Lower Tal formation, Mandhali formation and Jhamarkotra formation) lies in the fact that their depositional ages are estimated from Paleoproterozoic to Early Cambrian [*Valdiya*, 1982; *Singh et al.*, 1999; *Ray*, 2006; *Sarangi et al.*, 2006]. This time range witnessed some of the important evolutionary changes in the early Earth, for example, increase in atmospheric oxygen level, growth of continental crust, seawater oxygenation and changes in the biosphere. Dating of black shales, similar to any other sedimentary deposits, is challenging as the age information retained by various radiometric geochronometers is often compounded by signatures from their provenances. In this regard, Re-Os chronometer has been proved successful to provide reliable ages for black shales. The Re and Os contained in the organic-rich shales are by and large authigenic in nature and hence, the ^{187}Re-^{187}Os isotopic systematics in well preserved samples can yield their depositional ages [*Ravizza and Turekian*, 1989; *Kendall et al.*, 2009a]. Further, the application of Re-Os chronometer has a merit that it dates the sedimentary deposits, whereas most of the radiometric approaches rely on volcanic ashes/ clay minerals. In light of this, in this study, Re-Os dating method has been employed to constrain the depositional ages of black shales from the three different geological regions cited above. This dating technique also enables to reconstruct the marine

^{187}Os/^{188}Os ratio during deposition period of these shales. These paleo-seawater ^{187}Os/^{188}Os ratios along with the existing literature knowledge can be helpful to evaluate the potential of seawater ^{187}Os/^{188}Os as a proxy to track the atmospheric oxygen evolution trend.

In addition to depositional ages and paleo-seawater conditions, the Re-Os isotopic systematics of shales from these three locations also has the merit to address some key issues of regional to global significance. For example, the chronology of the Vindhyan Supergroup has been a matter of great interest and debate in recent times as it can provide key information on the temporal evolution of life in our planet. Subsequent to the discovery of small shelly fossils [*Azmi*, 1998; *Seilacher et al.,* 1998], which are often found in the Early Cambrian deposits, in the Paleoproterozoic sediments of the Vindhyan Supergroup [*Ray*, 2006], there has been considerable efforts to constrain the depositional ages of various formations of the Vindhyan, particularly that of the Lower Vindhyan. However, there exists insufficient information on the ages of the Upper Vindhyan. Precise chronology of the Upper Vindhyan will be useful in establishing interrelation of ages between Upper and Lower Vindhyan. This information on the ages of Vindhyan Supergroup is required to place time constrain to the sedimentary hiatus between Lower-Upper Vindhyan, which has been inferred from sedimentological signatures of the two groups [*Prakash and Dalela*, 1982; *Ram et al*., 1996]. Similar to black shales from the Vindhyan, the Re-Os isotopic systematics of black shales from the Lesser Himalaya holds potential to provide information on their deposition ages to provide a well constrained age of the formation present above the Pc-C boundary. Re-Os systematics of these shales can also be useful in providing information on the redox state of seawater near the Pc-C boundary and to provide correlation between inner and outer Lesser Himalaya. The time span near the Pc-C boundary is an important period in terms of evolution of life as the "Cambrian explosion" shifted the biosphere towards dominance of multi-cellular life. Despite its global importance, the cause for triggering the Cambrian explosion and seawater chemistry during this period has been remained unclear. In light of this, the work in this thesis is aimed to investigate the abundances of Re and

Os and Os isotopes along with geochemical signatures of the black shale deposited around the Pc-C boundary in the outer LH. Further, black shales from inner LH have also been investigated to constrain their ages to correlate them with that of the formations of the outer LH. In an attempt to derive information pertaining to paleo-seawater during middle Proterozoic, black shales from the Lower Aravalli have been investigated in this study for Re-Os systematics.

Recognizing the importance of geochemical and isotopic signatures of black shales in providing information on various regional aspects of the Vindhyan, Himalaya and Aravalli Supergroup, this chapter is sub-sectioned into four parts, *viz*. (i) constraining the depositional age of the (Upper) Vindhyan Supergroup and Lesser Himalaya using Re-Os chronometer (ii) oxic-anoxic condition of seawater at around Precambrian-Cambrian boundary using Re-Os composition of black shales from the Lesser Himalaya, (iii) Re-Os systematics of Aravalli shales to asses the impact of black shales weathering on the Re-Os chronometer and finally, (iv) evaluating the possibility of tracking atmospheric oxygen evolution trend during the Precambrian using past seawater ^{187}Os/^{188}Os as a proxy.

3.2. VINDHYAN SUPERGROUP

The Vindhyan Supergroup is less metamorphosed and undeformed sedimentary succession deposited mainly in the shallow marine conditions [*Mitra*, 1996; *Ramakrishnan and Vaidyanadhan*, 2008]. These sedimentary deposits preserve valuable information on past marine conditions from Mesoproterozoic to Vendian [*Ray*, 2006]; however, lack of *reliable* radiometric ages of rocks from the Vindhyan Supergroup particularly that of the Upper Vindhyan, prevents their application to extract useful information pertaining to earth history from them.

Table 3-1: *Radiometric ages for the various sedimentary successions of the Vindhyan Supergroup. All the ages, except those from this study and Srivastava and Rajgopalan [1988], reported for the Kaimur are based on dating of Kimberlite pipe that intrudes to the Kaimur sandstones.*

		Startigraphic Layer	Age (Ma)	Dating Scheme	Reference
Vindhyan Supergroup	**Upper Vindhyan**	**Bhander**	771-1070	Pb-Pb	*Malone et al., 2008*
			650-750	Sr isotopic startigraphy	*Ray et al., 2003*
			650 ± 770	Pb-Pb	*Ray et al., 2003*
			~550	K-Ar	*Crawford and Compston, 1970*
		Rewa	710 ± 120	F-T	*Srivastava and Rajgopalan, 1988*
		Kaimur	**1196 ± 41**	**Re-Os**	***This Study***
			1073 ± 14	Ar-Ar	*Geogory et al., 2006*
			1067 ± 31	Rb-Sr	*Kumar et al., 1993*
			1044 ± 22	Rb-Sr	*Smith, 1992*
			1072 ± 169	K-Ar	*Srivastava and Rajgopalan, 1988*
			1071 ± 160	F-T	*Srivastava and Rajgopalan, 1988*
			1630 ± 353	Rb-Sr	*Paul, 1979*
			947 ± 30	K-Ar	*Paul et al., 1975*
			1170 ± 46	K-Ar	*Paul et al., 1975*
			1116 ± 12	K-Ar	*Crawford and Compston, 1970*
			1056	K-Ar	*Crawford and Compston, 1970*
			940 ± 30	K-Ar	*Vinogradov et al., 1964*
	Lower Vindhyan (Semri)	**Rohtas**	1599 ± 48	Pb-Pb	*Sarangi et al., 2004*
			1601 ± 130	U-Pb	*Ray et al., 2003*
			1400 ± 70	K-Ar	*Vinogradov et al., 1964*
		Khenjua	1599 ± 8	U-Pb	*Rasmussen et al., 2002*
			1483 ± 15	Rb-Sr	*Kumar et al., 2001*
			1461 ± 14	Rb-Sr	*Kumar et al., 2001*
			1504 ± 15	Rb-Sr	*Kumar et al., 2001*
			1080 ± 40	K-Ar	*Vinogradov et al., 1964*
			1110 ± 70	K-Ar	*Vinogradov et al., 1964*
		Mirzapur	1729 ± 110	Pb-Pb	*Sarangi et al., 2004*
			1628 ± 8	U-Pb	*Rasmussen et al., 2002*
			1631± 5 (and 1)	U-Pb	*Ray et al., 2002*
			1014 ± 18	Rb-Sr	*Bansal et al., 1999*
			1243 ± 218	F-T	*Srivastava and Rajgopalan, 1988*

Subsequent to the finding of Cambrian-like fossils with annulated tubes, embryo-like globules, calcified cyanobacteria by *Azmi* [1998] in the Rohtas and the triploblastic worm burrows by *Seilacher et al.* [1998] in the Chorhat Formation, number of efforts were made to constrain the depositional age of the Lower (Semri) Vindhyan (Table 3-1). In an attempt to date the gluconites from the Lower Vindhyan near Chitrakut using Rb-Sr isotopic systematics, *Kumar et al.* [2001] found a near isochron line corresponding to an age of 1485±14 Ma. Realizing the intricacies involved with the Rb-Sr dating of gluconites, which is expected to provide lower age than the startigraphic age, the authors suggested the onset of the earliest Vindhyan sedimentation not later than 1600±50 Ma. A similar conclusion, but with precise information came from the U-Pb zircon age from the Kajrahat and Rohtasgarh limestones from the Lower Vindhyan, which constrained the depositional ages of these successions to 1631±5 Ma and 1631±1 Ma respectively [*Ray et al.*, 2002]. Consistent with these results, *Rasmussen et al.* [2002] reported the depositional age of 1628±8 Ma and 1599±8 Ma for the Chorhat sandstone based on the U-Pb geochronology of zircons. The robustness of these ages for the Lower Vindhyan got strengthened with the subsequent Pb-Pb ages (~1600 Ma) reported for the Semri group [*Ray et al.*, 2003; *Sarangi et al.*, 2004; *Bengston et al.*, 2009]. These radiometric dates reported for the Semri group are found to be consistently clustered around 1600 Ma, providing good age control for the Lower Vindhyan [*Kumar et al.*, 2001; *Rasmussen et al.*, 2002; *Ray et al.*, 2002, 2003; *Sarangi et al.*, 2004; *Bengston et al.*, 2009].

On contrary to the Semri group, reliable depositional ages for the Upper Vindhyan successions are limited (Table 3-1). The depositional age of the Bhander, the uppermost group of the Vindhyan, has been suggested to be ~650 Ma [*Ray et al.*, 2003] based on Pb-Pb age of carbonates and Sr isotope startigraphy. This suggestion of age seems to be in accord with marked age range [*Srivastava*, 2009] for the Sirbu Shales (850-630 Ma) and the Upper Bhander (630-542 Ma), based on the record of bio-markers. However, recent (U-Pb of zircon) study of *Malone et al.* [2008] indicated an age range of 771-1070 Ma for the Bhander group. These age ranges are consistent with that (700-1100 Ma) inferred based on the Churia-Tawunia fossils by *Kumar and Srivastava* [1997]. Similar to the Bhander, few depositional ages reported for lowermost sequence of the Upper Vindhyan, *i.e.* Kaimur group also show wide range [~900-1600 Ma; *Gregory et al.*, 2006 *and references therein*; *Azmi et al.*, 2008]. Most of these radiometric ages for the Upper Vindhyan come from the dating of the Majhgawan Kimberlite pipe that intrudes to the Kaimur sandstones, providing a lower limit for the actual depositional ages. Excluding one reported age (1630±353 Ma; Table 3-1) associated with large error, the ages suggested for the Kaimur based on radiometric dating of Majhgawan Kimberlite pipe ranges between 947±30 Ma and 1170±46 Ma and cluster around ~1050 Ma (Table 3-1). These dates obtained using Rb-Sr, Ar-Ar and K-Ar systematics of intrusions of the Kimberlite pipe provide a intruding time of the pipe into the Kaimur sandstones, which constrains only a lower limit for the depositional age of the Kaimur group. A few depositional ages reported for the Kaimur group are associated with large errors [*Srivastava and Rajgopalan,* 1988]. The insufficient age information available for the Upper Vindhyan particularly that for the Kaimur group demands more studies pertaining to their chronology, which would provide not only their depositional ages but also the useful information on the time gap, if any, in sedimentation between the Lower and the Upper Vindhyan. Towards this, direct dating of sedimentary layers using suitable geochrometer will be essential to obtain a precise age.

The Re-Os isotopic systematics of sedimentary rocks, such as organic rich shales has found successful to determine their depositional ages [*Ravizza and Turekian*, 1989; *Singh et al.*, 1999; *Selby and Creaser*, 2003; *Kendall et al*., 2009a]. The Re and Os, as discussed earlier, preserved in the black shales are mostly authigenic in nature with insignificant contribution from detrital and/or extraterrestrial particulates and hence the growth of ^{187}Os corresponding to decay of ^{187}Re provides a precise depositional age for the shales. Therefore, the Re-Os geochronometer of black shales can be used to gain better age information for the sedimentary deposit of the Upper Vindhyan. In this contribution, attempts were made to constrain the depositional age of the Kaimur group using Re-Os chronometer of Bijaigarh shales.

3.2.1. Re-Os Geochronology for the Bijaigarh Shales, Kaimur group

The Kaimur group is an important succession of the Vindhyan Supergroup as it overlies on the Rohtas sub-group, where the small shelly fossils were discovered and also, the depositional age of the Kaimur can be useful to infer about the time gap in the sedimentary depositions exists between the Semri and Kaimur. In this section, Re-Os geochronological approach to constrain the age for the Kaimur group is provided.

Table 3-2: *Re-Os isotopic systematics of the Bijaigarh shales, Kaimur group, Vindhyan Supergroup.*

Sample ID	Re	Os	^{187}Re/^{188}Os		^{187}Os/^{188}Os	
	ng/g	*pg/g*		$\pm 1\sigma_\mu$		$\pm 1\sigma_\mu$
V99-1A	14.4	397	323	2	6.705	0.004
V99-1A/R	14.5	440	293	2	6.649	0.012
V99-4A	14.1	472	260	1	6.348	0.007
V99-5A	5.8	217	206	1	4.664	0.021
V99-5A/R	5.6	231	180	1	4.326	0.011
V99-6A	3.8	123	277	2	6.814	0.033
V99-7A	11.5	383	255	2	5.987	0.009
V99-9A	1.7	45	395	5	8.728	0.021
V99-10A	12.8	424	260	2	6.164	0.011
V99-11A	2.7	222	80	1	2.948	0.005
V99-1*	13.1	556	168	2	3.838	0.006
V99-3*	4.3	90	666	7	14.597	0.029
V99-3/R*	4.5	91	677	7	14.398	0.023
V99-4*	13.5	421	269	3	5.803	0.005
V99-5*	16.7	710	172	2	4.110	0.101
V99-6*	3.0	99	237	2	5.155	0.006
V99-9*	2.0	47	488	5	10.309	0.014
V99-10*	16.6	491	297	3	6.457	0.010
V99-11*	5.1	334	100	1	2.873	0.019
V99-12*	10.3	182	1020	10	21.207	0.043

*Samples were analyzed by Dr. S. K. Singh at CRPG, France. See text for details.

3.2.1.1. Re, Os and their isotopes

The Re, Os and ^{187}Os/^{188}Os analyzed for the black shales from the Kaimur group is listed in Table 3-2. The Re concentration in these shales varies significantly from 1.7 to 16.7 ng/g with an average value of 8.8±5.4 ng/g, whereas the Os concentration ranges between 45 and 710 pg/g with a mean value of ~300 pg/g. The average Re/Os ratio for these shales are found to be 32±11, significantly higher compared to that of the mantle and meteorites (~1) and the average crustal value (~10) [*Esser and Turekian*, 1993]. The mean Re/Os ratio observed for the Bijaigarh shales are found to be similar to that reported (~25) for the earlier Cambrian shales from the Lesser Himalaya [*Singh et al.*, 1999]. The average ^{187}Re/^{188}Os value for the black shales studies in this work is found to be 331, lower by an order to that of the contemporary seawater [~4100; *Pierson-Wickmann et al.,* 2002]. However, the average value of ^{187}Re/^{188}Os of the black shales is comparable with that reported for Paleoproterozoic shales from geological deposits from other locations [*Yang et al.*, 2009]. The ^{187}Os/^{188}Os ratio for the black shales shows wide variation, ranging from 2.873 to 21.207 (Table 3-2).

3.2.1.2. Re-Os isochron

For the Re-Os analysis of the Bijaigarh shales, two hand specimens of each sample collected from the Amjhore pyrite mine were powdered separately. One set of powdered samples is analyzed at PRL, India during this study, whereas other set were measured for their Re, Os concentrations and ^{187}Os/^{188}Os by Dr. Sunil Kumar Singh at CRPG, France (Table 3-2). Further, some of the black shale samples are measured in duplicates using same powdered aliquot. Some of the samples from these two sets found to have different Re, Os elemental and isotopic compositions (Table 3-2). This shows that samples are heterogeneous at hand specimen scale as they are separate powdered aliquots of two different hand specimens of the black shales from the Kaimur group. This could be due to presence of pyrite nodules of difference sizes which are disseminated unevenly in these shales. This observation warrants the need of Re and Os measurement of black shales in the same aliquot to get a precise Re-Os ages and hence the preliminary results [*Singh et al*., 2002]on Re and Os measured in different aliquots of Bijaigarh shales required reanalysis of Re and Os of these shales in the same aliquot. The Re-Os isochron line of all the black shale samples measured both at PRL and CRPG is plotted in Fig. 3.1. Both set of Re-Os data measured for Bijaigarh shales using N-TIMS at PRL, India and CRPG, France fall on a single line. This ensures the reliability of the measurements as these measurements have been done at two different laboratories using different spikes. Again, these Re-Os data for both set of samples measured provide large spread in ^{187}Os/^{188}Os (~3-21) and ^{187}Re/^{188}Os (~80-1000) values (Table 3-2), required to get a precise isochron. The presence of good correlation between ^{187}Re/^{188}Os and ^{187}Os/^{188}Os for the Bijaigarh shales confirms close system behavior of Re and Os in them. As discussed earlier (*c.f.*

Chapter 1), in a closed Re-Os system with insignificant detrital Re and Os contribution, the growth of ^{187}Os due to decay of ^{187}Re in black shales subsequent to its deposition can be accounted to obtain depositional age for the rock using the following equation,

$$\left(\frac{^{187}Os}{^{188}Os}\right)_t = \left(\frac{^{187}Os}{^{188}Os}\right)_i + \left(\frac{^{187}\mathrm{Re}}{^{188}Os}\right)_t \times \left(e^{\lambda t} - 1\right) \qquad \text{------------- (3-1)}$$

where, (^{187}Os/^{188}Os)$_t$ and (^{187}Os/^{188}Os)$_i$ are the Os isotopic ratios of black shales of age t at present and at their depositional time (initial ^{187}Os/^{188}Os) respectively. λ represents the decay constant of ^{187}Re. Equation (3-1) represents a linear relation between ^{187}Os/^{188}Os and ^{187}Re/^{188}Os of the black shales; the slope of the straight line (Isochron) fit between these two ratios provides information about their depositional time, whereas the y-intercept gives the Os isotopic composition of the depositional basin at the time of their deposition. The basic assumptions to get an isochron are : (i) after the deposition the black shales have remained closed for Re and Os, (ii) initial isotope composition (^{187}Os/^{188}Os) were homogeneous and (iii) Re/Os ratios of these rocks are hetergeneous to get an spread in ^{187}Os/^{188}Os.

The Re-Os isochron line obtained (Fig. 3.1) for Bijaigarh shales, based on a bidirectional-error weighted regression line fit [using *Isoplot* 3.0 software; *Ludwig*, 2003], provides a depositional age of 1196 ± 41 Ma (using equation 3-1) for this black shale layer from the Kaimur group. This age is based on a half life of 41.6 Ga for ^{187}Re, which corresponds to a decay constant of 1.666×10^{-11} yr^{-1} [*Ludwig*, 2003]. The initial ^{187}Os/^{188}Os ratio obtained from the y-intercept of the Re-Os isochron is 0.74±0.27 (Fig. 3.1). This initial Os isotopic ratio is expected to be the ^{187}Os/^{188}Os of the seawater during the deposition time of the Bijaigarh shales. This inference can be challenged owing to the leaching of non-authigenic osmium from the black shales during their dissolution with inverse aqua regia. However, recent study of Selby and Creaser [2003] have found that leaching of authigenic CrO_3-H_2SO_4 provides a range of initial ratio (0.39-0.55) for black shales from the Exshaw formation, Canada overlaps with that found using inverse aqua regia [0.53±0.07; *Creaser et al.*, 2002].

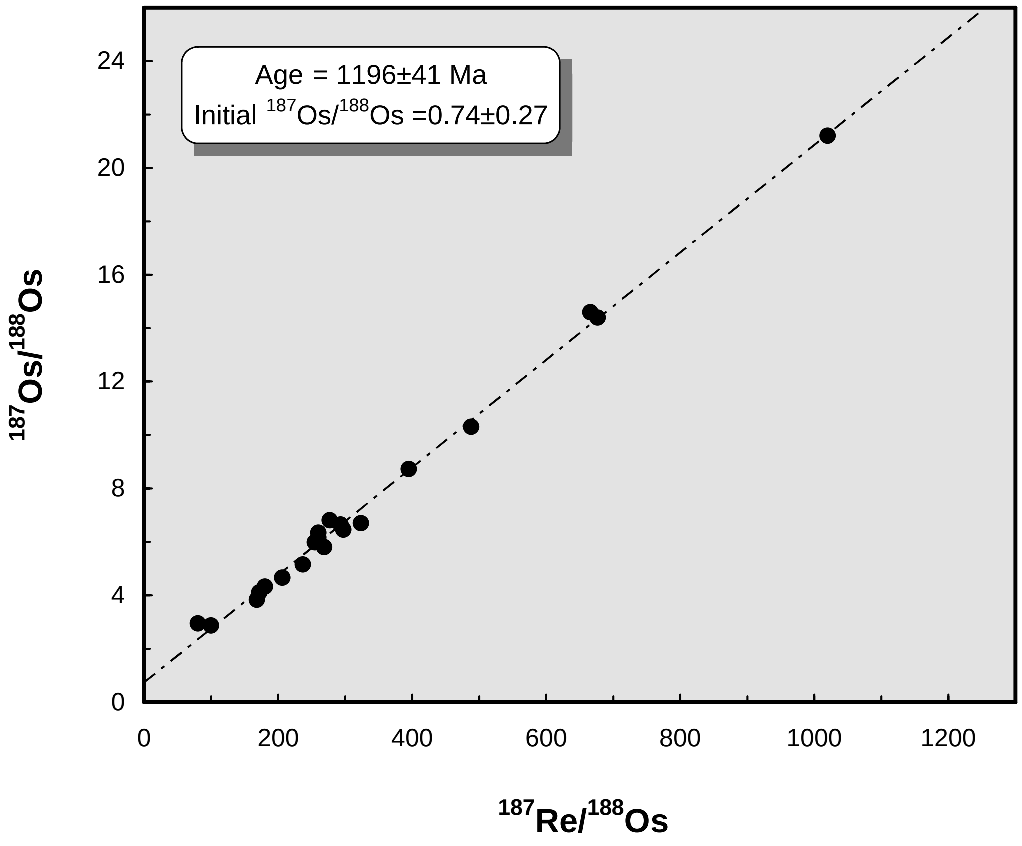

Figure 3.1: *Re-Os isochron for the black shales from the Bijaigarh shales, Kaimur group.*

The present study of Re-Os ages of black shales has been carried out using inverse aqua regia as dissolution medium, which though can leach some fraction of detrital osmium from the shale, the uncertainties associated with depositional age and the initial $^{187}Os/^{188}Os$ could be insignificant. Hence, the initial $^{187}Os/^{188}Os$ found from the isochron with its associated uncertainty provides the seawater Os isotopic composition during the time of their deposition. This initial $^{187}Os/^{188}Os$ ratio is found to be significantly higher compared to that (~0.1) obtained for black shales and pyrites from (Transvaal Supergroup, South Africa and Kola Peninsula, Russia) the Paleoproterozoic [*Hannah et al.*, 2004, 2008], but lower compared to that (~1.0) reported for Neoproterozoic, (Lesser Himalaya, India and South China) sedimentary organic deposits [*Singh et al.*, 1999; *Li et al.*, 2003]. Implication of this observation is linked with the temporal changes in the osmium supply from the continents to the seawater at various periods of the Proterozoic and will be detailed in a subsequent section of this chapter.

The Re-Os depositional age of 1196 ± 41 Ma obtained for the Kaimur group in this study overlaps with the K-Ar ages [1072 ± 169 Ma; *Srivastava and Rajgopalan,* 1988] and F-T ages reported for Vindhyan gluconites [1071 ± 160 Ma; *Srivastava and Rajgopalan,* 1988], but is older compared to the most of the reported ages clustering around 1050 Ma for the Kimberlite pipe (Table 3-1) that intrudes into the Kaimur sandstones. The ages of samples from the pipe are expected to be younger as it intrudes the existing sedimentary succession. For example, the recent Ar-Ar age [1073.5 ± 13.7 Ma; *Gregory et al.*, 2006] reported for the phlogopite separates from the Kimberlite pipe is younger by ~100 Ma compared to present Re-Os age. However, this Re-Os age for the Kaimur group is found to be consistent with the reported K-Ar age of the pipe of 1170 ± 46 Ma [*Paul et al.*, 1975] and overlaps with the Kimerlite pipe age reported using Rb-Sr [1630 ± 353Ma; *Paul,* 1979]. Hence, the depositional age (~1200 Ma) of the Kaimur group obtained from the Re-Os geochronometer in this study are in accordance with the lower age limit constrained for the Kaimur *via* radiometric ages of the samples from the Kimberlite pipe (Table

3-1). Along with constraining the depositional age for the Kaimur, the Re-Os age obtained for the Bijaigarh shales also provides an upper age limit for the Rewa group, for which radiometric ages are lacking.

3.2.2. Sedimentary Hiatus between the Semri and Kaimur groups

The ages for the Vindhyan sediments, including the Re-Os age for the Kaimur black shales from this study, are compiled from various studies and are listed in Table 3-1. Broadly, these radiometric ages indicate a depositional age of ~1600 Ma for the Lower Vindhyan, whereas ~1200 Ma for the lower section of the Upper Vindhyan. This large age gap between the Lower and Upper Vindhyan, as observed by earlier workers [*Ray et al.*, 2003; *Ray*, 2006] indicates existence of a sedimentary hiatus of ~400 Ma at the Rohtas-Kaimur junction. The occurrence of hiatus between the Rohtas and Kaimur is also inferred [*Prakash and Dalela*, 1982] from the presence of highly weathered surface with nodular shales often passing into laterite and bauxite zones at the boundary. These sedimentological evidences led to the suggestion that the Rohtas formation got eroded and deformed prior to the deposition of Kaimur sediments. The sedimentation cycle post-Lower Vindhyan was observed [*Ram et al.*, 1996] to be significantly different; the basin was drained out subsequent to the deposition of Lower Vindhyan causing long period of erosion leading to a regional unconformity at the Lower-Upper Vindhyan boundary. Ram et al. [1996] suggested a significant change in the provenance of the sediments from the Lower and Upper Vindhyan; for example, the sediments from the Lower Vindhyan were mainly from the near-by locations of the Bundelkhand province, whereas the provenance of Upper Vindhyan sediments located along the southern basinal margin of the Vindhyan basin inclusive of uplifted lower Vindhyans sediments. A similar change in the provenance between the Semri and Kaimur group is also inferred from the abrupt increase in the Nd isotopic composition of sediments across the Semri-Kaimur boundary [*Chakrabarti et al.*, 2007]. This change of sediment provenance is also advocated by the younger Nd model age of the Kaimur (2.5 Ga) compared to the Semri (3.0 Ga) group with existence of angular unconformity between two groups [*Chakrabarti et al.*, 2007].

The existence of this hiatus near the Rohtas-Kaimur boundary was also recognized in earlier studies, however, the time gap for the hiatus was inferred to be during ~1100-900 Ma [*Valdiya*, 1982]. Therefore, this unconformity was suggested [*Valdiya*, 1982] to be a result of crustal disturbance, a change contemporaneous to that observed in the Gothic orogeny (1100-900 Ma) of Europe and the Gordonian orogeny (1000 Ma) of Africa. The renewed chronology available for the Vindhyan (Table 3-1) constrains the sedimentary gap between *ca*. 1600 to 1200 Ma and hence, may not be correlated with orogenic events suggested earlier. The presence of sedimentary hiatus at the Rohtas-Kaimur junction has been suggested to be resuted from tectonic activites, such as rifting and convergence of the Bundelkhand and Bhandara-Bastar cratons [*Mishra*, 2011]. This tectonic activity could have changed the depositional settings of the Vindhyan, such as the volcanogenic sedimentary sequences of the Semri were invoked to deposit on the rifted platform of the Bundelkhand craton, whereas the sediments of the Upper Vindhyan during the final phase of convergence [*Mishra*, 2011]. Exposure of the lithosphere resulting from intercontinental collisions coupled with variations in sea level can led to a sedimentary hiatus of large time gap. This proposition of role of tectonics and sea level variation to result sedimentary hiatus at ~1600 Ma in the Vindhyan Supergoup is contemporaneous to erosional unconformity observed in the Sao Francisco craton and Aracuai fold belt of eastern Brazil [*Martins-Neto et al.*, 2001]. The erosional unconformity between 1500 and 950 Ma observed in the eastern Brazil [*Martins-Neto et al.*, 2001] has been related to tectonic changes associated with sea level variations. Further, the role of tectonic disturbance in resulting a sedimentary hiatus between the Semri and Kaimur group also seem to be evident from the changes observed in depositional settings and provenances of sediments of the Kaimur compared to that of the Rohtas [*Ram et al.*, 1996; *Chakrabarti et al.*, 2007].

3.3. Lesser Himalaya

Perturbations in the global biogeochemical cycles have been found responsible to trigger most of the biological transformations of the planet. Biological diversifications are very often found to be followed by mass extinction events, resulting from the internal and/or external causes. Events of this kind and their causes hold the key to understand and reconstruct the evolution history of life. One such event of significant biological interest occurred at around the Pc-C boundary. This biological change around the Pc-C boundary was inferred from the distinct records of Neoproterozoic soft-bodies Ediacarian biota and Cambrian small shelly fossils. This drastic change towards multi-cellular life was possibly the last explosive evolutionary change in the planet [*Steiner et al.*, 2001]. However, the exact cause for the diversification of biotas near the Pc-C boundary has remained poorly understood. In India, Pc-C boundary has been identified between the Krol and Tal formations of the outer Lesser Himalaya. However, this boundary lacks reliable radiometric age except one Re-Os age in which black shale layer in the lower Tal formation above the Pc-C boundary has been dated to 535±11 [*Singh et al*., 1999]. In this study an effort has been made to date a black shale layer present above the boundary but much closer to it to provide a reliable age of the boundary. Further, black shales from the Mandhali formation of the inner Lesser Himalaya have also been studied to correlate with those from the outer belt.

Studies concerning the causes of the anoxia of seawater at around the Pc-C boundary that led to the Cambrian explosion has suggested various possibilities. The supply of poorly ventilated bottom water to the surface is one of them [*Brasier*, 1989; *Wille et al*., 2008]. This proposition finds support from the negative excursion in the δ^{13}C at around Pc-C, which has been explained in terms of supply of the deep water depleted in δ^{13}C. This hypothesis however has been debated due to absence of such excursion in δ^{13}C in early Cambrian [*Brasier*, 1995] and long time periods (1 Ma) of the excursion [*Kump*, 1991]. Alternative hypothesis suggested to explain this include the release and oxidation of methane-hydrate stored in marine sediments [*Erwin*, 1993] and enhanced hydrothermal activities near the Pc-C [*Steiner et al*., 2001; *Jiang et al*., 2007].

Table 3-3: *Major elemental composition of black shales from inner and outer belts of the Lesser Himalaya. The outer belt samples are from an underground mine, whereas the inner belt samples are from a road cut.*

	Sample ID	**Al**	**Ca**	**Fe**	**Mg**	**Ti**	**TN**	**TC**	**C_{org}**	**C_{inorg}**
						wt%				
Outer Belt	**UK99-1**	3.56	5.47	1.79	1.38	0.24	0.17	8.19	7.34	0.84
	UK99-2	4.28	1.73	2.38	1.20	0.28	0.20	8.45	8.00	0.45
	UK99-3	3.66	2.54	1.39	1.30	0.24	0.17	6.35	5.67	0.68
	UK99-4	4.20	2.28	1.71	1.47	0.29	0.18	5.73	4.96	0.77
	UK99-5	3.59	1.76	2.12	1.35	0.23	0.19	6.15	5.37	0.78
	UK99-6	4.10	3.10	1.59	1.51	0.29	0.17	6.55	5.63	0.92
	UK99-7	3.68	4.35	1.75	1.49	0.23	0.15	7.08	6.29	0.79
	UK99-8	4.01	3.25	1.70	1.68	0.30	0.18	6.19	5.24	0.95
	Average	3.89 ± 0.29	3.06 ± 1.30	1.80 ± 0.31	1.42 ± 0.15	0.26 ± 0.03	0.18 ± 0.02	6.84 ± 0.99	6.06 ± 1.08	0.77 ± 0.16
Inner Belt	**UK99-9**	6.73	0.04	0.77	0.38	0.46	0.14	3.91	3.86	0.05
	UK99-10	5.77	0.03	1.29	0.33	0.42	0.14	4.51	4.49	0.02
	UK99-11	5.77	0.03	0.62	0.33	0.44	0.13	4.33	4.31	0.02
	UK99-12	6.81	0.03	0.58	0.37	0.46	0.13	4.61	4.60	0.01
	UK99-13	6.90	0.03	0.68	0.37	0.48	0.12	2.89	2.87	0.02
	UK99-14	7.21	0.03	0.74	0.39	0.47	0.13	2.59	2.58	0.01
	UK99-15	5.54	0.03	0.68	0.31	0.39	0.13	5.51	5.50	0.01
	Average	6.39 ± 0.67	0.03 ± 0.00	0.76 ± 0.24	0.35 ± 0.03	0.45 ± 0.03	0.13 ± 0.01	4.05 ± 1.02	4.03 ± 1.02	0.02 ± 0.01
	PAAS	10.01	0.93	5.05	1.33	0.60				

Table 3-4: Trace elemental composition of black shales from the Lesser Himalaya.

	Sample ID	Ba	Cr	Mn	Sr	Co	Cu	Ni	Zn	V	U	Mo	Re	Os
							µg/g						ng/g	
Outer Belt	UK99-1	208	1160	171	140	34	178	209	83	2316	37	18	191	8.4
	UK99-2	1042	1653	130	79	40	372	398	224	4651	31	22	382	20.2
	UK99-3	270	1104	132	76	31	163	193	86	1365	19	21	190	9.3
	UK99-4	316	965	137	66	30	185	223	92	3230	19	32	236	11.4
	UK99-5	228	2288	124	59	30	334	368	2008	5946	17	30	209	23.0
	UK99-6	201	1526	167	96	31	436	393	1457	4598	33	76	311	18.1
	UK99-7	166	1457	141	188	28	451	374	2671	3711	56	81	270	16.4
	UK99-8	*n.a.*	982	185	84	32	186	231	295	3570	19	37	259	12.0
	Mean	347 ± 310	1392 ± 444	148 ± 22	99 ± 44	32 ± 4	288 ± 123	299 ± 92	865 ± 1033	3674 ± 1432	29 ± 13	39 ± 25	256 ± 66	15 ± 5
Inner Belt	UK99-9	491	110	2	34	35	21	13	51	145	6	2	33	0.27
	UK99-10	422	118	*b.d.*	30	32	19	11	31	137	5	3	33	0.46
	UK99-11	442	115	*b.d.*	29	36	18	15	30	136	5	2	29	0.40
	UK99-12	522	117	2	36	32	16	13	30	156	5	3	33	0.40
	UK99-13	527	123	5	37	33	15	11	30	139	5	2	21	0.34
	UK99-14	515	114	3	42	33	15	12	31	141	6	2	18	0.32
	UK99-15	386	110	*b.d.*	27	30	25	12	34	130	5	2	34	0.54
	Mean	472 ± 56	115 ± 5	3 ± 2	34 ± 5	33 ± 2	18 ± 4	13 ± 1	34 ± 8	141 ± 8	5 ± 0	2 ± 1	29 ± 7	0.39 ± 0.09
	PAAS	650	110	852	200	23	50	55	85	150	3.1	1	-	-

In this study, efforts were made to constrain the depositional ages for the black shales deposited in the inner and outer belts of the LH using Re-Os chronometer. The Re-Os isotopic systematics of these shales placed above and below the Pc-C boundary along with their geochemical composition enables to infer about the state of seawater around the Pc-C boundary and their causes.

3.3.1. Geochemistry of Black shales

The chemical composition of black shales measured for the shales from the inner and outer belts of the LH measured in this study are provided in Table 3-3 and 3-4. The shales from the two belts showed distinctly different chemical composition. The average C_{org} concentrations of the shales from the outer (6%) and inner (4%) belt of LH are much higher compared to the lower limit of 1% C_{org} for a rock to fall in black shale category [*Arthur and Sageman*, 1994]. The lithogenic major elements, Al (6.39±0.67%) and Ti (0.45±0.03%) concentrations of the inner belt of the LH are observed to be higher compared to that of the outer belts (3.89±0.29% and 0.26±0.03% respectively). In contrast to these elements, the average concentrations of other major elements and most of the trace elements are found to be significantly higher in the outer belts than that of the inner belt (Table 3-3; 3-4). The range of concentrations of Ba in the outer belt (166-1042 μg/g), however overlaps with that of the inner belts (386-527 μg/g). The average concentrations of most of the trace elements with redox-sensitive behavior, *e.g.* V, U, Mo, Re, Os in the outer belts are enriched by about an order compared to that of the inner belt shales. A similar observation of enrichment of trace elements above, but near the Pc-C boundary has been documented in various other sedimentary formations globally [*Jiang et al.*, 2007 and *references therein*]. The average composition of most of trace elements of these shales is found to be comparable or higher to that of the Post-Archean Australian shales [PAAS; *Taylor and McLennan*, 1985].

3.3.2. Re-Os systematics

The concentrations of Re and Os along with the $^{187}Os/^{188}Os$ ratios of the black shales from the inner and outer belts of LH analyzed in this study are given in Table

3-5. Similar to the trace element abundances (Table 3-4), the concentrations of Re and Os in the shales from these two formation shows remarkable difference. The average Re concentration of the shales from the outer belt (256±66 ng/g) is found to be ~10 times higher than that of the inner belt (29±7 ng/g). About 40 times enrichment of Os in the shales from the outer belt (14.8±5.3 ng/g) is observed compared to that of the inner belt (0.39±0.09 ng/g) of LH. These trends of Re and Os enrichment above, but near the Pc-C boundary is consistent with the trends observed for other redox-sensitive, as discussed earlier (Table 3-4). The Re/Os ratio of the black shales from the outer belt are found to vary from 9 to 23, lower compared to the inner belt shales, which show a range of 56-121. The range of ^{187}Os/^{188}Os observed for the black shales from the outer belt are found to be lower compared to that of the inner belt (Table 3-5). This observation of high radiogenic Os isotopic composition of the inner belt of LH is consistent with their corresponding higher Re/Os ratio compared to that of the black shales from the outer belt.

Table 3-5: Re, Os, ^{187}Re/^{188}Os and ^{187}Os/^{188}Os values of the black shales from the Lesser Himalaya.

	Sample ID	**Re** ng/g	**Os** pg/g	**^{187}Re/^{188}Os**		**^{187}Os/^{188}Os**	
					$\pm 1\sigma_{\mu}$		$\pm 1\sigma_{\mu}$
Outer Belt	**UK99-1**	191	8403	136.99	1.11	2.043	0.008
	UK99-2	382	20160	112.33	0.59	1.892	0.002
	UK99-3	190	9282	121.63	0.62	1.901	0.004
	UK99-4	236	11440	124.39	0.87	2.048	0.002
	UK99-5	209	23021	50.82	0.36	1.363	0.001
	UK99-6	311	18054	101.86	0.86	1.869	0.011
	UK99-7	270	16362	96.29	0.33	1.748	0.002
	UK99-8	259	11971	131.26	0.36	2.116	0.004
	Average	256 ± 66	14837 ± 5345	109 ± 27		1.873 ± 0.238	
Inner Belt	**UK99-9**	33	273	939.23	5.47	4.865	0.007
	UK99-10	33	464	545.00	6.65	4.628	0.022
	UK99-11	29	395	573.33	6.65	4.713	0.014
	UK99-12	33	397	646.81	5.66	5.027	0.011
	UK99-13	21	339	477.11	1.91	4.977	0.006
	UK99-14	18	320	433.11	0.82	4.746	0.007
	UK99-15	34	541	461.05	3.04	4.098	0.013
	Average	29 ± 7	390 ± 91	582 ± 174		4.722 ± 0.310	

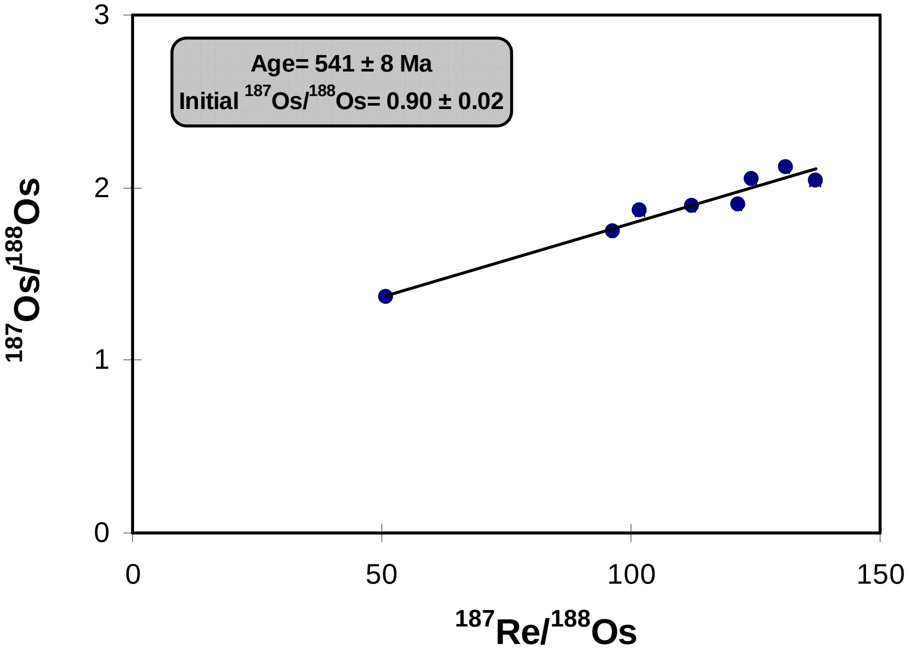

Figure 3.2: *Re-Os isochron of black shales above, but near the Krol-Tal boundary, Lesser Himalaya.*

3.3.3. Re-Os Isochrones

One of the foci of this study is to constrain the depositional ages of black shales from the LH using Re-Os isotopic systematics and to infer about the state of anoxia of seawater during the period of their deposition. In light of this, Re-Os elemental and isotopic ratios from three successions from the LH deposited around the Pc-C [*Present study*; *Singh et al.*, 1999] are compared. The Re-Os systematics of black shales following few Ma of the Pc-C boundary is from the study of *Singh et al.* [1999]. The authors constrained the depositional ages for the succession using Re-Os chronometer to 535±11 Ma with an initial $^{187}Os/^{188}Os$ of 1.181±0.024, using a Williamson bi-directional error weighted statistical analysis. In this work, a similar approach is followed as that of *Singh et al.* [1999] to find the depositional age of black shales and initial $^{187}Os/^{188}Os$ values for better comparison between the shales from different horizons.

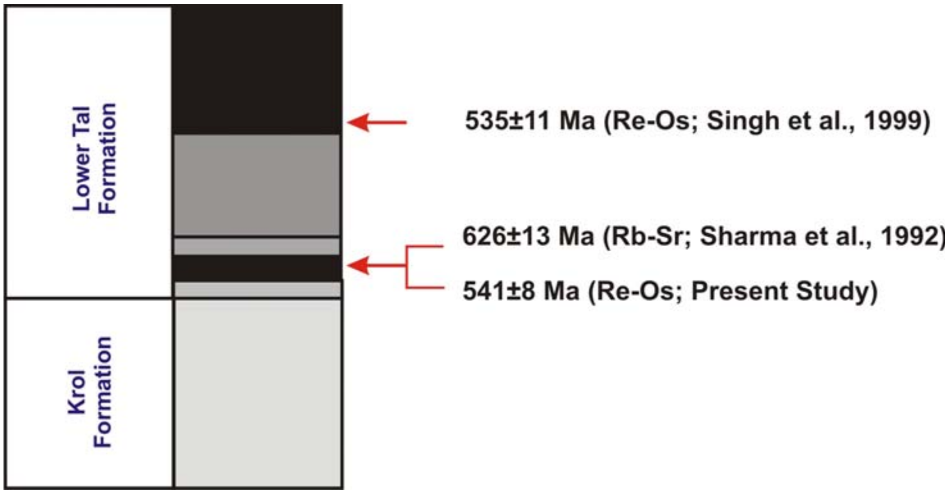

Figure 3.3: *Available Chronological information for the Krol-Lower Tal formation, Lesser Himalaya.*

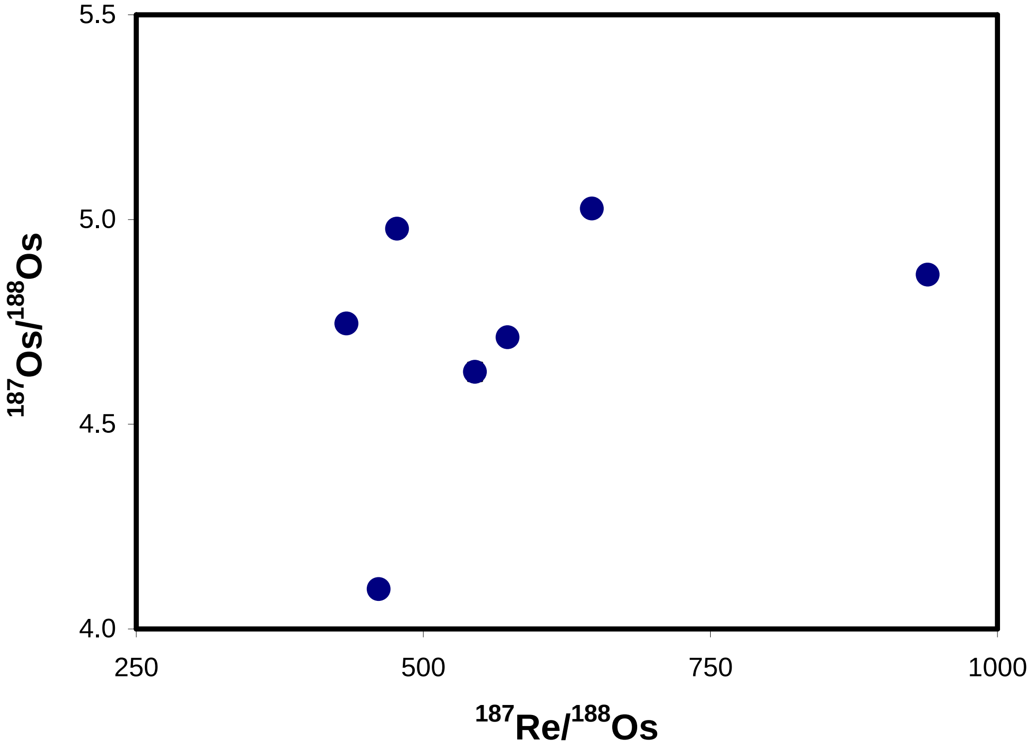

Figure 3.4: *^{187}Re/^{188}Os-^{187}Os/^{188}Os plot of the black shales from the Mandhali formation, inner belt of the Lesser Himalaya. Large scatter in the data does not allow reliable estimate of depositional age for the formation.*

The ^{187}Re/^{188}Os and ^{187}Os/^{188}Os for the black shales from the outer belt of the LH above, but closer to the Pc-C boundary vary from 51 to 137 and 1.363 to 2.116 respectively. The Re-Os isochron for these shales are plotted in Fig. 3.2. A straight line fit of the data between the ^{187}Re/^{188}Os and ^{187}Os/^{188}Os for these shales with good correlation coefficient (r^2= 0.95) confirm that they remained closed with respect to Re and Os since their deposition and hence, retains the age information. The Re-Os isochron provides a depositional age of 541±8 Ma [λ_{187Re}=1.64×10^{-11} yr^{-1}; *Lindner et al.*, 1989] estimated following the approach of *Singh et al.* [1999], so that comparison of both layers of black shales can be done. The y-intercept of the Re-Os isochron of the Lower Tal shales analyzed in this study provides an initial isotopic ratio of 0.90±0.02. Available radiometric ages of the stratigraphy for the lithology near Pc-C (Krol-Tal) boundary has been provided in Fig. 3.3. The age obtained for black shale close to Pc-C boundary in this study are consistent with the ages of 535±11 Ma reported for the shales exposed above this horizon [*Singh et al.*, 1999]. It matches quite well with the reported ages [~542 Ma; *Amthor et al.*, 2003] for Pc-C boundary across the various world-wide exposures [*Amthor et al.*, 2003; *Bowring et al.*, 2003; *Grotzinger et al.*, 1995; *Singh et al.*, 1999]. Rb-Sr age of the black shales [*Sharma et al.*, 1992] of the same layer (Fig. 3.3) is inconsistent with their Re-Os age obtained in this study. It has been shown [*Dickin*, 2005] based on the results of various studies that Rb-Sr systematics fail to provide depositional ages of the sedimentary rocks.

The initial ^{187}Os/^{188}Os ratio obtained in this work (0.90±0.02) is found to be low compared to that reported for the overlying Early Cambrian shale sequence [1.181±0.024; *Singh et al.,* 1999]. The lower initial ^{187}Os/^{188}Os ratio near the Pc-C boundary could arise due to enhanced supply of mantle-like osmium to the seawater. A similar inference was also drawn by *Jiang et al.* [2007], based on the Re-Os chronometer of black shales from the south China. There exits a possibility that the initial Os isotopic compositions obtained in this study could have affected from the leaching of non-hydrogenous osmium during the whole-rock dissolution of the rock for osmium purification using inverse aqua regia procedure [*Selby and Creaser*, 2003]. However, this possibility is less likely as the osmium concentration of these shales (~15 ng/g) are higher by few orders compared to average Os value (50 pg/g) for the continental crust.

The ^{187}Re/^{188}Os of black shales from the inner belt of LH (Mandhali formation) vary from 433 to 939, higher compared to the ranges observed for the black shales from the outer belt, however the ^{187}Os/^{188}Os of these black shales from the Mandhali formations of LH show less variation (4.098-5.027). The ^{187}Re/^{188}Os vs ^{187}Os/^{188}Os plot of these shales show a large scatter without any discernible trend, indicating that assumption of closed system behaviour of Re and Os in these black shales are not valid. The scatter of data (Fig. 3.4) indicates loss of Re and Os from the shales during post-depositional processes. This "open system" behavior of the black shale from the inner belt with respect to Re-Os isotopic systematics precludes their use to derive age information for this sedimentary deposit (Fig. 3.4) and hence, could not provide precise date for these shales. As has been mentined in chapter 2, the black shales used in this study were collected from road cut after removing ~1 m surface exposures to get a fresh and unaltered sample. The "open system" behavior of these black shales with respect to Re-Os systematics indicates that it is difficult to get fresh black shales from surface exposures. Even roving part of the surface exposed section does not help. It is clear that to ensure the closed system behaviour black shale samples from underground mine and/or from drilled core section are essential for dating the sedimentary layer.

3.3.4. Oxic-anoxic conditions at around Pc-C boundary

Earlier studies have suggested an intense anoxic condition in seawater for a few Ma following the Pc-C boundary [*Brasier*, 1995; *Steiner et al.*, 2001; *Jiang et al.*, 2007; *Wille et al.*, 2008]. This high anoxia resulted in mass extinction followed by a large extent of biological diversity, known as "Cambrian explosion". Hence, the anoxicity of the seawater near the Pc-C holds a key role in structuring the evolution of multi-cellular life in the Earth. Despite its global importance, the cause which triggered the state of anoxia at ~540 Ma has been remained unclear. Study of *Jiang et* *al.* [2007], based on geochemical composition of black shales from the South China, suggested an enhanced discharge of hydrothermal fluids to the ocean, which might have affected the biosphere during the Cambrian explosion. This proposition is consistent with the conclusion of few more studies on this regard [*Steiner et al.*, 2001]. More recently, *Wille et al.* [2008], however, based on Mo isotopic studies of black shales deposited near the Pc-C boundary, concluded that the upwelling of sulphidic rich deep water to the surface water caused the anoxia in seawater and the mass extinction, consistent with the suggestion of *Brasier* [1995].

The abundances of Re, Os and other redox-sensitive elements of black shales deposited during [*Present Study*] and after few Ma [*Singh et al.*, 1999] of the Pc-C boundary are compared in this study to infer about the redox state of seawater near the Pc-C boundary. The black shales from the Lower Tal studied in this study lies ~ 3m above the Pc-C boundary [*Sharma et al.*, 1992]. The geochemical and Os isotopic composition of these shales, with Re-Os depositional age of 541±8 Ma, are considered to represent the seawater redox state during Pc-C boundary. Another layer of black shales also exists above the present studied black shale horizon and both the layers are separated by a layer of phosphrite. *Singh et al.* [1999] constrained the depositional ages of these shales to 535±11 Ma. Though ages of both the shales overlaps, the geologically overlying sequence certainly deposited after the shales studied in this study and hence, preserve signatures of deposition after few Ma after the Pc-C boundary. Hence, the black shale sequence studied for Re-Os chronometer by *Singh et al.* [1999] from the Lower Tal represents seawater conditions following few Ma of the Pc-C. Both of these sequences of black shales were from underground mines and provide good isochrones, confirming their close system behavior with respect to Re-Os systematics. The black shales collected close to Pc-C boundary has significantly higher Os/C_{org} (pg/g/wt%) ratios, (645±263) compared to (16±15) those collected from overlying sequence [535 Ma; *Singh et al.*, 1999]. The Os/C_{org} ratio during Pc-C is also found to be significantly higher than that observed for black shales from the Mandhali formations, inner belt of LH representing Neoproterozoic seawater conditions (88±97); however, this observation is not extended to infer about the anoxicity as the black shales from the inner belt of LH are found to be “open” with respect to their Re-Os isotopic systematics subsequent to their deposition. The higher values of the Os/C_{org} of the shales that deposited during the Pc-C could have arisen due to various reasons, which include changes in sedimentation rates, dilution effects due to $CaCO_3$ or quartz, post depositional alterations and changes in redox state in water. Among these possibilities, the anoxicity of the seawater near the Pc-C boundary seem to be the possible cause for higher Os/C_{org} at around the Pc-C. Earlier studies have documented that the seawater was anoxic near the Pc-C boundary [*Wille et al.*, 2008]. This proposition is supported by the redox-sensitive geochemical indices, *e.g.* V/Cr and V/(V+Ni) [*Jones and Manning*, 1994; *Wignall*, 1994; *Rimmer*, 2004] of these black shales. Vandium (V^{+4}) has high affinity to incorporate itself into organic carbon in reducing conditions and hence, enhancing its concentration in sediments deposited in anoxic conditions. Contrary to the redox-sensitive nature of vanadium, Cr in black shales are mostly of detrital nature, as it in often found to be incorporated with clastic sediments where Cr substitute Al in the clays [*Jones and Manning*, 1994]. Owing to difference in their geochemical properties, V/Cr ratio found extensive use to infer about the paleo-oxygenation of seawater. *Dill* [1986] suggested that V/Cr of shales with values in excess of 2 indicates an anoxic condition, whereas a value <1.0 shows an oxic condition [*Wignall*, 1994]. The average V/Cr ratio for the black shales analyzed in this work is 2.6±0.8 during Pc-C. The values of V/Cr (higher than 1.0) of black shales show that the seawater was highly anoxic during Pc-C, a result consistent with that concluded from the Re and Os ratios of the shales. These inferences also draw support from the average ratio of V/(V+Ni) for the black shales. It has been suggested, based on observation of large datasets of V and Ni in marine sedimentary deposits [*Wignall*, 1994], that a value greater than 0.84 for V/(V+Ni) indicates anoxic depositional basin of the sediments. The average V/(V+Ni) for the shales during in this study are found to be ~0.92, indicating their anoxic conditions. In summary, the elemental compositions of the black shales from the LH are deposited in anoxic conditions with the shales during Pc-C period are indicating an intense anoxic depositional environment.

A useful approach to infer about the cause for the anoxia of seawater during the Pc-C could be to compare the initial ^{187}Os/^{188}Os ratios obtained from the Re-Os isochrones. The initial ^{187}Os/^{188}Os, as discussed in the previous section, is expected to provide the seawater osmium isotopic composition during their deposition. The study of *Singh et al.* [1999] inferred an initial ^{187}Os/^{188}Os of 1.181±0.024 after a few Ma of the Pc-C (535±11 Ma). The present study found relative lower value (0.90±0.02) of ^{187}Os/^{188}Os for the seawater at the Pc-C (541±8 Ma). The lower osmium isotopic composition at the Pc-C indicates enriched supply from its unradiogenic sources, *e.g.* mantle and cosmic dusts. This observation of the lower seawater ^{187}Os/^{188}Os coupled with the results from few earlier studies [*Mao et al.*, 2002; *Li et al.*, 2003; *Jiang et al.*, 2007] seem to indicate an enhanced supply of the hydrothermal venting and alteration of seafloor basalt to the seawater near the Pc-C boundary. This proposition is also evident from the temporal variation in the ^{187}Re/^{188}Os values of the shales from the three sequences. The ^{187}Re/^{188}Os, depending on compatibility of Re and Os during melting, has distinctly different values in the mantle and the crustal rocks. The ^{187}Re/^{188}Os ratio for the mantle (0.4) is few orders less compared to the crustal materials, *e.g.* for upper continental crust ^{187}Re/^{188}Os ~50 [*Yang et al.*, 2009]. The ^{187}Re/^{188}Os for the black shales during (51 to 137) and after few Ma (74 to 522) of the Pc-C is found to be different with fairly lower range during the Pc-C boundary. The lower ^{87}Re/^{188}Os of the shales during Pc-C hints relatively enhanced contribution from the mantle (or, cosmic dust), consistent with the inferences from the initial ^{187}Os/^{188}Os results. Therefore, based on the Re-Os isotopic systematics of black shales from three succession, this study infers that the seawater at Pc-C was highly anoxic compared to a few Ma post-Pc-C and the cause for this anoxia seem to be resulted from enhanced supply from the hydrothermal venting to the seawater during that time.

3.4. ARAVALLI SUPERGROUP

Aravalli Supergroup represents a sedimentary deposition of Proterozoic period and hence archive the information related to ocean chemistry, atmospheric evolution etc of that time period. As part of this thesis, black shales were collected from the Jhamarkotra Formation of the Lower Aravalli to date them using Re-Os systematics. These samples were collected from fresh road cut near Udaipur after removing their surface exposures to get fresh samples of black shales.

3.4.1. Geochemistry of Lower Aravalli Shales

The composition of the black shales from the Jhamarkotra formation, Lower Aravalli analyzed in this work is listed in Table 3-6. The average organic carbon, C_{org} concentration for these shales is 6.1±0.3%, higher compared to the minimum C_{org} values (1%) defined for black shales [*Arthur and Sageman*, 1994]. The mean value of the major elements of the Lower Aravalli shales show a depleted value compared to the average for the post-Archean Australian shales [PAAS; *Taylor and McLennan*, 1985]. Similar to these elements, Ba, Mn, Sr, Zn concentrations also are lower compared to the average shale (Table 3-6). In contrast, the average abundances of Cr, Co, Cu, Ni, V, U, Mo for these shales are higher or comparable to that of PAAS (Table 3-6). These Aravalli shales are observed to have negligible inorganic carbonate content. The significant difference in the abundances of various chemical parameters in the black shales from the Lower Aravalli compared to average post-Archean shales could have arisen due to significantly different depositional environment of the shales and/or post-depositional alterations of the shales. Post-depositional alteration, such as due to weathering process, is expected to increase the Al content of the black shales. However, the average Al content of these shales is found to be low compared to the PAAS values. Based on low Al content of these shales, the possibility of chemical alteration of shales can not be ruled out as shales can have relatively low Al content since their deposition. This proposition seems to be valid as the preliminary results on the silica concentration of these shales carried out using XRF are found to be high (~80%).

Table 3-6: Geochemistry of black shales from the Jhamarkotra formation, Lower Aravalli, India.

SampleID	Al	Ca	Fe	Mg	Ti	C_{inorg}	C_{org}	TN
	wt%							
LA06-33	2.78	0.06	0.65	0.32	0.25	0.01	6.08	0.06
LA06-34	2.80	0.06	0.23	0.40	0.15	0.01	5.96	0.05
LA06-35	3.61	0.07	0.38	0.50	0.23	0.01	5.74	0.05
LA06-36	3.74	0.05	0.15	0.50	0.22	0.01	6.44	0.06
LA06-37	3.67	0.04	0.78	0.50	0.21	0.01	6.45	0.06
LA06-38	3.93	0.06	0.29	0.57	0.22	0.01	6.13	0.06
Average	3.42±0.50	0.06±0.01	0.41±0.25	0.46±0.09	0.21±0.03	0.01±0.00	6.13±0.28	0.06±0.01
PAAS	10.01*	0.93	5.05	1.33	0.60	-	-	-

**Mean Al value for Black shales: 7.00% [Vine and Tourtelot, 1970]*

PAAS stands for average chemical composition of Post-Archean Australian shales [Taylor and McLennan, 1985].

SampleID	Ba	Cr	Mn	Sr	Co	Cu	Ni	Zn	V	U	Mo
	μg/g										
LA06-33	241	114	4	81	26	89	55	63	801	11	21
LA06-34	306	156	b.d.	77	20	38	30	64	940	12	12
LA06-35	447	142	1	76	25	38	25	64	1223	16	17
LA06-36	456	184	9	73	21	68	34	58	1335	14	5
LA06-37	395	162	11	122	22	107	66	66	1287	14	35
LA06-38	426	212	7	82	25	93	41	70	1368	17	23
Average	378±86	162±34	7±4	85±18	23±3	72±29	42±15	64±4	1159±233	14±2	19±10
PAAS	650	110	852	200	23	50	55	85	150	3.1	1

3.4.2. Re, Os and $^{187}Os/^{188}Os$ of Lower Aravalli Shales

Table 3-7: Re, Os concentrations and $^{187}Os/^{188}Os$ values of black shales from the Jhamarkotra formation, Lower Aravalli.

Sample ID	[Re]	[Os]	$^{187}Os/^{188}Os$		$^{187}Re/^{188}Os$		Model Age, Ga
	pg/g			±1σ		±1σ	
LA06-30	863	537	3.456	0.010	11.1	0.06	15.8
LA06-31	127	287	3.962	0.017	3.2	0.02	47.5
LA06-33	2347	1203	7.407	0.048	18.3	0.15	20.2
LA06-34	506	2602	9.480	0.046	2.1	0.01	102.7
LA06-36	163	1927	7.612	0.028	0.8	0.01	140.4
LA06-37	175	3057	8.502	0.013	0.6	0.00	165.1
LA06-38	2426	2240	9.847	0.036	11.8	0.08	36.1
LA10-1	234	189	8.607	0.015	12.5	0.07	31.1
LA10-2	266	295	9.992	0.024	9.9	0.06	41.5
LA10-3	232	325	10.513	0.014	8.1	0.04	49.8
LA10-4	384	1025	9.755	0.066	4.1	0.04	73.1
LA10-5	338	2124	8.969	0.019	1.7	0.01	111.4
LA10-6	497	4317	6.947	0.005	1.0	0.01	121.5
LA10-8	42222	1258	7.256	0.008	311.8	1.59	1.4
LA10-9	4117	4711	7.431	0.004	8.2	0.04	38.3
LA10-10	632	1731	8.881	0.004	3.8	0.02	72.4

The concentrations of Re and Os and $^{187}Os/^{188}Os$ of the black shales from the Lower Aravalli are given in Table 3-7. The Os concentrations for these shales (n=16) vary significantly, ranging from 189 to 4711 pg/g, with an average value of 1739±1402 pg/g (Fig. 3.5). These Os cocentrations for the Aravalli shales overlaps with that reported for shales from various other geological formations [*Singh et al.*, 1999; *Hannah et al.*, 2004; *Kendall et al.*, 2004; *Kato et al.*, 2009; *Yang et al.*, 2009]. Re concentrations of black shales of the Jhamarkotra display a range of 127 to 42222 pg/g, with many of them having lower Re concentration. These concentrations are lower compared to the Re concentration of black shales from the Vindhyan and the Lesser Himalaya analayzed in this study having similar C_{org} content. Many of these shales have Re concentrations lower than their Os concentrations (Table 3-7) not expected for average black shales. Among the samples analyzed, one sample has high concentration of Re (42 ng/g) compared to others. The average Re/Os ratio for the Lower Aravalli shales is 2.5, which is significantly lower compared to corresponding

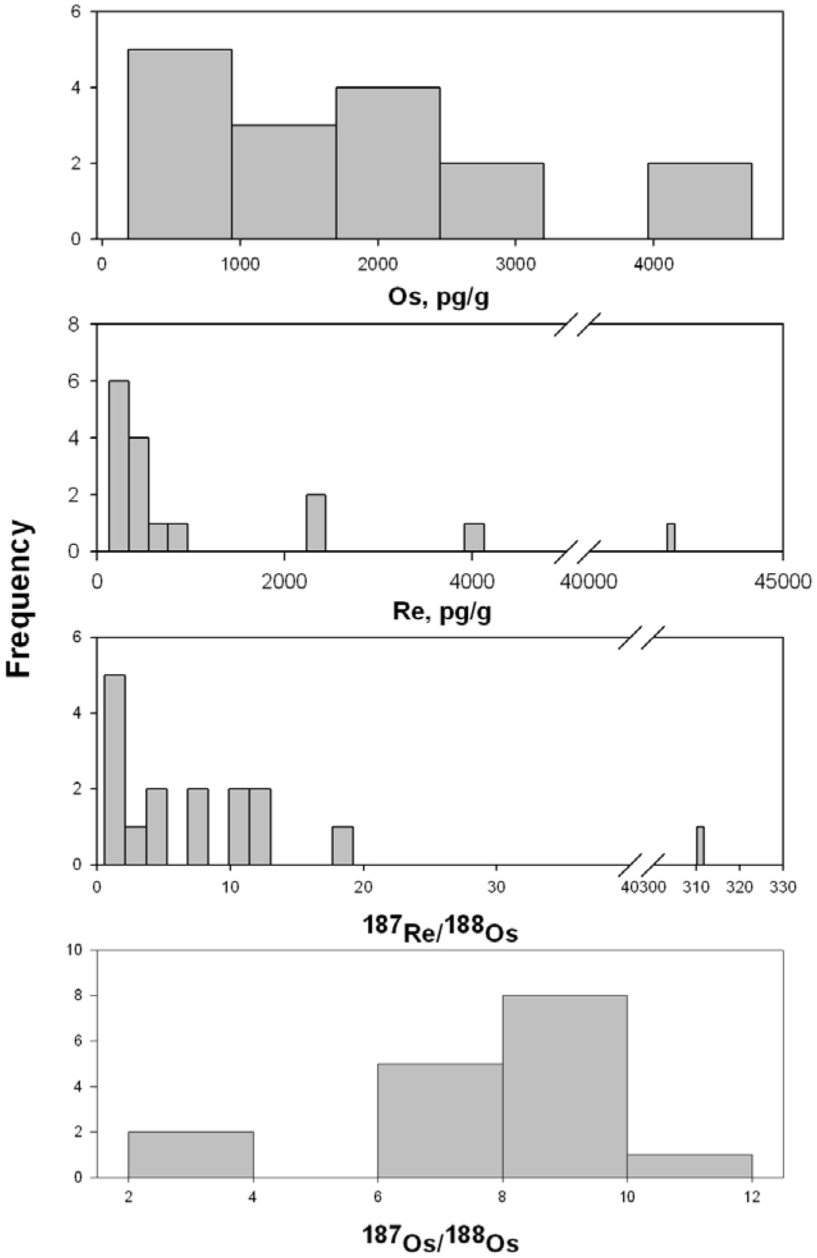

Figure 3.5: *Frequency distribution of Re-Os elemental and isotopic compositions of black shales from the Lower Aravalli.*

average value (~160) for organic-rich sediments [*Peucker-Ehrenbrink and Jahn*, 2001]. The lower Re content in these shales with similar ^{188}Os content as that reported for black shales of 2000 Ma age [*Yang et al*., 2009] indicates loss of Re from these shales subsequent to their deposition. The loss of Re from the shales could have arisen from the chemical weathering of these black shales, which are easily weatherable due to presence of labile organic carbons. The low Re in these shales also brings out the higher mobility of Re compared to Os during weathering of black shales, consistent with earlier reported conclusions [*Jaffe et al.*, 2002; *Pierson-Wickmann et al.*, 2002].

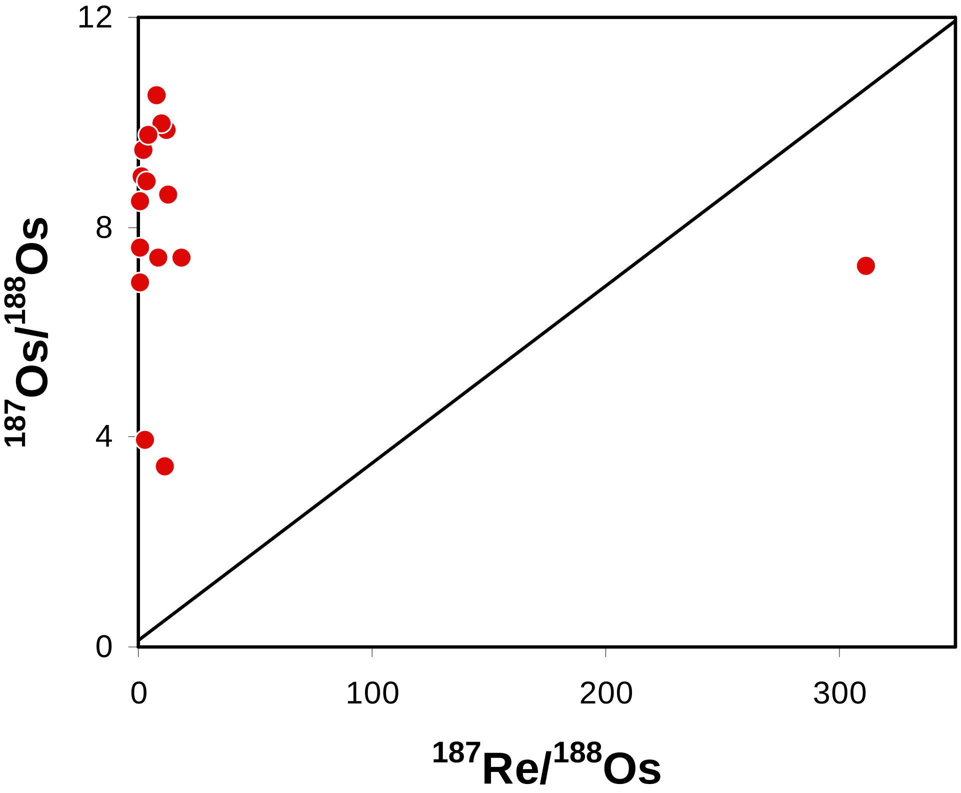

Figure 3.6: *$^{187}Re/^{188}Os$-$^{187}Os/^{188}Os$ plot of the Aravalli shales. A reference line of 2000 Ma with an initial value of 0.13 is also given. All the data (except one point) fall far left of the line with a lower $^{187}Re/^{188}Os$ ratio. If these shales are 2000 Ma old as reported for Jhamarkotra formation, then this indicates significant loss of Re from the shales.*

Efforts were made in this study to estimate the loss of Re from black shales of the Lower Aravalli since their deposition due to weathering. For this estimation, it was assumed that the depositional age for these shales is 2000 Ma similar to that suggested for the Jhamarkotra Formation [*Sarangi et al.*, 2006] and that themarine

$^{187}Os/^{188}Os$ at the time of deposition of these shale could be ~0.13 as estimated by *Hannah et al.* [2008] using shales of similar age. Based on this initial $^{187}Os/^{188}Os$ and the measured $^{187}Os/^{188}Os$ and $^{187}Re/^{188}Os$ in the Lower Aravalli black shales, model ages of their deposition were estimated (Table 3-7). The estimated model ages of these shales are impossibly high, except for one sample which has a model age of 1.4 Ga. Extremely high model ages of these shales are due to their lower Re content. This observation is also evident in $^{187}Re/^{188}Os$ vs. $^{187}Os/^{188}Os$ plot (Fig. 3.6), where all but one sample fall far left from the reference line of 2000 Ma with an initial value of 0.13 and cluster along y-axis. This also indicates loss of Re from them. Lower $^{187}Re/^{187}Os$ of these shales could also result from gain of Os after their deposition, however, this proposition is unlikely considering the measured concentration of these black shales. This inference is evident from the comparable Os concentration in these shales with that of similar ages from other locations [*Yang et al.*, 2009] and also with black shales of different ages [*Singh et al.*, 1999; *Hannah et al.*, 2004; *Kendall et al.*, 2004; *Kato et al.*, 2009; *Yang et al.*, 2009] as discussed earlier. One of the samples (LA10-8) does have higher Re content (Fig. 3.8) with lower model age indicating that other samples are less preserved compared to LA10-8 and have lost Re during weathering following their exposure.

It is evident from the above discussion that Re has been lost preferentially over Os from the black shales of Lower Aravalli. The loss of Re from these shales during weathering processes has been estimated assuming their deposition age ~2000 Ma and initial $^{187}Os/^{188}Os$ ~0.13 as discussed earlier and using the measured $^{187}Os/^{188}Os$ of these shales. Further it was assumed that no osmium was lost from the shales since their deposition. As Re and Os has strong association with organic matter, its quiet unlikely that only Re, but not Os will be lost from the black shales; however, as the Os measured values are comparable with that reported for shales from other geological formations, the loss of Os from these shales is expected to be relatively low. Therefore, as there can be loss of Os during post-depositional events, the present estimates of loss of Re from the shales are lower limit only. To obtain an age of 2000 Ma for the shales with measured Os and $^{187}Os/^{188}Os$ values, average Re concentration of ~42 ng/g is required (Table 3-8). Comparing these required Re values with the measured Re values of the shales, it was estimated that more than 95% of Re is lost from most of the shales. These estimates of Re loss in black shales possibly due to weathering are comparable with that reported based on weathering profile studies [*Jaffe et al.*, 2002; *Pierson-Wickmann et al.*, 2002]. The comparable Os composition with that of the Precambrian shales coupled with significant loss in Re from the Lower Aravalli shales indicates higher mobility of Re compared to Os during weathering, a result contradictory to the observations of *Peucker-Ehrenbrink and Hannigan* [2000], but consistent with the results of few earlier studies [*Jaffe et al.*, 2002; *Pierson-Wickmann et al.*, 2002].

Table 3-8: Estimation of loss of Re for the shales considering their age to be 2000 Ma and assuming insignificant loss of Os.

Sample ID	Measured [Re], pg/g	Required ^{187}Re/^{188}Os	Required [Re], pg/g	Loss of Re (%)
LA06-30	863	99	7663	88.7
LA06-31	127	114	4507	97.2
LA06-33	2347	216	27654	91.5
LA06-34	506	277	67418	99.2
LA06-36	163	222	44871	99.6
LA06-37	175	248	75232	99.8
LA06-38	2426	288	59103	95.9
LA10-1	234	251	4687	95.0
LA10-2	266	292	7814	96.6
LA10-3	232	308	8809	97.4
LA10-4	384	285	26943	98.6
LA10-5	338	262	53624	99.4
LA10-6	497	202	95811	99.5
LA10-8	42222	211	28585	-47.7
LA10-9	4117	216	108362	96.2
LA10-10	632	259	43514	98.5

Re-Os study conducted on the black shales from the inner Lesser Himalaya and the Lower Aravalli indicate their open system behavior for Re and Os. In both cases, samples were collected from a fresh road cut after removing ~1 m of their surface exposures in order to get fresh and unweathered samples. In hand specimen, though they were looking fresh, they have not remained closed for Re and Os. Significant amount of Re in case of the Lower Aravalli black shales and both Re and Os from inner Lesser Himalayan black shales have been lost during weathering subsequent to their exposure. The samples collected from the exposed section did not provide the isochron on the other hand the samples collected from underground mines such as from the Vindhyan and the outer Lesser Himalaya has provided good isochrones. Therefore, it is essential to collect samples either from underground mines or after core drilling to get fresh black shale samples suitable for Re-Os dating.

3.5. PAST SEAWATER ^{187}Os/^{188}Os: EVOLUTION TREND OF ATMOSPHERIC OXYGEN LEVEL

The present day seawater ^{187}Os/^{188}Os value (~1.06) is dominated by its supply from radiogenic osmium resulted from the oxidative weathering of the continents [*Peucker-Ehrenbrink and Ravizza*, 2000; *McDaniel et al.*, 2004]. Owing to the oxidative weathering nature of osmium, its relative supply to the seawater must have varied over time depending on the atmospheric oxygen concentration resulting in the variation in the seawater osmium isotopic composition over the past. It is well established that atmospheric oxygen concentration has varied with time [*Canfield et al.*, 2000; *Farquhar et al.*, 2000; *Farquhar and Wing*, 2003; *Kah et al.*, 2004; *Canfield*, 2005; *Campbell and Allen, 2008; Frei et al.,* 2009]. Atmospheric oxygen has increased from its zero level in the Archean to present atmospheric level. Absence of oxygen from atmosphere would inhibit the continental weathering of Os and hence its supply from continent to ocean resulting in non-radiogenic marine Os isotope composition. Temporal increase in atmospheric oxygen level would increase the continental supply of radiogenic Os to the ocean causing an increase in marine Os isotope composition. Therefore, the temporal variations of seawater ^{187}Os/^{188}Os seem to have the potential to track the atmospheric oxygen evolution trend. To evaluate this proposition, past seawater ^{187}Os/^{188}Os values inferred from the initial isotopic ratios obtained from Re-Os isochrones and expected to provide seawater composition at the

Table 3-9: Compilation of initial $^{187}Os/^{188}Os$ from earlier studies inferred from Re-Os isochrones of various Precambrian black shales.

Sl. No.	Age of Black shale (Ma)	Initial $^{187}Os/^{188}Os$	Reference
1	535 ± 11	0.8 ± 0.04	Jiang et al., 2007
2	535 ± 11	1.181 ± 0.024	Singh et al.,1999
3	**541 ± 8**	**0.90 ± 0.02**	**This Study**
4	541 ± 16	0.78 ± 0.19	Mao et al., 2002
5	542 ± 11	0.84 ± 0.12	Li et al., 2003
6	608 ± 5	0.62 ± 0.03	Kendall et al., 2004
7	623 ± 18	0.78 ± 0.1	Schaefer and Burgess, 2002
8	640.7 ± 4.7	1 ± 0.05	Kendall et al., 2009b
9	643 ± 2.4	0.95 ± 0.01	Kendall et al., 2006
10	657.2 ± 5.4	0.82 ± 0.03	Kendall et al., 2006
11	1100 ± 77	0.33 ± 0.3	Azmy et al., 2008
12	1107 ± 12	0.28 ± 0.13	Rooney et al., 2010
13	**1196 ± 41**	**0.74 ± 0.27**	**This study**
14	1361 ± 21	0.29 ± 0.18	Kendall et al., 2009c
15	2004 ± 9	0.133 ± 0.02	Hannah et al., 2008
16	2316 ± 7	0.1121 ± 0.0012	Hannah et al., 2004
17	2501.1 ± 8.2	0.04 ± 0.06	Anbar et al., 2007
18	2550	0.1296	Wille et al., 2007
19	2695 ± 14	0.15 ± 0.16	Yang et al.,2009
20	2763 ± 16	0.115 ± 0.011	Kato et al., 2009

time of deposition of the black shales are compiled from earlier reported studies on Re-Os age of Precambrian black shales (Table 3-9) and obtained from this study. Based on these data, marine $^{187}Os/^{188}Os$ ratio evolution with time has been reconstructed between 2.6 and 0.54 Ga (Fig. 3.7). Envelop in Fig. 3.7 Show the uncertainties associated with the estimated marine Os isotope composition. By 0.54 Ga atmospheric oxygen has attained a value close to present atmospheric level (PAL) and hence marine Os isotope composition has not been extended beyond Pc-C boundary. Marine $^{187}Os/^{188}Os$ during Paleoproterozoic, as expected, is non-radiogenic (Fig. 3.7). In absence of oxygen, supply of radiogenic continental Os was zero resulting in non-radiogenic marine Os isotope composition. With the increase in atmospheric level, marine $^{187}Os/^{188}Os$ started growing steadily upto the Pc-C boundary (Fig. 3.7). The rise in seawater $^{187}Os/^{188}Os$ indicates enhanced supply of radiogenic osmium from continents due to increase in the intensity of oxidative

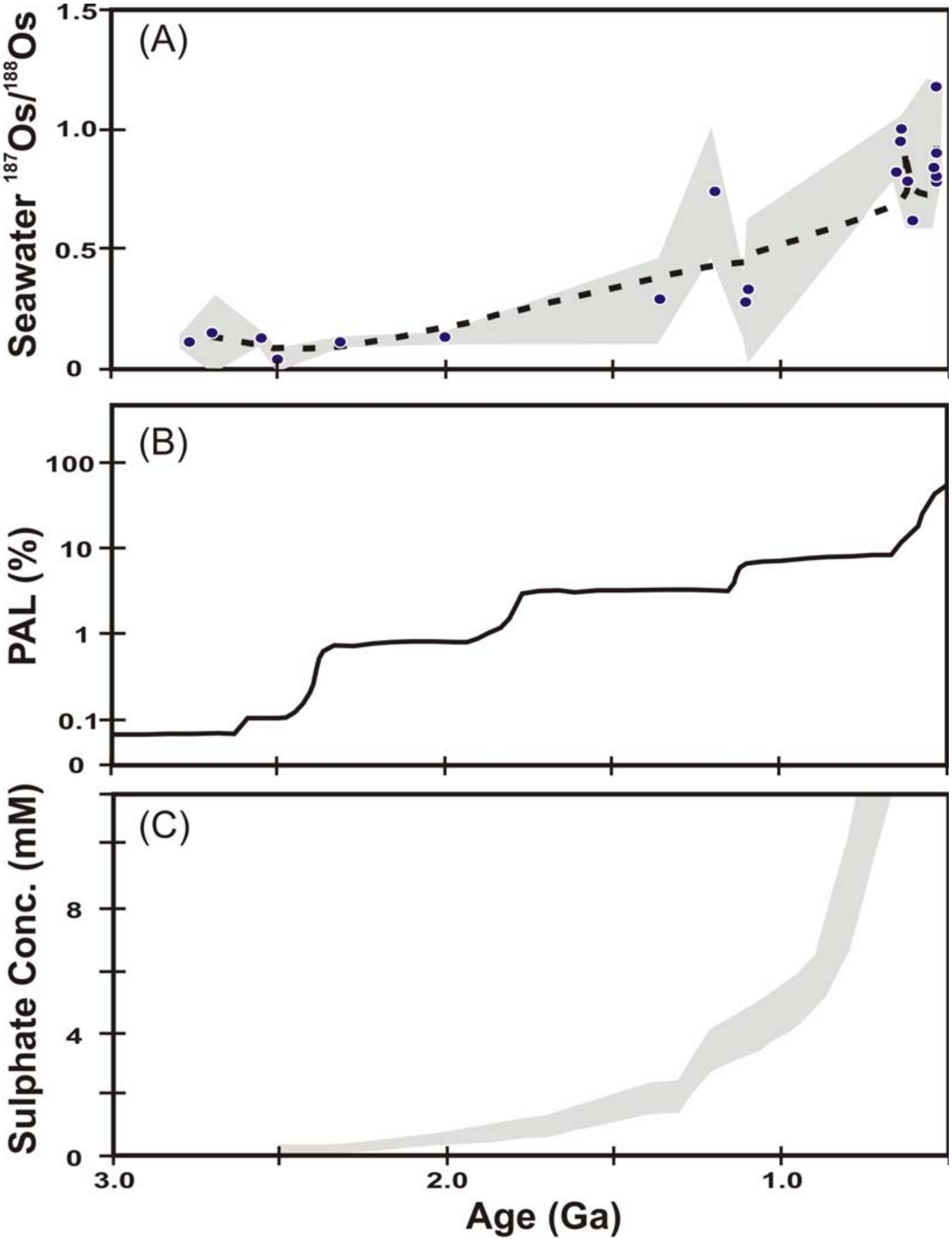

Figure 3.7: *Temporal variation in seawater ^{187}Os/^{188}Os, compiled from reported Re-Os isochrones along with those of the present study [panel A; Data source: c.f. Table 3-8], show a good correlation with the atmospheric Oxygen evolution trend [panel B; Campbell and Allen, 2008] and the seawater sulphate concentration levels [panel C; Kah et al., 2004]. This resemblance hints the potential of seawater ^{187}Os/^{188}Os as a proxy to track the atmospheric oxygen evolution. The dotted line in panel A represents overall (3-point moving average) trend of seawater ^{187}Os/^{188}Os and the shaded portion shows the uncertainty associated with the data.*

weathering *i.e.* rise in atmospheric oxygen concentrations. At an oxygen concentration more than 10^{-5} times of present atmospheric level (PAL), the oxidative weathering in the continents can trigger [*Farquhar and Wing*, 2003] and hence, the rise of $^{187}Os/^{188}Os$ indicates an atmospheric oxygen level more than 10^{-5} of PAL. This trend of $^{187}Os/^{188}Os$ as a proxy for atmospheric oxygen evolution suggests that the rise of oxygen was not straight-forward and monotonic, particularly prior to 2.4 Ga (Great Oxidation Event: GOE) event. This trend finds promising correlation with available records of atmospheric Oxygen evolution trend based on the other proxies and confirming the potential of seawater $^{187}Os/^{188}Os$ as a proxy for evolution of oxygen (Fig. 3.7).

The application of osmium isotopes as a proxy to track the atmospheric oxygen level can be challenged as Os isotope composition of seawater could increase with time if its flux from non-radiogenic sources, hydrothermal and cosmic dust decreases. There is paucity of information on the temporal variations in Os fluxes from the hydrothermal and comic dust, however, model calculations to balance the seawater $^{87}Sr/^{86}Sr$ indicates that the hydrothermal flux of Sr remained fairly constant for last 3.0 Ga [*Godderis and Veizer*, 2000] which could be true for Os too as hydrothermal flux of any element is governed by formation of new crust in the ocean. For last ~100 Ma, the cosmic dust flux remained fairly constant, but it can have possibly higher flux during Precambrian periods [*Anderson*, 1993]. If so, then it would lead to lower the seawater $^{187}Os/^{188}Os$. Information of this kind will be useful to extend the application of osmium isotopes as a proxy for oxygen rise, particularly prior to 2.4 Ga. Another limitation for the use of $^{187}Os/^{188}Os$ to track oxygen evolution can arise from possibly low residence time of Os during Proterozoic [*Kendall et al*., 2009a]. In contemporary timescale, the reducing sediments from sub-oxic ocean basin, such as from the Japan Sea [*Dalai et al*., 2005], the Santa Barbara Basin [*Williams and Turekian*, 2004] are found to preserve the global seawater osmium signature as that of oxic sediments and hence, the issue of low residence time of osmium should not affect the inferences that are drawn from black shales younger than 2.4 Ga, where the seawater was not completely anoxic. The approach of inferring paleo-seawater ^{187}Os/^{188}Os from the y-intercept of Re-Os isochrones can be critical if significant fraction of osmium leached during Os purification chemistry is detrital, which in turn can challenge the application of osmium as a proxy for tracking atmospheric oxygen level. Further, a lower residence time of osmium in anoxic condition may not have significant impact on tracking oxygen trend, as anoxic seawater are expected to receive osmium from only its non-radiogenic sources. However, the success of osmium isotopes as a suitable proxy can be advanced with more knowledge on these less explored issues.

Table 3-10: Sr, Nd and their isotope composition in silicate fraction of black shales from the Lesser Himalaya, Upper Vindhyan and the Lower Aravalli.

	Sample ID	[Sr], μg/g	^{87}Sr/^{86}Sr	[Nd] , μg/g	ε_{Nd}
LH (Outer)	**UK98-2**	45	0.78608	15.8	-18.0
	UK98-3	22	0.82208	4.9	-16.7
	UK98-17	44	0.76752	24.6	-15.8
	UK98-18	50	0.76385	27.7	-16.0
	UK99-4	17	0.97918	*n.a.*	*n.a.*
	UK99-5	14	0.98523	18.8	-17.0
	UK99-6	21	0.92646	7.2	-17.5
	UK99-7	76	0.76903	*n.a.*	*n.a.*
Vindhyan	**V99-1**	38	0.90595	24.5	-19.7
	V99-2	40	0.85460	31.6	-19.2
	V99-3	31	0.95471	28.0	-18.0
	V99-4	35	0.92022	22.4	-19.5
	V99-10	47	0.87779	27.5	-19.8
Aravalli	**LA06-30**	160	0.78744	23.3	-26.6
	LA06-33	108	0.79480	16.2	-25.4
	LA06-35	34	0.90603	22.1	-26.8
	LA06-37	116	0.77410	22.4	-25.3
	LA06-38	45	0.86659	17.8	-25.3

Average Values

LH	36±22	0.850±097	16.5±9.1	-16.9±0.9
Upper Vindhyan	38±6	0.903±039	26.8±3.5	-19.3±0.7
Lower Aravalli	93±53	0.826±057	20.4±3.1	-25.9±0.7

3.5. Sr-Nd ISOTOPES OF BLACK SHALES

A large fraction of matrix of black shales is clastic material derived from continental weathering. These clastic materials preserve in them the source information from where they are derived. Provenance of these shales could vary in response to varying tectonic activity and climate. Change in the provenance to sedimentary basins in past holds clue to understand the erosion processes, their variations and related causes. In light of this, efforts are made in this study to identify the provenance of detrital material of black shales of the Lower Aravalli, Upper Vindhyan and the Lesser Himalaya. Towards this, Sr and Nd isotopic compositions of silicate fractions of black shales are investigated. Sr and Nd isotopes of sediments found extensive application as a proxy of their provenances [*Tripathy et al*., 2010a and *references therein*]. The Sr and Nd isotopes in silicate fraction of the black shales analyzed in this study are given in Table 3-10. The $^{87}Sr/^{86}Sr$ ratios of black shales from the Lesser Himalaya, Upper Vindhyan and the Aravalli show wide ranges of 0.764-0.985, 0.855-0.955, and 0.774-0.906 respectively and overlap with each other. These ratios do not show promising trends with their corresponding ages [Fig. 3.8;

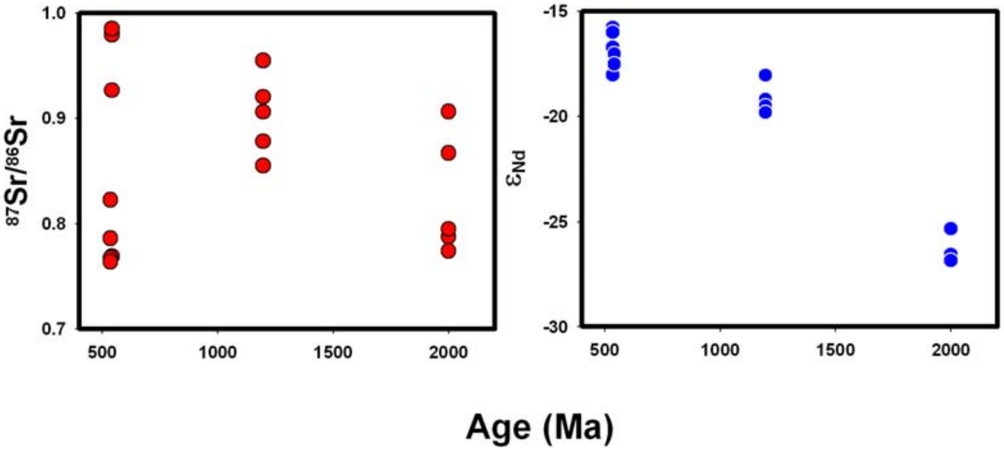

Figure 3.8: *Plot of $^{87}Sr/^{86}Sr$ and ε_{Nd} of the black shales from the Lesser Himalaya, Upper Vindhyan and the Lower Aravalli against their depositional ages. ε_{Nd} show an increasing trend with their corresponding depositional ages; indicating clastic material of older sedimentary rocks are sourced from less evolved continental crust having less radiogenic Nd. The $^{87}Sr/^{86}Sr$ of the shales shows no promising trend with their depositional ages.*

Sarangi et al., 2006; *Singh et al.*, 1999, *Present study*]. In contrast to Sr isotopes, ε_{Nd} values of the black shales show an increasing trend with their depositional ages (Fig. 3-8).

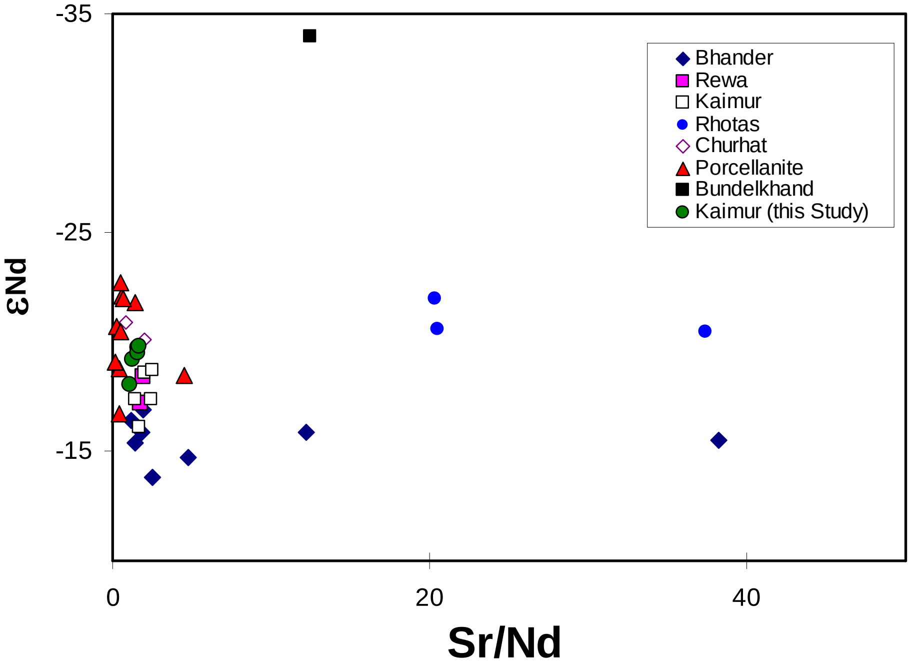

Figure 3.9: *Mixing plot of Sr/Nd-ε_{Nd} of the Bijaigarh shales along with the data of few possible sources of these shales and other group of the Vindhyan Supergroup reported by Chakrabarti et al. [2007].*

The average ^{87}Sr/^{86}Sr and ε_{Nd} values for the black shales from the Lower Aravalli are 0.826±0.057 and -25.9±0.7 respectively (Table 3-10). The possible sources for the sediments deposited in the Jhamarkotra formation are Mewar gneiss and/or weathered products from the Delwara formations. There has been paucity of information on the Sr isotopic composition of possible provenances of the Aravalli shales, limited data available for Mewar gneiss indicates average ^{87}Sr/^{86}Sr ratio as low as ~0.722 [*Gopalan et al.*, 1990] compared to the average ^{87}Sr/^{86}Sr ratios of black shales of the Lower Aravalli (0.826). In contrast to ^{87}Sr/^{86}Sr, the ε_{Nd} of these black shales are found to be bracketed by the average ε_{Nd} values reported for the biotite gneisses and the amphibolites of the Aravalli basement [-21±14; *Gopalan et al.*, 1990] and the basal mafic rocks [-19±7; *Ahmad et al.*, 2008]. The comparison of

Nd isotopic compositions of these geological units with that of the shales (-25.9) indicates the basal mafic rocks of the Aravalli Supergroup as the dominant provenance for the Jhamarkotra formation. However, to better source identification more data on the $^{87}Sr/^{86}Sr$ and ε_{Nd} of the possible sources are required.

The average $^{87}Sr/^{86}Sr$ and ε_{Nd} values for the Bijaigarh shales from the Upper Vindhyan are 0.903±0.039 and -19.3±0.7 respectively (Table 3-10). The average ε_{Nd} values obtained in this study for the shales from the Kaimur group are consistent with earlier reported values for the Kaimur sandstones [-17.6±1.0; *Chakrabarti et al*., 2007], but significantly radiogenic in Nd compared to that reported for the Rohtas sub-group [-21.0±0.8; *Chakrabarti et al*., 2007]. This confirms that the sources of these subgroups are significantly different, despite the Kaimur group overlies on the Rohtas sub-group. To infer about the sources of the sediments of the Kaimur group, a mixing plot of ε_{Nd} and Sr/Nd is plotted along with its few possible sources (Fig. 3.9). The possible sources for the sedimentary deposits of the Kaimur group could be Bundelkhand granites, Bijawar Group, Mahakoshal Group and Chhotanagapur granite gneiss [*Paikaray et al*., 2008; *Mishra and Sen*, 2010]. Fig. 3.9 shows that the single data available for the Bundelkhand granites falls far away from the Kaimur shales, questioning its possibility as a dominant source for the Kaimur sediments. However, this proposition can only be confirmed through larger dataset of both $^{87}Sr/^{86}Sr$ and ε_{Nd} of these granites. Based on the paleocurrent direction and geochemistry of sili-clastic rocks of the Kaimur group, *Mishra and Sen* [2010] suggested the Chhotanagapur granite gneiss as the major source for these sedimentary rocks. However, the proposition of the Chhotanagapur granite gneiss as provenance for the sediments of the Kaimur deposit can not be evaluated in this study, owing to lack of Sr, Nd elemental and isotopic data for these geological units.

In this study, attempts were also made to infer about the provenance of the Lesser Himalayan sediments preserved in the Lower Tal formation. *Ahmad et al.* [2000] recognized two distinct fields for Sr-Nd isotopic composition of sediments from the Higher Himalaya and the Outer LH and the Inner LH (Fig. 3.10). These authors found remarkable change in Sr and Nd isotopic composition in the sedimentary deposits of the Higher and Lesser Himalaya, as a consequence of tectonic activities at ~500 Ma. The ε_{Nd} ratios of sedimentary records of the inner LH are found to have less radiogenic composition (ε_{Nd} ~-25) with large spread in $^{87}Sr/^{86}Sr$, suggesting their Late Archean, or an earliest Proterozoic sources [*Ahmad et al.*, 2000; *Richards et al*., 2005]. These isotopic compositions are distinctly different compared to that from the HH and the outer LH (Fig. 3.10). The Nd isotopic ratios of HH and the outer LH sediments is highly radiogenic (ε_{Nd} ~-15), indicating their Archean (Indian Cratons) sources. The Sr-Nd isotopic compositions of most of the shales from the Lower Tal formation fall in the field of HH and the outer LH sediments, suggesting their similar source. These observations indicate that the detritus sediments of the black shales of the Lower Tal are derived from a Archean source, such as the Indian Cratons.

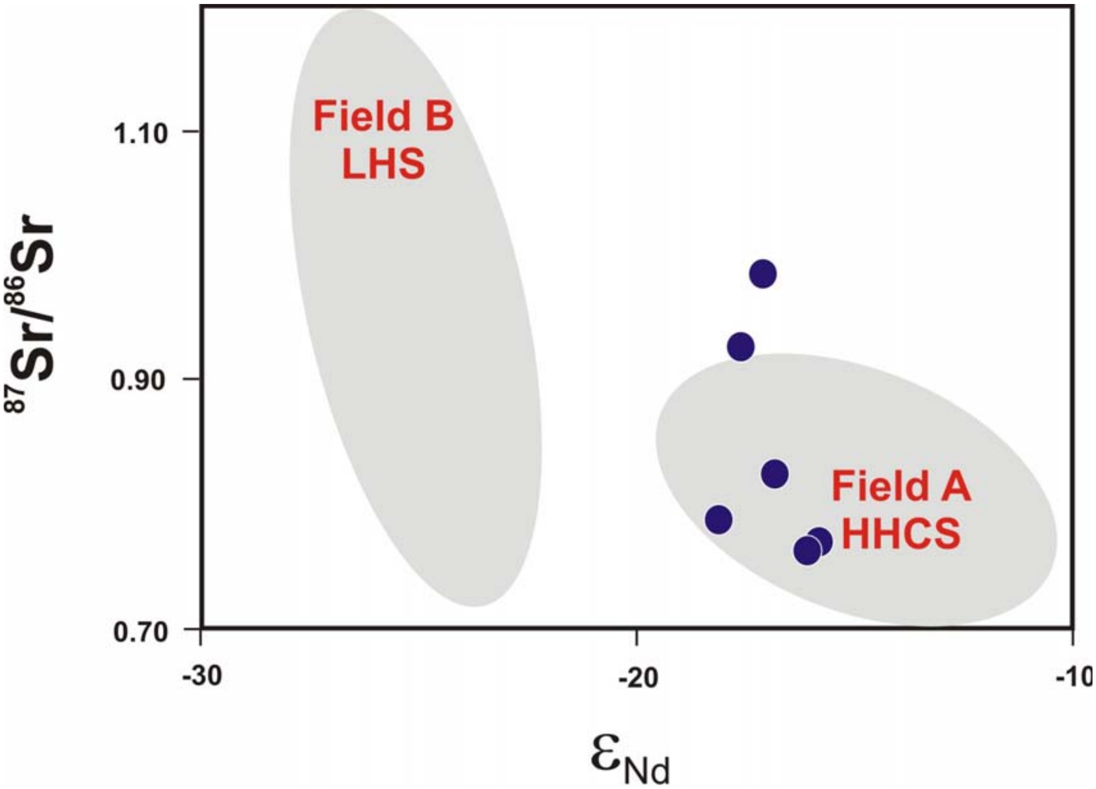

Figure 3.10: *Mixing plot of Sr-Nd isotopes of the black shales (blue circles) from the Lower Tal formation, Lesser Himalaya. The field A and field B is the range reported by Ahmad et al. [2000] for the HH+Outer LH and the Inner LH sediments respectively.*

CHAPTER 4

Chemical and Sr-Nd isotopic composition of the Bay of Bengal Sediments: Impact of Climate on Erosion

4.1. INTRODUCTION

The Bay of Bengal (BoB) receives sediments from various sources such as the Himalaya, Trans-Himalayan plutonic belt (TPB; Mishmi Hills), Indo-Burman Ranges and the Peninsular India through the major rivers, the Brahmaputra, Ganga, Irrawaddy, Salween, Godavari, Mahanadi and the Krishna. These river basins receive rainfall either during the southwest (summer), the northeast (winter) monsoons or during both. There are evidences to show that the intensity of these monsoons varied over millennial timescale [*Duplessy*, 1982; *Prell and Kutzbach*, 1987; *Sarkar et al.*, 1990; *Tiwari et al.*, 2005; *Herzschuh*, 2006]. These variations in turn have the potential to influence the erosion pattern over the source regions and the sediment delivery to the BoB. Therefore, the variations in the sources of sediments deposited in the BoB hold clues to changes in the monsoon intensity.

In earlier studies, temporal variations in the provenance of sediments of the BoB have been reconstructed using Sr-Nd isotopes [*France-Lanord et al.*, 1993; Colin *et al.*, 1999; *Pierson-Wickmann et al.*, 2001; *Ahmad et al.*, 2005; *Kessarkar et al.*, 2005; *Galy et al.*, 2008a]. Over Ma timescale, the sources of sediments to the BoB have remained roughly the same since the Miocene [*Bouquillon et al.*, 1990; *France-Lanord et al.*, 1993]. The sources are dominated by contributions from the Higher Himalaya (HH) with subordinate supply from the Lesser Himalaya (LH). However, on millennial timescale, there are evidences of variations in the provenance of sediments in the BoB related to climatic changes [*Colin et al.*, 1999; *Goodbred*, 2003; *Ahmad et al.*, 2005; *Bookhagen et al.*, 2005; *Bookhagen and Burbank*, 2006; *Kessarkar et al.*, 2005; *Clift et al.*, 2008; *Rahaman et al.*, 2009]. This is consistent with the important role that climate has on the present-day erosion over the Himalaya, with most of sediments delivered to the BoB by rivers during the southwest monsoon [*Islam et al.*, 1999; *Goodbred*, 2003]. In contrast, some of the studies carried out in the Nepal Himalaya [*Burbank et al.*, 2003], have decoupled climate and erosion and have highlighted the important control of tectonics on erosion. Compared to the Himalaya, there has been paucity of information on the paleo-erosion pattern of the Peninsular India river basins and their controlling factors. Based on clay mineralogy and Sr-Nd isotopes of marine sediments from the south-west margin of India, *Kessarkar et al.* [2003] concluded that these sediments are mainly from the Peninsular India and the Himalaya/Trans-Himalaya (Indus basin) and that their provenances and transport pathways remained the same during the late Pleistocene and Holocene.

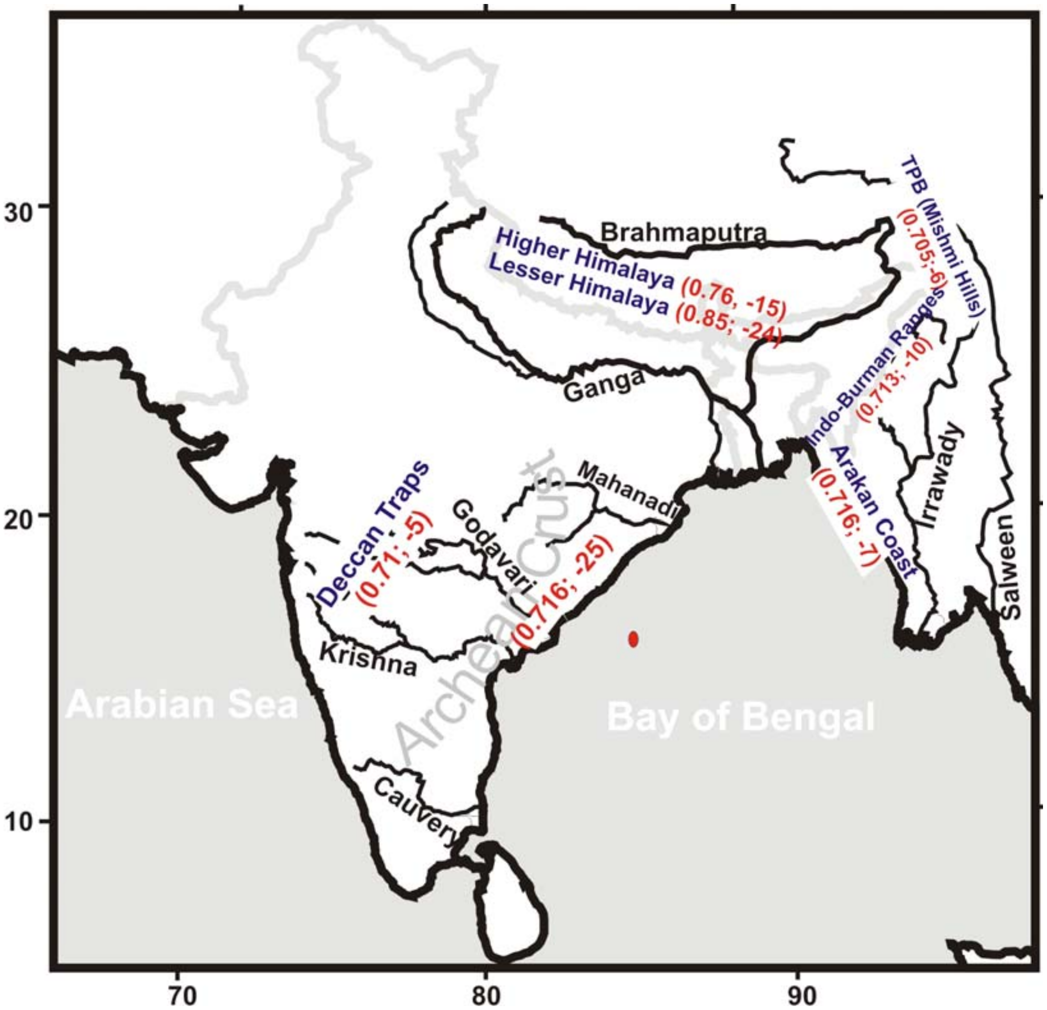

Figure 4.1: *The Map shows the location of the sediment core SK187/PC33 in the Bay of Bengal. The various sources of sediments to the core site with their characteristic* $^{87}Sr/^{86}Sr$ *and* ε_{Nd} *are also shown [Data Source: Colin et al., 1999, 2006; Ahmad et al., 2009; Singh et al., 2008].*

These limited information on the monsoon-erosion relation in the Himalaya and the Peninsular India regions, warrant a detailed study. The western Bengal fan receives sediments predominantly from the Himalaya and the Peninsular India and

Table 4-1: Basin characteristics and Sr, Nd isotopic composition of sediments at the outflow of major rivers contributing sediments to the BoB.

Basin	**River**	**Major Litho-units**	**Area**	**Runoff**	**Water discharge**	**Sediment flux**	**Sediments**	
			10^6 km^2	mm/yr	km^3/yr	10^6 tons/yr	**^{87}Sr/^{86}Sr**	ε_{Nd}
Himalaya	Ganga[1,2]	HH, LH	0.95	619	460	520	0.762 to 0.782	-16.1 to -18.1
	Brahmaputra[1,3]	HH, LH, TPB, Indo-Burmese Ranges	0.58	1087	630	540	0.721 to 0.749	-13.6 to -16.9
	Lower Meghna[1]		-	-	-	-	0.738 to 0.753	-14.8 to -17.4
Peninsular India	Mahanadi	Archean Crust	0.132	500	66	60	-	-
	Godavari[4]	Deccan Trap, Archean Crust	0.31	350	92	170	0.720 to 0.730	-14.8 to -17.4
	Krishna[4]		0.252	266	67	16		
	Pennar[4]	Archean Crust	0.02	-	2	-	0.752 to 0.761	-21.7 to -23.7
Indo-Burman Ranges	Irrawady[5]	Indo-Burmese Ranges, Arakan Mountains	0.414	1034	428	355[$]	0.713	-10.7
	Salween	TPB, Indo-Burmese Ranges	0.325	649	211	337[$]	-	-

Hydrological parameters from *http://www.gemswater.org/atlas-gwq/table3-e.html*; [$] *Robinson et al.*, 2006.
Sr and Nd isotopic data for the sediment of the rivers at their outflow are from [1] *Galy and France-Lanord*, 2001; [2] *Singh et al.*, 2008; [3] *Singh and France-Lanord*, 2002; [4] *Ahmad et al.*, 2009; [5] *Colin et al.*, 1999.

hence it can be used to investigate the past erosion pattern of these source regions. In the present study, efforts are made to track the provenances of the sediments from western BoB and their variations before, during and after the Last Glacial Maximum (LGM hereafter) and to identify the processes controlling the variations, based on sediment magnetic susceptibility (MS), chemical and Sr and Nd isotope compositions.

4.2. RESULTS

The core logs showed the core to be turbidite free. The lithology is mainly silty-clay and it does not show any significant changes with depth. The core location presently receives sediments predominantly from the Himalaya and the Peninsular India. The present core therefore is strategically situated to study the erosional process over the Himalayan and Peninsular Indian regions. The Sr and Nd isotopic compositions of these two source regimes are distinctly different (Fig. 4.1; Table 4-1) and hence, changes in the provenance of sediments and/or in their relative contributions will be reflected in the Sr and Nd isotope composition of sediments. This makes Sr and Nd isotope composition of the sediments a good proxy to quantify the relative contributions from these two sources, the Himalaya and the Peninsular India.

The depth-age relation for the core SK187/PC33 has been constrained using ^{14}C ages of bulk inorganic carbonates as discussed in Chapter 2. The measured ^{14}C ages (Table 4-2) were calibrated using Calib 5.2 [*Stuiver and Reimer*, 1993] with a reservoir age correction of ΔR = -60±50 [*Dutta et al.*, 2001].

Table 4-2: ^{14}C ages of inorganic carbon from the core SK187/PC33.

Sample code	**Depth** (cmbsf)	**Radiocarbon ages** (years BP)	**Calibrated ^{14}C age** (years BP)
PRLCH-725	54±17	7788 ± 295	8361 ± 953
PRLCH-766	281±16	13573 ± 302	15727 ± 1277
PRLCH-770	316±8	13964 ± 325	16171 ± 1333
PRLCH-776	466±23	14286 ± 355	16728 ± 1572
PRLCH-777	621±30	21242 ± 610	24840 ± 1613

Table 4-3: Geochemical compositions of bulk sediments from the SK187/PC33 core.

SampleID	Na	K	Ca	Mg	Al	Fe	Ti	Ba	Cr	Mn	Sr	Co	Cu	Ni	Zn	V
	(Wt %)							(µg/g)								
10-12cm	1.14	1.95	0.97	1.93	8.96	6.54	0.57	358	117	10946	97	32	66	75	152	130
18-20cm	1.05	2.19	1.37	1.29	7.44	4.05	0.56	407	96	1190	111	21	31	48	140	90
28-30cm	1.12	2.20	1.16	1.98	8.83	6.42	0.57	401	117	1400	105	30	62	69	156	125
109-111cm	1.03	2.14	0.74	1.64	7.95	6.22	0.55	385	124	1727	93	32	70	89	130	119
149-151cm	1.13	2.43	0.87	1.80	8.85	5.63	0.55	461	120	1351	105	27	57	77	120	115
201-203cm	1.08	2.49	1.96	1.69	8.47	4.88	0.45	449	109	856	133	22	45	61	138	106
221-223cm	0.54	1.07	22.71	1.15	2.50	2.17	0.37	239	35	2361	2749	16	8	32	56	30
249-251cm	1.16	2.33	1.64	1.80	8.82	5.78	0.50	559	110	977	133	26	66	79	132	112
300-302cm	0.97	1.99	2.31	1.62	7.89	5.57	0.45	533	103	1014	150	26	59	78	124	108
320-322cm	1.10	1.88	13.41	2.59	6.28	3.97	0.34	363	85	1685	531	23	36	68	397	77
350-352cm	1.29	2.70	7.48	3.37	8.63	4.69	0.38	365	86	1689	500	22	44	63	546	78
400-402cm	1.36	2.07	10.75	2.68	6.41	3.87	0.36	520	95	1572	186	24	40	79	461	78
440-442cm	0.74	1.03	29.37	1.62	2.84	1.84	0.16	231	37	3111	4159	10	16	28	250	34
450-452cm	0.99	2.43	4.25	1.66	8.27	4.97	0.44	383	102	1648	262	25	44	68	104	105
500-502cm	1.02	3.08	2.75	1.94	8.22	4.47	0.50	463	89	941	123	25	36	64	99	99
550-552cm	1.68	2.03	6.11	2.10	6.15	2.52	0.27	365	60	662	213	16	16	39	333	49
600-602cm	1.42	2.04	11.50	3.36	6.80	4.42	0.50	409	107	1589	434	26	41	70	545	104
650-652cm	0.97	2.01	6.24	2.11	7.30	4.88	0.41	551	90	2543	318	33	56	87	188	115
700-702cm	1.10	2.15	4.62	2.11	7.77	4.84	0.48	489	88	1782	233	33	53	79	158	112
750-752cm	1.46	2.40	2.87	1.70	7.75	3.84	0.38	429	67	1440	173	21	27	45	110	83
800-802cm	1.35	2.42	8.12	3.39	8.13	4.86	0.31	406	103	1926	254	29	40	77	467	89
849-851cm	1.11	2.05	2.92	1.54	6.81	3.57	0.40	401	71	1765	187	21	25	46	144	79
899-901cm	1.02	1.69	16.22	2.60	5.57	3.69	0.29	365	66	1396	886	24	37	62	418	56
949-951cm	1.06	2.52	2.59	1.78	7.87	4.82	0.39	497	84	1217	150	33	44	68	114	103
999-1001cm	0.84	1.57	4.79	1.70	4.55	2.63	0.21	338	50	1096	170	15	27	38	278	53
1049-1051cm	1.16	2.67	2.60	1.70	8.07	4.46	0.38	437	77	883	144	22	37	43	97	94
1099-1101cm	1.18	3.03	2.40	1.85	8.72	4.98	0.43	487	83	1026	153	24	41	53	109	103
1149-1151cm	1.65	2.61	2.25	1.45	7.55	3.68	0.42	409	61	615	147	19	24	37	83	73
1199-1201cm	2.39	1.97	1.89	0.80	6.00	1.86	0.22	340	26	284	156	9	7	15	93	35
1219-1221cm	1.06	2.72	2.25	1.94	9.19	4.87	0.43	434	83	753	123	22	42	47	160	96

Table 4-4: Comparison of Geochemical compositions of the BoB sediments analyzed in this study with that reported for its possible riverine sedimentary sources.

Basin	**Sediment Type**	**Al (%)**	**Fe (%)**	**Ti (%)**	**Mg (%)**	**K (%)**	**Ca (%)**	**Na (%)**
Ganga[$,#]	*Bank*	4.2 ± 1.0	2.0 ± 0.8	0.5	0.7 ± 0.3	1.7 ± 0.4	2.1 ± 1.4	1.1 ± 0.3
	Suspended	7.6 ± 1.0	4.5 ± 0.5	0.3 ± 0.1	1.8 ± 0.3	2.4 ± 0.6	3.1 ± 1.7	0.8 ± 0.3
Brahmaputra*	*Bank*	6.0 ± 0.4	3.1 ± 0.4	0.4 ± 0.1	1.0 ± 0.2	1.9 ± 0.2	1.9 ± 0.4	1.5 ± 0.1
	Suspended	8.3 ± 1.4	5.1 ± 2.1	0.6 ± 0.5	1.7 ± 0.7	2.4 ± 0.3	1.6 ± 0.4	1.2 ± 0.2
Lower Meghna[#]	*Suspended*	9.9 ± 0.5	5.5 ± 0.2	0.5 ± 0.01	1.8 ± 0.1	2.9 ± 0.2	1.4 ± 0.4	0.8 ± 0.2
Godavari-Krishna[&,@]	*core-tops at Mouth*	8.0 ± 0.4	6.4 ± 0.3	0.8 ± 0.1	1.5 ± 0.1	1.7 ± 0.01	2.0 ± 0.3	0.8 ± 0.3
Bay of Bengal[+]	SK187/PC33	7.3 ± 1.7	4.4 ± 1.3	0.4 ± 0.1	2.0 ± 0.6	2.2 ± 0.5	6.0 ± 6.8	1.2 ± 0.3

Data Source: [$]*Rai, 2008;* [#]*Galy and France-Lanord, 2001; *Singh and France-Lanord, 2002;* [&]*Das and Krishnaswami, 2007;* [@]*Pattan et al., 2008;* [+]*Present Study.*

Sediment Basin	**Ba**	**V**	**Cr**	**Cu**	**Ni**	**Zn**	**Sr**	**Co**	**Mn**
	µg/g								
Ganga	348	86	52	21	20	46	116	-	400
Brahamaputra	347	137	100	17	47	47	270	-	600
Godavari-Krishna	205	192	129	91	84	151	140	30	800
SK187/PC33	416 ± 79	88 ± 28	85 ± 26	40 ± 17	59 ± 19	210 ± 147	439 ± 857	24 ± 6	1715 ± 1843

Table 4-5: $CaCO_3$, C_{org} and total nitrogen content in the BoB sediments from the SK187/PC33 core.

Depth (cm)	$CaCO_3$	C_{org} (wt %)	TN
2-4	3.3	0.7	0.07
10-12	1.7	1.1	0.12
18-20	1.5	0.8	0.07
28-30	1.1	1.0	0.08
38-40	2.1	0.8	0.06
48-50	3.0	0.3	0.00
58-60	2.4	0.7	0.05
68-70	2.8	0.7	0.07
78-80	3.7	0.5	0.04
89-91	2.2	1.2	0.13
109-111	1.2	1.3	0.12
111-113	1.5	1.5	0.13
121-123	1.1	1.1	0.07
129-131	2.5	0.6	0.05
141-143	1.2	1.1	0.07
149-151	1.5	0.1	0.09
161-163	1.6	1.6	0.42
169-171	1.1	1.4	0.13
181-183	4.9	0.9	0.07
189-191	0.9	1.2	0.12
201-203	3.8	1.2	0.08
209-211	19.6	0.5	0.06
221-223	50.5	0.3	0.02
229-231	2.2	1.2	0.12
241-243	1.1	0.6	0.11
249-251	3.1	1.3	0.12
260-262	2.9	1.1	0.09
270-272	14.5	0.5	0.04
280-282	2.4	1.2	0.10
290-292	3.9	-	-
300-302	4.9	1.0	0.10
310-312	7.7	0.3	0.08
320-322	23.0	1.1	0.07
330-332	13.9	2.9	0.23
340-342	6.0	0.8	0.04
350-352	6.0	0.5	0.04
360-362	6.0	1.2	0.07
370-372	7.1	0.5	0.05
380-382	7.4	-	-
390-392	6.2	1.5	0.14
400-402	13.8	0.8	0.06
410-412	5.7	0.6	0.05
420-422	6.0	0.4	0.03
430-432	15.9	0.7	0.06
440-442	53.9	6.7	0.04
450-452	10.0	1.3	0.11
460-462	6.6	0.2	0.02
470-472	8.3	1.1	0.09
480-482	3.0	2.1	0.08
490-492	2.9	1.7	0.08
500-502	7.1	0.6	0.00
510-512	4.5	0.8	0.07
520-522	7.3	1.2	0.08
530-532	0.2	-	-
540-542	12.9	0.8	0.15
550-552	5.2	0.2	0.00
560-562	7.7	0.9	0.07
570-572	7.3	-	-
580-582	12.1	1.1	0.06
590-592	21.6	-	-
600-602	14.3	0.8	0.21
610-612	11.2	0.8	0.06
620-622	9.7	0.6	0.06
630-632	10.4	0.9	0.08
640-642	6.9	0.3	0.03
650-652	14.1	1.1	8.86
660-662	10.1	1.2	0.12
670-672	7.0	0.6	0.05
680-682	11.2	0.8	0.07
690-692	6.1	0.4	0.03
700-702	10.2	0.9	0.09
710-712	6.0	-	-
720-722	4.9	0.1	0.00
730-732	5.7	-	-
740-742	8.5	-	-
750-752	5.9	0.5	0.03
760-762	7.5	-	-
770-772	16.2	-	-
780-782	13.7	0.6	0.03
790-792	6.2	-	-
800-802	8.3	1.1	0.12
810-812	8.0	-	-
819-821	6.5	1.3	0.11
829-831	5.2	-	-
839-841	5.2	-	-
849-851	5.2	0.6	0.05
859-861	5.3	-	-
869-871	5.4	-	-
879-881	6.4	1.5	0.12
889-891	6.9	-	-
899-901	27.9	-	-
909-911	7.6	0.3	0.03
919-921	10.7	0.3	0.03
929-931	4.9	-	-
939-941	5.1	-	-
949-951	5.7	1.0	0.09
959-961	11.4	-	-
969-971	8.7	-	-
979-981	15.6	-	-
989-991	13.1	-	-
999-1001	7.0	1.2	0.08
1009-1011	6.7	-	-
1019-1021	7.3	0.1	0.01
1029-1031	7.3	-	-
1039-1041	5.1	-	-
1049-1051	6.3	0.4	0.03
1059-1061	5.4	-	-
1069-1071	5.3	-	-
1079-1081	6.2	0.6	0.04
1089-1091	5.5	-	-
1099-1101	5.6	0.7	0.04
1109-1111	4.8	-	-
1119-1121	5.0	1.0	0.08
1129-1131	4.5	-	-
1139-1141	4.2	-	-
1149-1151	3.3	0.2	0.03
1159-1161	3.3	-	-
1169-1171	2.6	-	-
1179-1181	1.6	0.2	-
1189-1191	1.6	-	-
1199-1201	1.7	0.2	-
1209-1211	4.0	-	-
1219-1221	3.9	0.6	0.05

The concentrations of major and trace elements in bulk sediments of the core SK187/PC33 are given in Table 4-3. The concentrations of these geochemical parameters show significant depth variations. The major elements, Na (0.54-2.39), K (1.03-3.08), Ca (0.74-29.37), Mg (0.80-3.39), Al (2.50-9.19), Fe (1.84-6.54), Ti (0.16-0.57) vary widely in the depth profile of SK187/PC33 core. The average concentration of these elements (Table 4-4), barring Ca, in the SK187/PC33 core overlaps with the values reported for its possible sediment sources, *viz*. the Ganga, Brahmaputra and the Godavari-Krishna Rivers. Contrasting to other major elements, the average value of Ca (6.0±6.8 %) for the BoB sediments is observed to be high with large variation compared to that reported for the Himalayan and the Peninsular rivers. The high Ca value compared to its detrital sources is expected as significant amount of Ca to the sediment is supplied from the authigenic $CaCO_3$.

Similar to the major elements, the mean values for most trace elements (V, Cr, Cu, Ni) of the BoB sediments fall between the typical value reported for the Ganga, Brahmaputra and the Godavari-Krishna river sediments [Table 4-4; *Pattan et al.*, 2008]. Exception to these are Ba, Sr, Zn and Mn which are higher compared to that for its possible detrital sources as significant amount of these elements are contributed by the authigenic components. The $CaCO_3$, organic carbon and total nitrogen content for the SK187/PC33 analyzed in this study are provided in the Table 4-5. The $CaCO_3$ concentration for this core ranges widely from 0.2 to 53.9% with a mean value of 7.4 %, higher compared to the inorganic carbonate content [~3%; *Galy and France-Lanord*, 2001] of the sediments of the Lower Meghna, combined flow of the Ganga and Brahmaputra river system in the Bangladesh. The average organic carbon content of the BoB sediments is 0.9%, comparable with the average C_{org} value (0.85%) reported for the Bengal fan sediments [*France-Lanord and Derry*, 1997], but slightly higher compared to that of the suspended river sediments of Lower Meghna [0.6%; *Aucour et al.*, 2006]. The average total nitrogen content of the sediments analyzed in this study is found to be 0.2%. The magnetic susceptibilty (MS) of the core SK187/PC33 ranges from 14 to 68 in 10^{-8} m^3/kg units (Table 4-6), comparable to earlier reported values for sediments from the western BoB [*Kessarkar et al.*, 2005]. This values of MS of SK187/PC33 are intermediate to the continental fluvial sediments reported for the Ganga and Godavari basins [*Sangode et al.*, 2007], indicating their dominating control on the MS values of the BoB sediments.

Table 4-6: Magnetic susceptibility (MS) of sediments from the core SK187/PC33*.

Depth (cmbsf)	MS 10^{-8} m^3/kg	Depth (cmbsf)	MS 10^{-8} m^3/kg	Depth (cmbsf)	MS 10^{-8} m^3/kg
6-8	25.6	**424-426**	22.1	**833-835**	23.7
12-14	29.7	**452-454**	18.7	**835-837**	24.6
22-24	33.9	**476-478**	29.9	**837-839**	23.6
30-32	33.7	**510-512**	25.0	**855-857**	26.5
38-40	27.4	**512-514**	24.6	**857-859**	25.5
50-52	24.2	**556-558**	34.0	**931-933**	19.2
56-58	20.7	**568-570**	33.0	**933-935**	21.8
70-72	23.5	**578-580**	52.0	**935-937**	22.3
82-83	36.8	**592-594**	35.1	**937-939**	20.0
91-93	34.5	**612-614**	24.6	**941-943**	20.4
97-99	25.0	**624-626**	34.7	**943-945**	20.5
109-111	33.3	**632-634**	31.1	**959-961**	19.8
121-123	30.9	**644-646**	37.5	**961-963**	26.8
173-175	18.4	**648-650**	36.3	**967-969**	27.0
183-185	17.7	**660-662**	21.7	**969-971**	24.0
185-187	17.9	**670-672**	28.3	**1001-1003**	33.0
211-213	14.0	**678-680**	23.1	**1019-1021**	45.3
221-223	15.3	**690-692**	46.6	**1029-1031**	24.0
262-264	14.7	**700-702**	43.3	**1049-1051**	22.5
268-270	20.1	**710-712**	26.3	**1077-1079**	18.3
274-276	15.3	**732-734**	23.4	**1081-1083**	17.6
284-286	17.1	**760-762**	35.6	**1099-1101**	18.0
300-302	22.2	**770-772**	30.4	**1109-1111**	22.6
308-310	19.8	**790-792**	23.1	**1127-1129**	28.4
316-318	14.3	**798-800**	24.3	**1139-1141**	21.4
336-338	14.2	**810-812**	40.0	**1151-1153**	68.0
346-348	20.3	**820-821**	34.0	**1187-1189**	47.1
362-364	16.9	**821-823**	25.9	**1201-1203**	46.8
372-374	20.4	**827-829**	20.6	**1211-1213**	22.3
402-404	23.3	**831-833**	22.2	**1217-1219**	30.4

**measured at frequency 0.47 kHz*

The Sr, Nd concentrations in the silicate fraction and their $^{87}Sr/^{86}Sr$ and ε_{Nd} values also show significant variations with depth (Fig. 4.2; Table 4-7). The abundances of Sr and Nd vary from 43 to 172 µg/g and from 13 to 63 µg/g respectively whereas the $^{87}Sr/^{86}Sr$ ratios vary from 0.72528 to 0.75732 and ε_{Nd} from

-21.1 to -13.7 (Table 4-7). The Sr isotope composition of these sediments is very radiogenic with values generally exceeding 0.735 (Table 4-7), with corresponding ε_{Nd} values often less than (-15). These values are within the range of isotopic composition of various sources supplying sediments to the core site (Fig. 4.3), though a dominance of the Himalayan source, as supplied by the Lower Meghna, exists (see Discussion). Among the 36 samples analysed for Sr and Nd isotopic composition, two samples at depths of 221-223, 440-442 cmbsf show a sharp decrease in the ε_{Nd} (and increase in $^{87}Sr/^{86}Sr$ ratios) compared to samples from adjacent depths (Table 4-7). The cause for these ε_{Nd} and $^{87}Sr/^{86}Sr$ anomalies is unclear. It may be the result of a unique event, such as significant sediment delivery during flood events from a tributary flowing through lithology with low ε_{Nd} and high $^{87}Sr/^{86}Sr$ such as the Mahanadi and Pennar rivers draining Archean crust. These two samples have not been considered in the analysis of the isotope data to determine their general trend with depth (Fig. 4.2).

4.3. DISCUSSIONS

4.3.1 $^{87}Sr/^{86}Sr$ and ε_{Nd} in contemporary sediment sources to the BoB

The different sediment sources to the BoB show characteristic Sr and Nd isotopic compositions (Fig. 4.1, Table 4-1). For example, Himalayan rivers (such as the Ganga) supply sediments with highly radiogenic Sr and less radiogenic Nd compared to that of the sediments from the TPB, the Indo-Burmese ranges, the Arakan mountains and the Deccan Plateau, which are less radiogenic in Sr and more radiogenic in Nd [Table 4-1, Fig. 4.1; *France-Lanord et al.*, 1993; *Colin et al.*, 1999, 2006; *Galy and France-Lanord*, 2001; *Singh and France-Lanord*, 2002; *Singh et al.*, 2008; *Ahmad et al.*, 2009]. The Godavari and the Krishna rivers drain the basaltic terrain of the Deccan traps upstream and the Archean cratons downstream. Therefore, the Sr and Nd isotopic composition of these river sediments [0.720 to 0.730 and -12.0 to -18.2 respectively; *Ahmad et al.*, 2009] depend on the relative contribution from these two sources. The representative Sr, Nd isotope compositions for the Archean crust (Fig. 4.1) used in this study are 0.716 and -25 respectively, compiled from earlier studies [*Kessarkar et al.*, 2003, 2005].

Table 4-7: Sr, Nd concentrations and their isotope composition of the BoB sediments in their silicate fractions of the SK187/PC33 core.

Depth (cmbsf)	**Sr (μg/g)**	**^{87}Sr/^{86}Sr**	**Nd (μg/g)**	ε_{Nd}
10-12	56	0.74041	17	-15.5
18-20	87	0.75051	22	-16.9
28-30	57	0.74089	18	-14.6
109-111	58	0.74212	19	-15.4
149-151	59	0.74457	18	-15.9
201-203	43	0.74522	19	-15.8
221-223	73	0.75732	63	-21.1
249-251	60	0.73759	13	-15.7
300-302	69	0.73528	13	-15.8
320-322	98	0.73483	19	-15.1
340-342	49	0.74273	17	-15.8
350-352	82	0.75150	24	-15.8
360-362	43	0.74621	14	-15.6
400-402	87	0.73768	19	-15.3
440-442	84	0.74422	24	-19.6
450-452	82	0.73475	19	-14.9
490-492	58	0.74248	17	-16.5
500-502	71	0.75515	21	-16.5
510-512	54	0.74009	17	-15.4
550-552	123	0.73594	18	-14.6
600-602	104	0.72861	37	-15.0
650-652	99	0.72528	19	-13.7
700-702	101	0.72750	19	-14.5
750-752	127	0.73573	20	-14.5
800-802	83	0.73284	20	-13.8
849-851	101	0.73638	24	-15.5
889-891	54	0.73062	13	-14.9
899-901	68	0.74026	17	-17.1
909-911	61	0.73310	16	-14.0
949-951	97	0.73679	*n.a.*	*n.a.*
999-1001	89	0.73851	21	-14.9
1049-1051	111	0.74016	21	-15.5
1099-1101	105	0.73865	18	-15.9
1149-1151	145	0.73334	27	-14.7
1199-1201	172	0.72903	13	-14.5
1219-1221	116	0.73669	23	-14.8

n.a.: Not Analyzed.; Errors on Sr and Nd isotopic compositions are better than 10 ppm.

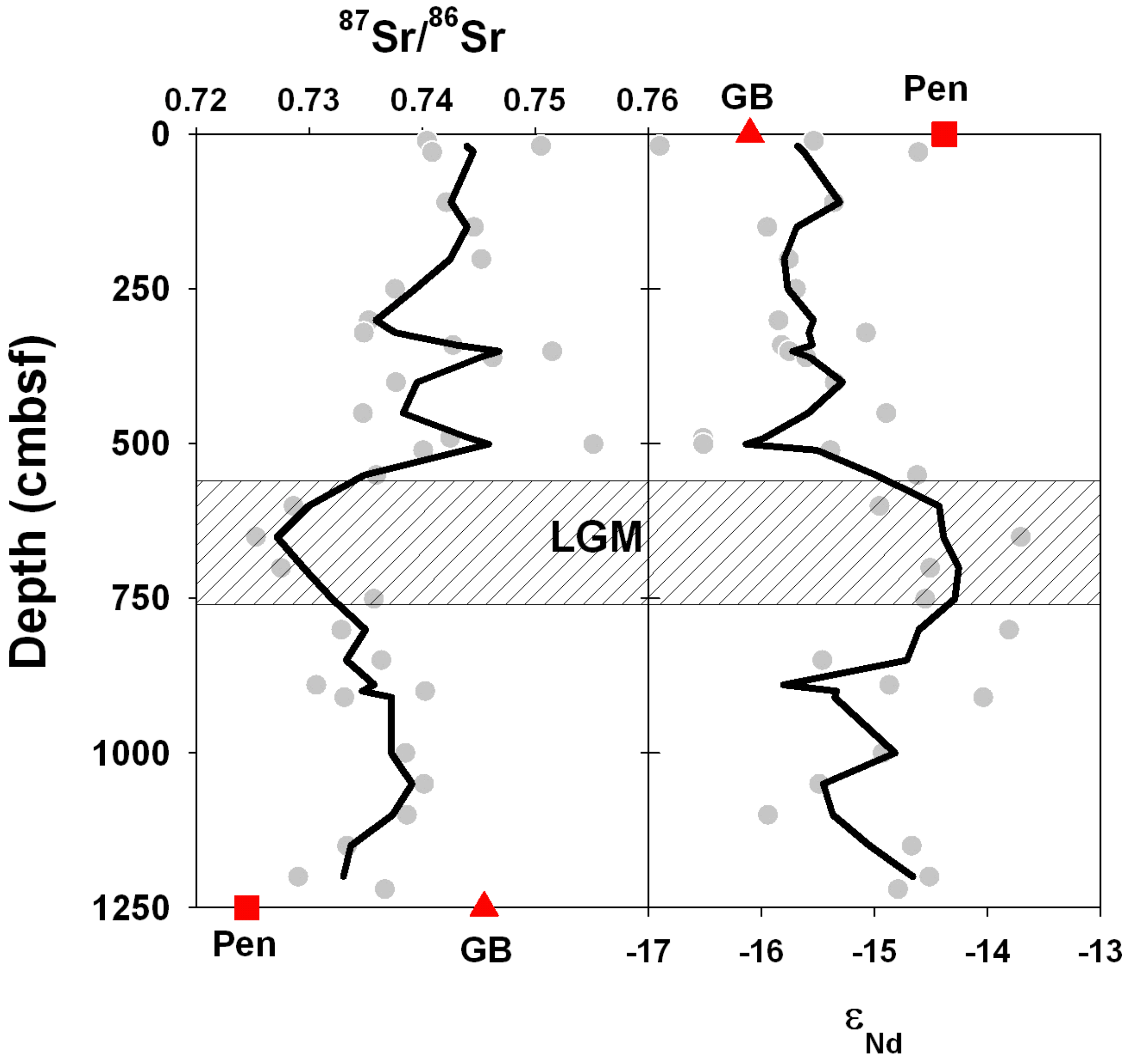

Figure 4.2: *Depth profile of Sr and Nd isotope composition of sediments from the core SK187/PC33 (dots). The solid line is the 3-point moving average of the data. Data show a dip in* $^{87}Sr/^{86}Sr$ *and a hump in* ε_{Nd} *excursions at ~600 cmbsf coinciding with the Last Glacial Maximum. Two anomalous samples at depth ~220 and 440 cmbsf are not included. The squares in the figure represent the average Sr-Nd isotopic values for the contemporary Peninsular Indian river sediments (PEN; Ahmad et al., 2009) and the combined flow (Lower Meghna) of G-B river sediments (Triangle (GB); Galy and France-Lanord, 2001).*

4.3.2. Sr-Nd isotope composition and Chemical Index of Alterations (CIA)

Sr-Nd isotope pair has been used extensively to apportion the soures of marine sediments [*Tripathy et al.*, 2010a and *references therein*]. Despite its wide application in source identification It has been always a concern whether isotope composition of sediments preserves the source signature or gets fractionated during chemical weathering [*Tripathy et al.*, 2010a and *references therein*]. To check if the sediments of the BoB retain the isotope signature of their corresponding sources or get altered during chemical weathering, Sr and Nd isotope compositions of these sediments are compared with their chemical index of alteration (CIA). CIA provides information on the intensity of chemical weathering the sediments have undergone [*Nesbitt and Young*, 1982] and is defined as,

$$CIA = 100 \times \left(\frac{Al_2O_3}{Na_2O + K_2O + CaO^* + Al_2O_3} \right) \text{---------} \ (4\text{-}1)$$

where, all the elemental compositions are in molar units and the CaO* represents the non-carbonate CaO concentrations in the sediments. CaO* is estimated by subtracting CaO content estimated using inorganic carbonates (assuming insignificant dolomite content in the BoB sediments) from the measured CaO of bulk sediments. All the samples except one (with CIA 17) have CIA values between 29 and 64. The average CIA value of of BoB sediments analysed is 47±12. The average value for the CIA of the BoB sediments is intermediate to that reported for its source rocks from the Higher Himalaya [53±7; Rai, 2008], Lesser Himalaya [52±7; Rai, 2008] and the Deccan basalts [~37 (Range: 35-44); *Das and Krishnaswami*, 2007]. To evaluate the impact of chemical weathering on the Sr-Nd isotopic compositions of the BoB sediments, CIA of the sediments is plotted against their isotopic values (Fig. 4.4). The scatter plot of CIA with Sr-Nd isotopes do not show any significant trend, confirming that chemical weathering have not affected the Sr and Nd isotopic composition of the sediments and therefore, can be used to track their provenances and their relative contributions to the studied core location in the past.

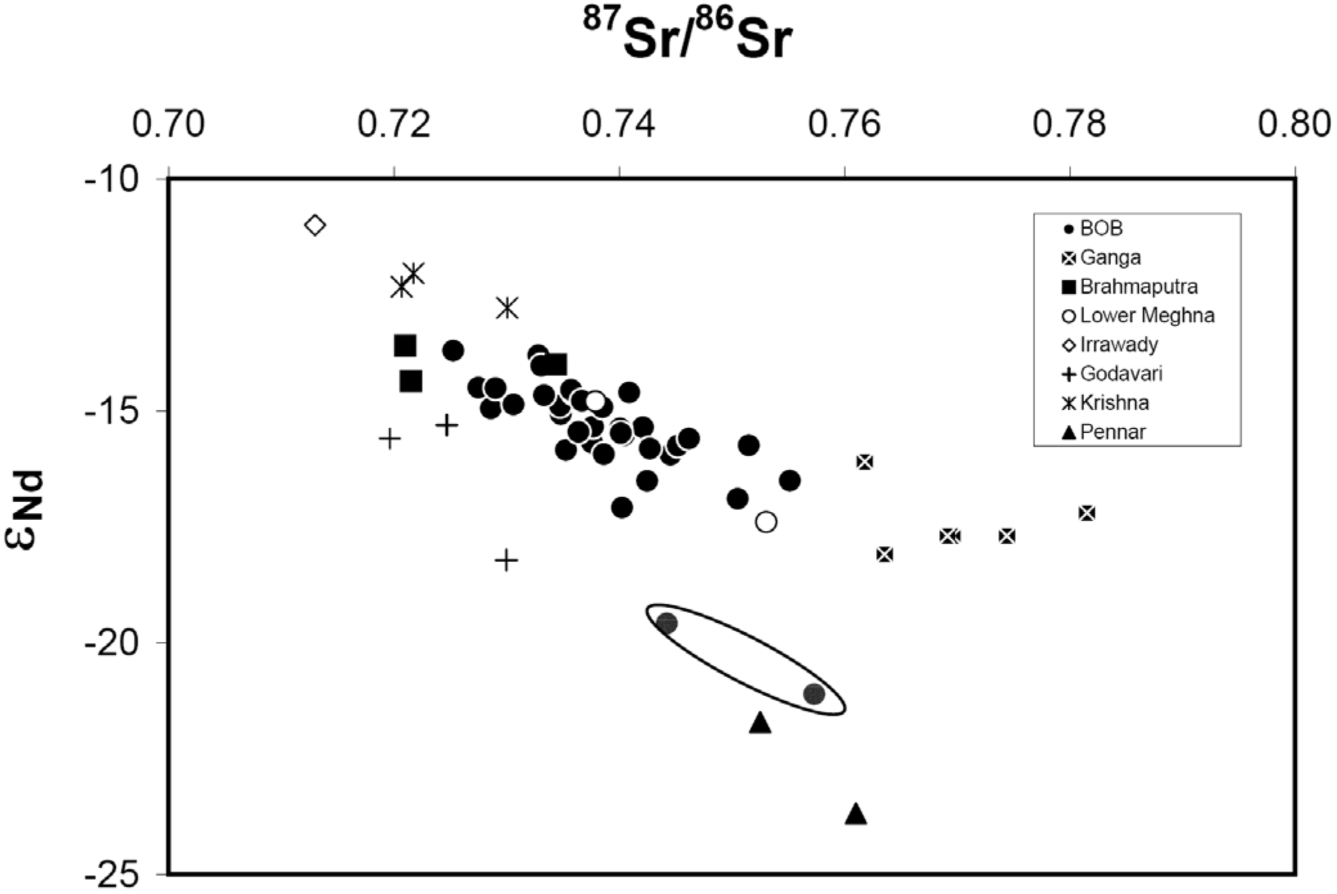

Figure 4.3: *$^{87}Sr/^{86}Sr$ vs. ε_{Nd} of the sediments from core SK187/PC33. The isotope composition of various sources contributing to these sediments is also given. The Sr and Nd isotope composition of SK187/PC33 sediments falls within the isotopic values of riverine sediments from the Himalaya and the Peninsular India. The two samples (encircled) having low ε_{Nd} seem to be anomalous and could be deposited by flood events in particular rivers such as the Mahanadi or the Pennar flowing though an Archean crust with radiogenic Sr and unradiogenic Nd.*

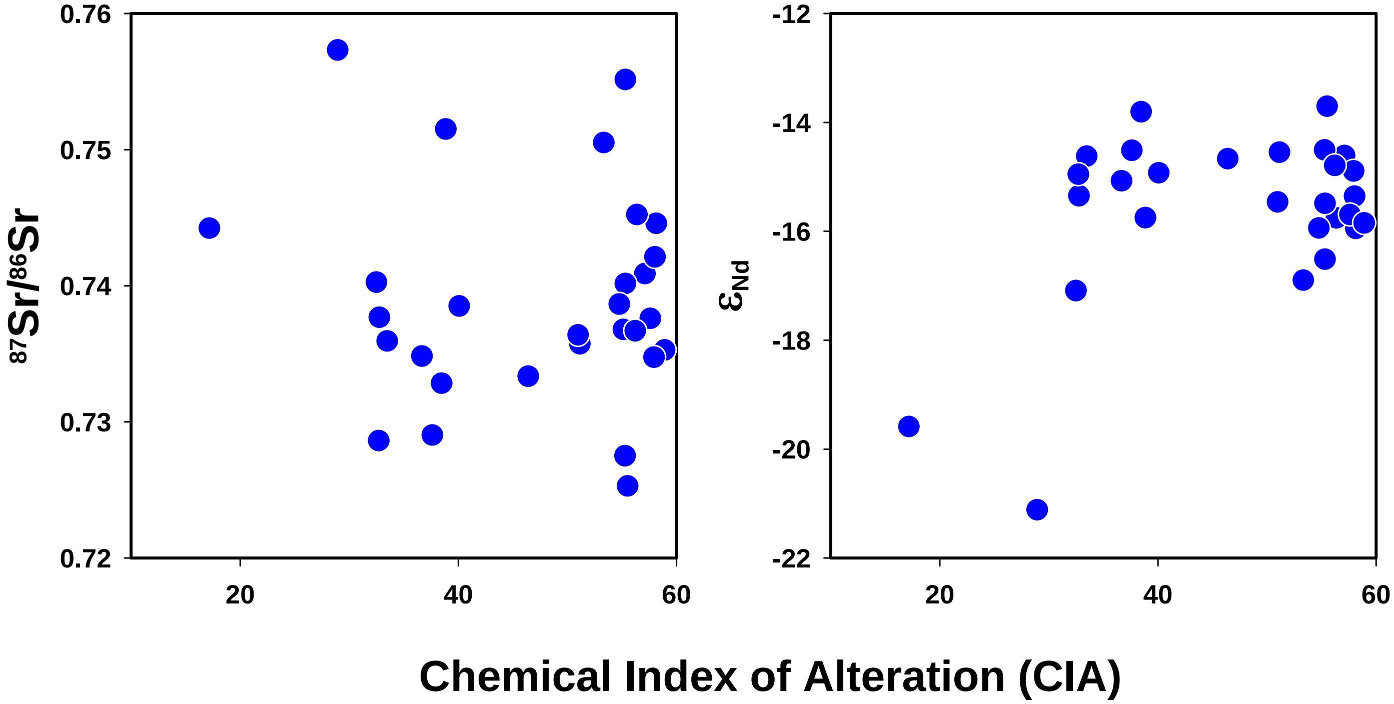

Figure 4.4: *Chemical index of alteration (CIA) and* $^{87}Sr/^{86}Sr$ (ε_{Nd}) *of the sediments from the SK187/PC33 showed no systematic trend between them; confirming that these isotopic ratios of the BoB sediments have not been altered due to chemical weathering.*

4.3.3 Temporal variations in the erosion pattern of Himalaya and Peninsular river basins of India

4.3.3.1 Depth-Age model

The availability of an age-depth model for the SK187/PC33 core is a prerequisite to infer the temporal variations of the sources supplying sediments to the core location and to make comparison with known climatic events. The depth-age model for the BoB sediments in this study has been established based on ^{14}C of total inorganic carbon. Since the ^{14}C analyses were made on bulk carbonates, there could be an overestimation of the ages due to potential contribution of dead carbon from detrital carbonates. Earlier studies on ^{14}C measurements in coarse and fine fractions of bulk carbonates showed that the finer fractions (comprising primarily of carbonate powder and nanoplanktons) were generally older than the coarser fractions (mature forams) by ~3 ka [*Sarkar*, 1989; *Sarkar et al.*, 1990]. The older age in the finer fraction was attributed to incorporation of dead detrital carbonates. Subsequently, *Tiwari et al.* [2005] by comparing $\delta^{18}O$ spike in two cores, one dated by AMS on forams and the other (near-by core) by ^{14}C on total carbonates, suggested that the age differ by ~3 ka, the AMS dates being younger. An independent estimation of age correction on the BoB sediments can be obtained from the inorganic carbon contents of sediment sources and that in the SK187/PC33 core. The average carbonate content (expressed as $CaCO_3$) is 8.6% in the five sections of SK187/PC33 analysed for ^{14}C, compared to ~3% in the Lower Meghna sediments [*Galy and France-Lanord*, 2001]. Dilution of SK187/PC33 carbonates with the dead riverine carbonate would overestimate the age by ~3.5 ka. The comparison of the pattern of MS profiles of the core analyzed in this study with that in an AMS ^{14}C dated core from the western BoB [*Kessakar et al.*, 2005], provides another approach to constrain the age-depth model. This approach essentially uses MS as a stratigraphic marker [*Ninkovich et al.*, 1966; *Bloemendal et al.*, 1995]. Matching the prominent changes in the MS profiles in the top layers of the two cores (assuming that they are synchronous) indicates that the bulk carbonate ages of SK187/PC33 are older by ~4 ka. The AMS dated western BoB core [*Kessarkar et al.*, 2005] had an age reversal at ~100 cm, therefore the MS pattern of the two cores below this depth are not compared. In this study, samples having comparable calcium carbonate content (~8 %) were analyzed for ^{14}C chronology so that the level of correction due to presence of detrital carbonate could be similar. Thus, based on available evidences, the bulk radiocarbon ages measured in the study could be ~3-4 ka older than actual ages. This suggests that the depositional age of the sample at depth 621 cmbsf, for which the measured ^{14}C calendar age is ~24 ka (Table 4-2), could be about 20 ka representing the LGM. In addition to the five samples in Table 4-2 one sample from 222 cmbsf depth with high $CaCO_3$ (~50 %) content was also analyzed for ^{14}C. This sample yielded an age of 22000 ± 600 yr (PRLCH-724) significantly different that expected based on the age-depth model of the sample in Table 4-2. It is worth mentioning here that this sample also has anomalous $^{87}Sr/^{86}Sr$ and ε_{Nd} values (Table 4-3; Fig. 4.3). As a result, this data is not included for the depth-age relation.

The age distribution with depth in the core suggests that the LGM (18-21 ka) occurs at the depth range of ~600-700 cmbsf. The sedimentation rate of the core varies with depth with the lowest value at around LGM (460-620 cmbsf; 0.2 mm/yr) and about an order of magnitude higher (2.7 mm/yr) following the LGM (320-460 cmbsf). Similar pattern in sedimentation, with high rates following the LGM have also been reported by *Kessarkar et al.* [2005] and *Galy et al.* [2008a].

4.3.3.2. Temporal variations in geochemical and Sr-Nd isotopic signatures in the BoB sediments

The depth profiles of Sr and Nd isotope compositions of the core show significant temporal variations (Fig. 4.2). The range in $^{87}Sr/^{86}Sr$ (0.725-0.757) and ε_{Nd} (-13.7 to -16.9) indicate the dominance of the Himalayan source with minor contributions from the Peninsular Indian regions (Fig. 4.3). The $^{87}Sr/^{86}Sr$ and ε_{Nd} of the SK187/PC33 sediments (Table 4-7) are bracketed by sediments from the Ganga, Brahmaputra and rivers from the Peninsular India and overlap with a few available data of the Lower Meghna (combined flow of the Ganga and the Brahmaputra in Bangladesh) indicating these rivers to be the major sediment supplier to the core site (Fig. 4.3). This inference is also borne out from the mixing plot between K/Al and

Fe/Al of the BoB sediments (Fig. 4.5). Most of the data points fall in the mixing curve of the Ganga-Brahmaputra [GB; *Galy and France-Lanord*, 2001] and Godavari-Krishna [GK; *Pattan et al.*, 2008] river sediment values, confirming their dominance in regulating the sedimentary budget at the studied location. A few data in Fig. 4-5 lie outside the mixing zone of the GK-GB river system, possibly indicates their source from the Archean crust through Mahanadi and Pennar river systems. This proposition draws support from the anomalous Sr-Nd isotopic signature of two of these outlier samples, as discussed earlier.

The Sr-Nd isotopes depth profiles (Fig. 4.2) show a striking change in isotopic compositions around 600 cmbsf. Considering the age model of the sediment core, this major change in $^{87}Sr/^{86}Sr$ and ε_{Nd} coincide with the LGM. The $^{87}Sr/^{86}Sr$ of the samples during LGM is ~0.725 compared to their interglacial values of ~0.745 (Fig. 4.2). The less radiogenic $^{87}Sr/^{86}Sr$ of the sediments during LGM indicate a relatively reduced supply of sediments from the Himalayan rivers, particularly that of the Ganga (which is characterized by a highly radiogenic Sr signature; Table 4-1) compared to that during pre- and post-LGM relative to the Peninsular Indian rivers. This inference based on the $^{87}Sr/^{86}Sr$ data is also supported from the trend of ε_{Nd} values which shows a broad hump (~ -14) during the LGM compared to pre- and post-LGM values (-16; Fig. 4.2). The concomitant changes in both $^{87}Sr/^{86}Sr$ and ε_{Nd} argue in favor of provenance changes and not due to particle sorting/weathering processes [*c.f. Walter et al.*, 2000; *Tutken et al.*, 2002; *Colin et al.*, 2006].

Similar to Sr-Nd isotopic signatures, the Fe/Al and V/Al ratios and MS (Fig. 4.6) of the sediment core also show significant variations with depth (time) indicating changes in relative proportion of sediments supplied from various sources. The Sr, Nd isotopes-based inference that the sediment contribution to the core site from the Himalayan source is relatively diminished during LGM is also confirmed by the V/Al and Fe/Al ratios. Distinctly higher V/Al and Fe/Al [$(60\text{-}70)\times10^{-4}$ and 1.01±0.21; *Pattan et al.*, 2008] characterize the rivers flowing through the Peninsular India compared to that of the G-B sediments [$V/Al = (20\text{-}25) \times 10^{-4}$ and $Fe/Al = 0.44\pm0.10$; *Pattan et al.*, 2008]. The humps in V/Al and Fe/Al profiles observed during LGM in

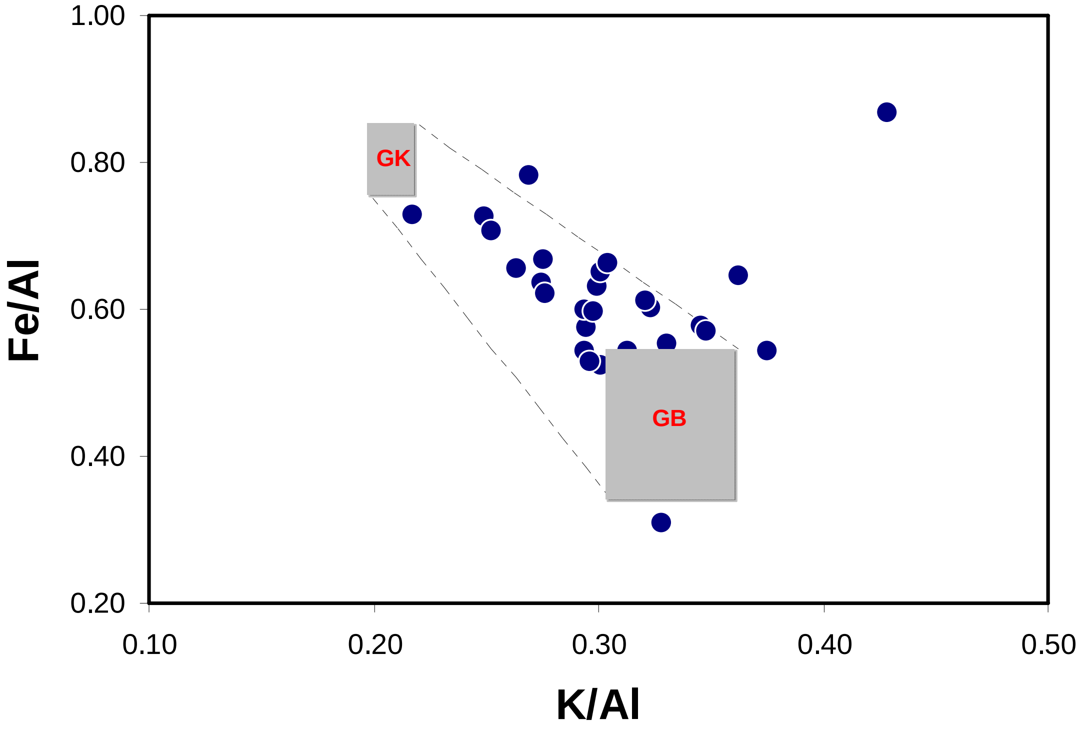

Figure 4.5: *Mixing plot of K/Al and Fe/Al of the BoB sediments indicates their sediment supply dominated by the Ganga-Brahmaputra (GB) and Godavari-Krishna (GK) river systems. The data for the GB and GK river sediments are from Galy and France-Lanord, 2001 and Pattan et al., 2008.*

SK187/PC33 (Fig. 4.6) attest to the relatively enhanced sediment supply from the Peninsular Indian Rivers. This is also supported by the variation in the MS values. The magnetic susceptibility of sediments depends mainly on the abundance of detrital magnetic minerals present in them. The low carbonate content of the sediments from SK187/PC33 ensures that the magnetic susceptibility is a good tool to infer sediment provenance changes in the past [*Bloemendal et al.*, 1993]. Temporal variations of MS of the sediments show an increasing trend at around LGM (Fig. 4.6), suggesting higher abundances of ferromagnetic minerals (such as magnetite) and Fe-bearing silicates in the sediments. A very likely source for the high MS values during LGM is the relatively enhanced contribution of sediments from the Peninsular Indian region. This inference draws support from the significantly higher MS values for the fluvial

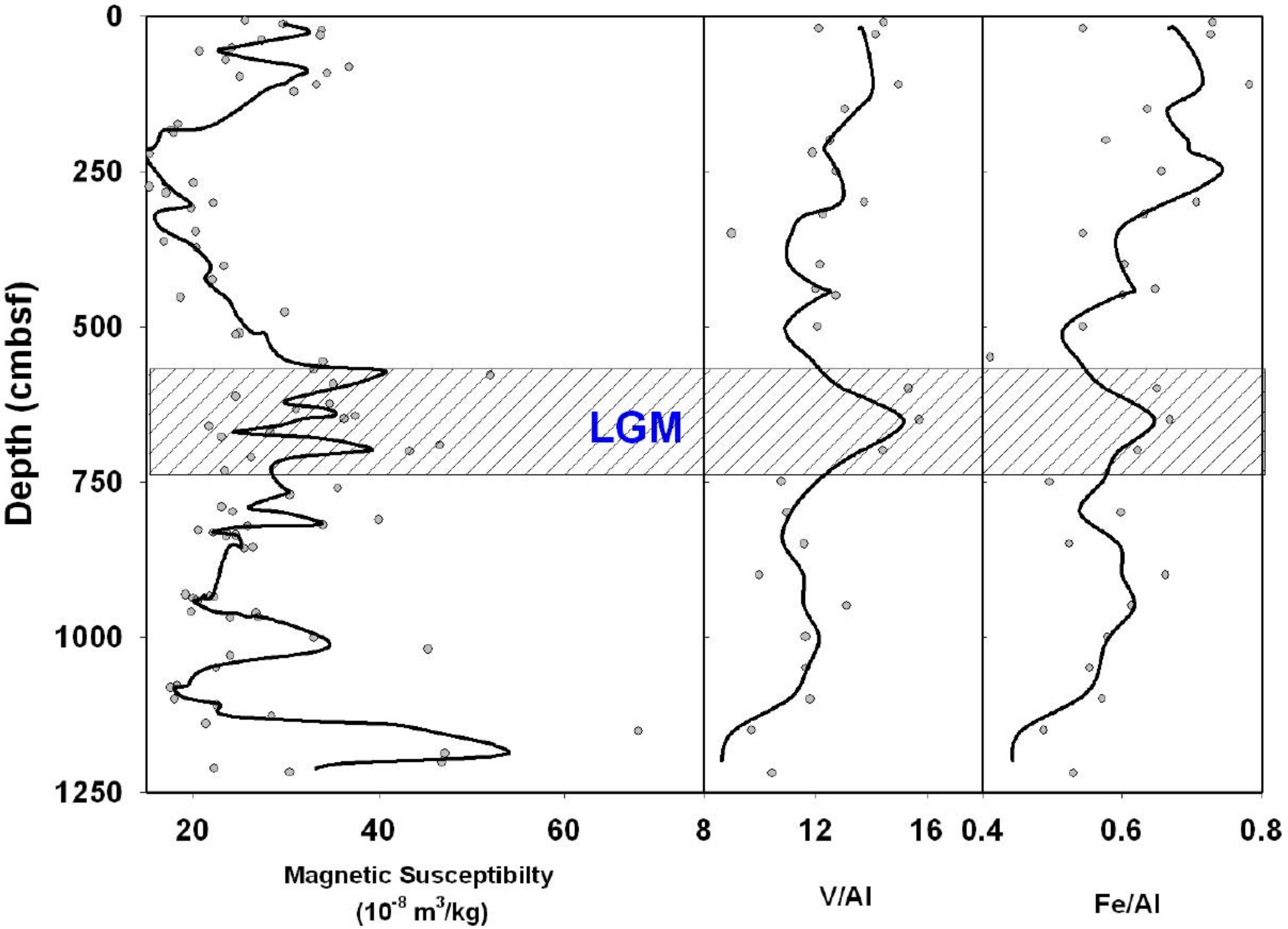

Figure 4.6: *Depth profiles of magnetic susceptibility (MS), Fe/Al and V/Al ratios for the SK187/PC33 sediments. The higher values of MS, V/Al and Fe/Al during the LGM indicate a relatively lower contribution from the Himalaya. The solid line is the 3-point moving average of the data.*

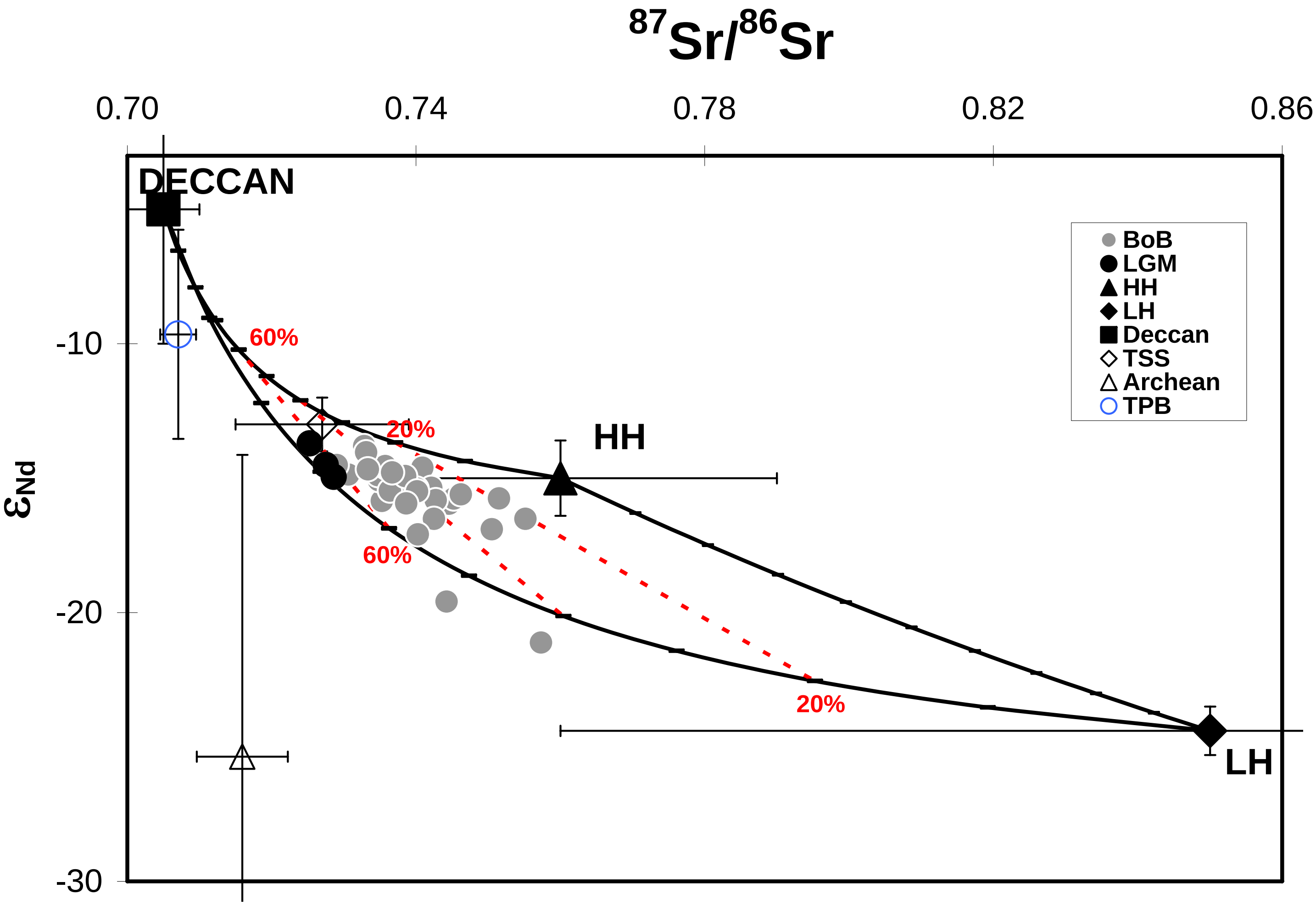

Figure 4.7: *Sr and Nd isotopic mixing plot for the SK187/PC33 sediments along with isotopic values of their dominant sedimentary sources. The dominance of the Himalayan sources, particularly HH, is observed for most of the samples with enhanced contribution from the Deccan traps during the LGM. The hyperbolic curve shown is the mixing trend among the sources calculated using the average Sr, Nd concentrations and isotope ratios of the Deccan (228 µg/g, 11 µg/g, 0.705, -5), HH (80 µg/g, 18 µg/g, 0.76, -15) and the LH (94 µg/g, 26 µg/g, 0.85, -24.4) respectively. The representative isotopic values for the sedimentary sources are from Singh et al. (2008), except for the TPB (Average of predominantly TPB flowing (Lohit and Dibang) river sediments; Singh and France-Lanord, 2002) and Archean terrains [Compiled from Kessarkar et al., 2003, 2005].*

sediments from Peninsular Indian regions compared to that from the sediments from the river basins of the Himalaya [*Sangode et al.*, 2007]. The high MS value for the sediments from the Peninsular India particularly that for weathered products of the Deccan basalts, is due to the abundance of titanomagnetite with minor hematite [*Courtillot et al.*, 1986; *Sager and Hall*, 1990]. A similar high MS value during LGM in the western Bengal fan was also reported by *Sangode et al.* [2001] and this change was attributed to weakening of sediment contribution from the Himalaya.

The above discussion, based on the isotope and trace element composition of the core SK187/PC33 along with its magnetic susceptibility reveal significant variations in the relative supply of sediments from the Himalaya and the Peninsular India over glacial-interglacial timescale. However, this conclusion rests on the assumption that the isotopic and chemical characteristics of these sources did not change since the LGM. This assumption seem to be valid for the G-B rivers as the Sr-Nd isotope ratios of the BoB sediments near the mouth of this river system has remained roughly the same since the LGM [*Galy et al.*, 2008a]. *Rahaman et al.* [2009], however, observed significant excursion in $^{87}Sr/^{86}Sr$ (and ε_{Nd}) in sediments of the Ganga upstream, during the LGM. If this finding is typical of the entire G-B basin, then it would require that the relative proportion of G-B sediments in the SK187/PC33 core during LGM would have to be lower than that estimated based on their present-day $^{87}Sr/^{86}Sr$ ratios.

The rivers draining the Peninsular India flow through multiple lithologies (Archean crust and Deccan traps) with their own distinct Sr-Nd isotope composition. Therefore, any change in the relative proportion of sediments from these two lithologies can alter the Sr-Nd isotopic signature of the peninsular sediments being delivered to the BoB. However, there is no evidence at present to suggest that the provenance of sediments of the Peninsular Indian rivers has changed in the past [*Kessarkar et al*., 2003]. Increase in NE monsoon during LGM could enhance supply from the peninsular river basins. But this could result in a decrease of ε_{Nd} unlike what has been observed in this study. Fig. 4.7 shows the Sr-Nd isotopic composition of the SK187/PC33 sediments along with the isotopic compositions of their dominant sources (*viz.* Higher Himalayan Crystallines, Lesser Himalayan silicates, Deccan traps and Archean). The dispersion of sediment data in the plot shows that their supply to the present core site is mainly from the HH, LH and the Deccan traps throughout the core length. The mixing curve (Fig. 4.7) among the major sources show that ~40% of the sediments are supplied from the Deccan and rest from the HH and the LH. However, the sediments deposited during LGM, with lower $^{87}Sr/^{86}Sr$ and high ε_{Nd} values, have relatively larger contribution of sediments from the Peninsular India (both Deccan traps and Archean crust) sources. The relative proportion of Peninsular India sediments to the core site during LGM (~60%; Fig. 4.7) increases significantly compared to that during the interglacial periods (~40%). The LGM shift in the SK187/PC33 sediments lean towards the mixing curve of Deccan and LH (Fig. 4.7), indicating relatively enhanced contribution from LH than that of HH during LGM. This is consistent with the results of *Rahaman et al.* [2009].

4.3.4. Impact of climate on continental Erosion

The excursions in Sr and Nd isotope composition of the sediments during LGM is compatible with the Asian monsoon strength variability *[Fig 4.8; Prell and Kutzbach*, 1987; *Herzschuh*, 2006]. Climatic records show that during the LGM the intensity of the SW monsoon decreased [*Prell and Kutzbach*, 1987; *Herzschuh*, 2006) and that of NE monsoon increased [*Prell et al.*, 1980; *Duplessy*, 1982; *Sarkar et al.*, 1990; *Tiwari et al.*, 2005]. The decrease in intensity of SW monsoon during LGM would limit its penetration into the Higher Himalaya, which is the dominant source of sediments to the Ganga and the Brahmaputra at present [*Singh et al.*, 2008]. In addition, during the LGM the extent of glacial cover over the Higher Himalaya was larger [*Owen et al.*, 2002], further limiting physical erosion in the region. In contrast, there are evidences that during the LGM the NE monsoon was more intense [*Duplessy*, 1982; *Prell and Kutzbach*, 1987; *Sarkar et al.*, 1990; *Tiwari et al.*, 2005]. This situation enhanced the sediment delivery from the rivers draining the Peninsular India and part of the drainage basin of the Brahmaputra (TPB), all of which have

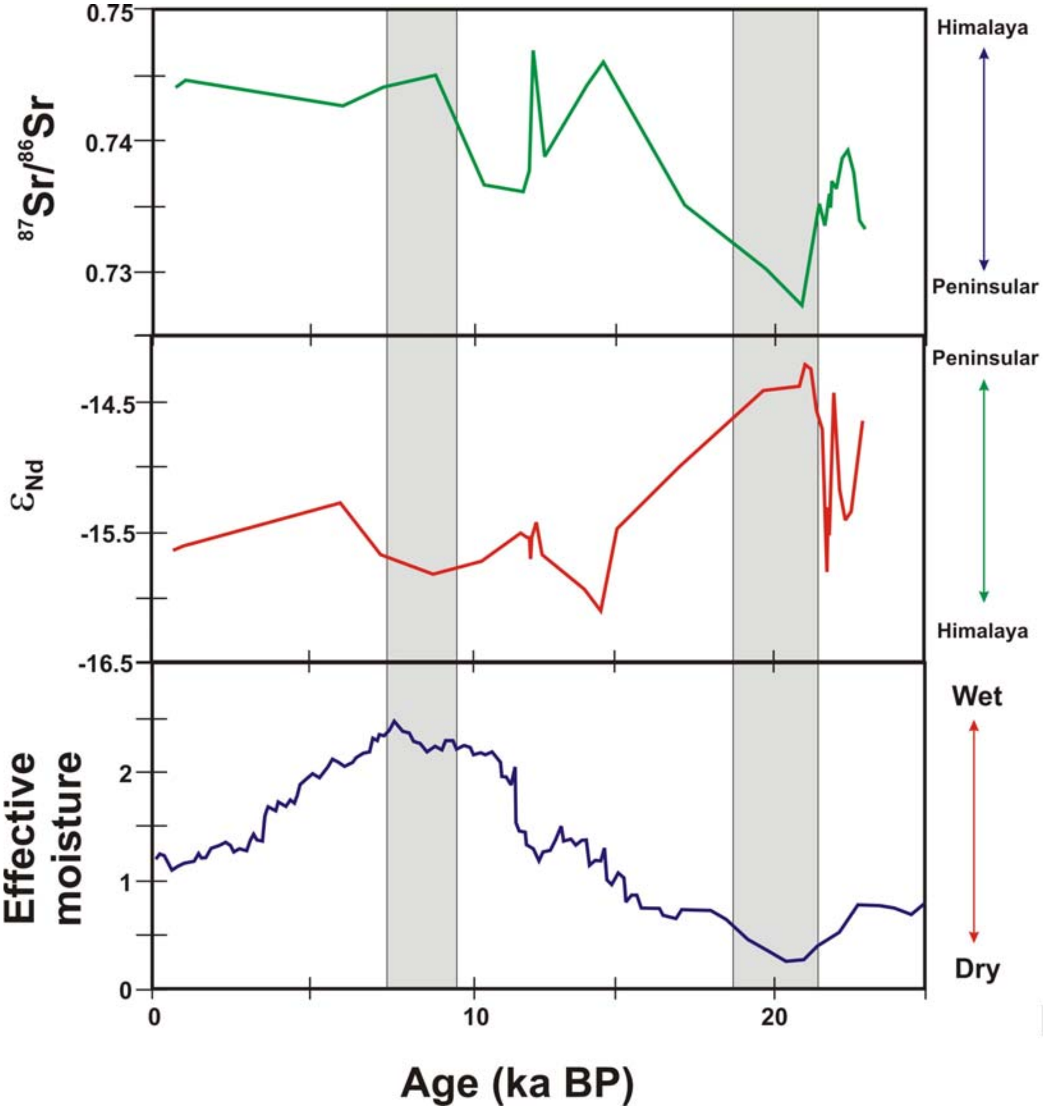

Figure 4.8: *Temporal variation of 3-point moving average of $^{87}Sr/^{86}Sr$ and ε_{Nd} of sediments from the SK187/PC33 core shows a close resemblance with regional monsoon strength (effective moisture) variability [Herzschuh, 2006]. The Sr-Nd isotopes show major change at ~20 ka and 9 ka, which coincides with weakening of monsoon at LGM and strengthening of monsoon during Holocene period respectively.*

lower ^{87}Sr/^{86}Sr and higher ε_{Nd} (Fig. 4.1). Thus, the combination of decrease in SW monsoon and increase in NE monsoon during LGM contributed to decrease the relative proportion of sediments from the Himalaya to the core site, resulting in the ^{87}Sr/^{86}Sr dip and ε_{Nd} hump (Fig. 4.8). Though the age-depth resolution of the core studied is not good enough, a similar link of monsoon strength and variability in erosion pattern is observed in the Sr-Nd isotopic profile of SK187/PC33 at ~9 ka. The BoB sediments showed an increase in their $^{87}Sr/^{86}Sr$ value and decrease in ε_{Nd} value during Holocene (Fig. 4.8). The radiogenic Sr and less radiogenic Nd isotopic composition of the BoB sediments during Holocene compared to that during post-Holocene periods indicate enhanced sediment contribution from the Himalaya, which are highly radiogenic in $^{87}Sr/^{86}Sr$ and less radiogenic in ε_{Nd} values (Fig. 4.1). The enhanced contribution from the Himalaya during Holocene coincides with the intensification of monsoon during these periods (Fig. 4.8), confirming a strong link of monsoon and erosion over a ka timescale. A relation between monsoon activity and sediment supply is consistent with the results of *Bookhagen and Burbank* [2006], who have shown that intensification of monsoon enhances sediment supply from the HH. Further, the recent study of *Rahaman et al.* [2009] on a sediment core from the Ganga plain showed a decrease in sediment contribution from the HH to the Ganga plain during the LGM, supporting the observation of the current study.

An alternative hypothesis to explain the observed variation in the relative proportion of sediment from the Himalaya and the Peninsular India is to invoke the role of hydrography and sea level changes in the Bay of Bengal in the dispersion of sediments. It can be argued that sediments from the Himalaya were transported directly to the central BoB during LGM due to lower sea level resulting in lower sediment proportion from the Himalaya at the core site. This proposition can be ruled out in case of sediments from the western BoB and particularly from the core site of SK187/PC33, as this core is from a water depth of ~3000 m and during LGM the Eastern Indian Coastal Current (EICC) was southwestward [*Sarkar et al.*, 1990; *Schott and McCreary*, 2001; *Tiwari et al.*, 2005]. The EICC was directed N-S during LGM and hence, is expected to have focused more sediments from the Himalayan rivers to the western BoB compared to present-day, where the EICC is directed S-N. If so, the western BoB would have received higher proportion of Himalayan sediments during the LGMunder the influence of N-S directed EICC.

The variations in the Sr and Nd isotope composition of core SK187/PC33 attest to the significant relation between climatic variation and continental erosion.

This hypothesis is also supported by earlier results on the variation of the Nd isotope composition of seawater and bulk sediments in the Bay of Bengal and in the Indian Ocean during the LGM and the Holocene [*Burton and Vance*, 2000; *Stoll et al.*, 2007; *Gourlan et al.*, 2010). *Burton and Vance* [2000] and *Stoll et al.* [2007] attributed changes in the Nd isotopic composition of seawater and bulk sediments during LGM to reduced erosional fluxes from the Himalaya caused by decrease in rainfall. This is consistent with the observation of this study.

Clift et al. [2008] investigated ε_{Nd} of sediments from the Indus delta. Their results show variability consistent to those observed in this study i.e. decrease in ε_{Nd} following LGM. This decrease can be attributed to relatively higher contribution of sediments from the Himalaya, particularly that from the Ganga basin, due to increase in monsoon intensity and decrease in snow cover. This interpretation is also supported by earlier observations of two-fold increase in the sediment supply from the Himalaya to the Bengal basin during these periods [*Goodbred and Kuehl*, 2000]. In contrast to this, the results of *Galy et al.* [2008a], based on Sr and Nd isotopic signatures of sediments from the channel-levee system in Bengal Fan, reported constancy in their sources since LGM. The reason behind this difference is unclear. One possible cause could be that the sampling site of *Galy et al.* [2008a] is a channel-levee system, where sediments can undergo recycling. Further, the core site of *Galy et al.* [2008a] receives sediments predominantly from G-B river, whereas the core SK187/PC33 receives sediments from the G-B rivers along with Peninsular Indian rivers and hence is able to better trace the signals of source variability.

The physical (MS), chemical and isotopic signature of SK187/PC33 showed a reduced Himalayan contribution to the BoB during LGM. These signatures of change in erosion pattern of the Himalaya during LGM are well preserved in the BOB sediments, which demonstrate the high efficiency of the Himalayan Rivers in transferring the sediments from their source (Himalaya) to the sink (BoB) with an insignificant time-lag between production of sediment in the Himalaya and their deposition in BoB. This observation hints lower residence time of the sediment of the

Himalayan rivers in the plain, far less compared to that (~100 ka) proposed by *Granet et al.* [2007] based on the U-Th data of the sediments of the Gandak river.

4.4. CONCLUSIONS

The sediments from a core in the western Bay of Bengal are characterized by highly radiogenic Sr and low ε_{Nd} values. This suggests relatively higher contribution of Himalayan-derived sediments to the core site than those from Peninsular India. The Sr and Nd isotope compositions show significant temporal variations suggesting considerable changes in the relative contributions from the Himalaya and the Peninsular India sources in the past. These variations in $^{87}Sr/^{86}Sr$ and ε_{Nd} support the hypothesis that during LGM, sediment contribution from the Himalaya was reduced due to decreased intensity of SW monsoon and increased extent of glacial cover over the High Himalaya.

CHAPTER 5

Chemical Erosion Rates of the Ganga Headwater Basins: An Inversion Model Approach

5.1. INTRODUCTION

The chemistry of river water is a combination of inputs from multiple sources that includes chemical weathering of silicates, carbonates and other lithologies of the drainage basin and atmospheric deposition. Apportionment of the chemical composition of rivers into its various sources is required to derive silicate and carbonate erosion rates (SER and CER) of their basins; data that are needed to determine CO_2 draw-down from the atmosphere. Such studies are a growing field of geochemical research in recent years due to the link between CO_2 draw-down from the atmosphere and global climate [*Ebelmen*, 1845; *Chamberlin*, 1899; *Walker et al.*, 1981; *Berner et al.*, 1983; *Raymo et al.*, 1988]. Among the major global river basins, those draining young orogenic belts, such as the Himalaya, have been suggested to contribute significantly to the enhanced CO_2 drawdown caused by the rapid uplift of the mountains and conducive climate [*Raymo and Ruddiman*, 1992; *Edmond and Huh*, 1997 *and references therein*; *Galy and France-Lanord*, 1999; *Krishnaswami et al.*, 1999; *Dalai et al.*, 2002; *Bickle et al.*, 2003; *Jacobson et al.*, 2003; *Quade et al.*, 2003; *Singh et al.*, 2005; *Tipper et al.*, 2006]. The Ganga, Brahmaputra and the Indus are the three major river systems draining the southern slopes of the Himalaya. These rivers supply large amounts of suspended and dissolved material to the adjacent seas and thus contribute significantly to the global geochemical and carbon cycles [*Raymo et al.*, 1988; *Sarin et al.*, 1989; *Raymo and Ruddiman*, 1992; *Pande et al.*, 1994; *France-Lanord and Derry*, 1997; *Karim and Veizer*, 2000; *Singh et al.*, 2005; *Galy et al.*, 2008b]. Among the various materials supplied to the Bay of Bengal by the Ganga-Brahmaputra river system, organic carbon is a key component [*Galy et al.*, 2007, 2008b], as its burial has been suggested to be another important sink of atmospheric CO_2 over geological time scale [*France-Lanord and Derry*, 1997]. Of the three river systems, the Ganga River is studied more extensively [*Sarin and Krishnaswami*, 1984; *Sarin et al.*, 1989, 1992; *Krishnaswami et al.*, 1992, 1999; *Harris et al.*, 1998; *Galy and France-Lanord*, 1999; *Galy et al.*, 1999; *English et al.*, 2000; *Bickle et al.*, 2001, 2003, 2005; *Dalai et al.*, 2002, 2003; *Evans et al.*, 2001; *West et al.*, 2002; *Oliver et al.*, 2003; *Quade et al.*, 2003; *Tipper et al.*, 2006; *Rai et* *al.*, 2010; *Tripathy et al.*, 2010b]. These studies constrain the role of these rivers in contributing to the global CO_2 draw-down, dissolved elemental fluxes and marine $^{87}Sr/^{86}Sr$ evolution. The various sub-basins of the Ganga have been studied by different groups, for example, the headwaters of the Ganga, the Bhagirathi, the Alaknanda and the Yamuna by *Sarin et al.* [1989, 1992]; *Krishnaswami et al.* [1992, 1999]; *Dalai et al.* [2002, 2003]; *Bickle et al.* [2003, 2005], the Ghaghra sub-basin by *Galy and France-Lanord* [1999]; *Galy et al.* [1999]; *English et al.* [2000], the Gandak sub-basin by *Galy and France-Lanord* [1999]; *Galy et al.* [1999]; *Tipper et al.* [2006] and the Kosi sub-basin by *Harris et al.* [1998]; *Oliver et al.* [2003]; *Quade et al.* [2003]. In addition to these tributaries, the Ganga in the plain has also been studied in some detail by *Galy and France-Lanord* [1999], *Galy et al.* [1999], and *Rai et al.* [2010]. These studies were carried out on minor to sub-basin scale of the Ganga tributaries or sub-tributaries to understand the chemical erosion pattern and their impact to global atmospheric budget.

The available results show that in most of the Ganga tributaries in the Himalaya the budgets of dissolved major element are dominated by carbonate weathering [*Sarin et al.*, 1989] with silicate weathering playing a subordinate role. The contributions of silicate derived cations to the elemental budgets of these rivers show significant spatial variability and the magnitude of silicate weathering highlights its importance as a driver of the Cenozoic global cooling. The studies concerning the erosion in the Ganga system are limited to one or two sub-basins of the Ganga [*Sarin et al.*, 1992; *Galy and France-Lanord*, 1999; *English et al.*, 2000; *Dalai et al.*, 2002; *Oliver et al.*, 2003; *Quade et al.*, 2003; *Bickle et al.*, 2005; *Tripathy et al*., 2010b]. A comprehensive study encompassing all the sub-basins of the Ganga headwaters would useful in gaining better information on the contemporary weathering processes and the factors influencing them over the entire Himalaya. In light of this, in the present study, the existing geochemical and isotopic information on the various sub-basins of the Ganga headwaters are reanalyzed. These geochemical and isotopic compositions of the dissolved solutes have been used to apportion their sources by both forward and inverse models and to derive SER and

CER. Further, a unique approach based on the inverse model has been developed to evaluate the magnitude of calcite precipitation in the various basins.

5.2. THE GANGA BASIN

5.2.1 Geology

The lithology of the river basins of the Ganga system in the Himalaya are broadly classified into four litho-tectonic units [*Gansser, 1964*; *Valdiya*, 1980; *Colchen et al*., 1986; *Le Fort*, 1989]. These are discussed in detail in many of the earlier publications on river water chemistry [*Sarin et al.*, 1989; *English et al.*, 2000; *Dalai et al.*, 2002; *Bickle et al.*, 2003, 2005; *Singh et al.*, 2008]. Briefly, these are

1. The Tethyan Sedimentary Series (TSS): The TSS outcrop towards north of the Higher Himalaya, has cold, dry climate and sparse vegetation with an average elevation of 4900 m. The TSS is composed of less altered limestones, amphibole calc-silicates with biotite, muscovite and chlorite outcrops [*Colchen et al.*, 1986]. The metamorphism of these rocks reaches lower greenschists facies near the boundary of the HH and TSS and their metamorphic grade decreases towards the north of TSS [*Tipper et al.*, 2006; *Crouzet et al*., 2007]. No evaporites have been reported in TSS region drained by the Ganga headwaters [*Bordet et al., 1971*]. Anthropogenic interference is expected to be negligible in these regions as they are sparsely populated. Some of the source waters of the Alaknanda, Ghaghra, Gandak and the Kosi drain the TSS.
2. Higher Himalaya (HH): The main component of the Higher Himalayan unit is high-grade granitoid gneisses, schist, granites, and marbles [*Gansser*, 1964; *Le Fort*, 1989] with minor amounts of carbonates and calc-silicates. The HH has an average elevation of 4700 m and about 30% of the HH area is covered with snow and glaciers [*Pandey et al.*, 1999; *Vance et al.*, 2003].
3. Lesser Himalaya (LH): Low grade sedimentary and crystalline rocks make up the LH. Greywacks, shales, slates, limestones and dolomites are found in LH. The exposed crystalline rocks in LH are gneisses, granites, schists, calc-

silicates and amphibolites [*Valdiya, 1980; Le Fort*, 1989; *Thakur and Rawat, 1992*].

4. Siwaliks: The Siwaliks is composed of the eroded materials from the HH and LH, transported by the Himalayan Rivers [*Quade et al.*, 1997].

To better evaluate the impact of lithology on erosion the exposure areas of silicate and carbonate lithologies in the drainages were inferred from geological maps [*Valdiya*, 1980], alluvial clast count [*English et al.*, 2000; *Quade et al.*, 2003] and non-carbonate contents of the suspended sediments [*Galy and France-Lanord*, 1999]. The silicate exposure areas in the various sub-basins of the Ganga are listed in Table 5-1, which shows that the Bhagirathi and the Kosi basins have relatively larger exposures of silicates.

Table 5-1: Silicate bed rock exposure area for the tributaries of the Ganga.

River	Silicate bedrock exposure area (%)	Method
Alaknanda	91	*Quantified from the map of Valdiya* [1980]
Bhagirathi	95	*Quantified from the map of Valdiya* [1980]
Yamuna	75	*Quantified from the map of Valdiya* [1980]
Kosi (Arun)	98	*Alluvial Clast counts by Quade et al.* [2003]
Gandak	< 95-60%	*non-carbonate content in suspended sediments by France-Lanord et al.* [2003]
Ghaghra	75%	*Alluvial Clast counts by English et al.* [2000]

5.2.2 Hydrology

The river “Ganga” is formed at Devprayag by the confluence of the Bhagirathi and the Alaknanda (Fig. 5.1). The mainstream Ganga enters the plain at Hardwar after cutting across the Siwaliks ranges. In the plain, the Ganga is joined by a number of tributaries from its right bank (the Ramganga, the Gomti, the Ghaghra, the Gandak and the Kosi) and from the left bank (the Yamuna, the Tons and the Son; Fig. 5.1). The Himalayan catchment of the Ganga tributaries has a runoff of about 1 m/y and accounts for ~54% of its water discharge [*Singh et al.*, 2008], with a maximum of ~1.55 m/y in the Gandak sub-basin and minimum of 0.50 m/y over the headwaters of the Kosi sub-basin (Table 5-2). The balance water to the Ganga is supplied from the peninsular and plain regions.

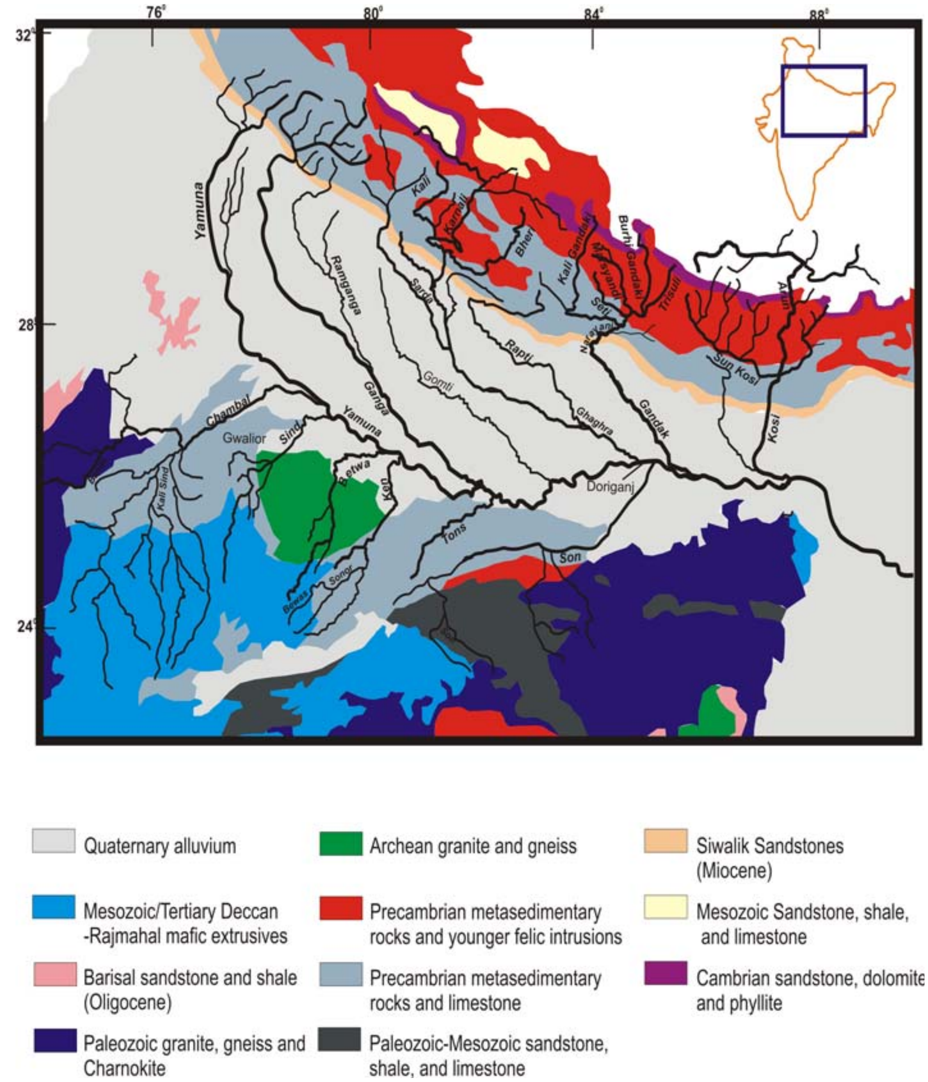

Figure 5.1: *Geological map of the drainage basins of the Ganga and its major tributaries [modified after Sarin et al., 1989; Mukherjee et al., 2009].*

5.2.3 Sources of Data

A large number of geochemical studies of the Ganga river have been carried out during the last two decades following the studies of *Handa* [1972] and *Sarin and Krishnaswami* [1984]. The existing data on the stream chemistry of Ganga headwaters [*Sarin et al.*, 1989, 1992; *Krishnaswami et al.*, 1992, 1999; *Harris et al.*, 1998; *Galy and France-Lanord*, 1999; *Galy et al.*, 1999; *English et al.*, 2000; *Dalai et al.*, 2002, 2003; *Bickle et al.*, 2003, 2005; *Oliver et al.*, 2003; *Quade et al.*, 2003; *Tipper et al.*, 2006] are compiled for this study and the data used to estimate contributions from various sources and chemical erosion rates are given in Appendix (Table S1).

Table 5-2: Sources of the data and details of the tributaries of the Ganga in the Himalaya.

River	Elevation (m)	Drainage Area (10^3 km^2)	Water Discharge (10^{12} l/y)	Location	Runoff m/y	Lithology	Source of data
Bhagirathi	3812[1]	7.8	8.3	Devprayag[7]	1.06	LH+HH	7, 11, 12, 16, 18
Alaknanda	3800[2]	11.8	14.1	Bhagwan[7]	1.19	LH+HH+TSS	7, 11, 12, 16, 18
Ganga	-	19.6	22.4	Rishikesh[7]	1.14	LH+HH+TSS	7, 8, 11, 13, 15, 16, 18
Yamuna	300-6400	9.6[3]	10.8	Batamandi[8]	1.13	LH+HH	8, 15
Ghaghra	100[5] - >5000[4]	42.9	42.7	Chisapani[9]	1.00	LH+HH+TSS	6, 10, 14
Gandak	200-7000[5]	31.8	49.4	Narayan Ghat[10]	1.55	LH+HH+TSS	10, 14, 20
Kosi	400-5500	28.2	13.3	Turkeghat[9]	0.47	LH+HH+TSS	4, 17, 19

[1]*Pandey et al.*, 1999; [2]*Singh and Hasnain*, 1998; [3]*Dalai*, 2001; [4]*Oliver et al.*, 2003; [5]*Galy*, 1999; [6]*English et al.*, 2000; [7]*Krishnaswami et al.*, 1999; [8]*Dalai et al.*, 2002; [9]*GRDC discharge metadata set* (http://grdc.bafg.de/); [10]*Galy and France-Lanord*, 1999; [11]*Sarin et al.*, 1989; [12]*Sarin et al.*, 1992; [13]*Krishnaswami et al.*, 1992; [14]*Galy et al.*, 1999; [15]*Dalai et al.*, 2003; [16]*Bickle et al.*, 2003; [17]*Quade et al.*, 2003; [18]*Bickle et al.*, 2005; [19]*Harris et al.*, 1998; [20]*Tipper et al.*, 2006.

5.3. Chemistry and ^{87}Sr/^{86}Sr of the Ganga headwaters

Ternary plots of the data (Fig. 5.2) show that with respect to anions most of the samples fall near the HCO_3 apex compared to $Cl+SO_4$ and Si apex and with respect to cations towards the Ca apex. These results coupled with the observation that (Ca+Mg) charge is roughly balanced by HCO_3, suggests that solute budget of these rivers is dominated by carbonate weathering, a conclusion derived by earlier workers [*Sarin et al.*, 1989; *Krishnaswami and Singh*, 1998; *Galy and France-Lanord*, 1999; *Dalai et al.*, 2002]. Exception to the general trend are some samples of the Ghaghra and a few from the Gandak and Kosi, which fall near the (Na+K) apex indicating comparatively higher contribution from silicates and/or halites [*Galy and France-Lanord*, 1999]. The latter option is less likely due to the lower abundance of ($Cl+SO_4$) in their anion budget. The higher silicate weathering in the Ghaghra basin is consistent with the lower Na content of its suspended loads compared to that in the other streams [*Pierson-Wickmann*, 2000; *Lupker et al.*, 2009]. The physical erosion

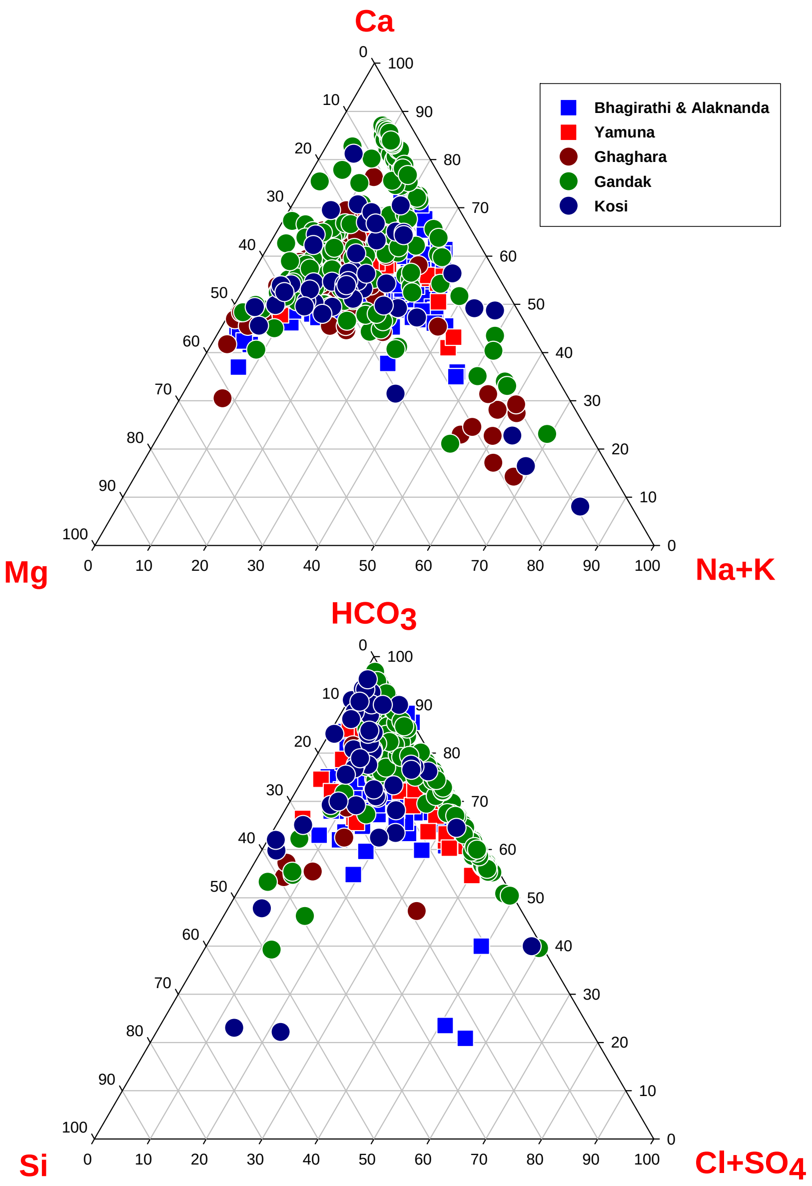

Figure 5.2: *Ternary diagram of the chemical composition (in molar units) of the Ganga headwaters. The data suggests dominance of carbonate weathering in the basin.*

rate in the Ghaghra is estimated to be low compared to the Gandak and Kosi [*Singh et al.*, 2008]. The higher silicate contribution to the Ghaghra water, despite relatively lower physical erosion, therefore can be attributed to transport limited intense chemical weathering in the basin.

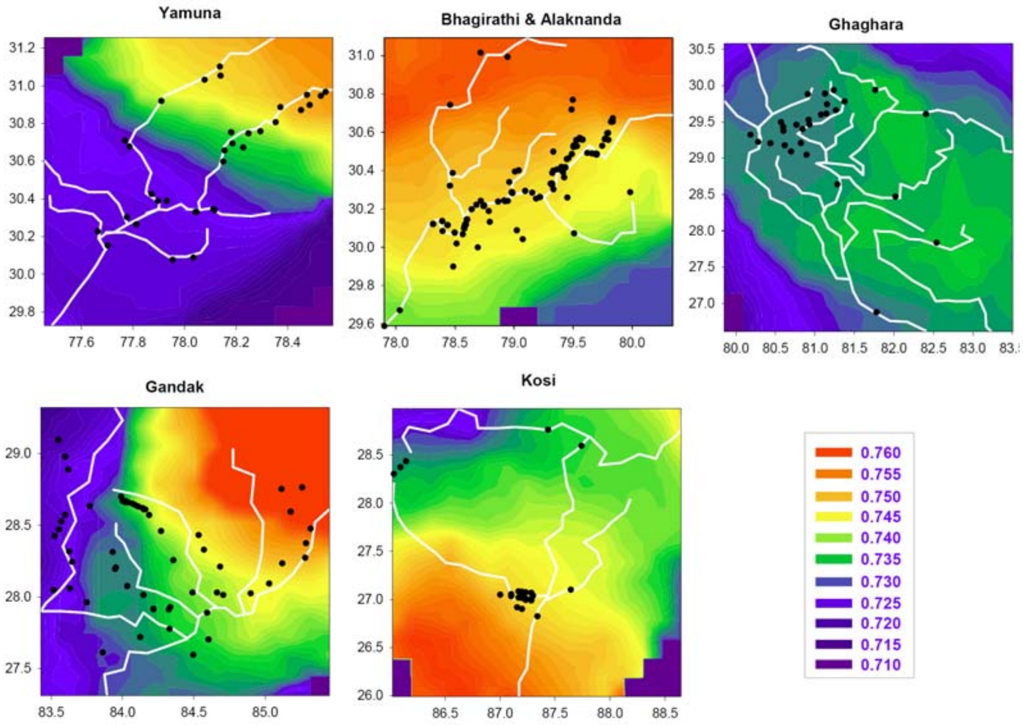

Figure 5.3: *Spatial variation of dissolved ^{87}Sr/^{86}Sr for the different tributaries of the Ganga headwaters. Higher ^{87}Sr/^{86}Sr values indicate relatively high silicate weathering especially in the Kosi and Bhagirathi basins. The black dots in the figure represent the sampling points used to construct the contours.*

The spatial variability of dissolved ^{87}Sr/^{86}Sr among the headwaters synthesized from available data [*Galy et al.*, 1999; *Krishnaswami et al.*, 1999; *English et al.*, 2000; *Bickle et al.*, 2003, 2005; *Dalai et al.*, 2003; *Oliver et al.*, 2003; *Quade et al.*, 2003] is shown in Fig. 5.3. All the Ganga headwaters have distinguishably higher ^{87}Sr/^{86}Sr (0.722 to 0.782) compared to the "average" global river [0.712; *Krishnaswami et al.*, 1992; *Palmer and Edmond*, 1992]. The Sr isotopic ratio shows wide variation among the various sub-basins of the Ganga. Between the Bhagirathi and the Alaknanda, the source waters of the Ganga, the Bhagirathi is more radiogenic, though the Alaknanda with lower ^{87}Sr/^{86}Sr exerts larger control on the ^{87}Sr/^{86}Sr of the Ganga after their confluence at Devprayag due to its higher Sr flux. The Kosi River supplies waters with the most radiogenic Sr to the mainstream of the Ganga (Fig. 5.3). The source of the high ^{87}Sr/^{86}Sr in the Ganga water is a topic of debate, though there seems to be a convergence that it is dominated by supply from highly radiogenic Precambrian granites and gneisses [*Krishnaswami et al.*, 1992; *Galy and France-Lanord*, 1999; *Bickle et al.*, 2003]. It is also borne out that metamorphosed carbonates enriched in radiogenic Sr could be important locally [*Palmer and Edmond*, 1992; *Quade et al.*, 1997; *Singh et al*., 1998; *Bickle et al*., 2001].

5.4. Source apportionment

One of the objectives of this study is to apportion the sources of cations and Sr to the headwaters of the Ganga following a uniform approach for all the sub-basins. The contribution of sources to dissolved major ions budget in rivers can be derived either by forward modeling [*Galy and France-Lanord*, 1999; *Krishnaswami et al.*, 1999; *Dalai et al*., 2002; *Quade et al*., 2003; *Singh et al*., 2005; *Tipper et al*., 2006] using suitable proxies, such as, Na_s, ($Na_s = Na_r – Cl_r$) or Mg [*Das et al.*, 2005] or by inverse modeling [*Negrel et al.*, 1993; *Gaillardet et al.*, 1999; *Millot et al.*, 2003; *Wu et al.*, 2005; *Moon et al.*, 2007]. Earlier studies in the Himalaya by and large employed the forward model for source apportionment [*Galy and France-Lanord*, 1999; *Krishnaswami et al.*, 1999; *Dalai et al.*, 2002; *Singh et al.*, 2005; *Tipper et al.*, 2006]. In this study, the inverse model has been used to apportion the sources of the dissolved material to the Ganga headwaters and its Himalayan tributaries. Further, the results obtained by the inverse model are compared with those derived from the forward model and their implications discussed. A key difference between the two models is that in the forward model the release ratios of various major ions from the source rocks to the rivers is assumed whereas in the inverse model it is the best fit derived by iteration of the measured data.

For source apportionment Na normalized elemental ratios are used because Na behaves conservatively in river systems; in addition its sources are better constrained. In basins where Na budget is difficult to constrain due to presence of alkaline and saline salts Mg and Si have been used as indices of silicate weathering [*Das et al.*, 2005; *Rai et al.*, 2010; *Rengarajan et al.*, 2009]. Ca, the most abundant cation in rivers, is not used as the normalizing element as it can behave nonconservatively; it may be removed from solution by calcite precipitation particularly during low flow periods. In addition, Ca and Mg in the rivers are derived from multiple sources. Similarly the use of K is also limited, as it is bio-reactive element and both Mg and K are known to be affected by secondary mineral formation processes in the basin [*Galy and France-Lanord*, 1999].

5.4.1 Forward Model

The forward modeling approach assumes that dissolved Na in rivers is derived from two sources, (atmosphere+halite) and silicate weathering and that the (atmosphere+halite) contribution of Na is equal to that of dissolved Cl. This makes the silicate derived Na (Na_s) to be equal to

$$Na_s = Na_r - Cl_r \qquad \text{-------} \quad 5\text{-}1$$

where, Na_r and Cl_r are the concentrations of dissolved Na and Cl in the rivers.

Na_s along with assumed ratios of (Ca/Na) and (Mg/Na) released from the silicates to rivers [*Krishnaswami et al.*, 1999] are used to estimate the cations derived from silicate weathering to river waters. Generally, the release ratios of Ca/Na and Mg/Na are taken to be their average abundance ratios in the silicates of the basin. The model therefore assumes congruent weathering of Na, Ca and Mg from silicates. However, in some of the Himalayan studies [*Singh et al.*, 1998; *Krishnaswami et al.*, 1999; *Dalai et al.*, 2002], the elemental ratios of Ca, Sr, Mg used in the forward model are based on the composition of bed rock, soil profiles and tributaries draining predominantly silicates. In these studies, therefore there is no assumption of congruent weathering. Cations derived from silicates are as given below:

$$Na_s = Na_r - Cl_r$$

$$K_s = K_r \qquad \text{-----} \quad 5\text{-}2$$

$$Ca_s = Na_s \times \left(\frac{Ca}{Na}\right)_{sol} \qquad \text{-----} \quad 5\text{-}3$$

$$Mg_s = Na_s \times \left(\frac{Mg}{Na}\right)_{sol} \qquad \text{-----} \quad 5\text{-}4$$

where, $\left(\frac{X}{Na}\right)_{sol}$ is the molar ratio with which the element X is released to rivers from the silicate rocks. The estimates of silicate derived cations by the forward model therefore depend critically on the $\left(\frac{X}{Na}\right)_{sol}$ ratio used in the calculation. This ratio, though varies widely in parent rocks [*Krishnaswami et al.*, 1999], it is expected to average out in large river basins, such as the basins of the Himalayan tributaries of the Ganga. The fraction of dissolved cations supplied from silicates to the river ($Cat_S = 100 \times \left(\frac{Na_s + K_s + Mg_s + Ca_s}{Na_r + K_r + Mg_r + Ca_r}\right)$) was estimated following the approach of *Krishnaswami et al.* [1999].

5.4.2 Inverse Modeling

Inverse model has also been used to derive the cation contribution from different sources to river waters [*Negrel et al.*, 1993; *Gaillardet et al.*, 1999; *Millot et al.*, 2003; *Wu et al.*, 2005; *Moon et al.*, 2007]. The inverse model calculates not only the contribution of various sources to the solute budget of the river but also the best values for elemental ratios of the end members [*Negrel et al.*, 1993]. The calculations rely on a set of mass balance equations which defines the relation between observed data and the model parameters, e.g.,

$$\left(\frac{X}{Na}\right)_r = \sum_{i=1}^{n}\left(\frac{X}{Na}\right)_i \times f_i(Na) \qquad \text{-----} \quad 5\text{-}5$$

where, X=Cl, Ca, Mg, Sr, HCO_3 and

$$\left[\frac{^{87}Sr}{^{86}Sr} \times \left\{\frac{Sr}{Na}\right\}\right]_r = \sum_{i=1}^{n}\left(\frac{^{87}Sr}{^{86}Sr}\right)_i \times \left(\frac{Sr}{Na}\right)_i \times f_i(Na) \qquad \text{-----} \quad 5\text{-}6$$

where, $\left(\frac{X}{Na}\right)_i$ is the molar ratio with which the element X is released to rivers from the end member *i*. In this study, four end-members (n=4) are considered, (i) silicates, (ii) carbonates+gypsum, (iii) atmosphere+halites and (iv) hot springs and $f_i(Na)$ is the fraction of Na in the river contributed from source i.

$$\sum_{i=1}^{n} f_i(Na) = 1 \qquad \text{-----} \quad 5\text{-}7$$

In general, equations (5-5 to 5-7) can be written as $d = g(p)$, where *d* and *p* are the data and model spaces respectively. The model spaces are assumed to follow log-normal probability distribution. A non-linear weighted fit of equations (5-5 to 5-7) was obtained using the Quasi-Newton method [*Tarantola*, 2005], which provided the best possible set for the model parameters and the covariance (i.e, uncertainties) associated with them.

Table 5-3: Comparison of results obtained from inverse model used in this study and those of Millot et al. (2003) using same set of end-members.

	Cat_s (%)		**Cat_c (%)**		**Sr_s (%)**		**Sr_c (%)**	
	Millot	Present	Millot	Present	Millot	Present	Millot	Present
CAN96-5	8	9	90	76	19	17	77	89
CAN96-6	11	10	82	83	11	10	49	51
CAN96-7	6	6	94	79	14	11	86	87
CAN96-15	7	8	92	97	12	11	88	84
CAN96-25	16	18	71	64	15	25	44	55
CAN96-26	7	7	93	95	15	10	85	88
CAN96-37	13	15	85	73	17	26	78	78
CAN96-38	16	20	79	73	15	28	62	62
CAN96-42	26	31	72	72	11	35	86	49

Millot: Millot et al. (2003); Present: Present Model

The consistency of the approach was checked by analysing the data of the Mackenzie River which were analysed earlier by *Millot et al.* [2003] using inverse model to estimate contributions from different sources. The *a-priori* input for various ratios used in the present study is the same as that used by *Millot et al.* [2003]. For $^{87}Sr/^{86}Sr$ of the silicate end-member, a value of (0.73±0.01) is used, as the same is not reported by *Millot et al.* [2003]. The results obtained in this study (Table 5-3; Fig. 5.4) are in good agreement with those of *Millot et al.* [2003] for silicates and carbonates, suggesting that the approach followed in this work are consistent with earlier studies.

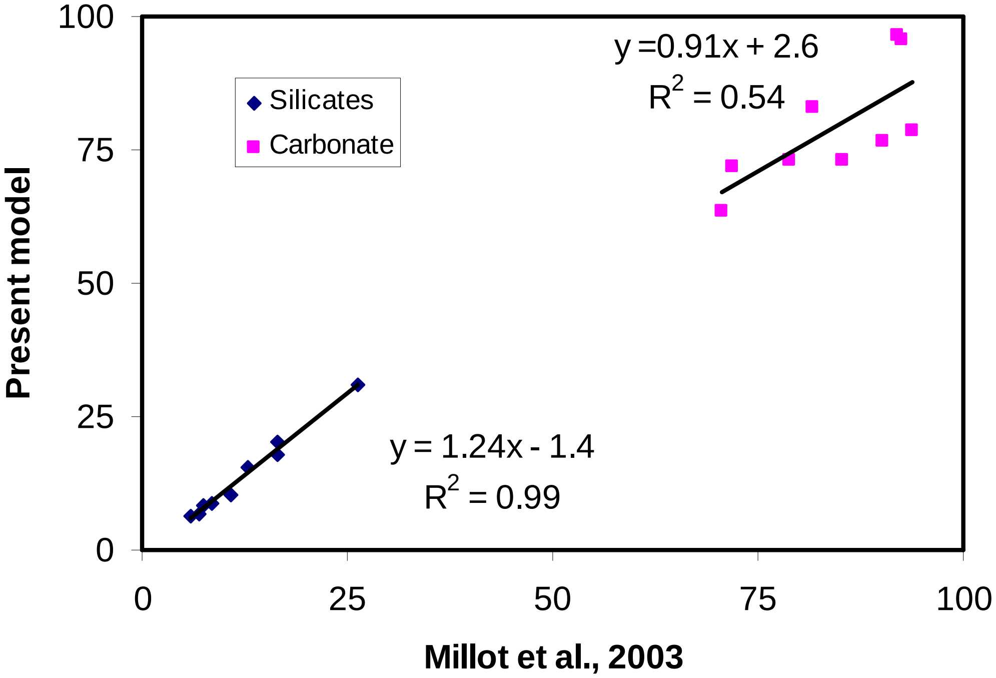

Figure 5.4: *Reanalysis of Mackenzie river water data. Correlation between results obtained based on the present analysis and those of Millot et al. [2003] using the same end members. The good correlation between the two sets of data indicates consistency of both the models.*

The use of inverse modeling to apportion the sources of dissolved components of rivers can be done based either on the data of the entire samples of the basin [*Moon et al.*, 2007] or a single sample at a time [*Negrel et al.*, 1993]. In this study, all samples of a sub-basin are modeled together to yield a number of mass balance equations which can provide the best fit for the *a-posteriori* end member values for the basin. Further, the source apportionment using the inverse model was done for the main stream and for the large tributaries in the Himalayan catchment for the monsoon and non-monsoon samples separately (*c.f.* Appendix). Samples with anomalous compositions and from small streams are not considered in the modeling. Silicate and carbonate contributions to the solute budget are calculated after obtaining the *a-posteriori* model parameters for different sources.

5.4.2.1 *A-priori* values of end members

Na is used for normalization in both the inverse model and the forward model. The elemental and isotopic ratios for atmospheric input were calculated from the rainwater composition reported for the Himalayan regions [*Galy and France-Lanord,* 1999; *Galy et al.*, 1999]. The elemental ratios for the silicate end member were taken to be the same as those used by *Krishnaswami et al.* [1999]. The abundance ratios of various elements in the carbonate end member are based on the chemical composition of Pre-Cambrian carbonates from the Lesser Himalaya [*Singh et al.*, 1998; *Bickle et al.*, 2001]. Sodium concentrations in ten carbonate samples for which other elemental abundances data are reported by *Singh et al.* [1998] was determined in this study and are provided in Table 5-4. Gypsum and carbonate end members were combined owing to similarity in their elemental ratios [*Moon et al.*, 2007].

Table 5-4 Sodium concentration in 0.1N HCl leach of Himalayan carbonates.

SampleID	**UK94-97**	**UK95-7**	**KU92-22**	**UK95-6**	**UK95-19**	**UK95-23**	**KU92-13**	**UK95-24**	**HP94-43**	**UK95-3**
Na (%)	0.016	0.023	0.001	0.008	0.001	0.005	0.005	0.004	0.003	0.003

The *a-priori* end member values used are listed in Table 5-5. The end member composition of the hot springs is from *Evans et al.* [2001, 2004]. The *a-priori* ratios of carbonates have large uncertainties due to significant spread in their composition. To assess the effect of the wide range in elemental ratios in carbonates on the results,

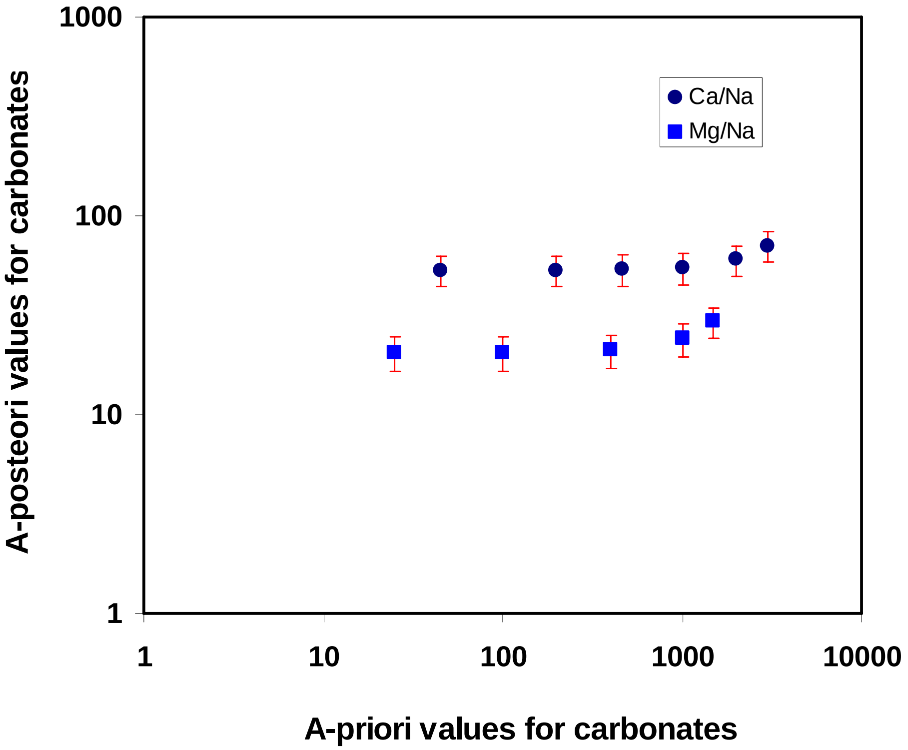

Figure 5.5: *Sensitivity test for the inverse model using a wide range of a-priori ratios for the carbonate end members, the convergence of the a-posteriori value for different a-priori ratios indicates that the model is nearly independent of the a-priori values.*

a sensitivity test of the inverse model was done for the monsoon samples of the Ganga at Rishikesh by varying the *a-priori* Ca/Na ratios by nearly two orders of magnitude (3000, 2000, 1000, 460, 200, 45) while keeping other ratios unchanged. Despite the orders of magnitude difference in the *a-priori* Ca/Na values, the calculated *a-posteriori* ratios converged to nearly the same value (Fig. 5.5). Similarly, the *a-posteriori* Mg/Na ratios also converged to nearly the same value despite a variation in the *a-priori* values from 1500 to 25. These tests (Fig. 5.5) establish that the model results are not critically dependent on the assigned *a-priori* values of Ca/Na and Mg/Na. A similar sensitivity test was also carried out for $f_i(Na)$ by using three different sets of *a-priori* values for $f_i(Na)$ [(0.5±0.4, 0.4±0.4, 0.2±0.1) for rain; (0.7±0.6, 0.6±0.5, 0.7±0.2) for silicates; (0.35±0.25, 0.25±0.2, 0.2±0.1) for carbonates and (0.35±0.3, 0.3±0.2, 0.15±0.1) for hot springs] for the monsoon samples of the Ganga (Rishikesh). These three different sets of *a-priori* values of $f_i(Na)$ converged to statistically same *a-posteriori* values after the inversion. This suggests that the results of the inverse model are nearly independent of the *a-priori* data on $f_i(Na)$ and $\left(\frac{X}{Na}\right)$ values.

Table 5-5: *A-priori* molar ratio for the various ends members and associated uncertainties (1σ).

	Rain[1,2]	Silicates[3]	Carbonates[4,5]	HotSprings[6]
Cl/Na	*0.74±0.1*	*0.00*	*0.00*	*1.2*±0.3
Ca/Na	*2.2±0.11*	*0.7±0.3*	*3000±2000*	*4.4±0.8*
Mg/Na	*0.6±0.1*	*0.3±0.2*	*1500±1000*	*0.024±0.012*
Sr/Na	*2.1±0.5*	*2.0±0.8*	*350±200*	*1.2±0.13*
^{87}Sr/^{86}Sr	*0.714±0.004*	*0.8±0.2*	*0.715±0.02*	*0.77±0.02*
Alk/Na	*6.8±0.5*	*2±1*	*8000±4000*	*10±4*

Errors are ±1σ; Sr/Na is in nM/μM units; [1]*Galy and France-Lanord*, 1999; [2]*Galy et al.*, 1999; [3]*Krishnaswami et al.*, 1999; [4]Present study; [5]*Singh et al.*, 1998; [6]*Evans et al.*, 2001

5.4.2.2 *A-posteriori* results

Table 5-6 lists the *a-posteriori* values obtained for the different sub-basins of the Ganga during monsoon and their comparison with the *a-priori* values (Table 5-5). The monsoon samples have been used for comparison as in some of these rivers, there is a possibility of loss of Ca as calcite during non-monsoon. The results of the inversion model show spatial variability in Ca/Na values for the silicate end member of different sub-basins. The *a-posteriori* $\left(\frac{Ca}{Na}\right)_{sol}$ for the Kosi (0.36±0.14) and the Ghaghra (0.29±0.12) overlaps within errors with that reported [0.41±0.18; *English et al.*, 2000; *Quade et al.*, 2003] for streams draining predominantly silicate terrain in the central and the western Nepal Himalaya. Similarly, the *a-posteriori* $\left(\frac{Ca}{Na}\right)_{sol}$

Table 5-6: *A-posteriori* results from the inverse model for monsoon samples of the Ganga tributaries.

Bhagirathi

	Rain	Silicates	Carbonates	Hotspring
Cl/Na	0.76 ± 0.10	0 ± 0	0 ± 0	0.87 ± 0.18
Ca/Na	2.19 ± 0.11	0.68 ± 0.29	154 ± 36	4.73 ± 0.84
Mg/Na	0.60 ± 0.10	0.20 ± 0.13	76 ± 17	0.02 ± 0.01
Sr/Na	2.31 ± 0.54	1.35 ± 0.49	210 ± 49	1.14 ± 0.13
$^{87}Sr/^{86}Sr$	0.714 ± 0.004	0.801 ± 0.020	0.720 ± 0.018	0.770 ± 0.020
HCO_3/Na	6.64 ± 0.49	1.29 ± 0.63	304 ± 71	9.51 ± 3.38

Alaknanda

	Rain	Silicates	Carbonates	Hotspring
Cl/Na	0.71 ± 0.09	0 ± 0	0 ± 0	0.83 ± 0.17
Ca/Na	2.18 ± 0.11	0.64 ± 0.27	137 ± 27	4.48 ± 0.81
Mg/Na	0.66 ± 0.11	0.43 ± 0.27	44 ± 10	0.02 ± 0.01
Sr/Na	2.00 ± 0.46	1.21 ± 0.46	155 ± 30	1.14 ± 0.13
$^{87}Sr/^{86}Sr$	0.714 ± 0.004	0.800 ± 0.020	0.719 ± 0.016	0.770 ± 0.020
HCO_3/Na	6.73 ± 0.49	1.63 ± 0.80	329 ± 64	10.11 ± 3.95

Ganga (Rishikesh)

	Rain	Silicates	Carbonates	Hotspring
Cl/Na	0.83 ± 0.09	0 ± 0	0 ± 0	0.72 ± 0.14
Ca/Na	2.18 ± 0.11	0.70 ± 0.28	71 ± 12	5.06 ± 0.87
Mg/Na	0.63 ± 0.10	0.36 ± 0.19	29 ± 5	0.02 ± 0.01
Sr/Na	2.31 ± 0.53	1.14 ± 0.40	107 ± 18	1.13 ± 0.13
$^{87}Sr/^{86}Sr$	0.714 ± 0.004	0.800 ± 0.020	0.721 ± 0.015	0.770 ± 0.020
HCO_3/Na	6.60 ± 0.48	1.36 ± 0.64	161 ± 29	13.58 ± 4.27

Yamuna

	Rain	Silicates	Carbonates	Hotspring
Cl/Na	0.92 ± 0.09	0 ± 0	0 ± 0	0.57 ± 0.08
Ca/Na	2.28 ± 0.11	0.56 ± 0.16	27 ± 4	4.42 ± 0.01
Mg/Na	0.71 ± 0.10	0.09 ± 0.05	14 ± 2	0.03 ± 0.02
Sr/Na	2.08 ± 0.05	1.53 ± 0.22	48 ± 6	0.90 ± 0.10
$^{87}Sr/^{86}Sr$	0.714 ± 0.004	0.803 ± 0.019	0.725 ± 0.014	0.766 ± 0.020
HCO_3/Na	6.45 ± 0.47	1.79 ± 0.53	40 ± 6	16.17 ± 1.55

Ghaghra (Karnali)

	Rain	Silicates	Carbonates	Hotspring
Cl/Na	0.80 ± 0.10	0 ± 0	0 ± 0	1.54 ± 0.33
Ca/Na	2.17 ± 0.11	0.29 ± 0.12	65 ± 18	3.68 ± 0.65
Mg/Na	0.61 ± 0.10	0.41 ± 0.25	262 ± 62	0.02 ± 0.01
Sr/Na	2.05 ± 0.49	1.54 ± 0.46	351 ± 84	1.15 ± 0.13
$^{87}Sr/^{86}Sr$	0.714 ± 0.004	0.799 ± 0.020	0.715 ± 0.018	0.770 ± 0.020
HCO_3/Na	6.74 ± 0.49	1.32 ± 0.61	504 ± 122	8.06 ± 3.18

Gandak (Trisuli)

	Rain	Silicates	Carbonates	Hotspring
Cl/Na	0.98 ± 0.10	0 ± 0	0 ± 0	0.58 ± 0.09
Ca/Na	2.17 ± 0.11	0.50 ± 0.20	54 ± 9	6.77 ± 0.99
Mg/Na	0.80 ± 0.11	0.32 ± 0.12	11 ± 2	0.02 ± 0.01
Sr/Na	1.98 ± 0.44	1.46 ± 0.51	110 ± 18	1.12 ± 0.13
$^{87}Sr/^{86}Sr$	0.714 ± 0.004	0.800 ± 0.020	0.716 ± 0.015	0.769 ± 0.020
HCO_3/Na	6.45 ± 0.46	1.21 ± 0.57	109 ± 20	19.15 ± 3.45

Kosi (Arun)

	Rain	Silicates	Carbonates	Hotspring
Cl/Na	0.89 ± 0.10	0 ± 0	0 ± 0	0.95 ± 0.19
Ca/Na	2.15 ± 0.11	0.36 ± 0.14	29 ± 7	3.93 ± 0.69
Mg/Na	0.54 ± 0.08	0.07 ± 0.04	11 ± 2	0.02 ± 0.01
Sr/Na	4.02 ± 0.61	1.56 ± 0.31	49 ± 11	1.14 ± 0.13
$^{87}Sr/^{86}Sr$	0.714 ± 0.004	0.794 ± 0.019	0.707 ± 0.019	0.769 ± 0.020
HCO_3/Na	6.16 ± 0.43	0.68 ± 0.31	69 ± 15	5.71 ± 2.06

Sr/Na ratios are in nM/μM and other ratios are in μM/μM.

values for the Bhagirathi (0.68±0.29), Alaknanda (0.64±0.27), Ganga (Rishikesh) (0.70±0.28) and the Yamuna (0.56±0.16) are the same within errors and are consistent with the value of (0.70±0.30) used by *Krishnaswami et al.* [1999] for these rivers, based on (Ca/Na) of parent rocks, soil profiles and streams flowing predominantly through silicate terrain in the central Himalaya. A critical look at the *a-posteriori* values of Ca/Na for these different sub-basins, however seems to indicate that they are systematically lower compared to the *a-priori* ratios, though they overlap within their uncertainties.

The *a-posteriori* $\left(\frac{Mg}{Na}\right)_{sol}$ for the Gandak and Ghaghra basins (Table 5-6) are similar and consistent with the ratios of rivers (0.24±0.10) draining the central Himalaya containing non-carbonate sediments [*Quade et al.*, 2003]. The $\left(\frac{Mg}{Na}\right)_{sol}$ for the Bhagirathi, Alaknanda and the Ganga rivers is very close to the estimated ratio of (0.3±0.2) [*Krishnaswami et al.*, 1999]. The *a-posteriori* $\left(\frac{Sr}{Na}\right)_{sol}$ values for different rivers are nearly the same within errors (1.35±0.49; 1.21±0.46; 1.14±0.40; 1.53±0.22; 1.54±0.46; 1.46±0.51; 1.56±0.31 for Bhagirathi, Alaknanda, Ganga (Rishikesh), Yamuna, Ghaghra, Gandak and Kosi respectively), however all these values are lower compared to the average Sr/Na ratio of the silicate bed rocks (2.0±0.8) [*Krishnaswami et al.*, 1999]. This suggests the possibility of incongruent weathering of silicates in the Himalayan catchment of the Ganga with Na being weathered preferentially over Sr. The inverse model provides the best fit release ratios of the elements from silicates based on measured compositions and therefore is better suited to evaluate the role of incongruent release of elements during weathering. This is unlike the forward model which estimates the contribution of silicates to the dissolved Sr based on the assumed release ratios, generally assumed to be the same as the bed rocks. A similar difference between the results obtained using the forward and the inverse models were also reported for the Red river basin [*Moon et al.*, 2007].

Table 5-7: Source apportionment for cations and Sr (in %) and silicate, carbonate erosion rates* for the streams.

	Cat$_{rain}$	Cat$_{s}$	Cat$_{c}$	Cat$_{spring}$	Sr$_{rain}$	Sr$_{s}$	Sr$_{c}$	Sr$_{spring}$	Ca loss (%)	SER	CER	CO_2 drawdown
										tons/km^2/yr		10^5 moles/km^2/yr
Bhagirathi	10 ± 4	29 ± 5	52 ± 9	11 ± 4	8 ± 3	22 ± 5	68 ± 5	3 ± 1	8 ± 3	11.1	36.4	2.1
Alaknanda	7 ± 3	21 ± 2	71 ± 9	6 ± 1	5 ± 2	15 ± 5	79 ± 6	2 ± 0	23 ± 8	12.2	52.5	2.2
Ganga	9 ± 3	21 ± 4	69 ± 9	10 ± 8	6 ± 2	13 ± 4	79 ± 4	2 ± 2	25 ± 8	13.0	45.6	2.3
Yamuna	11 ± 5	22 ± 11	50 ± 18	16 ± 8	8 ± 5	17 ± 9	71 ± 11	4 ± 3	22 ± 7	13.5	38.0	1.6
Ghaghra	9 ± 1	24 ± 6	60 ± 9	8 ± 1	6 ± 1	20 ± 7	72 ± 8	2 ± 0	-	13.6	54.7	3.3
Gandak	14 ± 9	23 ± 6	52 ± 12	19 ± 11	6 ± 4	14 ± 6	77 ± 9	3 ± 2	36 ± 4	17.6	92.3	3.6
Kosi	10 ± 8	36 ± 8	50 ± 15	8 ± 6	16 ± 14	35 ± 11	47 ± 19	2 ± 2	16 ± 5	9.9	12.4	2.5

The source contribution from different end members for cations and Sr listed are the average of both monsoon and non-monsoon samples (Appendix S2) for each sub-basin. Erosion rates are estimated based on high flow samples for the river Bhagirathi (Devprayag), Alaknanda (Devprayag), Ganga (Rishikesh), Yamuna (Before confluence with Aglar), Ghaghra (Chisapani), Gandak (Narayan Ghat) and Kosi (Ulleri Khola).

*Based on results from the inverse model; Errors are ±σ.

5.5. Chemical Erosion in the Ganga Headwaters

The chemical weathering of silicate minerals is a major sink for atmospheric CO_2 on million year scale and the chemical erosion rate of silicates of the Ganga basin is important to assess the impact of the Himalaya on the global CO_2 budget.

5.5.1. Sources of dissolved cations and Sr

The fractions of dissolved cations supplied to the headwaters and tributaries of the Ganga from atmosphere, silicates, (carbonates+gypsum) and hot springs estimated based on the inverse model are listed in Table S2 of Appendix. The estimated silicate cations (Cat_s) from the inverse model for the Ganga at Rishikesh (21%; Table 5-7) is similar to that reported earlier (~25 %) based on the forward model [*Krishnaswami et al.*, 1999; *Dalai et al.*, 2002]. The range of Cat_s, (20-28%) for the Yamuna upstream basin [*Dalai et al.*, 2002] brackets the value of 22% derived in the present work. Similarly, the Cat_s for the Gandak (~20%) and Ghaghra (~20%) estimated based on the forward model using the data set of *Galy and France-Lanord* [1999] are consistent with those of the present study within uncertainties (23% and 24% respectively). The estimated Cat_s for the Kosi (36%) in this study is comparable with earlier reported values (33-43%) [*Quade et al.*, 2003]. Among the rivers studied, Cat_s is the highest for the Kosi followed by the Bhagirathi (Fig. 5.6) a result consistent with the lithology of the Kosi basin, with more aerial coverage of silicate rocks.

A closer look at the comparison of the forward and inverse model results, however indicates that the Cat_s values of almost all rivers derived from the inverse model are systematically lower than those based on the forward model. To check on this, statistical analysis of the Cat_s data derived for both the models was carried out using the Williamson bivariate statistical method. These analysis shows that the Cat_s derived from the inverse and forward models are linearly correlated with a slope of 0.81±0.07 (1σ, Fig. 5.7) significantly lower than the equiline. As a result the Cat_s and SER derived from the inverse model are lower than that estimated from the forward model. The difference in the results obtained from the two models can be explained in

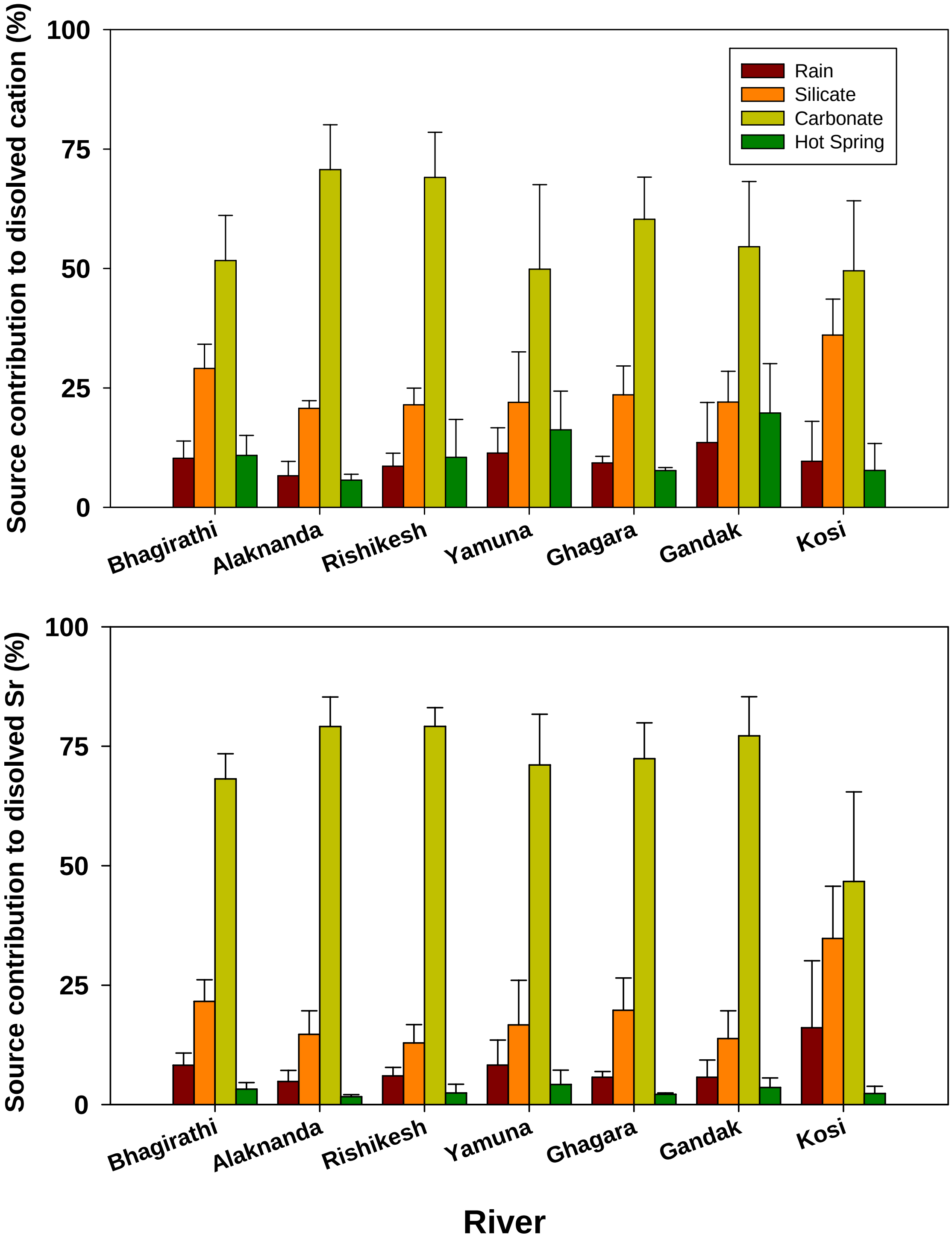

Figure 5.6: *Bar diagram of contribution from different sources to dissolved cations and Sr to the various tributaries of the Ganga based on the inverse model.*

terms of differences in their elemental release ratios. The inverse model provides the best fit for the release ratios based on measured chemical composition of the rivers whereas in the forward model the release ratios are assumed based on that in parent rocks or a combination of parent rocks, soil profiles and rivers draining monolithological terrains. Further, in the forward model, the role of hot springs in contributing to the water chemistry is not considered.

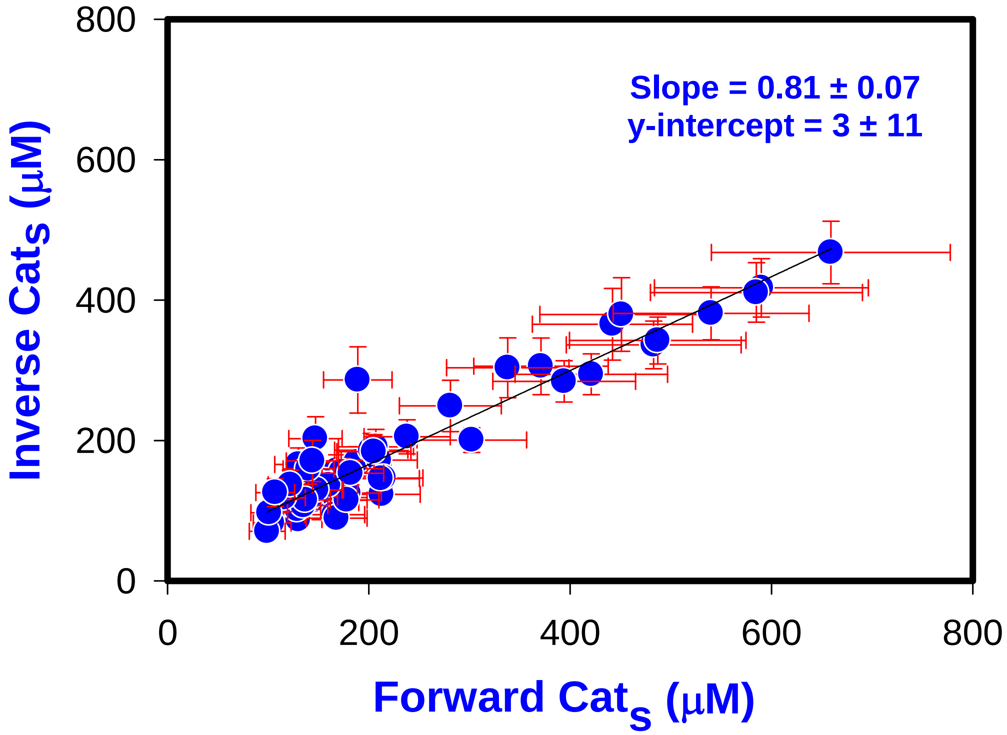

Figure 5.7: *Correlation between Cat$_s$ (μM) obtained by the forward and inverse models. Cat$_s$ derived using the inverse model is lower compared to that derived from the forward model. This disagreement in the results from the models is attributed to differences in the assumed and derived end member values.*

The relative contribution of Sr from silicate weathering to the rivers ($Sr_s = 100 \times$ (silicate derived Sr (nM))/Sr$_r$) follows a pattern similar to that of Cat$_s$. Analogous to Cat$_s$, the Sr$_s$ is highest for the Kosi. The Sr budget of the Gandak is dominated by carbonates, consistent with the geology of its basin. The range in Sr$_s$ based on the inverse model, though are systematically low, overlaps with the estimates of Sr$_s$ based on the forward model (13-65%) for these rivers [*Galy et al.*, 1999]. The present approach for apportioning the sources of dissolved Sr of the

Ganga headwaters using inverse model enables to quantify all possible contribution for Sr, which was otherwise not possible using forward models [*Krishnaswami et al*., 1999].

The estimated contribution from hot springs differs among the sub-basins of the Ganga (Table 5-7) and is the highest for the Gandak River. The present estimates of Sr_{spring} are low compared that reported by *Evans et al.* [2001, 2004] for the tributaries of the Gandak. The possible reason for this difference could be regional effect of hot springs on river geochemistry. The contribution of Sr from the hot springs to the Ganga headwaters is low (~3%) and is in agreement with the earlier reported values for the Alaknanda [*Bickle et al*., 2005].

5.5.2. Calcite Precipitation from the rivers

The river Ganga and its tributaries are known to be super-saturated with respect to calcite particularly during their lean flow [*Sarin et al.*, 1989; *Galy and France-Lanord*, 1999; *English et al.*, 2000; *Dalai et al.*, 2002; *Jacobson et al.*, 2002]. The precipitation of calcite from rivers can not only complicate the apportionment of dissolved Ca and to a lesser extent Mg and Sr to various sources but also can underestimate the CER on sub-basin scales and the quantification of this process provides a better understanding of the riverine alkalinity budget. Recognizing the importance of this, a few earlier studies [*Jacobson et al.*, 2002] have estimated Ca removal from the Ganga based on modeling the degree of variation of the dissolved Ca/Mg and Ca/Sr ratios. In this work, an attempt has been made using the inverse model to quantify the Ca removal from the streams during their lean flow. It is assumed that (1) the Ca/Mg release ratio from different end members have remained the same during different seasons and (2) the riverine Mg and Sr concentrations remain unaffected by calcite precipitation. The latter assumption may not be strictly valid due to minor incorporation of Mg and Sr in calcite. The removal of both Mg and Sr, however is not expected to impact their budget significantly considering that their distribution coefficient in calcite is far less than one [*Rimstidt et al.*, 1998].

Calcite saturation-indices for the Ganga tributaries indicate that most of them are supersaturated during lean flow. Therefore, the measured Ca and HCO_3

concentrations of such tributaries during their lean flow are likely to be affected by calcite precipitation. Hence, in the inverse model source apportionment of the non-monsoon (NM) samples was done independent of Ca and HCO_3. After obtaining best fit values for Mg/Na and the fraction of Na contributed from each source ($\left(\frac{Mg}{Na}\right)_i^{NM}$, $f_i^{NM}(Na)$); Ca/Na for the source i is estimated using the following equation.

$$\left(\frac{Ca}{Na}\right)_i^{NM} = \left(\frac{Mg}{Na}\right)_i^{NM} \times \left(\frac{Ca}{Mg}\right)_i^{M} \qquad \text{-----} \quad 5\text{-}8$$

where $\left(\frac{Ca}{Mg}\right)_i^{M}$ is the molar ratio of Ca/Mg released from source i during monsoon (M).

From this ratio, the Ca content of the river prior to calcite precipitation, $(\mathrm{Ca})_{\mathrm{orig}}$ can be calculated as,

$$(\mathrm{Ca})_{\mathrm{orig}} = \sum_{i=1}^{4} \left(\frac{Ca}{Na}\right)_i^{NM} \times f_i^{NM}(Na) \qquad \text{-----} \quad 5\text{-}9$$

The fractional loss of Ca from the river due to calcite precipitation during non-monsoon is calculated from the difference between $(\mathrm{Ca})_{\mathrm{orig}}$ and measured Ca (Ca_r).

$$\text{Ca loss} = \left(\frac{(Ca)_{orig} - (Ca)_r}{(Ca)_{orig}}\right) \qquad \text{-----} \quad 5\text{-}10$$

This approach to estimate Ca loss largely depends on the inverse model to provide consistent results, when Ca and HCO_3 are not included in the calculation. To test this, the monsoon samples were modeled twice, once with Ca and HCO_3 data and the second time without them. The results of both the analysis are the same (Table 5-8) suggesting that excluding the Ca and HCO_3 data from the model calculation does not affect the source apportionment estimates significantly.

Table 5-8: The results obtained from the inverse model with and without using Ca and alkalinity for the monsoon samples of the Ganga at Rishikesh are listed (in μM) here.

Sample ID	Na$_{rain}$	Na$_{s}$	Na$_{c}$	Na$_{spring}$	Mg$_{rain}$	Mg$_{s}$	Mg$_{c}$	Mg$_{spring}$	Sr$_{rain}$	Sr$_{s}$	Sr$_{c}$	Sr$_{spring}$
AK36	13	64	6	11	8	23	175	0	31	72	639	13
	13	59	12	9	8	23	175	0	24	74	646	18
AK121	22	56	4	13	14	20	108	0	50	64	394	15
	20	55	8	13	13	21	109	0	38	68	401	24
TA4	6	30	3	12	4	11	100	0	13	34	366	14
	9	29	7	6	5	11	96	0	16	36	353	12
RW98-34	21	69	5	8	13	25	137	0	48	78	501	9
	17	64	10	10	11	24	141	0	33	80	520	19
RW99-6	24	71	5	6	15	25	144	0	56	80	528	7
	16	66	11	13	10	25	155	0	31	82	573	24
RW99-59	16	47	4	9	10	17	114	0	36	54	418	11
	14	44	8	9	9	17	115	0	27	55	426	18
Ganga3	22	28	4	5	14	10	128	0	51	32	468	5
	12	24	10	13	8	9	139	0	23	30	513	25
AK175	9	52	3	11	5	19	89	0	20	59	326	13
	11	51	6	7	7	19	86	0	21	63	319	13
AK211	6	49	3	10	4	18	102	0	15	56	373	11
	9	48	7	5	6	18	97	0	17	59	360	10

The first row for each sample represents the results of inversion using all chemical parameters (Cl/Na, Ca/Na, Mg/Na, Sr/Na, HCO$_3$/Na, ^{87}Sr/^{86}Sr) and the second row (highlighted) contains results for all chemical ratios, except Ca/Na and HCO$_3$/Na. The results are observed to be same in both methods.

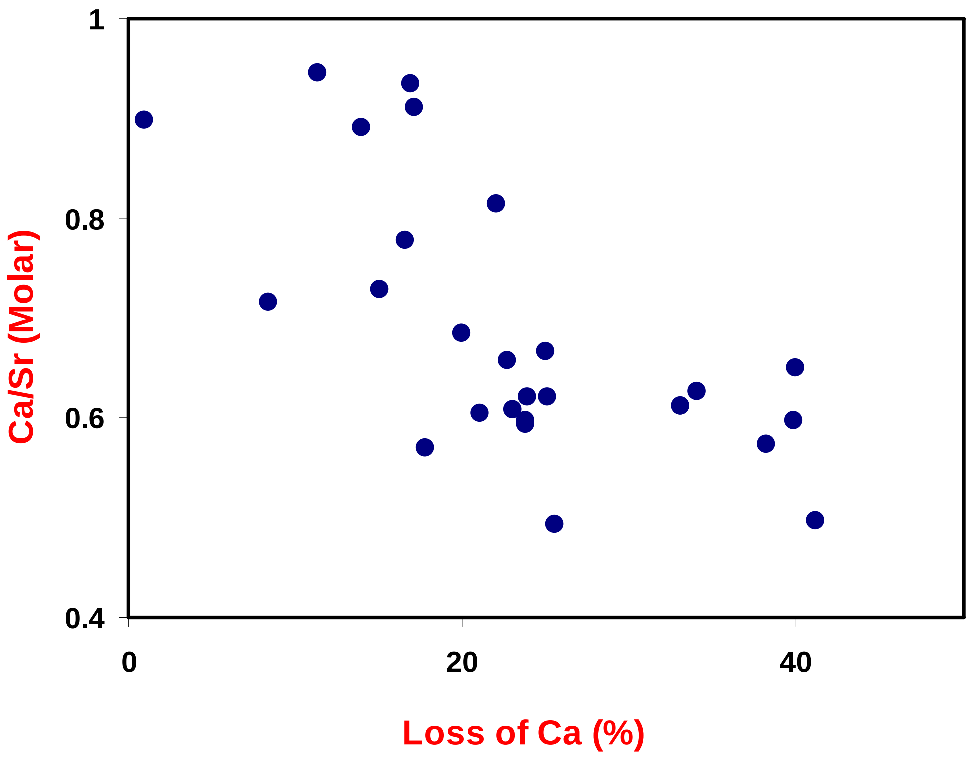

Figure 5.8: *Estimated loss of Ca shows a decreasing trend with measured Ca/Sr of the Ganga, consistent with lowering of Ca due to calcite precipitation in the sub-basins.*

The amount of Ca loss for different rivers is listed in Appendix S2 of Supplementary Materials. The Ca removal from the Ganga headwaters ranges from ~10-40 % and is highest for the Gandak (Table 5-7). The high calcite precipitation in the Gandak could be due to high carbonate weathering in the basin, which is dominated by carbonates. The present estimate of Ca loss for the Yamuna (~22%) is consistent with the upper limits (~50%) provided by *Dalai et al.* [2002]. Further, the Ca loss estimated for the Ganga tributaries in this work based on the inverse model is comparable with that reported by *Jacobson et al.* [2002]. The extent of Ca removal from the Ganga rivers is also evident from their Ca/Sr ratios (Fig. 5.8). The observed decrease in riverine Ca/Sr with increasing Ca loss indicates the impact of calcite precipitation which lowers the Ca abundance of the rivers, similar to those reported for various rivers of the Ganga system [*Sarin et al.*, 1989; *Dalai et al.*, 2002; *Jacobson et al.*, 2002; *Bickle et al.*, 2005]. The estimates for Ca removal suggests Ca eroded from one sub-basin can be deposited in a subsequent one and can result in possible underestimation of the chemical weathering rates in some of these basins, if calculated based on the non-monsoon data. This non-conservative behaviour of Ca in the Ganga river system also hampers the potential of Sr/Ca as a proxy for silicate weathering.

Based on calcite saturation-index, *Sarin et al.* [1989] indicated that the Ganga headwaters are largely under-saturated with respect to calcite, particularly during high flow periods. This supports the assumption used in the above calculation, viz insignificant removal of Ca during high flow period from the Ganga headwaters. However, a few subsequent studies [*Bickle et al.*, 2005; *Tipper et al.*, 2006] indicate towards calcite super-saturation in some of the rivers (Source waters of the Alaknanda and the Marsyandi) flowing through TSS during high flow periods. In such a case, the present estimate of Ca loss, particularly in these tributaries will be a lower limit.

5.5.3 Control of silicate weathering on $^{87}Sr/^{86}Sr$

The potential of $^{87}Sr/^{86}Sr$ to serve as a proxy of silicate weathering in the Himalayan basin has remained a topic of debate [*Harris*, 1995; *Blum et al.*, 1998; *Jacobson and Blum*, 2000; *Quade et al*., 2003]. Highly radiogenic Sr in the Himalayan silicates makes it possible to use dissolved $^{87}Sr/^{86}Sr$ of the Himalayan rivers as a proxy of silicate weathering, however, the presence of metamorphosed carbonates in the Himalaya with highly radiogenic Sr questions this application. The cations derived from silicates (Cat_s) estimated using the inverse model and measured $^{87}Sr/^{86}Sr$ show an overall positive correlation (Fig. 5.9) for the headwaters of the Ganga. The majority of the riverine $^{87}Sr/^{86}Sr$ for the Ganga headwaters (encircled with blue ellipse in Fig. 5.9) increase with Cat_s. This observation seems to suggest that $^{87}Sr/^{86}Sr$ in the Ganga is largely controlled by the intensity of silicate weathering in the basin [*Krishnaswami and Singh*, 1998]. However, a few samples from the upstream of the Gandak and the Arun (tributary of the Kosi) follow an increasing trend (red ellipse in Fig. 5.9) with lower slope. The possible reason for this different trend could be the difference in Sr isotopic composition of bedrocks present in their corresponding basins compared to the other Ganga headwaters. These streams of the Kosi [*Quade et al.*, 2003] and Gandak [*Galy et al.*, 1999] with low $^{87}Sr/^{86}Sr$ drain through TSS, which are known to have silicates with less radiogenic Sr [*Oliver et al.*, 2000]. Hence, any increase in silicate weathering in the basin (TSS) of these streams can enhance fraction of cations released from silicates with limited increase in $^{87}Sr/^{86}Sr$, i.e., with relatively lower slope compared to the streams draining LH and HH (Fig. 5.9).

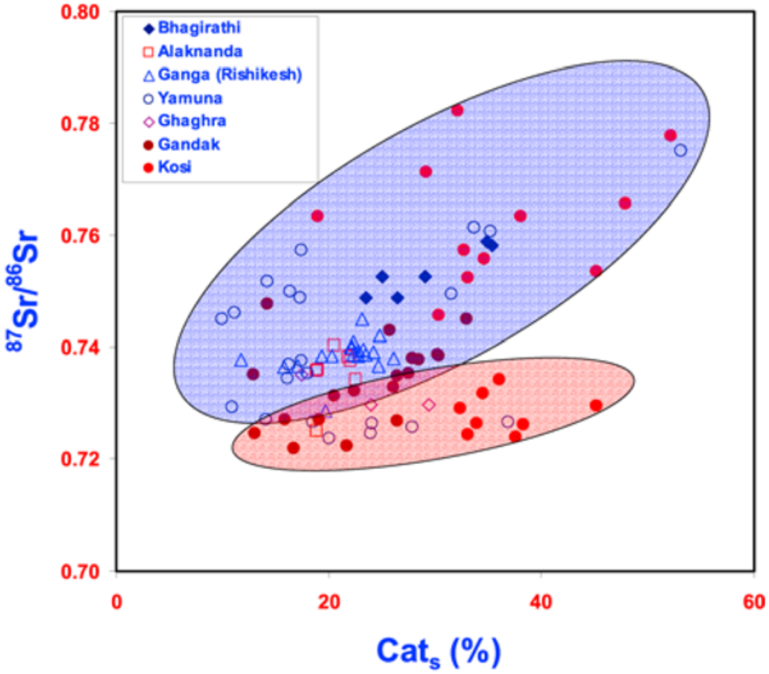

Figure 5.9: *The variation of $^{87}Sr/^{86}Sr$ vs. Cat_s. It is seen that Cat_s and $^{87}Sr/^{86}Sr$ covary indicating their source of radiogenic Sr is dominated by silicates and the $^{87}Sr/^{86}Sr$ has the potential to be a tracer for silicate weathering. There seems to exist two trends for the Ganga, i.e. (1) for majority of Ganga headwaters enveloped with blue ellipse and (2) streams flowing through the TSS or the Siwaliks, which are characterized by lower radiogenic Sr for silicates (red ellipse).*

5.5.4. Erosion rates

The silicate and carbonate erosion rates in the drainage basins are calculated based on the inverse model derived silicate and carbonate cations, Si concentration during high flow and their annual runoff (Table 5-7) using the following relations.

$$SER = \left(\frac{Q}{A}\right) \times \left(Na_s + K_s + Ca_s + Mg_s + SiO_2\right) \qquad \text{-----} \quad 5\text{-}11$$

$$CER = \left(\frac{Q}{A}\right) \times \left(Na_c + Ca_c + Mg_c + \left(CO_3\right)_c\right) \qquad \text{-----} \quad 5\text{-}12$$

SER and CER are in tons/km^2/yr.

$$CO_2 consumptionrate = \left(\frac{Q}{A}\right) \times \left(Na_s + K_s + 2 \times (Ca_s + Mg_s)\right) \quad \text{-----} \quad 5\text{-}13$$

CO_2 consumption rates are in moles/km^2/yr.

where, *Q* is the annual water discharge and *A* is the drainage area of the river.

Both SER and CER in the sub-basins of the Ganga are significantly higher compared to other Himalayan rivers (the Brahmaputra and Indus) and the global average (Fig. 5.10). These SER values of orogenic belts, e.g. the Himalaya and Andes, are higher compared to those reported for the rivers draining the shield areas [*Edmond and Huh*, 1997].

The erosion rates estimated in this study are the highest for the river Yamuna and are similar to the earlier estimates of *Dalai et al.* [2002]. However, the SER of the Yamuna show a significant spatial variation. The SER of the Yamuna downstream the confluence of the tributary Aglar is very high, however, up-stream of this confluence (above Batamandi) its SER is similar to that of other tributaries of the Ganga (Table 5-7). This large spatial variation in SER of the Yamuna sub-basin is intriguing possible reasons could be anthropogenic inputs by its downstream tributaries or large supply of dissolved material from saline/alkaline soils as observed for rivers in the Ganga plain and penisular India [*Rengarajan et al.*, 2009, Rai et al., 2010]. In this study, the erosion rates of the Yamuna before the confluence with the Aglar are considered as the representative value for the basin (Table 5-7).

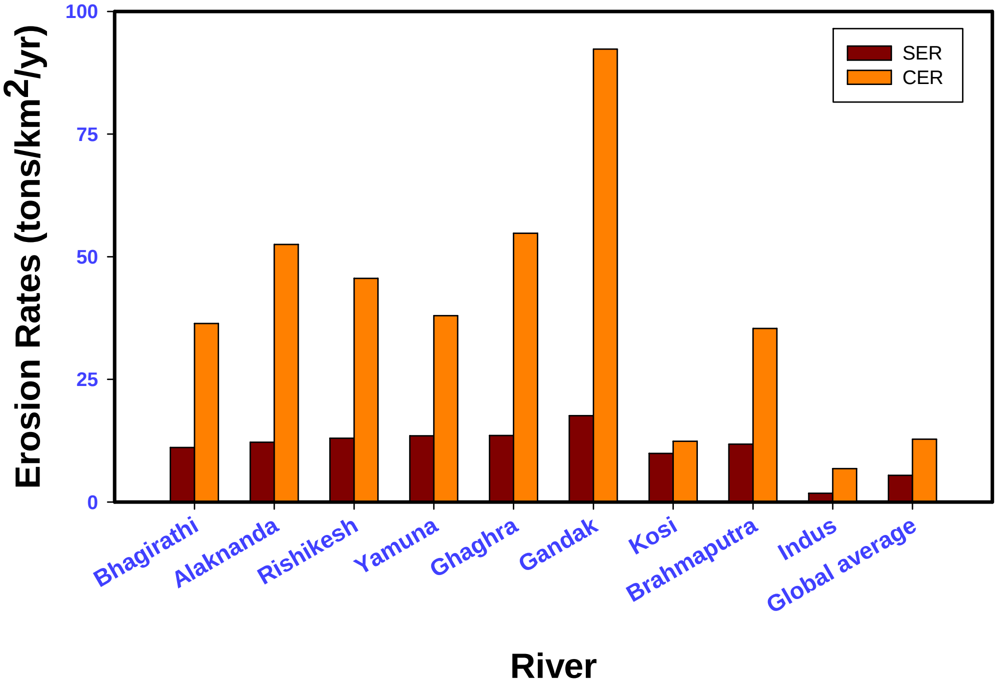

Figure 5.10: *Comparison of silicate and carbonate erosion rates in different tributaries of the Ganga River with global average and other Himalayan rivers.*

The SER of the Ganga headwaters are high compared to that of global average [5.5 tons/km^2/yr; *Gaillardet et al.*, 1999]. The high erosion rates in the drainage of the Ganga headwaters follow the intense physical erosion rates resulting from higher relief and runoff over the basin. The SER and CER for the Kosi are comparable, but unlike other Himalayan tributaries of the Ganga, where carbonate weathering dominates the river chemistry.

The CO_2 consumption rate due to the silicate weathering estimated (using Equation 5-13) in this study ranges between 1.6×10^5 moles/km^2/yr (Yamuna before confluence with Aglar) and 3.6×10^5 moles/km^2/yr (Gandak) for the Ganga headwaters (Table 5-7). The estimated CO_2 consumption rate due to silicate weathering in the Himalayan streams of the Ganga are distinctly higher compared to that of the global average [0.9×10^5 moles/km^2/yr; *Gaillardet et al.*, 1999]. These estimates are high compared to other Himalayan rivers such as the Indus [0.6×10^5

moles/km^2/yr; *Gaillardet et al.*, 1999], but low compared to that of the Brahmaputra river [6.0×10^5 moles/km^2/yr; *Singh et al.*, 2005].

5.5.5. Controlling factors for chemical weathering in the Ganga basin

The chemical weathering and its intensity in any basin depends on many factors including relief, stream power, lithology, runoff, temperature and vegetation [*Garrels and Mackenzie*, 1971]. The contribution of each of these parameters to the chemical weathering varies from basin to basin and it is greatly debated in case of the Himalayan rivers. This study underscores the importance of lithology in controlling the cation budget derived from them in the basin. This interpretation is well supported by the high Cat_s and Sr_s values for those rivers (the Kosi and the Bhagirathi) where silicate bedrock dominates drainage basin (Table 5-1).

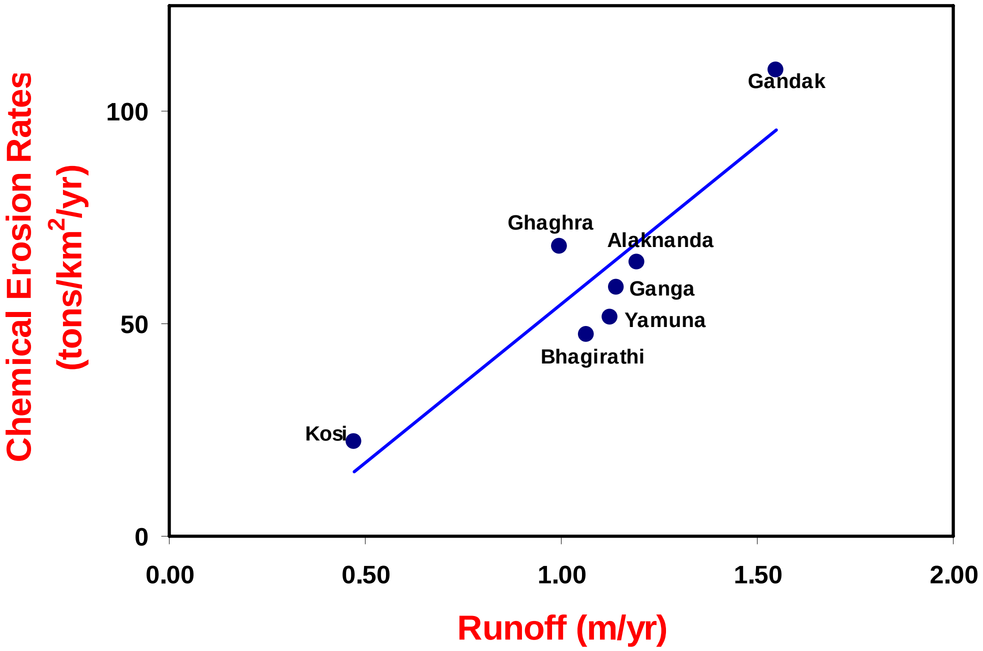

Figure 5.11: *Scatter diagram of chemical erosion rates and the runoff for the Ganga tributaries. The data show significant correlation indicating runoff to be the important factors controlling the erosion pattern over the Ganga*.

The estimated SER values for the Ganga tributaries range between 10-18 tons/km^2/yr and is high compared to global average. It is important to note that despite large variability in hydrogeological parameters e.g. rainfall, lithology among the sub-basins, their SER fall in a narrow range (10-14 tons/km^2/yr, except 18 tons/km^2/yr for the Gandak) possibly due to balancing of the impact of individual controlling factors in different sub-basins. The highest SER of the Gandak among the Ganga tributaries (Table 5-7) is well supported by very high physical erosion in this sub-basin [*Singh et al.*, 2008]. To understand the primary controlling factor of chemical erosion rate in the Ganga basin, chemical erosion rates of the sub-basins are plotted with runoff (Fig. 5.11). A significant positive correlation between them suggests the importance of runoff in controlling the chemical erosion in the Ganga. Similar observation was also reported over Nepal Himalaya [*France-Lanord et al.*, 2003].

Further, the SER of the Ganga sub-basins are compared with the rivers draining the Deccan traps. The silicate of the Ganga basin is composed of granite and gneisses where as the Deccan drainage consists of basalts. The estimated SER for most of the tributaries of the Ganga (~12 tons/km^2/y) using inverse modeling is comparable with that reported for the Krishna River [14 tons/km^2/yr, *Das et al.*, 2005]. The drainage basin of the Krishna is largely composed of the Basaltic rock; whereas the Himalaya contains only ~66% of silicate rock [*Amiotte-Suchet et al.*, 2003]. The silicate exposure area for the Ganga headwater basin is estimated, using data from Table 5-1, to be ~70%. Silicate exposure area (~70%) normalized SER of the Ganga basin, ~17 tons/km^2/yr, is higher compared to that of the Krishna River despite the fact that the Krishna river basin is mainly composed of easily weatherable basaltic rocks compared to the granitic rocks present in the Himalaya. This suggests that the high silicate erosion rate of the Himalaya compared to Deccan Rivers could be due to its high relief.

5.5.6 Flux from the Himalaya to the Ganga mainstream

The Ganga drains about 1060×10^3 km^2 of area [*Galy and France-Lanord*, 1999] before it merges with the Brahmaputra in the Bangladesh, out of which ~176×10^3 km^2 of drainage area falls over the Himalaya and forms drainage of the Ganga headwaters [*Singh et al.*, 2008]. To estimate the contribution from the Ganga headwaters in the Himalaya to the total dissolved load flux of Ganga at its mouth, the total dissolved load flux (in monsoon) from the headwaters of the Ganga to the mainstream is quantified. The annual total dissolved solid (TDS) flux (=TDS of the tributaries at mouth × annual water discharge) of the Ganga at the mouth is estimated to be ~57 million tons, out of this ~33 million tons is estimated to be supplied by the headwaters. This suggests that the Himalayan drainage of the Ganga, constituting only ~17% of the drainage, supply ~60% of the dissolved material to the Ganga. Rest of the dissolved flux (~40%) of the Ganga is derived from the rivers flowing through the plains and peninsular area (~83%) indicating lower erosion rates in the Plain and Peninsular drainages. The high chemical erosion rates for the Ganga headwaters could be an effect of high relief and rainfall over the Himalaya compared to that in the plains.

5.6. Conclusions

A number of studies on the headwaters and tributaries of the Ganga have been reported on their geochemical and isotopic properties to infer about erosion rates and their relation with atmospheric CO_2 drawdown rate. In the present work, a large number of sub-basin scale studies of the Ganga in the Himalaya was compiled and modeled together to infer about ongoing chemical erosion rates in the headwater basins.

The $^{87}Sr/^{86}Sr$ of the Ganga headwaters is highly radiogenic with high Sr content compared to the global average. Among the tributaries of the Ganga, the Kosi and the Bhagirathi supply water with the highly radiogenic Sr to the Ganga mainstream indicating intense silicate erosion in their basins. The sources of dissolved cations were quantified for these streams using both inverse and forward models. Silicate cations, Cat_s, derived using the inverse model are always lower than that derived based on the forward model indicating differences in the assumed and derived end member values. The highest Cat_s value (36%) among these rivers was found for the Kosi, consistent with the dominance of silicate lithology in its drainage.

For the Gandak, about ~20% of the dissolved cations is supplied by the hot springs. Highest carbonate derived Sr, Sr_c, is estimated for the Gandak sub-basin, which is in agreement with geology of the basin. The source contributions to the total dissolved cation and Sr budgets, hence, seem to be governed mainly by its lithology.

The Ganga headwater and tributaries get supersaturated with respect to calcite during non-monsoon seasons. The Ca removal during lean flow was estimated for these streams using the inverse model and plausible assumptions regarding Mg/Ca release ratios during different season. The loss of Ca is found to be maximum for the Gandak River. On an average, the Ca loss in these streams ranges from ~10-40 % and hence, can result in underestimation of the chemical weathering rates of these basins.

The SER and CER were estimated for the Ganga headwater basins draining the Himalaya. These estimates confirm the earlier reports that they are significantly higher compared to the global average and also from other Himalayan rivers. The high SER for the tributaries of the Ganga result due to high physical erosion over these sub-basins. The chemical weathering in the headwater basins of the Ganga seems to be controlled largely by their lithology, relief and rainfall. The Himalayan drainage of the Ganga supplies ~55% of water discharge and ~60% of dissolved material at its outflow draining only through ~17% of total area.

CHAPTER 6

Summary and Future Perspectives

The major objectives of this thesis were to provide reliable radiometric ages of the sedimentary sequences of the Vindhyan, Lesser Himalaya and the Aravalli and characterize the temporal variation of the provenances of the sediments from the western Bay of Bengal and their relation with the varying climate. Further, developing an inverse method to estimate the contemporary erosion rates was another objective of this study. To achieve these objectives, major and trace elemental geochemistry and radiogenic isotopes of osmium, strontium and neodymium have been used to decode the signatures of past events preserved in sedimentary archives of different depositional ages and environment. Black shales from the Vindhyan, Lesser Himalaya and the Aravalli have been investigated in this study for their Re, Os concentrations and their Os isotopic compositions to constrain their depositional ages and to reconstruct the marine $^{187}Os/^{188}Os$ evolution trend from Paleoproterozoic to Early Cambrian. This information on seawater osmium isotopic ratios in the past is used to evaluate its potential as a proxy for tracking atmospheric oxygen evolution trend. In this thesis, Sr-Nd isotopes are employed to infer the provenances of sediments, their temporal variations and the factors controlling them. For this, sediments from a piston core raised from the western Bay of Bengal are analyzed for their Sr-Nd isotopic compositions along with their geochemical parameters. The focus to carry out this research is to understand the erosion-climate link over a millennial timescale. Further, efforts were made in this study to develop an inverse method to apportion the sources of dissolved load using their Sr isotopes along with major ion data available in literature to estimate chemical erosion rates of the Ganga headwaters and their controlling factors. The major outcomes of this thesis are summarized below.

6.1. Studies on ages of Black shales using Re-Os chronometer

The Re-Os isotopic systematics of the black shales from the Lower Aravalli show a scatter relation between $^{187}Re/^{188}Os$ and $^{187}Os/^{188}Os$ and hence, provide no meaningful age information on these shales. This observation indicates that the Re and Os of the shales, which are collected from a road cut have not been remained closed subsequent to their deposition. Assuming an age of 2000 Ma for these shales as reported for Jhamarkotra formation and insignificant post-depositional loss of osmium, it is estimated that ~95% of Re is lost from these sedimentary rocks during weathering followed by their exposure. This estimate provides a lower estimate of Re loss during weathering processes, as these black shales could lose part of their Os also during weathering. This work indicates higher mobility of Re compared to Os during weathering.

The Re-Os isotopic systematics of black shales from the Kaimur group, Upper Vindhyan yields an excellent isochron and provides their precise depositional ages of 1196±41 Ma with an initial $^{187}Os/^{188}Os$ of 0.74±0.27. This Re-Os age not only provides the depositional ages for the Kaimur group, but also constrains the age limit for the initiation of sedimentation of the other members of the upper Vindhayn such as Rewa and Bhander groups, for which reliable ages are scarce. The Re-Os age of ~1200 Ma for the Kaimur group compared with the age of the Rohtas group (~1600 Ma) confirms the existence of a sedimentary hiatus of 400 Ma age gap between these two groups. This long sedimentary gap could have resulted as a consequence of tectonic perturbations at ~1600 Ma.

The Re-Os chronometer of the black shales from the Lower Tal formation near the Pc-C boundary of the Lesser Himalaya provides an age of 541±8 Ma, which matches very closely with the reported age for the Pc-C boundary from other parts of the world. The high Re and Os concentration in these shales compared to that of overlying sequences of black shales, indicates highly anoxic condition of seawater at the Pc-C boundary. The Re-Os isochron provided initial $^{187}Os/^{188}Os$ of the depositional basin to be 0.90 ± 0.02, lower compared to that (1.181 ± 0.024) reported after few Ma of their deposition. The lower osmium isotopic ratio of the seawater at the Pc-C boundary indicates enhanced supply from its unradiogenic source possibly from hydrothermal vents to the seawater.

Similar to the Lower Aravalli, Re and Os in black shales collected from an exposed section of the Inner belt of the LH found to remain not closed subsequent to their deposition and hence preclude to provide meaningful Re-Os depositional age for this geological succession. Re-Os elemental and isotopic study of the Lower Aravalli and the Inner LH indicate the requirement of fresh black shales either collected from underground mines or coring for dating them using this chronometer.

Obtained information on the paleo-seawater $^{187}Os/^{188}Os$ from the Re-Os isochrones, along with existing literature data, are used to evaluate the feasibility of tracking atmospheric oxygen evolution trend using osmium isotopes. Increase in seawater $^{187}Os/^{188}Os$ ratio from non-radiogenic value during Early Proterozoic when oxygen was not present in the atmosphere to a ratio close to 1.0 during Early Cambrian when oxygen reached to a level similar to that of present day indicate that marine $^{187}Os/^{188}Os$ evolution have the potential of tracking atmospheric oxygen level particularly during Precambrian period. Temporal variation of seawater $^{187}Os/^{188}Os$ show a close resemblance with the available atmospheric oxygen trend obtained from various other proxies. This attests to the potential of seawater $^{187}Os/^{188}Os$ to track the atmospheric oxygen trend.

6.2. Studies on Provenance of sediments and Erosion-Climate link

In this thesis, sediments from a piston core SK187/PC33 from the western Himalaya are analyzed for their geochemical, magnetic susceptibility and Sr-Nd isotopic compositions to track their sources. Property plot between elemental ratios of K/Al and Fe/Al and the mixing plot between Sr-Nd isotopes confirms the Himalaya and the Peninsular India as the major supplier of sediments to the present core location. Significant variations of the Sr and Nd isotopic composition and corresponding magnetic susceptibility and elemental ratios, such as Fe/Al and V/Al are observed in the sediment core with depth (time) indicating variable contributions from sources. The observed changes in the sediment provenance correlate well with the climatic record of the region, highlighting the important influence of climate over erosion. Relatively lower $^{87}Sr/^{86}Sr$ and higher ε_{Nd} corresponding to the LGM suggests proportionally reduced sediment contribution from the Himalaya during LGM. Erosion rate over the Himalaya decreased during LGM due to combined influence of reduced intensity of the southwest monsoon and larger extent of glaciations over the

Higher Himalaya, the main source of sediments to the Bay of Bengal. This proposition of erosion-climate coupling also draws support from the inference of relatively enhanced sediment supply from the Himalaya during the Holocene period, where the southwest monsoon was stronger compared to that of the LGM.

6.3. Development of inverse method to study the sources of river water solutes and chemical erosion rates

In this thesis, an inverse method to apportion the sources of solutes of the Ganga headwaters was developed successfully. Available data on chemical and Sr isotopic composition of the headwaters of the Ganga and its tributaries in the Himalaya are analyzed using inverse model and compared with those estimated using forward models. The estimates of silicate derived cations based on the inverse model are lower on average by ~20% than that derived from the forward model, a result attributable to differences in the release ratios of major ions between the two models. The inverse model yields the best fit values for the release ratio of various major ions based on measured river chemistry and therefore is more likely to be representative of the basins; unlike the forward model in which the release ratios are assumed. Among the various tributaries, the Kosi and the Bhagirathi have relatively larger contribution from silicate weathering to the cation budget with high ^{87}Sr/^{86}Sr, consistent with the lithology of their basins which is dominated by silicates. The Ganga river system in the Himalaya is known to be supersaturated with respect to calcite during lean flow periods. The inverse model calculates the extent of Ca loss to be between ~10-40% with the highest for the tributary Gandak. The silicate and carbonate erosion rates for these Himalayan rivers are relatively higher, in the range of 9.9 to 17.6 and 12.4 to 92.3 tons/km^2/yr respectively, compared to average values of 5.5 and 12.9 tons/km^2/yr for the global rivers. The higher chemical erosion rates in these river basins could be due to intense physical erosion caused by their higher relief and runoff.

6.4. Future Perspectives

Studies carried out in this thesis have addressed the issues related to ages and provenances of sedimentary deposits from India and their implications to infer about atmospheric oxygen evolution trend and controlling factors of continental erosion (both physical and chemical). However, there exist some areas related to this work, which needs future work. These include

(i) This thesis constrained the depositional age of Kaimur group using Re-Os chronometer. This depositional age though provides a much needed age information on the Upper Vindhyan, but efforts to obtain Re-Os depositional age for the shales of the uppermost group, *viz*. Bhander and Rewa groups in future will be essential to provide the complete sedimentation period of the sedimentary deposit of the Vindhyan Supergroup.

(ii) The Re-Os isotopic composition of black shales that are collected from road cuts showed significant loss of Re and Os due to post-depositional processes, such as weathering. Samples collected from drill cores will be useful in constraining depositional ages of black shales using this dating scheme. In future, application of Re-Os chronometer to date drill core samples of black shales from the Aravalli, Cuddaph, Dharwar craton and the Inner Lesser Himalaya would be useful to assign precise depositional age for these Precambrian sedimentary records and to reconstruct more robust seawater ^{187}Os/^{188}Os evolution curve during the Precambrian.

(iii) This thesis work indicated the significant potential of past seawater ^{187}Os/^{188}Os as a proxy to trace the atmospheric oxygen evolution trend. Paleo-atmospheric oxygen evolution trend can be tracked more accurately by attempting a coupled study of Os and Mo isotope composition the black shales of various ages.

(iv) The Sr-Nd isotopes of the Bay of Bengal sediments show provenance changes during LGM, confirming an erosion-climate link over a millennial timescale. A similar change in provenance is also expected in river basins draining through multi-lithology terrains. In future, it will be interesting to employ Sr-Nd isotopes to reconstruct the past changes in provenances of river sediments, particularly that of the Ganga, Brahmaputra and the Godavari near their outflows. These informations will be useful in understanding the temporal variations of Sr-Nd isotopic compositions of the Bay of Bengal sediments.

(v) Efforts should be made to extend the application of inverse model to provenance study of the marine and river basin sediments.

Appendix

Table S1: Details of the samples and their location, sampling period with chemical and isotopic compositions. The elemental compositions listed here are in the units of μM, except for Sr (nM).

SampleID	Location	Date	Na^+	K^+	Ca^{++}	Mg^{++}	$^{87}Sr/^{86}Sr$	Sr	Cl^-	HCO_3^-	SO_4^{--}	SiO_2	Reference
AK31e	Uttarkashi	May-96	83	32	318	141	0.74921	471	22	666	162	104	10
AK32e	Tehri	May-96	87	33	332	145	0.75016	465	19	722	158	94	10
AK178	Devprayag	Aug-03	70	36	292	94	0.74883	311	15	585	128	106	10
AK208	Devprayag	Aug-03	64	39	256	86	0.75251	289	12	477	139	90	10
5	After confluence of Bhilangana	Apr-89	154	51	377	136	0.75830	420	37	833	170	136	2, 6
23	Devprayag	Apr-89	154	51	385	134	0.75890	529	39	873	164	139	2, 6
AK179	Devprayag	Aug-03	58	50	408	118	0.73809	349	10	955	87	91	13
AK207	Devprayag	Aug-03	52	34	393	113	0.73594	393	9	908	82	83	13
AK104e	Devprayag	Sep-97	83	40	392	188	0.74029	483	23	1047	98	122	10
AK123	Devprayag	Aug-98	65	36	412	135	0.73568	453	16	1010	83	106	10
AK169	Devprayag	Sep-98	70	34	403	143	0.73744	463	11	974	99	102	10
AK33e	Devprayag	May-96	78	36	555	162	0.72493	766	12	1306	108	84	10
24	Devprayag	Apr-89	107	51	429	175	0.73850	644	21	1106	132	110	2, 6
AK54	Devprayag	May-97	114	39	435	169	0.73417	635	19	1047	126	98	10
AK36	Rishikesh	May-96	94	38	546	180	0.72863	788	19	1280	134	92	10
AK121	Rishikesh	Aug-98	95	39	407	160	0.74006	504	28	1014	105	128	10
TA4	Rishikesh	Jul-96	51	38	384	109	0.73659	413	13	852	96	81	10
RW98-34	Rishikesh	Oct-98	102	45	452	195	0.73856	626	23	1035	165	151	8, 9
RW99-6	Rishikesh	Jun-99	106	46	446	176	0.73657	712	25	1014	204	81	8, 9
RW99-59	Rishikesh	Sep-99	76	37	397	150	0.73849	507	20	891	145	116	8, 9
Ganga3	Rishikesh	Sep-82	59	38	353	153	0.73650	580	23	894	121	109	1, 3
AK175	Rishikesh	Sep-98	75	35	348	116	0.74209	404	15	793	102	113	13
AK211	Rishikesh	Aug-03	69	37	381	121	0.73847	439	12	859	108	98	13
AK43	Rishikesh	May-97	117	42	437	179	0.73782	672	88	714	160	94	10
AK101	Rishikesh	May-97	149	41	447	182	0.73791	739	31	1071	161	118	10
AK120	Rishikesh	Oct-97	139	47	452	252	0.73858	728	31	1215	164	133	10
RK1096	Rishikesh	Oct-96	122	56	482	217	0.73836	733	38	1177	168	131	10
RK1196	Rishikesh	Nov-96	208	49	623	406	0.74502	1003	35	1713	268	149	10

RK1296	Rishikesh	Dec-96	156	49	537	247	0.73937	904	31	1295	211	136	10
RK197	Rishikesh	Jan-97	169	49	558	261	0.73961	918	34	1362	219	136	10
RK297	Rishikesh	Feb-97	180	52	573	269	0.73919	961	35	1380	233	124	10
Ganga 3	Rishikesh	Mar-82	145	40	398	239	0.73990	800	42	1004	162	152	1, 3
Ganga 3'	Rishikesh	Nov-82	137	52	544	238	0.74080	760	21	1382	-	-	1, 3
RW98-26	Godu Gad (Purola-Mori Road)	Oct-98	89	49.3	133	53	0.77495	259	9	450	19	200	8, 9
RW98-27	Pabar (U. of confluence with Tons)	Jun-99	64	45.1	182	35	0.76059	200	14	383	62	116	8, 9
RW98-28	Tons (D. of Mori)	Oct-98	73	45.4	189	40	0.76145	221	24	383	58	119	8, 9
RW98-29	Tons (Tiuni)	Oct-98	78	45.7	221	50	0.74954	256	20	495	62	138	8, 9
RW98-30	Tons (Minas, after confluence)	Oct-98	98	37.4	436	160	0.73676	594	27	990	100	163	8, 9
RW98-31	Shej Khad (Minas)	Oct-98	125	22.5	727	254	0.72927	1071	30	1575	159	206	8, 9
RW98-32	Tons (Kalsi, U. of confluence)	Oct-98	152	52.4	808	411	0.72693	2196	27	1395	581	186	8, 9
RW98-16	Yamuna (Hanuman Chatti)	Oct-98	67	56	388	100	0.75158	381	30	780	113	92	8, 9
RW98-20	Yamuna (D. of Pali Gad Bridge)	Oct-98	89	55	392	104	0.75725	412	36	855	100	112	8, 9
RW98-25	Yamuna (Barkot)	Oct-98	110	52	406	133	0.74985	422	52	960	76	126	8, 9
RW98-22	Yamuna (U. of Naugaon)	Oct-98	117	52	422	133	0.74887	468	53	990	76	127	8, 9
RW98-15	Yamuna (U. of Barni Gad's confluence)	Oct-98	108	50	500	186	0.74598	386	50	1260	72	140	8, 9
RW98-14	Yamuna (D. of Barni Gad's confluence)	Oct-98	110	48	525	211	0.74495	402	50	1445	63	144	8, 9
RW98-12	Yamuna (D. of Nainbag)	Oct-98	136	35	504	167	0.73757	903	46	1260	66	176	8, 9
RW98-1	Yamuna (Rampur Mandi, Paonta sahib)	Oct-98	112	46	481	171	0.73518	728	29	1085	101	167	8, 9
RW99-58	Yamuna (Rampur Mandi, Paonta sahib)	Sep-99	92	42	452	130	0.73446	522	24	1039	100	137	8, 9
RW98-4	Yamuna (D. of Bata's confluence, Batamandi)	Oct-98	255	52	1019	497	0.72356	1802	60	2369	333	211	8, 9
RW99-55	Yamuna (D. of Bata's confluence, Batamandi)	Sep-99	262	61	920	344	0.72447	1484	67	2900	288	183	8, 9
RW98-33	Yamuna (Yamuna Nagar, Saharanpur)	Oct-98	213	61	928	451	0.72657	1513	58	2250	268	220	8, 9
RW99-54	Yamuna (Yamuna Nagar, Saharanpur)	Sep-99	122	58	500	173	0.72624	895	32	1520	192	146	8, 9
RW99-31	Yamuna (D. of Ton's confluence)	Jun-99	175	44	720	310	0.72556	1461	75	1357	405	96	8, 9
RW99-7	Yamuna (Yamuna Nagar, Saharanpur)	Jun-99	242	85	948	448	0.72657	1664	56	2608	321	204	8, 9
Karnali below the Seti	Karnali below the Seti	Apr-97	196	54	249	534	0.72957	855	54	1350	115	108	7

Karnali above Thuli Gad	Karnali above Thuli Gad	Apr-97	168	35	254	584	0.72968	975	45	1362	117	120	7
Karnali at Chisapani	Karnali at Chisapani	Apr-97	123	47	308	581	0.73499	959	44	1487	133	102	7
LO256	Syagru Bensi	Jun-93	80	29	355	88	0.72220	620	23	784	87	60	4, 5
LO258	Betrawati	Jun-93	84	28	327	76	0.72680	670	18	739	75	64	4, 5
TRI 19/6	Betrawati	Jun-93	56	24	296	56	0.72700	410	16	644	56	51	4, 5
LO316	Adamghat	Jun-93	94	32	370	84	0.73480	720	19	889	62	93	4, 5
LO304	Gumaune	Jun-93	119	35	505	152	0.72700	970	63	1121	140	84	4, 5
TRI 15/7	Betrawati	Jul-93	44	39	409	49	0.72460	480	14	897	41	57	4, 5
TRI 1/8	Betrawati	Aug-93	54	51	341	51	0.73130	410	15	784	42	82	4, 5
TRI 15/8	Betrawati	Aug-93	67	39	324	49	0.73210	390	19	737	46	75	4, 5
TRI 1/9	Betrawati	Sep-93	93	48	278	77	0.73280	390	43	694	54	73	4, 5
TRI 15/9	Betrawati	Sep-93	71	29	255	65	0.73530	390	17	610	55	94	4, 5
TRI 1/10	Betrawati	Oct-93	94	35	257	73	0.73750	420	26	642	57	107	4, 5
TRI 15/10	Betrawati	Oct-93	124	33	319	94	0.73490	510	35	766	85	114	4, 5
TRI 1/11	Betrawati	Nov-93	129	37	318	93	0.73490	520	33	779	84	116	4, 5
TRI 1/12	Betrawati	Dec-93	170	38	376	117	0.73450	630	49	911	111	127	4, 5
TRI 4/4	Betrawati	Apr-94	200	43	418	136	0.73310	730	49	1027	133	125	4, 5
LO310	Ramdi	Jun-93	113	50	762	362	0.73500	1310	73	1911	212	75	4, 5
LO306	Kot	Jun-93	101	50	635	338	0.74770	1020	56	1651	191	78	4, 5
LO312	Kotre Bazar	Jun-93	87	57	738	332	0.72180	1580	42	1893	171	107	4, 5
LO302	Sarang Ghat	Jun-93	102	51	636	322	0.74300	860	33	1688	174	120	4, 5
LO308	Narayan Ghat	Jun-93	114	51	602	244	0.73600	940	60	1458	169	96	4, 5
NH1	Narayan Ghat	Mar-93	230	50	739	439	0.73650	1390	245	2038	245		4, 5
NAG49	Narayan Ghat	Dec-95	185	68	777	429	0.73640	1250	214	2143	214		4, 5
Ab.Pikhuwa Khola	Ab.Pikhuwa Khola	Jan-99	291	43	552	130	0.72422	1010	71	1212	162	137	11
Ab.Khandapp Khola	Ab.Khandapp Khola	Jan-99	344	54	562	151	0.72385	1070	76	1175	164	137	11
Ab.Sabaya Khola	Ab.Sabaya Khola	Jan-99	312	52	496	134	0.72597	1160	68	1100	151	145	11
Ab.Yankuwa Khola	Ab.Yankuwa Khola	Jan-99	236	41	468	123	0.72632	810	46	1012	129	160	11
Below Piluwa Khola	Below Piluwa Khola	Jan-99	348	77	687	185	0.73422	1100	57	1337	253	161	11
Below Lekuwa Khola	Below Lekuwa Khola	Jan-99	276	42	450	109	0.72894	880	100	987	126	151	11
Ab.Pikhuwa Khola	Ab.Pikhuwa Khola	Jan-99	282	53	519	138	0.73173	960	65	1200	145	162	11
Ab.Ulleri Khola	Ab.Ulleri Khola	Jan-99	320	35	461	94	0.72946	880	45	1075	126	157	11
BK58	85.91^0; 27.88^0	Sep-99	53	20	246	70	0.74568	340	5	539	152	95	12
BK60	85.90^0; 27.89^0	Sep-99	63	22	313	119	0.75234	260	2	601	136	81	12
BK62	85.88^0; 27.82^0	Sep-99	48	29	280	155	0.76341	260	12	735	75	92	12
BK64	85.88^0; 27.76^0	Sep-99	51	32	232	154	0.77122	190	6	752	65	88	12
BK74a	85.71^0; 27.64^0	Sep-99	42	25	221	103	0.78224	170	1	651	47	107	12
BK85	85.88^0; 27.87^0	Oct-99	66	24	249	103	0.75352	320	2	492	91	94	12

BK86	85.88^0; 27.86^0	Oct-99	75	28	285	153	0.75568	350	8	725	87	115	12
BK89	85.87^0; 27.83^0	Oct-99	71	30	312	163	0.75732	350	6	962	90	114	12
BK133	85.77^0; 27.72^0	Nov-99	80	30	273	151	0.76572	300	1	734	74	137	12
BK134	85.78^0; 27.73^0	Nov-99	81	34	340	185	0.76328	360	3	910	81	86	12
SK3	87.15^0; 26.92^0	Nov-99	117	42	346	132	0.77770	370	9	903	86	178	12

Table S2: Contributions from different sources to the chemical composition of river waters and estimated Ca loss for non-monsoon samples (with an assumption that the streams are undersaturated during high flow period).

		%Na$_R$	**%Na$_S$**	**%Na$_C$**	**%Na$_{Springs}$**	**%Cat$_R$**	**%Cat$_S$**	**%Cat$_C$**	**%Cat$_{Spring}$**	**%Sr$_R$**	**%Sr$_S$**	**%Sr$_C$**	**%Sr$_{Spring}$**	**^{87}Sr/^{86}Sr**	**%Ca loss**
Bhagirathi	**AK178**	25	66	2	7	14	23	62	6	10	16	69	1	0.74883	
	AK208	19	71	2	8	10	25	61	7	8	18	72	2	0.75251	
	AK178	11	72	2	16	6	26	50	13	6	22	73	4	0.74883	
	AK208	11	75	2	12	6	29	51	10	6	23	72	3	0.75251	
	5	18	70	2	10	14	35	37	12	12	29	60	4	0.75830	1
	23	14	70	2	14	11	35	49	17	7	23	64	5	0.75890	15
Alaknanda	**AK179**	11	74	3	12	4	22	57	6	4	15	88	2	0.73809	
	AK207	12	73	4	11	4	19	67	5	3	12	86	2	0.73594	
	AK104e	29	61	3	7	13	21	62	5	10	13	77	1	0.74029	
	AK123	19	64	4	13	7	19	67	7	6	11	82	2	0.73568	
	AK169	13	76	3	8	6	22	68	5	4	14	82	1	0.73744	
	AK33e	13	75	5	8	5	19	81	4	3	9	75	1	0.72493	
	24	14	73	3	9	7	22	83	7	5	21	73	2	0.73850	25
	AK54	13	77	3	8	7	22	79	6	5	24	70	2	0.73417	20
Ganga (Rishikesh)	**AK36**	14	68	6	12	6	20	70	8	4	9	81	2	0.72863	
	AK121	23	59	4	14	12	22	53	12	10	13	78	3	0.74006	
	TA4	11	59	7	24	4	17	59	13	3	8	89	3	0.73659	
	RW98-34	20	67	5	8	10	23	60	6	8	13	80	1	0.73856	
	RW99-6	23	67	5	6	12	25	64	5	8	11	74	1	0.73657	

	RW99-59	21	62	5	12	9	20	60	9	7	11	82	2	0.73849	
	Ganga3	38	47	7	8	14	16	73	5	9	5	81	1	0.73650	
	AK175	11	69	4	15	6	25	54	12	5	15	81	3	0.74209	
	AK211	9	72	5	14	4	23	58	10	3	13	85	3	0.73847	
	AK43	18	24	12	46	10	12	76	41	6	6	77	9	0.73782	40
	AK101	13	68	9	9	9	26	72	10	6	18	70	2	0.73791	21
	AK120	16	64	11	9	9	22	74	8	6	16	79	2	0.73858	25
	RK1096	18	54	13	15	9	19	76	12	6	12	80	3	0.73836	23
	RK1196	14	70	10	6	8	23	71	6	6	19	80	2	0.74502	24
	RK1296	14	66	12	8	8	23	80	8	5	15	77	2	0.73937	24
	RK197	14	66	11	8	8	23	77	8	5	16	77	2	0.73961	23
	RK297	14	67	11	8	8	24	77	8	5	16	76	2	0.73919	24
	Ganga 3	18	57	11	13	11	22	86	14	7	14	78	3	0.73990	41
	Ganga 3	12	70	12	6	6	22	71	5	4	17	80	1	0.74080	8
Yamuna	**RW98-26**	7	84	3	6	7	53	36	10	5	44	52	2	0.77495	
	RW98-27	11	66	3	19	9	35	28	21	7	32	53	6	0.76059	
	RW98-28	26	59	3	12	21	34	25	14	18	30	46	4	0.76145	
	RW98-29	16	61	4	19	13	32	31	20	10	28	56	5	0.74954	
	RW98-30	17	50	10	23	9	16	57	17	6	13	81	3	0.73676	
	RW98-31	11	49	15	25	5	11	70	15	3	9	85	3	0.72927	
	RW98-32	17	59	21	3	7	14	93	2	2	6	70	0	0.72693	
	RW98-16	24	28	9	38	11	14	43	23	9	8	81	6	0.75158	
	RW98-20	25	38	7	30	14	17	41	23	11	13	73	6	0.75725	
	RW98-25	37	35	5	23	23	16	35	20	20	14	67	5	0.74985	
	RW98-22	35	38	6	21	23	17	37	19	18	14	67	5	0.74887	
	RW98-15	25	25	5	45	13	11	29	31	15	11	73	11	0.74598	
	RW98-14	20	23	6	51	10	10	29	34	12	10	76	13	0.74495	
	RW98-12	25	50	9	16	16	17	63	14	8	11	68	2	0.73757	
	RW98-1	16	54	11	19	9	18	61	15	5	13	78	3	0.73518	
	RW99-58	9	48	9	33	5	16	51	23	3	13	81	5	0.73446	
	RW98-4	23	69	2	6	12	20	61	4	6	18	75	1	0.72356	
	RW99-55	13	68	2	17	8	24	55	15	4	22	71	4	0.72447	

	RW98-33	25	65	2	9	12	18	59	6	7	17	78	1	0.72657	
	RW99-54	12	68	2	18	7	24	62	13	3	17	71	3	0.72624	
	RW99-31	18	54	4	24	9	28	71	14	5	10	80	3	0.72556	26
	RW99-7	16	71	3	9	8	37	59	6	5	16	80	2	0.72657	18
Ghagara (Karnali)	**Karnali below the Seti**	15	75	1	9	11	29	51	8	7	26	66	2	0.72957	
	Karnali above Thuli Gad	15	75	1	9	9	24	62	7	5	20	71	2	0.72968	
	Karnali at Chisapani	18	65	2	14	8	17	68	8	5	13	80	2	0.73499	
Gandak															
Trisuli	**LO256**	24	62	6	8	14	22	55	9	6	12	81	1	0.72220	
	LO258	18	71	6	6	11	26	61	8	4	13	77	1	0.72680	
	TRI 19/6	18	57	6	19	9	19	48	20	5	11	83	3	0.72700	
	LO316	15	71	5	8	10	26	59	11	4	13	78	1	0.73480	
	LO304	47	43	6	4	27	16	56	4	11	8	78	1	0.72700	
	TRI 15/7	8	39	9	44	3	13	48	28	1	5	90	5	0.72460	
	TRI 1/8	11	52	6	32	5	21	43	27	3	10	86	5	0.73130	
	TRI 15/8	13	56	4	27	7	22	38	29	5	14	77	5	0.73210	
	TRI 1/9	41	48	2	9	30	26	30	13	19	17	64	2	0.73280	
	TRI 15/9	18	67	4	11	12	27	43	15	7	18	77	2	0.73530	
	TRI 1/10	11	63	7	19	20	28	49	30	5	19	71	5	0.73782	33
	TRI 15/10	12	63	6	19	24	28	46	31	6	21	68	5	0.73791	34
	TRI 1/11	11	66	6	17	22	30	46	30	5	22	68	5	0.73858	33
	TRI 1/12	11	63	5	20	25	30	44	37	6	23	65	6	0.73836	40
	TRI 4/4	11	68	5	16	24	33	44	31	6	25	64	5	0.74502	38
Kali	**LO310**	18	53	1	27	6	13	72	13	3	9	82	3	0.73500	
	LO306	21	56	1	22	7	14	67	10	4	11	86	3	0.74770	
Seti	**LO312**	31	49	2	18	8	17	77	7	4	3	84	1	0.72180	
	LO302	14	68	1	18	5	26	50	9	3	10	93	2	0.74300	
Narayani	**LO308**	20	56	1	24	8	17	62	14	5	15	76	3	0.73600	
	NH1	18	42	3	37	11	16	81	31	6	13	73	7	0.73650	42
	NAG49	18	37	4	41	9	13	78	27	6	11	78	7	0.73640	34
Kosi															

Arun	**Ab.Pikhuwa Khola**	16	70	3	11	17	33	37	15	18	32	44	4	0.72422	
	Ab.Khandapp Khola	15	74	3	8	18	38	32	13	20	37	40	3	0.72385	
	Ab.Sabaya Khola	19	74	3	5	22	38	37	7	20	31	38	1	0.72597	
	Ab.Yankuwa Khola	11	75	4	11	11	34	40	14	13	34	52	3	0.72632	
	Below Piluwa Khola	8	78	3	10	8	36	38	14	10	39	53	4	0.73422	
	Below Lekuwa Khola	28	61	2	9	33	32	24	13	36	30	29	3	0.72894	
	Ab.Pikhuwa Khola	15	72	3	10	16	35	38	14	18	33	46	3	0.73173	
	Ab.Ulleri Khola	7	82	2	9	9	45	31	16	10	46	38	4	0.72946	
Bhote Kosi	**BK58**	25	71	2	2	13	30	47	1	51	28	12	0	0.74568	
	BK60	6	91	2	2	3	33	56	1	17	55	24	0	0.75234	
	BK62	19	54	3	24	7	19	63	11	45	25	27	5	0.76341	
	BK64	4	79	3	14	2	29	64	7	14	53	35	4	0.77122	
	BK74a	3	92	3	2	1	32	69	1	11	57	34	0	0.78224	
	BK85	4	84	10	3	2	45	67	2	2	25	64	1	0.75352	17
	BK86	13	67	11	9	7	35	67	6	6	21	72	2	0.75568	22
	BK89	11	70	12	7	5	33	66	4	5	20	76	2	0.75732	14
	BK133	2	89	9	1	1	48	57	1	1	34	71	0	0.76572	17
	BK134	5	81	11	3	2	38	61	2	2	26	76	1	0.76328	11
	SK3	9	78	6	7	7	52	47	6	6	35	56	3	0.7777	17

References

Aharon P., Schiodlowski M. and Singh I. (1987) Chronostratigraphic markers in the end-Precambrian carbon isotope record of the Lesser Himalaya. Nature, 327, 699-702.

Ahmad S. M., Anil Babu G., Padmakumari V. M., Dayal A. M., Sukhija and B. S., Nagabhushanam P. (2005) Sr, Nd isotopic evidence of terrigenous flux variations in the Bay of Bengal: Implications of monsoons during the last ~34,000 years. Geophyical Research Letters, 32, 1-4.

Ahmad S. M., Padmakumari V. and Anil Babu G. (2009) Strontium and neodymium isotopic compositions in sediments fom Godavari, Krishna and Pennar rivers. Current Science, 97, 1766-1769.

Ahmad T., Harris N., Bickle M., Chapman H., Bunbury J. and Prince C. (2000) Isotopic constraints on the structural relationships between the Lesser Himalayan Series and the High Himalayan Crystalline Series, Garhwal Himalaya, Geological Society of America Bulletin, 112, 467– 477.

Ahmad T., Dragusanu C. and Tanaka T. (2008) Provenance of Proterozoic Basal Aravalli volcanic rocks from Rajasthan, Northwestern India: Nd isotopes evidence for enriched mantle reservoirs. Precambrian Research, 162, 150-159.

Amiotte-Suchet P., Probst J., and Ludwig W. (2003) Worldwide distribution of continental rock lithology: Implications for the atmospheric/soil CO_2 uptake by continental weathering and alkalinity river transport to the oceans. Global Biogeochemical Cycles, 17, 1038, doi: 10.1029/2002GB001891.

Amthor J., Grotzinger J., Schroder S., Bowring S., Ramezani J., Martin M. and Matter A. (2003) Extinction of *Cloudina* and *Namacalathus* at the Precambrian-Cambrian boundary in Oman. Geology, 31, 431-434.

Anbar A., Duan Y., Lyons T., Arnold G., Kendall B., Creaser R., Kaufman A., Gordon G., Scott C., Garvin J. and Buick R. (2007) A whiff of oxygen before the great oxidation event? Science, 317, 1903-1906.

Anderson D. (1993) Helium-3 from the Mantle: Primordial signal or cosmic dust? Science, 261, 170-176.

Arthur M. and Sageman B. (1994) Marine black shales: depositional mechanisms and environments of ancient deposits. Annual Review of Earth and Planetary Sciences, 22, 499–551.

Aucour A., France-Lanord C., Pedoja K., Pierson-Wickmann A.-C. and Sheppard S. M. F. (2006) Fluxes and sources of particulate organic carbon in the Ganga-Brahmaputra river system, Global Biogeochemical Cycles, 20, GB2006, doi:10.1029/2004GB002324.

Auden J. B. (1933) Vindhyan sedimentation in the Son Valley, Mirzapur District. Memoir of the Geological Survey of India, 62, 141-250.

Awasthi N. (1970) Some aspects of the Krol Formation of the Himalaya, India. Contributions to Minerology and Petrology, 28, 198-220.

Azmi R.J. (1983) Microfauna and age of the Lower Tal Phosphorite of Mussoorie Syncline, Garhwal Lesser Himalaya, India. Himalayan Geology, 11, 373–409.

Azmi R.J. (1998) Discovery of Lower Cambrian small shelly fossils and brachiopods from the Lower Vindhyan of the Son Valley, Central India. Journal of Geological Society of India, 52, 381-389.

Azmi R.J., Joshi D., Tiwari B., Joshi M. and Srivastava S. (2008) A synoptic view on the current discordant geo- and biochronological ages of the Vindhyan Supergroup, central India. Himalayan Geology, 29, 177-191.

Azmy K., Kendall B., Creaser R. A., Heaman L., Misi A. and De Oliveira T. F. (2008) Global correlation of the Vazante Group, Sa˜o Francisco Basin, Brazil: Re–Os and U–Pb radiometric age constraints. Precambrian Research, 164, 160–172.

Banerjee D. and Narain M. (1976) Trace fossils in the Lower Tal formation of Mussoorie and their environmental significance. Journal of Sedimentary Research, 46, 234-239.

Banerjee D., Schidlowski M., Siebert F. and Brasier M. (1997) Geochemical changes across the Proterozoic–Cambrian transition in the Durmala phosphorite mine section, Mussoorie Hills, Garhwal Himalaya, India. Palaeogeography Palaeoclimatology Palaeoecology, 132, 183–194.

Bansal M., Vijan A.R., Mahar Y.S., Ghosh N., Krishna, Prasad S. and Prabhy B. (1999) Rb-Sr dating of Lower Vindhyan sediments from Son Valley, Madhya Pradesh, India. Indian Mineralogist, 33, 1-9.

Bekker A., Holland H.D.,Wang P.-L., Rumble III D., Stein H.J., Hannah J.L., Coetzee L.L. and Beukes, N.J. (2004) Dating the rise of atmospheric oxygen. Nature, 427, 117–120.

Bengston S., Belivanova V., Rasmussen B. and Whitehouse M. (2009) The controversial "Cambrian" fossils of the Vindhyan are real but more than a billion years older. Proceedings of the National Academy of Sciences of the United States of America, 106, 7729-7734.

Berner R. A., Lasaga A. C., and Garrels R. M. (1983) The carbonate–silicate geochemical cycle and its effect on atmospheric carbon dioxide over the past 100 million years, American Journal of Science, 283, 641– 683.

Bhushan R., Chakraborty S. and Krishnaswami S. (1994) Physical Research Laboratory (Chemistry) Radiocarbon Date list I. Radiocarbon, 36, 251-256.

Bhushan R., Dutta K. and Somayajulu B.L.K. (2001) Concentrations and burial fluxes of organic and inorganic carbon on the eastern margins of the Arabian Sea, Marine Geology, 178, 95-113.

Bickle M. J., Harris N. B. W., Bunbury J. M., Chapman H. J., Fairchild I. J. and Ahmad T. (2001) Controls on the ^{87}Sr/^{86}Sr ratio of carbonates in the Garhwal Himalaya, Headwaters of the Ganges. The Journal of Geology, 109, 737-753.

Bickle M. J., Bunbury J., Chapman H. J., Harris N. B. W., Fairchild I. J. and Ahmad T. (2003) Fluxes of Sr into the headwaters of the Ganges. Geochimica et Cosmochimica Acta, 67, 2567-2584.

Bickle M. J., Chapman H. J., Bunbury J., Harris N. B. W., Fairchild I. J., Ahmad T. and Pomies C. (2005) Relative contributions of silicate and carbonate rocks to riverine Sr fluxes in the headwaters of the Ganges. Geochimica et Cosmochimica Acta, 69, 2221-2240.

Biju-Sekhar S., Yokoyama K., Pandit M., Okudaira T., Yoshida M. and Santosh M. (2003) Late Paleoproterozoic magmatism in Delhi fold belt, NW India and its implication : evidence from EPMA chemical ages of zircons. Journal of Asian Earth Sciences, 22, 189-207.

Birck J.L., Roy Barman M. and Capmas F. (1997) Re–Os isotopic measurements at the Femtomole level in natural samples. Geostandards Newsletter, 20, 19–27.

Bloemendal J., King J., Hunt A., Demenocal P. and Hayashida A. (1993) Origin of the sedimentary magnetic record at Ocean drilling program sites on the Owen ridge, western Arabian sea. Journal of Geophyical Research, 98, 4199-4219.

Bloemendal J., Liu X. and Rolph T. (1995) Correlation of the magnetic susceptibility startigraphy of Chinese loess and the marine oxygen isotope record: chronological and palaeoclimatic implications. Earth and Planetary Science Letters, 131, 371-380.

Blum J. D., Gazis C. A., Jacobson A. D. and Chamberlain C. P. (1998) Carbonate versus silicate weathering in the Raikhot watershed within the high Himalayan crystalline series. Geology, 26, 411–414.

Bookhagen B., and Burbank D.W. (2006), Topography, relief, and TRMM-derived rainfall variations along the Himalaya, Geophyical Research Letters, 33, L08405, doi:10.1029/2006GL026037.

Bookhagen B., Thiede R. C. and Strecker M. R. (2005) Late Quaternary intensified monsoon phases control landscape evolution in the northwest Himalaya, Geology, 33, 149-152.

Bordet P., Colchen M., Krummenacher D., Le Fort P., Mouterde R. and Remy M. (1971) Recherches Ge´ologiques dans l'Himalaya du Ne´pal, Re´gion de le Thakkhola. Centre National de la Recherche Scientifique, Paris.

Bouquillon A., France-Lanord C., Michard A. and Tiercelin J. J. (1990) Sedimentology and isotopic chemistry of the Bengal Fan sediments: the denudation of the Himalaya, Proceedings of the Ocean Drilling Program, Scientific Results, Leg 116, 43-58.

Bowring S. A., Grotzinger J. P., Isachen C. E., Knoll A. H., Pelechaty S. M. and Kolosov P. (1993) Calibrating rates of Early Cambrian evolution. Science, 261, 1293–1298.

Bowring S.A., Myrow P.M., Landing E. and Ramezani E. (2003) Geochronological constraints on terminal Neoproterozoic events and the rise of the metazoans. NASA Astrobiology Institute General Meeting Abstracts 113–114.

Brasier M.D. (1989) On mass extinctions and faunal turnover near the end of the Precambrian, I*n* Mass extinctions: Processes and evidence (Ed. Donovan S.K.): London, Belhaven Press, 73–88.

Brasier M.D. (1995) The basal Cambrian transition and Cambrian bio-events (from terminal Proterozoic extinctions to Cambrian biomeres), *In* Global events and event stratigraphy in the Phanerozoic (Ed. Walliser O.H.): Berlin, Springer-Verlag, 113–138.

Brasier M. D. and Singh P. (1987) Microfossils and Precambrian-Cambrian boundary stratigraphy at Maldeota, Lesser Himalaya. Geological Magazine 124, 323–345.

Brasier M. D., Cowie J. and Taylor M. (1994) Decision on the Precambrian-Cambrian boundary stratotype. Episodes, 17, 3–8.

Burbank D. W., Blythe A. E., Putkonen J., Pratt-Sitaula B., Gabet E., Oskin M., Barros A. and Ojha, T. P. (2003) Decoupling of erosion and precipitation in the Himalayas, Nature, 426, 652-655.

Burton K. W. and Vance D. (2000) Glacial-interglacial variations in the neodymium isotope composition of seawater in the Bay of Bengal recorded by planktonic foraminifera, Earth and Planetary Science Letters, 176, 425-441.

Campbell I. and Allen C. (2008) Formation of supercontinents linked to increases in atmospheric oxygen. Nature Geoscience 1, 554-558.

Canfield D., Habicht K. and Thamdrup B. (2000) The Archean sulfur cycle and the early history of atmospheric oxygen. Science, 288, 658-661.

Canfield DE. (2005) The early history of atmospheric oxygen: homage to Robert M. Garrels. Annual Review of Earth and Planetary Sciences, 33, 1–36.

Chakrabarti R., Basu A. and Chakrabarti A. (2007) Trace element and Nd isotopic evidence for sediment sources in the mid-Proterozoic Vindhyan Basin, central India. Precambrian Research, 159, 260-274.

Chamberlin T. C. (1899) An attempt to frame a working hypothesis of the cause of glacial periods on an atmospheric basis. The Journal of Geology, 7, 545–584.

Chen C., Sedwick P. and Sharma M. (2009) Anthropogenic osmium in rain and snow reveals global-scale atmospheric contamination. Proceedings of the National Academy of Sciences of the United States of America, 106, 7724-7728.

Choudhary A.K., Gopalan K. and Sastry C.A. (1984) Present status of geochronology of the Precambrian rocks of Rajasthan. Tectonophysics, 105, 131–140.

Clift P. D., Giosan L., Blusztajn J., Campbell I. H., Allen C., Pringle M., Tabrez A. R., Danish M., Rabbani M. M., Alizai C. A. and Lückge A. (2008) Holocene erosion of the Lesser Himalaya triggered by intensified summer monsoon, Geology, 36, 79-82.

Cohen A. S., Coe A. L., Bartlett J. M. and Hawkesworth C. J. (1999) Precise Re–Os ages of organic-rich mudrocks and the Os isotope composition of Jurassic seawater. Earth and Planetary Science Letters, 167, 159–173.

Colchen M., Le Fort P. and Pecher A. (1986) Notice explicative de la carte ge´ologique Annapurna-Manaslu-Ganesh Himalaya du Ne´pal.au

1:200.000e bilingue: Franc¸ais–English.. Centre National de la Recherche Scientifique.

Colin C., Turpin L., Bertaux J., Desprairies A. and Kissel C. (1999) Erosional history of the Himalayan and Burman ranges during the last two glacial-interglacial cycles, Earth and Planetary Science Letters, 171, 647-660.

Colin C., Turpin L., Blamart D., Frank N., Kisel C. and Duchamp S. (2006) Evolution of weathering patterns in the Indo-Burman Ranges over 280 kyr: Effects of sediment provenance on ^{87}Sr/^{86}Sr ratios tracer, Geochemistry Geophyics Geosystem, 7, doi:10.1029/2005GC000962.

Colodner D., Sachs J., Ravizza G., Turekian K. K., Edmond J. M. and Boyle E. (1993) The geochemical cycle of rhenium: A reconnaissance. Earth and Planetary Science Letters ,117, 205–221.

Courtillot V., Besse J., Vandamme D., Montigny R., Jaeger J. and Cappetta H. (1986) Deccan flood basalts at Cretaceous/Tertiary boundary? Earth and Planetary Science Letters, 80, 361-374.

Crawford A.R. and Compston W. (1970) The age of the Vindhyan System of Peninsular India. Quarterly Journal of Geological Society, 125, 251–371.

Creaser R. A., Papanastassiou D. A. and Wasserburg G. J. (1991) Negative thermal ion mass spectrometry of osmium, rhenium and iridium. Geochimica et Cosmochimica Acta, 55, 397–401.

Creaser R. A., Sannigrahi P., Chacko T. and Selby D. (2002) Further evaluation of the Re–Os geochronometer in organic-rich sedimentary rocks: a test of hydrocarbon maturation effects in the Exshaw Formation, Western Canada Sedimentary Basin. Geochimica et Cosmochimica Acta, 66, 3441–3452.

Crouzet C., Dunkl I., Paudel L., Arkai P., Rainer T. M., Balogh K. and Appel E. (2007) Temperature and age constraints on the metamorphism of the Tethyan Himalaya in central Nepal: A multidisciplinary approach. Journal of Asian Earth Sciences, 30, 113-130.

Curray J. R. (1994) Sediment volume and mass beneath the Bay of Bengal. Earth and Planetary Science Letters, 125, 371-383.

Curray J. R., Emmel F. J. and Moore D. G. (2003) The Bengal Fan: Morphology, geometry, stratigraphy, history and processes. Marine and Petroleum Geology, 19, 1191-1223.

Dalai T.K. (2001) Major ions, stable isotopes, $^{87}Sr/^{86}Sr$ and Re in the headwaters of the Yamuna: Implications to chemical weathering in the Himalaya. Ph.D. Dissertation, M.S. University of Baroda, Vadodara, India.

Dalai T. K. and Ravizza G. (2010) Investigation of an early Pleistocene marine Osmium isotope record from the Eastern Equatorial Pacific. Geochimica et Cosmochimica Acta, 74, 4332-4345.

Dalai T. K., Krishnaswami S., and Sarin M. M. (2002) Major ion chemistry in the headwaters of the Yamuna river system: Chemical weathering, its temperature dependence and CO_2 consumption in the Himalaya. Geochimica et Cosmochimica Acta, 66, 3397-3416.

Dalai T. K., Singh S. K., Trivedi J. R. and Krishnaswami S. (2002) Dissolved rhenium in the Yamuna River System and the Ganga in the Himalaya: Role of black shale weathering on the budgets of Re, Os, and U in rivers and CO2 in the atmosphere. Geochimica et Cosmochimica Acta, 66, 29-43.

Dalai T. K., Krishnaswami S. and Kumar A. (2003) Sr and $^{87}Sr/^{86}Sr$ in the Yamuna River System in the Himalaya: Sources, fluxes, and controls on Sr isotope composition. Geochimica et Cosmochimica Acta, 67, 2931-2948.

Dalai T. K., Rengarajan R. and Patel P. P. (2004) Sediment geochemistry of the Yamuna River System in the Himalaya: Implications to weathering and transport. Geochemical Journal, 38, 441-453.

Dalai T. K., Suzuki K., Minagawa M. and Nozaki Y. (2005) Variations in seawater osmium isotope composition since the last glacial maximum: A case study from the Japan Sea. Chemical Geology, 220, 303-314.

Das A., Krishnaswami S., Sarin M. M. and Pande K. (2005) Chemical weathering in the Krishna Basin and Western Ghats of the Deccan Traps, India: Rates of basalt weathering and their controls. Geochimica et Cosmochimica Acta, 69, 2067-2084.

Das A. and Krishnaswami S. (2007) Elemental geochemistry of river sediments from the Deccan Traps, India: Implications to sources of elements and their mobility during basalt–water interaction. Chemical Geology, 242, 232–254.

Deb M. and Thorpe R.A. (2004) Geochronological constraints inthe Precambrian geology of Rajasthan and their metallogenic implications. *In* Sediment-Hosted Lead–Zinc Sulphide Deposits (Eds. Deb, M., Goodfellow, W.D.). Narosa Publishing House, New Delhi, 246–263.

Dickin A. (2005) Radiogenic Isotope Geology. Second Edition, Cambridge Publications, 492 pp.

Dill H., 1986. Metallogenesis of early Paleozoic graptolite shales from the Graefenthal Horst (Northern Bavaria-Federal Republic of Germany). Economic Geology, 81, 889–903.

Duplessy J. C. (1982) Glacial to interglacial contrasts in the northern Indian Ocean, Nature, 295, 494-498.

Dutta K., Bhushan R. and Somayajulu B. L. K. (2001) ΔR correction values for the northern Indian Ocean. Radiocarbon, 43, 483-488.

Ebelmen J. (1845) Sur les produits de la de´composition des especes mine´rales de famille des silicates. Annales des Mines, 7, 3– 66.

Edmond J. M. and Huh Y. (1997) Chemical weathering yields from basement and orogenic terrains in hot and cold climates. In Tectonic Uplift and Climate Change (Ed. Ruddiman, W.F.), Plenum Press, New York, 329-351.

English N.B., Quade J., DeCelles P. G. and Garizone C.N. (2000) Geological control of Sr and major element chemistry in Himalayan rivers, Nepal. Geochimica et Cosmochimica Acta, 64, 2549-2566.

Erwin D.H. (1993) The great Paleozoic crisis: Life and death in the Permian: New York, Columbia University Press, 327 pp.

Esser B. K. and Turekian K. K. (1993) The osmium isotopic composition of the continental crust. Geochimica et Cosmochimica Acta, 57, 3093–3104.

Evans M. J., Derry L. A., Anderson S. P. and France-Lanord C. (2001) Hydrothermal source of radiogenic Sr to Himalayan rivers. Geology, 29, 803–806.

Evans M. J., Derry L. A. and France-Lanord C. (2004) Geothermal fluxes of alkalinity in the Narayani river system of central Nepal. Geochemistry Geophyics Geosystem, 5, Q08011, doi:10.1029/2004GC000719.

Farquhar J. and Wing B. (2003) Multiple sulfur isotopes and the evolution of the atmosphere. Earth and Planetary Science Letters, 213, 1-13.

Farquhar J., Bao H. and Thiemens M. (2000) Atmospheric influence of Earth's earliest sulfur cycle, Science, 289, 756-758.

Faure G. (1986) Principles of Isotope Geology. 2nd Edition. Wiley, Hoboken, N.J., 608 pp.

France-Lanord C. and Derry L. A. (1997) Organic carbon burial forcing of the carbon cycle from Himalayan erosion. Nature, 390, 65-67.

France-Lanord C., Evans M., Hurtrez J., and Riotte J. (2003) Annual dissolved fluxes from Central Nepal rivers: Budget of chemical erosion in the Himalayas. Comptes Rendus Geosciences, 335, 1131-1140.

France-Lanord C., Derry L. and Michard A. (1993) Evolution of the Himalaya since Miocene time: Isotopic and sedimentologic evidence from the Bengal Fan. *In* Himalayan Tectonics (Ed. Treloar P. J. and Searle M. P.) Special Publication, Geological Society, London, 74, 603–621.

Frei R., Gaucher C., Poulton S. and Canfield D. (2009) Fluctuations in Precambrian atmospheric oxygenation recorded by chromium isotopes. Nature 461, 250-253.

Frimmel H. E. (2005) Archean atmospheric evolution: evidence from the Witwatersrand gold fields, South Africa. Earth-Science Reviews, 70, 1-46.

Gaillardet J., Dupre B., Louvat P. and Allegre C. J. (1999) Global silicate weathering and CO_2 consumption rates deduced from the chemistry of large rivers. Chemical Geology, 159, 3-30.

Galy A. (1999) Etude geochimique de l'erosion actuelle de la chaine Himalayenne, Ph. D. thesis, 464 pp., Inst. Natl. Polytech. De Lorrain, Vandoeuvre-lees-Nancy, France.

Galy A. and France-Lanord C. (1999) Weathering processes in the Ganges-Brahmaputra basin and the riverine alkalinity budget. Chemical Geology, 159, 31-60.

Galy A. and France-Lanord C. (2001) Higher erosion rates in the Himalaya: Geochemical constraints on riverine fluxes. *Geology*, 29, 23-26.

Galy A., France-Lanord C. and Derry L. A. (1999) The strontium isotopic budget of Himalayan Rivers in Nepal and Bangladesh. Geochimica et Cosmochimica Acta, 63, 1905-1925.

Galy V., France-Lanord C., Beyssac O., Faure P., Kudrass H. and Palhol F. (2007) Efficient organic carbon burial in the Bengal fan sustained by the Himalayan erosion system. Nature, 450, 407-411, doi: 10.1038/nature06273.

Galy V., Francois L., France-Lanord C., Faure P., Kudrass H., Palhol F. and Singh S. K. (2008a) C4 plants decline in the Himalayan basin since the Last Glacial Maximum. Quaternary Science Reviews, 27, 1396-1409.

Galy V., France-Lanord C. and Lartiges B. (2008b) Loading and fate of prticulate organic carbon from the Himalaya to the Ganga-Brahmaputra delta. Geochimica et Cosmochimica Acta, 72, 1767-1787.

Galy V., France-Lanord C., Peucker-Ehrenbrink B. and Huyghe P. (2010) Sr-Nd-Os evidence for a stable erosion regime in the Himalaya during the past 12 Myr. Earth and Planetary Science Letters, 290, 474-480.

Gansser A. (1964) Geology of the Himalayas. Intersciences Publishers, L.U.

Garrels R.M. and Mackenzie F. (1971) Evolution of Sedimentary Rocks. Norton W.W. & Co., New York, 397 pp.

Godderis Y. and Veizer J. (2000) Tectonics control of chemical and isotopic composition of ancient oceans: The impact of continental growth. American Journal of Science, 300, 434-461.

Goldstein S L, O'Nions R K (1981) Nd and Sr isotopic relationships in pelagic clays and ferromanganese deposits. Nature, 292, 324-327.

Goodbred S. L. Jr. (2003) Response of the Ganges dispersal system to climate change: a source-to-sink view since the last interstade. Sedimentary Geology, 162, 83-104.

Goodbred S.L. Jr. and Kuehl S.A. (2000) The significance of large sediment supply, active tectonism, and eustasy on margin sequence development: Late Quaternary stratigraphy and evolution of the Ganges-Brahmaputra delta. Sedimentary Geology, 133, 227–248.

Gopalan K., Macdougall J.D., Roy A.B. and Murali A.V. (1990) Sm-Nd evidence for 3.3 Ga old rocks in Rajasthan, NW India. Precambrian Research, 48, 287–297.

Gourlan A., Meynadier L., Allegre C., Tapponnier P., Birck J. and Joron J. (2010) Northern Hemisphere climate control of the Bengali rivers discharge during the past 4 Ma. Quaternary Science Reviews, 29, 2484-2498.

Granet M., Chabaux F., Stille P., France-Lanord C.and Pelt E. (2007) Time-series of sedimentary transfer and weathering processes from U-series nuclides: Clues from the Himalayan rivers. Earth and Planetary Science Letters, 261, 389-406.

Gregory L.C., Meert J.G., Pradhan V., Pandit M.K., Tamrat E. and Malone S.J. (2006) A paleomagnetic and geochronologic study of the Majhgawan Kimberlite, India: Implications for the age of the Vindhyan SuperGroup. Precambrian Research, 149, 65–75.

Grotzinger J.P., Bowring B.Z., Saylor B.Z., and Kaufman A.J. (1995) Biostratigraphic and geochronologic constraints on early animal evolution. Science, 270, 598–604.

Handa R.K. (1972) Geochemistry of the Ganga river water. Indian Geohydrology, 2, 71–78.

Hannah J.L., Bekker A., Stein H.J., Markey R.J. and Holland H.D. (2004) Primitive Os and 2316 Ma age for marine shale: implications for Paleoproterozoic glacial events and the rise of atmospheric oxygen. Earth and Planetary Science Letters, 225, 43–52.

Hannah J.L., Stein H.J., Zimmerman A., Yang G., Melezhik V.A., and Melezhik V.A. (2008). Precise 2004±9 Ma Re–Os age for Pechenga black shale: Comparison of sulfides and organic material. Geochimica et Cosmochimica Acta, 70, A228.

Harris N. (1995) Significance of weathering Himalayan metasedimentary rocks and leucogranites for the Sr isotope evolution of seawater during the early Mioce*ne.* Geology, *23*, *79*5–798.

Harris N., Bickle M., Chapman H., Fairchild I. and Bunbury J. (1998) The significance of Himalayan rivers for silicate weathering rates: Evidence from the Bhote Kosi tributary. Chemical Geology, 144, 205-220.

Heron A. (1953) Geology of Central Rajputana. Mem. Geol. Surv. India, 79, 339 pp.

Herzschuh U. (2006) Palaeo-moisture evolution in monsoonal Central Asia during the last 50,000 years. Quaternary Science Reviews, 25, 163-178.

http://www.gemswater.org/atlas-gwq/table3-e.html

Hughes N., Peng S., Bhargava O., Ahluwalia A., Walia S., Myrow P. and Parcha S. (2005) Cambrian biostratigraphy of the Tal group, Lesser Himalaya, India, and early Tsanglangpuan (late early Cambrian) trilobites from the Nigali Dhar syncline. Geological Magazine, 142, 57-80.

Islam M. R., Begum S. F., Yamaguchi Y. and Ogawa K. (1999) The Ganges and Brahmaputra rivers in Bangladesh: Basin denudation and sedimentation, Hydrological Processes, 13, 2907-2923.

Jacobson A. D., and Blum J. D. (2000) Ca/Sr and ^{87}Sr/^{86}Sr geochemistry of disseminated calcite in Himalayan silicate rocks from Nanga Parbat: Influence on river-water chemistry. Geology, 28, 463–466.

Jacobson A. D., Blum J. D., Page Chamberlain C., Craw D. and Koons P. O. (2003) Climatic and tectonic controls on chemical weathering in the New Zealand southern Alps. Geochimica et Cosmochimica Acta, 67, 29-46.

Jacobson A. D., Blum J. D. and Walter L. M. (2002) Reconciling the elemental and Sr isotope composition of Himalayan weathering fluxes: Insights from the carbonate geochemistry of stream waters. Geochimica et Cosmochimica Acta, 66, 3417-3429.

Jaffe L.A., Peucker-Ehrenbrink B. and Petsch S.T. (2002) Mobility of rhenium, platinum group elements and organic carbon during black shale weathering. Earth and Planetary Science Letters, 198, 339–353.

Jiang G., Sohl L. and Christie-Blick N. (2003) Neoproterozoic stratigraphic comparision of the Lesser Himalaya (India) and Yangtze block (south China): Paleogeographic implications. Geology 31, 917-920.

Jiang S., Yang J., Ling H., Chen Y., Feng H., Zhao K. and Ni P. (2007) Extreme enrichment of polymetallic Ni–Mo–PGE–Au in lower Cambrian black shales of South China: An Os isotope and PGE geochemical investigation. Palaeogeography Palaeoclimatology Palaeoecology, 254, 217–228.

Jiang S., Pi D., Heubeck C., Frimmel H., Liu Y., Deng H., Ling H. and Yang J. (2009) Early Cambrian ocean anoxia in south China. Nature, 459, E5-E6.

Jones B. and Manning D.A.C. (1994) Comparison of geochemical indices used for the interpretation of palaeoredox conditions in ancient mudstones. Chemical Geology, 111, 111 –129.

Kah L.C., Lyons T.W. and Frank T.D. (2004) Evidence for low marine sulphate and the protracted oxygenation of the Proterozoic biosphere. Nature, 431, 834–838.

Karim A. and Veizer J. (2000) Weathering processes in the Indus River Basin: implications from riverine carbon, sulfur, oxygen, and strontium isotopes. Chemical Geology, 170, 153-177.

Kasting J. (2001) The rise of atmospheric oxygen. Science, 293, 819-820.

Kato Y., Suzuki K., Nakamura K., Hickman A., Nedachi M., Kusakabe M., Bevacqua D. and Ohmoto H. (2009) Hematite formation by oxygenated groundwater more than 2.76 billion years ago. Earth and Planetary Science Letters, 278, 40-49.

Kaufman A., Jiang G., Christie-Blick N., Banerjee D. and Rai V. (2006) Stable isotope record of the terminal Neoproterozoic Krol platform in the Lesser Himalayas of the northern India. Precambrian Research, 147, 156-185.

Kendall B.S., Creaser R.A., Ross G.M. and Selby D. (2004) Constraints on the timing of Marinoan Snowball Earth glaciation by 187Re–187Os dating of a Neoproterozoic, post-glacial black shale in Western Canada. Earth and Planetary Science Letters, 222, 729–740.

Kendall B.S., Creaser R.A. and Selby D. (2006) Re–Os geochronology of postglacial black shales in Australia: constraints on the timing of “Sturtian” glaciation. Geology, 34, 729–732.

Kendall B., Creaser R. and Selby D. (2009a) ^{187}Re-^{187}Os geochronology of Precambrian organic-rich sedimentary rocks. *In* Global Neoproterozoic Petroleum Systems: The Emerging Potential in North Africa (Eds. Craig J., Thurow J., Thusu B.,Whitham A., Abutarruma Y.). Geological Society, London, Special Publications, 326, 85–107.

Kendall B., Creaser R. A., Gordon G. W. and Anbar A. D. (2009b) Re–Os and Mo isotope systematics of black shales from the Middle Proterozoic Velkerri and Wollogorang Formations, McArthur Basin, northern Australia. Geochimica et Cosmochimica Acta, 73, 2534–2558.

Kendall B., Creaser R. A., Calver C. R., Raub T. D. and Evans D. (2009c) Correlation of Sturtian diamictite successions in southern Australia and northwestern Tasmania by Re–Os black shale geochronology and the ambiguity of “Sturtian”-type diamictite-cap carbonate pairs as chronostratigraphic marker horizons. Precambrian Research, 172, 301–310.

Kessarkar P. M., Rao V. P., Ahmad S. M. and Anil Babu G. (2003) Clay minerals and Sr-Nd isotopes of the sediments along the western margin of India and their Implication for sediment provenance. Marine Geology, 202, 55-69.

Kessarkar P. M., Rao V. P., Ahmad S. M., Patil S. K., Anil Kumar A., Anil Babu G., Chakraborty S. and Soundar Rajan, R. (2005) Changing sedimentary environment during the Late Quaternary: Sedimentological and isotopic evidence from the distal Bengal Fan. Deep Sea Research, 52, 1591-1615.

Krishnaswami S., Trivedi J. R., Sarin M. M., Ramesh R. and Sharma K. K. (1992) Strontium isotopes and rubidium in the Ganga-Brahmaputra river system: weathering in the Himalaya, fluxes to the Bay of Bengal and contributions to the evolution of oceanic ^{87}Sr/^{86}Sr. Earth and Planetary Science Letters, 109, 243-253.

Krishnaswami S. and Singh S. K. (1998) Silicate and carbonate weathering in the drainage basins of the Ganga-Ghaghara-Indus headwaters: Contributions to major ion and Sr isotope geochemistry. Proceedings of the Indian National Science Academy, 107, 283–291.

Krishnaswami S., Singh S.K. and Dalai T. (1999) Silicate weathering in the Himalaya: Role in contributing to major ions and radiogenic Sr to the Bay of Bengal. *In* Ocean Science, Trends and Future Directions (Ed. Somayajulu B.L.K.), Indian National Science Academy and Akademia International, New Delhi, 23–51.

Kuehl S. A., Hariu T. M. and Moore W. S. (1989) Shelf sedimentation off the Ganges-Brahmaputra river system: evidence for sediment bypassing to the Bengal fan. Geology, 17, 1132-1135.

Kumar S and Srivastava P (1997) A note on the carbonaceous megafossils from the Neoproterozoic Bhander Group, Maihar area, M. P. Journal of Paleontological Society of India, 42, 141–146.

Kumar A., Kumari P., Dayal A.M., Murthy D.S.N. and Gopalan K. (1993) Rb–Sr ages of Proterozoic kimberlites of India: evidence for contemporaneous emplacements. Precambrian Research, 62, 227–237.

Kumar A., Gopalan K. and Rajgopalan G. (2001) Age of the Lower Vindhyan sediments, Central India. Current Science, 81, 806–809.

Kump L.R. (1991) Interpreting carbon-isotope excursions: Strangelove oceans. Geology, 19, 299–302.

La Fond E. (1957) The Swatch of No Ground. Bulletin of National Institute of Sciences of India, 11, 84-89.

Le Fort P. (1989) The Himalayan orogenic segment. In: Sengo¨r, A.M.C. Ed.., Tectonic evolution of the Tethyan regions. Proceedings of the NATO ASI meeting, Istanbul, October 1985. Reidel Publ.

Li S.-R., Xiao Q.-Y., Shen J.-F., Sun L., Liu B. and Yan B.-K. (2003). Rhenium–osmium isotope constraints on the age and source of the platinum mineralization in the Lower Cambrian black rock series of Hunan–Guizhou provinces, China. Science in China (Series D) 46, 919–927.

Lindner M., Leich D. A., Russ G. P., Bazan J. M. and Borg R. J. (1989) Direct determination of the half life of 187Re. Geochimica et Cosmochimica Acta, 53, 1597–1606.

Ludwig K.R. (2003) User's manual for Isoplot 3.0. A Geochronological toolkit for Microsoft Excel, Berkeley Geochronology Center Special Publication, 4, 70 pp.

Luguet A., Nowell G. and Pearson D. (2008) ^{184}Os/^{188}Os and ^{186}Os/^{188}Os measurements by Negative Thermal Ionisation Mass Spectrometry (N-TIMS): Effects of interfering element and mass fractionation corrections on data accuracy and precision. Chemical Geology, 248, 342-362.

Lupker M., France-Lanord C., Lave J. and Galy V. (2009) Spatial variation of weathering in the Ganga basin. Geochimica et Cosmochimica Acta, 67, A803.

Malone S., Meert J., Banerjee D., Pandit M., Tamrat E., Kamenov G., Pradhan V. and Sohl L. (2008) Paleomagnetism and Detrital zircon geochronology of the upper Vindhyan sequence, Son Valley and Rajasthan, India: A ca. 1000 Ma closure age for the purana basins? Precambrian Research 164, 137-159.

Mao J., Lehmann B., Du A., Zhang G., Ma D., Wang Y., Zeng M. and Kerrich, R., (2002) Re–Os dating of polymetallic Ni–Mo–PGE–Au mineralization in Lower Cambrian black shales of South China and its geologic significance. Economic Geology, 97, 1051–1061.

Martins-Neto M., Pedrosa-Soares A. and Lima S. (2001) Tectno-sedimentary evolution of sedimentary basins from Late Paleoproterozoic to late Neoproterozoic in the Sao Francisco craton and Aracuai fold belt, eastern Brazil. Sedimentary Geology 141-142, 343-370.

Mazumdar A., Banerjee D.M., Schidlowski M. and Balram V. (1999) Rare-earth elements and stable isotopic geochemistry of Early Cambrian, Lower Tal chert-phosphorite of Krol Belt, Lesser Himalaya, India. Chemical Geology, 156, 275–297.

McCall G. (2006) The Vendian (Edicaran) in the geological record: Enigmas in geology’s prelude to the Cambrian explosion. Earth-Science Reviews, 77, 1-229.

McDaniel D. K., Walker R. J., Hemming S. R., Horan M. F., Becker H. and Grauch R. I. (2004) Sources of osmium to the modern oceans: new evidence from the 190Pt–186Os system. Geochimica et Cosmochimica Acta, 68, 1243–1252.

Milliman J. and Meade R. (1983) World Delivery of River Sediment to the Oceans. The Journal of Geology, 1, 1-21.

Milliman J. and Syvitski P. (1992) Geomorphic/Tectonic control of sediment discharge to the ocean: the importance of small mountainous rivers. The Journal of Geology, 100, 525-544.

Millot R., Gaillardet J., Dupré B. and Allègre C. J. (2003) Northern latitude chemical weathering rates: clues from the Mackenzie River Basin, Canada. Geochimica et Cosmochimica Acta, 67, 1305-1329.

Mishra D. (2011) Long hiatus in Proterozoic sedimentation in India: Vindhyan, Cuddapah and Pakhal Basins-A plate tectonic model. Journal of Geological Society of India, 77, 17-25.

Mishra M. and Sen S. (2010) Geochemical signatures of Mesoproterozoic silici-clastic rocks of the Kaimur Group of the Vindhyan Supergroup, Central India. Chinese Journal of Geochemistry, 29, 21-32.

Mitra N. D. (1996) Some problems of Vindhyan Geology; Memoirs of the Geological Society of India, 36, 1-4.

Mondal M.E.A., Goswami J.N., Deomurari M.P. and Sharma K.K. (2002) Ion microprobe ^{207}Pb/^{206}Pb ages of zircons from the Bundelkhand massif, northern India: implications for crustal evolution of the Bundelkhand-Aravalli protocontinent. Precambrian Research, 117, 85-100.

Moon S., Huh Y., Qin J. and van Pho N. (2007) Chemical weathering in the Hong (Red) River basin: Rates of silicate weathering and their controlling factors. Geochimica et Cosmochimica Acta, 71, 1411-1430.

Mukherjee A., Fryar A. E. and Thomas W. A. (2009) Geological, geomorphic and hydrological framework and evolution of the Bengal basin, India and Bangladesh. Journal of Asian Earth Sciences, 34, 227-244.

Negrel P., Allegre C. J., Dupre B. and Lewin E. (1993) Erosion sources determined by inversion of major and trace element ratios and strontium isotopic ratios in river water: the Congo Basin case. Earth and Planetary Science Letters, 120, 59-76.

Nesbitt H.W. and Young G.M. (1982) Early Proterozoic climates and plate motions inferred from major element chemistry of lutites, Nature, 299, 715– 717.

Nier A. (1937) The isotopic constitution of osmium. Physical Reviews, 52, 885-885.

Ninkovich D., Opdyke N., Heezen B. and Foster J. (1966) Palaeomagnetic startigraphy, rates of deposition and tephrachronology in North Pacific deep-sea sediments. Earth and Planetary Science Letters, 1, 476-492.

Ohmoto H. (1996) Evidence in pre-2.2 Ga paleosols for the early evolution of atmospheric oxygen and terrestrial biota. Geology 24, 1135-1138.

Ohmoto H., Watanabe Y., Ikemi H., Poulson S.R. and Taylor B.E. (2006) Sulphur isotope evidence for an oxic Archaean atmosphere. Nature, 442, 908–911.

Oliver L., Harris N., Bickle M., Chapman H., Dise N. and Horstwood M. (2003) Silicate weathering rates decoupled from the ^{87}Sr ratio of the dissolved load during Himalayan erosion. Chemical Geology, 201, 119-139.

Owen L. A., Finkel R. C. and Caffee M. W. (2002) A note on the extent of glaciation throughout the Himalaya during the global Last Glacial Maximum. Quaternary Science Reviews, 21, 147-157.

Oxburgh R. (2001) Residence time of osmium in the oceans. Geochemistry Geophysics Geosystems, 2, 1018.

Paikaray S., Banerjee S. and Mukherji (2008) Geochemistry of shales from the Paleoproterozoic to Neoproterozoic Vindhyan Supergroup: Implications on provenance, tectonics and paleoweathering. Journal of Asian Earth Sciences 32, 34–48.

Palmer M. R. and Edmond J. M. (1992) Controls over the strontium isotope composition of river water. Geochimica et Cosmochimica Acta, 56, 2099-2111.

Pande K., Sarin M. M., Trivedi J. R., Krishnaswami S. and Sharma K.K. (1994) The Indus river system (India-Pakistan): Major-ion chemistry, uranium and strontium isotopes. Chemical Geology, 116, 245-259.

Pandey S. K., Singh A. K. and Hasnain S. I. (1999) Weathering and geochemical processes controlling solute acquisition in Ganga Headwater-Bhagirathi River, Garhwal Himalaya, India. Aquatic Geochemistry, 5, 357-379.

Papineau D., Purohit R., Goldberg T., Pi D., Shields G., Bhu H., Steele A. and Fogel M. (2009) High primary productivity and nitrogen cycling after the Paleoproterozoic phosphogenic event in the Aravalli Supergroup, India. Precambrian Research, 171, 37-56.

Pattan J.N., Parthiban G., Prakash Babu C. and Khadge N.H. (2008) A note on geochemistry of surface sediments from Krishna-Godavari basin, East coast of India. Journal of Geological Society of India, 71, 107-114.

Paul D.K. (1979) Isotopic composition of strontium in Indian kimberlites. Geochimica et Cosmochimica Acta, 43, 389–394.

Paul D.K., Potts P.J., Gibson I.L. and Harris P.G. (1975) Rare-earth abundances in Indian kimberlite. Earth and Planetary Science Letters, 25, 151–158.

Pauquay F., Ravizza G., Dalai T. and Peucker-Ehrenbrink B. (2008) Determining chrondritic impactor size from the marine osmium isotope record. Science, 320, 214-218.

Pegram W., Krishnaswami S., Ravizza G. and Turekian K. (1992) The record of seawater ^{187}Os/^{188}Os variation through the Cenozoic. Earth and Planetary Science Letters, 113, 569-576.

Peucker-Ehrenbrink B. and Hannigan R. E. (2000) Effects of black shale weathering on the mobility of rhenium and platinum group elements. Geology, 28, 475–478.

Peucker-Ehrenbrink B. and Jahn B. (2001) Rhenium–osmium isotope systematics and platinum group element concentrations: Loess and the upper continental crust. Geochemistry Geophysics Geosystems, 2(10), 1061.

Peucker-Ehrenbrink B. and Ravizza G. (2000) The marine osmium isotope record. Terra Nova, 12, 205–219.

Pierson-Wickmann A. (2000) Le cycle de l'osmium et dy rhenium pendant l'erosion himalayenne, Ph. D. thesis, 246 pp., Inst. Natl. Polytech. De Lorrain, Vandoeuvre-lees-Nancy, France.

Pierson-Wickmann A.-C., Reisberg L., France-Lanord C. and Kudrass H. R. (2001) Os-Sr-Nd results from sediments in the Bay of Bengal: Implications for sediment transport and the marine Os record, Paleoceanography, 16, 435-444.

Pierson-Wickmann A.C., Reisberg L., France-Landord C. (2002) Behavior of Re and Os during low-temperature alteration: results from Himalayan soils and altered black shales. Geochimica et Cosmochimica Acta 66, 1539–1548.

Prakash R. and Dalela I. (1982) Stratigrahy of the Vindhyan in Uttar Pradesh: A Brief Review. 55-79. (Eds.Valdiya K.S., Bhatia S. B. and Gaur V. K.). Hindustan Publishing Corporation, India.

Prell W. L. and Kutzbach J. E. (1987) Monsoon variability over the past 150, 000 years. Journal of Geophyical Research, 92, 8411-8425.

Prell W. L., Hutson W., Williams D. F., Be A. W. H., Geitzenauer K. and Molfino B. (1980) Surface circulation of the Indian Ocean during the last Glacial Maximum approximately 18,000 yr B.P., Quaternary Research, 14, 309–336.

Quade J., Roe L., DeCelles P.G. and Ojha T.P. (1997) The late neogene ^{87}Sr/^{86}Sr record of lowland Himalayan rivers. Science, 276, 1828-1831.

Quade J., English N. and DeCelles P. G. (2003) Silicate versus carbonate weathering in the Himalaya: a comparison of the Arun and Seti River watersheds. Chemical Geology, 202, 275-296.

Rahaman W. and Singh S. K. (2010) Rhenium in rivers and estuaries of India: Sources, transport and behavior. Marine Chemistry, 118, 1-10.

Rahaman W., Singh S. K., Sinha R. and Tandon S. K. (2009) Climate control on erosion distribution over the Himalaya during the past ~100 ka. Geology, 37, 559-562.

Rahaman W., Singh S. K. and Raghav S. (2010) Dissolved Mo and U in rivers and estuaries of India: Implications to geochemistry of redox-sensitive elements and their marine budgets. Chemical Geology, 278, 160-172.

Rai S.K. (2008), Isotopic and Geochemical studies of Ancient and Modern sediments. Ph.D. Dissertation, M.S. University of Baroda, Vadodara, India.

Rai S.K., Singh S. K. and Krishnaswami S. (2010) Chemical weathering in the plain and peninsular sub-basins of the Ganga drainage: Impact on the major ion chemistry and elemental fluxes of the Ganga. Geochimica et Cosmochimica Acta, 74, 234-2355, doi 10.1016/j.gca.2010.01.008.

Ram J., Shukla S., Pramanik A., Varma B., Chandra G. and Murthy A. (1996) Recent investigations in the Vindhyan Basin: Implications for the Basin Tectonics. *In:* Recent Advances in Vindhyan Geology (Ed. Bhattacharyya A.) Memoir Geological Socoety of India, 36, 267-286.

Ramakrishnan M. and Vaidyanadhan R. (2008) Geology of India. Geological Society of India. Volume 1, 556 pp.

Ramaswamy V. and Nair R. (1994) Fluxes of material to the Arabian Sea and Bay of Bengal- sediment trap studies. Proceedings of the Indian Academy of sciences (Earth and Planetary Sciences) 103, 189-210.

Rasmussen B., Bose P.K., Sarkar S., Banerjee S., Fletcher I.R. and McNaughton N.J. (2002) 1.6 Ga U–Pb zircon ages for the Chorhat Sandstone, Lower Vindhyan, India: possible implications for early evolution of animals. Geology, 30, 103–106.

Rasmussen B. (2005) Radiometric dating of sedimentary rocks: the application of diagenetic xenotime geochronology. Earth-Science Reviews, 68, 197–243.

Ravizza G. and Esser B.K. (1993) A possible link between the seawater osmium isotope record and weathering of ancient sedimentary organic matter. Chemical Geology, 107, 255–258.

Ravizza G. and Turekian K. K. (1989) Application of the ^{187}Re–^{187}Os system to black shale geochronometry. Geochimica et Cosmochimica Acta, 53, 3257–3262.

Ravizza G. and Peucker-Ehrenbrink B. (2003) Chemostratigraphic evidence of Deccan volcanism from the marine osmium isotope record. Science, 302, 1392–1395.

Ray J.S., Martin M.W., Veizer J., Bowring S.A. (2002) U–Pb zircon dating and Sr isotope systematics of the Vindhyan Supergroup, India. Geology, 30, 131–134.

Ray J.S., Veizer J. and Davis W. J. (2003) C, O, Sr and Pb isotope systematics of carbonate sequences of the Vindhyan Supergroup, India: age diagenesis, correlations and implications for global events. Precambrian Research, 121, 103-140.

Ray J.S. (2006) Age of the Vindhyan SuperGroup: a review of recent findings. Journal of Earth System Science, 115, 149–160.

Raymo M. E. and Ruddiman W. F. (1992) Tectonic forcing of late Cenozoic climate. Nature, 359, 117-122.

Raymo M. E., Ruddiman W. F. and Froelich P.N. (1988) Influence of late Cenezoic mountain building on ocean geochemical cycles. Geology, 16, 649-653.

Rengarajan R., Singh S.K., Sarin M.M., and S. Krishnaswami (2009), Strontium isotopes and major ion chemistry in the Chambal River system, India: Implications to silicate erosion rates of the Ganga. *Chem. Geo.*, 260, 87-101.

Richards A., Argles T., Harris N., Parrish R., Ahmad T., Darbyshire F and Draganits E. (2005) Himalayan architecture constrained by isotopic tracers from clastic sediments. Earth and Planetary Science Letters, 236, 773-796.

Richter F. M., Rowley D. B. and DePaolo D. J. (1992) Sr isotope evolution of seawater: the role of tectonics. Earth and Planetary Science Letters, 109, 11–23.

Rimmer *S.* (2004) Geochemical paleoredox indicators in Devonian-Mississippian black shales, Central Appalachian Basin (USA). Chemical Geology 206, 373-391.

Rimstidt, J. D., Balog A., and Webb J. (1998) Distribution of trace elements between carbonate minerals and aqueous solutions. Geochimica et Cosmochimica Acta, 62, 1851-1863.

Robinson R.A.J., Bird M. I., Oo N. W., Lu X. X., Hoey T. B., Swe A. and Tun T. (2006) Reanalysis of the 19th century hydrology and sediment load dataset for the Irrawaddy River, Myanmar, Geophysical Research Abstracts, 8, 10097.

Rooney A., Selby D., Houzay J. and Renne P. (2010) Re–Os geochronology of a Mesoproterozoic sedimentary succession, Taoudeni basin, Mauritania: Implications for basin-wide correlations and Re–Os organic-rich sediments systematics. Earth and Planetary Science Letters, 289, 486-496.

Rouxel O., Bekker A. and Edwards K. (2005) Iron isotope constraints on the Archean and Paleoproterozoic ocean redox state. Science 307, 1088-1091.

Roy A. B. and Jakhar S. R. (2002) Geology of Rajasthan (Norhwest India) Precambrian to Recent. Scientific Publishers (India), Jodhpur. 421 pp.

Roy A.B. and Kroner A. (1996) Single zircon eveporation ages constraining the growth of the Archaean Aravalli craton, Northwestern Indian shield. Geological Magazine, 133, 333–342.

Sager, W. and Hall, S. (1990) Magnetic properties of black mud turbidites from ODP Leg 116, Distal Bengal Fan, Indian Ocean. *In*: Proceedings of the ocean Drilling Programme, Scientific results (Eds Cochran, J. et al.), 116, 317-336.

Sangode, S., Suresh, N. and Bagati T. (2001) Godavari source in the Bengal fan sediments: Resulst from magnetic susceptibility dispersal pattern. Current Science, 80, 660-664.

Sangode S., Sinha R., Phartiyal B., Chauhan O., Mazari R., Bagati T., Suresh N., Mishra S., Kumar R. and Bhattacharjee P. (2007) Environmental magnetic studies on some quaternary sediments of varied depositional settings in the Indian sub-continent. Quaternary International, 159, 102-118.

Sarangi S., Gopalan K. and Kumar S. (2004) Pb-Pb age of earliest megascopic eukaryotic alga bearing Rohtas Formation, Vindhyan Supergroup, India: Implications for Precambrian atmospheric oxygen evolution. Precambrian Research, 132, 107-121.

Sarangi S., Gopalan K., Roy A. B., Sreenivas B. and Sharma S. D. (2006) Pb-Pb Age of the carbonates of Jhamarkotra Formation: Constrains on the age of the Aravalli Supergroup. Journal of Geological Society of India, 67, 442-446.

Sarin, M. M., and Krishnaswami S. (1984) Major ion chemistry of the Ganga-Brahmaputra river systems, India. Nature, 312, 538-541.

Sarin M. M., Krishnaswami S., Dilli K., Somayajulu B. L. K. and Moore W. S. (1989) Major ion chemistry of the Ganga-Brahmaputra river system: weathering processes and fluxes to the Bay of Bengal. Geochimica et Cosmochimica Acta, 53, 997-1009.

Sarin M. M., Krishnaswami S., Trivedi J. R. and Sharma K. K. (1992) Major ion chemistry of the Ganga source waters: Weathering in the high altitude Himalaya. Proceedings of the Indian National Science Academy (Earth and Planetary Sciences), 101, 89-98.

Sarkar A. (1989) Oxygen and Carbon isotopes in Indian Ocean sediments and their Palaeoclimatic implications, Ph D. Thesis, Gujarat University, 55-57.

Sarkar A., Ramesh R., Bhattacharya S. K. and Rajagopalan G. (1990) Oxygen isotope evidence for a stronger winter monsoon current during the last glaciation. Nature, 343, 549-551.

Schaefer B. F. and Burgess J. M. (2003) Re–Os isotopic age constraints on deposition in the Neoproterozoic Amadeus Basin: implications for the ‘Snowball Earth’.Journal of the Geological Society, London, 160, 825–828.

Schott F. A. and McCreary Jr. J. P. (2001) The monsoon circulation of the Indian Ocean. Progress in Oceanography, 51, 1 – 123.

Seilacher A., Bose P.K. and Pflüger F. (1998) Triploblastic animals more than 1 billion years age: trace fossil evidence from India. Science, 282, 80-83.

Selby D. and Creaser R. A. (2003) Re–Os geochronology of organic-rich sediments: an evaluation of organic matter analysis methods. Chemical Geology, 200, 225–240.

Selby D. and Creaser R.A. (2005) Direct radiometric dating of the Devonian-Mississippian time-scale boundary using the Re–Os black shale geochronometer. Geology 33, 545–548.

Shankar D., Vinayachandran P. N. and Unnikrishnan A. S. (2002) The monsoon currents in the north Indian Ocean. Progress in Oceanography, 52, 63-120.

Shanker R., Kumar G., Mathur V. K. and Joshi A. (1993) Stratigraphy of Blaini, Infra Krol, Krol and Tal Succession, Krol Belt, Lesser Himalaya. Indian Journal of Petroleum Geology, 2, 99–136.

Sharma K. K., Rao D. R., Azmi R. J., Gopalan K., and Pantulu G. V. C. (1992) Precambrian–Cambrian boundary in the Tal Formation of Garhwal Lesser Himalaya: Rb-Sr age evidence from black shales underlying phosphorites. Current Science, 62, 528–530.

Shetye S. R., Gouveia A.D., Shenoi S. S. C., Sundar D., Michael G. S. and Nampoothiri G. (1993) The western boundary current of the seasonal subtropical gyre in the Bay of Bengal. Journal of Geophysical Research, 98, 945–954.

Shirey S. B. and Walker R. J. (1995) Carius tube digestion for low-blank rhenium–osmium analysis. Analytical Chemistry, 67, 2136–2141.

Singh S. K. (1999) Isotopic and geochemical studies of the Lesser Himalayan sedimentaries. Ph.D. dissertation, M.S. University of Baroda, 160 pp.

Singh S. K. and France-Lanord C. (2002) Tracing the distribution of erosion in the Brahmaputra watershed from isotopic compositions of stream sediments. Earth and Planetary Science Letters, 202, 645– 662.

Singh, S. K., Trivedi J. R., Pande K., Ramesh R. and Krishnaswami S. (1998) Chemical and Strontium, Oxygen, and Carbon Isotopic Compositions of Carbonates from the Lesser Himalaya: Implications to the Strontium Isotope Composition of the Source Waters of the Ganga, Ghaghara, and the Indus Rivers. Geochimica et Cosmochimica Acta, 62, 743-755.

Singh S.K., Trivedi J.R. and Krishnaswami S. (1999) Re-Os isotope systematics in black shales from the Lesser Himalaya: Their chronology and role in the ^{187}Os/^{188}Os evolution of seawater. Geochimica et Cosmochimica Acta 63, 2381–2392.

Singh S.K., Rai S. K. and Trivedi J.R. (2002) ^{187}Re-^{187}Os systematics of black shales from the Vindhyans: Implications to their geochronology. 10th ISMAS-WS, Puri, 242-244.

Singh, S. K., Sarin M. M. and C. France-Lanord (2005) Chemical erosion in the eastern Himalaya: Major ion composition of the Brahmaputra and δ^{13}C of dissolved inorganic carbon. Geochimica et Cosmochimica Acta, 69, 3573-3588.

Singh S.K., Rai S.K. and Krishnaswami S. (2008) Sr and Nd isotopes in river sediments from the Ganga Basin: Sediment Provenance and Hotspots of Physical Erosion, Journal of Geophyical Research, 113, F03006.

Singh, A. K. and Hasnain S. I. (1998) Major ion chemistry and weathering control in a high altitude basin: Alaknanda River, Garhwal Himalaya, India. Hydrological Sciences Journal, 43, 825-843.

Singh I. (1980) The Bijaigarh Shale, Vindhyan System (Precambrian), India-An example of a lagoonal deposit. Sedimentary Geology, 25, 83-103.

Smith, C.B., 1992. The age of the Majhgawan Pipe, India. Scott Smith Petrology, 9.

Smoliar M., Walker R. and Morgan J. (1996) Re–Os ages of Group IIA, IIIA, IVA, and IVB iron meteorites. Science, 271, 1099–1102.

Sreenivas B., Das Sharma S., Kumar B., Patil D., Roy A. and Srinivasan R. (2001) Positive $\delta^{13}C$ excursion in carbonate and organic fractions from the Paleoproterozoic Aravalli supergroup, Northwestern India. Precambrian Research, 106, 277-290.

Srivastava A.P. and Rajagopalan G. (1988) F-T ages of Vindhyan glauconitic sandstone beds exposed around Rawatbhata area, Rajasthan. Journal of Geological Society of India, 32, 527–529.

Srivastava P. (2009) Trachyhystrichosphaera: An age-marker acanthomorph from the Bhander group, upper Vindhyan, Rajasthan. Journal of Earth System Science, 118, 575-582.

Steiner M., Wallis E., Erdtmann B., Zhao Y. and Yang R. (2001) Submarine-hydrothermal exhalative ore layers in black shales from south China and associated fossils-insights into a Lower Cambrian facies and bio-evolution. Palaeogeography Palaeoclimatography Palaeoecology 169, 165-191.

Stoll H. M., Vence D. and Arevalos A. (2007) Records of the Nd isotope composition of seawater from the Bay of Bengal: Implications for the impact of Northern Hemisphere cooling on ITCZ movement. Earth and Planetary Science Letters, 255, 213-228.

Stuiver M. and Reimer P. J. (1993) Extended ^{14}C data base and revised CALIB 3.0 ^{14}C age calibration program. Radiocarbon, 35, 215-230.

Tarantola A. (2005) The least square criterion. In: Inverse problem theory and methods for model parameter estimation. Society for Industrial and Applied Mathematics, Philadelphia, 68-72.

Taylor S.R. and McLennan S.M. (1985) The continental crust: Its composition and evolution. Oxford, UK, Blackwell, 312 pp.

Thakur V. C. and Rawat B. S. (1992), Geological Map of Western Himalaya, Wadia Institute of Himalayan Geology, Dehradun, 22.

Tipper E. T., Bickle M. J., Galy A., West A. J., Pomies C. and Chapman H. J. (2006) The short term climatic sensitivity of carbonate and silicate weathering fluxes: Insight from seasonal variations in river chemistry. Geochimica et Cosmochimica Acta, 70, 2737-2754.

Tiwari M., Ramesh R., Somayajulu B. L. K., Jull A. J. T. and Burr G. S. (2005) Early deglacial (~19-17 ka) strengthening of the northeast monsoon. Geophyical Research Letters, 32, 1-4.

Trapp E., Kaufmann B., Mezger K., Korn M. and Weyer D. (2004) Numerical calibration of the Devonian–Mississippian boundary: Two new U–Pb isotope dilution-thermal ionization mass spectrometry single-zircon ages from Hasselbachtal (Sauerland, Germany). Geology, 32, 857–860.

Tripathy G. R., Singh S. K. and Krishnaswami S. (2010a) Sr and Nd isotopes as tracers of Chemical and Physical erosion. *In* Handbook of Environemental isotope Geochemistry (Ed. M. Baskaran), Springer-Verlag Publications (In Press).

Tripathy G. R., Goswami V., Singh S. K. and Chakrapani G. J. (2010b) Temporal Variations in Sr and ^{87}Sr/^{86}Sr of the Ganga headwaters: estimates of dissolved Sr flux to the mainstream. Hydrological Processes, 24, 1159-1171, doi: 10.1002/hyp.7572.

Trivedi J., Singh S. K. and Krishnaswami S. (1999) ^{187}Re-^{187}Os in Lesser Himlaya sediments: Measurement techniques and preliminary results. Proceedings of the Indian National Science Academy (Earth and Planetary Sciences), 108, 179-187.

Turgeon S.C., Creaser R.A. and Algeo T.J. (2007) Re–Os depositional ages and seawater Os estimates for the Frasnian–Famennian boundary: implications for weathering rates,land plant evolution, and extinction mechanisms. Earth and Planetary Science Letters, 261,649–661.

Tutken T., Eisenhauer A., Wiegand B. and Hansen B. T. (2002) Glacial-interglacial cycles in Sr and Nd isotopic composition of Arctic marine sediments triggered by the Svalbard/Barents Sea ice sheet, Marine Geology, 182, 351-372.

Valdiya K. (1980) Geology of Kuman Lesser Himalaya. Wadia Institute of Himalayan Geology, Dehradun, 291 pp.

Valdiya K. (1982) Tectonic prespective of the Vindhyanchal Region. 23-29. In: Geology of Vindhyanchal (Eds. Valdiya K.S., Bhatia S. B. and Gaur V. K.). Hindustan Publishing Corporation, India.

Vance D., Bickle M., Ivy-Ochs S. and Kubuik P. W. (2003) Erosion and exhumation in the Himalaya from cosmogenic isotope inventories of river sediments. Earth and Planetary Science Letters, 206, 273-288.

Venkatachala B., Sharma M. and Shukla M. (1996) Age and life of the Vindhyans-Facts and Conjectures. *In:* Recent Advances in Vindhyan Geology (Ed. Bhattacharyya A.) Memoir Geological Socoety of India, 36, 137-165.

Vine J.D. and Tourtelot E.B. (1970) Geochemistry of black shale deposits—A summary report. Economic Geology, 65, 253–272.

Vinogradov A.P., Tugarinov A.I., Zhikov C.I., Stanikova N.I., Bibikova E.V. and Khorre K. (1964) Geochonology of Indian Precambrian. Report of 22nd International Geological Congress, New Delhi, vol. 10, pp. 553–567.

Volkening J., Walczyk T. and Heumann K. (1991) Osmium isotope ratio determinations by negative thermal ionization mass spectrometry. International Journal of Mass Spectrometry and Ion Processes, 105, 147-159.

Walczyk T., Hebeda E. and Heumann K. (1991) Osmium isotope ratio measurements by negative thermal ionization mass spectrometry (NTI-MS) Improvement in precision and enhancement in emission by introducing oxygen or freons into the ion source. Fresenius Journal of Analytical Chemistry, 341, 537-541.

Walker J. C. G., Hays P. B. and Kasting J.F. (1981) A negative feedback mechanism for the long-term stabilization of Earth's surface temperature. Journal of Geophyical Research, 86, 9776-9782.

Walter H. J., Hegner E., Diekmann B., Kuhn G. and van der loeff M. M. (2000) Provenance and transport of terrigenous sediment in the south Atlantic Ocean and their relations to glacial and interglacial cycles: Nd and Sr isotopic evidence. Geochimica et Cosmochimica Acta, 64, 3813-3827.

West A. J., Bickle M. J., Collins R. and Brasington J. (2002) Small-catchment perspective on Himalayan weathering fluxes. Geology, 30, 355–358.

Wiedenbeck M. and Goswami J. (1994) High precision ^{207}Pb/^{206}Pb zircon geochronology using a small ion microprobe. Geochimica et Cosmochimica Acta, 58, 2135-2145.

Wiedenbeck M., Goswami J. and Roy A. (1996) Stabilization of the Aravalli craton of northwestern India at 2.5 Ga: An ion microprobe zircon study. Chemical Geology, 129, 325-340.

Wignall P.B. (1994) Black shales: New York, Oxford University Press, 127 pp.

Wille M., Kramers J. Nagler T., Beukes N., Schroder S., Meisel T., Lacassie J. and Voegelin A. (2007) Evidence for a gradual rise of oxygen between 2.6 and 2.5 Ga from Mo isotopes and Re-PGE signatures in shales. Geochimica et Cosmochimica Acta, 71, 2417–2435.

Wille M., Nagler T., Lehmann B., Schroder S. and Kramers J. (2008) Hydrogen sulphide release to surface waters at the Precambrian/Cambrian boundary. Nature, 453, 767-769.

Williams G. and Turekian K. (2004) The glacial-interglacial variation of seawater osmium isotopes as recorded in Santa Barbara Basin. Earth and Planetary Science Letters, 228, 379– 389.

Wu L., Huh Y., Qin J., Du G. and van Der Lee S. (2005) Chemical weathering in the Upper Huang He (Yellow River) draining the eastern Qinghai-Tibet Plateau. Geochimica et Cosmochimica Acta, 69, 5279-5294.

Yang G., Hannah J. L., Zimmerman A., Stein H. J. and Bekker A. (2009) Re–Os depositional age for Archean carbonaceous slates from the southwestern Superior Province: challenges and insights. Earth and Planetary Science Letters, 280, 83–92.

LIST OF PUBLICATIONS

1. **Gyana Ranjan Tripathy**, and Singh S. K. (2010) Chemical Erosion Rates of the Ganga headwater basin: Reassessment based on inversion of dissolved major ions, Sr and $^{87}Sr/^{86}Sr$. Geochemistry Geophysics Geosystems, 11, Q03013, DOI: 10.1029/2009GC002862.
2. **Gyana Ranjan Tripathy**, Goswami V., Singh S.K. and Chakrapani G.J. (2010) Temporal variations in Sr and $^{87}Sr/^{86}Sr$ of the Ganga headwaters: Estimates of dissolved Sr flux to the mainstream. Hydrological Processes, 24, 1159-1171. DOI: 10.1002/hyp.7572.
3. **Gyana Ranjan Tripathy**, Singh S.K., Bhushan R. and Ramaswamy V., "Sr-Nd isotope signatures of Bay of Bengal Sediments: Impact of Climate on Erosion", Geochemical Journal (Article in Press).
4. **Gyana Ranjan Tripathy**, Sunil Kumar Singh and S. Krishnaswami. Sr and Nd isotopes as tracers of Chemical and Physical erosion. In "Handbook of Environemental isotope Geochemistry" Edited by M. Baskaran, Springer Publications (Article in Press).

ABSTRACTS (in Conferences and Symposiums)

1. **Gyana Ranjan Tripathy**, Vineet Goswami, Sunil Kumar Singh and G J Chakrapani (2008) Seasonal variation of major ions, Sr and $^{87}Sr/^{86}Sr$ in the Ganga headwaters, International conference on "Terrestrial planets: Evolution through time", India.
2. **Gyana Ranjan Tripathy**, Sunil Kumar Singh and V Ramaswamy (2008) Tracking the provenance of sediments of the Bay of Bengal through their Sr concentration and $^{87}Sr/^{86}Sr$, International conference on "Terrestrial planets: Evolution through time", India.
3. **Gyana Ranjan Tripathy**, Sunil Kumar Singh and V Ramaswamy (2008) Past erosion pattern of the Himalaya: Inferences from Sr-Nd isotopic signature of sediments of the Bay of Bengal, International symposium on "Mountain Building and Climate-Tectonic Interaction", Wadia Institute of Himalayan Geology, Dehradun, India.

PUBLICATIONS

Geochemistry
Geophysics
Geosystems
G3
AN ELECTRONIC JOURNAL OF THE EARTH SCIENCES
Published by AGU and the Geochemical Society

Article
Volume 11, Number 3
24 March 2010
Q03013, doi:10.1029/2009GC002862
ISSN: 1525-2027

Chemical erosion rates of river basins of the Ganga system in the Himalaya: Reanalysis based on inversion of dissolved major ions, Sr, and ^{87}Sr/^{86}Sr

Gyana Ranjan Tripathy and Sunil Kumar Singh
Geosciences Division, Physical Research Laboratory, Ahmedabad 380009, India (gyana@prl.res.in)

[1] Available data on chemical and Sr isotopic composition of the headwaters of the Ganga and its tributaries in the Himalaya are analyzed using inverse and the forward models to quantify the silicate and carbonate erosion rates in their basins and to parameterize the controlling factors of contemporary chemical erosion. The estimates of silicate-derived cations based on the inverse model are lower on average by ~20% than that derived from the forward model, a result attributable to differences in the release ratios of major ions between the two models. The inverse model yields the best fit values for the release ratio of various major ions based on measured river chemistry and therefore is more likely to be representative of the basins, unlike the forward model, in which the release ratios are assumed. Among the various tributaries, the Kosi and the Bhagirathi have relatively larger contributions from silicate weathering to the cation budget with high ^{87}Sr/^{86}Sr, consistent with the lithologies of their basins, which are dominated by silicates. The Ganga river system in the Himalaya is known to be supersaturated with respect to calcite during lean flow periods. The inverse model calculates the extent of Ca loss to be between ~10%–40% with the highest for the Gandak. The silicate and carbonate erosion rates for these Himalayan rivers are relatively higher, in the ranges of 9.9–17.6 and 12.4–92.3 tons/km^2/yr, respectively, compared to other global rivers. The higher chemical erosion rates in these river basins could be due to intense physical erosion caused by their higher relief and runoff.

Components: 12,053 words, 9 figures, 5 tables.

Keywords: Ganga River; ^{87}Sr/^{86}Sr; inverse model; silicate erosion rates.

Index Terms: 1815 Hydrology: Erosion (0483); 5419 Planetary Sciences: Solid Surface Planets: Hydrology and fluvial processes (0483); 0744 Cryosphere: Rivers (0483).

Received 16 September 2009; **Revised** 12 January 2010; **Accepted** 21 January 2010; **Published** 24 March 2010.

Tripathy, G. R., and S. K. Singh (2010), Chemical erosion rates of river basins of the Ganga system in the Himalaya: Reanalysis based on inversion of dissolved major ions, Sr, and ^{87}Sr/^{86}Sr, *Geochem. Geophys. Geosyst.*, *11*, Q03013, doi:10.1029/2009GC002862.

1. Introduction

[2] The chemistry of river water is a combination of inputs from multiple sources that includes chemical weathering of silicates, carbonates and other lithologies of the drainage basin and atmospheric deposition. Apportionment of the chemical composition of rivers into its various sources is required to derive silicate and carbonate erosion rates (SER and CER) of their basins; data that are

needed to determine CO_2 drawdown from the atmosphere. Such studies are a growing field of geochemical research in recent years due to the link between CO_2 drawdown from the atmosphere and global climate [*Ebelmen*, 1845; *Chamberlin*, 1899; *Walker et al.*, 1981; *Berner et al.*, 1983; *Raymo et al.*, 1988]. Among the major global river basins, those draining young orogenic belts, such as the Himalaya, have been suggested to contribute significantly to the enhanced CO_2 drawdown caused by the rapid uplift of the mountains and conducive climate [*Raymo and Ruddiman*, 1992; *Edmond and Huh*, 1997, and references therein; *Galy and France-Lanord*, 1999; *Krishnaswami et al.*, 1999; *Dalai et al.*, 2002; *Bickle et al.*, 2003; *Jacobson et al.*, 2003; *Quade et al.*, 2003; *Singh et al.*, 2005; *Tipper et al.*, 2006]. The Ganga, Brahmaputra and the Indus are the three major river systems draining the southern slopes of the Himalaya. These rivers supply large amounts of suspended and dissolved material to the adjacent seas and thus contribute significantly to the global geochemical and carbon cycles [*Raymo et al.*, 1988; *Sarin et al.*, 1989; *Raymo and Ruddiman*, 1992; *Pande et al.*, 1994; *France-Lanord and Derry*, 1997; *Karim and Veizer*, 2000; *Singh et al.*, 2005; *Galy et al.*, 2008]. Among the various materials supplied to the Bay of Bengal by the Ganga-Brahmaputra river system, organic carbon is a key component [*Galy et al.*, 2007, 2008], as its burial has been suggested to be another important sink of atmospheric CO_2 over geological time scale [*France-Lanord and Derry*, 1997]. Of the three river systems, the Ganga River is studied more extensively [*Sarin and Krishnaswami*, 1984; *Sarin et al.*, 1989, 1992; *Krishnaswami et al.*, 1992, 1999; *Harris et al.*, 1998; *Galy and France-Lanord*, 1999; *Galy et al.*, 1999; *English et al.*, 2000; *Bickle et al.*, 2001, 2003, 2005; *Dalai et al.*, 2002, 2003; *Evans et al.*, 2001; *West et al.*, 2002; *Oliver et al.*, 2003; *Quade et al.*, 2003; *Tipper et al.*, 2006; *Rai et al.*, 2010; *Tripathy et al.*, 2010]. These studies constrain the role of these rivers in contributing to the global CO_2 drawdown, dissolved elemental fluxes and marine $^{87}Sr/^{86}Sr$ evolution. The various subbasins of the Ganga have been studied by different groups, for example, the headwaters of the Ganga, the Bhagirathi, the Alaknanda and the Yamuna by *Sarin et al.* [1989, 1992], *Krishnaswami et al.* [1992, 1999], *Dalai et al.* [2002, 2003], and *Bickle et al.* [2003, 2005]; the Ghaghra subbasin by *Galy and France-Lanord* [1999], *Galy et al.* [1999], and *English et al.* [2000]; the Gandak subbasin by *Galy and France-Lanord* [1999], *Galy et al.* [1999], and *Tipper et al.* [2006]; and the Kosi subbasin by *Harris et al.* [1998], *Oliver et al.* [2003], and *Quade et al.* [2003]. In addition to these tributaries, the Ganga in the plain has also been studied in some detail by *Galy and France-Lanord* [1999], *Galy et al.* [1999], and *Rai et al.* [2010]. These studies were carried out either on individual minor river basins or on relatively large river systems of the Ganga tributaries or subtributaries to understand the processes regulating the chemical erosion of the basin, specifically to quantify the contribution from different lithological units to the stream chemistry.

[3] The available results show that in most of the Ganga tributaries in the Himalaya the budgets of dissolved major element are dominated by carbonate weathering [*Sarin et al.*, 1989] with silicate weathering playing a subordinate role. The contributions of silicate derived cations to the elemental budgets of these rivers show significant spatial variability and the magnitude of silicate weathering highlights its importance as a driver of the Cenozoic global cooling. The studies concerning the erosion in the Ganga system are limited to one or two subbasins of the Ganga [*Sarin et al.*, 1992; *Galy and France-Lanord*, 1999; *English et al.*, 2000; *Dalai et al.*, 2002; *Oliver et al.*, 2003; *Quade et al.*, 2003; *Bickle et al.*, 2005; *Tripathy et al.*, 2010]. A detailed and coordinated study encompassing all the subbasins of the Ganga headwaters would provide a better understanding of the contemporary weathering processes and the factors influencing them over the entire Himalaya. Realizing this, in the present study, the existing geochemical and isotopic information on the various subbasins of the Ganga headwaters are reanalyzed. This has been done by both forward and inverse models for source apportionment of the dissolved solutes and to derive SER and CER. Further, a unique approach based on the inverse model has been developed to evaluate the magnitude of calcite precipitation in the various basins.

2. Ganga Basin

2.1. Geology

[4] The lithology of the river basins of the Ganga system in the Himalaya are broadly classified into four lithotectonic units [*Gansser*, 1964; *Valdiya*, 1980; *Colchen et al.*, 1986; *Le Fort*, 1989]. These are discussed in detail in many of the earlier publications on river water chemistry [*Sarin et al.*, 1989; *English et al.*, 2000; *Dalai et al.*, 2002; *Bickle et al.*, 2003, 2005; *Singh et al.*, 2008]. Briefly, these are as follows:

[5] 1. The Tethyan Sedimentary Series (TSS) outcrop toward north of the Higher Himalaya has cold,

Table 1a. Silicate Bed Rock Exposure Area for the Tributaries of the Ganga

River	Silicate Bedrock Exposure Area (%)	Method
Alaknanda	91	quantified from the map of *Valdiya* [1980]
Bhagirathi	95	quantified from the map of *Valdiya* [1980]
Yamuna	75	quantified from the map of *Valdiya* [1980]
Kosi (Arun)	98	alluvial clast counts by *Quade et al.* [2003]
Gandak	<95–60	noncarbonate content in suspended sediments by *France-Lanord et al.* [2003]
Ghaghra	75	alluvial clast counts by *English et al.* [2000]

dry climate and sparse vegetation with an average elevation of 4900 m. The TSS is composed of less altered limestones, amphibole calc-silicates with biotite, muscovite and chlorite outcrops [*Colchen et al.*, 1986]. The metamorphism of these rocks reaches lower greenschists facies near the boundary of the HH and TSS and their metamorphic grade decreases toward the north of TSS [*Tipper et al.*, 2006; *Crouzet et al.*, 2007]. No evaporites have been reported in TSS region drained by the Ganga headwaters [*Bordet et al.*, 1971]. Anthropogenic interference is expected to be negligible in these regions as they are sparsely populated. Some of the source waters of the Alaknanda, Ghaghra, Gandak and the Kosi drain the TSS.

[6] 2. The main component of the Higher Himalayan (HH) unit is high-grade granitoid gneisses, schist, granites, and marbles [*Gansser*, 1964; *Le Fort*, 1989] with minor amounts of carbonates and calc-silicates. The HH has an average elevation of 4700 m and about 30% of the HH area is covered with snow and glaciers [*Pandey et al.*, 1999; *Vance et al.*, 2003].

[7] 3. Low-grade sedimentary and crystalline rocks make up the Lesser Himalaya (LH). Greywacks, shales, slates, limestones and dolomites are found in LH. The exposed crystalline rocks in LH are gneisses, granites, schists, calc-silicates and amphibolites [*Valdiya*, 1980; *Le Fort*, 1989; *Thakur and Rawat*, 1992].

[8] 4. The Siwaliks is composed of the eroded materials from the HH and LH, transported by the Himalayan Rivers [*Quade et al.*, 1997].

[9] To better evaluate the impact of lithology on erosion the exposure areas of silicate and carbonate lithologies in the drainages were inferred from geological maps [*Valdiya*, 1980], alluvial clast count [*English et al.*, 2000; *Quade et al.*, 2003] and noncarbonate contents of the suspended sediments [*France-Lanord et al.*, 2003]. The silicate exposure areas in the various subbasins of the Ganga are listed in Table 1a, which shows that the Bhagirathi and the Kosi basins have relatively larger exposures of silicates.

2.2. Hydrology

[10] The river "Ganga" is formed at Devprayag by the confluence of the Bhagirathi and the Alaknanda (Figure 1a). The mainstream Ganga enters the plain at Hardwar after cutting across the Siwaliks ranges. In the plain, the Ganga is joined by a number of tributaries from its right bank (the Ramganga, the Gomti, the Ghaghra, the Gandak and the Kosi) and from the left bank (the Yamuna, the Tons and the Son (Figure 1b)).

[11] The hydrological and climatic parameters and basin characteristics such as rainfall, elevation, mean annual air temperature, river gradient vary significantly over the entire stretch of the Ganga basin [*Rao*, 1975]. These parameters are presented in Figures 1b–1f. The water discharge shows large monthly variation with peak during monsoon (Figure S1 and Data Set S1 in the auxiliary material).[1] Rainfall during the southwest monsoon (June–September) is the major source of water to the Ganga system. The Himalayan catchment of the Ganga tributaries has a runoff of about 1 m/yr and accounts for ~54% of its water discharge [*Singh et al.*, 2008], with a maximum of ~1.55 m/yr in the Gandak subbasin and minimum of 0.50 m/yr over the headwaters of the Kosi subbasin (Table 1b). The balance water to the Ganga is supplied from the peninsular and plain regions.

2.3. Sources of Data

[12] A large number of geochemical studies of the Ganga river have been carried out during the last two decades following the studies of *Handa* [1972] and *Sarin and Krishnaswami* [1984]. The existing data on the stream chemistry of Ganga headwaters [*Sarin et al.*, 1989, 1992; *Krishnaswami et al.*,

---

[1] Auxiliary material data sets are available at ftp://ftp.agu.org/apend/gc/2009gc002862. Other auxiliary materials are available in the HTML.

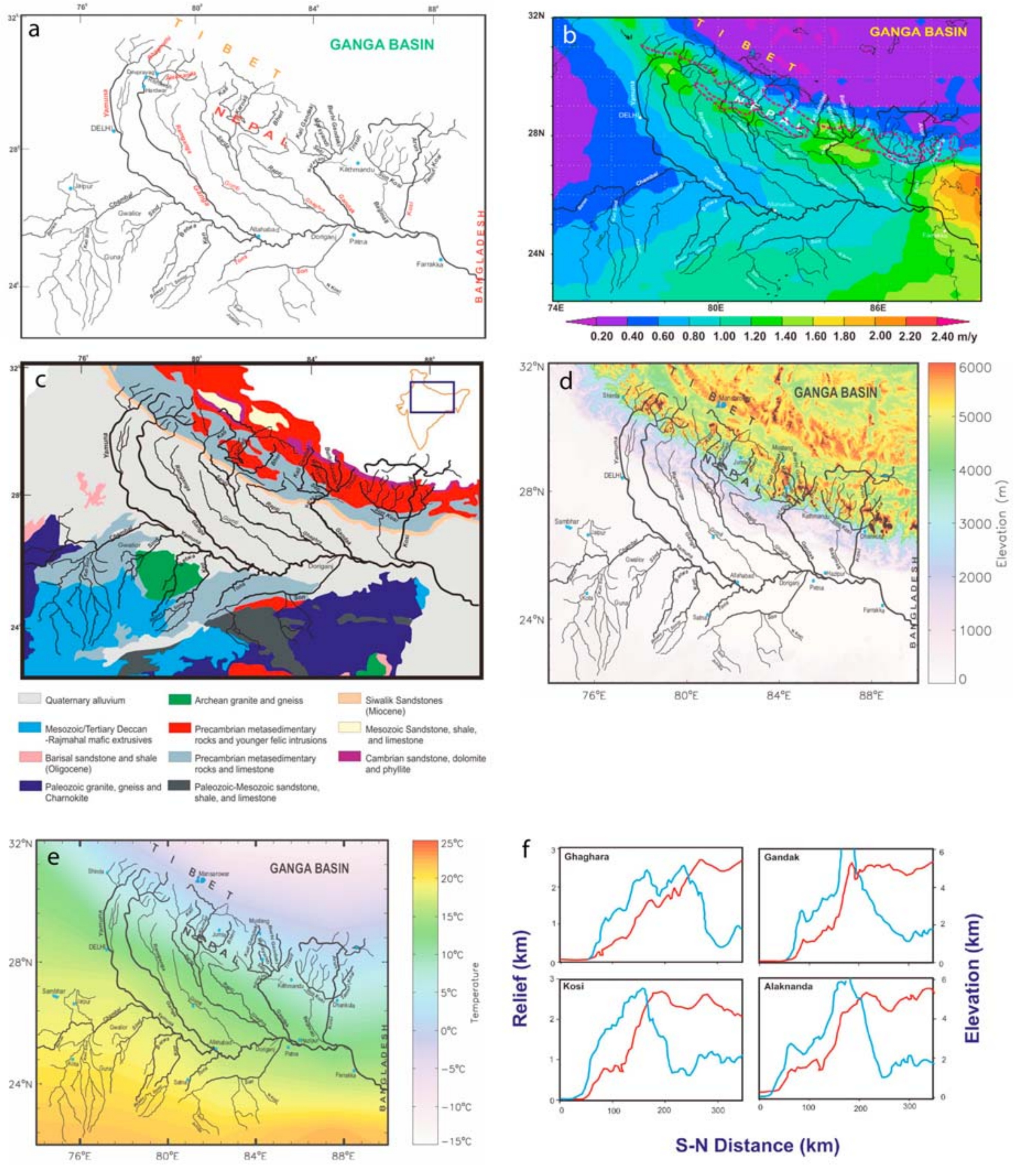

Figure 1. (a) Map of the drainage basins of the Ganga and its major tributaries. (b) Annual rainfall pattern over the Ganga basin (red line shows the MCT) (TRMM, http://disc2.nascom.nasa.gov/Giovanni/tovas/TRMM_V6.3B43.shtml) (modified after *Singh et al.* [2008]). Besides the maximum near the mouth of the Ganga, two more precipitation maxima are observed in the basins of the Ganga headwaters, one in the beginning of the Higher Himalaya (near the Gandak) and the other over the Lesser Himalaya (near Rishikesh). Precipitation shows an ENE-WSW gradient. (c) Geological map of the drainage basin of the Ganga (modified after *Sarin et al.* [1989] and *Mukherjee et al.* [2009]). (d) High-resolution (1 km gridded) elevation map of the Ganga basin (data from http://www.ngdc.noaa.gov/cgi-bin/mgg/ff/nph-newform.pl/mgg/topo/customdatacd). (e) Shaded color diagram (5° × 5° resolution) of the annual surface temperature over the Ganga basin (data from http://www.ngdc.noaa.gov/). (f) Elevation (red line) and relief (blue line) profiles for the different tributaries of the Ganga [*Bookhagen and Burbank*, 2006]. The zero value in the *x* axis represents beginning of the Himalaya, i.e., the southern point of the Siwalik; it represents the large variations in the relief and elevation of the river basin from its origin to the Ganga plain region.

Table 1b. Sources of the Data and Details of the Tributaries of the Ganga in the Himalaya[a]

River	Elevation (m) (Reference)	Drainage Area (10^3 km^2) (Reference)	Annual Discharge: Discharge (10^{12} L/yr)	Annual Discharge: Location (Reference)	Runoff (m/yr)	Lithology	Source of Data
Bhagirathi	3812 (1)	7.8	8.3	Devprayag (7)	1.06	LH+HH	7, 11, 12, 16, 18
Alaknanda	3800 (2)	11.8	14.1	Bhagwan (7)	1.19	LH+HH+TSS	7, 11, 12, 16, 18
Ganga	-	19.6	22.4	Rishikesh (7)	1.14	LH+HH+TSS	7, 8, 11, 13, 15, 16, 18
Yamuna	300–6400	9.6 (3)	10.8	Batamandi (8)	1.13	LH+HH	8, 15
Ghaghra	100 (5) to >5000 (4)	42.9	42.7	Chisapani (9)	1.00	LH+HH+TSS	6, 10, 14
Gandak	200–7000 (5)	31.8	49.4	Narayan Ghat (10)	1.55	LH+HH+TSS	10, 14, 20
Kosi	400–5500	28.2	13.3	Turkeghat (9)	0.47	LH+HH+TSS	4, 17, 19

[a] References are as follows: 1, *Pandey et al.* [1999]; 2, *Singh and Hasnain* [1998]; 3, *Dalai* [2001]; 4, *Oliver et al.* [2003]; 5, *Galy* [1999]; 6, *English et al.* [2000]; 7, *Krishnaswami et al.* [1999]; 8, *Dalai et al.* [2002]; 9, GRDC discharge metadata set (http://www.grdc.sr.unh.edu); 10, *Galy and France-Lanord* [1999]; 11, *Sarin et al.* [1989]; 12, *Sarin et al.* [1992]; 13, *Krishnaswami et al.* [1992]; 14, *Galy et al.* [1999]; 15, *Dalai et al.* [2003]; 16, *Bickle et al.* [2003]; 17, *Quade et al.* [2003]; 18, *Bickle et al.* [2005]; 19, *Harris et al.* [1998]; 20, *Tipper et al.* [2006].

1992, 1999; *Harris et al.*, 1998; *Galy and France-Lanord*, 1999; *Galy et al.*, 1999; *English et al.*, 2000; *Dalai et al.*, 2002, 2003; *Bickle et al.*, 2003, 2005; *Oliver et al.*, 2003; *Quade et al.*, 2003; *Tipper et al.*, 2006] are compiled for this study and the data used to estimate contributions from various sources and chemical erosion rates are given in the auxiliary material (Data Set S2).

3. Chemistry and ^{87}Sr/^{86}Sr of the Ganga Headwaters

[13] Ternary plots of the data (Figure 2) show that with respect to anions most of the samples fall near the HCO_3 apex compared to Cl + SO_4 and Si apex and with respect to cations toward the Ca apex. These results coupled with the observation that (Ca + Mg) charge is roughly balanced by HCO_3, suggests that solute budget of these rivers is dominated by carbonate weathering, a conclusion derived by earlier workers [*Sarin et al.*, 1989; *Krishnaswami and Singh*, 1998; *Galy and France-Lanord*, 1999; *Dalai et al.*, 2002]. Exception to the general trend are some samples of the Ghaghra and a few from the Gandak and Kosi, which fall near the (Na + K) apex indicating comparatively higher contribution from silicates and/or halites [*Galy and France-Lanord*, 1999]. The latter option is less likely due to the lower abundance of (Cl + SO_4) in their anion budget. The higher silicate weathering in the Ghaghra basin is consistent with the lower Na content of its suspended loads compared to that in the other streams [*Pierson-Wickmann*, 2000; *Lupker et al.*, 2009]. The physical erosion rate in the Ghaghra is estimated to be low compared to the Gandak and Kosi [*Singh et al.*, 2008]. The higher silicate contribution to the Ghaghra water, despite relatively lower physical erosion, therefore can be attributed to transport limited intense chemical weathering in the basin.

[14] The spatial variability of dissolved ^{87}Sr/^{86}Sr among the headwaters synthesized from available data [*Galy et al.*, 1999; *Krishnaswami et al.*, 1999; *English et al.*, 2000; *Bickle et al.*, 2003, 2005; *Dalai et al.*, 2003; *Oliver et al.*, 2003; *Quade et al.*, 2003] is shown in Figure 3. All the Ganga headwaters have distinguishably higher ^{87}Sr/^{86}Sr (0.722 to 0.782) compared to the "average" global river (0.712 [*Krishnaswami et al.*, 1992; *Palmer and Edmond*, 1992]). The Sr isotopic ratio shows wide variation among the various subbasins of the Ganga. Between the Bhagirathi and the Alaknanda, the source waters of the Ganga, the Bhagirathi is more radiogenic, though the Alaknanda with lower ^{87}Sr/^{86}Sr exerts larger control on the ^{87}Sr/^{86}Sr of the Ganga after their confluence at Devprayag due to its higher Sr flux. The Kosi River supplies waters with the most radiogenic Sr to the mainstream of the Ganga (Figure 3). The source of the high ^{87}Sr/^{86}Sr in the Ganga water is a topic of debate, though there seems to be a convergence that it is dominated by supply from highly radiogenic Precambrian granites and gneisses [*Krishnaswami et al.*, 1992; *Galy and France-Lanord*, 1999; *Bickle et al.*, 2003]. It is also borne out that metamorphosed carbonates enriched in radiogenic Sr could be important locally [*Palmer and Edmond*, 1992; *Quade et al.*, 1997; *Singh et al.*, 1998; *Bickle et al.*, 2001].

4. Source Apportionment

[15] One of the objectives of this study is to apportion the sources of cations and Sr to the headwaters of the Ganga following a uniform approach for all the subbasins. The contribution of

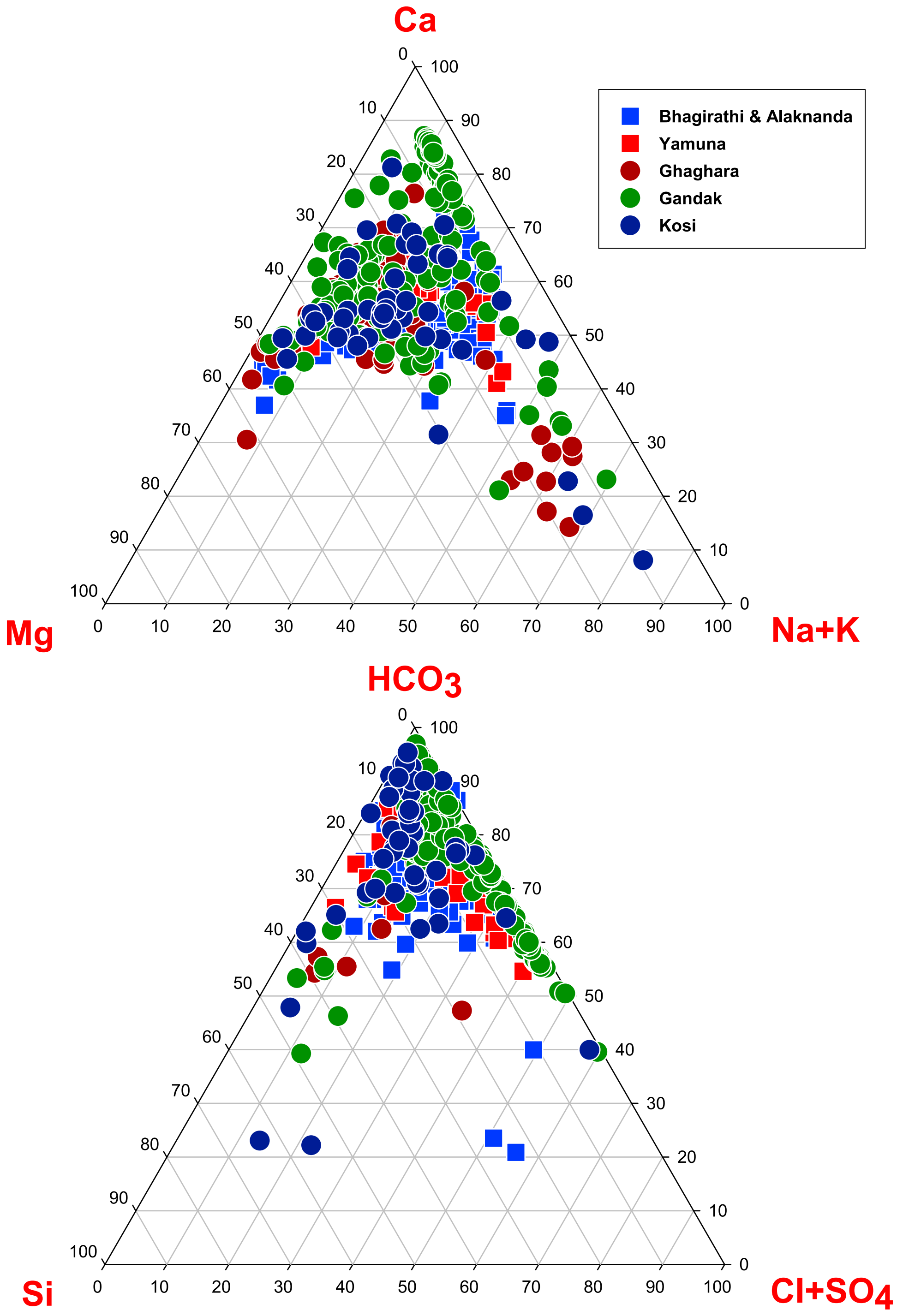

Figure 2. Ternary diagram of the chemical composition (in molar units) of the Ganga headwaters. The data suggests dominance of carbonate weathering in the basin.

sources to dissolved major ions budget in rivers can be derived either by forward modeling [*Galy and France-Lanord*, 1999; *Krishnaswami et al.*, 1999; *Dalai et al.*, 2002; *Quade et al.*, 2003; *Singh et al.*, 2005; *Tipper et al.*, 2006] using suitable proxies, such as Na_s, ($Na_s = Na_r - Cl_r$) or Mg [*Das et al.*, 2005] or by inverse modeling [*Negrel et al.*, 1993; *Gaillardet et al.*, 1999; *Millot et al.*, 2003; *Wu et al.*, 2005; *Moon et al.*, 2007]. Earlier studies in the Himalaya by and large employed the forward model for source apportionment [*Galy and France-Lanord*, 1999; *Krishnaswami et al.*, 1999; *Dalai et al.*, 2002; *Singh et al.*, 2005; *Tipper et al.*, 2006]. In this study, the inverse model has been used to

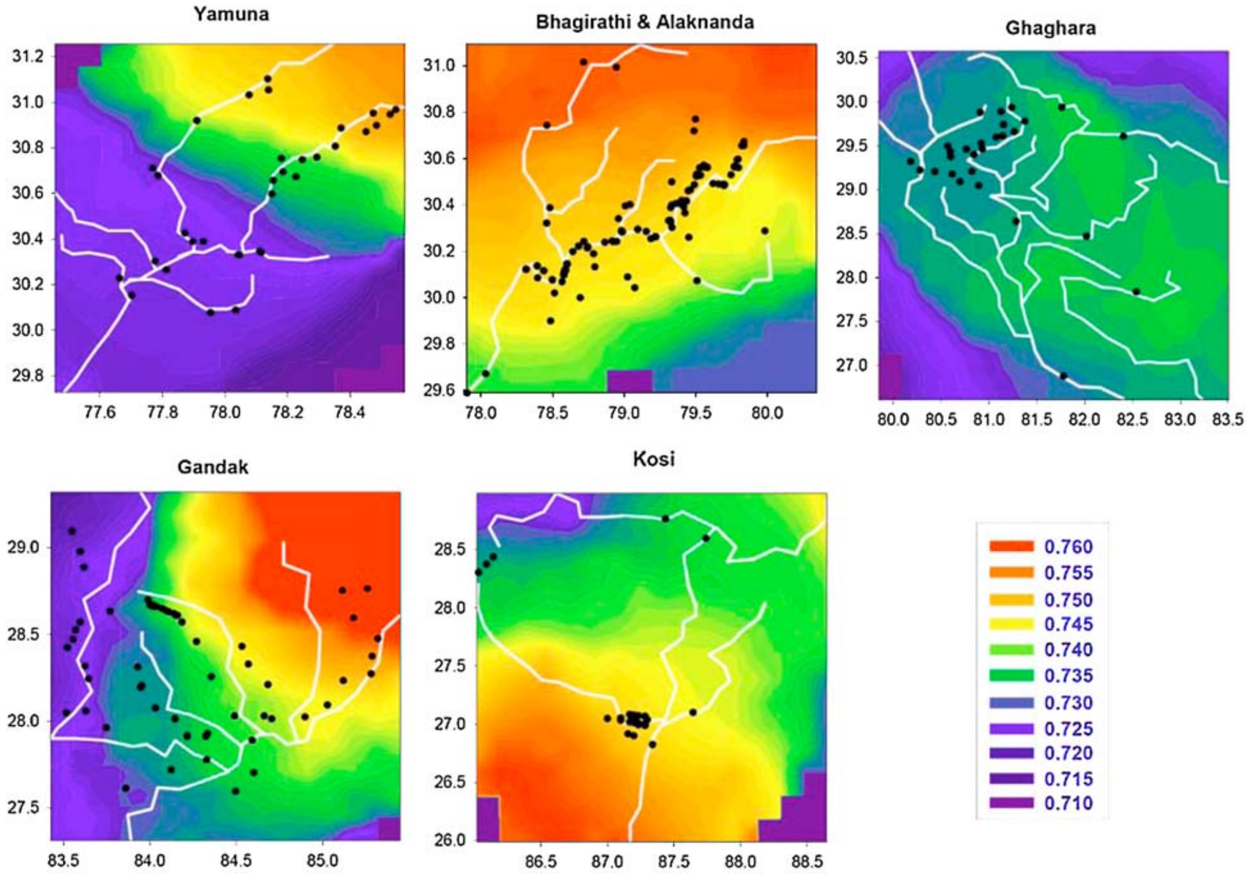

Figure 3. Spatial variation of dissolved $^{87}Sr/^{86}Sr$ for the different tributaries of the Ganga headwaters. Higher $^{87}Sr/^{86}Sr$ values indicate relatively high silicate weathering, especially in the Kosi and Bhagirathi basins. The black dots represent the sampling points used to construct the contours.

apportion the sources of the dissolved material to the Ganga headwaters and its Himalayan tributaries. Further, the results obtained by the inverse model are compared with those derived from the forward model and their implications discussed. A key difference between the two models is that in the forward model the release ratios of various major ions from the source rocks to the rivers is assumed whereas in the inverse model it is the best fit derived by iteration of the measured data.

[16] For source apportionment Na normalized elemental ratios are used because Na behaves conservatively in river systems; in addition its sources are better constrained. In basins where Na budget is difficult to constrain due to presence of alkaline and saline salts Mg and Si have been used as indices of silicate weathering [*Das et al.*, 2005; *Rengarajan et al.*, 2009; *Rai et al.*, 2010]. Ca, the most abundant cation in rivers, is not used as the normalizing element as it can behave nonconservatively; it may be removed from solution by calcite precipitation particularly during low-flow periods. In addition, Ca and Mg in the rivers are derived from multiple sources. Similarly the use of K is also limited, as it is bioreactive element and both Mg and K are known to be affected by secondary mineral formation processes in the basin [*Galy and France-Lanord*, 1999].

4.1. Forward Model

[17] The forward modeling approach assumes that dissolved Na in rivers is derived from two sources, (atmosphere + halite) and silicate weathering and that the (atmosphere + halite) contribution of Na is equal to that of dissolved Cl. This makes the silicate derived Na (Na_s) to be equal to

$$Na_s = Na_r - Cl_r \qquad (1)$$

where Na_r and Cl_r are the concentrations of dissolved Na and Cl in the rivers.

[18] Na_s along with assumed ratios of (Ca/Na) and (Mg/Na) released from the silicates to rivers [*Krishnaswami et al.*, 1999] are used to estimate

the cations derived from silicate weathering to river waters. Generally, the release ratios of Ca/Na and Mg/Na are taken to be their average abundance ratios in the silicates of the basin. The model therefore assumes congruent weathering of Na, Ca and Mg from silicates. However, in some of the Himalayan studies [*Singh et al.*, 1998; *Krishnaswami et al.*, 1999; *Dalai et al.*, 2002], the elemental ratios of Ca, Sr, Mg used in the forward model are based on the composition of bed rock, soil profiles and tributaries draining predominantly silicates. In these studies, therefore there is no assumption of congruent weathering. Cations derived from silicates are as given below:

$$\begin{aligned} Na_s &= Na_r - Cl_r \\ K_s &= K_r \end{aligned} \qquad (2)$$

$$Ca_s = Na_s \times \left(\frac{Ca}{Na}\right)_{sol} \qquad (3)$$

$$Mg_s = Na_s \times \left(\frac{Mg}{Na}\right)_{sol} \qquad (4)$$

where $(X/Na)_{sol}$ is the molar ratio with which the element X is released to rivers from the silicate rocks. The estimates of silicate derived cations by the forward model therefore depend critically on the $(X/Na)_{sol}$ ratio used in the calculation. This ratio, though varies widely in parent rocks [*Krishnaswami et al.*, 1999], it is expected to average out in large river basins, such as the basins of the Himalayan tributaries of the Ganga. The fraction of dissolved cations supplied from silicates to the river ($Cat_s = 100 \times [(Na_s + K_s + Mg_s + Ca_s)/(Na_r + K_r + Mg_r + Ca_r)]$) was estimated following the approach of *Krishnaswami et al.* [1999].

4.2. Inverse Modeling

[19] Inverse model has also been used to derive the cation contribution from different sources to river waters [*Negrel et al.*, 1993; *Gaillardet et al.*, 1999; *Millot et al.*, 2003; *Wu et al.*, 2005; *Moon et al.*, 2007]. The inverse model calculates not only the contribution of various sources to the solute budget of the river but also the best values for elemental ratios of the end-members [*Negrel et al.*, 1993]. The calculations rely on a set of mass balance equations which defines the relation between observed data and the model parameters, e.g.,

$$\left(\frac{X}{Na}\right)_r = \sum_{i=1}^{n} \left(\frac{X}{Na}\right)_i \times f_i(Na) \qquad (5)$$

where X = Cl, Ca, Mg, Sr, HCO_3 and

$$\left[\frac{^{87}Sr}{^{86}Sr} \times \left\{\frac{Sr}{Na}\right\}\right]_r = \sum_{i=1}^{n} \left(\frac{^{87}Sr}{^{86}Sr}\right)_i \times \left(\frac{Sr}{Na}\right)_i \times f_i(Na) \qquad (6)$$

where $(X/Na)_i$ is the molar ratio with which the element X is released to rivers from the end-member i. In this study, four end-members (n = 4) are considered, (1) silicates, (2) carbonates + gypsum, (3) atmosphere + halites, and (4) hot springs, and $f_i(Na)$ is the fraction of Na in the river contributed from source i.

$$\sum_{i=1}^{n} f_i(Na) = 1 \qquad (7)$$

[20] In general, equations (5)–(7) can be written as $d = g(p)$, where d and p are the data and model spaces, respectively. The model spaces are assumed to follow lognormal probability distribution. A nonlinear weighted fit of equations (5)–(7) was obtained using the Quasi-Newton method [*Tarantola*, 2005], which provided the best possible set for the model parameters and the covariance (i.e., uncertainties) associated with them.

[21] The consistency of the approach was checked by analyzing the data of the Mackenzie River which were analyzed earlier by *Millot et al.* [2003] using inverse model to estimate contributions from different sources. The a priori input for various ratios used in the present study is the same as that used by *Millot et al.* [2003]. For $^{87}Sr/^{86}Sr$ of the silicate end-member, a value of (0.73 ± 0.01) is used, as the same is not reported by *Millot et al.* [2003]. The results obtained in this study (Data Set S3 of the auxiliary material and Figure 4a) are in good agreement with those of *Millot et al.* [2003] for silicates and carbonates, suggesting that the approach followed in this work are consistent with earlier studies.

[22] The use of inverse modeling to apportion the sources of dissolved components of rivers can be done based either on the data of the entire samples of the basin [*Moon et al.*, 2007] or a single sample at a time [*Negrel et al.*, 1993]. In this study, all samples of a subbasin are modeled together to yield a number of mass balance equations which can provide the best fit for the a posteriori end-member values for the basin. Further, the source apportionment using the inverse model was done for the mainstream and for the large tributaries in the Himalayan catchment for the monsoon and non-monsoon samples separately (Data Set S2 of the

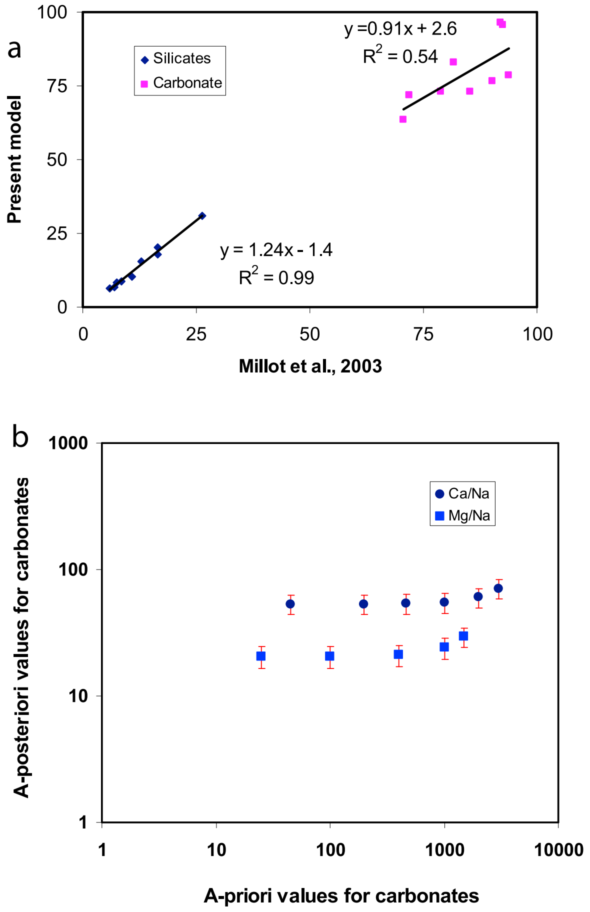

Figure 4. (a) Reanalysis of Mackenzie river water data. Correlation between results obtained based on the present analysis and those of *Millot et al.* [2003] using the same end-members. The good correlation between the two sets of data indicates consistency of both the models. (b) Sensitivity test for the inverse model using a wide range of a priori ratios for the carbonate end-members, the convergence of the a posteriori value for different a priori ratios indicates that the model is nearly independent of the a priori values.

auxiliary material). Samples with anomalous compositions and from small streams are not considered in the modeling. Silicate and carbonate contributions to the solute budget are calculated after obtaining the a posteriori model parameters for different sources.

4.2.1. A Priori Values of End-Members

[23] Na is used for normalization in both the inverse model and the forward model. The elemental and isotopic ratios for atmospheric input were calculated from the rainwater composition reported for the Himalayan regions [*Galy and France-Lanord*, 1999; *Galy et al.*, 1999]. The elemental ratios for the silicate end-member were taken to be the same as those used by *Krishnaswami et al.* [1999]. The abundance ratios of various elements in the carbonate end-member are based on the chemical composition of Precambrian carbonates from the Lesser Himalaya [*Singh et al.*, 1998; *Bickle et al.*, 2001]. Sodium concentration in ten carbonate samples for which other elemental abundances data are reported by *Singh et al.* [1998] was determined in this study. Gypsum and carbonate end-members were combined owing to similarity in their elemental ratios [*Moon et al.*, 2007].

[24] The a priori end-member values used are listed in Table 2. The end-member composition of the hot springs is from *Evans et al.* [2001, 2004]. The a priori ratios of carbonates have large uncertainties due to significant spread in their composition. To assess the effect of the wide range in elemental ratios in carbonates on the results, a sensitivity test of the inverse model was done for the monsoon samples of the Ganga at Rishikesh by varying the a priori Ca/Na ratios by nearly two orders of magnitude (3000, 2000, 1000, 460, 200, 45) while keeping other ratios unchanged. Despite the orders of magnitude difference in the a priori Ca/Na values, the calculated a posteriori ratios converged to nearly the same value (Figure 4b). Similarly, the a posteriori Mg/Na ratios also converged to nearly the same value despite a variation in the a priori values from 1500 to 25. These tests (Figure 4b) establish that the model results are not critically dependent on the assigned a priori values of Ca/Na and Mg/Na. A similar sensitivity test was also carried out for $f_i(Na)$ by using three different sets of a priori values for $f_i(Na)$ ((0.5 ± 0.4, 0.4 ± 0.4, 0.2 ± 0.1) for rain; (0.7 ± 0.6, 0.6 ± 0.5, 0.7 ± 0.2) for silicates; (0.35 ± 0.25, 0.25 ± 0.2, 0.2 ± 0.1) for carbonates and (0.35 ± 0.3, 0.3 ± 0.2, 0.15 ± 0.1) for hot springs) for the monsoon samples of the Ganga (Rishikesh). These three different sets of a priori values of $f_i(Na)$ converged to statistically same a posteriori values after the inversion. This suggests that the results of the inverse model are nearly independent of the a priori data on $f_i(Na)$ and (X/Na) values.

4.2.2. A Posteriori Results

[25] Table 3 lists the a posteriori values obtained for the different subbasins of the Ganga during monsoon, and they are compared with the a priori values (Table 2). The monsoon samples have been used for comparison as in some of these rivers, there is a possibility of loss of Ca as calcite during

Table 2. A Priori Molar Ratio for the Various End-Members and Associated Uncertainties[a]

	Rain[b,c]	Silicates[d]	Carbonates[e,f]	Hot Springs[g]
Cl/Na	0.74 ± 0.1	0.00	0.00	1.2 ± 0.3
Ca/Na	2.2 ± 0.11	0.7 ± 0.3	3000 ± 2000	4.4 ± 0.8
Mg/Na	0.6 ± 0.1	0.3 ± 0.2	1500 ± 1000	0.024 ± 0.012
Sr/Na	2.1 ± 0.5	2.0 ± 0.8	350 ± 200	1.2 ± 0.13
$^{87}Sr/^{86}Sr$	0.714 ± 0.004	0.8 ± 0.2	0.715 ± 0.02	0.77 ± 0.02
Alk/Na	6.8 ± 0.5	2 ± 1	8000 ± 4000	10 ± 4

[a] Errors are $\pm 1\sigma$; Sr/Na is in nM/μM units.
[b] *Galy and France-Lanord* [1999].
[c] *Galy et al.* [1999].
[d] *Krishnaswami et al.* [1999].
[e] Present study.
[f] *Singh et al.* [1998].
[g] *Evans et al.* [2001].

nonmonsoon. The results of the inversion model show spatial variability in Ca/Na values for the silicate end-member of different subbasins. The a posteriori $(Ca/Na)_{sol}$ for the Kosi (0.36 ± 0.14) and the Ghaghra (0.29 ± 0.12) overlaps within errors with that reported (0.41 ± 0.18 [*English et al.*, 2000; *Quade et al.*, 2003]) for streams draining predominantly silicate terrain in the central and the western Nepal Himalaya. Similarly, the a posteriori $(Ca/Na)_{sol}$ values for the Bhagirathi (0.68 ± 0.29), Alaknanda (0.64 ± 0.27), Ganga (Rishikesh) (0.70 ± 0.28) and the Yamuna (0.56 ± 0.16) are the same within errors and are consistent with the value of (0.70 ± 0.30) used by *Krishnaswami et al.* [1999] for these rivers, based on (Ca/Na) of parent rocks, soil profiles and streams flowing predominantly through silicate terrain in the central Himalaya. A critical look at the a posteriori values of Ca/Na for these different subbasins, however seems to indicate that they are systematically lower compared to the a priori ratios, though they overlap within their uncertainties.

[26] The a posteriori $(Mg/Na)_{sol}$ for the Gandak and Ghaghra basins (Table 3) are similar and consistent with the ratios of rivers (0.24 ± 0.10) draining the central Himalaya containing noncarbonate sediments [*Quade et al.*, 2003]. The $(Mg/Na)_{sol}$ for the Bhagirathi, Alaknanda and the Ganga rivers is very close to the estimated ratio of (0.3 ± 0.2) [*Krishnaswami et al.*, 1999]. The a posteriori $(Sr/Na)_{sol}$ values for different rivers are nearly the same within errors (1.35 ± 0.49, 1.21 ± 0.46, 1.14 ± 0.40, 1.53 ± 0.22, 1.54 ± 0.46, 1.46 ± 0.51, and 1.56 ± 0.31 for Bhagirathi, Alaknanda, Ganga (Rishikesh), Yamuna, Ghaghra, Gandak, and Kosi, respectively), however all these values are lower compared to the average Sr/Na ratio of the silicate bed rocks (2.0 ± 0.8) [*Krishnaswami et al.*, 1999]. This suggests the possibility of incongruent weathering of silicates in the Himalayan catchment of the Ganga with Na being weathered preferentially over Sr. The inverse model provides the best fit release ratios of the elements from silicates based on measured compositions and therefore is better suited to evaluate the role of incongruent release of elements during weathering. This is unlike the forward model which estimates the contribution of silicates to the dissolved Sr based on the assumed release ratios, generally assumed to be the same as the bed rocks. A similar difference between the results obtained using the forward and the inverse models were also reported for the Red river basin [*Moon et al.*, 2007].

5. Chemical Erosion in the Ganga Headwaters

[27] The chemical weathering of silicate minerals is a major sink for atmospheric CO_2 on million year scale and the chemical erosion rate of silicates of the Ganga basin is important to assess the impact of the Himalaya on the global CO_2 budget.

5.1. Sources of Dissolved Cations and Sr

[28] The fractions of dissolved cations supplied to the headwaters and tributaries of the Ganga from atmosphere, silicates, (carbonates + gypsum) and hot springs estimated based on the inverse model are listed in Data Set S4 of the auxiliary material. The estimated silicate cations (Cat_s) from the inverse model for the Ganga at Rishikesh (21% (Table 4)) is similar to that reported earlier (~25%) based on the forward model [*Krishnaswami et al.*, 1999; *Dalai et al.*, 2002]. The range of Cat_s (20%–28%) for the Yamuna upstream basin [*Dalai et al.*, 2002]

Table 3. A Posteriori Results From the Inverse Model for Monsoon Samples of the Ganga Tributaries[a]

	Rain	Silicates	Carbonates	Hot Spring
Bhagirathi				
Cl/Na	0.76 ± 0.10	0 ± 0	0 ± 0	0.87 ± 0.18
Ca/Na	2.19 ± 0.11	0.68 ± 0.29	154 ± 36	4.73 ± 0.84
Mg/Na	0.60 ± 0.10	0.20 ± 0.13	76 ± 17	0.02 ± 0.01
Sr/Na	2.31 ± 0.54	1.35 ± 0.49	210 ± 49	1.14 ± 0.13
^{87}Sr/^{86}Sr	0.714 ± 0.004	0.801 ± 0.020	0.720 ± 0.018	0.770 ± 0.020
HCO$_3$/Na	6.64 ± 0.49	1.29 ± 0.63	304 ± 71	9.51 ± 3.38
Alaknanda				
Cl/Na	0.71 ± 0.09	0 ± 0	0 ± 0	0.83 ± 0.17
Ca/Na	2.18 ± 0.11	0.64 ± 0.27	137 ± 27	4.48 ± 0.81
Mg/Na	0.66 ± 0.11	0.43 ± 0.27	44 ± 10	0.02 ± 0.01
Sr/Na	2.00 ± 0.46	1.21 ± 0.46	155 ± 30	1.14 ± 0.13
^{87}Sr/^{86}Sr	0.714 ± 0.004	0.800 ± 0.020	0.719 ± 0.016	0.770 ± 0.020
HCO$_3$/Na	6.73 ± 0.49	1.63 ± 0.80	329 ± 64	10.11 ± 3.95
Ganga (Rishikesh)				
Cl/Na	0.83 ± 0.09	0 ± 0	0 ± 0	0.72 ± 0.14
Ca/Na	2.18 ± 0.11	0.70 ± 0.28	71 ± 12	5.06 ± 0.87
Mg/Na	0.63 ± 0.10	0.36 ± 0.19	29 ± 5	0.02 ± 0.01
Sr/Na	2.31 ± 0.53	1.14 ± 0.40	107 ± 18	1.13 ± 0.13
^{87}Sr/^{86}Sr	0.714 ± 0.004	0.800 ± 0.020	0.721 ± 0.015	0.770 ± 0.020
HCO$_3$/Na	6.60 ± 0.48	1.36 ± 0.64	161 ± 29	13.58 ± 4.27
Yamuna				
Cl/Na	0.92 ± 0.09	0 ± 0	0 ± 0	0.57 ± 0.08
Ca/Na	2.28 ± 0.11	0.56 ± 0.16	27 ± 4	4.42 ± 0.01
Mg/Na	0.71 ± 0.10	0.09 ± 0.05	14 ± 2	0.03 ± 0.02
Sr/Na	2.08 ± 0.05	1.53 ± 0.22	48 ± 6	0.90 ± 0.10
^{87}Sr/^{86}Sr	0.714 ± 0.004	0.803 ± 0.019	0.725 ± 0.014	0.766 ± 0.020
HCO$_3$/Na	6.45 ± 0.47	1.79 ± 0.53	40 ± 6	16.17 ± 1.55
Ghaghra (Karnali)				
Cl/Na	0.80 ± 0.10	0 ± 0	0 ± 0	1.54 ± 0.33
Ca/Na	2.17 ± 0.11	0.29 ± 0.12	65 ± 18	3.68 ± 0.65
Mg/Na	0.61 ± 0.10	0.41 ± 0.25	262 ± 62	0.02 ± 0.01
Sr/Na	2.05 ± 0.49	1.54 ± 0.46	351 ± 84	1.15 ± 0.13
^{87}Sr/^{86}Sr	0.714 ± 0.004	0.799 ± 0.020	0.715 ± 0.018	0.770 ± 0.020
HCO$_3$/Na	6.74 ± 0.49	1.32 ± 0.61	504 ± 122	8.06 ± 3.18
Gandak (Trisuli)				
Cl/Na	0.98 ± 0.10	0 ± 0	0 ± 0	0.58 ± 0.09
Ca/Na	2.17 ± 0.11	0.50 ± 0.20	54 ± 9	6.77 ± 0.99
Mg/Na	0.80 ± 0.11	0.32 ± 0.12	11 ± 2	0.02 ± 0.01
Sr/Na	1.98 ± 0.44	1.46 ± 0.51	110 ± 18	1.12 ± 0.13
^{87}Sr/^{86}Sr	0.714 ± 0.004	0.800 ± 0.020	0.716 ± 0.015	0.769 ± 0.020
HCO$_3$/Na	6.45 ± 0.46	1.21 ± 0.57	109 ± 20	19.15 ± 3.45
Kosi (Arun)				
Cl/Na	0.89 ± 0.10	0 ± 0	0 ± 0	0.95 ± 0.19
Ca/Na	2.15 ± 0.11	0.36 ± 0.14	29 ± 7	3.93 ± 0.69
Mg/Na	0.54 ± 0.08	0.07 ± 0.04	11 ± 2	0.02 ± 0.01
Sr/Na	4.02 ± 0.61	1.56 ± 0.31	49 ± 11	1.14 ± 0.13
^{87}Sr/^{86}Sr	0.714 ± 0.004	0.794 ± 0.019	0.707 ± 0.019	0.769 ± 0.020
HCO$_3$/Na	6.16 ± 0.43	0.68 ± 0.31	69 ± 15	5.71 ± 2.06

[a] Sr/Na ratios are in nM/μM and other ratios are in μM/μM.

brackets the value of 22% derived in the present work. Similarly, the Cat$_s$ for the Gandak (~20%) and Ghaghra (~20%) estimated based on the forward model using the data set of *Galy and France-Lanord* [1999] are consistent with those of the present study within uncertainties (23% and 24%, respectively). The estimated Cat$_s$ for the Kosi (36%) in this study is comparable with earlier

Table 4. Source Apportionment for Cations and Sr and Silicate and Carbonate Erosion Rates for the Streams[a]

	Cat_{rain}	Cat_s	Cat_c	Cat_{spring}	Sr_{rain}	Sr_s	Sr_c	Sr_{spring}	Ca Loss (%)	SER (tons/km^2/yr)	CER (tons/km^2/yr)	CO_2 Drawdown (10^5 moles/km^2/yr)
Bhagirathi	10 ± 4	29 ± 5	52 ± 9	11 ± 4	8 ± 3	22 ± 5	68 ± 5	3 ± 1	8 ± 3	11.1	36.4	2.1
Alaknanda	7 ± 3	21 ± 2	71 ± 9	6 ± 1	5 ± 2	15 ± 5	79 ± 6	2 ± 0	23 ± 8	12.2	52.5	2.2
Rishikesh	9 ± 3	21 ± 4	69 ± 9	10 ± 8	6 ± 2	13 ± 4	79 ± 4	2 ± 2	25 ± 8	13.0	45.6	2.3
Yamuna	11 ± 5	22 ± 11	50 ± 18	16 ± 8	8 ± 5	17 ± 9	71 ± 11	4 ± 3	22 ± 7	13.5	38.0	1.6
Ghaghra	9 ± 1	24 ± 6	60 ± 9	8 ± 1	6 ± 1	20 ± 7	72 ± 8	2 ± 0	-	13.6	54.7	3.3
Gandak	14 ± 9	23 ± 6	52 ± 12	19 ± 11	6 ± 4	14 ± 6	77 ± 9	3 ± 2	36 ± 4	17.6	92.3	3.6
Kosi	10 ± 8	36 ± 8	50 ± 15	8 ± 6	16 ± 14	35 ± 11	47 ± 19	2 ± 2	16 ± 5	9.9	12.4	2.5

[a] Based on results from the inverse model. Errors are ±σ. The source contributions from different end-members for cations and Sr listed are the average of both monsoon and nonmonsoon samples (Data Set S4) for each subbasin. Erosion rates are estimated based on high-flow samples for the river Bhagirathi (Devprayag), Alaknanda (Devprayag), Ganga (Rishikesh), Yamuna (before confluence with Aglar), Ghaghra (Chisapani), Gandak (Narayan Ghat), and Kosi (Ulleri Khola).

reported values (33%–43%) [*Quade et al.*, 2003]. Among the rivers studied, Cat_s is the highest for the Kosi followed by the Bhagirathi (Figure 5a) a result consistent with the lithology of the Kosi basin, with more aerial coverage of silicate rocks.

[29] A closer look at the comparison of the forward and inverse model results, however indicates that the Cat_s values of almost all rivers derived from the inverse model are systematically lower than those based on the forward model. To check on this, statistical analysis of the Cat_s data derived for both the models was carried out using the Williamson bivariate statistical method. This analysis shows that the Cat_s derived from the inverse and forward models are linearly correlated with a slope of 0.81 ± 0.07 significantly lower than the equiline (1σ, Figure 6). As a result the Cat_s and SER derived from the inverse model are lower than that estimated from the forward model. The difference in the results obtained from the two models can be explained in terms of differences in their elemental release ratios. The inverse model provides the best fit for the release ratios based on measured chemical composition of the rivers whereas in the forward model the release ratios are assumed based on that in parent rocks or a combination of parent rocks, soil profiles and rivers draining monolithological terrains. Further, in the forward model, the role of hot springs in contributing to the water chemistry is not considered.

[30] The relative contribution of Sr from silicate weathering to the rivers (Sr_s = 100 × (silicate derived Sr (nM))/Sr_r) follows a pattern similar to that of Cat_s. Analogous to Cat_s, the Sr_s is highest for the Kosi. The Sr budget of the Gandak is dominated by carbonates, consistent with the geology of its basin. The range in Sr_s based on the inverse model, though are systematically low, overlaps with the estimates of Sr_s based on the forward model (13%–65%) for these rivers [*Galy et al.*, 1999].

[31] The estimated contribution from hot springs differs among the subbasins of the Ganga (Table 4) and is the highest for the Gandak River. The present estimates of Sr_{spring} are low compared that reported by *Evans et al.* [2001, 2004] for the tributaries of the Gandak. The possible reason for this difference could be regional effect of hot springs on river geochemistry. The contribution of Sr from the hot springs to the Ganga headwaters is low (~3%) and is in agreement with the earlier reported values for the Alaknanda [*Bickle et al.*, 2005].

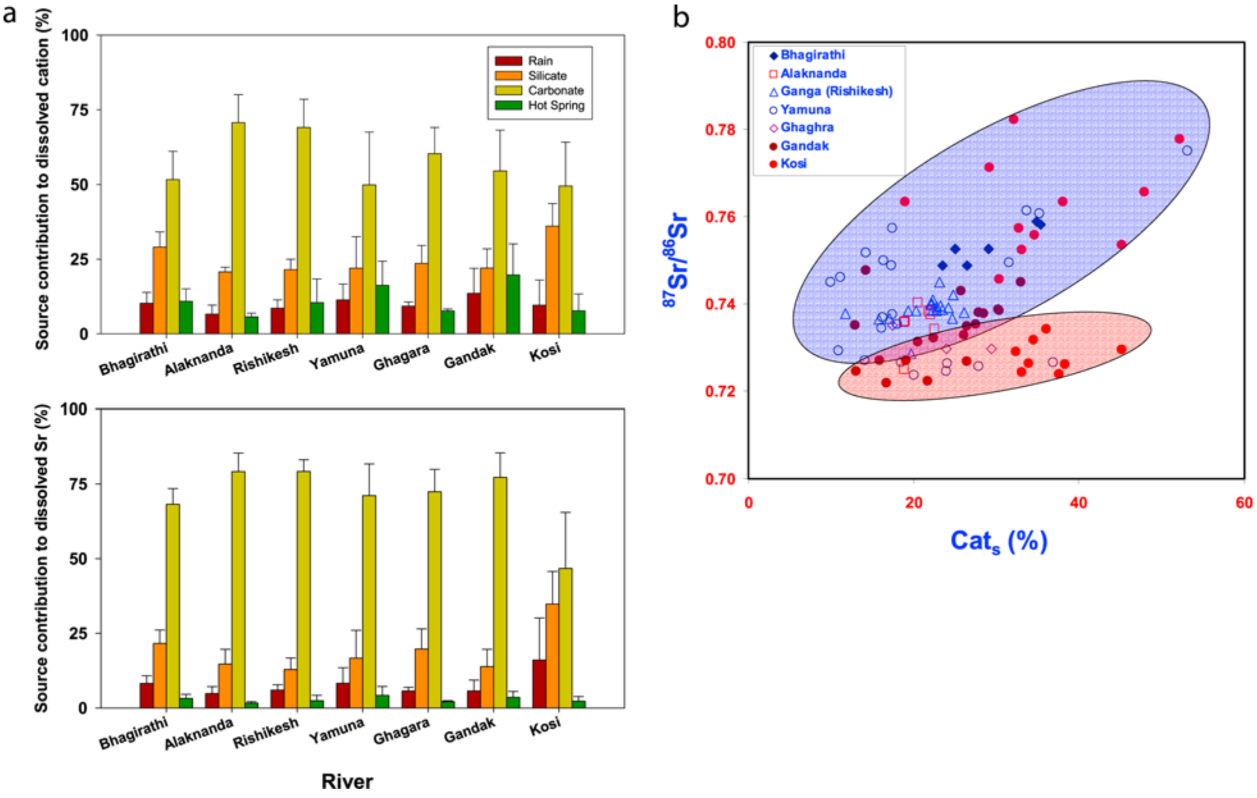

Figure 5. (a) Bar diagram of contribution from different sources to dissolved cations and Sr to the various tributaries of the Ganga based on the inverse model. (b) The variation of $^{87}Sr/^{86}Sr$ versus Cat_s. It is seen that Cat_s and $^{87}Sr/^{86}Sr$ covary, indicating that their source of radiogenic Sr is dominated by silicates and the $^{87}Sr/^{86}Sr$ has the potential to be a tracer for silicate weathering. There seems to exist two trends for the Ganga: (1) for the majority of Ganga headwaters enveloped with blue ellipse and (2) streams flowing through the TSS or the Siwaliks, which are characterized by lower radiogenic Sr for silicates (red ellipse).

5.2. Calcite Precipitation From the Rivers

[32] The river Ganga and its tributaries are known to be supersaturated with respect to calcite particularly during their lean flow [*Sarin et al.*, 1989; *Galy and France-Lanord*, 1999; *English et al.*, 2000; *Dalai et al.*, 2002; *Jacobson et al.*, 2002]. The precipitation of calcite from rivers cannot only complicate the apportionment of dissolved Ca and to a lesser extent Mg and Sr to various sources but also can underestimate the CER on subbasin scales and the quantification of this process provides a better understanding of the riverine alkalinity budget. Recognizing the importance of this, a few earlier studies [*Jacobson et al.*, 2002] have estimated Ca removal from the Ganga based on modeling the degree of variation of the dissolved Ca/Mg and Ca/Sr ratios. In this work, an attempt has been made using the inverse model to quantify the Ca removal from the streams during their lean flow. It is assumed that (1) the Ca/Mg release ratio from different end-members have remained the

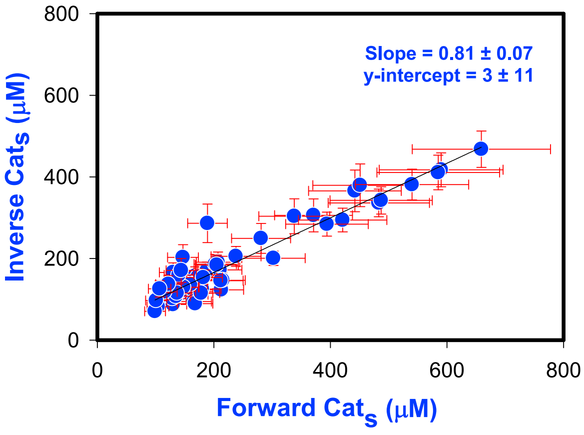

Figure 6. Correlation between Cat_s (µM) obtained by the forward and inverse models. Cat_s derived using the inverse model is lower compared to that derived from the forward model. This disagreement in the results from the models is attributed to differences in the assumed and derived end-member values.

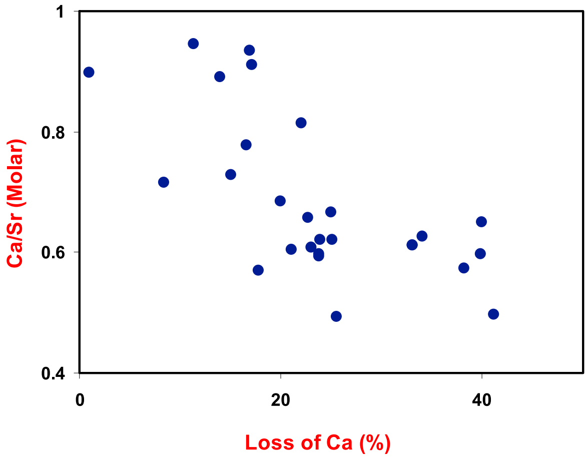

Figure 7. Estimated loss of Ca shows a decreasing trend with measured Ca/Sr of the Ganga, consistent with lowering of Ca due to calcite precipitation in the subbasins.

same during different seasons and (2) the riverine Mg and Sr concentrations remain unaffected by calcite precipitation. The latter assumption may not be strictly valid due to minor incorporation of Mg and Sr in calcite. The removal of both Mg and Sr, however is not expected to impact their budget significantly considering that their distribution coefficient in calcite is far less than one [*Rimstidt et al.*, 1998].

[33] Calcite saturation indices for the Ganga tributaries indicate that most of them are supersaturated during lean flow. Therefore, the measured Ca and HCO_3 concentrations of such tributaries during their lean flow are likely to be affected by calcite precipitation. Hence, in the inverse model source apportionment of the nonmonsoon (NM) samples was done independent of Ca and HCO_3. After obtaining best fit values for Mg/Na and the fraction of Na contributed from each source ($(Mg/Na)_i^{NM}$, $f_i^{NM}(Na)$); Ca/Na for the source i is estimated using the following equation.

$$\left(\frac{Ca}{Na}\right)_i^{NM} = \left(\frac{Mg}{Na}\right)_i^{NM} \times \left(\frac{Ca}{Mg}\right)_i^{M} \tag{8}$$

where $(Ca/Mg)_i^M$ is the molar ratio of Ca/Mg released from source i during monsoon (M).

[34] From this ratio, the Ca content of the river prior to calcite precipitation, $(Ca)_{orig}$ can be calculated as,

$$(\mathrm{Ca})_{\mathrm{orig}} = \sum_{i=1}^{4} \left(\frac{Ca}{Na}\right)_i^{NM} \times f_i^{NM}(Na) \tag{9}$$

The fractional loss of Ca from the river due to calcite precipitation during nonmonsoon is calculated from the difference between $(Ca)_{orig}$ and measured Ca (Ca_r).

$$\mathrm{Ca\ loss} = \left(\frac{(Ca)_{orig} - (Ca)_r}{(Ca)_{orig}}\right) \tag{10}$$

[35] This approach to estimate Ca loss largely depends on the inverse model to provide consistent results, when Ca and HCO_3 are not included in the calculation. To test this, the monsoon samples were modeled twice, once with Ca and HCO_3 data and the second time without them. The results of both the analysis are the same (Data Set S5 of the auxiliary material) suggesting that excluding the Ca and HCO_3 data from the model calculation does not affect the source apportionment estimates significantly.

[36] The amount of Ca loss for different rivers is listed in Data Set S4 of the auxiliary material. The Ca removal from the Ganga headwaters ranges from ~10%–40% and is highest for the Gandak (Table 4). The high calcite precipitation in the Gandak could be due to high carbonate weathering in the basin, which is dominated by carbonates. The present estimate of Ca loss for the Yamuna (~22%) is consistent with the upper limits (~50%) provided by *Dalai et al.* [2002]. Further, the Ca loss estimated for the Ganga tributaries in this work based on the inverse model is comparable with that reported by *Jacobson et al.* [2002]. The extent of Ca removal from the Ganga rivers is also evident from their Ca/Sr ratios (Figure 7). The observed decrease in riverine Ca/Sr with increasing Ca loss indicates the impact of calcite precipitation which lowers the Ca abundance of the rivers, similar to those reported for various rivers of the Ganga system [*Sarin et al.*, 1989; *Dalai et al.*, 2002; *Jacobson et al.*, 2002; *Bickle et al.*, 2005]. The estimates for Ca removal suggests Ca eroded from one subbasin can be deposited in a subsequent one and can result in possible underestimation of the chemical weathering rates in some of these basins, if calculated based on the nonmonsoon data. This nonconservative behavior of Ca in the Ganga river system also hampers the potential of Sr/Ca as a proxy for silicate weathering.

[37] Based on calcite saturation index, *Sarin et al.* [1989] indicated that the Ganga headwaters are largely undersaturated with respect to calcite, particularly during high-flow periods. This supports

the assumption used in the above calculation, namely, insignificant removal of Ca during high-flow period from the Ganga headwaters. However, a few subsequent studies [*Bickle et al.*, 2005; *Tipper et al.*, 2006] indicate toward calcite supersaturation in some of the rivers (Source waters of the Alaknanda and the Marsyandi) flowing through TSS during high-flow periods. In such a case, the present estimate of Ca loss, particularly in these tributaries will be a lower limit.

5.3. Control of Silicate Weathering on ^{87}Sr/^{86}Sr

[38] The potential of ^{87}Sr/^{86}Sr to serve as a proxy of silicate weathering in the Himalayan basin has remained a topic of debate [*Harris*, 1995; *Blum et al.*, 1998; *Jacobson and Blum*, 2000; *Quade et al.*, 2003]. Highly radiogenic Sr in the Himalayan silicates makes it possible to use dissolved ^{87}Sr/^{86}Sr of the Himalayan rivers as a proxy of silicate weathering, however, the presence of metamorphosed carbonates in the Himalaya with highly radiogenic Sr questions this application. The cations derived from silicates (Cat_s) estimated using the inverse model and measured ^{87}Sr/^{86}Sr show an overall positive correlation (Figure 5b) for the headwaters of the Ganga. The majority of the riverine ^{87}Sr/^{86}Sr for the Ganga headwaters (encircled with blue ellipse in Figure 5b) increase with Cat_s. This observation seems to suggest that ^{87}Sr/^{86}Sr in the Ganga is largely controlled by the intensity of silicate weathering in the basin [*Krishnaswami and Singh*, 1998]. However, a few samples from the upstream of the Gandak and the Arun (tributary of the Kosi) follow an increasing trend (red ellipse in Figure 5b) with lower slope. The possible reason for this different trend could be the difference in Sr isotopic composition of bedrocks present in their corresponding basins compared to the other Ganga headwaters. These streams of the Kosi [*Quade et al.*, 2003] and Gandak [*Galy et al.*, 1999] with low ^{87}Sr/^{86}Sr drain through TSS, which are known to have silicates with less radiogenic Sr [*Oliver et al.*, 2003]. Hence, any increase in silicate weathering in the basin (TSS) of these streams can enhance fraction of cations released from silicates with limited increase in ^{87}Sr/^{86}Sr, i.e., with relatively lower slope compared to the streams draining LH and HH (Figure 5b).

5.4. Erosion Rates

[39] The silicate and carbonate erosion rates in the drainage basins are calculated based on the inverse model derived silicate and carbonate cations, Si concentration during high flow and their annual runoff (Table 4) using the following relations.

$$SER = \left(\frac{Q}{A}\right) \times (Na_s + K_s + Ca_s + Mg_s + SiO_2) \qquad (11)$$

$$CER = \left(\frac{Q}{A}\right) \times \left(Na_c + Ca_c + Mg_c + (CO_3)_c\right) \qquad (12)$$

$$\mathrm{CO_2\ consumption\ rate} = \left(\frac{Q}{A}\right) \times (Na_s + K_s + 2 \times (Ca_s + Mg_s)) \qquad (13)$$

where Q is the annual water discharge and A is the drainage area of the river. SER and CER are in tons/km^2/yr, and CO_2 consumption rates are in moles/km^2/yr.

[40] Both SER and CER in the subbasins of the Ganga are significantly higher compared to other Himalayan rivers (the Brahmaputra and Indus) and the global average (Figure 8). These SER values of orogenic belts, e.g., the Himalaya and Andes, are higher compared to those reported for the rivers draining the shield areas [*Edmond and Huh*, 1997].

[41] The erosion rates estimated in this study are the highest for the river Yamuna and are similar to the earlier estimates of *Dalai et al.* [2002]. However, the SER of the Yamuna show a significant spatial variation. The SER of the Yamuna downstream the confluence of the tributary Aglar is very high, however, upstream of this confluence (above Batamandi) its SER is similar to that of other tributaries of the Ganga (Table 4). This large spatial variation in SER of the Yamuna subbasin is intriguing possible reasons could be anthropogenic inputs by its downstream tributaries or large supply of dissolved material from saline/alkaline soils as observed for rivers in the Ganga plain and penisular India [*Rengarajan et al.*, 2009; *Rai et al.*, 2010]. In this study, the erosion rates of the Yamuna before the confluence with the Aglar are considered as the representative value for the basin (Table 4).

[42] The SER of the Ganga headwaters are high compared to that of global average (5.4 tons/km^2/yr [*Gaillardet et al.*, 1999]). The high erosion rates in the drainage of the Ganga headwaters follow the intense physical erosion rates resulting from higher relief and runoff over the basin. The SER and CER for the Kosi are comparable, but unlike other

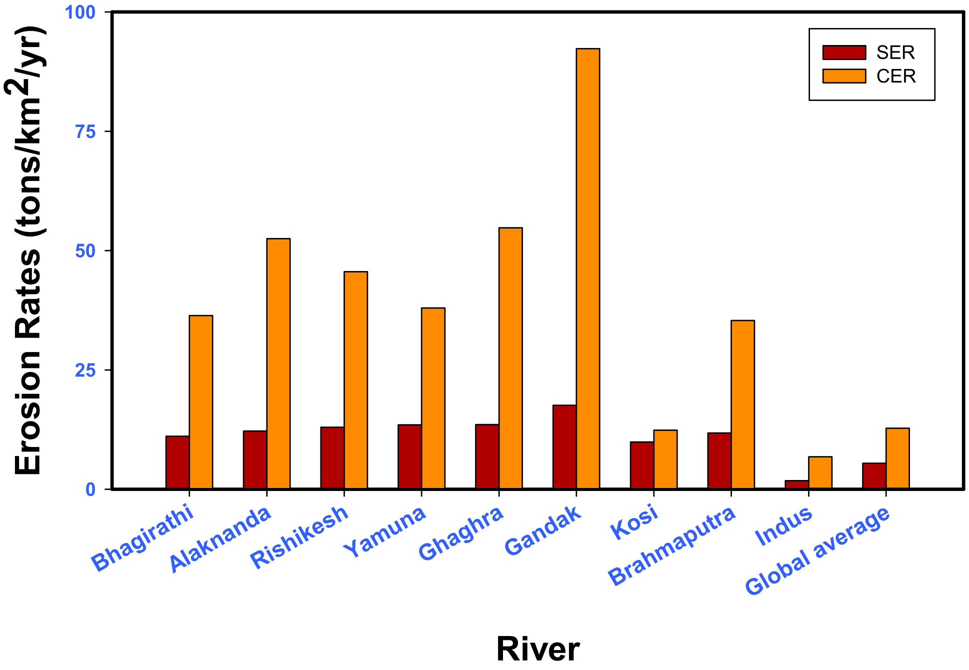

Figure 8. Comparison of silicate and carbonate erosion rates in different tributaries of the Ganga River with global average and other Himalayan rivers.

Himalayan tributaries of the Ganga, where carbonate weathering dominates the river chemistry.

[43] The CO_2 consumption rate due to the silicate weathering estimated (using equation (13)) in this study ranges between 1.6 × 10^5 moles/km^2/yr (Yamuna before confluence with Aglar) and 3.6 × 10^5 moles/km^2/yr (Gandak) for the Ganga headwaters (Table 4). The estimated CO_2 consumption rate due to silicate weathering in the Himalayan streams of the Ganga are distinctly higher compared to that of the global average (0.9 × 10^5 moles/km^2/yr [*Gaillardet et al.*, 1999]). These estimates are high compared to other Himalayan rivers such as the Indus (0.6 × 10^5 moles/km^2/yr [*Gaillardet et al.*, 1999]), but low compared to that of the Brahmaputra river (6.0 × 10^5 moles/km^2/yr [*Singh et al.*, 2005]).

5.5. Controlling Factors for Chemical Weathering in the Ganga Basin

[44] The chemical weathering and its intensity in any basin depends on many factors including relief, stream power, lithology, runoff, temperature and vegetation [*Garrels and Mackenzie*, 1971]. The contribution of each of these parameters to the chemical weathering varies from basin to basin and it is greatly debated in case of the Himalayan rivers. This study underscores the importance of lithology in controlling the cation budget derived from them in the basin. This interpretation is well supported by the high Cat_s and Sr_s values for those rivers (the Kosi and the Bhagirathi) where silicate bedrock dominates drainage basin (Table 1a).

[45] The estimated SER values for the Ganga tributaries range between 10 and 18 tons/km^2/yr and is high compared to global average. It is important to note that despite large variability in hydrogeological parameters e.g., rainfall, lithology among the subbasins, their SER fall in a narrow range (10–14 tons/km^2/yr, except 18 tons/km^2/yr for the Gandak) possibly due to balancing of the impact of individual controlling factors in different subbasins. The highest SER of the Gandak among the Ganga tributaries (Table 4) is well supported by very high physical erosion in this subbasin [*Singh et al.*, 2008]. To understand the primary controlling factor of chemical erosion rate in the Ganga basin, chemical erosion rates of the subbasins are plotted with runoff (Figure 9). A significant positive correlation between them suggests the importance of runoff in controlling the chemical erosion in the Ganga. Similar observation was also reported over Nepal Himalaya [*France-Lanord et al.*, 2003].

[46] Further, the SER of the Ganga subbasins are compared with the rivers draining the Deccan traps. The silicate of the Ganga basin is composed of granite and gneisses where as the Deccan drainage

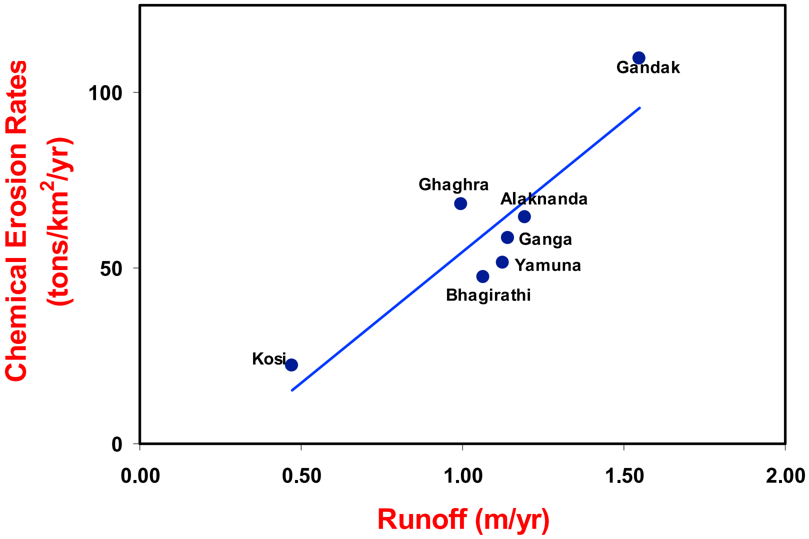

Figure 9. Scatter diagram of chemical erosion rates and the runoff for the Ganga tributaries. The data show significant correlation indicating runoff to be the important factors controlling the erosion pattern over the Ganga.

consists of basalts. The estimated SER for most of the tributaries of the Ganga (~12 tons/km^2/yr) using inverse modeling is comparable with that reported for the Krishna River (14 tons/km^2/yr [*Das et al.*, 2005]). The drainage basin of the Krishna is largely composed of the Basaltic rock; whereas the Himalaya contains only ~66% of silicate rock [*Amiotte Suchet et al.*, 2003]. The silicate exposure area for the Ganga headwater basin is estimated, using data from Table 1, to be ~70%. Silicate exposure area (~70%) normalized SER of the Ganga basin, ~17 tons/km^2/yr, is higher compared to that of the Krishna River despite the fact that the Krishna river basin is mainly composed of easily weatherable basaltic rocks compared to the granitic rocks present in the Himalaya. This suggests that the high silicate erosion rate of the Himalaya compared to Deccan Rivers could be due to its high relief.

5.6. Flux From the Himalaya to the Ganga Mainstream

[47] The Ganga drains about 1060 × 10^3 km^2 of area [*Galy and France-Lanord*, 1999] before it merges with the Brahmaputra in the Bangladesh, out of which ~176 × 10^3 km^2 of drainage area falls over the Himalaya and forms drainage of the Ganga headwaters [*Singh et al.*, 2008]. To estimate the contribution from the Ganga headwaters in the Himalaya to the total dissolved load flux of Ganga at its mouth, the total dissolved load flux (in monsoon) from the headwaters of the Ganga to the mainstream is quantified. The annual total dissolved solid (TDS) flux (= TDS of the tributaries at mouth × annual water discharge) of the Ganga at the mouth is estimated to be ~57 million tons, out of this ~33 million tons is estimated to be supplied by the headwaters. This suggests that the Himalayan drainage of the Ganga, constituting only ~17% of the drainage, supply ~60% of the dissolved material to the Ganga. Rest of the dissolved flux (~40%) of the Ganga is derived from the rivers flowing through the plains and peninsular area (~83%) indicating lower erosion rates in the Plain and Peninsular drainages. The high chemical erosion rates for the Ganga headwaters could be an effect of high relief and rainfall over the Himalaya compared to that in the plains.

6. Conclusions

[48] A number of studies on the headwaters and tributaries of the Ganga have been reported on their geochemical and isotopic properties to infer about erosion rates and their relation with atmospheric CO$_2$ drawdown rate. In the present work, a large number of subbasin-scale studies of the Ganga in the Himalaya was compiled and modeled together to infer about ongoing chemical erosion rates in the headwater basins.

[49] The ^{87}Sr/^{86}Sr of the Ganga headwaters is highly radiogenic with high Sr content compared to the global average. Among the tributaries of the Ganga, the Kosi and the Bhagirathi supply water

with the highly radiogenic Sr to the Ganga mainstream indicating intense silicate erosion in their basins. The sources of dissolved cations were quantified for these streams using both inverse and forward models. Silicate cations, Cat_s, derived using the inverse model are always lower than that derived based on the forward model indicating differences in the assumed and derived end-member values. The highest Cat_s value (36%) among these rivers was found for the Kosi, consistent with the dominance of silicate lithology in its drainage. For the Gandak, about ~20% of the dissolved cations is supplied by the hot springs. Highest carbonate derived Sr, Sr_c, is estimated for the Gandak subbasin, which is in agreement with geology of the basin. The source contributions to the total dissolved cation and Sr budgets, hence, seem to be governed mainly by its lithology.

[50] The Ganga headwater and tributaries get supersaturated with respect to calcite during nonmonsoon seasons. The Ca removal during lean flow was estimated for these streams using the inverse model and plausible assumptions regarding Mg/Ca release ratios during different season. The loss of Ca is found to be maximum for the Gandak River. On an average, the Ca loss in these streams ranges from ~10%–40% and hence, can result in underestimation of the chemical weathering rates of these basins.

[51] The SER and CER were estimated for the Ganga headwater basins draining the Himalaya. These estimates confirm the earlier reports that they are significantly higher compared to the global average and also from other Himalayan rivers. The high SER for the tributaries of the Ganga result due to high physical erosion over these subbasins. The chemical weathering in the headwater basins of the Ganga seems to be controlled largely by their lithology, relief and rainfall. The Himalayan drainage of the Ganga supplies ~55% of water discharge and ~60% of dissolved material at its outflow draining only through ~17% of total area.

Acknowledgments

[52] Discussions with S. Krishnaswami helped improve this manuscript significantly. Authors thank Albert Tarantola for suggestions on the use of inverse model and Subimal Deb and Sanat Kumar Das for help with in computer programming. The suggestions of Vincent Salters, the Editor, and comments from Bernhard Peucker-Ehrenbrink, Mike Bickle, and two anonymous reviewers were useful in improving this manuscript.

References

Amiotte Suchet, P., J.-L. Probst, and W. Ludwig (2003), Worldwide distribution of continental rock lithology: Implications for the atmospheric/soil CO_2 uptake by continental weathering and alkalinity river transport to the oceans, *Global Biogeochem. Cycles*, *17*(2), 1038, doi:10.1029/2002GB001891.

Berner, R. A., A. C. Lasaga, and R. M. Garrels (1983), The carbonate–silicate geochemical cycle and its effect on atmospheric carbon dioxide over the past 100 million years, *Am. J. Sci.*, *283*, 641–683.

Bickle, M. J., N. B. W. Harris, J. M. Bunbury, H. J. Chapman, I. J. Fairchild, and T. Ahmad (2001), Controls on the $^{87}Sr/^{86}Sr$ ratio of carbonates in the Garhwal Himalaya, headwaters of the Ganges, *J. Geol.*, *109*, 737–753, doi:10.1086/323192.

Bickle, M. J., J. Bunbury, H. J. Chapman, N. B. W. Harris, I. J. Fairchild, and T. Ahmad (2003), Fluxes of Sr into the headwaters of the Ganges, *Geochim. Cosmochim. Acta*, *67*, 2567–2584, doi:10.1016/S0016-7037(03)00029-2.

Bickle, M. J., H. J. Chapman, J. Bunbury, N. B. W. Harris, I. J. Fairchild, T. Ahmad, and C. Pomies (2005), Relative contributions of silicate and carbonate rocks to riverine Sr fluxes in the headwaters of the Ganges, *Geochim. Cosmochim. Acta*, *69*, 2221–2240, doi:10.1016/j.gca.2004.11.019.

Blum, J. D., C. A. Gazis, A. D. Jacobson, and C. P. Chamberlain (1998), Carbonate versus silicate weathering in the Raikhot watershed within the high Himalayan crystalline series, *Geology*, *26*, 411–414, doi:10.1130/0091-7613(1998)026<0411:CVSWIT>2.3.CO;2.

Bookhagen, B., and D. W. Burbank (2006), Topography, relief, and TRMM-derived rainfall variations along the Himalaya, *Geophys. Res. Lett.*, *33*, L08405, doi:10.1029/2006GL026037.

Bordet, P., M. Colchen, D. Krummenacher, P. Le Fort, R. Mouterde, and M. Remy (1971), *Recherches Géologiques dans l'Himalaya du Népal, Région de le Thakkhola*, Cent. Natl. de la Rech. Sci., Paris.

Chamberlin, T. C. (1899), An attempt to frame a working hypothesis of the cause of glacial periods on an atmospheric basis, *J. Geol.*, *7*, 545–584, doi:10.1086/608449.

Colchen, M., P. Le Fort, and A. Pecher (1986), Notice explicative de la carte géologique Annapurna-Manaslu-Ganesh Himalaya du Népal, au 1:200.000e (bilingue: Français–English), Cent. Natl. de la Rech. Sci., Paris.

Crouzet, C., I. Dunkl, L. Paudel, P. Arkai, T. M. Rainer, K. Balogh, and E. Appel (2007), Temperature and age constraints on the metamorphism of the Tethyan Himalaya in central Nepal: A multidisciplinary approach, *J. Asian Earth Sci.*, *30*, 113–130, doi:10.1016/j.jseaes.2006.07.014.

Dalai, T. K. (2001), Major ions, stable isotopes, $^{87}Sr/^{86}Sr$ and Re in the headwaters of the Yamuna: Implications to chemical weathering in the Himalaya, Ph.D. dissertation, Maharaja Sayajirao Univ. of Baroda, Vadodara, India.

Dalai, T. K., S. Krishnaswami, and M. M. Sarin (2002), Major ion chemistry in the headwaters of the Yamuna river system: Chemical weathering, its temperature dependence and CO_2 consumption in the Himalaya, *Geochim. Cosmochim. Acta*, *66*, 3397–3416, doi:10.1016/S0016-7037(02)00937-7.

Dalai, T. K., S. Krishnaswami, and A. Kumar (2003), Sr and $^{87}Sr/^{86}Sr$ in the Yamuna River System in the Himalaya: Sources, fluxes, and controls on Sr isotope composition, *Geochim. Cosmochim. Acta*, *67*, 2931–2948, doi:10.1016/S0016-7037(03)00203-5.

Das, A., S. Krishnaswami, M. M. Sarin, and K. Pande (2005), Chemical weathering in the Krishna Basin and Western Ghats of the Deccan Traps, India: Rates of basalt weathering and their controls, *Geochim. Cosmochim. Acta*, *69*, 2067–2084, doi:10.1016/j.gca.2004.10.014.

Ebelmen, J. (1845), Sur les produits de la décomposition des especes minérales de famille des silicates, *Ann. Mines*, *7*, 3–66.

Edmond, J. M., and Y. Huh (1997), Chemical weathering yields from basement and orogenic terrains in hot and cold climates, in *Tectonic Uplift and Climate Change*, edited by W. F. Ruddiman, pp. 329–351, Plenum, New York.

English, N. B., J. Quade, P. G. DeCelles, and C. N. Garizone (2000), Geological control of Sr and major element chemistry in Himalayan rivers, Nepal, *Geochim. Cosmochim. Acta*, *64*, 2549–2566, doi:10.1016/S0016-7037(00)00379-3.

Evans, M. J., L. A. Derry, S. P. Anderson, and C. France-Lanord (2001), Hydrothermal source of radiogenic Sr to Himalayan rivers, *Geology*, *29*, 803–806, doi:10.1130/0091-7613(2001)029<0803:HSORST>2.0.CO;2.

Evans, M. J., L. A. Derry, and C. France-Lanord (2004), Geothermal fluxes of alkalinity in the Narayani river system of central Nepal, *Geochem. Geophys. Geosyst.*, *5*, Q08011, doi:10.1029/2004GC000719.

France-Lanord, C., and L. A. Derry (1997), Organic carbon burial forcing of the carbon cycle from Himalayan erosion, *Nature*, *390*, 65–67, doi:10.1038/36324.

France-Lanord, C., M. Evans, J. Hurtrez, and J. Riotte (2003), Annual dissolved fluxes from central Nepal rivers: Budget of chemical erosion in the Himalayas, *C. R. Geosci.*, *335*, 1131–1140, doi:10.1016/j.crte.2003.09.014.

Gaillardet, J., B. Dupre, P. Louvat, and C. J. Allegre (1999), Global silicate weathering and CO_2 consumption rates deduced from the chemistry of large rivers, *Chem. Geol.*, *159*, 3–30, doi:10.1016/S0009-2541(99)00031-5.

Galy, A. (1999), Etude geochimique de l'erosion actuelle de la chaine Himalayenne, Ph.D. thesis, 464 pp., Inst. Natl. Polytech. de Lorraine, Vandoeuvre-les-Nancy, France.

Galy, A., and C. France-Lanord (1999), Weathering processes in the Ganges-Brahmaputra basin and the riverine alkalinity budget, *Chem. Geol.*, *159*, 31–60, doi:10.1016/S0009-2541(99)00033-9.

Galy, A., C. France-Lanord, and L. A. Derry (1999), The strontium isotopic budget of Himalayan Rivers in Nepal and Bangladesh, *Geochim. Cosmochim. Acta*, *63*, 1905–1925, doi:10.1016/S0016-7037(99)00081-2.

Galy, V., C. France-Lanord, O. Beyssac, P. Faure, H. Kudrass, and F. Palhol (2007), Efficient organic carbon burial in the Bengal fan sustained by the Himalayan erosion system, *Nature*, *450*, 407–411, doi:10.1038/nature06273.

Galy, V., C. France-Lanord, and B. Lartiges (2008), Loading and fate of particulate organic carbon from the Himalaya to the Ganga-Brahmaputra delta, *Geochim. Cosmochim. Acta*, *72*, 1767–1787, doi:10.1016/j.gca.2008.01.027.

Gansser, A. (1964), *Geology of the Himalayas*, Interscience, London.

Garrels, R. M., and F. Mackenzie (1971), *Evolution of Sedimentary Rocks*, 397 pp., W.W. Norton, New York.

Handa, R. K. (1972), Geochemistry of the Ganga river water, *Indian Geohydrol.*, *2*, 71–78.

Harris, N. (1995), Significance of weathering Himalayan metasedimentary rocks and leucogranites for the Sr isotope evolution of seawater during the early Miocene, *Geology*, *23*, 795–798, doi:10.1130/0091-7613(1995)023<0795:SOWHMR>2.3.CO;2.

Harris, N., M. Bickle, H. Chapman, I. Fairchild, and J. Bunbury (1998), The significance of Himalayan rivers for silicate weathering rates: Evidence from the Bhote Kosi tributary, *Chem. Geol.*, *144*, 205–220, doi:10.1016/S0009-2541(97)00132-0.

Jacobson, A. D., and J. D. Blum (2000), Ca/Sr and $^{87}Sr/^{86}Sr$ geochemistry of disseminated calcite in Himalayan silicate rocks from Nanga Parbat: Influence on river-water chemistry, *Geology*, *28*, 463–466, doi:10.1130/0091-7613(2000)28<463:SASGOD>2.0.CO;2.

Jacobson, A. D., J. D. Blum, and L. M. Walter (2002), Reconciling the elemental and Sr isotope composition of Himalayan weathering fluxes: Insights from the carbonate geochemistry of stream waters, *Geochim. Cosmochim. Acta*, *66*, 3417–3429, doi:10.1016/S0016-7037(02)00951-1.

Jacobson, A. D., J. D. Blum, C. Page Chamberlain, D. Craw, and P. O. Koons (2003), Climatic and tectonic controls on chemical weathering in the New Zealand southern Alps, *Geochim. Cosmochim. Acta*, *67*, 29–46, doi:10.1016/S0016-7037(02)01053-0.

Karim, A., and J. Veizer (2000), Weathering processes in the Indus River Basin: Implications from riverine carbon, sulfur, oxygen, and strontium isotopes, *Chem. Geol.*, *170*, 153–177, doi:10.1016/S0009-2541(99)00246-6.

Krishnaswami, S., and S. K. Singh (1998), Silicate and carbonate weathering in the drainage basins of the Ganga-Ghaghara-Indus headwaters: Contributions to major ion and Sr isotope geochemistry, *Proc. Indian Acad. Sci.*, *107*, 283–291.

Krishnaswami, S., J. R. Trivedi, M. M. Sarin, R. Ramesh, and K. K. Sharma (1992), Strontium isotopes and rubidium in the Ganga-Brahmaputra river system: Weathering in the Himalaya, fluxes to the Bay of Bengal and contributions to the evolution of oceanic $^{87}Sr/^{86}Sr$, *Earth Planet. Sci. Lett.*, *109*, 243–253, doi:10.1016/0012-821X(92)90087-C.

Krishnaswami, S., S. K. Singh, and T. Dalai (1999), Silicate weathering in the Himalaya: Role in contributing to major ions and radiogenic Sr to the Bay of Bengal, in *Ocean Science, Trends and Future Directions*, edited by B. L. K. Somayajulu, pp. 23–51, Indian Natl. Sci. Acad. and Akad. Int., New Delhi.

Le Fort, P. (1989), The Himalayan orogenic segment, in *Tectonic Evolution of the Tethyan Regions: Proceedings of the NATO ASI Meeting, Istanbul, October 1985*, edited by A. M. C. Sengör, pp. 289–386, D. Reidel, Dordrecht, Netherlands.

Lupker, M., C. France-Lanord, J. Lave, and V. Galy (2009), Spatial variation of weathering in the Ganga basin, *Geochim. Cosmochim. Acta*, *67*, A803.

Millot, R., J. Gaillardet, B. Dupré, and C. J. Allègre (2003), Northern latitude chemical weathering rates: Clues from the Mackenzie River Basin, Canada, *Geochim. Cosmochim. Acta*, *67*, 1305–1329, doi:10.1016/S0016-7037(02)01207-3.

Moon, S., Y. Huh, J. Qin, and N. van Pho (2007), Chemical weathering in the Hong (Red) River basin: Rates of silicate weathering and their controlling factors, *Geochim. Cosmochim. Acta*, *71*, 1411–1430, doi:10.1016/j.gca.2006.12.004.

Mukherjee, A., A. E. Fryar, and W. A. Thomas (2009), Geological, geomorphic and hydrological framework and evolution of the Bengal basin, India and Bangladesh, *J. Asian Earth Sci.*, *34*, 227–244, doi:10.1016/j.jseaes.2008.05.011.

Negrel, P., C. J. Allegre, B. Dupre, and E. Lewin (1993), Erosion sources determined by inversion of major and trace element ratios and strontium isotopic ratios in river water: The Congo Basin case, *Earth Planet. Sci. Lett.*, *120*, 59–76, doi:10.1016/0012-821X(93)90023-3.

Oliver, L., N. Harris, M. Bickle, H. Chapman, N. Dise, and M. Horstwood (2003), Silicate weathering rates decoupled from the ^{87}Sr ratio of the dissolved load during Himalayan erosion, *Chem. Geol.*, *201*, 119–139, doi:10.1016/S0009-2541(03)00236-5.

Palmer, M. R., and J. M. Edmond (1992), Controls over the strontium isotope composition of river water, *Geochim. Cosmochim. Acta*, *56*, 2099–2111, doi:10.1016/0016-7037(92)90332-D.

Pande, K., M. M. Sarin, J. R. Trivedi, S. Krishnaswami, and K. K. Sharma (1994), The Indus river system (India-Pakistan): Major-ion chemistry, uranium and strontium isotopes, *Chem. Geol.*, *116*, 245–259, doi:10.1016/0009-2541(94)90017-5.

Pandey, S. K., A. K. Singh, and S. I. Hasnain (1999), Weathering and geochemical processes controlling solute acquisition in Ganga Headwater-Bhagirathi River, Garhwal Himalaya, India, *Aquat. Geochem.*, *5*, 357–379, doi:10.1023/A:1009698016548.

Pierson-Wickmann, A. (2000), Le cycle de l'osmium et dy rhenium pendant l'erosion himalayenne, Ph.D. thesis, 246 pp., Inst. Natl. Polytech. de Lorraine, Vandoeuvre-les-Nancy, France.

Quade, J., L. Roe, P. G. DeCelles, and T. P. Ojha (1997), The late neogene ^{87}Sr/^{86}Sr record of lowland Himalayan rivers, *Science*, *276*, 1828–1831, doi:10.1126/science.276.5320.1828.

Quade, J., N. English, and P. G. DeCelles (2003), Silicate versus carbonate weathering in the Himalaya: A comparison of the Arun and Seti River watersheds, *Chem. Geol.*, *202*, 275–296, doi:10.1016/j.chemgeo.2002.05.002.

Rai, S. K., S. K. Singh, and S. Krishnaswami (2010), Chemical weathering in the plain and peninsular sub-basins of the Ganga drainage: Impact on the major ion chemistry and elemental fluxes of the Ganga, *Geochim. Cosmochim. Acta*, doi:10.1016/j.gca.2010.01.008, in press.

Rao, K. L. (1975), *India's Water Wealth*, 267 pp., Orient Longman, New Delhi.

Raymo, M. E., and W. F. Ruddiman (1992), Tectonic forcing of late Cenozoic climate, *Nature*, *359*, 117–122, doi:10.1038/359117a0.

Raymo, M. E., W. F. Ruddiman, and P. N. Froelich (1988), Influence of late Cenezoic mountain building on ocean geochemical cycles, *Geology*, *16*, 649–653, doi:10.1130/0091-7613(1988)016<0649:IOLCMB>2.3.CO;2.

Rengarajan, R., S. K. Singh, M. M. Sarin, and S. Krishnaswami (2009), Strontium isotopes and major ion chemistry in the Chambal River system, India: Implications to silicate erosion rates of the Ganga, *Chem. Geol.*, *260*, 87–101, doi:10.1016/j.chemgeo.2008.12.013.

Rimstidt, J. D., A. Balog, and J. Webb (1998), Distribution of trace elements between carbonate minerals and aqueous solutions, *Geochim. Cosmochim. Acta*, *62*, 1851–1863, doi:10.1016/S0016-7037(98)00125-2.

Sarin, M. M., and S. Krishnaswami (1984), Major ion chemistry of the Ganga-Brahmaputra river systems, India, *Nature*, *312*, 538–541, doi:10.1038/312538a0.

Sarin, M. M., S. Krishnaswami, K. Dilli, B. L. K. Somayajulu, and W. S. Moore (1989), Major ion chemistry of the Ganga-Brahmaputra river system: Weathering processes and fluxes to the Bay of Bengal, *Geochim. Cosmochim. Acta*, *53*, 997–1009, doi:10.1016/0016-7037(89)90205-6.

Sarin, M. M., S. Krishnaswami, J. R. Trivedi, and K. K. Sharma (1992), Major ion chemistry of the Ganga source waters: Weathering in the high altitude Himalaya, *Proc. Indian Acad. Sci. Earth Planet. Sci.*, *101*, 89–98.

Singh, A. K., and S. I. Hasnain (1998), Major ion chemistry and weathering control in a high altitude basin: Alaknanda River, Garhwal Himalaya, India, *Hydrol. Sci. J.*, *43*, 825–843.

Singh, S. K., J. R. Trivedi, K. Pande, R. Ramesh, and S. Krishnaswami (1998), Chemical and strontium, oxygen, and carbon isotopic compositions of carbonates from the Lesser Himalaya: Implications to the strontium isotope composition of the source waters of the Ganga, Ghaghara, and the Indus rivers, *Geochim. Cosmochim. Acta*, *62*, 743–755, doi:10.1016/S0016-7037(97)00381-5.

Singh, S. K., M. M. Sarin, and C. France-Lanord (2005), Chemical erosion in the eastern Himalaya: Major ion composition of the Brahmaputra and δ^{13}C of dissolved inorganic carbon, *Geochim. Cosmochim. Acta*, *69*, 3573–3588, doi:10.1016/j.gca.2005.02.033.

Singh, S. K., S. K. Rai, and S. Krishnaswami (2008), Sr and Nd isotopes in river sediments from the Ganga basin: Sediment provenance and spatial variability in physical erosion, *J. Geophys. Res.*, *113*, F03006, doi:10.1029/2007JF000909.

Tarantola, A. (2005), The least square criterion, in *Inverse Problem Theory and Methods for Model Parameter Estimation*, pp. 68–72, Soc. for Ind. and Appl. Math., Philadelphia, Pa.

Thakur, V. C., and B. S. Rawat (1992), *Geological map of western Himalaya*, 22 pp., Wadia Inst. of Himalayan Geol., Dehradun, India.

Tipper, E. T., M. J. Bickle, A. Galy, A. J. West, C. Pomies, and H. J. Chapman (2006), The short term climatic sensitivity of carbonate and silicate weathering fluxes: Insight from seasonal variations in river chemistry, *Geochim. Cosmochim. Acta*, *70*, 2737–2754, doi:10.1016/j.gca.2006.03.005.

Tripathy, G. R., V. Goswami, S. K. Singh, and G. J. Chakrapani (2010), Temporal variations in Sr and ^{87}Sr/^{86}Sr of the Ganga headwaters: Estimates of dissolved Sr flux to the mainstream, *Hydrol. Processes*, doi:10.1002/hyp.7572, in press.

Valdiya, K. S. (1980), *Geology of Kumaun Lesser Himalaya*, 291 pp., Wadia Inst. of Himalayan Geol., Dehradun, India.

Vance, D., M. Bickle, S. Ivy-Ochs, and P. W. Kubuik (2003), Erosion and exhumation in the Himalaya from cosmogenic isotope inventories of river sediments, *Earth Planet. Sci. Lett.*, *206*, 273–288, doi:10.1016/S0012-821X(02)01102-0.

Walker, J. C. G., P. B. Hays, and J. F. Kasting (1981), A negative feedback mechanism for the long-term stabilization of Earth's surface temperature, *J. Geophys. Res.*, *86*, 9776–9782, doi:10.1029/JC086iC10p09776.

West, A. J., M. J. Bickle, R. Collins, and J. Brasington (2002), Small-catchment perspective on Himalayan weathering fluxes, *Geology*, *30*, 355–358, doi:10.1130/0091-7613(2002)030<0355:SCPOHW>2.0.CO;2.

Wu, L., Y. Huh, J. Qin, G. Du, and S. van Der Lee (2005), Chemical weathering in the Upper Huang He (Yellow River) draining the eastern Qinghai-Tibet Plateau, *Geochim. Cosmochim. Acta*, *69*, 5279–5294, doi:10.1016/j.gca.2005.07.001.

HYDROLOGICAL PROCESSES
Hydrol. Process. **24**, 1159–1171 (2010)
DOI: 10.1002/hyp.7572

Temporal variations in Sr and ^{87}Sr/^{86}Sr of the Ganga headwaters: estimates of dissolved Sr flux to the mainstream

Gyana Ranjan Tripathy,[1]* Vineet Goswami,[1] Sunil Kumar Singh[1] and G. J. Chakrapani[2]
[1] *Geosciences Division, Physical Research Laboratory, Ahmedabad-380009, India*
[2] *Department of Earth Sciences, Indian Institute of Technology, Roorkee, India*

Abstract:

The headwaters of the Ganga (the Alaknanda, Bhagirathi and the Ganga) were analysed for their dissolved major ions, Sr and ^{87}Sr/^{86}Sr on a biweekly to monthly basis over a period of one year to determine their temporal variations and the factors contributing to them. The concentrations of major ions and Sr show significant seasonal variation with lower values during monsoon period in all the three rivers. A similar trend is also observed for ^{87}Sr/^{86}Sr and Na*/Ca (Na* $=$Na$_r$−Cl$_r$) suggesting relatively lower contribution of Sr and Na from silicates (which are more radiogenic in Sr) during monsoon. Budget calculations show that silicate derived dissolved Sr (Sr$_s$) in the river Ganga, Alaknanda and the Bhagirathi varied from 10 ± 4 to 27 ± 11, 7 ± 3 to 30 ± 12, 16 ± 6 to 57 ± 23% of measured Sr respectively with lower values during monsoon. The relative decrease in silicate erosion compared to carbonate during monsoon can result from several factors, these include higher dissolution kinetics of the carbonates, lower water–rock interaction time and availability of larger area for weathering.

The annual discharge weighted Sr flux derived from the time series data is higher by ~20% from that based on peak flow Sr, and lower by ~40% compared to that derived from lean flow Sr concentration. The area-normalized annual flux of dissolved Sr from the Ganga at Rishikesh is about five times its flux at Rajshahi (Bangladesh) and a few other major global rivers, such as the Amazon, indicating higher erosion rate over the Himalaya.

KEY WORDS Ganga River; ^{87}Sr/^{86}Sr; temporal variation; silicate weathering

Received 23 November 2008; Accepted 4 November 2009

INTRODUCTION

One of the hypotheses suggested to explain global cooling during the Cenozoic is increased CO$_2$ consumption due to enhanced silicate weathering in young orogenic belts such as the Himalaya (Raymo *et al*., 1988; Raymo and Ruddiman, 1992). This hypothesis draws support from the increasing trend of oceanic ^{87}Sr/^{86}Sr since the last ~40 Ma which has been attributed to enhanced silicate weathering in the Himalaya (Raymo and Ruddiman, 1992; Richter *et al*., 1992; McCauley and DePaolo, 1997). Based on several studies on the Himalayan rivers, particularly the Ganga–Brahmaputra (Krishnaswami *et al*., 1992; Palmer and Edmond, 1992; Blum *et al*., 1998; Harris *et al*., 1998; Galy *et al*., 1999; English *et al*., 2000; Dalai *et al*., 2003; Oliver *et al*., 2003; Quade *et al*., 2003; Bickle *et al*., 2005; Singh *et al*., 2006; Tipper *et al*., 2006; Hren *et al*., 2007; Rai and Singh, 2007), it is validated that these rivers supply more radiogenic Sr with moderate Sr concentration to the Bay of Bengal. The suggested sources for the high radiogenic Sr to the rivers include the silicates of the Lesser and the Higher Himalaya (Krishnaswami *et al*., 1992; Singh *et al*., 1998; Galy *et al*., 1999; Oliver *et al*., 2003; Bickle *et al*., 2005), metamorphosed carbonates (Palmer and Edmond, 1992; Quade *et al*., 1997; Bickle *et al*., 2001) and vein calcites (Jacobson and Blum, 2000). More recent studies and budget estimates, however, seem to converge on the suggestion that the dominant source of radiogenic Sr to the Ganga–Brahmaputra Rivers is silicates and the role of metamorphosed carbonates in contributing to radiogenic Sr is insignificant on a basin-wide scale (Dalai *et al*., 2003; Oliver *et al*., 2003; Bickle *et al*., 2005; Singh *et al*., 2006). Further, much of the earlier studies on the estimates of average ^{87}Sr/^{86}Sr of the Ganga River and the annual fluxes of major ions and Sr from it to the Bay of Bengal are based on a single or a few measurements over a year. Considering that the discharge of the Ganga and the Brahmaputra Rivers varies by more than an order of magnitude over an annual cycle with maximum during the monsoon, such flux estimates and average ^{87}Sr/^{86}Sr could have significant uncertainties. A few available studies on Sr and ^{87}Sr/^{86}Sr indeed show seasonal cycles in these rivers (Galy *et al*., 1999; Bickle *et al*., 2003; Dalai *et al*., 2003; Tipper *et al*., 2006; Rai and Singh, 2007). Therefore attempts to determine annual fluxes of major ions and Sr isotopes would require time series analysis of river water geochemistry.

Recently, Bickle *et al*. (2003) carried out sampling in the Ganga headwater basin to quantify the seasonal and temporal variations in the fluxes of dissolved

---

* Correspondence to: Gyana Ranjan Tripathy, Geosciences Division, Physical Research Laboratory, Ahmedabad, India.
E-mail: gyana@prl.res.in

Sr and to determine the contribution of major lithotectonic units in the Himalaya to the Sr and ^{87}Sr budgets. This study reports relatively more intense weathering of carbonates during the monsoon, confirming the earlier observations of Krishnaswami *et al.* (1999) based on synthesis of available results. Tipper *et al.* (2006) and Rai and Singh (2007), showed considerable temporal variation in ^{87}Sr/^{86}Sr in the tributaries of the Gandak and the Brahmaputra mainstream respectively. Temporal variation of riverine ^{87}Sr/^{86}Sr was also used to track flash floods in the Brahmaputra river (Rai and Singh, 2007) and Mediterranean watershed in Southern France (Petelet–Giraud and Negrel, 2007).

The present study deals with the temporal and spatial variations in dissolved major ions, Sr and ^{87}Sr/^{86}Sr of the Bhagirathi, Alaknanda and the Ganga at the foot-hills of the Himalaya. These rivers were sampled biweekly (once in two weeks) to monthly intervals at three stations to quantify temporal variations in their chemical properties and assess the impact of water discharge on the elemental fluxes. Efforts are also made to apportion the sources of dissolved cations and Sr over the year and to estimate discharge-weighted flux of Sr and ^{87}Sr/^{86}Sr of the Ganga exiting the Himalaya at Rishikesh. Further, the study also attempts to bring out the role of water discharge in controlling the riverine ^{87}Sr/^{86}Sr, as the water discharge varies by a factor of ∼20 over an annual cycle.

GEOHYDROLOGY OF THE BASIN

The Bhagirathi River originates from the Gangotri glacier at an elevation of 3812 m and flows over a catchment area of 7811 km^2 (of which 2328 km^2 is annually snow covered) in the central Himalaya before its confluence with the Alaknanda River at Devprayag (Figure 1) to form the river Ganga (Pandey *et al.*, 1999). The Alaknanda River originates from the glaciers of Satopanth and the Bhagirathi Kharak at an elevation of 3800 m and flows over $11{\cdot}8 \times 10^3$ km^2 (Singh and Hasnain, 1998). The annual rainfall in the Alaknanda basin is 1000–1600 mm (Singh and Hasnain, 1998). About 65% of total water discharge of the Ganga at Devprayag is supplied by the Alaknanda River. The discharge of the Bhagirathi at Maneri and the Alaknanda at Srinagar varies from ∼20 to 400 m^3/s and 90 to 2000 m^3/s over the year respectively (Chakrapani and Saini, 2009), whereas for the Ganga at Rishikesh it ranges between 200 and 2500 m^3/s (Figure 2).

The Bhagirathi River drains the Higher Himalaya(HH) and the Lesser Himalaya (LH) (Valdiya, 1980). The lithology of the HH is composed mainly of high-grade gneisses, schists, granites, marbles with limited carbonates and calc-silicate rocks (Figure 1). The LH is composed mainly of sedimentary and crystalline rocks that include gneisses, granites, greywackes, shales, slates, limestones and dolomites (Singh *et al.*, 1998). In addition to the HH and LH, the Alaknanda River also flows through Tethyan Sedimentary Series (TSS). The TSS is

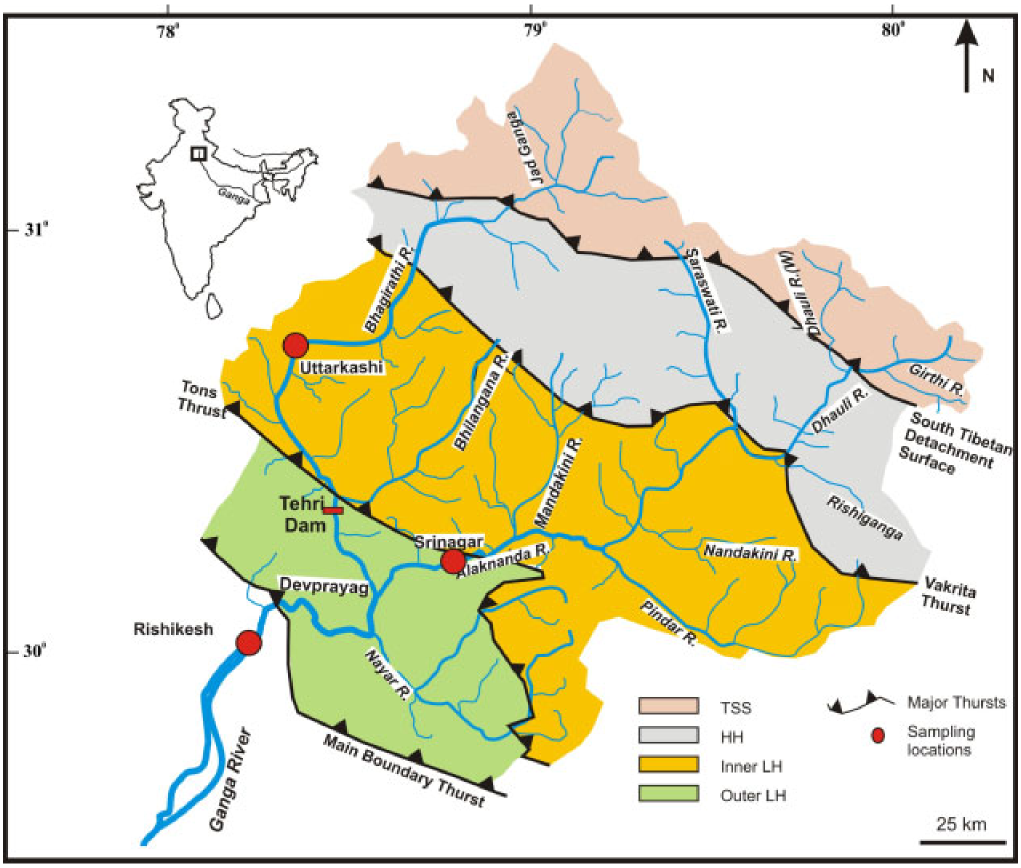

Figure 1. Lithology of the drainage basin of the Ganga (modified after Bickle *et al.*, 2003). Rectangle on the map of India shows the study area

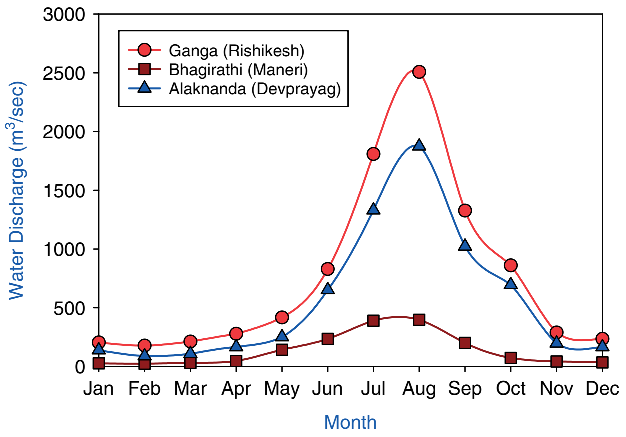

Figure 2. Water discharge of the Ganga at Rishikesh, Alaknanda at Srinagar and Bhagirathi at Maneri during sampling periods. Discharge of these rivers peaks during monsoon (July–September) and is ~20 times more compared to lean flow season (December–Febraury)

composed of metamorphosed impure limestone and siliclastic rocks such as pyrite rich black shales and contains amphibole calc-silicates with biotite, muscovite and chlorite outcrops above the south Tibetan detachment zone. No evaporite exposures have been reported in TSS (Tipper *et al.*, 2006).

MATERIALS AND METHODS

Water samples were collected from the Bhagirathi, Alaknanda and the Ganga Rivers at Uttarkashi (78·46 °E, 30·74 °N), Srinagar (78·74 °E, 30·22 °N) and Rishikesh (78·31 °E, 30·12 °N) respectively for a period of one year during July 2004–July 2005 at biweekly to monthly intervals. Samples were filtered onsite through 0·45 μM cellulose nitrate membrane filters and stored in cleaned polypropylene bottles (Chakrapani *et al.*, 2009). An unacidified aliquot of ~30 ml was brought to the Physical Research Laboratory (PRL), a few months after sample collection, where measurements for major ions, Sr concentration and its isotopic composition were carried out.

The strontium concentration and isotopic composition is measured using Isoprobe-T Thermal Ionization Mass Spectrometer in static multi-collection mode at PRL. Towards this, Sr is separated from a known weight of unacidified water samples after equilibrating them with ^{84}Sr spike. Pure Sr was extracted by passing them through Sr specific resin (Rai and Singh, 2007). The measured ^{87}Sr/^{86}Sr is corrected for instrumental mass fractionation by normalizing ^{86}Sr/^{88}Sr to 0·1194. The mean ^{87}Sr/^{86}Sr of the standard NBS987 based on repeat measurements during this study is 0·710230 ± 0·000026 (2σ, $n = 72$). The total procedural blank for Sr is ~1 ng, insignificant compared to total Sr measured. The Cl^- concentrations in the samples were measured using ion chromatography (Dionex 500), cations by atomic absorption spectrophotometry (AAS) and inductively coupled plasma atomic emission spectrometry (ICP-AES), except for samples from Rishikesh for which cations were also measured by ion chromatography using CS12 column (Dionex 500). The analytical precision for the measurements of major ions is better than ±4%. The net inorganic charge balance (NICB) in most of the samples (44 out of 48) is better than ±10%. The charge imbalance in a few samples may have resulted due to presence of unanalysed ions (PO_4, NH_4 and organic ligands). While this study was in progress, the major ion compositions of the samples were reported by Chakrapani *et al.* (2009). Their data agree with those measured in this study within 10–15% with a few outliers.

RESULTS

The concentration of dissolved major ions, Sr and ^{87}Sr/^{86}Sr of the Ganga at Rishikesh, Bhagirathi at Uttarkashi and the Alaknanda at Srinagar are given in Table I. The Sr and ^{87}Sr/^{86}Sr in the Ganga headwaters show significant variation among the biweekly samples with lower Sr during monsoon. The Sr in the Bhagirathi River ranges from 192 to 736 nM, whereas for the Alaknanda and the Ganga it lies between 500–856 nM and 236–1707 nM respectively (Table I). Majority of the samples have Sr in excess of 500 nM, however a few samples of the Ganga and the Bhagirathi have much lower concentrations (Table I). This could be a result of dilution caused by flash flood during heavy rainfall. This hypothesis is supported by the low Ca, Mg and Na concentrations in the same samples. The ^{87}Sr/^{86}Sr of the Bhagirathi samples are marginally more radiogenic than the Alaknanda and the Ganga, however, their ranges overlap with each other. The ^{87}Sr/^{86}Sr of the Ganga at Rishikesh varies from 0·72795 to 0·74078 with lower values during monsoon (Figure 3). The ^{87}Sr/^{86}Sr of the Alaknanda and the Bhagirathi range between 0·72448 and 0·74242, 0·72932 and 0·75746 respectively and are consistent with data available in literature (Krishnaswami *et al.*, 1992, 1999; Palmer and Edmond, 1992; Bickle *et al.*, 2003, 2005).

The concentrations of major ions show significant variations among the three rivers (Table I), however all of them have similar seasonal trends with low concentrations during monsoon. The concentrations, on an average decrease by a factor of about two during monsoon compared to non-monsoon period, this decrease is far less than the ~20 times increase in water discharge during monsoon. The molar abundance of major ions follows the trend: $Ca^{+2} > Mg^{+2} > Na^{+} > K^{+}$. Among the cations (Ca+Mg) accounts for ~80%, confirming earlier interpretations (Sarin *et al.*, 1989) of carbonate dominated weathering in the Ganga headwater basins.

DISCUSSION

Temporal variation in Sr and ^{87}Sr/^{86}Sr

The Sr budget of the Ganga River water is mainly governed by the inputs from weathering of radiogenic

Table I. Temporal variation of major ions, Sr and ^{87}Sr/^{86}Sr of the Ganga headwaters

		Date of sampling (2004–2005)	Water discharge km^3 per sampling interval	Na	K	Ca	Mg	Cl	^{87}Sr/^{86}Sr	[Sr], nM
				μM						
Ganga	RK1	19 July	1.56	57	47	405	150	23	0·73807	457
	RK3	2 August	2.17	58	79	522	128	22	0·72795	667
	RK5	16 August	2.17	66	74	482	154	26	0·73599	517
	RK7	30 August	2.17	228	40	682	452	58	0·73752	1643
	RK9	13 September	1.72	157	48	516	285	45	0·73745	1062
	RK11	27 September	1.72	84	58	330	137	66	0·73633	236
	RK13	11 October	1.12	251	60	691	456	84	0·73620	1707
	RK-15	25 October	1.12	279	75	789	496	98	0·74078	1351
	RK17	27 December	0.38	159	55	501	236	42	0·73946	889
	RK20	17 January	0.38	254	70	758	458	88	0·73922	1338
	RK22	31 January	0.61	244	66	703	420	95	0·73942	1258
	RK24	14 February	0.18	296	77	807	500	128	0·73992	1308
	RK25	21 February	0.18	289	70	802	505	124	0·74003	1370
	RK27	7 March	0.18	300	67	806	487	144	0·73985	1365
	RK29	21 March	0.23	188	58	561	326	75	0·74000	993
	RK31	5 April	0.23	179	54	506	266	66	0·73998	926
	RK33	19 April	0.28	214	62	628	349	90	0·73896	1089
	RK35	3 May	0.28	221	61	689	397	92	0·73798	1215
	RK38	23 May	0.72	160	50	580	299	59	0·73523	1037
	RK40	6 June	1.08	76	49	563	151	21	0·72804	877
	RK42	21 June	1.08	123	53	650	210	58	0·73003	998
	RK43	28 June	1.08	92	72	652	155	46	0·72891	874
	RK44	5 July	1.56	88	72	620	146	47	0·72894	822
	RK46	19 July	1.56	114	76	560	197	53	0·73575	889
Alaknanda	SN-1	19 July	1.15	68	57	410	143	23	0·73611	542
	SN-5	16 August	4.86	51	95	540	167	20	0·73347	530
	SN-11	27 September	2.65	85	48	343	131	24	0·73772	500
	SN-17	8 November	2.31	168	61	501	228	84	0·74096	753
	SN-22	27 December	0.43	164	59	498	230	56	0·74065	764
	SN-25	17 January	0.36	181	61	543	245	83	0·74044	856
	SN-29	14 February	0.12	173	60	513	241	61	0·74242	756
	SN-31	28 February	0.12	194	67	531	245	80	0·74224	795
	SN-33	14 March	0.28	159	61	474	208	66	0·74107	749
	SN-38	19 April	1.08	61	47	361	138	22	0·73680	532
	SN-43	13 June	1.69	115	62	474	191	42	0·73867	624
	SN-44	5 July	1.15	46	47	483	127	18	0·72953	576
	SN-46	19 July	1.15	56	55	550	125	28	0·72448	782
Bhagirathi	UK-1	19 July	0.34	20	10	568	42	43	0·72932	192
	UK-5	16 August	1.03	55	177	590	95	16	0·74386	426
	UK-9	13 September	0.52	43	44	248	115	8	0·74588	439
	UK-13	11 October	0.19	90	48	435	206	15	0·74919	692
	UK-17	8 November	0.11	45	51	208	82	7	0·73006	201
	UK-22	31 January	0.16	164	57	386	160	33	0·75421	625
	UK-28	14 March	0.14	276	68	461	185	64	0·75746	736
	UK-35	3 May	0.49	174	60	361	151	36	0·75330	582
	UK-41	13 June	0.61	118	48	353	162	29	0·74883	567
	UK-44	5 July	0.34	33	61	175	73	13	0·74013	233
	UK-46	19 July	0.34	45	59	231	90	13	0·74630	307

silicates and less radiogenic carbonates (Galy *et al*., 1999; Krishnaswami *et al*., 1999; Bickle *et al*., 2005). The elemental and isotopic composition of the silicates and carbonates present in the upstream of the Ganga basin are listed in Table II (Krishnaswami *et al*., 1999; Jacobson *et al*., 2002; Singh *et al*., 2008). The average ^{87}Sr/^{86}Sr of silicates (0·79 ± 0·06) and carbonates (0·715 ± 0·01) present in the basin (Krishnaswami *et al*., 1999; Singh *et al*., 2008) is significantly different and hence, can be used to assess temporal variation in their relative contributions to dissolved Sr. The representative ^{87}Sr/^{86}Sr for silicates and carbonates of the Himalaya used in this study are the average of the data available in literature, after statistically rejecting few outliers. The Sr isotopic composition of rivers shows significant temporal variation with less radiogenic values during monsoon (Figure 3). The lower ^{87}Sr/^{86}Sr during monsoon seem to indicate relatively larger Sr contribution from the weathering of carbonates, which are less radiogenic in Sr.

A mixing diagram of ^{87}Sr/^{86}Sr versus 1/Sr for the Bhagirathi and the Alaknanda is plotted in Figure 4. The

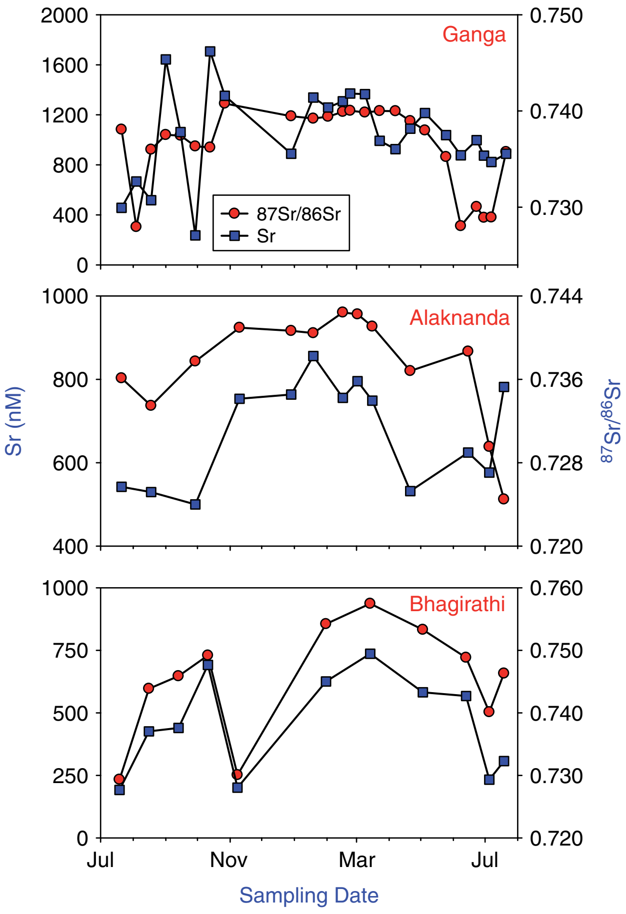

Figure 3. Temporal variation in Sr and ^{87}Sr/^{86}Sr in the three rivers. The general decrease in ^{87}Sr/^{86}Sr during monsoon indicates relatively higher contribution from carbonate weathering

figures indicate a two end member mixing; between the more radiogenic silicate and the less radiogenic carbonate end members. It is, however, observed from the trends in Figure 4 that lower ^{87}Sr/^{86}Sr have lower Sr content, unlike commonly observed mixing trends, in which the low ^{87}Sr/^{86}Sr is associated with high Sr. Such a reverse trend in the mixing plot is a combined effect of decrease in Sr concentration resulting from dilution effect and variation in relative intensities of weathering carbonates and silicates. As discussed in an earlier section, in this study measurements have been made at the same locations over a year. The results show decrease in both Sr concentration and ^{87}Sr/^{86}Sr during monsoon. This is attributed to relative increase in carbonate weathering (which lowers ^{87}Sr/^{86}Sr of rivers, see the later discussion for more details) and dilution of Sr concentration due to increase in water discharge (Figure 4).

Figure 5 shows the variation in Na*/Ca of these river waters during the sampling period. Na* is conventionally taken to represent Na derived from silicate weathering

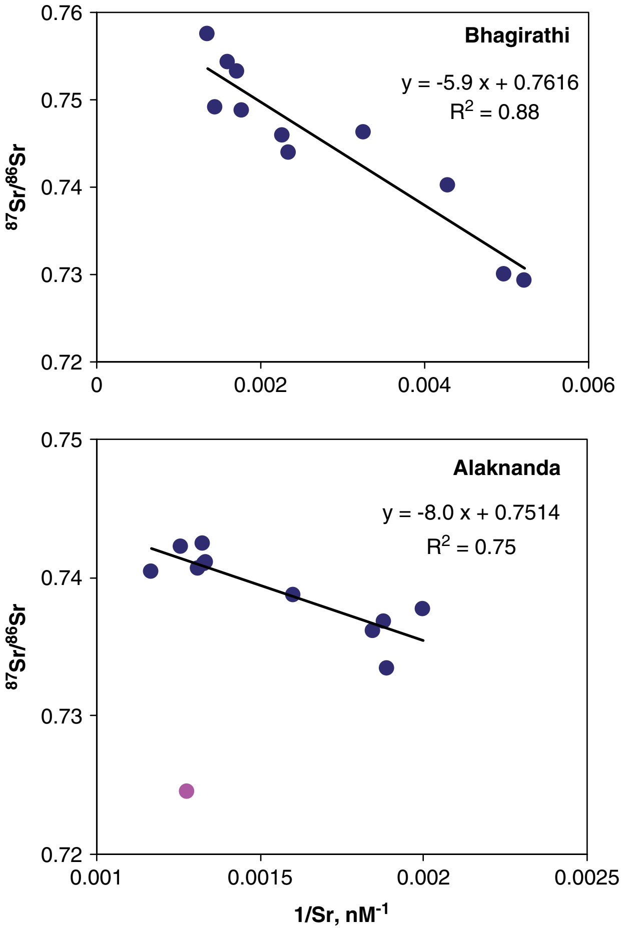

Figure 4. Mixing plot between ^{87}Sr/^{86}Sr and 1/Sr for the Alaknanda and Bhagirathi Rivers (excluding the anomalous sample (circle) from the Alaknanda). Lower ^{87}Sr/^{86}Sr is typical of carbonate end member, whereas silicate end member is characterized by more radiogenic ^{87}Sr/^{86}Sr. Negative slope is due to dilution of Sr during monsoon

Table II. Elemental ratios (molar) and Sr isotopic composition of silicates and carbonates in the basin (Krishnaswami *et al*., 1999; Jacobson *et al*., 2002; Singh *et al*., 2008)

	Silicates			Carbonates	
	HH	*LH*		*HH*	*LH*
	Granites/gneisses	Granites/gneisses	metasediments		
Ca/Na	0·32 ± 0·29 (45)	0·46 ± 0·28 (61)	0·44 ± 0·31 (61)	—	—
Mg/Na	0·31 ± 0·28 (37)	0·65 ± 0·45 (57)	0·52 ± 0·32 (71)	—	—
Sr/Na	1·22 ± 0·65 (48)	1·23 ± 0·60 (39)	—	—	—
Ca/Sr	0·20 ± 0·13 (78)	0·28 ± 0·15 (65)		4·1 ± 5·3 (19)	5·8 ± 5·3 (104)
^{87}Sr/^{86}Sr	0·757 ± 0·017 (122)	0·824 ± 0·071 (95)		0·720 ± 0·010 (19)	0·715 ± 0·01

Numbers in the paranthesis show the number of data used for compilation.

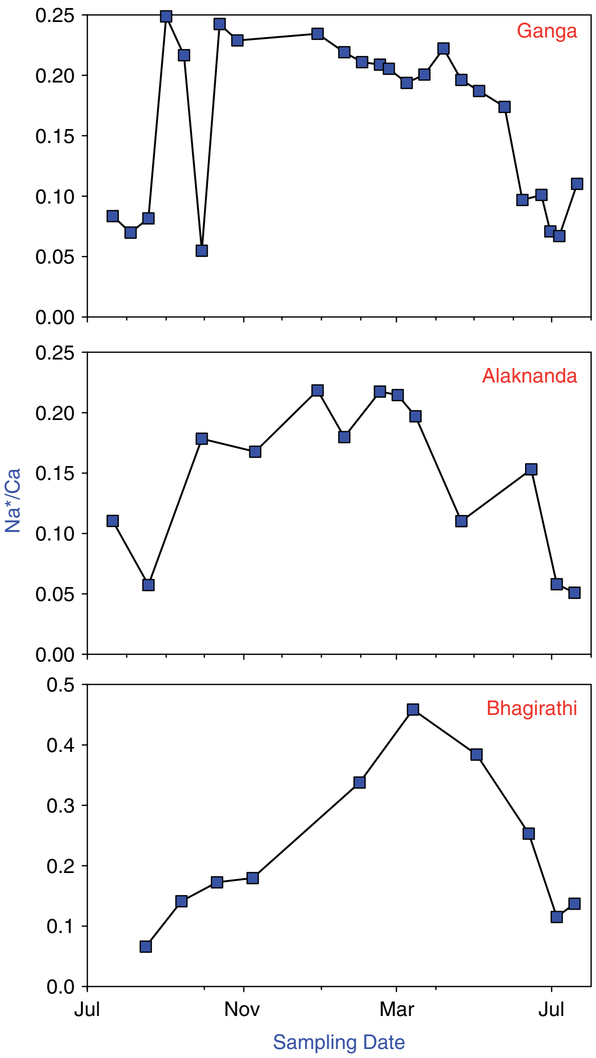

Figure 5. Temporal variation in Na*/Ca in the three rivers. This variation is result of variation in relative contribution from carbonates and silicates during different season. The decrease during monsoon indicates proportionally higher contribution from carbonate weathering

(Na* = Na_r-Cl_r, Krishnaswami *et al.*, 1999). Na*/Ca shows similar seasonal variation in all the three rivers, with lower values during monsoon. Several factors can contribute to this observation; these include relatively higher carbonate weathering during monsoon, enhanced calcite precipitation (Jacobson *et al.*, 2002) and/or relatively more silicate weathering during non-monsoon. Calculation of calcite saturation index (CSI) indicates that all these samples are undersaturated in calcite (Chakrapani *et al.*, 2009), ruling out the possibility of carbonate precipitation as a cause for the observed trend. Figure 6 is a mixing plot between (Na*/Ca) and Sr isotope composition. It indicates two end member mixing, one with high Na*/Ca and high $^{87}Sr/^{86}Sr$ (silicates) and the other with low Na*/Ca and low $^{87}Sr/^{86}Sr$ (carbonates and/or calc-silicates). The y-intercept in this mixing plot should represent the characteristic $^{87}Sr/^{86}Sr$ of non-Na bearing minerals (e.g. carbonates and calc-silicates) present in the basin. The relatively higher $^{87}Sr/^{86}Sr$ value compared to carbonates corresponding to zero Na*/Ca for the Bhagirathi River, unlike in the Alaknanda River, resulted due to significant contribution from non-Na bearing silicates (calc-silicates, Singh *et al.*, 2002) with high $^{87}Sr/^{86}Sr$ values to the dissolved phase. The good correlation between Na*/Ca-$^{87}Sr/^{86}Sr$ suggests the important role of silicate weathering in contributing radiogenic $^{87}Sr/^{86}Sr$ to the waters.

Decadal variability. The Sr concentration and $^{87}Sr/^{86}Sr$ of the Ganga at Rishikesh measured in this study are compared with available data for the same months for

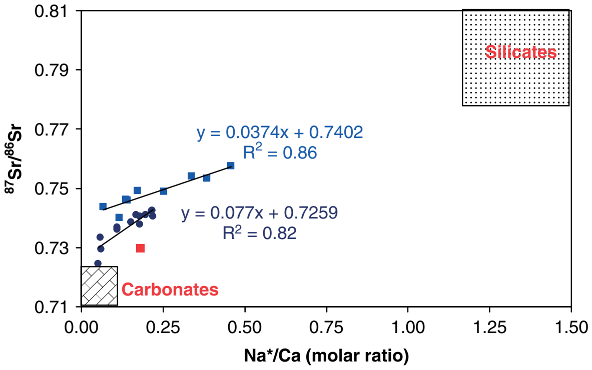

Figure 6. Plot of Na*/Ca versus $^{87}Sr/^{86}Sr$ for the Alaknanda (circles) and Bhagirathi River (sqaures). y-intercepts of the Bhagirathi and the Alaknanda represent $^{87}Sr/^{86}Sr$ contribution from non-Na bearing minerals (calc-silicates and carbonates together). One of the Bhagirathi samples (falling outside the trend) is anomalous and is not included in the regression. The range for Na*/Ca and $^{87}Sr/^{86}Sr$ shown for end members are from Krishnaswami *et al.*, and Table II

Table III. Decadal variation of dissolved Sr and $^{87}Sr/^{86}Sr$ of the Ganga River at Rishikesh

Period	[Sr], nM	$^{87}Sr/^{86}Sr$	Reference
Ganga (Rishikesh)			
September 1982	580	0·7365	Krishnaswami *et al.*, 1992
September 1996	610	0·74585	Bickle *et al.*, 2003
September 1999	507	0·73849	Dalai *et al.*, 2003
13 September 2004	1062	0·73745	This study
27 September 2004	236	0·73633	This study
October 1996	733	0·73836	Bickle *et al.*, 2003
October 1998	626	0·73856	Dalai *et al.*, 2003
11 October 2004	1707	0·73620	This study
25 October 2004	1351	0·74078	This study
March 1982	800	0·7399	Krishnaswami *et al.*, 1992
March 1998	924	0·742239	Bickle *et al.*, 2003
14 March 2005	1089	0·73896	This study
28 March 2005	1215	0·73798	This study
April 1989	676	0·7425	Krishnaswami *et al.*, 1999
April 1999	815	—	Bickle *et al.*, 2003
April 2005	1037	0·73523	This Study
June 1997	435	0·73477	Bickle *et al.*, 2003
June 1999	712	0·73657	Dalai *et al.*, 2003
6 June 2005	998	0·73003	This study
13 June 2005	874	0·72891	This study

The systematically high Sr values observed in this study could be an impact of Tehri dam on the Ganga River geochemistry.

this location. The comparison spans for a period of about 25 years (Table III). The decadal variability in $^{87}Sr/^{86}Sr$ for the same month sampling is typically $\sim \pm 0{\cdot}002$ units, though the range in some months (e.g. Sept) is much wider $\sim$0·01 units. The magnitude of this variability is less than the seasonal trend measured during 2004–2005 (Table I, Figure 3).

The temporal variation in dissolved $^{87}Sr/^{86}Sr$ observed in this study for 2004–2005 and by Bickle *et al.* (2003) for 1996 and 1999 show similar seasonal trends, though there are indications of interannual variations, with lower $^{87}Sr/^{86}Sr$ during late and early monsoon in 2004–2005. Interannual variations are also observed in Sr concentration and are found to be systematically higher in this study compared to previously reported data (Table III). This interannual variations in $^{87}Sr/^{86}Sr$ and Sr could have resulted from relative variation in the intensity and spatial pattern of rainfall resulting in varying contribution from small tributaries. The other possible cause for these variations is the impact of Tehri dam built on the Bhagirathi (Figure 1), the highest Dam in Asia situated downstream the confluence of Bhagirathi and Bhilangana. Impact of this dam on the Ganga River geochemistry is quite likely as the dam has significantly influenced its water discharge (Chakrapani *et al.*, 1999). This inference is well supported by the observed changes (Bahuguna *et al.*, 2008) in the aquatic micro invertebrate diversity of the Bhagirathi during 2004–2005, same time period as the present study.

Causes for temporal variation in $^{87}Sr/^{86}Sr$

The majority of geochemical studies on the Himalayan rivers (Sarin *et al.*, 1989; Krishnaswami *et al.*, 1992, 1999; Dalai *et al.*, 2002, 2003; Bickle *et al.*, 2003, 2005; Singh *et al.*, 2005, 2006; Hren *et al.*, 2007) are based on single or a few season sampling, which constrains assessment of temporal variations in solute chemistry and its impact on estimates of annual erosion rates and their associated CO_2 consumption fluxes. The seasonality of erosion pattern in a river basin is a complex process and depends on several factors. In addition to relative variations in bedrock weathering as discussed in the earlier section, the river geochemistry can also show a seasonal trend due to variations in the temperature and in mixing proportion of various sources (e.g. glacier melt in summer, impact of base flow and zonation in rainfall pattern). The temperature in the Ganga, Bhagirathi and the Alaknanda River basins varies significantly from 5 to 25 °C over an annual cycle. The temperature variation from 5 to 25 °C can enhance the dissolution rate of silicate and carbonate minerals by 3–4 times (Velbel, 1993; White and Blum, 1995; Alkattan *et al.*, 1998; White *et al.*, 1999) and hence, can impart seasonal variations in the weathering pattern of the basin. However, the impact of temperature on weathering seem to have minimal effect in the Ganga headwaters, as the months (May and July) with most significant changes in riverine $^{87}Sr/^{86}Sr$ and Na*/Ca (Figures 3 and 5) have similar temperatures (20 and 18 °C; Bickle *et al.*, 2003). Contribution of glacial melt to the Ganga River show temporal variation, higher during summer compared to winter and hence could be responsible for part of the temporal variation in riverine $^{87}Sr/^{86}Sr$. However, variation between premonsoon (May–June) and monsoon (July–September) compositions of river water could not be explained by meltwater variation. Another factor which affects the relative proportion of silicate/carbonate weathering is the exposed area available for weathering. During monsoon, water interacts with the rocks exposed in the entire drainage while during non-monsoon, it shrinks mainly to the rivers. This increase in exposed area available for weathering during monsoon increases intensity of chemical weathering (both carbonate and silicate) in the basin. However, the weathering of carbonates is relatively higher compared to resistant silicates, due to higher weathering kinetics of the former. The dissolution rate of silicates and carbonates differ by about 7 orders, e.g. the approximate time for dissolving a 1-mm sphere of calcite mineral (10^{-1} years) is far less than the silicates ($\sim 10^{7}$ years; Drever, 1997). Despite the fact that proportion of silicate versus carbonate exposures remains the same through out the year for given drainage, the effective area of erosion increases during monsoon due to surface runoff. The higher surface runoff during monsoon triggers an increase in the chemical weathering in the basin, however relative increase of silicate erosion rate of the basin is found to be less compared to carbonates during monsoon due to lower water/rock interaction time. On the contrary, the relative weathering rate of silicates increases during lean flow period possibly due to relatively higher contribution from groundwater, which leaches more silicates due to larger rock–water interaction time. The variation in weathering of bedrocks with season is found to be an important factor for seasonal variation in the chemistry of river water during geochemical studies in different river basins (Douglas, 2006; Tipper *et al.*, 2006; Rai and Singh, 2007).

Previous geochemical and isotopic studies on the Ganga headwaters, particularly on the Alaknanda River, have reported large seasonal variations from individual sub-basins (Bickle *et al.*, 2003, 2005). These results brought out the seasonal changes in $^{87}Sr/^{86}Sr$ of these streams which could result due to differences in mixing proportions from the sub-basin and/or change in the weathering rates of bedrocks. The $^{87}Sr/^{86}Sr$ and Na*/Ca for LH and HH rocks have a wide range and they overlap with each other (Table II). The seasonal changes in the $^{87}Sr/^{86}Sr$ and Na*/Ca (Figures 3 and 5) for the Bhagirathi River at Uttarkashi, which receives contribution mostly from the HH, can be explained by varying relative contributions from the silicate and carbonate minerals only. The seasonality in bedrock weathering and its impact on river geochemistry establish the importance of seasonal study of river water to quantify the annual elemental fluxes and CO_2 consumption rates.

Apportioning the sources of the dissolved material

The contribution of various sources to dissolved elemental and strontium budget in rivers can be derived either by the forward modeling (Galy *et al.*, 1999; Krishnaswami *et al.*, 1999) using suitable proxies, such as, Na*, ($Na^* = Na_r - Cl_r$) or by inverse modeling (Negrel *et al.*, 1993). In this study, the forward model has been used to apportion the sources of dissolved major ions and Sr to the Ganga headwaters.

Forward modeling approach relies on the basis that dissolved Na in rivers is derived only from two sources, (atmosphere+halite) and silicate weathering. The (atmosphere+halite) contribution of Na is generally taken to be equal to that of Cl, making the silicate derived Na (Na* or Na_s) equal to

$$Na^* = Na_s = Na_r - Cl_r \tag{1}$$

where Na_r and Cl_r is the concentration of Na and Cl in rivers.

Na* along with assumed elemental ratios of Ca/Na, Mg/Na and Sr/Na that are released during the weathering of silicate rocks to rivers (Krishnaswami *et al.*, 1999) are used to estimate the fraction of cations and strontium derived from silicate weathering. The release ratios of different elements during weathering is inferred from their average abundance ratios in the silicate rocks of the basin, chemistry of small tributaries draining the silicate dominated terrain and soil profiles, as followed by Krishnaswami *et al.* (1999). The contribution of major ions and Sr from the silicate weathering to the streams can be estimated following Krishnaswami *et al.* (1999), briefly,

$$K_s = 0{\cdot}85 \times K_r \tag{2}$$

$$Ca_s = Na^* \times \left(\frac{Ca}{Na}\right)_s \tag{3}$$

$$Mg_s = Na^* \times \left(\frac{Mg}{Na}\right)_s \tag{4}$$

$$Sr_s = Na^* \times \left(\frac{Sr}{Na}\right)_s \tag{5}$$

where $\left(\frac{Ca}{Na}\right)_s$, $\left(\frac{Mg}{Na}\right)_s$, and $\left(\frac{Sr}{Na}\right)_s$ are the Na normalized ratios with which Ca, Mg and Sr are released to rivers from silicates.

The estimated silicate contribution (Equations (1)–(5)) depends critically on the Ca/Na, Mg/Na and Sr/Na used for calculation. In this study, $\left(\frac{Sr}{Na}\right)_s$ is assumed to be $2{\cdot}0 \pm 0{\cdot}8$ nM/μM, whereas $\left(\frac{Ca}{Na}\right)_s$ and $\left(\frac{Mg}{Na}\right)_s$ are assumed to be $0{\cdot}7 \pm 0{\cdot}3$ and $0{\cdot}3 \pm 0{\cdot}2$ μM/μM respectively.

The fractions of total cations derived from silicate weathering, $Cat_s(\%) \left(= 100 \times \frac{(Na_s + K_s + Ca_s + Mg_s)}{Na_r + K_r + Ca_r + Mg_r}\right)$ for the Ganga, Alaknanda and the Bhagirathi range between 14 ± 3 to 30 ± 5, 13 ± 2 to 28 ± 5 and 24 ± 4 to 49 ± 9% respectively (Table IV). The estimates of Cat_s (in %) show significant seasonal variation (Figure 7), with higher values during lean flow period, indicating relatively enhanced silicate weathering contribution compared to that of carbonates consistent with Na*/Ca and $^{87}Sr/^{86}Sr$ variation (Figure 6). The various possible reasons for temporal variations in silicate/carbonate weathering are already discussed in the previous section.

Table IV. Silicate weathering contribution to the dissolved cations and Sr of the Ganga, Alaknanda and the Bhagirathi

Sample ID	Cat_s		Sr_s	
	μM	(%)	nM	%
Ganga (Rishikesh)				
RK-1	108	16 ± 3	68	15 ± 6
RK-3	140	18 ± 3	73	11 ± 4
RK-5	141	18 ± 3	79	15 ± 6
RK-7	373	27 ± 5	340	21 ± 8
RK-9	264	26 ± 5	224	21 ± 9
RK-11	86	14 ± 3	36	15 ± 7
RK-13	386	26 ± 5	335	20 ± 8
RK-15	424	26 ± 5	361	27 ± 11
RK-17	281	30 ± 5	235	26 ± 11
RK-20	392	25 ± 5	332	25 ± 10
RK-22	352	25 ± 5	297	24 ± 10
RK-24	402	24 ± 4	337	26 ± 10
RK-25	389	23 ± 4	330	24 ± 10
RK-27	369	22 ± 4	312	23 ± 9
RK-29	275	24 ± 4	225	23 ± 9
RK-31	271	27 ± 5	225	24 ± 10
RK-33	299	24 ± 4	246	23 ± 9
RK-35	309	23 ± 4	258	21 ± 9
RK-38	245	22 ± 4	202	19 ± 8
RK-40	150	18 ± 3	109	12 ± 5
RK-42	177	17 ± 3	131	13 ± 5
RK-43	154	16 ± 3	92	11 ± 4
RK-44	145	16 ± 3	83	10 ± 4
RK-46	188	20 ± 4	123	14 ± 6
Alaknanda (Srinagar)				
SN-1	139	20 ± 4	90	17 ± 7
SN-5	143	17 ± 3	62	12 ± 5
SN-11	163	27 ± 5	122	24 ± 10
SN-17	220	23 ± 4	168	22 ± 9
SN-22	267	28 ± 5	217	28 ± 12
SN-25	247	24 ± 4	195	23 ± 9
SN-29	274	28 ± 5	223	30 ± 12
SN-31	285	27 ± 5	228	29 ± 12
SN-33	238	26 ± 5	187	25 ± 10
SN-38	120	20 ± 4	80	15 ± 6
SN-43	198	24 ± 4	145	23 ± 9
SN-44	96	14 ± 3	57	10 ± 4
SN-46	103	13 ± 2	56	7 ± 3
Bhagirathi (Uttarkashi)				
UK-5	229	25 ± 5	78	18 ± 7
UK-9	107	24 ± 4	70	16 ± 6
UK-13	191	24 ± 4	150	22 ± 9
UK-17	117	31 ± 6	74	37 ± 15
UK-22	310	40 ± 7	261	42 ± 17
UK-28	481	49 ± 9	423	57 ± 23
UK-35	328	44 ± 8	277	48 ± 19
UK-41	219	32 ± 6	178	31 ± 13
UK-44	92	27 ± 5	40	17 ± 7
UK-46	113	27 ± 5	63	21 ± 8

Sr derived from silicates, Sr_s (%), in the Ganga, Alaknanda and the Bhagirathi in the time series samples

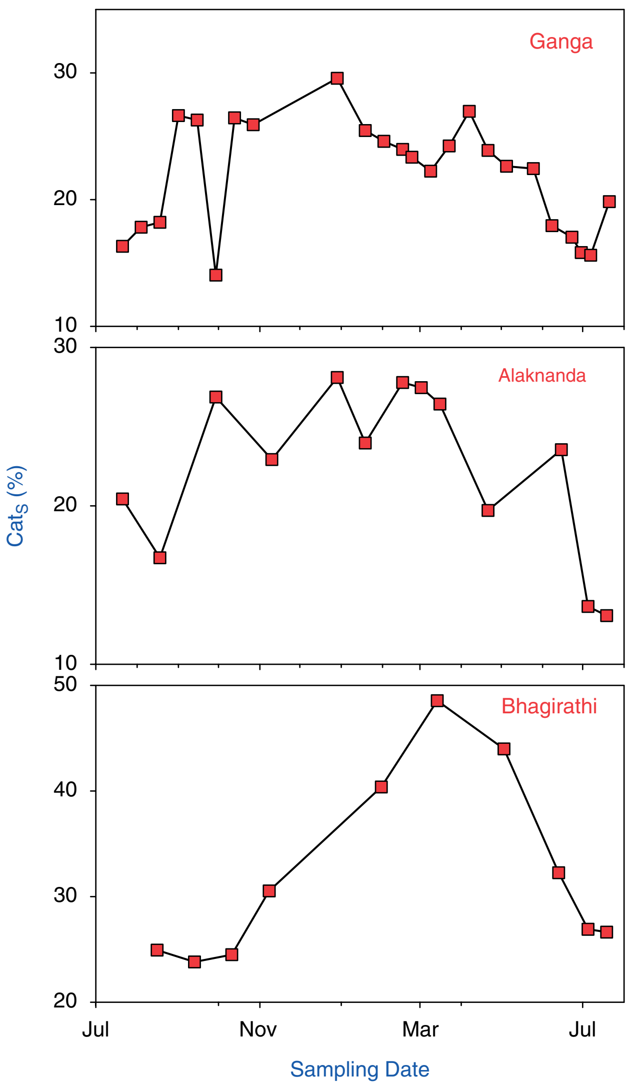

Figure 7. Seasonal variation in Cat$_s$ (%) for the Ganga, Alaknanda and the Bhagirathi. The low Cat$_s$ during monsoon indicates higher proportion of carbonate derived cations to the river water due to the combined effect of higher physical erosion, higher effective area available for erosion, and higher weatheribility of carbonates. It is important to note that both silicate and carbonate erosion rates increase during monsoon but the relative increase in the carbonate erosion rate is higher

over a year ranges between 10 ± 4 and 27 ± 11%, 7 ± 3 and 30 ± 12%, 16 ± 6 and 57 ± 23% respectively (Table IV). The uncertainties over Sr$_s$ are estimated by considering the errors on measurement and uncertainty in the $\left(\frac{\text{Sr}}{\text{Na}}\right)_s$ value. Despite of the large uncertainties, extremes of Sr$_s$ of individual rivers estimated over one year do not overlap with each other, indicating relative variation in silicate and carbonate weathering with season. Similar to seasonal trend of ^{87}Sr/^{86}Sr and Na*/Ca, Sr$_s$ (also %Sr$_s$) (Table IV) for these samples showed systematically lower values during monsoon. Sr$_s$ (also %Sr$_s$) of these streams show a decreasing trend with the water discharge over a period of one year (Figure 8); indicating relatively enhanced contribution of Sr from the weathering of carbonates during high flow period (Tipper *et al.*, 2006). Similar pattern for Sr with discharge was also observed for the Brahmaputra River (Rai and Singh, 2007). Estimated Sr$_s$ for the Bhagirathi, Alaknanda and the Ganga show an overall seasonal variation with higher Sr$_s$ during non-monsoon period (Figure 9) with more radiogenic ^{87}Sr/^{86}Sr suggestive of higher silicate contribution to dissolved Sr during non-monsoon. The above observations confirms that higher runoff during monsoon enhances the total chemical weathering.

Validity of these calculation were assessed by estimating back the riverine Sr isotope composition using the ^{87}Sr/^{86}Sr of silicate and carbonate endmembers and the estimated Sr$_s$ and Sr$_c$ (100−Sr$_s$) values in this study. The following mass balance equation is used to reproduce measured riverine ^{87}Sr/^{86}Sr value.

$$\left(\frac{^{87}\text{Sr}}{^{86}\text{Sr}}\right)_{River} = \left(\frac{^{87}\text{Sr}}{^{86}\text{Sr}}\right)_s \times \text{Sr}_s + \left(\frac{^{87}\text{Sr}}{^{86}\text{Sr}}\right)_c \times \text{Sr}_c \quad (6)$$

The estimated ^{87}Sr/^{86}Sr from the above equation for the Ganga (0·732 for RK-27), Alaknanda (0·737 for SN-29) and Bhagirathi (0·746 for UK-22) river for the month of February are found to be similar to their corresponding measured values (Table I) establishing the validity of the forward model. Further, a similar check for silicate derived Sr budget of the Ganga was carried out using the estimated Sr$_s$ for its tributaries, the Bhagirathi and the Alaknanda along with their relative annual water discharge contributions (the Alaknanda, f_{Alk} (63%) and the Bhagirathi, f_{Bhag} (37%)). In the present study, the Bhagirathi was sampled before its confluence with its largest tributary, the Bhilangana. Hence, the Sr$_s$ estimated at Uttarkashi is assumed to be similar to that of the Bhilangana and hence to that of at its outflow. Considering the Ganga at Rishikesh as binary mixing between the Bhagirathi and the Alaknanda, Sr$_S$ of the Ganga are derived using the relation,

$$(\text{Sr}_s)_{\text{Ganga}} = (\text{Sr}_s)_{\text{Alaknanda}} \times f_{\text{Alk}} + (\text{Sr}_s)_{\text{Bhagirathi}} \times f_{\text{Bhag}} \quad (7)$$

The Sr$_s$ of the Ganga estimated using Equation (7) compares well with the estimated Sr$_s$ of the corresponding Ganga sample (RK-5, Table IV). The above two calculations confirm the validity of the endmembers used in the calculation and that of the forward model itself.

A linear correlation between Sr$_s$ and ^{87}Sr/^{86}Sr is observed for the Ganga headwaters with high Sr$_s$ and ^{87}Sr/^{86}Sr values during lean flow period (Figure 10). The low ^{87}Sr/^{86}Sr values of the river during high flow period indicate relatively enhanced weathering of less radiogenic carbonates compared to the highly radiogenic silicate minerals. The enhanced carbonate weathering during the monsoon period is well supported by its faster dissolution kinetics (Lasaga *et al.*, 1994; Drever, 1997). The increase of ^{87}Sr/^{86}Sr with Sr$_s$ of these streams (Figure 10) also establishes the potential of Sr isotopic composition as a good proxy for silicate weathering in the Himalayan rivers. Further, assuming a linear relation between Sr$_s$ and ^{87}Sr/^{86}Sr for these streams, the Sr isotopic composition for the end members with 0% Sr$_s$ (Carbonates) and 100% Sr$_s$ (Silicates) are estimated. The

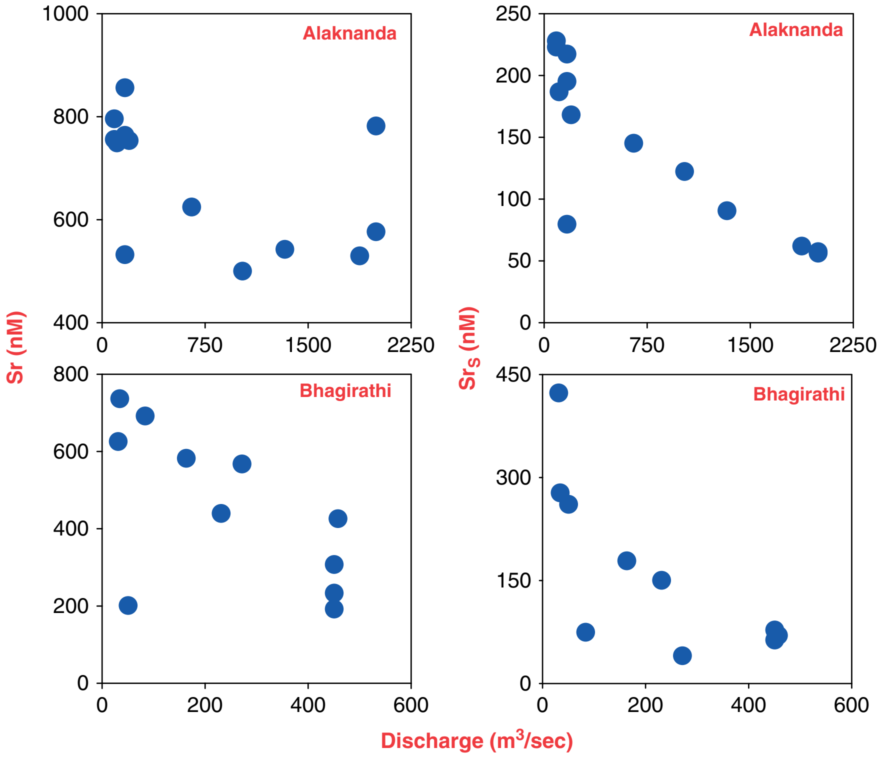

Figure 8. Variation in Sr and Sr$_S$ concentration with water discharge for the Alaknanda and the Bhagirathi. Both Sr and Sr$_S$ show decreasing trend with increase in discharge

estimated ^{87}Sr/^{86}Sr for the carbonate end member (i.e. 0% of Sr$_S$) derived from Sr$_s$-^{87}Sr/^{86}Sr relation of the streams Alaknanda and Ganga are similar (0·72) and matches well with the Sr isotopic composition of the carbonates (0·715 ± 0·01) found in the Himalaya (Singh *et al.*, 1998; Krishnaswami *et al.*, 1999). However, the estimated ^{87}Sr/^{86}Sr values for the end member with 0% of Sr$_s$ derived from the Bhagirathi River (0·74) is found to be higher than the Himalayan carbonates. As also observed in the Na*/Ca-^{87}Sr/^{86}Sr plot (Figure 6) for the Bhagirathi, the high ^{87}Sr/^{86}Sr value corresponding to 0% Sr$_s$ could have resulted from non-Na bearing silicates observed in the basin (Singh *et al.*, 2002). The silicate end member values estimated from the Bhagirathi (0·77), Alaknanda (0·79) and the Ganga (0·79) are similar to that of the Himalayan silicates (0·79 ± 0·06%).

The results of this work yield a discharge-weighted annual Sr$_s$ of 30 ± 5% for the Bhagirathi. The estimated Sr$_s$ in this study based on single data point are consistent with those reported earlier for same month (Krishnaswami *et al.*, 1999). However, the annual discharge-weighed Sr$_s$ for the Ganga (18 ± 2%) and the Alaknanda (17 ± 3%) are lower compared to those reported for single or limited season sampling (34%, Krishnaswami *et al.*, 1999; 23%, Dalai *et al.*, 2003; 50%, Bickle *et al.*, 2005 and 43 ± 17%, Singh *et al.*, 1998). This difference between discharge-weighted annual Sr$_s$ and that for single sampling establishes the importance of time series analysis of river geochemistry to estimate their fluxes to the mainstream.

Flux estimates

The riverine flux of dissolved strontium provides a measure of intensity of erosion in the basin, its controlling factors (France-Lanord *et al.*, 2003) and also its contribution to marine geochemical budget. Earlier estimates of fluxes are based mostly on a single or limited seasonal sampling (Krishnaswami *et al.*, 1992; Dalai *et al.*, 2003). Large temporal variation in water discharge and concentrations of dissolved ions over a year introduce large uncertainty in flux if estimated using single sample. In this study, the annual elemental fluxes of Sr and ^{87}Sr/^{86}Sr for the Ganga, Bhagirathi and the Alaknanda were calculated (Equations (6) and (7)) based on their time series data and available water discharges (Table V). The Sr flux calculations for the Bhagirathi and the Alaknanda were made at Devprayag assuming the Sr and ^{87}Sr/^{86}Sr values measured in the present study are representative values of the respective rivers before their confluence with the Ganga.

$$\text{Discharge} - \text{weighted annual Sr flux}$$
$$= \sum_{i=1}^{n} (Q_i \times \text{Sr}_i) \qquad (8)$$

$$\text{Discharge} - \text{weighted annual } ^{87}\text{Sr}/^{86}\text{Sr}$$
$$= \frac{\sum_{i=1}^{n} (Q_i \times \text{Sr}_i \times {}^{87}\text{Sr}/^{86}\text{Sr}_i)}{\sum_{i=1}^{n} (Q_i \times \text{Sr}_i)} \qquad (9)$$

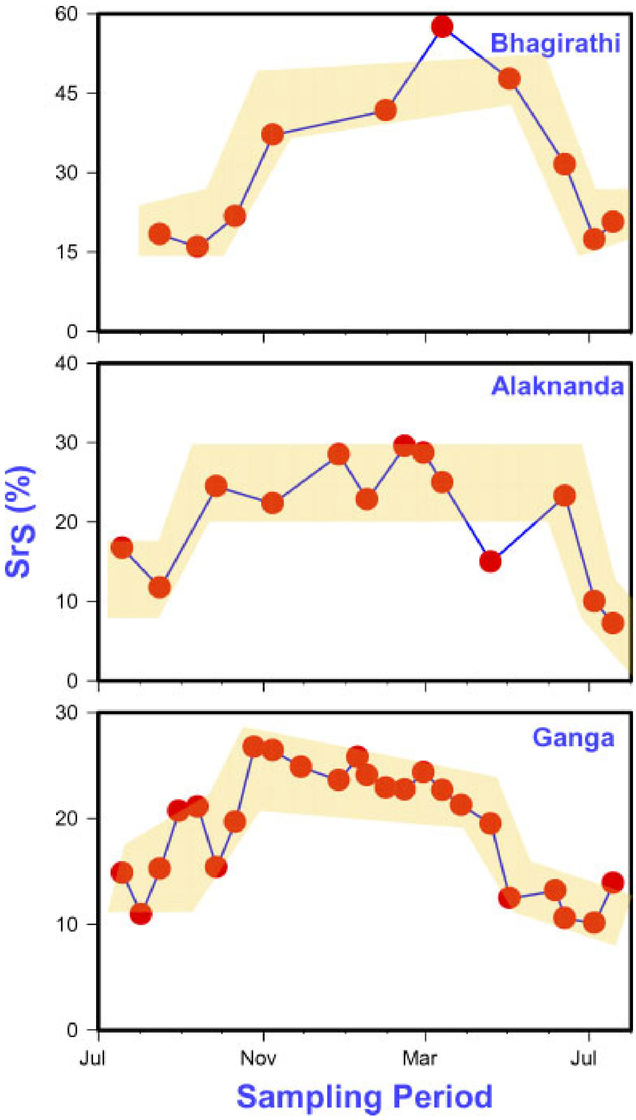

Figure 9. Seasonal variation in Sr_s (%) for the Ganga, Alaknanda and the Bhagirathi. The low Sr_s during monsoon indicates higher proportion of carbonate derived Sr to the river. The yellow band beneath the plot shows the overall seasonal trend of Sr_S. The sample of Bhagirathi from the month July is not included in the plot due to its anomalous signature (Na<Cl)

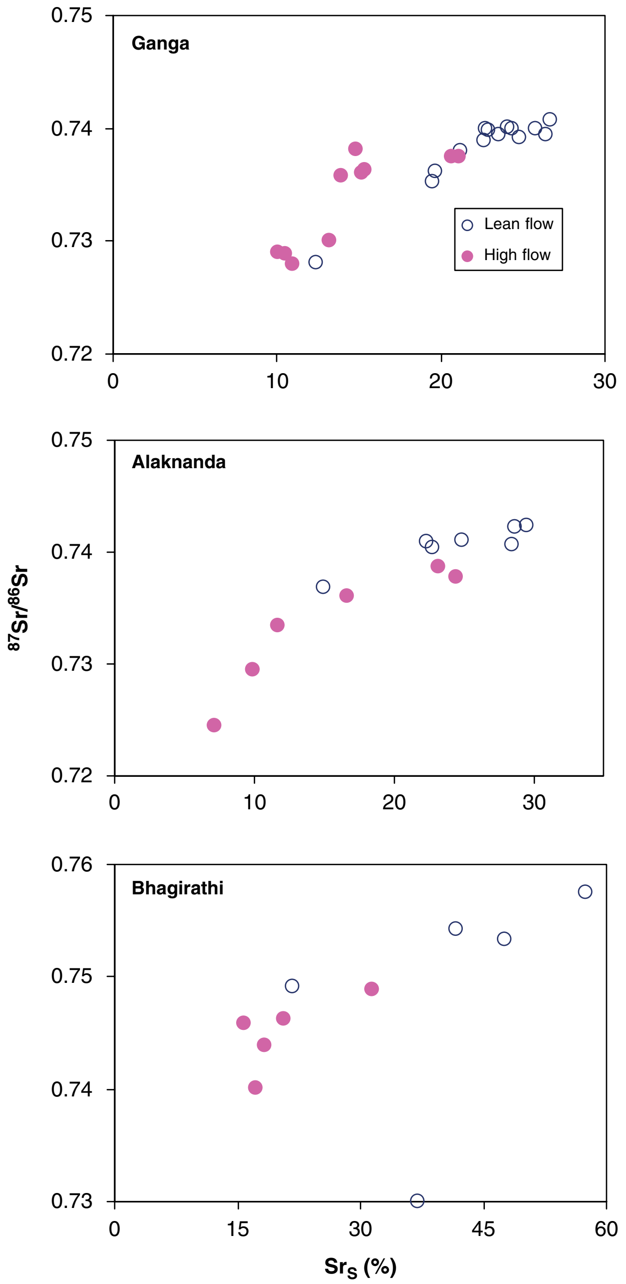

Figure 10. ^{87}Sr/^{86}Sr versus silicate derived Sr (Sr_s) for the three rivers. Good correlation between ^{87}Sr/^{86}Sr and Sr_s indicates that Sr isotope composition of the Ganga water can be used as proxy of silicate weathering

where, n is the total number of samples and Q_i is water discharge on the sampling date of ith sample.

To compare the discharge-weighed annual flux based on time series data and single sampling, the elemental fluxes are estimated using lowest Sr concentration sample of Alaknanda (SN-11), representing high flow period and highest Sr containing sample (SN-31), representing lean flow period. The discharge-weighed annual area-normalized elemental fluxes for the Alaknanda (888 moles/km^2/ year) is closer to that of the high flow period sample (735 moles/km^2/ year) compared to low period sample (1258 moles/km^2/ year). This observation indicates that in absence of time series sampling, the high flow period sample can provide a better estimate of annual area-normalized elemental fluxes of the river compared to that of lean flow sampling. However, estimates based on single season sampling can introduce an uncertainty of ∼15–40% on the annual flux calculations. The annual area-normalized elemental flux of Sr for the Ganga River at Rishikesh and the Alaknanda at Devprayag are significantly higher compared to that of the Ganga, Brahmaputra and the Indus (Table V). These values for the Ganga and Alaknanda are significantly higher compared to that of the Krishna River, which drains the Deccan traps (Das *et al*., 2006). The high Sr flux of the Ganga compared to the rivers draining the shield regions could have resulted due to high chemical erosion in the basin mediated by high physical erosion (relief) in this orogenic belt (Singh *et al*., 2008). These area-normalized Sr fluxes of the Ganga headwaters are

Table V. Discharge-weighted annual Sr flux of the Ganga headwaters and other global rivers

Stream	Drainage area (10^3 km^2)	Annual discharge (10^{12} L/year)	Sr flux		^{87}Sr/^{86}Sr
			(mol/km^2/ year)	10^6 mol/year	
Bhagirathi[a]	7·8	6·4	371	2·9	0·7479
Alaknanda[a]	11·8	17·3	888	10·5	0·7358
Ganga (Rishikesh)[a]	19·6	23·7	1135	22·3	0·7354
Ganga (Rishikesh)[b]			684	13·4	—
Ganga (Outflow)[c]	935	393	503	470	0·7239
Ganga (Rajshahi)[d]	1060	459	242	257	0·7291
Brahmaputra[e]	630	510	630	300	0·7192
Indus[f]	916	90	363	332	0·7110
Krishna[g]	259	30	521	135	0·7070
Amazon[f]	6112	6590	205	1252	0·7115

[a] Discharge-weighted annual Sr flux and ^{87}Sr/^{86}Sr; estimates are made assuming temporal variation of Sr in the Bhagirathi (Uttarkashi) and the Alaknanda (Srinagar) observed in the present study as their representative values at Devprayag. Hydrological parameters for the rivers before their confluence at Devprayag is taken from Krishnaswami *et al*., (1999); Chakrapani and Saini (2009).
[b] Discharge-weighted annual Sr flux from Rai and Singh (2007).
[c] Krishnaswami *et al*., (1992).
[d] Estimated from the sample (BGP 4) of August month of Galy *et al*., (1999).
[e] Singh *et al*., (2006); [f] Gaillardet *et al*., (1999); [g] Das *et al*., (2006).

high compared to global rivers, like the Amazon (Stallard and Edmond, 1987; Gaillardet *et al*., 1997). The chemical erosion in the basin supplies highly radiogenic Sr compared to other global river. The average discharge-weighted annual ^{87}Sr/^{86}Sr value for the Alaknanda and the Ganga at Rishikesh are less radiogenic compared to the Bhagirathi River.

CONCLUSIONS

A significant seasonal variation of dissolved major ions, Sr and ^{87}Sr/^{86}Sr were observed for the Ganga, the Alaknanda and the Bhagirathi. The concentrations of major ions and Sr of these rivers during monsoon period are found to be low compared to the non-monsoon. The high ^{87}Sr/^{86}Sr during the lean flow period indicates relatively higher contribution from silicate erosion to the riverine Sr budget. Unlike a mixing curve, an anti-correlation between ^{87}Sr/^{86}Sr and 1/Sr was observed; suggesting that the dissolved Sr content of these streams is controlled both by dilution effect and source variability during different seasons.

The source apportionment of the dissolved loads was carried out using forward model. Sr_s (%) estimated based on forward model for the Ganga, Alaknanda and the Bhagirathi range between 10 ± 4 and 27 ± 11, 7 ± 3 and 30 ± 12, 16 ± 6 and $57 \pm 23\%$ respectively with higher values during non-monsoon period. A similar seasonal trend is also observed for Cat_s of these streams. This indicates high carbonate erosion during monsoon due to larger area available for weathering, high weatherability of carbonates coupled with high physical erosion, less water–rock interaction time and higher rainfall over LH having higher exposures of carbonates. The discharge-weighted annual area-normalized dissolved Sr fluxes estimated for the Ganga and the Alaknanda are significantly high compared to those reported earlier for other global rivers; indicating significant control of orogenic belt such as the Himalaya on oceanic Sr budget.

ACKNOWLEDGEMENTS

This paper has benefited from discussion with S. Krishnaswami. A. K. Sudheer and Ashwini Kumar helped with the measurement of major ions. We thank the five anonymous reviewers and the associate editor for their comments and suggestions which helped to improve this manuscript significantly.

REFERENCES

Alkattan M, Oelkers EH, Dandurand J, Schott J. 1998. An experimental study of calcite and limestone dissolution rates as a function of pH from −1 to 3 and temperature from 25 to 80 °C. *Chemical Geology* **151**: 199–214.

Bahuguna M, Chauhan P, Sharma RC. 2008. Impact of Tehri Dam on aquatic macroinvertebrate diversity of Bhagirathi, Uttarakhand. *Journal of Environmental Science and Engineering* **50**: 41–50.

Bickle MJ, Bunbury J, Chapman HJ, Harris NBW, Fairchild IJ, Ahmad T. 2003. Fluxes of Sr into the headwaters of the Ganges. *Geochimica et Cosmochimica Acta* **67**: 2567–2584.

Bickle MJ, Chapman HJ, Bunbury J, Harris NBW, Fairchild IJ, Ahmad T, Pomies C. 2005. Relative contributions of silicate and carbonate rocks to riverine Sr fluxes in the headwaters of the Ganges. *Geochimica et Cosmochimica Acta* **69**: 2221–2240.

Bickle MJ, Harris NBW, Bunbury JM, Chapman HJ, Fairchild IJ, Ahmad T. 2001. Controls on the ^{87}Sr/^{86}Sr ratio of carbonates in the Garhwal Himalaya, Headwaters of the Ganges. *Journal of Geology* **109**: 737–753.

Blum JD, Gazis CA, Jacobson AD, Chamberlain CP. 1998. Carbonate versus silicate weathering in the Raikhot watershed within the high Himalayan crystalline series. *Geology* **26**: 411–414.

Chakrapani GJ, Saini RK. 2009. Temporal and spatial variations in water discharge and sediment load in the Alaknanda and Bhagirathi rivers in Himalaya, India. *Journal of Asian Earth Sciences* **35**: 545–553.

Chakrapani GJ, Saini RK, Yadav SK. 2009. Chemical weathering in the Alaknanda-Bhagirathi river basins in Himalayas, India. *Journal of Asian Earth Sciences* **34**: 347–362.

Dalai TK, Krishnaswami S, Kumar A. 2003. Sr and ^{87}Sr/^{86}Sr in the Yamuna River System in the Himalaya: Sources, fluxes, and controls on Sr isotope composition. *Geochimica et Cosmochimica Acta* **67**: 2931–2948.

Dalai TK, Krishnaswami S, Sarin MM. 2002. Major ion chemistry in the headwaters of the Yamuna river system: chemical weathering, its temperature dependence and CO_2 consumption in the Himalaya. *Geochimica et Cosmochimica Acta* **66**: 3397–3416.

Das A, Krishnaswami S, Kumar A. 2006. Sr and ^{87}Sr/^{86}Sr in rivers draining the deccan traps (India): implications to weathering, Sr fluxes, and the marine ^{87}Sr/^{86}Sr record around K/T. *Geochemistry Geophysics Geosystems* **7**: Q06014. DOI: 10.1029/2005GC001081.

Douglas TA. 2006. Seasonality of bedrock weathering chemistry and CO_2 consumption in a small watershed, the White River, Vermont. *Chemical Geology* **231**: 236–251.

Drever JI. 1997. *The Geochemistry of Natural Waters*, 3rd edn. Prentice Hall New Jersey; 215–234.

English NB, Quade J, DeCelles PG, Garizone CN. 2000. Geological control of Sr and major element chemistry in Himalayan rivers, Nepal. *Geochimica et Cosmochimica Acta* **64**: 2549–2566.

France-Lanord C, Evans M, Hurtrez J, Riotte J. 2003. Annual dissolved fluxes from Central Nepal rivers: budget of chemical erosion in the Himalayas. *Comptes Rendu Geosciences* **335**: 1131–1140.

Gaillardet J, Dupre B, Allegre CJ. 1997. Chemical and physical denudation in the Amazon river basin. *Chemical Geology* **142**: 141–173.

Gaillardet J, Dupre B, Louvat P, Allegre CJ. 1999. Global silicate weathering and CO_2 consumption rates deduced from the chemistry of large rivers. *Chemical Geology* **159**: 3–30.

Galy A, France-Lanord C, Derry LA. 1999. The strontium isotopic budget of Himalayan Rivers in Nepal and Bangladesh. *Geochimica et Cosmochimica Acta* **63**: 1905–1925.

Harris N, Bickle M, Chapman H, Fairchild I, Bunbury J. 1998. The significance of Himalayan rivers for silicate weathering rates: Evidence from the Bhote Kosi tributary. *Chemical Geology* **144**: 205–220.

Hren MT, Page Chamberlain C, Hilley GE, Blisniuk PM, Bookhagen B. 2007. Major ion chemistry of the Yarlung Tsangpo–Brahmaputra river: chemical weathering, erosion, and CO_2 consumption in the southern Tibetan plateau and eastern syntaxis of the Himalaya. *Geochimica et Cosmochimica Acta* **71**: 2907–2935.

Jacobson AD, Blum JD. 2000. Ca/Sr and ^{87}Sr/^{86}Sr geochemistry of disseminated calcite in Himalayan silicate rocks from Nanga Parbat: Influence on river-water chemistry. *Geology* **28**: 463–466.

Jacobson AD, Blum JD, Walter LM. 2002. Reconciling the elemental and Sr isotope composition of Himalayan weathering fluxes: insights from the carbonate geochemistry of streams waters. *Geochimica et Cosmochimica Acta* **66**: 3417–3429.

Krishnaswami S, Singh SK, Dalai T. 1999. Silicate weathering in the Himalaya: role in contributing to major ions and radiogenic Sr to the Bay of Bengal. In *Ocean Science, Trends and Future Directions*, Somayajulu BLK (ed.). Indian National Science Academy and Akademia International: New Delhi; 23–51.

Krishnaswami S, Trivedi JR, Sarin MM, Ramesh R, Sharma KK. 1992. Strontium isotopes and rubidium in the Ganga-Brahmaputra river system: weathering in the Himalaya, fluxes to the Bay of Bengal and contributions to the evolution of oceanic ^{87}Sr/^{86}Sr. *Earth and Planetary Science Letters* **109**: 243–253.

Lasaga AC, Soler JM, Ganor J, Burch TE. 1994. Chemical weathering rate laws and global geochemical cycles. *Geochimica et Cosmochimica Acta* **58**: 2361–2386.

McCauley SE, DePaolo DJ. 1997. The marine ^{87}Sr/^{86}Sr and δ^{18}O records, Himalayan Alkalinity Fluxes and Cenozoic climate models. In *Tectonic Uplift and Climate change*, Ruddiman WF (ed.). Plenum Press: New York; 428–467.

Negrel P, Allegre CJ, Dupre B, Lewin E. 1993. Erosion sources determined by inversion of major and trace element ratios and strontium isotopic ratios in river water: the Congo Basin case. *Earth and Planetary Science Letters* **120**: 59–76.

Oliver L, Harris N, Bickle M, Chapman H, Dise N, Horstwood M. 2003. Silicate weathering rates decoupled from the ^{87}Sr ratio of the dissolved load during Himalayan erosion. *Chemical Geology* **201**: 119–139.

Palmer MR, Edmond JM. 1992. Controls over the strontium isotope composition of river water. *Geochimica et Cosmochimica Acta* **56**: 2099–2111.

Pandey SK, Singh AK, Hasnain SI. 1999. Weathering and geochemical processes controlling solute acquisition in Ganga Headwater-Bhagirathi River, Garhwal Himalaya, India. *Aquatic Geochemistry* **5**: 357–379.

Petelet-Giraud E, Negrel P. 2007. Geochemical flood deconvolution in a Mediterrnean catchment (Herault, France) by Sr isotopes, major and trace elements. *Journal of Hydrology* **337**: 224–241.

Quade J, English N, DeCelles PG. 2003. Silicate versus carbonate weathering in the Himalaya: a comparison of the Arun and Seti River watersheds. *Chemical Geology* **202**: 275–296.

Quade J, Roe L, DeCelles PG, Ojha TP. 1997. The late neogene ^{87}Sr/^{86}Sr record of lowland Himalayan rivers. *Science* **276**: 1828–1831.

Rai SK, Singh SK. 2007. Temporal variation in Sr and ^{87}Sr/^{86}Sr of the Brahmaputra: implications for annual fluxes and tracking flash floods through chemical and isotope composition. *Geochemistry Geophysics Geosystems* **8**: Q08008. DOI:10.1029/2007GC001610.

Raymo ME, Ruddiman WF. 1992. Tectonic forcing of late Cenozoic climate. *Nature* **359**: 117–122.

Raymo ME, Ruddiman WF, Froelich PN. 1988. Influence of late Cenezoic mountain building on ocean geochemical cycles. *Geology* **16**: 649–653.

Richter FM, Rowley DB, DePaolo DJ. 1992. Sr isotope evolution of seawater: the role of tectonics. *Earth and Planetary Science Letters* **109**: 11–23.

Sarin MM, Krishnaswami S, Dilli K, Somayajulu BLK, Moore WS. 1989. Major ion chemistry of the Ganga-Brahmaputra river system: weathering processes and fluxes to the Bay of Bengal. *Geochimica et Cosmochimica Acta* **53**: 997–1009.

Singh AK, Hasnain SI. 1998. Major ion chemistry and weathering control in a high altitude basin: Alaknanda River, Garhwal Himalaya, India. *Hydrological Sciences-Journal* **43**: 825–843.

Singh SK, Kumar A, France-Lanord C. 2006. Sr and ^{87}Sr/^{86}Sr in waters and sediments of the Brahmaputra river system: Silicate weathering, CO_2 consumption and Sr flux. *Chemical Geology* **234**: 308–320.

Singh S, Mukherjee PK, Jain AK, Khanna PP, Saini NK, Kumar R. 2002. Source characterization and possible emplacement mechanism of collision-related Gangotri Leucogranite along Bhagirathi Valley, NW-Himalaya. In: Singh, S.2003. Granitiods of the Himalayan Collisional Belt. *Journal of the Virtual Explorer* **11**: 15–26.

Singh SK, Rai SK, Krishnaswami S. 2008. Sr and Nd isotopes in River sediments from the Ganga basin: sediment provenance and spatial variability in physical erosion. *Journal of Geophysical Research F: Earth Surface* **113**: F03006. DOI:10.1029/2007JF000909.

Singh SK, Sarin MM, France-Lanord C. 2005. Chemical erosion in the eastern Himalaya: major ion composition of the Brahmaputra and δ^{13}C of dissolved inorganic carbon. *Geochimica et Cosmochimica Acta* **69**: 3573–3588.

Singh SK, Trivedi JR, Pande K, Ramesh R, Krishnaswami S. 1998. Chemical and strontium, oxygen, and carbon isotopic compositions of carbonates from the Lesser Himalaya: implications to the strontium isotope composition of the source waters of the Ganga, Ghaghara, and the Indus rivers. *Geochimica et Cosmochimica Acta* **62**: 743–755.

Stallard RF, Edmond JM. 1987. Geochemistry of the Amazon: 3. Weathering chemistry and limits to dissolved inputs. *Journal of Geophyical Research* **92**: 8293–8302.

Tipper ET, Bickle MJ, Galy A, West AJ, Pomies C, Chapman HJ. 2006. The short term climatic sensitivity of carbonate and silicate weathering fluxes: Insight from seasonal variations in river chemistry. *Geochimica et Cosmochimica Acta* **70**: 2737–2754.

Valdiya KS. 1980. Geology of Kumaun Lesser Himalaya. *Geology of Kumaun Lesser Himalaya*: 291.

Velbel MA. 1993. Temperature dependence of silicate weathering in nature: How strong of a negative feedback on long term accumulation of atmospheric CO_2 and global greenhouse warming? *Geology* **21**: 1059–1062.

White AF, Blum AE. 1995. Effects of climate on chemical weathering rates in watersheds. *Geochimica et Cosmochimica Acta* **59**: 1729–1747.

White AF, Blum AE, Bullen TD, Vivit DV, Schultz M, Fitzpatrick J. 1999. The effect of temperature on experimental and natural chemical weathering rates of granitoid rocks. *Geochimica et Cosmochimica Acta* **63**: 3277–3291.

WAYNE STATE
UNIVERSITY
College of Liberal Arts and Sciences
Department of Geology

Mark Baskaran, Editor, *Handbook of Environmental Isotope Geochemistry* – Springer-Verlag

Prof. S. Krishnaswami
Geosciences Division
Physical Research Laboratory
Ahmedabad-380009
India

25th November 2010

Dear Swami,

Thanks for submitting your revised manuscript entitled “Chapter-24: **Sr and Nd Isotopes as Tracers of Chemical and Physical Erosion**.” I am pleased to inform you that your manuscript is accepted for publication in the *Handbook of Environmental Isotope Geochemistry* – Springer-Verlag. We anticipate having this volume printed by early spring 2011. The publisher will contact you with the Galley Proof once it is ready (in a few months).

Once again, I thank you for contributing to the Handbook.

Best regards,

M. Baskaran

Mark Baskaran

Accepted Manuscript (Style modified to include in Thesis)

Handbook of Environmental Isotope Geochemistry (*Ed. by Mark Baskaran*)
Springer-Verlag Publications

Sr and Nd Isotopes as Tracers of Chemical and Physical Erosion

Gyana Ranjan Tripathy, Sunil Kumar Singh and S Krishnaswami*
Geosciences Division, Physical Research Laboratory, Ahmedabad-380009, India
(*swami@prl.res.in)

ABSTRACT

The applications of radiogenic isotopes to investigate chemical and physical erosion processes, particularly in river basins of the Himalaya, have led to interesting inferences on the relationship between tectonics, weathering and climate. The chemical weathering studies rely more on Sr isotopes because of their widely different ratios in various end members, their uniform distribution in the oceans and the availability of continuous and robust record of marine $^{87}Sr/^{86}Sr$ through much of the geological past. The record for the Cenozoic shows steady increase in $^{87}Sr/^{86}Sr$; one of the hypotheses suggested to explain this is enhanced continental silicate weathering due to the uplift of the Himalaya. This hypothesis linking tectonics-weathering-climate, based on $^{87}Sr/^{86}Sr$ as an index of silicate weathering, however, is being challenged by the recent observations that there are a variety of carbonates in the river basins of the Himalaya with $^{87}Sr/^{86}Sr$ similar to that of silicates which have the potential to contribute significantly to the high $^{87}Sr/^{86}Sr$ of rivers such as the Ganga-Brahmaputra. Further, the non-stochiometric release of Sr isotopes during chemical weathering of minerals and rocks, the imbalance of Sr isotope budget in the oceans and temporal variations in riverine fluxes due to impact of glaciations all have compounded the problem.

Studies on the provenance of sediments and physical erosion pattern employ both Sr and Nd isotopes under the assumption that their source signatures are preserved in sediments. Though there are concerns on how well this assumption is satisfied especially by the Sr isotope system, both Sr and Nd systems are being used to learn about physical erosion in the Himalaya, its variability and causative factors. The results show that the major source of sediments to the Ganga plain and the Bay of Bengal is the Higher Himalayan Crystallines and that physical erosion among the various sub-basins is very heterogeneous with maximum rates in regions of intense precipitation and high relief. There are three such "hot-spots", one each in the basins of the Ganga, Brahmaputra and the Indus, which unload huge amount of sediments promoting rapid uplift of regions surrounding them and enhance chemical weathering by exposing fresh rock surfaces. The pattern of physical erosion and its temporal variations shows that it is influenced by climate change both on ky and My time scales though during the latter periods the erosion regime has been by and large stable. This article reviews investigations on the present and past chemical and physical erosion in river basins of the Himalaya using Sr and Nd isotope systematics in water and sediments.

1. INTRODUCTION

The Earth's continental surface is subject to continuous physical and chemical weathering and erosion by wind, water and glaciers. Physical weathering is the process of breakdown of rocks into finer fragments without affecting their composition, whereas chemical weathering is a complex process of conversion of rocks into its soluble and insoluble secondary products through water-rock interactions. The process of removal of soluble and particulate weathering products from the site of their formation to their final repository is erosion, though weathering and erosion are often used interchangeably. Erosion therefore plays an important role in exposing "fresh" rock and mineral surfaces in a drainage basin for weathering, a key factor regulating their chemical weathering rates (Stallard and Edmond 1983; Kump et al. 2000). A major driver of chemical weathering is carbonic acid formed by the solution of CO_2 in natural waters. Therefore, studies of chemical weathering are intimately linked to global carbon cycle. In recent years there have been several studies to determine the chemical erosion rates of major global river basins and the various factors regulating it, especially the role of tectonics and climate (Negrel et al. 1993; Derry and France-Lanord 1997; Edmond and Huh 1997; Gaillardet et al. 1997, 1999; Galy and France-Lanord 1999; Huh and Edmond 1999; Krishnaswami et al. 1999; Kump et al. 2000; Millot et al. 2002; Blum and Erel 2003; Dessert et al. 2003; Das et al. 2005; Bickle et al. 2005; Singh et al. 2005; West et al. 2005; Wu et al. 2005; Moon et al. 2007; Peucker-Ehrenbrink et al. 2010; Tripathy and Singh 2010). One of the key topics of interest in this area is silicate weathering of river basins, a major sink for atmospheric CO_2 on million year time scales. This makes the determination of silicate erosion rates (SER) of river basins and its temporal variations, an important component of studies on atmospheric CO_2 balance through time and its impact on long term global change, the tectonics-weathering-climate link (Walker et al. 1981; Berner et al. 1983; Raymo et al. 1988; Raymo and Ruddiman 1992; Ruddiman 1997; Kump et al. 2000). These studies though rely primarily on the chemical composition of dissolved phase of rivers, radiogenic isotopes, particularly $^{87}Sr/^{86}Sr$, have provided important additional insights into mineral and rock weathering processes that have implications to isotope geochemistry of rivers and oceans and contemporary and paleo-silicate erosion of continents. The unique isotope composition of minerals and rocks and the near conservative behavior of the isotope ratios in solution (unlike major elements which are prone to removal from solution by precipitation, ion-exchange and biological cycling) make the isotope techniques very useful to investigate kinetics of rock-water interactions in natural systems where the reactions often proceed at very slow rates (Blum and Erel 2003; Gaillardet 2008).

In contrast to studies on chemical erosion which rely mainly on the chemical and isotopic composition of dissolved phases, investigations on physical erosion (*e.g.* provenance studies) depend on chemical and isotopic signatures of sediments. Construction of the physical erosion pattern of sedimentary basins and its controlling factors requires tracking the source of sediments. Sr and Nd isotopes have been extensively used as provenance indicators of river and ocean sediments (Dia et al. 1992; Allegre et al. 1996; Pierson-Wickman et al. 2001; Singh and France-Lanord 2002; Clift 2006; Colin et al. 2006; Singh et al. 2008; Viers et al. 2008) ever since the pioneering study of Dasch (1969) on tracing the source of deep-sea surface sediments of the Atlantic using Sr isotopes. These isotope systems have become increasingly popular in such studies because their signatures among the various sources (end members) are often markedly different and easily distinguishable. Further, the application of these isotopes as provenance tracers is promoted by the property of the sediments to preserve in them the isotope composition of sources. There have been a number of Sr and Nd isotopic studies in river and ocean sediments from different basins to tag their provenances (*e.g.* Derry and France-Lanord 1997; Colin et al. 1999; Tutken et al. 2002; Clift et al. 2008; Singh et al. 2008) and their temporal variations to infer about factors controlling physical erosion in the past, particularly its link to regional changes in climate and/or tectonics (France-Lanord et al. 1993; Walter et al. 2000; Li et al. 2003; Clift et al. 2008; Rahaman et al. 2009; Galy et al. 2010). During the past decade, in addition to Sr-Nd, the applications of other isotope systems such as U series disequilibrium (Chabaux et al. 2008, Vigier and Bourdon this volume), Lu-Hf (Ma et al. 2010) and some of the non-traditional isotopes, *e.g.* Si, Mg and Ca (Reynolds, this volume; Tipper et al. 2008) are also being explored to investigate chemical and physical erosion.

This chapter reviews selected studies on the applications of Sr and Nd isotopes as tracers to investigate chemical and physical erosion with emphasis on river basins of the Himalaya. The topics addressed include chemical weathering of minerals and rocks, silicate erosion in river basins and sediment provenance studies and the relation among erosion, tectonics and climate.

2. CHEMICAL WEATHERING IN RIVER BASINS

2.1. Overview of Sr, Nd in Rocks and their isotope systematics

Strontium is an alkaline earth element with chemical properties similar to that of Ca. It occurs as a minor constituent in rock-forming minerals often replacing Ca or K. Sr has four naturally occurring isotopes, of these ^{87}Sr is radiogenic, produced from the radioactive decay of ^{87}Rb ($t_{1/2} = 4.88\times10^{10}$ years). Rb is an alkali element with properties similar to K, therefore it is more abundant in K-rich minerals. As a result, minerals with high K/Ca (~Rb/Sr) ratio develop more radiogenic Sr with time. Thus in a rock suite with minerals of the same age, those with high Rb and low Sr (*e.g.* biotite, muscovite) will have higher ^{87}Sr/^{86}Sr (refers to ^{87}Sr/^{86}Sr ratio) compared to minerals with low Rb and high Sr (*e.g.* plagioclase, apatite). During chemical weathering, Sr is generally more mobile than Rb; therefore, the Rb/Sr ratio of weathered residues is higher than that in parent rocks. The results of Dasch (1969) and subsequent studies on Rb-Sr abundances in weathering profiles developed on basalts and granites confirm this behavior with the weathered residues having higher Rb/Sr than the parent rocks. Preferential adsorption of Rb on clays can also contribute to the higher Rb/Sr in the weathered residues.

The Rare Earth Elements (REEs) occur as trace elements in major rock forming minerals and in higher concentrations in the accessory minerals, *e.g.* zircon, apatite, monazite and allanite. The concentrations of REEs vary widely in accessory minerals; they are often a minor constituent in zircon and apatite, but are a major component of REE bearing minerals such as monazite and allanite. The REEs are classified broadly into two groups, the LREE (light rare earth elements; La-Sm) and the HREE (heavy rare earth elements; Eu-Lu). Major rock forming minerals are relatively enriched in one of these two groups, for example feldspars and apatite are more abundant in LREE whereas pyroxenes and garnet prefer HREE. The concentrations of Sm and Nd in rock-forming minerals increase in the sequence in which they crystallize from magma, however due to the close similarity in the chemical properties between Sm and Nd their fractionation during geological processes is limited. As a result, the Sm/Nd abundance ratio in terrestrial rocks and minerals is within a narrow range (0.1-0.5), in contrast to Rb/Sr which varies widely, from 0.005 to 3 (Faure 1986).

Neodymium is a light rare-earth element having seven naturally occurring isotopes. Among these, ^{142}Nd and ^{143}Nd are radiogenic produced by the α-decay of ^{146}Sm ($t_{1/2} = 1.03\times10^{8}$ years) and ^{147}Sm ($t_{1/2} = 1.06\times10^{11}$ years), respectively. ^{146}Sm, because of its short half-life is now an extinct radionuclide; its signature however has been detected in meteorites through measurements of ^{142}Nd (Amelin and Rotenberg 2004; Anderasen and Sharma 2006). The ^{143}Nd/^{144}Nd ratio of minerals and rocks increases with time due to production of ^{143}Nd from ^{147}Sm, their ^{143}Nd/^{144}Nd, therefore depends on their Sm/Nd ratios and ages. The isotopic composition of Nd (^{143}Nd/^{144}Nd) is expressed in epsilon units (ε, DePaolo and Wasserburg 1976), which represents the relative deviation of ^{143}Nd/^{144}Nd in the sample from ^{143}Nd/^{144}Nd of the chondritic uniform reservoir (CHUR) in units of 10^4. ε is expressed as,

$$\varepsilon_{Nd}(0) = \left(\frac{\left({}^{143}Nd / {}^{144}Nd \right)_{sample}(0)}{\left({}^{143}Nd / {}^{144}Nd \right)_{CHUR}(0)} - 1 \right) \times 10^4$$

where $(^{143}\mathrm{Nd}/^{144}\mathrm{Nd})_{\mathrm{CHUR}}(0)$ and $(^{143}\mathrm{Nd}/^{144}\mathrm{Nd})_{\mathrm{sample}}(0)$ are the present day ^{143}Nd/^{144}Nd ratio of CHUR (= 0.512638; Jacobsen and Wasserburg 1980) and the sample, respectively. The normalization of Nd isotopic ratios of rocks with chondritic value provides information on the relative Sm/Nd ratio of their sources. For example, a negative epsilon value indicates that the rock is derived from sources lower in Sm/Nd than CHUR (Faure 1986). Further, as the Nd isotopic variations in natural systems are quite small, the ε notation provides a convenient approach to express and appreciate these small variations.

2.2. Behavior of Sr and Nd isotopes during Chemical Weathering of rocks and Mineral weathering kinetics

2.2.1. ^{87}Sr/^{86}Sr release during mineral and rock weathering: Laboratory and Field Studies

The major source of dissolved Sr to rivers is chemical weathering of silicates and carbonates in their drainage basins, with minor contribution from other lithologies such as evaporites. The silicates of bed rocks are an assemblage of minerals, which have different chemical and mineralogical composition and weathering properties. Each of these minerals has their own distinct ^{87}Sr/^{86}Sr corresponding to their age and Rb and Sr concentrations. During chemical weathering of silicate rocks, Sr isotopes from various minerals are released depending on their weathering rates and accessibility to weathering. As a result, Sr from easily weatherable minerals is expected to be released to solution initially from freshly exposed rock surfaces. The exposure of fresh rock surfaces is facilitated by physical erosion, tectonics and glaciations.

Studies on the release of Sr and ^{87}Sr/^{86}Sr during weathering of continental rocks and their subsequent behavior are being carried out (i) to determine their release pattern from minerals in the parent rock and its implications to mineral weathering rates and ^{87}Sr/^{86}Sr of rivers, (ii) to assess the relative roles of silicate and carbonate sources to their budget in river/ground water systems and to explore the possibility of using ^{87}Sr/^{86}Sr in rivers as a proxy for silicate weathering and (iii) to interpret Sr isotope records in marine archives. The ^{87}Sr/^{86}Sr of the oceans, as recorded in carbonate shells of marine sediments, is known to be steadily increasing since the Cenozoic (Burke et al. 1982; Veizer 1989; Richter et al. 1992). Delineating the sources responsible for this increase in terms of silicate/carbonate weathering can prove useful in deciphering the weathering history of continents and its role in atmospheric CO_2 drawdown.

Erel et al. (2004) conducted laboratory studies of granitoid weathering to determine trends in Sr isotope release with time and its implications to mineral weathering. These authors based on combined studies of major elements and Sr isotopes in minerals of a granitoid rock from Elat, Israel and in the solution from its weathering observed that during initial stages the granitoid dissolution is dominated by contributions from easily weatherable trace phases, calcites/apatites, followed by biotites in the intermediate stages and plagioclase during the later stages of weathering (Fig. 1). By comparing these laboratory experimental data with Sr isotope distribution in soil chronosequences from the Wind River and Sierra Nevada mountains, Erel et al. (2004) were able to deduce the temporal pattern of Sr release during granitoid weathering under natural conditions and from it the mineral dissolution sequence for the granite. The results showed that the easily weatherable trace phases in the granitoid, calcites and apatites are the major source of elements to solution from rock weathering during the initial few hundred years, biotites determining the supply from rock surfaces exposed to weathering a few hundreds to ~10,000 years and plagioclase accounting for much of the cations from surfaces that have been weathered for more than ~100,000 years.

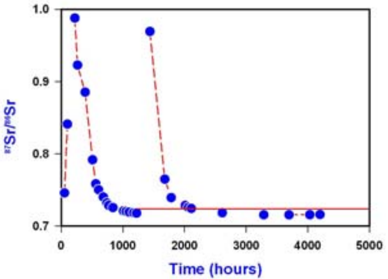

Figure 1: *The release pattern of $^{87}Sr/^{86}Sr$ during dissolution of a granitoid rock with time. The low $^{87}Sr/^{86}Sr$ during the early stage of dissolution is a result of preferential weathering of calcites; this is followed by a sharp peak in Sr isotopic ratio due to weathering of biotites. The straight line parallel to the X-axis is the $^{87}Sr/^{86}Sr$ of the whole rock. The weathered residue of the granitoid rock after ~1200 hrs of experiment was dried and subjected to further dissolution; this resulted in the second $^{87}Sr/^{86}Sr$ peak. Figure replotted from Erel et al. 2004.*

The distribution of Sr isotopes in different components of soil chronosequences provided independent evidences for the non-stochiometric release of Sr during rock weathering. Measurements of Sr isotopes (Blum and Erel 1995, 1997) in the exchangeable fractions and bulk soils from a granitic soil chronosequence developed on the Wind River Mountains (0.4-300 ky) showed very significant and systematic decrease in $^{87}Sr/^{86}Sr$ of the exchangeable pool with soil age (Fig. 2). The primary source of exchangeable Sr in the soil profile is that released during chemical weathering of rocks. This Sr, retained in the exchangeable sites of soils, can be released to solution by ion exchange with suitable reagents. Therefore the decrease in $^{87}Sr/^{86}Sr$ (from 0.7947 to 0.7114; Fig. 2) of the exchangeable pool with age suggests that $^{87}Sr/^{86}Sr$ released during the early stages of weathering was far more radiogenic than that released during the later stages. This was interpreted in terms of preferential weathering of biotites from freshly exposed rock surfaces (<20 ky), underscoring its importance as a source of highly radiogenic Sr to waters draining young rocks rich in biotite. These granites/gneisses were devoid of even trace amounts of calcite (Blum and Erel 1995) precluding it as a source for Sr in the early stages of weathering (*c.f.* Erel et al. 2004). The data also suggested that biotites weather much faster relative to plagioclase in young soils (~8 times) and that the trend gets reversed as the soil gets older, primarily due to depletion in the abundances of unweathered biotites (Blum and Erel 1995). More importantly, the non-stochiometric release of $^{87}Sr/^{86}Sr$ due to differences in mineral weathering rates led to the suggestion that exposure of new weathering surfaces (*e.g.* by glaciation and/or mountain uplift) can make the $^{87}Sr/^{86}Sr$ of rivers significantly more radiogenic for periods of ~20 ky following their exposure and thus elevate the riverine $^{87}Sr/^{86}Sr$ input to the oceans during such periods. This result also provides a mechanism to link global glaciations with Sr isotope evolution of the oceans (Armstrong 1971; Blum and Erel 1995, 1997; Zachos et al. 1999). More studies on Sr isotopes in granitic soil chronosequence from other locations however showed that the composition of the exchangeable Sr depended on the history of the profile. For example, in a profile from central Sierra Nevada (Bullen et al. 1997), developed on granitic alluvium the exchangeable $^{87}Sr/^{86}Sr$ was dominated by supply from plagioclase and K-feldspars and not biotite as was observed by Blum and Erel (1997). This difference was attributed to the absence of fresh biotites in the soil profile of Sierra Neveda, further attesting to the importance of biotite weathering from freshly exposed rock surfaces in contributing to highly radiogenic Sr to solutions.

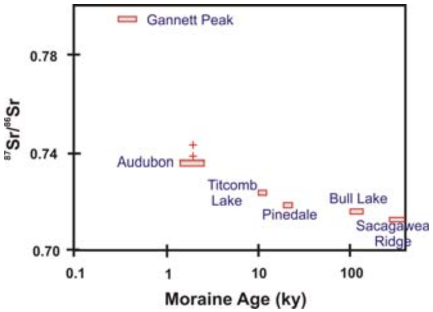

Figure 2: *Variations in the Sr isotopic ratio in the exchangeable fractions of a granitoid soil chronosequence developed on glacial moraines in the Wind River Range. The negative correlation between exchangeable $^{87}Sr/^{86}Sr$ and moraine age indicates release of more radiogenic $^{87}Sr/^{86}Sr$ from biotites during the early stage of weathering. The $^{87}Sr/^{86}Sr$ values for two stream water samples (marked as crosses) draining the Audubon till are also shown in the figure. Figure redrawn from Blum and Erel 1995.*

Analogous to field studies of rock weathering, mineral weathering experiments also brought out the role of non-stochiometric release of Sr isotope ratios during their early stages of dissolution. Brantley et al. (1998) in their dissolution experiments of feldspars observed that in the initial stages the release of Sr was not stochiometric and its isotope composition was different from that of the host mineral. This difference was explained in terms of contribution of Sr either from fluorite and zeolites, trace secondary phases in the feldspars and/or to preferential leaching of Sr from more easily weatherable sites of the primary mineral. The isotopic composition of the solution attained steady-state and became close to that of the host mineral with progressive dissolution. These results have led to the suggestion that non-stochiometric release of Sr and $^{87}Sr/^{86}Sr$ can also occur in natural systems, but only for short time periods ($< 10^3$ years) following the exposure of fresh mineral/rock surfaces for weathering. Taylor et al. (2000) also have reported similar non-stochiometric release of Sr and $^{87}Sr/^{86}Sr$ during early stages of dissolution of biotites and phlogopites (Fig. 3). These results were interpreted in terms of preferential dissolution of trace calcite in the primary minerals and materials from their interlayer sites, the later being more radiogenic as they concentrate Rb. Based on the results of these experiments the authors calculated the dissolution rate of ^{87}Sr to be marginally higher than that of ^{86}Sr in biotites and that steady state with respect to release of Sr isotopes would be reached in a few thousand years.

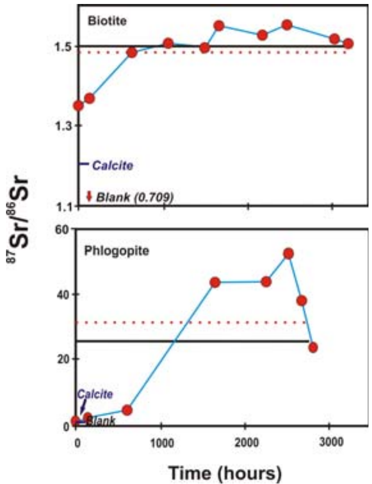

Figure 3: *The release pattern of $^{87}Sr/^{86}Sr$ in laboratory leaching experiments of biotite and phlogopite. The low Sr isotopic ratio during the initial stages of the experiment is a result of Sr release from trace calcite contained in the minerals. The solid (black) and dotted (red) lines in the figure represent the pre-experiment and post-experiment values of the minerals respectively. Figure redrawn from Taylor et al. 2000.*

The importance of trace calcic phases (*e.g.* calcite, apatite, and bytownite) in dominating the supply of Ca, Sr and Sr isotopes during granite weathering has also been demonstrated through field studies (Blum et al. 1998; Jacobson et al. 2002; Oliva et al. 2004). Results of Sr isotope measurements in rivers draining small catchments of the Himalaya suggest that vein calcites in granites of the basin can be an important source of Ca and Sr with high ^{87}Sr/^{86}Sr (Blum et al. 1998). The researches of Oliva et al. (2004) on chemical weathering of high elevation Estibere granitic watershed showed that trace calcic phases, epidote, bytownite, prehnite and apatite, contributed significantly to the Ca, Sr and Sr isotope fluxes. However, unlike in the crystallines of the Himalaya, the majority of trace calcic phases in the Estibere watershed is silicates and therefore contributes to silicate weathering and atmospheric CO_2 drawdown. Similarly, the studies of Aubert et al. (2001) in the Strengbach watershed (France) showed that the Sr and Nd isotope composition of streams and spring waters of the region can be interpreted in terms of two end member mixing, apatite and plagioclase. The authors also inferred that biotites and K-feldspars only have a "weak influence" on the Sr isotope budget of these waters (*c.f.* Blum and Erel 1995, Bullen et al. 1997). All these field and laboratory studies bring out the important role of trace calcic inclusions such as calcites, apatites and silicates (epidote, bytownite, prehnite) often contained in silicate rocks in supplying Ca and Sr and ^{87}Sr/^{86}Sr to streams during rock weathering. These results have vital implications on the use of Sr isotopes to track silicate weathering (see section 2.4).

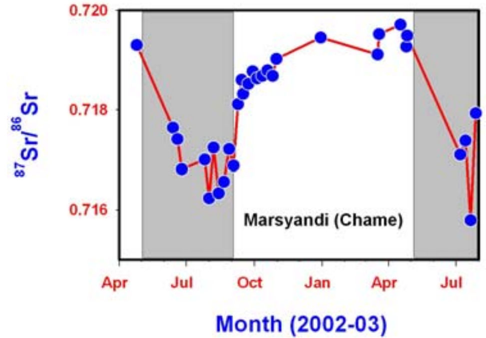

Figure 4: *Seasonal variations in ^{87}Sr/^{86}Sr of the Marsyandi River, Nepal, a sub-tributary of the Ganga river. The data show significantly lower ^{87}Sr/^{86}Sr ratio during monsoon (shaded zone) due to relatively more contribution of unradiogenic Sr from carbonates. Figure replotted from Tipper et al. 2006a.*

The impact of mineral weathering kinetics is also evident in the seasonal variations of ^{87}Sr/^{86}Sr of rivers. Tipper et al. (2006a) observed that during the monsoon season the ^{87}Sr/^{86}Sr of the headwater tributaries of the Marsyandi, a sub-tributary of the Ganga was less radiogenic compared to that during non-monsoon periods (Fig. 4) similar to that noted earlier by Krishnaswami et al (1999) and Bickle et al (2003) for the headwaters of the Ganga. The Sr isotopic composition of rivers in the Himalaya is determined by the mixing proportion of contributions from two major sources, marginally radiogenic sedimentary carbonates (^{87}Sr/^{86}Sr~0.715; Singh et al. 1998) and radiogenic silicates (with associated trace phases; ^{87}Sr/^{86}Sr ~0.75-0.80, Krishnaswami et al. 1999). The difference in weathering kinetics of silicates and carbonates and its climatic dependence is an important cause contributing to the seasonal variations in ^{87}Sr/^{86}Sr of rivers. The weathering rates of carbonates are significantly higher than silicates, this enhances their relative contribution to rivers during high runoff. Considering that Sr in sedimentary carbonates is generally far less radiogenic relative to Sr in silicates, higher proportion of Sr from such carbonates to rivers during monsoon would make the riverine Sr lower in ^{87}Sr/^{86}Sr. In contrast during dry periods when more time becomes available for water-rock interactions the contribution from silicates is relatively more than that during monsoon. Similar seasonal trends in riverine silicate cations and ^{87}Sr/^{86}Sr have been documented in a few other rivers (Moon et al. 2007; Rai and Singh 2007; Tripathy et al. 2010).

Thus the laboratory experiments and field data provide evidences to suggest that during weathering, particularly in early stages, Sr isotope composition of the solution can be significantly different from that of the parent material primarily due to differences in mineral weathering kinetics. Such non-stochiometric release of Sr isotopes can result in increasing ^{87}Sr/^{86}Sr of rivers, if minerals with highly radiogenic Sr isotope composition (*e.g.* biotite) are freshly exposed for weathering. These studies also establishes a link between dissolved fluxes of rivers and glaciation/mountain uplift as the exposure of fresh rock surfaces for weathering is promoted by tectonics, glaciation and intense physical erosion. Two other consequences of non-stochiometric release of Sr isotopes pertain to their applications in weathering and provenances studies. The finding that trace calcites and apatites can be important sources of Ca, Sr and radiogenic ^{87}Sr/^{86}Sr to rivers can constrain the use of ^{87}Sr/^{86}Sr as a proxy of silicate weathering if such contributions are major on a basin wide scale. Similarly the non-stochiometric release of ^{87}Sr/^{86}Sr to solution, if significant on a basin scale, it can result in the formation of sediments with ^{87}Sr/^{86}Sr different from that of parent material, a result that can challenge the use of ^{87}Sr/^{86}Sr as a provenance tracer.

2.2.2. REE (Sm/Nd) and ^{143}Nd/^{144}Nd release during mineral and rock weathering: Laboratory and Field Studies

Compared to Rb-Sr and ^{87}Sr/^{86}Sr, there are only a few investigations on the behavior of Sm-Nd and ^{143}Nd/^{144}Nd during progressive weathering of rocks. Generally, most of the REE in rocks, ~70-90%, is present in accessory minerals (*e.g.* allanite, monazite, sphene, zircon and apatite) and the reminder distributed among the primary rock forming minerals (Barun et al. 1993; Harlavan et al. 2009). Therefore studies on the release of REE during rock weathering serve as a probe to investigate their fractionation and to infer the weathering characteristics of the accessory minerals. Early investigations (Nesbitt 1979) based on the abundances and distribution of LREEs and HREEs in soil profiles developed on granodiorite demonstrated that during chemical weathering they are leached from the upper layers of soil depleting their concentrations relative to parent rocks. During their downward transport they get sequestered in the weathering products in the deeper layers enriching their abundances. The mobilization and fractionation behavior of the two groups of REEs during chemical weathering however, was found to be different and that it was determined by (i) the chemistry of soil water, pH and dissolved organic matter concentration. This is consistent with the subsequent studies that these two properties of water play an important role in regulating the concentration and mobilization of dissolved Nd in rivers (Section 2.3.2.), (ii) the abundance and weathering pattern of different accessory minerals in rocks hosting the REEs and (iii) the formation of secondary phases in the soil that sequester the REEs.

Subsequent studies based on different components of soil profiles and laboratory leaching experiments on granitoid weathering have by and large attested to the above findings (Nesbitt and Markovics 1997; Aubert et al. 2001; Harlaven and Erel 2002; Ma et al. 2007; Harlaven et al. 2009); solubilization of REEs from accessory minerals in the upper layers of the soil and their uptake in secondary phases in the deeper layers causing their redistribution within the soil column. The solubilization and transport of REEs was linked to the availability of organic matter.

The accessory minerals involved in the REE release were identified and their weathering sequence determined through inter-element/isotope association. For example, in the soil profile from Vosges Mountains, France (Aubert et al. 2001), the correlation of REEs with P and Th suggested apatite and monazite to be the main phases determining the mobilization and budget of REEs. Similarly, Harlavan and Erel (2002) in their laboratory experiments on the release of Pb isotopes, REEs and major elements during granitoid weathering observed that dissolution of allanite dominated REE supply to solution initially, followed by weathering of allanite, apatite and sphene in the later stages and contributions from dissolution of feldspar becoming prominent during the final stages. These results also provided weathering sequences for the accessory minerals as allanite > apatite > sphene. These findings were independently confirmed by Harlavan et al. (2009) based on their studies on REE abundances and Pb isotopes in the labile pool of soil chronosequences. These latter studies, as they were based on soil chronosequences, also provided time constraints on the processes governing REE mobilization and distribution in soils. Investigations on the mobilization and redistribution of REEs during intense weathering of basalts (Ma et al. 2007) also reveal similar pattern with extensive removal from the upper layers of soil and uptake in the deeper layers. The mobilization results in fractionation of LREEs from HREEs, the former group being relatively less mobile. As in earlier studies, the availability of organic matter was found to be a key factor in the mobilization of REEs and the formation of secondary phases such as phosphates and Fe-Mn oxy/hydroxides for their sequestration in deeper layers.

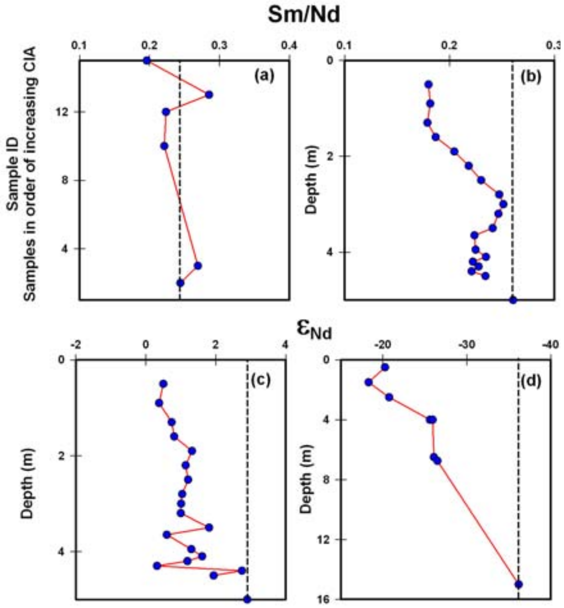

Figure 5: *The behavior of Sm/Nd and ε_{Nd} during chemical weathering as recorded in soil profiles. The results show different patterns. Figs a (Toorongo granodiorite, Australia; Nessbit and Markovics 1997) show that Sm/Nd remain nearly constant during weathering; whereas Figs b, c (Neogene basalts from South China; Ma et al. 2010) and d (granodiorite from southern Cameroon; Viers and Wasserburg 2004) show effects of preferential mobilization of Sm. The bottom and top sides of the figures show the least and most weathered rocks; the dashed straight line in the figure represents the bed rock value.*

Information on the behavior of Sm/Nd during weathering is derived mainly from studies of their distribution in soil profiles (Fig. 5). These results however do not show any consistent pattern on their relative mobilities. For example, Nesbitt and Markovics (1997) did not observe significant fractionation between Sm and Nd as a function of weathering intensity in the Toorango soil profile, Australia (Fig. 5a) relative to the parent granitoid rock though both elements were significantly mobilized by chemical weathering. These results led to the conclusion that in this profile chemical weathering has not affected the Sm-Nd chronology. In contrast, a number of studies (*e.g.* Ohlander et al. 2000; MacFarlane et al. 1994; Ma et al. 2010) report significant fractionation in Sm/Nd during chemical weathering. Ohlander et al. (2000) observed that during weathering of till, Nd is preferentially released over Sm from minerals with lower Sm/Nd (allanite, monazite) than the bulk soil leading to enhancement in the ε_{Nd} value, by up to four units, (~ -22 to -18) in the weathered till. MacFarlane et al. (1994) also observed preferential release of LREEs and fractionation of Nd isotopes and ^{147}Sm/^{144}Nd in two weathering profiles preserved between flows of the Mt. Roe basalts in Western Australia. Investigations of Sm/Nd and ε_{Nd} in soil profiles formed by intensive weathering of basalts (Ma et al. 2010) also showed effects of Sm/Nd fractionation with corresponding changes in ε_{Nd} values (Figs. 5b, c). Viers and Wasserburg (2004) investigated the behavior of Sm/Nd and Nd isotope composition during weathering of granite by analyzing a lateritic soil profile in a tropical watershed from Cameroon along with surface waters collected from the region. The results showed major changes in ε_{Nd}, from ~ -36 in the parent rock to -18 near the top of the soil profile (Fig. 5d), without any major shifts in Sm/Nd. These results were attributed to preferential dissolution of minerals such as feldspars and apatite with least radiogenic Nd.

The above studies thus suggest that an important source of REEs to solution during chemical weathering of rocks is dissolution of accessory minerals. The differences in mineral weathering rates can cause the Nd isotope composition of the solution and residual solids to be different from that of the parent rock. However, the changes observed in Nd isotopic ratios due to chemical weathering in the basins are often less compared to the variations observed among global sediments (Ma et al. 2010).

2.3. Dissolved Sr, ^{87}Sr/^{86}Sr, Nd and ε_{Nd} in Rivers

2.3.1. Sr and ^{87}Sr/^{86}Sr

The concentration of dissolved Sr and its isotopic composition have been measured in a large number of global rivers to learn about its behavior during weathering and transport, its flux to the oceans and its marine budget (Goldstein and Jacobsen 1987; Palmer and Edmond 1989; Trivedi et al. 1995; Gaillardet et al. 1999; Vance et al. 2009; Peucker-Ehrenbrink et al. 2010). The dissolved Sr concentration of major global rivers varies widely, by more than an order of magnitude, from ~0.21 to ~7.46 μM (Table 1). Among the major rivers (Table 1) Sr concentration is the highest for the Yellow and the lowest for the Orinoco, with the Yangtze delivering the maximum amount of Sr to the ocean, ~7 % of the global riverine Sr flux compared to its contribution of ~2.5 % to water discharge. The global discharge-weighted average concentration of Sr based on data in Table 1 (which make up ~44 % of global water discharge and ~33 % of drainage area) is ~0.94 μM; this corresponds to an annual flux of 36.5×10^9 mol/y consistent with some of the earlier estimates (Palmer and Edmond 1989; Vance et al. 2009; Table 1). This is expected considering that much of the data in Table 1 are from earlier compilations. More recently, Peucker-Ehrenbrink et al. (2010) have calculated following a different approach (by averaging Sr concentration on the basis of large scale drainage regions and extrapolating them) the contemporary supply of dissolved Sr to the ocean to be 47×10^9 mol/y, ~30% higher than the present and some of the earlier estimates (Table 1).

The major uncertainty in the flux estimates arises from the use of the available Sr data (Table 1) which are often based on a single or a few measurements in a river during a year, as the annual mean Sr concentration. Such an approach can be subject to significant errors because of short-term/seasonal variations in Sr abundance of rivers, in general it seems to show a decreasing trend with increasing water discharge. For example, Sr in the Brahmaputra measured at biweekly intervals over a period of ~10 months shows that it varies by a factor of ~2 (Rai and Singh 2007), similar to the range reported by Galy et al. (1999) and for some of the other major global rivers such as the Orinoco, Yukon, Mississippi and the Ganga (Palmer and Edmond 1989; Xu and Marcantonio 2007; Rai et al. 2010; Table 2). It is apparent from these data that the determination of Sr flux based on a single measurement in a river can differ from the annual average value by as much as ±50%. Other potential sources of uncertainty in the flux

Table 1: Dissolved Sr concentration and ^{87}Sr/^{86}Sr ratios of global rivers.

River	Water discharge km^3/y	Drainage Area 10^6 km^2	Sr nM	Sr flux 10^9 mol/y	^{87}Sr/^{86}Sr	Reference
Amazon	6590	6.112	310	2.04	0.71165	1
Zaire (Congo)	1200	3.698	313	0.38	0.71550	2
Orinoco	1135	1.1	210	0.24	0.71830	2
Mississippi	580	2.98	2130	1.24	0.70957	3
Parana	568	2.783	520	0.30	0.71390	4
Lena	525	2.49	1100	0.58	0.71048	1
Tocantins	372	0.757	380	0.14	0.72067	4
Amur	344	1.855	500	0.17	0.70923	5
St. Lawrence	337	1.02	1200	0.40	0.70962	6
Mackenzie	308	1.787	2740	0.84	0.71138	7
Columbia	236	0.669	982	0.23	0.71210	8
Danube	207	0.817	2760	0.57	0.70890	4
Yukon	200	0.849	1590	0.32	0.7137	4
Niger	154	1.2	250	0.04	0.71400	2
Fraser	112	0.22	913	0.10	0.71200	2
Rhine	69	0.224	6227	0.43	0.70920	2
		HT Rivers				
Yangtze (Chang Jiang)	928	1.808	2830	2.63	0.71032	9
Brahmaputra	510	0.58	730	0.37	0.71920	10
Ganga	493	1.05	560	0.28	0.72910	11
Irrawaddy*	486	0.41	-	-	0.71010	12
Mekong	467	0.795	3080	1.44	0.71035	9
Pearl	363	0.437	767	0.28	0.71190	2
Indus	238	0.47	3689	0.88	0.71110	13
Salween	211	0.325	1330	0.28	0.71405	9
Hong (Red)	123	0.12	1158	0.14	0.71284	14
Huang He (Yellow)	41	0.752	7458	0.31	0.71110	2
		Peninsular Indian Rivers				
Godavari	105	0.313	1375	0.14	0.7152	15
Mahanadi	66	0.132	704	0.05	0.71930	15
Narmada	39	0.102	2156	0.08	0.71140	15
Krishna	30	0.259	3742	0.11	0.71420	15
Kaveri (Cauvery)	21	0.088	2690	0.06	0.71498	16

Discharge-weighted Sr concentration and ^{87}Sr/^{86}Sr

HT Rivers	3860	7	1956	7.55	0.71179
Non-HT rivers	13199	29	641	-	0.71163
Global River	38857	110	939	36.5	0.71171

Earlier estimates of global river Sr and ^{87}Sr/^{86}Sr

Goldstein and Jacobson (1987)	705	-	0.7101
Palmer and Edmond (1989)	890	33.3	0.7119
Vance et al. (2009)	-	33.7	0.7114
Peucker-Ehrenbrink et al. (2010)	1220	47	0.7111

Average discharge-weighted Sr and ^{87}Sr/^{86}Sr values for global river are estimated based on the data in the Table. The discharge-weighted average Sr for rivers listed in the Table is taken to be the same for the mean global river, this value is multiplied by global water discharge to estimate global riverine Sr flux.

**For flux calculations, the Sr concentration of Irrawaddy is assumed to be the same as the mean of HT rivers.*

Hydrological parameters are from Pande et al. 1994, Gailladret et al. 1999 and Peucker-Ehrenbrink 2009. For the HT and Non-HT rivers are based on the data compiled in this study. Sr and ^{87}Sr/^{86}Sr data are from [1]Peucker-Ehrenbrink et al. 2010; [2]Palmer and Edmond 1989; [3]Xu and Marcantonio 2007; [4]Gailladret et al. 1999; [5]Moon et al. 2009; [6]Yang et al. 1996; [7]Millot et al. 2003; [8]Goldstein and Jacobsen 1987; [9]Noh et al. 2009; [10]Krishnaswami et al. 1992;[11]Galy et al. 1999; [12]Tipper et al., 2006b; [13]Pande et al. 1994; [14]Moon et al. 2007; [15]Trivedi et al. 1995; [16]Pattanaik et al. 2007.

estimates are (i) inter-annual variation in water discharge. The Ganga, for example shows a spread of ±20% in water discharge during decadal time scales (1950-1960; 1965-1973; http://www.grdc.sr.unh.edu)). This variation however is much higher, a factor of ~2 on a year to year basis and (ii) validity of calculating global flux by extrapolating Sr data from available measurements (Table 1) which represents only 40%-50% of global river discharge and about a third of drainage area. Such a calculation requires that the measured data is globally representative in terms of different factors that include discharge (climate), areal coverage and lithological distribution of the river basins. In this context, the available data (Table 1) may not have adequate representation of rivers from volcanic islands and island arcs.

The concentration of dissolved Sr in rivers is determined largely by the lithology of the drainage basin and the intensity of chemical weathering. In general, silicate and carbonates are the major lithologies of river basins with minor occurrence of evaporites and sulfides. The weathering kinetics of carbonates is much faster than that of silicates (Drever 1997); this can make carbonates an important source of Sr to rivers even if their areal exposure in river basins is relatively less and their Sr abundances comparable to that in silicates. The role of carbonates and silicates in determining the budget of Sr in rivers is borne out from the linear co-variation of dissolved Sr/Na with Ca/Na in several large and medium size global rivers (Gaillardet et al. 1999), attributable to mixing between a high Ca/Na, Sr/Na end member (carbonates) and a low Ca/Na, Sr/Na end member (silicates). Model calculations to constrain the silicate and carbonate derived Sr in rivers have met with challenges due to large variations in elemental ratios of end members and precipitation of calcite from water (*e.g.* Galy et al. 1999; Krishnaswami et al. 1999; Bickle et al. 2005). Some of these challenges, particularly those pertaining to end member values have been addressed through the use of inverse model (Negrel et al. 1993; Gaillardet et al. 1999; Moon et al. 2007; Tripathy and Singh 2010). The application of such a model (Tripathy and Singh 2010) to the headwaters of the Ganga system rivers in the Himalaya show that ~70% of dissolved Sr in them is derived from carbonates and ~20% from silicates, despite relatively low areal exposure of carbonates in the catchment (Amiotte Suchet et al. 2003; Tripathy and Singh 2010). The uncertainties in the estimates of Sr supply from silicates and carbonates and insufficient knowledge on the release ratios of Sr to (Na, K, Mg and Ca) from the major lithologies of the basin restricts the use of dissolved Sr in rivers as an index to derive silicate and carbonate erosion rates of their basins.

Table 2: Temporal variations in Sr and $^{87}Sr/^{86}Sr$ in rivers.

River	Location	Sr, nM	$^{87}Sr/^{86}Sr$	Reference
Ganga	**Patna**	1017-2270	0.7224-0.7249	Krishnaswami et al. 1992
	Rajshahi	560-2710	0.7235-0.7291	Galy et al. 1999
	Rajmahal	1122-2157	-	Rai et al. 2010
Brahmaputra	**Goalpara**	670-1082	0.7187-0.7197	Krishnaswami et al. 1992
	Chilmari	320-900	0.7218-0.7413	Galy et al. 1999
	Guwahati	604-1392	0.7159-0.7180	Rai and Singh 2007
Mekong	**Da Hai**	3080-5770	0.7098-0.7104	Noh et al. 2009
Orinoco	-	132-312	0.7175-0.7199	Palmer and Edmond 1989
Yukon	-	1116-2390	0.7136-0.7139	Palmer and Edmond 1989
Red	**Phu Tho**	1158-1413	0.7121-0.7128	Moon et al. 2007

The $^{87}Sr/^{86}Sr$ of the major rivers ranges from 0.7089 to 0.7291 (Table 1) with the highest value for the Ganga and the lowest for the Danube. The $^{87}Sr/^{86}Sr$ of rivers is determined by the mixing proportion of Sr contributed predominantly by silicates and carbonates in the catchment. The Sr isotopic composition of sedimentary carbonates is fairly well established and is generally unradiogenic, in the range of 0.705-0.709 (Veizer 1989; Allegre et al. 2010). Metamorphic alteration of carbonates however, can make their $^{87}Sr/^{86}Sr$ far more radiogenic, as has been observed in some of the carbonates from the Himalaya (Singh et al. 1998; Bickle et al. 2001). The limited range in $^{87}Sr/^{86}Sr$ of carbonates is in contrast to the Sr isotope composition of silicates which show a very wide range, from unradiogenic volcanic rocks to highly radiogenic granites and gneisses such as those from the Himalaya (Singh et al. 1998, 2008; Dalai et al. 2003). The $^{87}Sr/^{86}Sr$ of silicates in the drainage basin is often reflected in the isotopic composition of dissolved Sr in rivers draining them. The recent compilation of $^{87}Sr/^{86}Sr$ of dissolved Sr from large scale drainage regions (Peucker-Ehrenbrink et al. 2010) shows an overall increasing trend with bed rock ages of the region.

The Sr flux weighted $^{87}Sr/^{86}Sr$ for the global river is 0.7117 (based on data in Table 1), consistent with the value of 0.7119 (Palmer and Edmond 1989), but marginally more radiogenic than the values of 0.7114 and 0.7111 reported by Vance et al. (2009) and Peucker-Ehrenbrink et al. (2010). Analogous to Sr concentration, $^{87}Sr/^{86}Sr$ of rivers also show significant seasonal variations (Table 2). This can result from variations in the relative contribution of Sr from silicates and carbonates and/or from different tributaries. Whatever may be the cause for such variations, they highlight the need for long term monitoring of rivers along with their discharge to obtain representative global riverine Sr concentration and $^{87}Sr/^{86}Sr$.

The Sr elemental and isotopic data for the major rivers listed in Table 1 show distinctly high $^{87}Sr/^{86}Sr$ with moderate Sr concentration in the Ganga-Brahmaputra Rivers compared to the others. Identifying the source for the high $^{87}Sr/^{86}Sr$ in these rivers has been a topic of investigation and debate over the last few decades (Section 2.4.1.1.). The discharge weighted Sr concentration for the nine Himalayan-Tibetan rivers listed in Table-1 is 1.96 μM with a flux weighted $^{87}Sr/^{86}Sr$ of 0.7118. These rivers account for ~21% of global riverine Sr flux, disproportionately higher compared to their contribution to water discharge (~10 %).

2.3.2. Nd and ε_{Nd}

Studies on the concentration of dissolved Nd in rivers (0.20-0.45 μm filtered) and its isotopic geochemistry are limited compared to those of Sr. Initial studies of Nd concentration in river waters showed that it varies widely, from 0.02 to 21.8 nM, with a discharge-weighted average value of 0.28 nM for the global river (Goldstein and Jacobsen 1987). The concentration of Nd in these rivers was found to be inversely correlated with their pH and (Na+Ca) abundances; relationships that underscore the importance of water chemistry in determining the Nd concentration of rivers. Further, the measurements of Sm in these rivers indicated that its geochemical behavior is similar to that of Nd, though there was a minor fractionation between them. The Sm/Nd in solution was marginally higher (~10%) compared to that in suspended phases, suggestive of preferential release of Sm to solution. There was also a hint that the fractionation increased with pH, likely due to greater stability of Sm-carbonate complexes. The importance of pH in determining the abundances and fractionation of REEs in the dissolved load of rivers was also brought out in the studies of Gaillardet et al. (1997) in rivers of the Amazon basin and Tricca et al. (1999) for mature rivers of the Rhine valley. Some of the subsequent studies have provided an alternative explanation for the pH-REE relationship. Ingri et al. (2000) in their investigations of Kalix River observed that La concentrations are strongly correlated with DOC (dissolved organic carbon) and that high La and DOC abundances are associated with lower pH. These results led to the suggestion that DOC is the primary factor governing REE abundances in filtered river waters and that the REE-pH relation is a result of pH-DOC correlation. Subsequent studies have both supported (*e.g.* Johannesson et al. 2004; Shiller 2010) and challenged (*e.g.* Steinmann and Stille 2008) the REE-DOC relationship.

The role of colloids in contributing to REE abundances in filtered river water and its impact on REE behavior in rivers and estuaries became a topic of investigation following advances in analytical techniques for the study of colloids. Measurement of REEs in filtered river waters and their colloidal fractions (Ingri et al. 2000; Andersson et al. 2001) suggest that REEs are largely associated with colloids, with less than 5% in dissolved phase (<3 kD fraction). Both organic rich and inorganic (Fe oxyhydroxides) colloids have been suggested as potential 'carriers' of REEs. Barroux et al. (2006) and Steinmann and Stille (2008) have invoked the important role of REE-colloid interactions in determining the concentrations and fractionation of REEs in rivers. The observation that the Nd concentration in the Amazon increases linearly with water discharge led Barroux et al. (2006) to suggest that enhanced mobilization of particles and colloids during rain events can be a cause for the discharge-REE relationship. More recently, Steinmann and Stille (2008) have explained the steady increase in LREE depletion along the course of small rivers in Massif Central (France) in terms of precipitation of colloidal Fe-oxyhydroxides that preferentially scavenge LREE.

The behavior of dissolved Nd in estuaries determines the significance of rivers in contributing to the budget of Nd and its isotopes in the ocean. Investigations on the abundance and distribution of dissolved REEs in estuaries show their widespread removal in the low salinity regions due to coagulation and settling of colloids, the major carrier phase of dissolved Nd (Sholkovitz 1995; Sholkovitz and Szymczak 2000; Frank 2002; Jeandel et al. 2007; Porcelli et al. 2009). The budget of dissolved Nd and its isotopic composition in the oceans, therefore has to be supported by input from other sources such as desorption from river particulates and atmospheric dust and boundary exchange at the continental margins, among these the boundary exchange has been suggested as the dominant mode of supply (Tachikawa et al. 2003; Jeandel et al. 2007).

The ε_{Nd} values for rivers also show a wide range (-44 to +7) with a global Nd flux weighted riverine average of -8.4 (Goldstein and Jacobsen 1987). The ε_{Nd} of river water is often found to be similar to that of the bedrocks in their basin, and therefore correlates with the age of the rocks (Goldstein and Jacobsen 1987; Peucker-Ehrenbrink et al. 2010). There are however, minor differences in the ε_{Nd} values of dissolved and suspended loads of rivers, most likely a result of preferential weathering of phases with different Sm/Nd and ε_{Nd}. The ε_{Nd} of rivers shows an inverse relation with $^{87}Sr/^{86}Sr$ resulting from Nd and Sr isotope composition of rocks being weathered and mixing of various end members with different ε_{Nd} and $^{87}Sr/^{86}Sr$.

2.4. Silicate Erosion in River Basins

2.4.1. Contemporary Silicate Erosion in the Ganga-Brahmaputra System

Silicate weathering on land is a fundamental process that determines the supply of materials derived from crustal silicates to the oceans. This process is driven primarily by CO_2, making silicate weathering an important regulator of CO_2 budget over million year time scales and a key component of global carbon cycle. Therefore, changes in silicate weathering rates on long time scales can affect the atmospheric CO_2 budget and hence global climate. Recognizing the importance of silicate weathering on the exogenic cycles of elements, global carbon cycle and climate, there have been a number of investigations to determine silicate erosion rates (SER) and the factors regulating it. These investigations have been based both on small streams which by and large drain mono-lithologic terrains and large river systems which integrate contributions from their tributaries draining different lithologies. The studies on small streams are an approach to derive mineral weathering rates in natural settings, whereas larger river basins provide estimates of regional silicate erosion. The studies on large river basins, particularly those draining young orogenic belts such as the Himalaya have also been motivated by the hypothesis (Raymo et al. 1988; Raymo and Ruddiman 1992; Ruddiman 1997) that enhanced silicate weathering in this mountain belt can be the driver of global cooling during the Cenozoic, as the conducive monsoon climate, high relief and intense physical erosion of the region all can significantly enhance silicate weathering and associated atmospheric CO_2 drawdown. The steady increase in the Sr isotope composition of the oceans during the Cenozoic (Fig. 6) has been suggested as a major support for the tectonics-weathering-climate hypothesis (Raymo and Ruddiman 1992; Richter et al. 1992. Based on the present day Sr concentration and its isotopic composition of rivers draining the Himalayan-Tibet region), it is argued that the observed steady increase in the marine $^{87}Sr/^{86}Sr$ can result from silicate weathering in this region. This hypothesis invokes the use of Sr isotope composition of seawater as a proxy of silicate weathering on the continents. This suggestion has been a topic of debate as diverse and at times controversial sources have been proposed for Sr and its isotopes in rivers of the Himalaya (Edmond 1992; Krishnaswami et al. 1992; Palmer and Edmond 1992; Blum et al. 1998; Jacobson and Blum 2000; Bickle et al. 2001). If, however, the use of Sr isotopes as a proxy of silicate weathering is validated, it would also serve as a tool to investigate its past variations which are difficult to determine using other approaches.

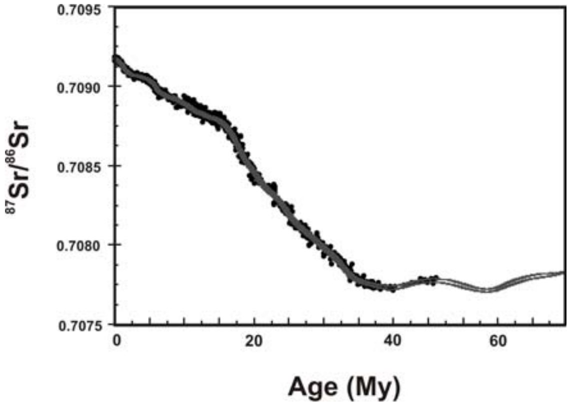

Figure 6: *Evolution of seawater $^{87}Sr/^{86}Sr$ since the last 70 My. Intense chemical weathering in the Himalaya is suggested as a potential cause for the steady increase in $^{87}Sr/^{86}Sr$ since 40 My (Raymo and Ruddiman 1992). Figure modified from Ravizza and Zachos 2003.*

The determination of contemporary SER relies on the chemical and isotopic composition of rivers. The chemistry of rivers is dominated by contributions from various lithologies of river basins and the kinetics of rock-water interaction. From the measured concentrations, the contributions from silicates, carbonates and evaporites are deduced using either the forward or the inverse model (Negrel et al. 1993; Singh et al. 1998; Galy and France-Lanord 1999; Gaillardet et al. 1999; Krishnaswami et al. 1999; Bickle et al. 2005; Singh et al. 2005; Wu et al. 2005; Hren et al. 2007; Tripathy and Singh 2010). In the forward model, Na* (Na corrected for Cl; $Na^* = Na_{riv} - Cl_{riv}$, where 'riv' refers to measured concentration in rivers) is used as an index of silicate weathering. This coupled with knowledge of release ratios of (K+Mg+Ca) to Na* from silicates in the basin to rivers is used to derive SER. The release ratios would depend on the silicate lithology of the basin and the nature of weathering (mineral specific/stochiometric) and therefore can have a wide range. In contrast, in the inverse model likely elemental ratios for various end members contributing to major cation abundances to rivers is assigned *a priori* and following the method of iteration and material balance considerations the best end member ratios that can generate the measured river water composition is derived. The removal of Ca from rivers by calcite precipitation can be a source of uncertainty in this approach. Both the forward and inverse methods have been widely used to derive contemporary SER and associated CO_2 consumption rates for various major rivers including the Ganga-Brahmaputra. The contemporary SER (calculated from the sum of cations derived from silicates and SiO_2) for the headwaters of the Ganga, Bhagirathi and Alaknanda range between 10 to 15 tons km^{-2} y^{-1} (Krishnaswami and Singh 2005), a factor of ~2-3 higher than the global average value of ~5.5 tons km^{-2} y^{-1} (Gaillardet et al. 1999). The higher SER in the headwater basins of the Ganga suggests more intense silicate erosion in these Himalayan basins (Galy and France-Lanord 1999; Krishnaswami et al. 1999). Independent estimates of SER have been obtained by France-Lanord and Derry (1997) and McCauley and DePaolo (1997) based on the deficiency in Na, K, Ca, and Mg in the Bay of Bengal sediments relative to that in crystallines of the Himalaya; these estimates generally are time-averaged values, unlike that based on river water data which are based on snap shot sampling.

2.4.1.1. Can $^{87}Sr/^{86}Sr$ be a proxy for silicate erosion?

Generally rivers draining old silicate rocks have lower Sr with higher $^{87}Sr/^{86}Sr$ compared to rivers weathering marine limestones/evaporites. The large difference in the $^{87}Sr/^{86}Sr$ among the different lithologies in the drainage basin promotes the use of Sr isotopes as a natural tracer to determine Sr contribution to rivers from various end members.

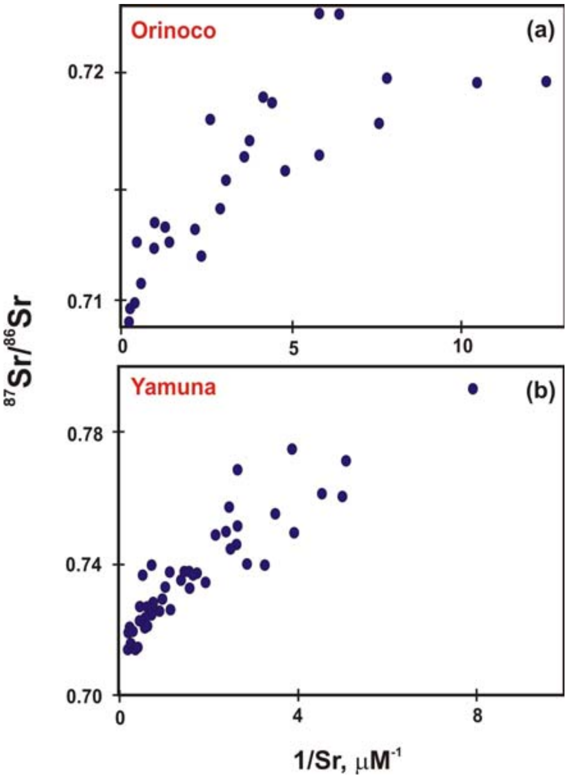

Figure 7: *Sr mixing plots for two major rivers, the Orinoco and the Yamuna headwaters. The near linear trend is suggestive of a two component mixing, the high* $^{87}Sr/^{86}Sr$ *and low Sr silicates with the low* $^{87}Sr/^{86}Sr$ *and high Sr carbonates. Figure redrawn from Palmer and Edmond 1989 and Dalai et al. 2003.*

Figures 7 (a and b) are examples of mixing plots for Sr isotopes in two river systems, the Orinoco and the Yamuna headwaters. The plots show an overall linear trend albeit some scatter, suggestive of two component mixing (Palmer and Edmond 1992; Dalai et al. 2003). From the mixing array, the Sr contribution to the rivers from the two end members can be determined if their Sr isotope composition are known and from it the SER of the basin if (Na+K+Ca+Mg)/Sr release ratios are known. Estimates of these release ratios are available based on different approaches and models (***e.g.*** Krishnaswami et al. 1999), however as mentioned earlier they are not well constrained. More importantly, such calculations generally assume that the high $^{87}Sr/^{86}Sr$ end member is silicates; ascertaining the validity of this assumption is critical to the application of $^{87}Sr/^{86}Sr$ as proxy for silicate weathering. Krishnaswami et al. (1992) and Dalai et al. (2003) based on the widespread occurrence of crystallines with highly radiogenic Sr isotope composition (~ 0.75-1.0) in the drainage basins of the headwaters of the Yamuna and the Ganga and the strong correlation between "silicate indices" and $^{87}Sr/^{86}Sr$ of these rivers (Fig. 8) suggested that the high $^{87}Sr/^{86}Sr$ end member is indeed silicates of the drainage basin. However, the occurrence of metamorphic carbonates and vein calcites in these river basins with highly radiogenic $^{87}Sr/^{86}Sr$ similar to that of the crystallines and considering that carbonates are more easily weatherable compared to silicates has challenged the assignment of high $^{87}Sr/^{86}Sr$ end member to silicates. These studies instead suggest that the metamorphosed carbonates and vein calcites to be the dominant sources of high $^{87}Sr/^{86}Sr$ to the rivers in the Himalaya (Palmer and Edmond 1992; Blum et al. 1998; Quade et al. 1997; Harris et al. 1998; Jacobson and Blum 2000; Oliver et al. 2003). Attempts to test the different components of this hypothesis have resulted in contrasting conclusions. Singh et al. (1998) measured Sr isotopic composition of Pre-Cambrian carbonates from the Lesser Himalaya to assess their role in contributing to the high $^{87}Sr/^{86}Sr$ of the Ganga-Yamuna source waters. Their results, though brought out the important role of metamorphism in considerably elevating the $^{87}Sr/^{86}Sr$ of these sedimentary carbonates locally, suggested that their weathering is unlikely to be a major source for the high $^{87}Sr/^{86}Sr$ to the headwaters of the Ganga on a basin wide scale. The results of Bickle et al. (2005) on the Sr isotopic composition of the Ganga headwater basins also show that it is dominated by contribution from weathering of silicates (~50 % of total Sr) with the balance from trace calcites (~10 %) and sedimentary carbonates (~35 %). In contrast, the work of Oliver et al. (2003) brought out the major role of metasedimentary carbonates as the source of elevated $^{87}Sr/^{86}Sr$ to the sub-tributaries of the Ganga (Bhote Kosi-Sun Kosi, Nepal). Their work based on downstream variations in the chemistry and $^{87}Sr/^{86}Sr$ of rivers and mass balance considerations demonstrated that the Paleo-Proterozoic impure carbonates with highly radiogenic Sr isotope composition are the significant contributor to the high $^{87}Sr/^{86}Sr$ of the Ganga river, accounting for a major fraction of their supply to the marine $^{87}Sr/^{86}Sr$. Thus, the available results on Sr isotope composition of metamorphosed carbonates from the Himalaya and their interpretation have led to diverging views on their role as a major source of high $^{87}Sr/^{86}Sr$ to the Ganga river on a basin wide scale.

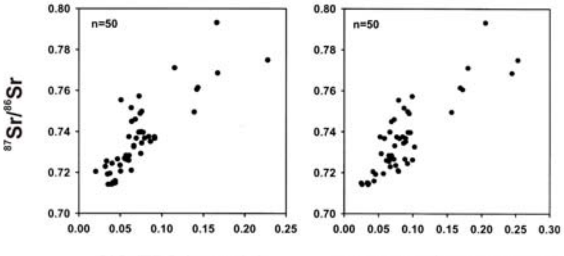

Figure 8: *Scatter diagrams of* $^{87}Sr/^{86}Sr$ *with other "silicate indices" (SiO_2/TDS and (Na*+K)/TZ$^+$) in the Yamuna headwaters. The good correlation between them has been interpreted to suggest that the high* $^{87}Sr/^{86}Sr$ *end member in these rivers is of silicate origin and that* $^{87}Sr/^{86}Sr$ *can serve as a proxy of silicate weathering. Figure from Dalai et al. 2003.*

In addition to metamorphosed carbonates, the significance of disseminated carbonates and vein calcites as sources of highly radiogenic Sr to the Ganga river also have been investigated. For example, Sr isotope studies (Jacobson et al. 2002) on glacial moraine chronosequences from the Himalaya containing trace carbonates demonstrated that their weathering can be a significant source of Ca, Sr and radiogenic Sr to rivers for thousands of years subsequent to their exposure. In addition, as mentioned earlier, there are also results which suggest that vein calcites in granites of the Himalaya can be an important source of Ca and Sr with high $^{87}Sr/^{86}Sr$ (Blum et al. 1998).

It is thus evident from the available results and interpretation that both silicates and carbonates can contribute to the high $^{87}Sr/^{86}Sr$ of the Ganga-Brahmaputra Rivers. However, their relative significance to the Sr isotope budget remains to be established quantitatively. This information is essential to decide on the applicability of Sr isotopes as a proxy of silicate erosion, one of the bases of the tectonics-weathering-climate hypothesis.

2.4.2. Seawater $^{87}Sr/^{86}Sr$ record during the Cenozoic: Impact of weathering in the Himalaya and Deccan Traps

Chemical weathering of continental crust and the supply of its products to the ocean is a key process regulating its chemical and isotopic evolution through time. The chemical and isotopic composition of the authigenic and biogenic components of marine sediments holds clues to temporal variations in continental inputs to the sea. Among these the Sr isotope records hold promise to retrieve continental weathering history.

The evolution of seawater Sr isotopic composition can be expressed using a balance equation involving the various Sr supply and removal terms. Early attempt in this direction was made by Brass (1976) to explain the variations in the oceanic $^{87}Sr/^{86}Sr$ over the past ~400 My based on changes in $^{87}Sr/^{86}Sr$ input from weathering of silicates and carbonates on continents. These mass balance calculations showed that the variations in seawater $^{87}Sr/^{86}Sr$ since the last 200 My can be attributed to changes in the $^{87}Sr/^{86}Sr$ supplied to the ocean from weathering of silicates on land; the ratio being dependent on the proportion of radiogenic Sr from old acidic rocks and unradiogenic Sr from young basic rocks. The mixing proportion of Sr from these two silicate lithologies can vary depending on their exposure to weathering which in turn is governed by processes such as tectonics/glaciation.

The Sr isotope evolution of the ocean was investigated in great detail during 1970-1990 which resulted in a robust and dense record of $^{87}Sr/^{86}Sr$ in marine carbonates since the Cenozoic (Fig. 6; Veizer 1989). Richter et al. (1992) based on these data developed a model to test the hypothesis (Raymo et al. 1988; Raymo and Ruddiman 1992) that silicate weathering in the Himalaya-Tibet (HT) is the primary factor contributing to the steady increase in the Sr isotope composition of the oceans during this period. In this model, the marine budget of Sr and its isotopes are determined by their supply from rivers, hydrothermal sources and diagenetic alteration/dissolution of carbonates from sediments and their removal to ocean floor *via* calcareous skeletons. Among the three input sources, Sr flux from diagenetic alteration/dissolution of carbonates is much less than the fluxes from the other two sources (Richter et al. 1992; Banner 2004) and therefore as an approximation this term is often neglected from the budget calculations. The mass balance equation for the rate of change of marine Sr isotope ratio is:

$$N\frac{dR_{SW}}{dt} = J_r(R_r - R_{SW}) + J_h(R_h - R_{SW}) \quad \text{----(1)}$$

where N is total Sr (in moles) in the ocean. J_r and J_h are the flux (moles/y) of Sr from the riverine and hydrothermal sources. R_{sw}, R_r and R_h are the $^{87}Sr/^{86}Sr$ of seawater, river and hydrothermal sources respectively. Equation (1) suggests that the $^{87}Sr/^{86}Sr$ of seawater is governed by the balance between supply of radiogenic Sr from rivers and unradiogenic mantle like Sr derived from hydrothermal sources. In the above equation the temporal changes in J_r, R_r and J_h are not known, though J_h is often assumed to be proportional to ocean floor production (Richter et al. 1992). The variations in either J_r or R_r or both can bring about changes in R_{sw} (Edmond 1992; Krishnaswami et al. 1992; Richter et al. 1992; Derry and France-Lanord 1997; McCauley and DePaolo 1997; Kump et al. 2000; Gaillardet 2008). Increase in J_r (riverine flux) would imply more intense continental weathering (Raymo et al. 1988) whereas increasing R_r would suggest change in the source material being weathered (Edmond 1992; Derry and France-Lanord 1997; Kump et al. 2000). Therefore to determine variations in the intensity of continental weathering, information on changes in R_r is required. These data are generally unavailable and therefore the equation is solved using reasonable assumptions. Richter et al. (1992) by solving equation (1) with the then available data on contemporary fluxes and ratios (Table 3) showed that the increase in the $^{87}Sr/^{86}Sr$ of seawater since the past ~40 My is due to enhanced supply of Sr and $^{87}Sr/^{86}Sr$ by rivers and that increase in both J_r and R_r are required to balance the evolution of R_{sw}. In their calculations they also evaluated the impact of temporal variations in J_h on the evolution of seawater $^{87}Sr/^{86}Sr$ and concluded that though changes in J_h could explain about half the change in R_{sw}, the evolutionary trend was not consistent with the observations.

Table 3: Numerical **(**Present day) values of various parameters used in seawater Sr budget model (Richter et al. 1992).

Parameter		
J_r	Riverine flux	3.3×10^{10} mol/y
J_h	Hydrothermal alteration flux	0.82×10^{10} mol/y
J_d	Digenetic flux	~0
J_{r0}	Riverine flux excluding HT rivers	2.2×10^{10} mol/y
J_{r1}	HT riverine flux	7.7×10^{9} mol/y
N	Total Sr in Ocean	1.25×10^{17} mol
R_r	Riverine $^{87}Sr/^{86}Sr$	0.711
R_h	Hydrothermal $^{87}Sr/^{86}Sr$	0.7030
R_d	Digenetic $^{87}Sr/^{86}Sr$	0.7084
R_{r0}	$^{87}Sr/^{86}Sr$ global rivers excluding HT rivers	0.710
R_{r1}	$^{87}Sr/^{86}Sr$ of HT rivers	0.7127

To further evaluate the role of Himalayan-Tibetan (HT) rivers on $^{87}Sr/^{86}Sr$ of oceans, the river water flux and Sr isotopic ratio terms in the above equation is split into two parts, one representing global rivers excluding those from HT and the other representing the extra flux (J_{r1}) with $^{87}Sr/^{86}Sr$, R_{r1} required to explain the observed variation in seawater Sr evolution (Richter et al. 1992). The modified equation is:

$$N\frac{dR_{SW}}{dt} = J_{ro}(R_{ro} - R_{SW}) + J_{r1}(R_{r1} - R_{SW}) + J_h(R_h - R_{SW}) \quad \text{----(2)}$$

where, J_{ro} and R_{ro} are the Sr flux and $^{87}Sr/^{86}Sr$ from the global rivers excluding those from the HT. The calculations showed that the Sr flux (J_{r1}) required to reproduce the sea water $^{87}Sr/^{86}Sr$ curve using present day value of R_{rl} is roughly consistent with that measured indicating that the HT rivers can be a dominant source to account for the marine Sr isotope evolution during the past ~40 My. These calculations and inferences derived from them rely on the compilation of riverine Sr flux and $^{87}Sr/^{86}Sr$ (*c.f.* Table 1), which as mentioned earlier can be subject to uncertainties arising from intra and inter-annual variations in Sr concentration and $^{87}Sr/^{86}Sr$ of rivers, water discharge and inadequate sampling of rivers from various major lithologies. These results and therefore the conclusions based on them maybe subject to revision as more robust data on Sr concentration of rivers and its isotopic composition become available. For example, subsequent to the work of Richter et al. (1992) there have been more measurements of Sr and $^{87}Sr/^{86}Sr$ in the HT rivers, particularly in the Ganga and the Brahmaputra during various seasons including peak discharge. These results show that the dissolved Sr concentration of the Ganga is much lower during peak discharge (0.56 μM; Galy et al. 1999) than the value used by Richter et al. (1992) in their model (1.58 μM), the corresponding $^{87}Sr/^{86}Sr$ values also being significantly different (0.7257-0.7291). The Brahmaputra at its mouth also exhibits a similar difference in its Sr concentration with a value of 0.32 μM (Galy et al. 1999) during peak flow compared to 0.93 μM used in the model (Richter et al. 1992). Considering that much of the annual water discharge of the Ganga (~75%) is during its peak flow, the Sr concentration measured during this period is likely to be more representative of its annual average concentration. Using this value for the Sr concentration of the Ganga yields a Sr flux weighted ^{87}Sr/^{86}Sr ratio of 0.7118 for the HT rivers, very close to ^{87}Sr/^{86}Sr of global rivers 0.7117 and lower than 0.7127, used in the model calculations (Richter et al. 1992). The use of the revised ^{87}Sr/^{86}Sr of the HT rivers in the model calculation suggest that the Sr flux (J_{r1}) required from the HT rivers would be significantly higher than the estimates of Richter et al. (1992) and their contemporary measured flux (Table 1). These observations underscore the importance of regular monitoring of rivers to obtain representative values for the annual average Sr concentration and ^{87}Sr/^{86}Sr.

The inferences of Richter et al. (1992) can be used to deduce the weathering history of continents if data on temporal variations of either J_r or R_r are available. Derry and France-Lanord (1996) obtained ^{87}Sr/^{86}Sr data for the Ganga during the past ~20 My based on Sr isotope record of the Ganga floodplain as preserved in the pedogenic clays of the Bay of Bengal sediments. The results showed significant temporal changes in the Sr isotopic ratio of the Ganga with highly radiogenic ratios during 1-7 My (~0.74) compared to ~0.72 during 0-1 and 7-20 My periods. The higher ^{87}Sr/^{86}Sr during 1-7 My requires a decrease in the riverine Sr flux during this period to balance the Sr isotope data of the oceans. This led to the suggestion that increase in ^{87}Sr/^{86}Sr of oceans need not be driven by a concomitant increase in riverine Sr flux and therefore continental weathering. Quade et al. (1997) also observed that the Sr isotopic composition of Himalayan rivers (Ganga, Indus) had varied with time based on ^{87}Sr/^{86}Sr of shells and paleosol carbonates from the Siwaliks, further attesting to the idea that the Sr isotope evolution of the oceans can be a result of variations in source composition.

Another recent development on Sr budget in the oceans is the finding that its hydrothermal flux is much less than that estimated earlier (~1.0×10^{10} mol/y; Palmer and Edmond 1989) and that the current estimate can support only about a third or less of Sr required to balance its budget in the oceans (Davis et al. 2003). This imbalance in the marine Sr budget therefore, requires that there has to be additional major source (s) of unradiogenic Sr to the oceans. Investigations on chemical weathering rates, Sr concentration and ^{87}Sr/^{86}Sr of rivers, groundwater and hydrothermal sources in volcanic islands and island arcs (Rad et al. 2007; Allegre et al. 2010) suggest that supply from these regions can be the 'missing source' of unradiogenic Sr to the oceans. Budget model for present day oceanic ^{87}Sr/^{86}Sr shows that hydrothermal sources contribute only ~27% of mantle-like unradiogenic Sr to the sea compared to ~73% from island arcs and volcanic islands (Allegre et al. 2010). Temporal variation in the Sr concentration from these sources to the sea can also impact the Sr isotope evolution of the ocean; however there is no data to evaluate this.

Analogous to the studies on the role of HT rivers on the ^{87}Sr/^{86}Sr of the oceans, the impact of weathering Deccan trap basalts was also assessed using data from rivers flowing through them and suitable models (Dessert et al. 2001; Das et al. 2006). The results of Dessert et al. (2001) showed an increase in seawater ^{87}Sr/^{86}Sr from 0.70782 to 0.70789 over a period of a few My after the Deccan eruption followed by a steady decrease. The initial increase was explained in terms of enhanced continental weathering by CO_2 (and hence temperature) released during the emplacement of the Deccan basalts. The subsequent decrease in the seawater ^{87}Sr/^{86}Sr is attributed to a combined effect of contribution of unradiogenic Sr from the weathering of Deccan basalts and decrease in atmospheric CO_2 which decreases continental weathering. Das et al. (2005; 2006) carried out major ion and Sr isotope studies on several rivers exclusively draining the Deccan Traps to investigate the role of their weathering on the evolution of marine ^{87}Sr/^{86}Sr at around K-T boundary and early Tertiary. Their results and model calculations showed that the supply of unradiogenic Sr from the Deccan basalt weathering caused the decline in seawater ^{87}Sr/^{86}Sr during the early Tertiary. As basalts are a source of unradiogenic Sr to the oceans, changes in their Sr contribution relative to that from old sialic rocks can modify the riverine ^{87}Sr/^{86}Sr which in turn can affect the Sr isotope composition of the oceans (Brass 1976; Taylor and Lasaga 1999). Such a relative change in weathering of silicate lithology can also bring about changes in oceanic ^{87}Sr/^{86}Sr without invoking changes in the intensity of chemical weathering on continents (Taylor and Lasaga 1999).

Thus, many of the above studies bring out the potential of Sr isotopes in oceans and rivers to provide information on contemporary and past global chemical weathering patterns and the role of weathering in the Himalaya and Deccan traps in contributing to the Sr isotope evolution of the oceans since the Cenozoic. The potential of Sr isotopes as a proxy of silicate weathering in the Himalaya however awaits quantitative information on the role of radiogenic carbonates as a source riverine ^{87}Sr/^{86}Sr and temporal variations in riverine ^{87}Sr/^{86}Sr.

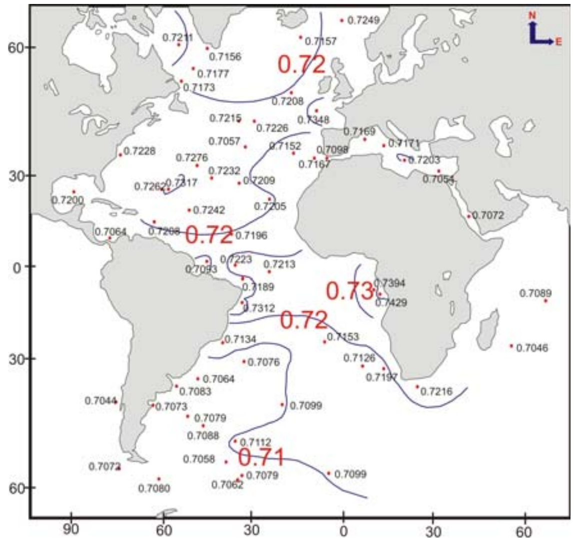

Figure 9: *^{87}Sr/^{86}Sr of Atlantic surface sediments. The ratio shows significant spatial variations which has been used to infer their provenances. Figure redrawn from Dasch 1969.*

3. PHYSICAL EROSION IN RIVER BASINS

Physical erosion is a key process that determines the geomorphology of the earth surface and chemical weathering intensity of river basins. The records of physical erosion contained in sediments hold clues to the spatial and temporal erosion pattern of the source region and its dependence on climatic and tectonic factors (***e.g.***, Dia et al. 1992; Asahara et al. 1999; Burbank et al. 2003; Singh et al. 2008; Rahaman et al. 2009; Galy et al. 2010). Over the years there have been a number of studies both in river and marine basins to decipher these patterns by tracking the sediment provenances through their geochemical, mineralogical and isotopic composition. The successful application of these proxies require their source signatures to be well preserved in the sediments, a requirement that has met with challenges because of chemical weathering of source rocks and size sorting of sediments. Many of the initial studies on sediment provenances were based on clay mineralogy. The clay minerals provide information more on their weathering provenances than their geological provenances (Dasch 1969) as they are the end products of chemical weathering of minerals present in source rocks.

Historically, the use of Sr isotopes as a proxy for sediment provenance was recognized and demonstrated during the 60's (Dasch 1969). The detailed study of spatial distribution of ^{87}Sr/^{86}Sr in surface sediments of the Atlantic (Dasch 1969; Fig. 9) showed large variations which were interpreted in terms of differences in their provenances. During the last few decades, radiogenic isotope ratios particularly ^{87}Sr/^{86}Sr and ε_{Nd} of sediments have often found applications as tracers to track the provenance of sediments (Goldstein and O'Nions 1981; France-Lanord et al. 1993; Winter et al. 1997; Pierson-Wickmann et al. 2001; Banner 2004; Yang et al. 2007; Singh et al. 2008; Viers et al. 2008; Ahmad et al. 2005, 2009; Galy et al. 2010). These isotope systems serve as reliable proxies for sediment provenance studies because of their distinctly different isotopic composition in different sources and the near preservation of the source isotope composition during weathering and transport. Processes that can affect the preservation of source isotope composition in sediments are chemical weathering and sediment transport. These processes are likely to influence the preservation of ^{87}Sr/^{86}Sr more than that of ^{143}Nd/^{144}Nd because (i) generally the isotopic composition of Nd is relatively more uniform among the minerals in the parent rock compared to ^{87}Sr/^{86}Sr as the fractionation between Sm and Nd is significantly less compared to Rb and Sr during mineral formation. Therefore, preferential dissolution of specific minerals during chemical weathering though can influence the preservation of source isotope composition of both Sr and Nd, the impact is likely to be more on ^{87}Sr/^{86}Sr and (ii) during transportation of sediments size sorting is common; if this results in mineralogical differences in the various size fractions, then the isotope composition of the sediment may differ from that of the source rock. Here again, the influence is likely to be more on ^{87}Sr/^{86}Sr because of its wider range among various minerals present in a parent rock compared to ε_{Nd}. Studies of soil profiles (*c.f.* Section 2.2.) and sediments (Tutken et al. 2002) have provided evidences for alteration of isotopic composition of source rock during weathering and transport (Fig. 10). These data indicate that between ^{87}Sr/^{86}Sr and ε_{Nd}, the later is less susceptible for alteration during weathering and transportation making it a more robust tracer for fingerprinting the provenance of sediments (Walter et al. 2000). Such differences in the behavior of Sr and Nd isotopes during weathering and transport have led to combine studies of Sr-Nd isotope systematics in sediments to derive more detailed information on sediment provenances and related sedimentary processes (*e.g.* Colin et al. 1999; Walter et al. 2000; Tutken et al. 2002; Singh et al. 2008).

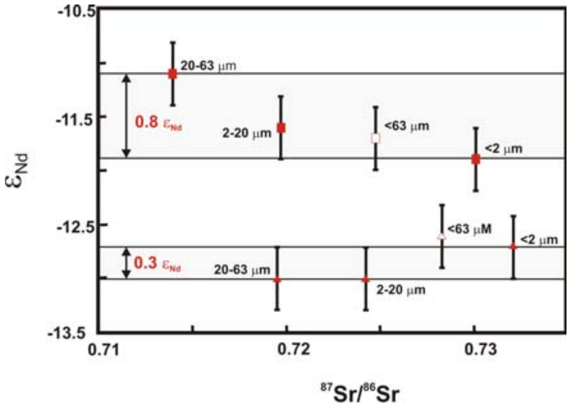

Figure 10: *Sr and Nd isotopic ratios in different size fractions separated from two Arctic sediment cores. The ^{87}Sr/^{86}Sr shows significant variation with size whereas ε_{Nd} is relatively constant. Figure modified from Tutken et al. 2002.*

Sr and Nd isotope compositions of riverine and marine sediments though are being used often to track their provenances, there are lingering questions about how well the source isotope signatures are preserved in them. Therefore to make the interpretation more robust preference should be for the use of multi-tracer approaches involving isotopic and chemical/mineralogical composition of sediments. Such approaches can also help in determining the factors contributing to the changes in the isotopic, chemical and mineralogical composition of sediments (France-Lanord et al. 1993; Colin et al. 1999; Singh and France-Lanord 2002; Viers et al. 2008).

3.1. Contemporary physical erosion pattern of River Basins in the Himalaya

The rate of physical erosion of river basins of the Himalaya, particularly the Ganga and the Brahmaputra is a topic of investigation in recent years because of their importance to the sediment budget of the ocean, the global carbon and geochemical cycles of various elements and to understand the physical erosion pattern of their sub-basins and their controlling factors.

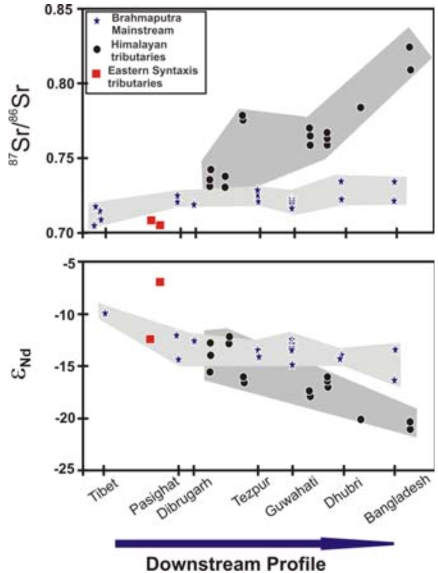

Figure 11: *Spatial variations in ^{87}Sr/^{86}Sr and ε_{Nd} of sediments of the Brahmaputra river system. The Sr-Nd isotopic signatures of the Brahmaputra mainstream sediments down stream Pasighat remains nearly uniform. Figure redrawn from Singh and France-Lanord 2002.*

Singh and France-Lanord (2002) and Singh et al. (2008) investigated the Sr-Nd isotopic composition of bank and suspended sediments of the Brahmaputra and the Ganga plain along with those of their tributaries to determine the sources of sediments to the main stream and their relative contributions. The Brahmaputra mainstream receives sediments from three sources, the Trans-Himalayan plutonic belt, the Lesser and the Higher Himalaya. The Sr-Nd isotopic composition of the Brahmaputra sediments is nearly uniform all along its course in the plain downstream Pasighat, in spite of contributions from the Himalayan tributaries with a wide range of Sr and Nd isotope composition (Fig. 11). This uniformity in ε_{Nd} and ^{87}Sr/^{86}Sr suggests that the sediment contributions from the Siang, draining the Eastern Syntaxis of the Himalaya and southern Tibet (Tsangpo) overwhelm that from other sources. Material balance calculations based on isotope data show that about half of the sediments of the Brahmaputra at its outflow are from the Siang resulting in intense localised erosion. Thus the sediment flux of the Brahmaputra is dominated by the Eastern Syntaxis "hot spot" where the physical erosion is controlled by runoff and relief (Singh and France-Lanord 2002; Singh 2006, 2007).

Subsequently, similar studies in the Ganga mainstream sediments and its tributaries show that their ^{87}Sr/^{86}Sr and ε_{Nd} values are close to or by and large within the range reported for the Higher Himalayan Crystallines (HH, Fig. 12). The Sr and Nd isotope mass balance of these sediments on the basis of a two component (Higher and Lesser Himalayan Crystallines) mixing suggests that the HH account for more than two thirds of the contemporary Ganga Plain sediments (Fig. 12), consistent with the results from sediments of the Bay of Bengal (France-Lanord et al. 1993; Derry and France-Lanord 1997; Galy et al. 2010). More interestingly, the Sr isotopic composition of the Ganga sediments showed significant spatial variation along the plain with a drastic decrease from 0.768 to 0.755 immediately following the confluence of the Ganga with the Gandak (Fig. 13). A similar feature was also recorded in the spatial distribution of ε_{Nd}. Budget calculations based on the isotopic composition of these sediments show that the Gandak sub-basin which occupies only ~5% of the total drainage area of the Ganga, accounts for about half of the of the Ganga sediments at its outflow. These results bring out the intense physical erosion of the Gandak basin due to the high relief and focused precipitation over its headwater basins in the Himalaya (Singh et al. 2008). This observation highlights the coupling between high rainfall and relief and high physical erosion rate of river basins, linking climate (rainfall) and tectonics (relief) with contemporary erosion pattern of the Himalaya.

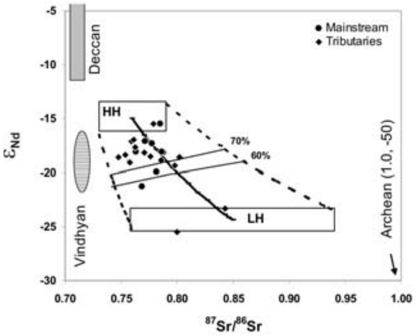

Figure 12: *Sr-Nd isotope mixing plot of river sediments from the Ganga plain. The isotopic composition of these sediments is interpreted in terms of a two component mixing, HH and LH. The isotopic compositions of sediments in their finer fractions (<4μm; triangles) and various other end members which can contribute to the Ganga sediments are also shown. Figure from Singh et al. 2008.*

The Sr and Nd isotope studies of sediments from various sub-basins of the three major global rivers draining the Himalaya, the Brahmaputra, the Ganga and the Indus show that physical erosion rates are quite high in sub-basins characterized by intense precipitation over regions of high relief, the Gandak, the Siang, and the Nanga-parbat (Leland et al. 1998; Clift et al. 2002; Singh and France-Lanord 2002; Singh 2006; Singh et al. 2008) and that the sediment fluxes of these major rivers are dominated by contributions from these "hot spots" of physical erosion. Such high and focused erosion in these hot spots is unloading huge amount of sediments from the Himalaya causing regions around them to uplift more rapidly compared to other regions (Molnar and England 1990; Montgomery 1994; Zeitler et al. 2001). Importantly, these results underscore the coupling among tectonics, climate and physical erosion. Further as physical and chemical erosion are linked (Bluth and Kump 1994; Edmond and Huh 1997; Gaillardet et al. 1999; Millot et al. 2002; Singh et al. 2005) these hotspots could also facilitate intense chemical weathering by continuously exposing 'fresh' rock surfaces.

3.2. Paleo-erosion in selected River basins of the Himalaya and its controlling factors

3.2.1. Shorter time (ky) scales

One of the key topics of interest in studies of physical erosion is its temporal variations and factors contributing to it. In this regard there have been a number of investigations in recent years to decipher the physical erosion history of the Himalaya and its link to tectonics and climate using river and marine sediments of Himalayan origin.

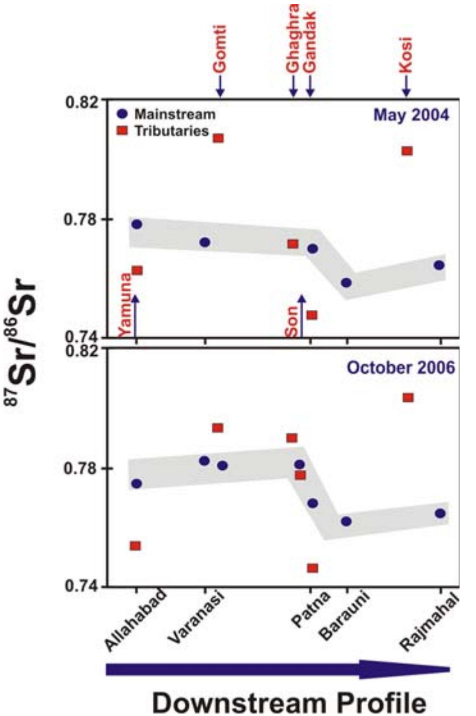

Figure 13: *Spatial variations (along the Ganga mainstream) in $^{87}Sr/^{86}Sr$ and ε_{Nd} of sediments from the Ganga and its tributaries. A major dip in the Sr isotopic ratio of the Ganga sediments is seen after the confluence of the Gandak, suggesting dominant supply of sediments to the Ganga mainstream from this tributary. Figure from Singh et al. 2008.*

Rahaman et al. (2009) derived temporal variations in the physical erosion pattern of the Ganga basin from depth profiles of Sr and Nd isotopes in the silicate fraction of a dated sediment core from the Ganga Plain. Both $^{87}Sr/^{86}Sr$ and ε_{Nd} exhibited significant variations with depth in the core, the range in their values, however, were bound by those for the Higher and the Lesser Himalayan Crystallines, the two major sediment sources to the Ganga plain. This led to the suggestion that the observed depth variations were due to differences in the mixing proportion of sediments from the Higher and Lesser Himalaya. Furthermore, the results also showed two major excursions in the Sr-Nd isotope composition at approximately 20 and 70 ky (Fig. 14), which were attributed to a decrease in the proportion of sediments from the Higher Himalaya caused by decrease in monsoon precipitation and an increase in glacial cover both of which result from lower solar insolation. Thus, the temporal variations in the relative sediment flux from the Higher and Lesser Himalaya were attributed to climate variability.

Colin et al. (1999; 2006) used Sr and Nd isotope composition along with clay mineralogy to constrain sediment sources to the Bay of Bengal and the Andaman Sea, to reconstruct the erosional history of the Indo–Burman ranges and to assess the role of climate changes (monsoon rainfall variations) on erosion. The geographical (spatial) distribution of Nd and Sr isotope composition in the Bay of Bengal and the Andaman Sea suggest that these basins receive sediments from several sources; the Ganga-Brahmaputra rivers dominating the supply to the western Bay of Bengal, the Himalayan and Indo-Burman ranges to the eastern Bay and the Irrawaddy River to the Andaman Basin. The sediments of the Andaman Sea and the Bay of Bengal deposited during the last glacial maximum (LGM) are characterized by more radiogenic $^{87}Sr/^{86}Sr$ compared to interglacial sediments with roughly the same ε_{Nd} (Fig. 15). The lack of concomitant changes in the Sr and Nd isotope composition led to interpret the $^{87}Sr/^{86}Sr$ results in terms of variations in chemical weathering intensity rather than to provenance changes (see section 2.2.). The more radiogenic $^{87}Sr/^{86}Sr$ during glacial periods at the core site was attributed to efficient transport of unaltered Rb-rich minerals exposed in the head water basin of the Irrawaddy river by glacier grinding.

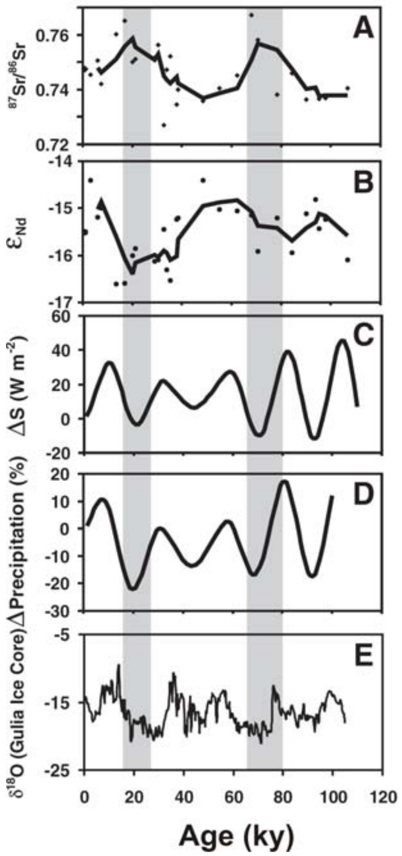

Figure 14: *Temporal variations in Sr and Nd isotopic ratios (panel A and B) of sediments from the Ganga plain during the past ~100 ky. These variations suggest relative changes in provenances (HH and LH) of the sediments and coincide with regional climatic changes (panel C: Solar insolation, panel D: Monsoon precipitation and panel E: Oxygen isotopic record of a Tibetan ice core), bringing out the role of climate on physical erosion of the Himalaya. Figure modified from Rahaman et al. 2009.*

The impact of climate variations on physical erosion in the Irrawaddy Basin was also brought out in the Sr-Nd isotope composition of sediments from a core raised from the Ninety East Ridge of the Bay of Bengal (Ahmad et al. 2005). The results showed concomitant temporal changes in $^{87}Sr/^{86}Sr$ and ε_{Nd} and that these changes overlapped with the records of Heinrich events. This led to suggest that these fluctuations in the isotope records are probably a result of relatively higher sediment contribution from the Irrawaddy river caused by intensification of NE monsoon in response to the cold events of the North Atlantic via an atmospheric teleconnection.

Analogous to the studies in the Bay of Bengal which receives sediments predominantly from the central and eastern Himalaya, there have also been investigations in the Indus delta and the Arabian Sea to decipher the erosional history of the western Himalaya. In one such study, Clift et al. (2008) observed significant temporal variations in the Nd isotope composition of sediments from the Indus delta with lesser radiogenic Nd in sediments younger than 14 ky. This suggested relatively increased sediment flux to these regions from sources with less radiogenic Nd, the Lesser and/or Greater (Higher) Himalaya compared to other sources (*e.g.* primitive arc rocks of the Indus suture and Trans-Himalaya) with LH dominating the contribution. This change in provenance of Indus sediments is attributed to change in the monsoon strength during these periods highlighting the importance of climate in regulating the erosion over western Himalaya over millennial time scales.

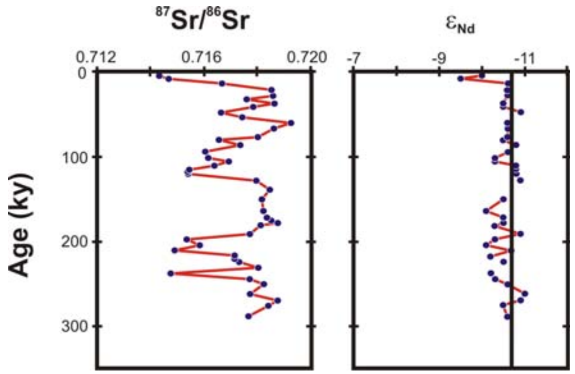

Figure 15: *Glacial-interglacial variations in Sr and Nd isotopic ratios of Andaman sea sediments. $^{87}Sr/^{86}Sr$ data show significant temporal variations, whereas ε_{Nd} is nearly uniform with depth. The straight line through ε_{Nd} data is the present-day ε_{Nd} value of the Irrawaddy river sediment. The lack of concomitant changes in $^{87}Sr/^{86}Sr$ and ε_{Nd} suggests that the variations in $^{87}Sr/^{86}Sr$ are a result of fractionation during weathering and transport rather than changes in provenance. Data Source: Colin et al. 2006.*

3.2.2. Longer time (My) scales

The Himalaya is one of the young and active mountain ranges and ranks first in the supply of sediments to the ocean (Milliman and Meade 1983; Milliman and Syvitski 1992). The temporal variation in the sediment supply from the Himalaya on million year time scales, particularly from its different sub-basins (*e.g.* Higher and Lesser Himalaya) and the factors regulating it have implications to global carbon cycle and therefore to climate. This has promoted studies on the pattern of physical erosion in the Himalaya and its variations over My time scales based mainly on Sr and Nd isotopic composition of sedimentary archives preserved in the Bay of Bengal and the Arabian Sea. In one such study, France-Lanord et al. (1993) investigated variations in the Sr and Nd isotopic ratios, together with stable isotopes and clay mineral abundances in a sediment core from the Bay of Bengal spanning 17 My time period. The results showed that the dominant source of these sediments is the Higher Himalayan Crystallines. The narrow range in Sr-Nd isotopic values of these sediments over their 17 My depositional history further suggested that their source remained nearly invariant despite significant changes in sedimentation rate, tectonic history and climate. In a more recent study, Galy et al. (2010) observed from the Sr and Nd isotopic composition of sediments deposited in the deep Bengal Fan that they were mainly derived from the High Himalaya Crystallines with sub-ordinate contributions from the Lesser Himalaya and Trans-Himalayan batholiths. Further, it was observed that the isotopic composition of sediments deposited during the recent 20 ky was very similar to that deposited during the past 12 My confirming the generally stable erosion regime of the Himalaya during this long time period. This stable erosion regime argues against any major impact on Himalayan erosion by glacier advance and retreat. The overall covariation between Sr and Nd isotope data further suggested that the isotope systematics were by and large, controlled by sediment provenances and not by changes in chemical weathering intensity. The near synchronicity between minor changes in erosion pattern during late Miocene and at the Plio-Pleistocene transition and climate parameters, precipitation and glacier development, brought out yet another example of climate-erosion link.

Clift and Blusztajn (2005) reconstructed the long-term erosional history of the Indus river system based on Nd isotope composition of the Arabian Sea sediments deposited during 30 My to present. The ε_{Nd} values showed a range from ~(-11) to ~(-9.5) during the period 30 My to 5 My ago. These values suggest a provenance dominated by Karakoram (ε_{Nd}: -10 to -11), in contrast to a Himalayan source which is characterized by less radiogenic ε_{Nd} (~-25 to ~-15). The ε_{Nd} values during 5 My to Late Pleistocene (~300 ky ago) showed a trend towards more negative values, from ~(-10 to ~-13) that require enhanced relative contribution from the Himalayan source at the expense of supply from the Karakoram or the Indus suture zone. The negative shift in ε_{Nd} has been explained in terms of capture of the ancestral Himalayan tributaries of the Ganga by the Indus. Currently much of the Himalayan sediments of the Indus river is supplied by its four large tributaries, the Sutlej, Ravi, Chennab and Jellum. It is suggested that ~5 My ago these rivers were part of the Ganga river system and not of the Indus drainage.

The above examples demonstrate the successful applications of Sr-Nd isotopes to reconstruct the erosion patterns of different sediment basins at various spatial and temporal scales. These studies also have brought out the links between the patterns of physical erosion and tectonic/climate changes.

4. FUTURE DIRECTIONS

This review addressed the applications of Sr and Nd isotope systems for investigating contemporary and past chemical (silicate) and physical erosion in river basins, particularly those from the Himalaya. Available results show that both these isotope systems, especially $^{143}Nd/^{144}Nd$, have been successfully used to track sediment sources and characterize physical erosion patterns, which have brought out the coupling between tectonics, erosion and climate. The use of Sr isotopes as a proxy for silicate weathering in the Himalaya has been controversial because of the presence of carbonates with highly radiogenic Sr similar to that of silicates, which makes it difficult to clearly identify the sources of radiogenic Sr to the rivers; resolving this issue would be an important challenge for the future. An approach to pursue this problem could be through a multi-tracer systematic study of rivers (major ions, Sr isotopes and other potential proxies of silicate/carbonate weathering, ***e.g.*** Ge, $^{234}U/^{238}U$, Ca and Mg isotopes) draining small and medium sized watersheds of the Himalaya with well characterized basin properties, lithology, mineralogy and temporal variations in water discharge. There have been a few investigations in this direction. For example, Chabaux et al. (2001) through measurements of U, Sr isotopes and major ions in selected Himalayan rivers concluded that "U activity ratios, in association with Sr isotope ratios, can be used to trace the sources of dissolved fluxes carried by these rivers". However, analogous to Sr isotopes, the role of trace phases in rocks in contributing to dissolved U in rivers can frustrate the interpretation of results. Another group of isotope tracers that may help in quantification of sources of alkaline earth elements to rivers is Ca and Mg isotopes (Tipper et al. 2008). Studies of these isotopes in rivers of the Himalayan-Tibetan Plateau indicate that in small rivers these isotopes hold promise to provide information on the sources of Ca and Mg whereas in large rivers the lithological control on the isotopic composition seem obscured by isotope fractionation during weathering and calcite precipitation. Better characterization of the impact of these processes on the isotope composition of Ca and Mg may provide a way forward for their application to quantify their sources to rivers.

Additional complexities on the use of Sr isotopes as silicate weathering proxy arise from their supply to rivers *via* hot springs. Studies on the role of hot springs in regulating river water chemistry and on the Sr isotopic budget of the Marsyandi river, a sub-tributary of the Ganga (Evans et al. 2001, 2004) have shown that they can be an important source of dissolved major ions and Sr with highly radiogenic $^{87}Sr/^{86}Sr$ to this river. An interesting aspect of this study has been the application of Ge/Si as a tracer to evaluate the hot spring contribution to the water flux and alkalinity of river. More detailed studies are required to quantitatively evaluate the role of hot springs in determining the budget of major ions and Sr isotopes on basin-wide and global scales.

The marine budget of strontium shows an imbalance between its supply and removal (Davis et al. 2003; Vance et al. 2009). Uncertainties in the estimates of hydrothermal and riverine fluxes and recent enhancement in riverine flux due to weathering of finely ground rock left behind by glaciers (Vance et al. 2009) can all contribute to this imbalance. Therefore, obtaining better estimates of mean Sr flux and $^{87}Sr/^{86}Sr$ to the ocean through temporally and spatially (lithology based) representative sampling of rivers from basins with different climate and physical features should provide better understanding of the Sr isotope budget of the oceans and their potential to yield information on continental weathering history. Similarly, ascertaining the relative variation in riverine fluxes between glacial and interglacial periods through investigations of weathering indices in dated sediments from selected basins can also contribute to better understanding of the marine geochemistry and budget of Sr.

Another source of dissolved Sr to the oceans which is not included in its marine budget calculations is sub-marine groundwater discharge (SGD), though its importance is getting increasingly recognized. For example, available results for the Bay of Bengal (Basu et al. 2001) indicate that SGD can be a very significant source of Sr to the bay, with moderately radiogenic Sr ($^{87}Sr/^{86}Sr$~0.715-0.720). More data for other coastal regions are needed to quantify the global significance of this input and its role in Sr isotope evolution of the oceans.

Recently, questions have been raised about the uplift-erosion-climate hypothesis based on depositional trends of dissolved $^{10}Be/^{9}Be$ in ocean sediments and Fe-Mn crusts during the past 12 My (Willenbring and Blanckenburg 2010). These trends do not show any significant temporal variation leading to infer that global weathering fluxes have not been interrupted by mountain building pulses during the late-Cenozoic era. A topic for future study could be reconciliation of these findings with the marine Sr isotope record which shows a steady increase during this period.

5. SUMMARY

Continental erosion, both physical and chemical, regulates global geochemical cycles, shapes Earth's surface morphology and influences its climate pattern. The global significance of erosion processes has led to several studies on them and their variations in space and time to learn about the evolutionary history of our planet. A topic of considerable interest in recent years in this field has been to understand the coupling between tectonics-erosion-climate. Radiogenic isotopes, particularly $^{87}Sr/^{86}Sr$ has proven to be a powerful tool in these investigations.

Chemical weathering of silicate minerals on continents is an important process that serves as a major sink for atmospheric CO_2 on My time scales. An important development on this topic has been the suggestion that enhanced silicate weathering in young orogenic belts such as the Himalaya is the driver of global cooling during the Cenozoic. This led to detailed investigations on silicate weathering, both present and past, particularly its relation with tectonics and climate. One of the key requirements in these studies is the availability of suitable proxies that can track changes in silicate weathering in the past. Sr isotope ratios recorded in carbonates of deep sea sediments hold clues to these variations, however deciphering them is challenging because of multiple sources supplying Sr to the sea and the assumptions required to interpret the Sr isotope record. For example, the Cenozoic increase in marine $^{87}Sr/^{86}Sr$ can result either from enhanced riverine Sr flux of constant $^{87}Sr/^{86}Sr$ or changes in its $^{87}Sr/^{86}Sr$ or both. Earlier studies argued in favor of increasing the riverine Sr flux and therefore intensity of silicate weathering to reproduce the marine Sr isotope record, whereas some of the later work suggested changing the riverine $^{87}Sr/^{86}Sr$ and therefore the source composition rather than the intensity of silicate weathering to explain the increase in seawater $^{87}Sr/^{86}Sr$. Sr isotope studies of clays and river carbonates formed during the past several My seem to support the later view, thereby challenging the proposition of enhanced silicate weathering during the Cenozoic. Another issue pertaining to the Sr isotope problem is the source of highly radiogenic Sr in rivers of the Himalaya; there have been both laboratory and field studies which demonstrate that trace calcites contained in granites and metamorphosed sedimentary carbonates dispersed in the drainage basins can also supply high radiogenic Sr to rivers. If the major source of radiogenic Sr to the Himalayan rivers is indeed trace calcites and metamorphosed carbonates, it would have serious repercussions on the use of Sr isotopes as a silicate proxy. Thus the multiple variables associated with the supply of Sr and $^{87}Sr/^{86}Sr$ to rivers and oceans have raised new challenges on the use of Sr isotopes to determine silicate weathering rates.

Physical Erosion is another key process that influences climate by regulating the transport and burial of organic carbon and determining chemical erosion rates. This has led to a number of studies on the physical erosion pattern of river basins, their variability in space and time and the factors controlling them. These studies rely mainly on Sr and Nd isotopes to determine the sediment provenances, under the assumption that the isotope signatures of sources are well preserved in the sediments. This assumption though is generally valid, there are evidences based both on laboratory and field studies that suggest non-stochiometric release of Sr and Nd isotopes during different stages of rock weathering; the release being governed by the weathering sequence of minerals in the rock. For example, it has been demonstrated that during early stages of granite weathering Sr isotopes are released preferentially from minerals such as calcites, apatites, bytownite and biotite contained in them. Similarly, the roles of island arcs and ocean islands in contributing unradiogenic Sr to the oceans and the release of Sr during enhanced chemical weathering of fresh and finely ground rocks produced by glaciers are being increasingly recognized.

The non-stochiometric release of Sr isotopes from rocks during their weathering though has raised concerns about its application as a provenance tracer, it has been used extensively often with Nd isotopes to investigate spatial and temporal variations in physical erosion pattern of river basins and factors controlling them. Nd being less mobile than Sr during weathering and transport its source composition is expected to be preserved better in sediments, therefore concomitant changes in both Sr and Nd isotopic composition of sediments is generally interpreted in terms of source variations. In recent years there have been many studies, using Sr and Nd isotope proxies, on the physical erosion pattern of river basins from the Himalaya because of their dominance in sediment flux to the ocean and major role in global carbon cycle. These studies identified HH to be the major source of sediments depositing at present and over the past several My in the Ganga Plain and the Bay of Bengal and that the erosional regime has been generally stable during this period. The primary factors controlling contemporary physical erosion in the Himalaya are relief and climate and that most of the erosion occurs in "hot spots" characterized by intense precipitation over regions of high relief. These hot spots unload huge amounts of sediments promoting more rapid uplift of regions around them thereby coupling tectonics and erosion. The past erosion pattern of the Himalaya deduced from the Sr and Nd isotope records in sediments from the Ganga Plain, the Bay of Bengal and the Arabian Sea all show that it was linked to climate changes both on ky and My time scales, however there was only limited impact of glacier advance and retreat on erosion. There are also evidences to demonstrate that capture of Ganga tributaries by the Indus contributed to changes in its erosion pattern during the past ~ 5 My. It is evident from the above examples that Sr and Nd isotope studies of contemporary and ancient sediments holds valuable information on their sources and controlling agents of physical erosion in respective basins. These studies also have underscored the importance of climate and tectonics in regulating continental erosion.

Acknowledgements

SK thanks the Indian National Science Academy, New Delhi for Senior Scientistship and the Director, PRL for logistical support. Reviews and comments from Prof. M. Baskaran and two anonymous reviewers have helped improve the article.

REFERENCES

Ahmad S, Babu G, Padmakumari V et al (2005) Sr, Nd isotopic evidence of terrigenous flux variations in the Bay of Bengal: Implications of monsoons during the last ~34,000 years. Geophys. Res. Lett. 32: 1-4.

Ahmad S, Padmakumari V, Babu G (2009) Strontium and neodymium isotopic compositions in sediments from Godavari, Krishna and Pennar rivers. Curr. Sci. 97: 1766-1769.

Allegre C, Dupre B, Negrel P et al (1996) Sr–Nd–Pb isotope systematics in Amazon and Congo River systems: Constraints about erosion processes. Chem. Geol. 131: 93–112.

Allegre C, Louvat P, Gaillardet J et al (2010) The fundamental role of island arc weathering in the oceanic Sr isotope budget. Earth Planet. Sci. Lett. 292: 51-56.

Amelin Y, Rotenberg E (2004) Sm-Nd systematics of chrondrites. Earth Planet. Sci. Lett. 223: 267-282.

Amiotte Suchet P, Probst J, Ludwig W (2003) Worldwide distribution of continental rock lithology: Implications for the atmospheric/soil CO_2 uptake by continental weathering and alkalinity river transport to the oceans. Global Biogeochem. Cycles 17: 1038, doi: 10.1029/2002GB001891.

Anderasen R, Sharma M (2006) Solar Nebula Heterogenity in p-process Samarium and Neodymium isotopes. Science 314:806-809.

Andersson P, Dahlqvist R, Ingri J et al (2001) The isotopic composition of Nd in a boreal river: A reflection of selective weathering and colloidal transport. Geochim. Cosmochim. Acta 65: 521–527.

Armstrong R L (1971) Glacial erosion and the variable isotopic composition of strontium in seawater. Nature 230: 132–134.

Asahara Y, Tanaka T, Kamioka H et al (1999) Provenance of the north Pacific sediments and process of source material transport as derived from Rb–Sr isotopic systematics. Chem. Geol. 158: 271–291.

Aubert D, Stille P, Probst A (2001) REE fractionation during granite weathering and removal by waters and suspended loads: Sr and Nd isotopic evidence. Geochim. Cosmochim. Acta 65: 387–406.

Banner J (2004) Radiogenic isotopes: systematics and applications to earth surface processes and chemical startigraphy. Earth Sci. Rev. 65: 141-194.

Barroux G, Sonke J, Boaventura G et al (2006) Seasonal dissolved rare earth element dynamics of the Amazon River main stem, its tributaries, and the Curuaí floodplain, Geochem. Geophys. Geosyst., 7, Q12005, doi:10.1029/2006GC001244.

Barun J J, Pagel M, Herbillon A et al (1993) Mobilization and redistribution of REEs and thorium in a syenitic lateritic profile: A mass balance study. Geochim. Cosmochim. Acta 57**:** 4419–4434.

Basu A, Jacobsen S, Poreda R et al (2001) Large groundwater strontium flux to the oceans from the Bengal basin and the marine strontium isotope record. Science 293: 1470-1473.

Berner R, Lasaga A, Garrels R (1983) The carbonate–silicate geochemical cycle and its effect on atmospheric carbon dioxide over the past 100 million years. Am. J. Sci. 283: 641–683.

Bickle M, Bunbury J, Chapman H et al (2003) Fluxes of Sr into the headwaters of the Ganges. Geochim. Cosmochim. Acta 67: 2567-2584.

Bickle M, Chapman H, Bunbury J et al (2005) Relative contributions of silicate and carbonate rocks to riverine Sr fluxes in the headwaters of the Ganges. Geochim. Cosmochim. Acta 69: 2221-2240.

Bickle M, Harris N, Bunbury J et al (2001) Controls on the $^{87}Sr/^{86}Sr$ ratio of carbonates in the Garhwal Himalaya, Headwaters of the Ganges. J. Geol. 109: 737-753.

Blum J D, Erel Y (1995) A silicate weathering mechanism linking increases in marine Sr-87/Sr-86 with global glaciation. Nature 373: 415–418.

Blum J D, Erel Y (1997) Rb-Sr isotope systematics of a granitic soil chronosequence: The importance of biotite weathering. Geochim. Cosmochim. Acta 61**:** 3193–3204.

Blum J D and Erel Y (2003) Radiogenic Isotopes in Weathering and Hydrology, pp.365-392. In Surface and Ground Water, Weathering and Soils (ed. J.I. Drever) Vol. 5 Treatise on Geochemistry (eds. Holland, H.D. and Turekian, K.K.), Elsevier-Pergamon, Oxford.

Blum J D, Gazis C A, Jacobson A et al (1998) Carbonate versus Silicate Weathering Rates in the Raikot Watershed within the High Himalayan Crystalline Series. Geology 26: 411-414.

Bluth G, Kump L (1994) Lithologic and climatologic controls of river chemistry. Geochim. Cosmochim. Acta 58:2341–2359.

Brantley S, Chesley J, Stillings L (1998) Isotopic ratios and release rates of strontium measured from weathering feldspars. Geochim. Cosmochim. Acta 62**:** 1493–1500.

Brass G W (1976) The variation of the marine $^{87}Sr/^{86}Sr$ ratio during Phanerozoic time; interpretation using a flux model. Geochim. Cosmochim. Acta 40: 721–730.

Bullen T, White A, Blum A et al (1997) Chemical weathering of a soil chronosequence on granitoid alluvium: II Mineralogic and isotopic constraints on the behavior of strontium. Geochim. Cosmochim. Acta 61**:** 291–306.

Burbank D, Blythe A, Putkonen J et al (2003) Decoupling of erosion and precipitation in the Himalayas, Nature, 426: 652-655.

Burke W, Denison R, Hetherington E et al (1982) Variation of seawater ^{87}Sr/^{86}Sr throughout Phanerozoic time. Geology 10: 516-519.

Chabaux F, Riotte J, Clauer N et al (2001) Isotopic tracing of the dissolved U fluxes of Himalayan rivers: Implications for present and past U budgets of the Ganges-Brahmaputra system. Geochim. Cosmochim. Acta 65: 3201-3217.

Chabaux F, Bourdon B, Riotte J (2008) U-series geochemistry in weathering profiles, river waters and lakes. In: Radioactivity in the Environment (Krishnaswami S. and Cochran J. (eds)), Elsevier, 13: 49-104.

Clift P (2006) Controls on the erosion of Cenozoic Asia and the flux of clastic sediment to the ocean. Earth Planet. Sci. Lett. 241: 571–590.

Clift P, Blusztajn J (2005) Reorganization of the western Himalayan river system after five million years ago. Nature 438: 1001–1003.

Clift P, Giosan L, Blusztajn J et al (2008) Holocene erosion of the Lesser Himalaya triggered by intensified summer monsoon. Geology 36: 79-82.

Clift P, Lee J, Hildebrand P et al (2002) Nd and Pb isotope variability in the Indus river system: Implications for crustal heterogeneity in the western Himalya. Earth Planet. Sci. Lett. 200: 91-106.

Colin C, Turpin L, Bertaux J et al (1999) Erosional history of the Himalayan and Burman ranges during the last two glacial-interglacial cycles. Earth Planet. Sci. Lett. 171: 647-660.

Colin C, Turpin L, Blamart D et al (2006) Evolution of weathering patterns in the Indo-Burman Ranges over 280 kyr: Effects of sediment provenance on ^{87}Sr/^{86}Sr ratios tracer. Geochem. Geophys. Geosyst. 7: doi: 10.1029/2005GC000962.

Dalai T, Krishnaswami S, Kumar A (2003) Sr and ^{87}Sr/^{86}Sr in the Yamuna River System in the Himalaya: Sources, fluxes, and controls on Sr isotope composition. Geochim. Cosmochim. Acta 67: 2931-2948.

Das A, Krishnaswami S, Kumar A (2006) Sr and ^{87}Sr/^{86}Sr in rivers draining the Deccan Traps (India): implications to weathering, Sr fluxes and marine ^{87}Sr/^{86}Sr record around K/T. Geochem. Geophys. Geosyst. 7: Q06014, doi: 10.1029/2005GC001081.

Das A, Krishnaswami S, Sarin M et al (2005) Chemical weathering in the Krishna Basin and Western Ghats of the Deccan Traps, India: Rates of basalt weathering and their controls. Geochim. Cosmochim. Acta 69: 2067-2084.

Dasch E (1969) Strontium isotopes in weathering profiles, deep-sea sediments, and sedimentary rocks. Geochim. Cosmochim. Acta 33**:** 1521–1552.

Davis A, Bickle M, Teagle D (2003) Imbalance in the oceanic strontium budget. Earth Planet. Sci. Lett. 211: 173-187.

DePaolo D, Wasserburg G (1976) Nd isotopic variations and petrogenetic models. Geophys. Res. Lett**.**, 3: 249–252.

Derry L, France-Lanord C (1996) Neogene Himalayan weathering history and river ^{87}Sr/^{86}Sr: Impact on the marine Sr record. Earth Planet. Sci. Lett. 142: 59-74.

Derry L, France-Lanord C (1997) Himalayan weathering and erosion fluxes: Climate and tectonic controls. In: Ruddiman W F (ed) Tectonic Uplift and Climate Change, Plenum, New York. 290–312.

Dessert C, Dupre B, Francois L et al (2001) Erosion of Deccan Traps determined by river geochemistry: Impact on the global climate and the ^{87}Sr/^{86}Sr ratio of sea water. Earth Planet. Sci. Lett. 188: 459–474.

Dessert C, Dupre B, Gaillardet J et al (2003) Basalt weathering laws and the impact of basalt weathering on the global carbon cycle. Chem. Geol. 20: 1–17.

Dia A, Dupré B, Allègre C (1992) Nd isotopes in Indian Ocean sediments used as a tracer of supply to the ocean and circulation paths. Mar. Geol. 103: 349–359.

Drever J (1997) The Geochemistry of Natural waters (3rd edition). Prentice Hall, pp 436.

Edmond J M (1992) Himalayan tectonics, weathering processes, and the strontium isotope record in marine limestone. Science 258: 1594–1597.

Edmond J, Huh Y (1997) Chemical weathering yields from basement and orogenic terrains in hot and cold climates. In: Ruddiman W F (ed) Tectonic Uplift and Climate Change. Plenum Press, New York. pp. 330–351.

Erel Y, Blum J D, Roueff E et al (2004) Lead and strontium isotopes as monitors of experimental granitoid mineral dissolution. Geochim. Cosmochim. Acta 68: 4649-4663.

Evans M, Derry L, Anderson S et al (2001) Hydrothermal source of radiogenic Sr to Himalayan rivers, Geology 29: 803–806.

Evans M, Derry L, France-Lanord C (2004) Geothermal fluxes of alkalinity in the Narayani river system of central Nepal. Geochem. Geophys. Geosyst., 5: Q08011, doi: 10.1029/2004GC000719.

Faure G (1986) Principles of Isotope Geology. 2nd Edition. Wiley, Hoboken, N.J.

France-Lanord C, Derry L (1997) Organic carbon burial forcing of the carbon cycle from Himalayan erosion. Nature 390: 65-67.

France-Lanord C, Derry L, Michard A (1993) Evolution of the Himalaya since Miocene time: Isotopic and sedimentologic evidence from the Bengal Fan. In: Treloar P J and Searle M (eds) Himalayan Tectonics. Geol. Soc. Spec. Publ. 74: 603–621.

Frank M (2002) Radiogenic isotopes: Tracers of past ocean circulation and erosional input. Rev. Geophys. 40. doi: 10.1029/2000RG000094.

Gaillardet J (2008) Isotope Geochemistry as a tool for deciphering kinetics of water-rock interaction. In: Brantley S, Kubicki J and White A (eds) Kinetics of water-rock interaction. Spinger, New York, Chapter 12: 611-674.

Gaillardet J, Dupre B, Allegre C (1997) Chemical and physical denudation in the Amazon river basin. Chem. Geol. 142: 141–173.

Gaillardet J, Dupre B, Louvat P et al (1999) Global silicate weathering and CO$_2$ consumption rates deduced from the chemistry of large rivers. Chem. Geol. 159: 3-30.

Galy A, France-Lanord C (1999) Weathering processes in the Ganges-Brahmaputra basin and the riverine alkalinity budget. Chem. Geol. 159: 31-60.

Galy A, France-Lanord C, Derry L (1999) The strontium isotopic budget of Himalayan Rivers in Nepal and Bangladesh. Geochim. Cosmochim. Acta 63: 1905-1925.

Galy V, France-Lanord C, Peucker-Ehrenbrink B et al (2010) Sr–Nd–Os evidence for a stable erosion regime in the Himalaya during the past 12 Myr. Earth Planet. Sci. Lett. 290: 474-480.

Goldstein S L, O'Nions R K (1981) Nd and Sr isotopic relationships in pelagic clays and ferromanganese deposits. Nature 292: 324-327.

Goldstein S L, Jacobsen S B (1987) The Nd and Sr isotopic systematics of river-water dissolved material: implications for the sources of Nd and Sr in the seawater. Chem. Geol. 66: 245–272.

Harlavan Y, Erel Y (2002) The release of Pb and REE from granitoids by the dissolution of accessory phases. Geochim. Cosmochim. Acta 66: 837–848.

Harlavan Y, Erel Y, Blum J D (2009) The coupled release of REE and Pb to the soil labile pool with time by weathering of accessory phases, Wind River Mountains, WY. Geochim. Cosmochim. Acta 73: 320-336.

Harris N, Bickle M, Chapman H et al (1998) The significance of Himalayan rivers for silicate weathering rates: Evidence from the Bhote Kosi tributary. Chem. Geol. 144: 205-220.

Hren M, Chamberlain C, Hilley G et al (2007) Major ion chemistry of the Yarlung Tsangpo-Brahmaputra river: chemical weathering, erosion, and CO$_2$ consumption in the southern Tibetan Plateau and eastern syntaxis of the Himalaya. Geochim. Cosmochim. Acta 71:2907−2935.

Huh Y, Edmond J (1999) The fluvial geochemistry of the rivers of Eastern Siberia: III Tributaries of the Lena and Anbar draining the basement terrain of the Siberian Craton and the Trans-Baikal Highlands. Geochim. Cosmochim. Acta 63**:** 967–987.

http://www.grdc.sr.unh.edu

Ingri J, Widerlund A, Land M et al. (2000) Temporal variations in the fractionation of the rare earth elements in a boreal river; the role of colloidal particles. Chem. Geol. 166: 23–45.

Jacobsen S and Wasserburg G (1980) Sm-Nd isotopic evolution of chondrites. Earth Planet. Sci. Lett 50: 139-155.

Jacobson A D, Blum J D (2000) The Ca/Sr and ^{87}Sr/^{86}Sr geochemistry of disseminated calcite in Himalayan silicate rocks from Nanga Parbat: Influence on river water chemistry. Geology 28: 463-466.

Jacobson A D, Blum J D, Chamberlain C P et al (2002) The Ca/Sr and Sr isotope systematics of a Himalayan glacial chronosequence: Carbonate versus silicate weathering rates as a function of landscape surface age. Geochim. Cosmochim. Acta 66: 13-27.

Jeandel C, Arsouze T, Lacan F et al. (2007) Isotopic Nd compositions and concentrations of the lithogenic inputs into the ocean: A compilation, with an emphasis on the margins. Chem. Geol. 239: 156–164.

Johannesson K, Tang J, Daniels J et al **(**2004) Rare earth element concentrations and speciation in organic-rich blackwaters of the Great Dismal Swamp, Virginia, USA. Chem. Geol. 209: 271-294.

Krishnaswami S, Singh S K (2005) Chemical weathering in the river basins of the Himalaya, India. Curr. Sci. 89: 841-849.

Krishnaswami S, Singh S K, Dalai T K (1999) Silicate weathering in the Himalaya: Role in contributing to major ions and radiogenic Sr to the Bay of Bengal. In: Somayajulu B L K (ed) Ocean Science, Trends and Future Directions, Indian National Science Academy and Akademia International, New Delhi, 23–51.

Krishnaswami S, Trivedi J R, Sarin M M et al (1992) Strontium isotopes and rubidium in the Ganga-Brahmaputra river system: weathering in the Himalaya, fluxes to the Bay of Bengal and contributions to the evolution of oceanic ^{87}Sr/^{86}Sr. Earth Planet. Sci. Lett. 109: 243-253.

Kump L R, Brantley S L, Arthur M A (2000) Chemical weathering, atmospheric CO$_2$ and climate. Annu. Rev. Earth Planet. Sci. 28**:** 611–667.

Leland J, Reid M R, Burbank D W et al (1998) Incision and differential bedrock uplift along the Indus River near Nanga Parbat, Pakistan Himalaya, from ^{10}Be and ^{26}Al exposure age dating of bedrock straths. Earth Planet. Sci. Lett. 154: 93–107.

Li X H, Wei G J, Shao L et al (2003) Geochemical and Nd isotopic variations in sediments of the South China Sea: a response to Cenozoic tectonism in SE Asia. Earth Planet. Sci. Lett. 211: 207–220.

Ma J, Wei G, Xu Y et al (2007) Mobilization and re-distribution of major and trace elements during extreme weathering of basalt in Hainan Island, South China. Geochim. Cosmochim. Acta 71: 3223-3237.

Ma J, Wei G, Xu Y et al (2010) Variations of Sr–Nd–Hf isotopic systematics in basalt during intensive weathering. Chem. Geol. 269: 376– 385.

MacFarlane A, Danielson A, Holland H et al (1994) REE chemistry and Sm-Nd systematics of late Archean weathering profiles in the Fortescue Group, Western Australia. Geochim. Cosmochim. Acta 58: 1777–1794.

McCauley S, DePaolo D (1997) The marine ^{87}Sr/^{86}Sr and δ^{18}O records, Himalayan alkalinity fluxes and Cenozoic climate records. In: Ruddiman W Tectonics uplift and Climate Change. Plenum Press, New York. pp. 428–467.

Milliman J, Meade R (1983) World-wide delivery of river sediment to the oceans. J Geol. 91: 1-21.

Milliman J D, Syvitski P M (1992) Geomorphic/Tectonic control of sediment discharge to the ocean: the importance of small mountainous rivers. J. Geol. 100: 525-544.

Millot R, Gaillardet J, Dupre B et al (2002) The global control of silicate weathering rates and the coupling with physical erosion: New insights from rivers of the Canadian Shield. Earth Planet. Sci. Lett. 196**:** 83–98.

Millot R, Gaillardet J, Dupre B et al (2003) Northern latitude chemical weathering rates: Clues from the Mackenzie River basin, Canada. Geochim. Cosmochim. Acta 67**:** 1305–1329.

Molnar P, England P (1990) Late Cenozoic uplift of mountain ranges and global climate change: Chicken or egg? Nature 346: 29–34.

Montgomery D R (1994) Valley incision and the uplift of mountain peaks. J. Geophys. Res. 99: 913–921.

Moon S, Huh Y, Qin J et al (2007) Chemical weathering in the Hong (Red) River basin: Rates of silicate weathering and their controlling factors. Geochim. Cosmochim. Acta 71: 1411-1430.

Moon S, Huh Y, Zitsev A (2009) Hydrochemistry of the Amur River: Weathering in a northern temperate basin. Aquat. Geochem. 15: 497-527.

Negrel P, Allegre C J, Dupre B et al (1993) Erosion sources determined by inversion of major and trace element ratios and strontium isotopic ratios in river water: the Congo Basin case. Earth Planet. Sci. Lett. 120: 59-76.

Nesbitt H (1979) Mobility and fractionation of rare earth elements during weathering of a granodiorite. Nature 279: 206-210.

Nesbitt H W, Markovics G (1997) Weathering of granodioritic crust, long-term storage of elements in weathering profiles, and petrogenesis of silicate minerals. Geochim. Cosmochim. Acta 61: 1653–1670.

Noh H, Huh Y, Qin J et al (2009) Chemical weathering in the three rivers region of Eastern Tibet. Geochim. Cosmochim. Acta 73**:** 1857–1877.

Ohlander B, Ingri J, Land M et al (2000) Change of Sm-Nd isotope composition during weathering of till. Geochim.Cosmochim. Acta 64: 813–820.

Oliva P, Dupre B, Martin F et al (2004) The role of trace minerals in chemical weathering in a high-elevation granitic watershed (Estibere, France): Chemical and mineralogical evidence. Geochim. Cosmochim. Acta 68: 2223–2243.

Oliver L, Harris N, Bickle M et al (2003) Silicate weathering rates decoupled from the $^{87}Sr/^{86}Sr$ ratio of the dissolved load during Himalayan erosion. Chem. Geol. 201: 119– 139.

Palmer M, Edmond J (1989) The strontium isotope budget of the modern ocean. Earth Planet. Sci. Lett. 92: 11–26.

Palmer M R, Edmond J M (1992) Controls over the strontium isotope composition of river water. Geochim. Cosmochim. Acta 56: 2099-2111.

Pande K, Sarin M M, Trivedi J R et al (1994) The Indus river system (India-Pakistan): Major-ion chemistry, uranium and strontium isotopes. Chem. Geol. 116: 245-259.

Pattanaik J, Balakrishnan S, Bhutani R et al (2007) Chemical and strontium isotopic composition of Kaveri, Palar and Ponnaiyar rivers: Significance to weathering of granulites and granitic gneisses of southern Peninsular India. Curr. Sci. 93: 523-531.

Peucker-Ehrenbrink B (2009) Land2Sea database of river drainage basin sizes, annual water discharges, and suspended sediment fluxes. Geochem. Geophys. Geosyst. 10: Q06014, doi:10.1029/2008GC002356.

Peucker-Ehrenbrink B, Miller M W, Arsouze T et al (2010) Continental bedrock and riverine fluxes of strontium and neodymium isotopes to the oceans. Geochem. Geophys. Geosyst. 11, Q03016, doi:10.1029/2009GC002869.

Pierson-Wickmann A C, Reisberg L, France-Lanord C et al (2001) Os-Sr-Nd results from sediments in the Bay of Bengal: Implications for sediment transport and the marine Os record. Paleoceanography 16: 435-444.

Porcelli D, Anderson P, Baskaran M et al (2009) The distribution of neodymium isotopes in Arctic Ocean basins. Geochim. Cosmochim. Acta 73: 2645-2659.

Quade, J, Roe L, DeCelles P et al (1997) The late neogene $^{87}Sr/^{86}Sr$ record of lowland Himalayan rivers. Science 276: 1828-1831.

Rad S, Allegre C, Lovat P (2007) Hidden erosion on volcanic islands. Earth Planet. Sci. Lett. 262: 109-124.

Rahaman W, Singh S K, Sinha R et al (2009) Climate control on erosion distribution over the Himalaya during the past ~100 ka. Geology 37: 559-562.

Rai S K, Singh S K (2007) Temporal variation in Sr and $^{87}Sr/^{86}Sr$ of the Brahmaputra: Implications for annual fluxes and tracking flash floods through chemical and isotope composition. Geochem. Geophys. Geosyst. 8, doi:10.1029/2007GC001610.

Rai S K, Singh S K, Krishnaswami S (2010) Chemical weathering in the plain and peninsular sub-basins of the Ganga: Impact on major ion chemistry and elemental fluxes Geochim. Cosmochim. Acta 74: 2340-2355.

Ravizza G, Zachos J. (2003) Records of Cenozoic Chemistry, pp.551-582. In The Oceans and Marine chemistry (ed. J.I. Drever) Vol. 6 Treatise on Geochemistry (eds. Holland, H.D. and Turekian, K.K.), Elsevier-Pergamon, Oxford.

Raymo M E, Ruddiman W F (1992) Tectonic forcing of late Cenozoic climate. Nature 359: 117-122.

Raymo M E, Ruddiman W F, Froelich P N (1988) Influence of late Cenozoic mountain building on ocean geochemical cycles. Geology 16: 649-653.

Reynolds B (This volume) Silicon isotopes as Tracers of Chemical Weathering. Handbook of Environmental Isotope Geochemistry (ed. Mark Baskaran), Chapter 22, Springer publications.

Richter F M, Rowley D B, DePaolo D J (1992) Sr isotope evolution of seawater: the role of tectonics. Earth Planet. Sci. Lett. 109: 11–23.

Ruddiman W (1997) Tectonic Uplift and Climate Change, Plenum, New York, pp 535.

Shiller A (2010) Dissolved rare earth elements in a seasonally snow-covered, alpine/subalpine watershed, Loch Vale, Colorado. Geochim. Cosmochim. Acta 74: 2040-2052.

Sholkovitz E (1995) The aquatic chemistry of rare earth elements in rivers and estuaries. Aquat. Geochem. 1: 1–34.

Sholkovitz E, Szymczak R (2000) The estuarine chemistry of rare earth elements: comparison of the Amazon, Fly, Sepik and the Gulf of Papua systems. Earth Planet. Sci. Lett. 179: 299-309.

Singh S K (2006) Spatial variability in erosion in the Brahmaputra basin: Causes and impacts. Curr. Sci. 90: 1271–1276.

Singh S K (2007) Erosion and Weathering in the Brahmaputra River System. In: Gupta A (ed) Large Rivers. John Wiley Publication, UK. pp. 373-393.

Singh S K, France-Lanord C (2002) Tracing the distribution of erosion in the Brahmaputra watershed from isotopic compositions of stream sediments. Earth Planet. Sci. Lett. 202: 645-662.

Singh S K, Rai S K, Krishnaswami S (2008) Sr and Nd isotopes in river sediments from the Ganga basin: Sediment provenance and spatial variability in physical erosion. J. Geophys. Res. 113: F03006, doi:10.1029/2007JF000909.

Singh S K, Sarin M M, France-Lanord C (2005) Chemical erosion in the eastern Himalaya: Major ion composition of the Brahmaputra and $\delta^{13}C$ of dissolved inorganic carbon. Geochim. Cosmochim. Acta 69: 3573-3588.

Singh S K, Trivedi J R, Pande K et al (1998) Chemical and Strontium, Oxygen, and Carbon Isotopic Compositions of Carbonates from the Lesser Himalaya: Implications to the Strontium Isotope Composition of the Source Waters of the Ganga, Ghaghara, and the Indus Rivers. Geochim. Cosmochim. Acta 62: 743-755.

Stallard R F, Edmond J M (1983) Geochemistry of the Amazon 2 J. Geophys. Res. 88: 9671–9688.

Steinmann M, Stille P (2008) Controls on transport and fractionation of the rare earth elements in stream water of a mixed basaltic-granitic catchment basin (Massif Central, France). Chem. Geol. 254: 1-18.

Tachikawa K, Athias V, Jeandel C (2003) Neodymium budget in the modern ocean and paleo-oceanographic implications. J. Geophys. Res. 108: 3254, doi:10.1029/1999JC000285.

Taylor A S, Blum J D, Lasaga A C et al (2000) Kinetics of dissolution and Sr release during biotite and phlogopite weathering. Geochim. Cosmochim. Acta 64: 1191-1208.

Taylor A S, Lasaga A C (1999) The role of basalt weathering in the Sr isotope budget of the oceans Chem. Geol. 161: 199-214.

Tipper E, Bickle M, Galy A et al (2006a) The short term climatic sensitivity of carbonate and silicate weathering fluxes: Insight from seasonal variations in river chemistry. Geochim. Cosmochim. Acta 70: 2737-2754.

Tipper E, Galy A, Gaillardet et al (2006b) The magnesium isotope budget of the modern ocean: Constraints from riverine magnesium isotope ratios. Earth Planet. Sci. Lett. 250: 241-253.

Tipper E, Galy A, Bickle M (2008) Calcium and magnesium isotope systematics in rivers draining the Himalaya-Tibetan-Plateau region: Lithological or fractionation control? Geochim. Cosmochim. Acta 72: 1057-1075.

Tricca A, Stille P, Steinmann M et al. (1999) Rare earth elements and Sr and Nd isotopic compositions of dissolved and suspended loads from small river systems in the Vosges mountains (France), the river Rhine and groundwater. Chem. Geol. 160: 139-158.

Tripathy G R, Goswami V, Singh S K et al (2010) Temporal variations in Sr and $^{87}Sr/^{86}Sr$ of the Ganga headwaters: estimate of dissolved Sr flux to the mainstream. Hydrol. Process. 24: 1159-1171, DOI: 10.1002/hyp.7572.

Tripathy G R, Singh S K (2010) Chemical erosion rates of river basins of the Ganga system in the Himalaya: Reanalysis based on inversion of dissolved major ions, Sr, and $^{87}Sr/^{86}Sr$. Geochem. Geophys.Geosyst. 11: doi: 10.1029/2009GC002862.

Trivedi J, Pande K, Krishnaswami S et al (1995) Sr isotopes in rivers of India and Pakistan: A reconnaissance study. Curr. Sci. 69: 171–178.

Tutken T, Eisenhauer A, Wiegand B et al (2002) Glacial-interglacial cycles in Sr and Nd isotopic composition of Arctic marine sediments triggered by the Svalbard/Barents Sea ice sheet. Mar. Geol. 182: 351-372.

Vance D, Teagle D, Foster G (2009) Variable Quaternary chemical weathering fluxes and imbalances in marine geochemical budgets. Nature 458: 493–496.

Veizer J (1989) Strontium isotopes in sea water through time. Annu. Rev. Earth Planet. Sci. 17: 141-168.

Viers J, Roddaz M, Filizola N et al (2008) Seasonal and provenance controls on Nd–Sr isotopic compositions of Amazon river suspended sediments and implications for Nd and Sr fluxes exported to the Atlantic Ocean. Earth Planet. Sci. Lett. 274: 511-523.

Viers J, Wasserburg G J (2004) Behavior of Sm and Nd in a lateritic soil profile. Geochim. Cosmochim. Acta 68: 2043–2054.

Vigier N, Bourdon B (This volume) Constraining chemical weathering using U-series Radionuclides as Tracers. Handbook of Environmental Isotope Geochemistry (Edited by Mark Baskaran), Chapter 25, Springer publications.

Walker J, Hays P, Kasting J (1981) A negative feedback mechanism for the long-term stabilization of Earth's surface temperature. J Geophy. Res. 86: 9776-9782.

Walter H J, Hegner E, Diekmann B et al (2000) Provenance and transport of terrigenous sediment in the south Atlantic Ocean and their relations to glacial and interglacial cycles: Nd and Sr isotopic evidence. Geochim. Cosmochim. Acta 64: 3813-3827.

West A J, Galy A, Bickle M (2005) Tectonic and climatic controls on silicate weathering. Earth Planet. Sci. Lett. 235: 211–228.

Willenbring J K, Blanckenburg F V (2010) Long-term stability of global erosion rates and weathering during late-Cenozoic cooling, Nature 465: 211-214.

Winter B, Johnson C, Clark D (1997) Strontium, neodymium and lead isotope variations of authigenic and silicate sediment components from the Late Cenozoic Arctic Ocean: Implications for sediment provenance and source of trace metals in sea water. Geochim. Cosmochim. Acta 61:4181-4200.

Wu L, Huh Y, Qin J et al (2005) Chemical weathering in the Upper Huang He (Yellow River) draining the eastern Qinghai-Tibet Plateau. Geochim. Cosmochim. Acta 69: 5279-5294.

Xu Y, Marcantonio F (2007) Strontium isotope variations in the lower Mississippi River and its estuarine mixing zone. Mar. Chem. 105: 118-128.

Yang C, Telmer K, Veizer J (1996) Chemical dynamics of the "St. Lawrence" riverine system: δD_{H2O}, $\delta^{18}O_{H2O}$, $\delta^{13}C_{DIC}$, $\delta^{34}S_{sulfate}$, and dissolved $^{87}Sr/^{86}Sr$. Geochim. Cosmochim. Acta 60: 851-866.

Yang S, Jiang S, Ling H et al (2007) Sr-Nd isotopic compositions of the Changjiang Sediments: Implications for tracing sediment sources. Sci China Ser D-Earth Sci 50:1556-1565.

Zachos J, Opdyke B, Quinn T et al (1999) Early Cenozoic glaciation, Antarctic weathering, and seawater $^{87}Sr/^{86}Sr$: is there a link? Chem. Geol. 161: 165-180.

Zeitler P, Koons P, Bishop M et al (2001) Erosion, Himalayan geodynamics, and the geomorphology of metamorphism, GSA Today 11: 4–9.

Internationally open and liberal   Indexed in "Current Contents"
GEOCHEMICAL JOURNAL
The Geochemical Society of Japan
e-mail : gj@geochem.jp (Geochemical Journal)

Montréal, Sunday, December 12, 2010

Dr. Gyana Ranjan Tripathy
Geosciences Division,
Physical Research Laboratory,
Ahmedabad 380009, India

Dear Dr. Gyana Ranjan Tripathy:

I am pleased to inform you that your paper " Sr-Nd isotope composition of the Bay of Bengal Sediments: Impact of Climate on Erosion in the Himalaya" by Gyana Ranjan Tripathy, Sunil Kumar Singh, Ravi Bhushan and V. Ramaswamy was recommended by Dr. Daniele Pinti for publication and has been accepted in *Geochemical Journal*. The date of acceptance is December 11th, 2010.

Please send to the Tokyo Office <gj@ori.u-tokyo.ac.jp> your manuscript. The publisher will send a galley proof directly to you. If the publisher will encounter any problem with quality of figures and tables, we will communicate with you as soon as possible. Please send to Tokyo for publishing the following items by e-mail:

- Five key words
- A running title
- Text files or MS-word files of text and tables
- Separate files with electronic figures (PS/EPS/AI/ JPG/TIFF or BMP formats)

Please notice that at http://www.geochem.jp/english/journal_e/index.html you have a very detailed "Instructions for Authors" with formats required and manuscript checklist.

Thank you for considering in *Geochemical Journal*.

Sincerely yours,

Daniele Luigi Pinti

Daniele L. PINTI, Vice-executive Editor
Geochemical Journal

Université du Québec à Montréal
Montréal, QC, H2X 3Y7, Canada
Tel: +1 514-987-3000 (2572)
Fax: +1 514 987 3635

Sr-Nd isotope composition of the Bay of Bengal Sediments: Impact of Climate on Erosion in the Himalaya

Gyana Ranjan Tripathy[1]*, Sunil Kumar Singh[1], Ravi Bhushan[1] and V. Ramaswamy[2]

[1]Geosciences Division, Physical Research Laboratory, Ahmedabad 380009, India
[2]National Institute of Oceanography, Dona Paula, Goa 403004, India

Revised Submission to *Geochemical Journal*, December, 2010

* Corresponding Author (gyana@prl.res.in)

ABSTRACT

A temporal high-resolution analysis of the Sr-Nd isotopic composition, the Fe, Al and V composition and the magnetic susceptibility (MS) has been carried out in a sediment core from the western Bay of Bengal to trace sedimentary sources. Significant variations of the Sr and Nd isotopic composition and corresponding MS and elemental Fe/Al and V/Al ratios are observed in the sediment core with depth (time) indicating variable contributions from sources. The observed changes in the sediment provenance correlate well with the climatic record of the region, highlighting the important influence of climate over erosion. Relatively lower $^{87}Sr/^{86}Sr$ and higher ε_{Nd} corresponding to the Last Glacial Maximum (LGM) suggests proportionally reduced sediment contribution from the Himalaya. Erosion rate over the Himalaya decreased during LGM due to combined influence of reduced intensity of the southwest monsoon and larger extent of glaciations over the Higher Himalaya, the main source of sediments to the Bay of Bengal.

Key Words: Himalaya; Bay of Bengal; Erosion; Climate; Sr-Nd isotopes.

1. INTRODUCTION

The Bay of Bengal (BoB) receives sediments from various sources including the Himalaya, Trans-Himalayan plutonic belt (TPB; Mishmi Hills), Indo-Burman Ranges and the Peninsular India through the major rivers, the Ganga, Brahmaputra, Irrawaddy, Salween, Godavari, Mahanadi and the Krishna. In these river basins, erosion is regulated by both the southwest (summer) and the northeast (winter) monsoons. There are evidences to show that the intensity of these monsoons varied over millennial timescale (Duplessy, 1982; Prell and Kutzbach, 1987; Sarkar *et al.*, 1990; Tiwari *et al.*, 2005; Herzschch, 2006). These variations in turn have the potential to influence the erosion pattern over the source regions and the sediment delivery to the BoB. Therefore, the variations in the sources of sediments deposited in the BoB hold clues to changes in the monsoon intensity.

In earlier studies, temporal variations in the provenance of sediments of the BoB have been tracked using Sr-Nd isotopes (France-Lanord *et al.*, 1993; Colin *et al.*, 1999; Pierson-Wickmann *et al.*, 2001; Ahmad *et al.*, 2005; Kessarkar *et al.*, 2005; Galy *et al.*, 2008). Over Ma time scale, the sources of sediments to the BoB have remained roughly the same since the Miocene (Bouquillon *et al.*, 1990; France-Lanord *et al.*, 1993). The sources are dominated by contributions from the Higher Himalaya (HH) with subordinate supply from the Lesser Himalaya (LH). However, on millennial timescale, there are evidences of variations in the provenance of sediments in the BoB related to climatic changes (Colin *et al.*, 1999; Goodbred, 2003; Ahmad *et al.*, 2005; Bookhagen *et al.*, 2005, 2006; Kessarkar *et al.*, 2005; Clift *et al.*, 2008; Rahaman *et al.*, 2009). This is consistent with the important role that climate has on the present-day erosion over the

Himalaya, with most of sediments delivered to the BoB by rivers during the southwest monsoon (Islam *et al.*, 1999; Goodbred, 2003). In contrast, some of the studies carried out in the Nepal Himalaya (Burbank *et al.*, 2003), have decoupled climate and erosion and have highlighted the important control of tectonics on erosion. Compared to the Himalaya, there has been paucity of information on the paleo-erosion pattern of the Peninsular India river basins and their controlling factors. Based on clay mineralogy and Sr-Nd isotopes of marine sediments from the south-west margin of India, Kessarkar *et al.* (2003) concluded that these sediments are mainly from the Peninsular India and the Himalaya (Indus basin) and that their provenances and transport pathways remained the same during the late Pleistocene and Holocene.

These limited information on the monsoon-erosion relation in the Himalaya and the Peninsular India regions, warrant a detailed study. The western Bengal fan receives sediments predominantly from the Himalaya and the Peninsular India and hence it can be used to investigate the past erosion pattern of these source regions. In the present study, efforts are made to track the provenances of the sediments from western BoB and their variations before, during and after the Last Glacial Maximum (LGM hereafter) and to identify the processes controlling the variations, based on sediment magnetic susceptibility (MS), chemical (Fe/Al and V/Al ratios) and Sr and Nd isotope compositions.

2. MATERIALS AND METHODS

The samples for this study are from a 12.8 m long piston core (SK187/PC33) collected from the western BoB (16° 16′ N, 84° 30′ E; Fig. 1) during the 187th expedition of the ORV *Sagar Kanya*. The core was raised from an abyssal plain at a water depth of 3003 m (Fig. 1). Immediately after recovery the core was subjected to non-invasive measurements using a Geotek® Multi-Sensor Core Logger. Continuous down-core measurements were made of P-Wave velocity, whole core bulk density using gamma-ray attenuation, magnetic susceptibility and non-contact electrical resistivity. The core logs showed the core to be turbidite free. The lithology is mainly silty-clay and it does not show any significant changes with depth. The core location presently receives sediments mainly from the Himalaya and the Peninsular India. The Sr and Nd isotopic compositions of these two source regimes are distinctly different (Fig. 1; Table 1) and hence, temporal changes in the provenance of sediments and/or in their relative contributions should be reflected in their Sr and Nd isotope composition.

The depth-age relation for the core SK187/PC33 has been constrained using ^{14}C ages of bulk inorganic carbonates. The low abundance of carbonates in the sediment samples required processing of ~100 grams of bulk sediment samples for ^{14}C analysis (Bhushan *et al.*, 1994). Briefly, the dried sediments were treated with H_3PO_4 in vacuum to convert the carbonate to CO_2. From the CO_2, benzene was synthesized for ^{14}C measurements and the ^{14}C activities were assayed using a low background liquid scintillation counter (Bhushan *et al.*, 1994). The calculated ^{14}C ages (Table 2) were calibrated using Calib 5.2 (Stuiver and Reimer, 1993) with a reservoir age correction of $\Delta R = -60\pm50$ (Dutta *et al.*, 2001).

The magnetic susceptibility of the sediments was measured at ~10 cm depth interval using a MS2 Bartington magnetic susceptibility meter calibrated at 0.47 kHz frequency (Kessakar *et al.*, 2005). Abundances of Al, Fe and V were measured using an ICP-AES (Jobin-Yvon, Ultima) after dissolving the water-washed sediments by repeated treatment with HF-HCl-HNO_3. The Sr and Nd concentrations and their isotopic compositions were measured in the silicate fraction of the sediments (Singh *et al.*, 2008) at ~50 cm intervals. Sediment samples were decarbonated by treating them with 0.6 N HCl at ~70°C followed by washing with distilled water. Initially, there were concerns about the effectiveness of the procedure in completely decarbonating the sediments, particularly samples with high $CaCO_3$ (e.g. 221-223, 440-442, 899-901 cmbsf; Tripathy *et al.*, 2008). Therefore, the high carbonate samples were reanalyzed after treating them one more time with 0.6 N HCl. The decarbonated and washed samples were ashed at 600ºC to combust the organic matter. The residue (silicate phase), spiked with ^{84}Sr and ^{150}Nd, was digested with HF, HCl and HNO_3. The samples were brought to complete solution and pure fractions of Sr and Nd were separated from the solution using conventional column chromatography (Singh *et al.*, 2008). The Sr and Nd isotope measurements were carried out using an ISOPROBE-T TIMS in static multi-collection mode. Sr and Nd data were normalized using $^{86}Sr/^{88}Sr$ (=0.1194) and $^{146}Nd/^{144}Nd$ (=0.7219) respectively. The average $^{87}Sr/^{86}Sr$ ratio of standard NBS 987 during the period of study was 0.710229±0.000014 (1σ, n=85) and $^{143}Nd/^{144}Nd$ for JNdi-1 Nd standard was 0.512102±0.000008 (1σ, n=13), within the recommended values. The differences in Sr and Nd isotopic ratios measured in replicates are insignificant compared to the range of values measured in the sediment (Table 3A). The total procedural blank for Sr and Nd were orders of magnitude lower than total Sr and Nd processed.

3. RESULTS

The concentrations of Al, Fe and V in total sediments of the core SK187/PC33 are given in Table 3A. The concentrations of Al, Fe and V vary from 2.5 to 9.2 wt%, 1.8 to 6.5 wt% and 30 to 130 μg/g respectively and show significant depth (temporal) variations. The MS of the core SK187/PC33 (Table 3B) ranges from 14 to 68 10^{-8} m^3/kg (Table 3B), comparable to earlier reported values for western BoB sediments (Kessarkar *et al.*, 2005).

The Sr, Nd concentrations in the silicate fraction and their $^{87}Sr/^{86}Sr$ and ε_{Nd} values also show significant variations with depth (Fig. 2; Table 3A). The abundances of Sr and Nd vary from 43 to 172 μg/g and from 13 to 63 μg/g respectively whereas the $^{87}Sr/^{86}Sr$ ratios vary from 0.72528 to 0.75732 and ε_{Nd} from -21.1 to -13.7 (Table 3A). The Sr isotope composition of these sediments is very radiogenic with values generally exceeding 0.735 (Table 3A), with corresponding ε_{Nd} values often less than (-15). These values are within the range of isotopic composition of various sources supplying sediments to the core site (Fig. 3), though a dominance of the Himalayan source, as supplied by the Lower Meghna, exists (see Discussion). Among the 36 samples analysed for Sr and Nd isotopic composition, two samples at depths of 222, 440 cmbsf show a sharp decrease in the ε_{Nd} (and increase in $^{87}Sr/^{86}Sr$ ratios) compared to samples from adjacent depths (Table 3A). The cause for these ε_{Nd} and $^{87}Sr/^{86}Sr$ anomalies is unclear. It may be the result of a unique event, such as significant sediment delivery during flood events from a tributary flowing through lithology with low ε_{Nd} and $^{87}Sr/^{86}Sr$ such as the Mahanadi and Pennar rivers draining Archean crust. These two samples have not been considered in the analysis of the isotope data to determine their general trend with depth (Fig. 2).

4. DISCUSSION

4.1 $^{87}Sr/^{86}Sr$ and ε_{Nd} in contemporary sediment sources to the BoB

The different sediment sources to the BoB show characteristic Sr and Nd isotopic compositions (Fig. 1, Table 1). For example, Himalayan rivers (such as the Ganga) supply sediments with highly radiogenic Sr and less radiogenic Nd compared to that of the sediments from the TPB, the Indo-Burmese ranges, the Arakan mountains and the Deccan Plateau, which are less radiogenic in Sr and more radiogenic in Nd (Table 1, Fig. 1; France-Lanord *et al.*, 1993; Colin *et al.*, 1999, 2006; Galy and France-Lanord, 2001; Singh and France-Lanord, 2002; Singh *et al.*, 2008; Ahmad *et al.*, 2009). The Godavari and the Krishna rivers drain the basaltic terrain of the Deccan traps upstream and the Archean cratons downstream. Therefore, the Sr and Nd isotopic composition of these river sediments (0.720 to 0.730 and -12.0 to -18.2 respectively; Ahmad *et al.*, 2009) depend on the relative contribution from these two sources. The representative Sr, Nd isotope compositions for the Archean crust (Fig. 1) used in this study are 0.716 and -25 respectively, compiled from earlier studies (Kessarkar *et al.*, 2003, 2005).

4.2 Temporal variations in the erosion pattern of Himalaya and Peninsular river basins of India

4.2.1 Depth-Age model

The availability of an age-depth model for the SK187/PC33 core is a prerequisite to infer the temporal variations of the sources supplying sediments to the core location. The depth-age model has been established based on ^{14}C of total inorganic carbon. The age distribution with depth in the core suggests that the LGM (18-21 ka) occurs at the depth range of ~600-700 cmbsf. The sedimentation rate of the core varies with depth with the lowest value at around LGM (460-620 cmbsf; 0.2 mm/yr) and about an order of magnitude higher (2.7 mm/yr) following the LGM (320-460 cmbsf). Similar pattern in sedimentation, with high rates following the LGM have also been reported by Kessarkar *et al.* (2005) and Galy *et al.* (2008).

Since the ^{14}C analyses were made in bulk carbonates, there could be an overestimation of the ages due to potential contribution of dead carbon from detrital carbonates. Earlier studies on ^{14}C measurements in coarse and fine fractions of bulk carbonates showed that the finer fractions (comprising primarily of carbonate powder and nanoplanktons) were generally older than the coarser fractions (mature forams) by ~3 ka (Sarkar, 1989; Sarkar *et al.*, 1990). The older age in the finer fraction was attributed to incorporation of dead detrital carbonates. Subsequently, Tiwari *et al.* (2005) by comparing δ^{18}O spike in two cores, one dated by AMS on forams and the other (near-by core) by ^{14}C on total carbonates, suggested that the age differ by ~3 ka, the AMS dates being younger. An independent estimation of age correction can be obtained from the inorganic carbon contents of sediment sources and that in the SK187/PC33 core. The average carbonate content (expressed as $CaCO_3$) is 8.6% in the five sections of SK187/PC33 analysed for ^{14}C, compared to ~3% in the Lower Meghna sediments (Galy and France-Lanord, 2001). Dilution of SK187/PC33 carbonates with the dead riverine carbonate would overestimate the age by ~3.5 ka. The comparison of the pattern of MS profiles of the core analyzed in this study with that in an AMS ^{14}C dated core from the western BoB (Kessakar *et al.*, 2005), provides another approach to constrain the age-depth model. This approach essentially uses MS as a stratigraphic marker (Ninkovich *et al.*, 1966; Bloemendal *et al.*, 2005). Matching the prominent changes in the MS profiles in the top layers of the two cores (assuming that they are synchronous) indicates that the bulk carbonate ages of SK187/PC33 are older by ~4 ka. The AMS dated western BoB core (Kessarkar *et al.*, 2005) had an age reversal at ~100 cm, therefore the MS pattern of the two cores below this depth are not compared. In this study, samples having comparable calcium carbonate content (~8 %) were analyzed for ^{14}C chronology so that the level of correction due to presence of detrital carbonate could be similar. Thus, based on available evidences, the bulk radiocarbon ages measured in the study could be ~3-4 ka older than actual ages. This suggests that the depositional age of the sample at depth 621 cmbsf, for which the measured ^{14}C calendar age is ~24 ka (Table 2), could be about 20 ka representing the LGM. In addition to the five samples in Table 2 one sample from 222 cmbsf depth with high $CaCO_3$ (~50 %) content was also analyzed for ^{14}C. This sample yielded an age of 22000 ± 600 yr (PRLCH-724) significantly different that expected based on the age-depth model of the sample in Table 2. It is worth mentioning here that this sample also has anomalous $^{87}Sr/^{86}Sr$ and ε_{Nd} values (Table 3; Fig. 3). As a result, this data is not included for the depth-age relation.

4.2.2 Temporal variations in geochemical and Sr-Nd isotopic signatures in the BoB sediments

The depth profiles of Sr and Nd isotope compositions of the core show significant temporal variations (Fig. 2). The range in $^{87}Sr/^{86}Sr$ (0.725-0.757) and ε_{Nd} (-13.7 to -16.9) indicate the dominance of the Himalayan source with minor contributions from the Peninsular Indian regions (Fig. 3). The $^{87}Sr/^{86}Sr$ and ε_{Nd} of the SK187/PC33 sediments (Table 3A) are bracketed by sediments from the Ganga, Brahmaputra and rivers from the Peninsular India and overlap with a few available data of the Lower Meghna (combined flow of the Ganga and the Brahmaputra in Bangladesh) indicating these rivers to be the major sediment supplier to the core site (Fig. 3).

The Sr-Nd isotopes depth profiles (Fig. 2) show a striking change in isotopic compositions around 600 cmbsf. Considering the age model of the sediment core, this major change in $^{87}Sr/^{86}Sr$ and ε_{Nd} coincide with the LGM. The $^{87}Sr/^{86}Sr$ of the samples during LGM is ~0.725 compared to their interglacial values of ~0.745 (Fig. 2). The less radiogenic $^{87}Sr/^{86}Sr$ of the sediments during LGM indicate a relatively reduced supply of sediments from the Himalayan rivers, particularly that of the Ganga (which is characterized by a highly radiogenic Sr signature; Table 1) compared to that during pre- and post-LGM relative to the Peninsular Indian rivers. This inference based on the $^{87}Sr/^{86}Sr$ data is also supported from the trend of ε_{Nd} values which shows a broad hump (~ -14) during the LGM compared to pre- and post-LGM values (-16; Fig. 2). The concomitant changes in both $^{87}Sr/^{86}Sr$ and ε_{Nd} argue in favor of provenance changes and not due to particle sorting/weathering processes (*c.f.* Walter *et al.*, 2000; Tutken *et al.*, 2002; Colin *et al.*, 2006).

Similar to Sr-Nd isotopic signatures, the Fe/Al and V/Al ratios and MS (Fig. 4) of the sediment core also show significant variations with depth (time) indicating changes in relative proportion of sediments supplied from various sources. The Sr, Nd isotopes-based inference that the sediment contribution to the core site from the Himalayan source is relatively diminished during LGM is also confirmed by the V/Al and Fe/Al ratios. Distinctly higher V/Al and Fe/Al ($(60\text{-}70)\times10^{-4}$ and 1.01±0.21; Pattan *et al.*, 2008) characterize the rivers flowing through the Peninsular India compared to that of the G-B sediments (V/Al = $(20\text{-}25) \times 10^{-4}$ and Fe/Al = 0.44±0.10; Pattan *et al.*, 2008). The humps in V/Al and Fe/Al profiles observed during LGM in SK187/PC33 (Fig. 4) attest to the relatively enhanced sediment supply from the Peninsular Indian rivers. This is also supported by the variation in the MS values. The magnetic susceptibility of sediments depends mainly on the abundance of detrital magnetic minerals present in them. The low carbonate content of the sediments from SK187/PC33 ensures that the magnetic susceptibility is a good tool to infer sediment provenance changes in the past (Bloemendal *et al.*, 1993). Temporal variations of MS of the sediments show an increasing trend at around LGM (Fig. 4), suggesting higher abundances of ferromagnetic minerals (such as magnetite) and Fe-bearing silicates in the sediments. A very likely source for the high MS values during LGM is the relatively enhanced contribution of sediments from the Peninsular Indian region. This inference draws support from the significantly higher MS values for the fluvial sediments from Peninsular Indian regions compared to that from the sediments from the river basins of the Himalaya (Sangode *et al.*, 2007). The high MS value for the sediments from the Peninsular India particularly that for weathered products of the Deccan basalts, is due to the abundance of titanomagnetite with minor hematite (Courtillot *et al.*, 1986; Sager and Hall, 1990). A similar high MS value during LGM in the western Bengal fan was also reported by Sangode *et al.* (2001) and this change was attributed to weakening of sediment contribution from the Himalaya.

The above discussion, based on the isotope and trace element composition of the core SK187/PC33 along with its magnetic susceptibility reveal significant variations in the relative supply of sediments from the Himalaya and the Peninsular India over glacial-interglacial timescale. However, this conclusion rests on the assumption that the isotopic and chemical characteristics of these sources did not change since the LGM. This assumption seem to be valid for the G-B rivers as the Sr-Nd isotope ratios of the BoB sediments near the mouth of this river system has remained roughly the same since the LGM (Galy *et al.*, 2008). Rahaman *et al.* (2009), however, observed significant excursion in $^{87}Sr/^{86}Sr$ (and ε_{Nd}) in sediments of the Ganga upstream, during the LGM. If this finding is typical of the entire G-B basin, then it would require that the relative proportion of G-B sediments in the SK187/PC33 core during LGM would have to be lower than that estimated based on their present-day $^{87}Sr/^{86}Sr$ ratios.

The rivers draining the Peninsular India flow through multiple lithologies (Archean crust and Deccan traps) with their own distinct Sr-Nd isotope composition. Therefore, any change in the relative proportion of sediments from these two lithologies can alter the Sr-Nd isotopic signature of the peninsular sediments being delivered to the BoB. However, there is no evidence at present to suggest that the provenance of sediments of the Peninsular Indian rivers has changed in the past (Kessakar *et al.*, 2003). Increase in NE monsoon during LGM could enhance supply from the peninsular river basins. But this could result in a decrease of ε_{Nd} unlike what has been observed in this study. Fig. 5 shows the Sr-Nd isotopic composition of the SK187/PC33 sediments along with the isotopic compositions of their dominant sources (*viz.* Higher Himalayan Crystallines, Lesser Himalayan silicates, Deccan traps and Archean). The dispersion of sediment data in the plot shows that their supply to the present core site is mainly from the HH, LH and the Deccan traps throughout the core length. The mixing curve (Fig. 5) among the major sources show that ~40% of the sediments are supplied from the Deccan and rest from the HH and the LH. However, the sediments deposited during LGM, with lower $^{87}Sr/^{86}Sr$ and high ε_{Nd} values, have relatively larger contribution of sediments from the Peninsular India (both Deccan traps and Archean crust) sources. The relative proportion of Peninsular India sediments to the core site during LGM (~60%; Fig. 5) increases significantly compared to that during the interglacial periods (~40%). The LGM shift in the SK187/PC33 sediments lean towards the mixing curve of Deccan and LH (Fig. 5), indicating relatively enhanced contribution from LH than that of HH during LGM. This is consistent with the results of Rahaman *et al.* (2009).

4.3 Impact of climate on continental Erosion

The excursions in Sr and Nd isotope composition of the sediments during LGM is compatible with the Asian monsoon strength variability (Prell and Kutzbach, 1987; Herzschuh, 2006). Climatic records show that during the LGM the intensity of the SW monsoon decreased (Prell and Kutzbach, 1987; Herzschuh, 2006) and that of NE monsoon increased (Duplessy, 1982; Prell *et al.*, 1990; Sarkar *et al.*, 1990; Tiwari *et al.*, 2005). The decrease in intensity of SW monsoon during LGM would limit its penetration into the Higher Himalaya, which is the dominant source of sediments to the Ganga and the Brahmaputra at present (Singh *et al.*, 2008). In addition, during the LGM the extent of glacial cover over the Higher Himalaya was larger (Owen *et al.*, 2002), further limiting physical erosion in the region. In contrast, there are evidences that during the LGM the NE monsoon was more intense (Duplessy, 1982; Prell and Kutzbach, 1987; Sarkar *et al.*, 1990; Tiwari *et al.*, 2005). This situation enhanced the sediment delivery from the rivers draining the Peninsular India and part of the drainage basin of the Brahmaputra (TPB), all of which have lower $^{87}Sr/^{86}Sr$ and higher ε_{Nd} (Fig. 1). Thus, the combination of decrease in SW monsoon and increase in NE monsoon during LGM contributed to decrease the relative proportion of sediments from the Himalaya to the core site, resulting in the $^{87}Sr/^{86}Sr$ dip and ε_{Nd} hump (Fig. 2). The link between monsoon activity and sediment supply is consistent with the results of Bookhagen *et al.* (2006), who have shown that intensification of monsoon enhances sediment supply from the HH. Further, the recent study of Rahaman *et al.* (2009) on a sediment core from the Ganga plain showed a decrease in sediment contribution from the HH to the Ganga plain during the LGM, supporting the observation of the current study.

An alternative, but unlikely hypothesis to explain the observed variation in the relative proportion of sediment from the Himalaya and the Peninsular India is to invoke the role of hydrography and sea level changes in the Bay of Bengal in the dispersion of sediments. It can be argued that sediments from the Himalaya were transported directly to the central BoB during LGM due to lower sea level resulting in lower sediment proportion from the Himalaya at the core site. This proposition can be ruled out in case of sediments from the western BoB and particularly from the core site of SK187/PC33, as this core is from a water depth of ~3000 m and during LGM the Eastern Indian Coastal Current (EICC) was southwestward (Sarkar *et al.*, 1990; Schott and McCreary, 2001; Tiwari *et al.*, 2005). The EICC was directed N-S during LGM and hence, is expected to have focused more sediments from the Himalayan rivers to the western BoB compared to present-day, where the EICC is directed S-N. If so, the western BoB would have received higher proportion of Himalayan sediments during the LGM, which is contrary to the observations of the present study.

The variations in the Sr and Nd isotope composition of core SK187/PC33 attest an existing relation between past climatic changes and continental erosion. This hypothesis is also supported by earlier results on the variation of the Nd isotope composition of seawater and bulk sediments in the Bay of Bengal and in the Indian Ocean during the LGM and the Holocene (Burton and Vance, 2000; Stoll *et al.*, 2007; Gourlan *et al.*, 2010). Burton and Vance (2000) and Stoll *et al.* (2007) attributed changes in the Nd isotopic composition of seawater and bulk sediments during LGM to reduced erosional fluxes from the Himalaya caused by decrease in rainfall. This is consistent with the observation of this study.

Clift *et al.* (2008) investigated ε_{Nd} of sediments from the Indus delta. Their results show variability consistent to those observed in this study i.e. decrease in ε_{Nd} following LGM. This decrease can be attributed to relatively higher contribution of sediments from the Himalaya, particularly that from the Ganga basin, due to increase in monsoon intensity and decrease in snow cover. This interpretation is also supported by earlier observations of two-fold increase in the sediment supply from the Himalaya to the Bengal basin during these periods (Goodbred and Kuehl, 2000). In contrast to this, the results of

Galy *et al.* (2008), based on Sr and Nd isotopic signatures of sediments from the channel-levee system in Bengal Fan, reported constancy in their sources since LGM. The reason behind this difference is unclear. One possible cause could be that the sampling site of Galy *et al.* (2008) is a channel-levee system, where sediments can undergo recycling. Further, the core site of Galy *et al.* (2008) receives sediments predominantly from G-B river, whereas the core SK187/PC33 receives sediments from the G-B rivers along with Peninsular Indian rivers and hence is able to better trace the signals of source variability.

The physical (MS), chemical and isotopic signature of SK187/PC33 showed a reduced Himalayan contribution to the BoB during LGM. These signatures of change in erosion pattern of the Himalaya during LGM are well preserved in the BOB sediments, which demonstrate the high efficiency of the Himalayan Rivers in transferring the sediments from their source (Himalaya) to the sink (BoB) with an insignificant time-lag between production of sediment in the Himalaya and their deposition in BoB. This observation hints that the residence time of the sediment of the Himalayan rivers in the plain seem to be very low, far less compared to that (~100 ka) proposed by Granet *et al.* (2007) based on the U-Th data of the sediments of the Gandak river.

5. CONCLUSIONS

The sediments from a core in the western Bay of Bengal are characterized by highly radiogenic Sr and low ε_{Nd} values. This suggests relatively higher contribution of Himalayan-derived sediments to the core site than those from Peninsular India. The Sr and Nd isotope compositions show significant temporal variations suggesting considerable changes in the relative contributions from the Himalaya and the Peninsular

India sources in the past. These variations in $^{87}Sr/^{86}Sr$ and ε_{Nd} support the hypothesis that during LGM, sediment contribution from the Himalaya was reduced due to decreased intensity of SW monsoon and increased extent of glacial cover over the High Himalaya.

ACKNOWLEDGEMENTS

Discussions with S. Krishnaswami helped improving the manuscript significantly. Thanks to M. M. Sarin for logistic support. M. G. Yadav and J. P. Bhavsar helped during ^{14}C measurements. Help of B. Srinivas and P. Kessarkar during geochemical and MS analyses is acknowledged. Thanks to the chief scientist and crew members of 187th cruise of ORV *Sagar Kanya* for their onboard help. We thank Daniele Pinti, the associate (and vice) editor and two anonymous reviewers for their constructive comments and suggestions. Financial assistance was provided by the Ministry of Earth Sciences for collection of piston cores under the BENFAN project. This is NIO contribution No. xxxx.

Reference:

Ahmad, S. M., Anil Babu, G., Padmakumari, V. M., Dayal, A. M., Sukhija and B. S., Nagabhushanam, P. (2005) Sr, Nd isotopic evidence of terrigenous flux variations in the Bay of Bengal: Implications of monsoons during the last ~34,000 years. *Geophys. Res. Lett.*, **32**, 1-4.

Ahmad, S. M., Padmakumari and Anil Babu, G. (2009) Strontium and neodymium isotopic compositions in sediments fom Godavari, Krishna and Pennar rivers. *Curr. Sci.*, **97**, 1766-1769.

Bhushan R., Chakraborty, S. and Krishnaswami, S. (1994) Physical Research Laboratory (Chemistry) Radiocarbon Date list I. *Radiocarbon*, **36**, 251-256.

Bloemendal, J., King, J., Hunt, A., Demenocal, P. and Hayashida, A. (1993) Origin of the sedimentary magnetic record at Ocean drilling program sites on the Owen ridge, western Arabian sea. *J. Geophys. Res.*, **98**, 4199-4219.

Bloemendal, J., Liu, X. And Rolph, T. (1995) Correlation of the magnetic susceptibility startigraphy of Chinese loess and the marine oxygen isotope record: chronological and palaeoclimatic implications. *Earth Planet. Sci. Lett.*, 131, 371-380.

Bookhagen, B., Fleitmann, D., Nishiizumi, K., Strecker, M. R. and Thiede, R. C. (2006) Holocene monsoonal dynamics and fluvial terrace formation in the northwest Himalaya, India, *Geology*, **34**, 601-604.

Bookhagen, B., Thiede, R. C. and Strecker, M. R. (2005) Late Quaternary intensified monsoon phases control landscape evolution in the northwest Himalaya, *Geology*, **33**, 149-152.

Bouquillon, A., France-Lanord, C., Michard, A. and Tiercelin, J. J. (1990) Sedimentology and isotopic chemistry of the Bengal Fan sediments: the denudation of the Himalaya, *Proc., scientific results*, ODP, Leg 116, distal Bengal Fan, 43-58.

Burbank, D. W., Blythe, A. E., Putkonen, J., Pratt-Sitaula, B., Gabet, E., Oskin, M., Barros, A. and Ojha, T. P. (2003) Decoupling of erosion and precipitation in the Himalayas, *Nature*, **426**, 652-655.

Burton, K. W. and Vance, D. (2000) Glacial-interglacial variations in the neodymium isotope composition of seawater in the Bay of Bengal recorded by planktonic foraminifera, *Earth Planet. Sci. Lett.*, **176**, 425-441.

Clift, P. D., Giosan, L., Blusztajn, J., Campbell, I. H., Allen, C., Pringle, M., Tabrez, A. R., Danish, M., Rabbani, M. M., Alizai, C. A., Lückge A. (2008) Holocene erosion of the Lesser Himalaya triggered by intensified summer monsoon, *Geology*, **36**, 79-82.

Colin, C., Turpin, L., Bertaux, J., Desprairies, A. and Kissel, C. (1999) Erosional history of the Himalayan and Burman ranges during the last two glacial-interglacial cycles, *Earth Planet. Sci. Lett.*, **171**, 647-660.

Colin, C., Turpin, L., Blamart, D., Frank, N., Kisel, C. and Duchamp, S. (2006) Evolution of weathering patterns in the Indo-Burman Ranges over 280 kyr: Effects of sediment provenance on ^{87}Sr/^{86}Sr ratios tracer, *Geochem. Geophys. Geosyst.,* **7**, doi:10.1029/2005GC000962.

Courtillot, V., Besse, J., Vandamme, D., Montigny, R., Jaeger, J. and Cappetta, H. (1986) Deccan flood basalts at Cretaceous/Tertiary boundary? *Earth Planet. Sci. Lett.*, **80**, 361-374.

Duplessy, J. C. (1982) Glacial to interglacial contrasts in the northern Indian Ocean, *Nature*, **295**, 494-498.

Dutta, K., Bhushan, R. and Somayajulu, B. L. K. (2001) ΔR correction values for the northern Indian Ocean, *Radiocarbon*, **43**, 483-488.

France-Lanord, C., Derry, L. and Michard, A. (1993) Evolution of the Himalaya since Miocene time: Isotopic and sedimentologic evidence from the Bengal Fan, in *Himalayan Tectonics*, edited by P. J. Treloar and M. Searle, *Geol. Soc. Spec. Publ.*, **74**, 603–621.

Galy, A. and France-Lanord, C. (2001) Higher erosion rates in the Himalaya: Geochemical constraints on riverine fluxes, *Geology*, **29**, 23-26.

Galy, V., Francois, L., France-Lanord, C., Faure, P., Kudrass, H., Palhol, F. and Singh, S. K. (2008) C4 plants decline in the Himalayan basin since the Last Glacial Maximum, *Quat. Sci. Rev.,* **27**, 1396-1409.

Goodbred, S. L., Jr. (2003) Response of the Ganges dispersal system to climate change: a source-to-sink view since the last interstade, *Sediment. Geol.*, **162**, 83-104.

Goodbred, S.L., Jr. and Kuehl, S.A. (2000) The significance of large sediment supply, active tectonism, and eustasy on margin sequence development: Late Quaternary stratigraphy and evolution of the Ganges-Brahmaputra delta. *Sediment. Geol.*, **133**, 227–248.

Gourlan, A., Meynadier, L., Allegre, C., Tapponnier, P., Birck, J. and Joron, J. (2010) Northern Hemisphere climate control of the Bengali rivers discharge during the past 4 Ma. Quaternary Science Reviews 29, 2484-2498.

Granet, M., F., Chabaux, P.,Stille, C.,France-Lanord and Pelt, E. (2007) Time-series of sedimentary transfer and weathering processes from U-series nuclides : Clues from the Himalayan rivers. *Earth Planet .Sci. Lett.*, **261**, 389-406.

Herzschuh, U. (2006) Palaeo-moisture evolution in monsoonal Central Asia during the last 50,000 years, *Quat. Sci. Rev.*, **25**, 163-178.

http://www.gemswater.org/atlas-gwq/table3-e.html

Islam, M. R., Begum, S. F., Yamaguchi, Y. and Ogawa, K. (1999) The Ganges and Brahmaputra rivers in Bangladesh: Basin denudation and sedimentation, *Hydrol. Proc.*, **13**, 2907-2923.

Kessarkar, P. M., Rao, V. P., Ahmad, S. M., Patil, S. K., Anil Kumar, A., Anil Babu, G., Chakraborty, S. and Soundar Rajan, R. (2005) Changing sedimentary environment during the Late Quaternary: Sedimentological and isotopic evidence from the distal Bengal Fan, *Deep Sea Res.*, **52**, 1591-1615.

Kessarkar, P. M., Rao, V. P., Ahmad, S. M. and Anil Babu G. (2003) Clay minerals and Sr-Nd isotopes of the sediments along the western margin of India and their Implication for sediment provenance, *Mar. Geol.*, **202**, 55-69.

Ninkovich, D., Opdyke, N., Heezen, B. and Foster, J. (1966) Palaeomagnetic startigraphy, rates of deposition and tephrachronology in North Pacific deep-sea sediments. *Earth Planet. Sci. Lett.,* **1**, 476-492.

Owen, L. A., Finkel, R. C. and Caffee, M. W. (2002) A note on the extent of glaciation throughout the Himalaya during the global Last Glacial Maximum, *Quat. Sci. Rev.*, **21**, 147-157.

Pattan, J.N., G., Parthiban, C., Prakash Babu and N.H., Khadge (2008) A note on geochemistry of surface sediments from Krishna-Godavari basin, East coast of India. *J. Geol. Soc. India.* **71**, 107-114.

Pierson-Wickmann, A.-C., Reisberg, L., France-Lanord, C. and Kudrass H. R. (2001) Os-Sr-Nd results from sediments in the Bay of Bengal: Implications for sediment transport and the marine Os record, *Paleoceanography*, **16**, 435-444.

Prell, W. L., Hutson, W., Williams, D. F., Be, A. W. H., Geitzenauer, K. and Molfino B. (1980) Surface circulation of the Indian Ocean during the last Glacial Maximum approximately 18,000 yr B.P., *Quat. Res.* **14**, 309– 336.

Prell, W. L. and Kutzbach, J. E. (1987) Monsoon variability over the past 150, 000 years, *J. Geophys. Res.*, **92**, 8411-8425.

Rahaman, W., Singh, S. K., Sinha, R. and Tandon, S. K. (2009) Climate control on erosion distribution over the Himalaya during the past ~100 ka, *Geology*, **37**, 559-562.

Robinson, R.A.J., Bird, M. I., Oo, N. W., Lu, X. X., Hoey, T. B., Swe, A. and Tun, T. (2006) Reanalysis of the 19th century hydrology and sediment load dataset for the Irrawaddy River, Myanmar, *Geophys. Res. Abstracts*, **8**, 10097.

Sager, W. and Hall, S. (1990) Magnetic properties of black mud turbidites from ODP Leg 116, Distal Bengal Fan, Indian Ocean. In: Proceedings of the ocean Drilling Programme, Scientific results (eds Cochran, J. et al.), **116**, 317-336.

Sarkar, A. (1989) Oxygen and Carbon isotopes in Indian Ocean sediments and their Palaeoclimatic implications, Ph D. Thesis, Gujarat University, 55-57.

Sarkar, A., Ramesh, R., Bhattacharya, S. K. and Rajagopalan, G. (1990) Oxygen isotope evidence for a stronger winter monsoon current during the last glaciation, *Nature*, **343**, 549-551.

Sangode, S., Suresh, N. and Bagati T. (2001) Godavari source in the Bengal fan sediments: Resulst from magnetic susceptibility dispersal pattern. *Curr. Sci.*, 80, 660-664.

Sangode, S., Sinha, R., Phartiyal, B., Chauhan, O., Mazari, R., Bagati, T., Suresh, N., Mishra, S., Kumar, R. and Bhattacharjee, P. (2007) Environmental magnetic studies on some quaternary sediments of varied depositional settings in the Indian sub-continent. *Quat. Int.*, **159**, 102-118.

Schott, F. A., and J. P. McCreary Jr. (2001) The monsoon circulation of the Indian Ocean, *Prog. Oceanogr.*, **51**, 1 – 123.

Singh, S. K. and France-Lanord, C. (2002) Tracing the distribution of erosion in the Brahmaputra watershed from isotopic compositions of stream sediments, *Earth Planet. Sci. Lett.*, **202**, 645-662.

Singh, S. K., Rai, S. K. and Krishnaswami, S. (2008) Sr and Nd isotopes in River sediments from the Ganga basin: Sediment provenance and spatial variability in physical erosion, *J. Geophys. Res.*, **113**, F03006, doi:10.1029/2007JF000909.

Stoll, H. M., Vence, D. and Arevalos, A. (2007) Records of the Nd isotope composition of seawater from the Bay of Bengal: Implications for the impact of Northern Hemisphere cooling on ITCZ movement, *Earth Planet. Sci. Lett.,* **255**, 213-228.

Stuiver, M. and Reimer, P. J. (1993) Extended ^{14}C data base and revised CALIB 3.0 ^{14}C age calibration program, *Radiocarbon*, **35**, 215-230.

Tiwari, M., Ramesh, R., Somayajulu, B. L. K., Jull, A. J. T. and Burr, G. S. (2005) Early deglacial (~19-17 ka) strengthening of the northeast monsoon, *Geophys. Res. Lett.*, **32**, 1-4.

Tripathy, G., Singh, S. and Ramaswamy, V. (2008) Tracking the provenance of sediments of the Bay of Bengal through their Sr concentration and $^{87}Sr/^{86}Sr$, Conference on "Terrestrial planets: Evolution through time", India.

Tutken, T., Eisenhauer, A., Wiegand, B. and Hansen, B. T. (2002) Glacial-interglacial cycles in Sr and Nd isotopic composition of Arctic marine sediments triggered by the Svalbard/Barents Sea ice sheet, *Mar. Geol.*, **182**, 351-372.

Walter, H. J., Hegner, E., Diekmann, B., Kuhn, G. and Rutgers van der loeff, M. M. (2000) Provenance and transport of terrigenous sediment in the south Atlantic Ocean and their relations to glacial and interglacial cycles: Nd and Sr isotopic evidence, *Geochim. Cosmochim. Acta*, **64**, 3813-3827.

Figure captions

Figure 1. Location of the sediment core SK187/PC33 (white circle marked) in the Bay of Bengal. The various sources of sediments to the core site with their characteristic $^{87}Sr/^{86}Sr$ and ε_{Nd} are also shown (Data Source: Colin *et al.*, 1999, 2006; Ahmad *et al.*, 2009; Singh *et al.*, 2008). Bathymetry data are from http://www.bodc.ac.uk/data/online_delivery/gebco/.

Figure 2. Depth profile of Sr and Nd isotope composition of sediments from the core SK187/PC33 (dots). The solid line is the 3-point moving average of the data. Data show a dip in $^{87}Sr/^{86}Sr$ and a hump in ε_{Nd} excursions at ~600 cmbsf coinciding with the Last Glacial Maximum. Two anomalous samples at depth ~220 and 440 cmbsf are not included. The squares in the figure represent the average Sr-Nd isotopic values for the contemporary Peninsular Indian river sediments (PEN; Ahmad *et al.*, 2009) and the combined flow (Lower Meghna) of G-B river sediments (Triangle (GB); Galy and France-Lanord, 2001).

Figure 3. $^{87}Sr/^{86}Sr$ vs. ε_{Nd} of the sediments from core SK187/PC33. The isotope composition of various sources contributing to these sediments is also given. The Sr and Nd isotope composition of SK187/PC33 sediments falls within the isotopic values of riverine sediments from the Himalaya and the Peninsular India. The two samples (encircled) having low ε_{Nd} seem to be anomalous and could be deposited by flood events

in particular rivers such as the Mahanadi or the Pennar flowing though an Archean crust with radiogenic Sr and unradiogenic Nd.

Figure 4. Depth profiles of magnetic susceptibility (MS), Fe/Al and V/Al ratios for the SK187/PC33 sediments. The higher values of MS, V/Al and Fe/Al during the LGM indicate a relatively lower contribution from the Himalaya. The solid line is the 3-point moving average of the data.

Figure 5. Sr and Nd isotopic mixing plot for the SK187/PC33 sediments along with isotopic values of their dominant sedimentary sources. The dominance of the Himalayan sources, particularly HH, is observed for most of the samples with enhanced contribution from the Deccan traps during the LGM. The hyperbolic curve shown is the mixing trend among the sources calculated using the average Sr, Nd concentrations and isotope ratios of the Deccan (228 μg/g, 11 μg/g, 0.705, -5), HH (80 μg/g, 18 μg/g, 0.76, -15) and the LH (94 μg/g, 26 μg/g, 0.85, -24.4) respectively. The representative isotopic values for the sedimentary sources are from Singh *et al.* (2008), except for the TPB (Average of predominantly TPB flowing (Lohit and Dibang) river sediments; Singh and France-Lanord, 2002) and Archean terrains (Compiled from Kessarkar *et al.*, 2003, 2005).

Table 1: Basin characteristics and Sr, Nd isotopic composition of sediments at the outflow of major rivers contributing sediments to the BoB.

Basin	**River**	**Major Litho-units**	**Area**	**Runoff**	**Water discharge**	**Sediment flux**	**Sediments**	
			10^6 km^2	mm/yr	km^3/yr	10^6 tons/yr	**^{87}Sr/^{86}Sr**	ε_{Nd}
Himalaya	Ganga[1,2]	HH, LH	0.95	619	460	520	0.762 to 0.782	-16.1 to -18.1
	Brahmaputra[1,3]	HH, LH, TPB, Indo-Burmese Ranges	0.58	1087	630	540	0.721 to 0.749	-13.6 to -16.9
	Lower Meghna[1]		-	-	-	-	0.738 to 0.753	-14.8 to -17.4
Peninsular India	Mahanadi	Archean Crust	0.132	500	66	60	-	-
	Godavari[4]	Deccan Trap, Archean Crust	0.31	350	92	170	0.720 to 0.730	-12.0 to -18.2
	Krishna[4]		0.252	266	67	16		
Indo-Burman Ranges	Irrawaddy[5]	Indo-Burmese Ranges, Arakan Mountains	0.414	1034	428	355[$]	0.713	-10.7
	Salween	TPB, Indo-Burmese Ranges	0.325	649	211	337[$]	-	-

Hydrological parameters from http://www.gemswater.org/atlas-gwq/table3-e.html; [$]Robinson *et al.*, 2006.

Sr and Nd isotopic data for the sediment of the rivers at their outflow are from [1]Galy and France-Lanord, 2001; [2]Singh *et al.*, 2008; [3]Singh and France-Lanord, 2002; [4]Ahmad *et al.*, 2009; [5]Colin *et al.*, 1999.

Table 2: ^{14}C ages of inorganic carbon from the core SK187/PC33.

Sample code	**Depth** (cmbsf)	**Radiocarbon ages** (yr BP)	**Calibrated ^{14}C age** (yr BP)
PRLCH-725	54±17	7788 ± 295	8361 ± 953
PRLCH-766	281±16	13573 ± 302	15727 ± 1277
PRLCH-770	316±8	13964 ± 325	16171 ± 1333
PRLCH-776	466±23	14286 ± 355	16728 ± 1572
PRLCH-777	621±30	21242 ± 610	24840 ± 1613

Table 3A: Elemental abundances$^{\$}$, Sr, Nd concentrations and their isotope composition$^{@}$ in the sediment core SK187/PC33.

Depth (cmbsf)	**Al**	**Fe**	**V**	**Sr**	**^{87}Sr/^{86}Sr**	**Nd**	ε_{Nd}
	(%wt)		**(μg/g)**	**(μg/g)**		**(μg/g)**	
10-12	8.96	6.54	130	56	0.74041	17	-15.5
18-20	7.44	4.05	90	87	0.75051	22	-16.9
28-30	8.83	6.42	125	57	0.74089	18	-14.6
109-111	7.95	6.22	119	58	0.74212	19	-15.4
149-151	8.85	5.63	115	59	0.74457	18	-15.9
201-203	8.47	4.88	106	43	0.74522	19	-15.8
221-223	2.50	2.17	30	73	0.75732	63	-21.1
249-251	8.82	5.78	112	60	0.73759	13	-15.7
300-302	7.89	5.57	108	69	0.73528	13	-15.8
320-322	6.28	3.97	77	98	0.73483	19	-15.1
340-342	*n.a.*	*n.a.*	*n.a.*	49	0.74273	17	-15.8
350-352	8.63	4.69	78	82	0.75150	24	-15.8
360-362	*n.a.*	*n.a.*	*n.a.*	43	0.74621	14	-15.6
400-402	6.41	3.87	78	87	0.73768	19	-15.3
440-442	2.84	1.84	34	84	0.74422	24	-19.6
450-452	8.27	4.97	105	82	0.73475	19	-14.9
490-492	*n.a.*	*n.a.*	*n.a.*	58	0.74248	17	-16.5
500-502	8.22	4.47	99	71	0.75515	21	-16.5
510-512	*n.a.*	*n.a.*	*n.a.*	54	0.74009	17	-15.4
550-552	6.15	2.52	49	123	0.73594	18	-14.6
600-602	6.80	4.42	104	104	0.72861	37	-15.0
650-652	7.30	4.88	115	99	0.72528	19	-13.7
700-702	7.77	4.84	112	101	0.72750	19	-14.5
750-752	7.75	3.84	83	127	0.73573	20	-14.5
800-802	8.13	4.86	89	83	0.73284	20	-13.8
849-851	6.81	3.57	79	101	0.73638	24	-15.5
889-891	*n.a.*	*n.a.*	*n.a.*	54	0.73062	13	-14.9
899-901	5.57	3.69	56	68	0.74026	17	-17.1
909-911	*n.a.*	*n.a.*	*n.a.*	61	0.73310	16	-14.0
949-951	7.87	4.82	103	97	0.73679	*n.a.*	*n.a.*
999-1001	4.55	2.63	53	89	0.73851	21	-14.9
1049-1051	8.07	4.46	94	111	0.74016	21	-15.5
1099-1101	8.72	4.98	103	105	0.73865	18	-15.9
1149-1151	7.55	3.68	73	145	0.73334	27	-14.7
1199-1201	6.00	1.86	35	172	0.72903	13	-14.5
1219-1221	9.19	4.87	96	116	0.73669	23	-14.8

n.a.: Not Analyzed.

$^{\$}$ *The concentrations of Al, Fe and V are measured in bulk sediments.*

$^{@}$*Sr, Nd and their isotopic compositions are measured in their silicate fractions. Errors on Sr and Nd isotopic compositions are better than 10 ppm.*

Table 3B: Magnetic susceptibility (MS) of sediments from the core SK187/PC33*.

Depth	MS 10^{-8} m^3/kg	Depth	MS 10^{-8} m^3/kg	Depth	MS 10^{-8} m^3/kg
6-8 cm	25.6	**424-426 cm**	22.1	**833-835 cm**	23.7
12-14 cm	29.7	**452-454 cm**	18.7	**835-837 cm**	24.6
22-24 cm	33.9	**476-478 cm**	29.9	**837-839 cm**	23.6
30-32 cm	33.7	**510-512 cm**	25.0	**855-857 cm**	26.5
38-40 cm	27.4	**512-514 cm**	24.6	**857-859 cm**	25.5
50-52 cm	24.2	**556-558 cm**	34.0	**931-933 cm**	19.2
56-58 cm	20.7	**568-570 cm**	33.0	**933-935 cm**	21.8
70-72 cm	23.5	**578-580 cm**	52.0	**935-937 cm**	22.3
82-83 cm	36.8	**592-594 cm**	35.1	**937-939 cm**	20.0
91-93 cm	34.5	**612-614 cm**	24.6	**941-943 cm**	20.4
97-99 cm	25.0	**624-626 cm**	34.7	**943-945 cm**	20.5
109-111 cm	33.3	**632-634 cm**	31.1	**959-961 cm**	19.8
121-123 cm	30.9	**644-646 cm**	37.5	**961-963 cm**	26.8
173-175 cm	18.4	**648-650 cm**	36.3	**967-969 cm**	27.0
183-185 cm	17.7	**660-662 cm**	21.7	**969-971 cm**	24.0
185-187 cm	17.9	**670-672 cm**	28.3	**1001-1003 cm**	33.0
211-213 cm	14.0	**678-680 cm**	23.1	**1019-1021 cm**	45.3
221-223 cm	15.3	**690-692 cm**	46.6	**1029-1031 cm**	24.0
262-264 cm	14.7	**700-702 cm**	43.3	**1049-1051 cm**	22.5
268-270 cm	20.1	**710-712 cm**	26.3	**1077-1079 cm**	18.3
274-276 cm	15.3	**732-734 cm**	23.4	**1081-1083 cm**	17.6
284-286 cm	17.1	**760-762 cm**	35.6	**1099-1101 cm**	18.0
300-302 cm	22.2	**770-772 cm**	30.4	**1109-1111 cm**	22.6
308-310 cm	19.8	**790-792 cm**	23.1	**1127-1129 cm**	28.4
316-318 cm	14.3	**798-800 cm**	24.3	**1139-1141 cm**	21.4
336-338 cm	14.2	**810-812 cm**	40.0	**1151-1153 cm**	68.0
346-348 cm	20.3	**820-821 cm**	34.0	**1187-1189 cm**	47.1
362-364 cm	16.9	**821-823 cm**	25.9	**1201-1203 cm**	46.8
372-374 cm	20.4	**827-829 cm**	20.6	**1211-1213 cm**	22.3
402-404 cm	23.3	**831-833 cm**	22.2	**1217-1219 cm**	30.4

*measured at frequency 0.47 kHz

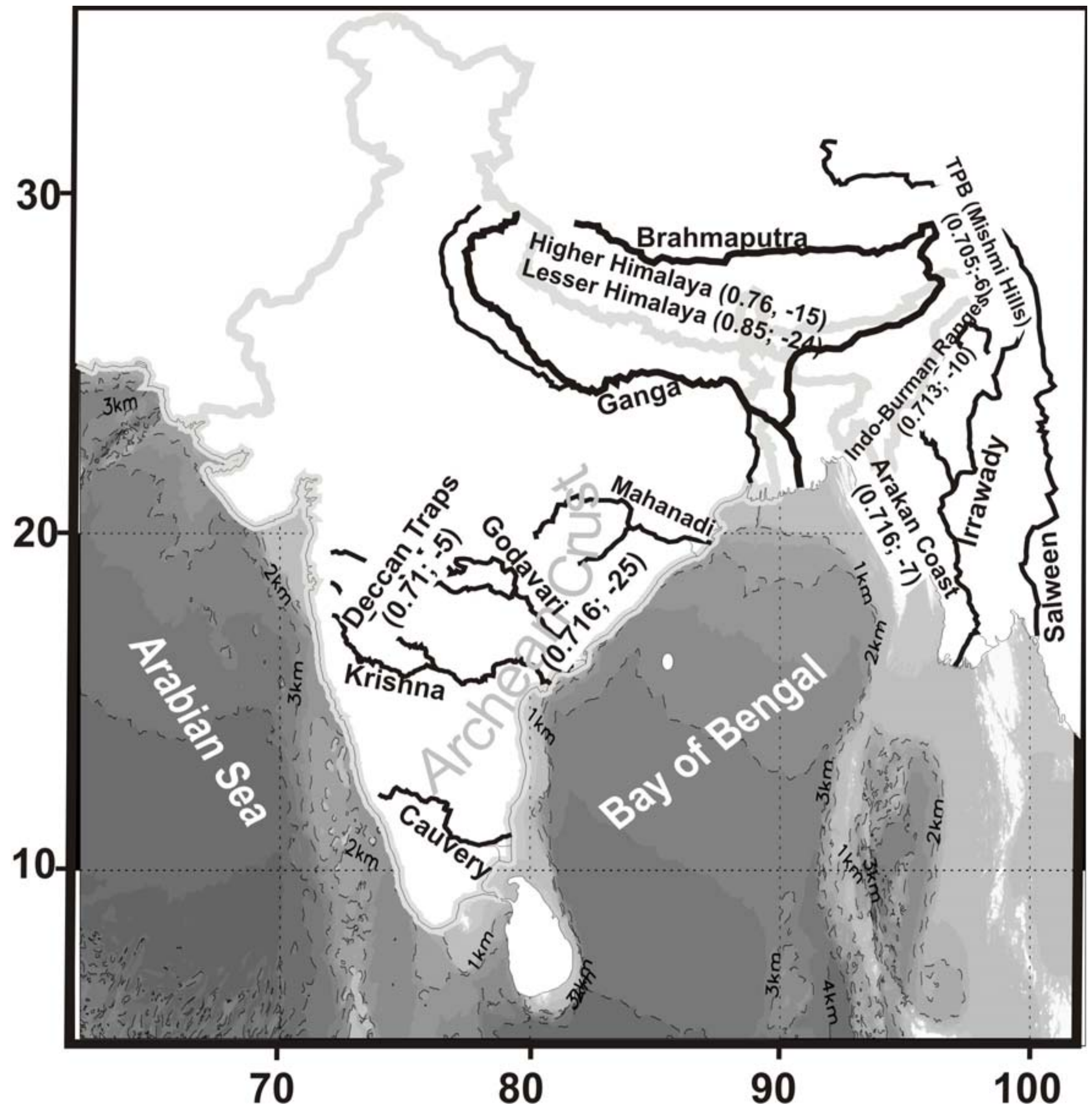
30
20
10
70
80
90
100
Brahmaputra
Higher Himalaya (0.76, -15)
Lesser Himalaya (0.85; -24)
TPB (Mishmi Hills) (0.705; -6)
Indo-Burman Ranges (0.713; -10)
Ganga
Irrawady
Salween
Arakan Coast (0.716; -7)
Mahanadi
Deccan Traps (0.71; -5)
Godavari
(0.716; -25)
Archean Crust
Krishna
Cauvery
Arabian Sea
Bay of Bengal
3km
2km
3km
2km
1km
1km
2km
1km
3km
2km
3km
1km
3km
3km
4km

Fig. 1

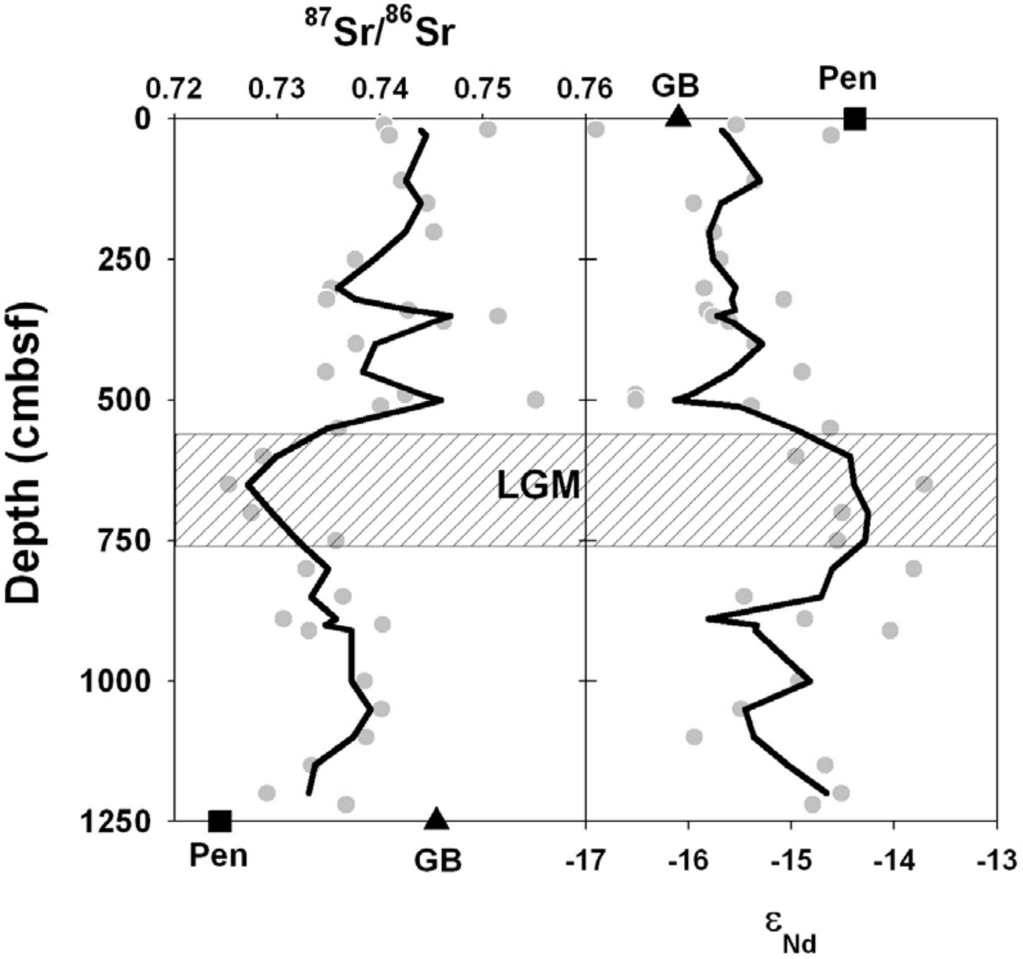

87Sr/86Sr
0.72
0.73
0.74
0.75
0.76
GB
Pen
0
250
500
750
1000
1250
Depth (cmbsf)
LGM
Pen
GB
-17
-16
-15
-14
-13
εNd

Fig. 2

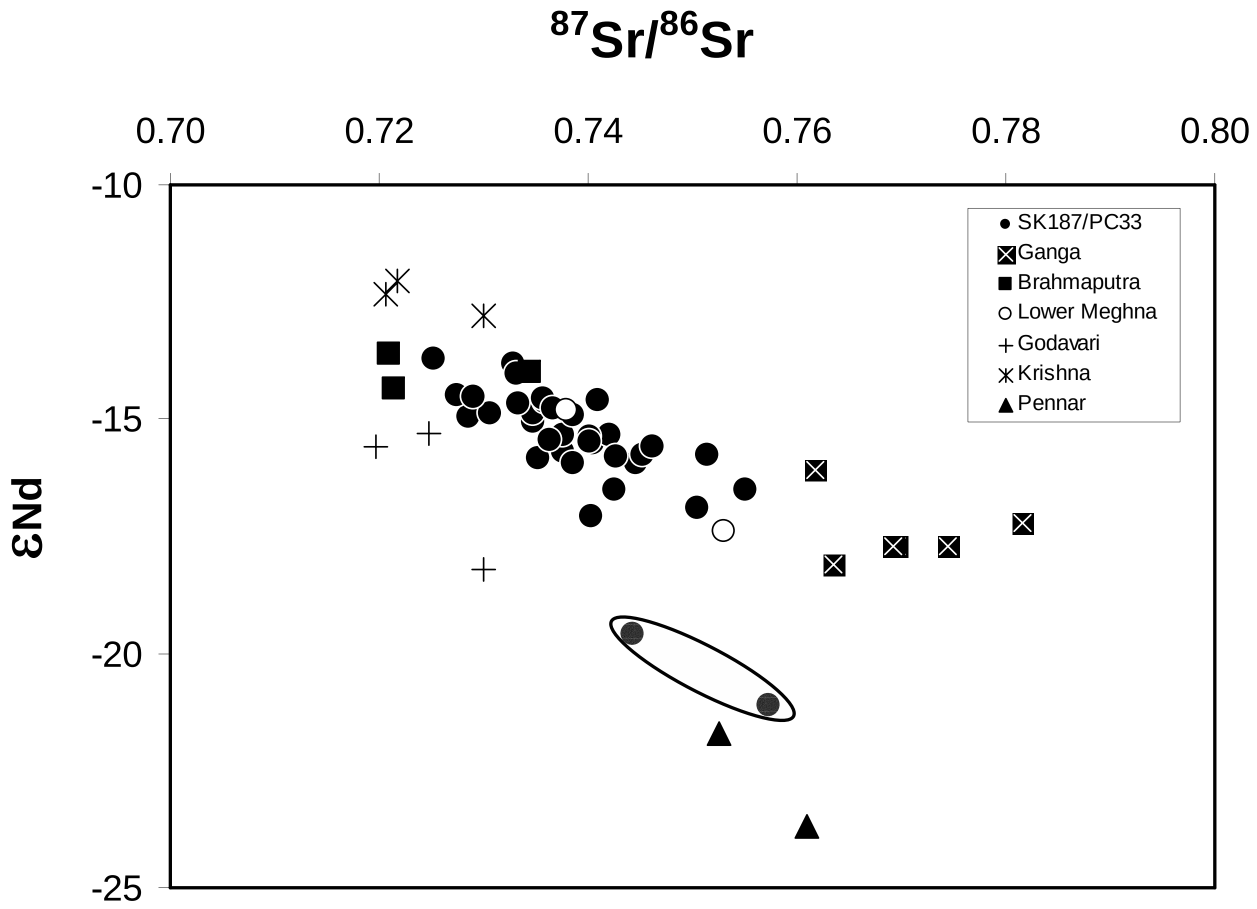

$^{87}Sr/^{86}Sr$
0.70
0.72
0.74
0.76
0.78
0.80
-10
-15
-20
-25
εNd
● SK187/PC33
☒ Ganga
■ Brahmaputra
○ Lower Meghna
+ Godavari
⁎ Krishna
▲ Pennar

Fig. 3

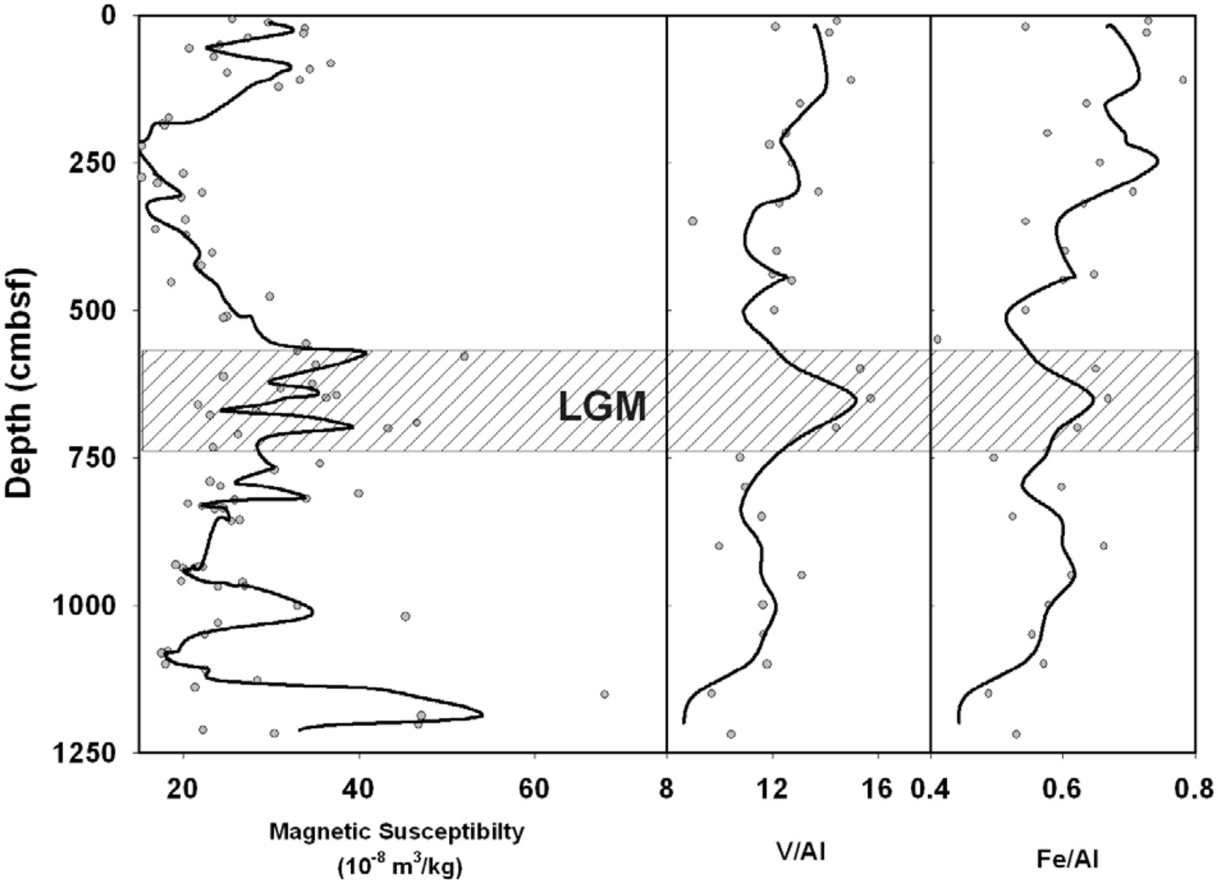

Depth (cmbsf)
0
250
500
750
1000
1250
LGM
20
40
60
8
12
16
0.4
0.6
0.8
Magnetic Susceptibilty
(10-8 m3/kg)
V/Al
Fe/Al

Fig. 4

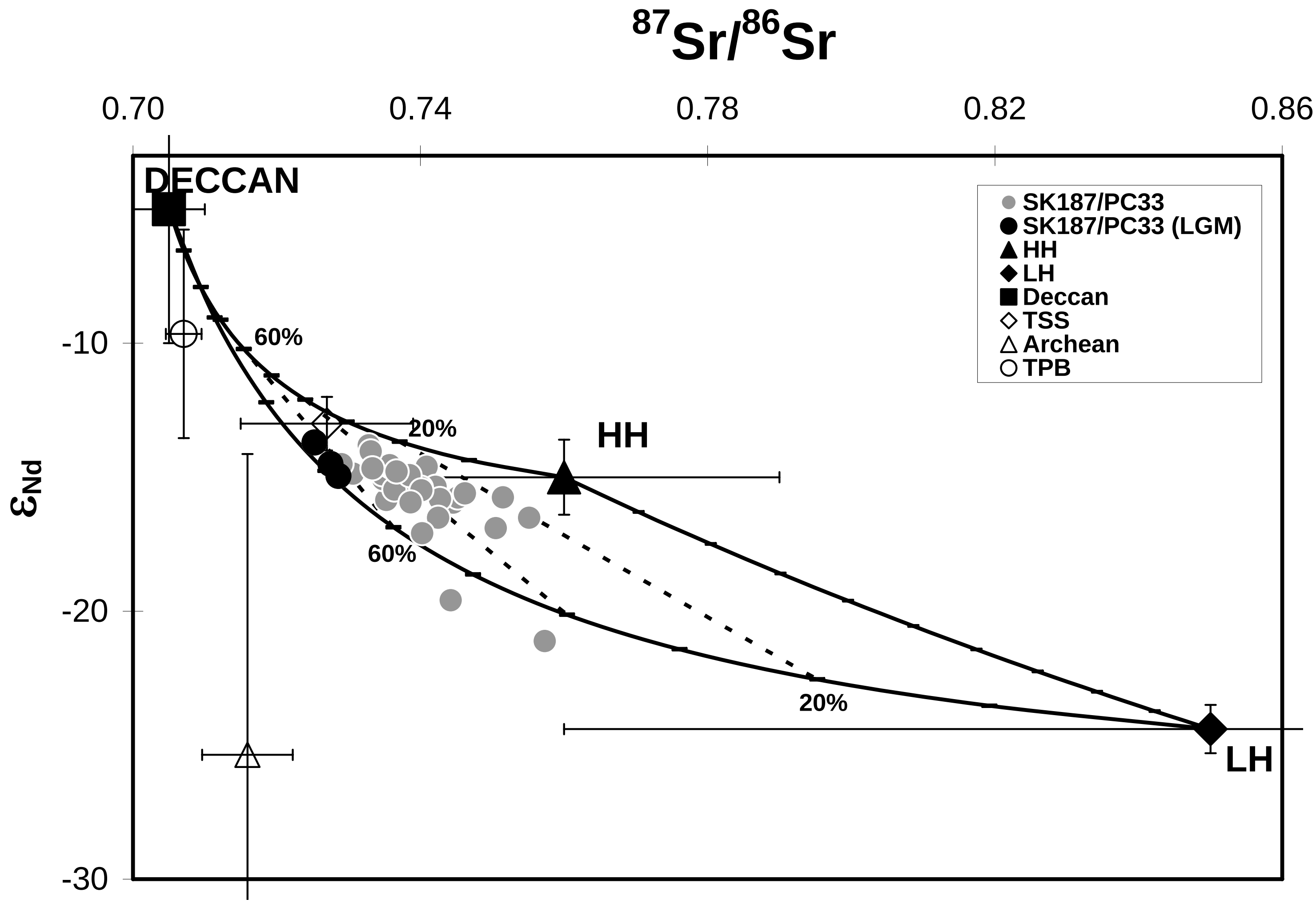
$^{87}Sr/^{86}Sr$
0.70
0.74
0.78
0.82
0.86
ε_{Nd}
-10
-20
-30
DECCAN
HH
LH
60%
20%
60%
20%
● SK187/PC33
● SK187/PC33 (LGM)
▲ HH
◆ LH
■ Deccan
◇ TSS
△ Archean
○ TPB

Fig. 5